

DISSERTATION ZUR ERLANGUNG DES DOKTORGRADES
DER FAKULTÄT FÜR CHEMIE UND PHARMAZIE
DER LUDWIG-MAXIMILIANS-UNIVERSITÄT MÜNCHEN

AZOLE-BASED ENERGETIC MATERIALS:
ADVANCES IN NITROGEN-RICH CHEMISTRY



Vorgelegt von

CARLOS H. MIRÓ SABATÉ

aus

Lleida (SPANIEN)

2008

Erklärung

Diese Dissertation wurde im Sinne von § 13 Abs. 3 bzw. 4 der Promotionsordnung vom 29. Januar 1998 von Prof. Dr. Thomas M. Klapötke betreut.

Ehrenwörtliche Versicherung

Diese Dissertation wurde selbständig, ohne unerlaubte Hilfsmittel erarbeitet.

München, den 25.07.08



(Carlos H. Miró Sabaté)

Dissertation eingereicht am: 25.07.08

1. Gutachter Prof. Dr. Thomas M. Klapötke

2. Gutacher Prof. Dr. Konstantin Karaghiosoff

Mündliche Prüfung am 08.09.08

Acknowledgements

First of all I would like to thank my mentor *Prof. Dr. Thomas M. Klapötke* for having given me the chance to do my Ph. D. studies in Munich and having kept positive about my suggestions and ideas and for the freedom in the research without which this work would have not been possible. Also for not having lost the nerves regardless many explosions.

I am specially thankful to *Prof. Dr. Konstantin Karaghiossof*. His enthusiasm and good mood have always helped me out of scientifically unpleasant situations. This work would have not been feasible without him working night and day on numerous NMR and X-ray measurements.

My lab colleagues in D3.107 (both old and new) as well as the rest of coworkers in the research group for the pleasant work atmosphere. Specially *Dr. Habil. Margaret-Jane Crawford* is thanked for her “Scottish” character.

My bachelor student *Moritz Ebespächer* and my research undergraduate students *Mihael Suhanji*, *Magdalena Rusan* and *Matthias Rasp*.

Dr. Jan M. Welch (“wee boy”) for being a good friend and for much help concerning everything to do with chemistry. Our team work is much appreciated here.

Dr. Chaza Darwich for putting up with my mood and for the nice publications together.

Dr. Georg Steinhauser for being the other guy at the back of the lab during 2007 and for the many enjoyable evenings at his place.

To *M. Sc. Vikas Verma* for his distinctive humor and for still calling me after two years of his departure and starting with the usual “Do you know who this is?” on the phone.

To *Dr. Zuraya González* (“Zuri”) for not letting me forget Spanish.

Carmen Nowak for his friendliness and much help with poster designing.

Irene Scheckenbach for much help concerning all the paper work, photocopies and faxing and for her nice character.

Gunnar Spiess and *Stefan Huber* for all the bomb calorimetry measurements and some sensitivity tests and for their easy-going character.

To *Dipl.-Chem. Norbert Mayer* and *Dipl.-Chem. Xaver Steeman* for his help with many different computer problems and for operating the high-speed camera.

To all the people that work or have worked at the analytical service (mass spectrometry, NMR and elemental analysis).

To my parents that have always trusted on me and have given me the chance to choose my way in live.

My two nephews *Gerard* and *Adrià* whose naivety helped me keep down to earth and remember what is important in live.

To the rest of my family, specially my three brothers and my two maternal grand-parents who died during the course of this work and unfortunately I could not attend their burial.

Last but not list financial support of my work by the Ludwig-Maximilian University of Munich (LMU), the Fonds der Chemischen Industrie (FCI), the European Research Office (ERO) of the U.S. Army Research Laboratory (ARL) and the Bundeswehr Research Institute for Materials, Explosives, Fuels and Lubricants (WIWEB) is also gratefully acknowledged.

*“Angesichts von Hindernissen mag die kürzeste Linie
zwischen zwei Punkten die krumme sein.”*

Bertolt Brecht aus *Leben des Galilei*

TABLE OF CONTENTS

	Page
TABLE OF CONTENTS.....	i
LIST OF FIGURES.....	vi
LIST OF TABLES.....	xii
LIST OF SCHEMES.....	xvi
CHAPTER I – INTRODUCTION TO EXPLOSIVE MATERIALS	
1.1 History of Explosives.....	1
1.2 Alternatives to TNT and Nitramine-Based Explosives.....	2
1.3 Less Powerful Energetic Materials (LPEMs).....	4
1.4 Heat Resistant Explosives.....	7
1.5 Explosives and Explosions	
1.5.1 Definitions and Types.....	7
1.6 DDT and SDT Transitions.....	9
1.7 Propellants.....	10
1.8 High Explosives.....	11
1.8.1 Primary Explosives.....	12
1.8.2 Secondary Explosives.....	13
1.8.3 Effect of Density in the Velocity of Detonation (V).....	14
1.9 Pyrotechnics.....	15
1.10 Decomposition of Explosives.....	16
1.11 Trends in Explosives Research: Azoles and Nitrogen-rich Chemistry.....	17
1.12 Summary of the Ph. D. Thesis.....	18
1.13 Testing of Energetic Materials.....	21
1.13.1 Thermal Stability.....	21
1.13.2 Standard (BAM) Tests.....	22
1.14 Definitions of Interest.....	23
1.15 References.....	24

CHAPTER II – 5-AMINOTETRAZOLES AND SILVER-BASED PRIMARIES	Page
2.1 Introduction.....	29
2.2 Synthesis.....	31
2.3 Vibrational and NMR Spectroscopy	33
2.4 Crystal Structures.....	37
2.5 Energetic Properties.....	53
2.6 Conclusions.....	56
2.7 Experimental Section.....	57
2.8 References.....	62

CHAPTER III – 5-NITRO-2*H*-TETRAZOLE PRIMARIES

3.1 Introduction.....	67
3.2 Synthesis.....	68
3.3 NMR and Vibrational Spectroscopy	70
3.4 Molecular Structures.....	72
3.5 Energetic Properties.....	85
3.6 Safety Note.....	92
3.7 Conclusions.....	93
3.8 Experimental Section.....	94
3.9 References.....	101

CHAPTER IV – 1,2,4-TRIAZOLIUM CATION-BASED ENERGETIC SALTS

4.1 Introduction	
4.1.1 General.....	105
4.1.2 Relationship between 3,4,5-triamino-1,2,4-triazole and 1,5-diamino-1 <i>H</i> -tetrazole.....	106
4.2 Synthesis of 3,4,5-triamino-1,2,4-triazolium Halogenides.....	108
4.3 Synthesis of 1-Methyl-3,4,5-triamino-1,2,4-triazolium Energetic Salts.....	109
4.4 Vibrational and NMR Spectroscopies.....	110
4.5 Molecular Structures.....	114
4.6 Physical and Energetic Properties.....	130
4.7 Conclusions.....	134
4.8 Experimental Section.....	136

4.9 References.....	143
---------------------	-----

CHAPTER V – TRIAZOLIUM AND TETRAZOLIUM PICRATE SALTS Page

5.1 Introduction.....	147
5.2 Synthesis.....	148
5.3 Vibrational Spectroscopy	150
5.4 NMR Spectroscopy.....	151
5.5 Molecular Structures.....	156
5.6 Energetic Properties.....	168
5.7 Long Term Stabilities of 1MATPic (60) and 13DMATPic (63)	175
5.8 Decomposition Gases.....	176
5.9 Conclusions.....	177
5.10 Experimental Section.....	178
5.11 References.....	185

CHAPTER VI – METHYLATED 5-AMINOTETRAZOLE DERIVATIVES

6.1 Introduction.....	188
6.2 Synthesis.....	189
6.3 Vibrational Spectroscopy	190
6.4 NMR Spectroscopy.....	192
6.5 Molecular Structures.....	194
6.6 Energetic Properties.....	205
6.7 Computational Methods.....	209
6.8 Decomposition Gases.....	210
6.9 Conclusions.....	211
6.10 Experimental Section.....	213
6.11 References.....	219

CHAPTER VII – 5,5′-AZOTETRAZOLE DERIVATIVES	Page
7.1 Introduction.....	223
7.2.1 Synthesis of 5,5′-Azotetrazolate Salts.....	224
7.2.2 Synthesis of Neutral 5,5′-Azotetrazoles.....	226
7.3 Vibrational and NMR Spectroscopy.....	227
7.4 Molecular Structures.....	232
7.5 Thermal and Energetic Properties.....	246
7.6 Long-term Stability and Response to Thermal Shock of 84	252
7.7 Decomposition Experiments.....	253
7.8 Conclusions.....	255
7.9 Experimental Section.....	256
7.10 References.....	264

CHAPTER VIII – 5,5′-HYDRAZINEBISTETRAZOLE DERIVATIVES

8.1 Introduction.....	268
8.2 Synthesis.....	269
8.3 Characterization	
8.3.1 Spectroscopic Discussion.....	271
8.3.2 Vibrational Spectroscopy.....	273
8.3.3 Molecular Structures.....	274
8.3.4 Thermal Stability and Energetic Properties of Nitrogen-rich Derivatives of 95	291
8.3.5 Thermal Stability and Energetic Properties of Metal Salts of 95	296
8.4 ESPs of 95 and its Methylated Derivatives.....	300
8.5 Koenen (Steel Sleeve Test) of 95	302
8.6 Long-term Stability and Response to Thermal Shock of 95	303
8.7 Decomposition Experiments of 95	304
8.8 Conclusions.....	305
8.9 Experimental Section.....	306
8.10 References.....	315

CHAPTER IX – SALTS OF 5-(5-NITROTETRAZOLE-2-YLMETHYL)-TETRAZOLE (WORK PROGRESS)

9.1 Introduction.....	319
9.2 Synthesis.....	320
9.3 NMR Spectroscopy.....	323
9.4 Vibrational Spectroscopy.....	325
9.5 Molecular Structures.....	327
9.6 Energetic Properties.....	341
9.7 Decomposition Gases.....	348
9.8 Conclusions.....	350
9.9 Experimental Section.....	351
9.10 References.....	359

Appendix A – Figures and Tables.....	363
Appendix B – Structure Parameters and Hydrogen-bonding.....	391
Appendix C – Crystal Structure Solution and Refinement.....	408
Appendix D – List of Compounds.....	429
Appendix E – List of Abbreviations.....	432

Curriculum Vitae

Full List of Publications

LIST OF FIGURES

Figure

- 1.1 Structure of commonly used secondary explosives.
- 1.2 Structure of high energy density materials (HEDMs).
- 1.3 Structure of less powerful energetic materials (LPEMs).
- 1.4 Classification of explosives.
- 1.5 Structure of commonly used primary explosives.
- 1.6 Goals of the work on azole-chemistry in regard to the application.
- 2.1 Structure of some commonly-used tetrazole-based ligands.
- 2.2 Crystals of 1,4-dimethyl-5-amino-1*H*-tetrazolium picrate (left) and of silver complex **19** (right).
- 2.3 Panel plot of the IR spectra of silver complexes.
- 2.4 Panel plot of the Raman spectra of silver complexes.
- 2.5 ^1H , ^{13}C and ^{14}N NMR spectra of **16** in $\text{DMSO}-d_6$.
- 2.6 ^{15}N NMR of the 5-amino-1*H*-tetrazolium cation in **5** measured in $\text{DMSO}-d_6$.
- 2.7a Asymmetric unit of **5** with the labelling scheme.
- 2.7b Asymmetric unit of **7** with the labelling scheme.
- 2.8a Hydrogen-bonding in the unit cell of **5**.
- 2.8b Hydrogen-bonding in the unit cell of **7**.
- 2.9 Ring graph-sets of interest in the crystal structure of **5**.
- 2.10 Ring graph-sets of interest in the crystal structure of **7**.
- 2.11a Full coordination around the Ag^+ cations in the crystal structure of **15**.
- 2.11b Ring graph-sets of interest in the crystal structure of **15**.
- 2.12 Heteronborane skeleton in the crystal structure of **15** and labelling scheme.
- 2.13 View of a supercell along the c -axis in the crystal structure of **15**.
- 2.14a Asymmetric unit of **17** with the labelling scheme.
- 2.14b Coordination around the Ag^+ cations in the crystal structure of **17**.
- 2.15 View of the unit cell along the c -axis in the crystal structure of **17**.
- 2.16 View of the asymmetric unit of **19** with the labelling scheme.
- 2.17 View of the unit cell of **19** along the b -axis.
- 2.18 View of the asymmetric unit of **20** with the labeling scheme.
- 2.19 Hydrogen-bonding and coordination around the Ag^+ cations in a layer in the crystal structure of **20**.
- 2.20 DSC thermograms for the disilver derivatives **13** and **14**.
- 3.1 Proton decoupled ^{15}N NMR spectrum of the free acid **31** (in $\text{DMSO}-d_6$).
- 3.2a Panel plot of the IR spectra of alkaline earth metal salts of 5-nitro-2*H*-tetrazole (**31**).
- 3.2b Panel plot of the Raman spectra of alkaline earth metal salts of 5-nitro-2*H*-tetrazole (**31**).
- 3.3a Full coordination around the Li^+ cations in the crystal structure of **LiNT** (**22**).
- 3.3b Simplified coordination around the Li^+ cations in the crystal structure of **LiNT** (**22**).

- 3.4 View of the unit cell of **LiNT** (22) along the *a*-axis with the hydrogen bonding.
- 3.5 View of the packing around the anion in the crystal structure of **NaNT** (23) with the numbering scheme.
- 3.6a Full coordination around the Na⁺ cations in the crystal structure of **NaNT** (23).
- 3.6b Simplified coordination around the Na⁺ cations in the crystal structure of **NaNT** (23).
- 3.7a Full coordination around the K⁺ cations in the crystal structure of **KNT** (24).
- 3.7b Simplified coordination around the K⁺ cations in the crystal structure of **KNT** (24).
- 3.8a View of the unit cell of **KNT** (24) along the *a*-axis.
- 3.8b Schematic representation of the zig-zag chains formed along the *b*-axis.
- 3.9a Full coordination around the Rb⁺ cations in the crystal structure of **RbNT** (25).
- 3.9b Simplified coordination around the Rb⁺ cations in the crystal structure of **RbNT** (25).
- 3.10 View of the unit cell of **RbNT** (25) along the *b*-axis.
- 3.11a Full coordination around the Cs⁺ cations in the crystal structure of **CsNT** (26).
- 3.11b Simplified coordination around the Cs⁺ cations in the crystal structure of **CsNT** (26).
- 3.12 View of a supercell in the crystal structure of **CsNT** (26) along the *a*-axis.
- 3.13a Asymmetric unit of **CaNT** (28) with the labeling scheme.
- 3.13b Simplified coordination around the Ca²⁺ cation in **CaNT** (28).
- 3.14 View of the unit cell of **CaNT** (28) along the *c*-axis.
- 3.15 Asymmetric unit of **5-NTH** (31) with the labeling scheme.
- 3.16 View of the unit cell of **5-NTH** (31) along the *a*-axis showing the graph-sets in the structure.
- 3.17 DSC plots of alkali metal salts of 5-nitro-2*H*-tetrazole.
- 3.18 Histogram comparing the energetic properties of **31** and **31b** with RDX.
- 3.19a Result of the explosion of **NaNT** (23) after the light touch of a plastic spatula
- 3.20a Result of the spontaneous explosion of anhydrous **SrNT** (29).
- 3.A1 View of the unit cell of **23** showing the hydrogen-bonding.
- 3.A2 Packing around the anion in the crystal structure of **24** with the numbering scheme.
- 3.A3 View of a “layer” in the crystal structure of **24**.
- 3.A4 Packing around the anion in the crystal structure of **25** with the numbering scheme.
- 3.A5 Packing around the anion in the crystal structure of **26** with the numbering scheme.
- 4.1 Structures of 1,5-diamino-1*H*-tetrazole (**48**) and 3,4,5-triamino-1,2,4-triazole (**49**).
- 4.2 Asymmetric unit of 2,4-dinitro-*O*-phenyloxyphtalimide (**51**).
- 4.3 Panel plot of the Raman spectra of methylguanazinium energetic salts.
- 4.4 Panel plot of the IR spectra of energetic guanazinium salts.
- 4.5 NMR labelling scheme.
- 4.6 ¹⁵N{¹H} NMR of the methylguanazinium cation in **47**, measured in [D₆]DMSO .
- 4.7 Asymmetric unit of a) **α-GzI** (**55a**), b) **β-GzI** (**55b**) and c) **41** with numbering scheme.
- 4.8 Layers in the structure of **α-GzI** (**55a**) with the contacts between perpendicular layers.
- 4.9 View of the unit cell of **β-GzI** (**55b**) along the *c*-axis.

- 4.10 a) View of the unit cell of **41** along the *c*-axis showing the layered structure b) Dimmer-pair representing a **R2,2(8)** motif hydrogen-bonding network
- 4.11 X-ray labeling for MeGz⁺ salts.
- 4.12 Asymmetric unit of **42** showing the numbering .
- 4.13 Hydrogen-bonding in a layer of **42**.
- 4.14 Asymmetric unit of **43** showing the numbering.
- 4.15 View of one of the layers showing the extensive hydrogen bonding in **43**.
- 4.16 Hydrogen bonding around the perchlorate anion in **44**.
- 4.17 View of one of the cations layers in **44**.
- 4.18 Asymmetric unit of **45a** showing the numbering .
- 4.19 Hydrogen-bonding around the 5,5'-azotetrazolate anion in **45a**.
- 4.20 Asymmetric unit of **46a** showing the numbering .
- 4.21 View of a layer with the corresponding hydrogen-bonding in **46a**.
- 4.22 Asymmetric unit of **47** showing the numbering .
- 4.23 Hydrogen-bonding in the structure of **47**.
- 4.24 DSC plots of **α -GzI (55a)**, **β -GzI (55b)** and **41**.
- 5.1 From left to right: formula structures of TNT, picric acid, 1,2,4-triazole and 1*H*-tetrazole.
- 5.2 Synthesis of **62** (Method 1).
- 5.3 IR spectra of selected azolium picrate salts.
- 5.4 Raman spectra of selected azolium picrate salts.
- 5.5 ¹H NMR spectrum of picrate salt **67** in DMSO-*d*₆.
- 5.6 ¹³C NMR spectrum of **61** in [D₆]DMSO with the assignments.
- 5.7 NMR labeling scheme for the triazolium and tetrazolium cations.
- 5.8 Coupled ¹⁵N NMR spectrum of **67** in DMSO-*d*₆ showing the N–H couplings at one bond.
- 5.9 Layers of cations and anions in the unit cell of **60** (view along the *a*-axis).
- 5.10 Hydrogen-bonding in the crystal structure of picrate salt **60**.
- 5.11 View of the unit cell of picrate salt **62** along the *b*-axis showing the hydrogen-bonding.
- 5.12 Hydrogen-bonding in the crystal structure of **62** showing some characteristic ring graph-sets.
- 5.13 Asymmetric unit of picrate salt **63** with the labeling scheme.
- 5.14 View of the unit cell of picrate salt **63** along the *b*-axis showing the hydrogen-bonding.
- 5.15 Molecular structure of **66** in the crystalline state.
- 5.16 Primary and secondary graph-sets of interest in **66**.
- 5.17 View of the unit cell of picrate salt **67** showing the stacks of cations and anions along the *b*-axis.
- 5.18 Hydrogen-bonding in the crystal structure of **67** showing some characteristic ring graph-sets.
- 5.19 Differential scanning calorimetry (DSC) plots for selected azolium picrate salts.
- 5.20 Thermal safety calorimetry (TSC) plots for **60** and **63**.
- 5.A1 Predicted decomposition gases for picrate salts **59**, **60**, **61**, **62**, **63** and **64**.
- 5.A2 Predicted decomposition gases for picrate salts **65**, **66**, **67** and for TNT and picric acid.

- 6.1 Structural formula of 5-aminotetrazoles.
- 6.2 Panel plot of the IR spectra of energetic salts of 2-methyl-5-aminotetrazole (**4**) and 1,3-dimethyl-5-aminotetrazole (**69**).
- 6.3 ^{15}N NMR spectrum of the 1,3-dimethyl-5-aminotetrazolium cation in compound **71**.
- 6.4 Hydrogen bonding in a layer in the crystal structure of compound **4**.
- 6.5 Hydrogen bonding in a layer of nitrate salt **12**.
- 6.6 Section of the hydrogen bonding in the crystal structure of perchlorate salt **11**.
- 6.7a View of the unit cell of iodide salt **70** along the *b* axis.
- 6.7b View of the unit cell of nitrate salt **71** along the *b* axis.
- 6.8a **C2,2(6)** chain networks in the crystal structure of nitrate salt **71**
- 6.8b Lateral view of one of the waved-layers of nitrate salt **71** formed along the *b* axis.
- 6.9 Formation of ring graph-sets in the crystal structure of perchlorate salt **72**.
- 6.10a Waves of anions and cations in the unit cell of azide salt **73** along the *b* axis
- 6.10b View of the hydrogen bonding in a layer of the azide salt **73**.
- 6.11 Hydrogen bonding in the crystal structure of dinitramide salt **74**.
- 6.12 “Flame test” of 1,3-dimethyl-5-aminotetrazolium salts **71–74**.
- 7.1 Pictures of 5,5′-azotetrazole derivatives: **14DMATZTh** (**81**), **1,1DMZT** (**91a**) and **2,2DMZT** (**92**).
- 7.2 a) Raman and b) IR spectra of selected 5,5′-azotetrazolate salts.
- 7.3 Solid state ^{15}N NMR spectrum of **81**.
- 7.4 Schematic representation of the disorder found in the 5,5′-azotetrazolate of **84**.
- 7.5 ^{15}N NMR spectrum of **91a** in $\text{DMSO}-d_7$.
- 7.6a View of the unit cell along the *b* axis in the crystal structure of **81**.
- 7.6b Hydrogen-bonding in a layer in the crystal structure of **81**.
- 7.7a Hydrogen-bonding between layers in the crystal structure of **83**.
- 7.7b Hydrogen-bonding in a layer in the crystal structure of **83**.
- 7.8 Asymmetric unit of **81** with hydrogen-bonding and the labelling .
- 7.9 Asymmetric unit of **83** showing the N11–N16 intramolecular hydrogen bond and the labelling .
- 7.10a View of an **R2,4(14)** hydrogen-bonding graph-set in the crystal structure of **83**.
- 7.10b View of an **R4,4(18)** hydrogen-bonding graph-set in the crystal structure of **83**.
- 7.11 Asymmetric unit of **86** with the labeling scheme.
- 7.12 Hydrogen-bonding around the azotetrazolate anion in the unit cell of **86**.
- 7.13 Hydrogen-bonding around the anion in the crystal structure of **88**.
- 7.14 Asymmetric unit of 5,5′-azotetrazolate **82** with the labelling .
- 7.15 Hydrogen-bonding around the anion in the structure of **82**.
- 7.16 Hydrogen-bonding around the guanazinium cation in the crystal structure of **84**.
- 7.17 Hydrogen-bonding around the 5,5′-azotetrazolate anion in the crystal structure of **85**.
- 7.18 Hydrogen-bonding between cations in the crystal structure of **85**.
- 7.19 Molecular structure of **91b**.

- 7.20 Unit cell of **91b** showing the hydrogen-bonding.
- 7.21 DSC plots for 5,5'-azotetrazolate salts at a heating rate of $\beta = 5\text{ }^{\circ}\text{C min}^{-1}$.
- 7.22 Radex plot for the long-term thermal stability of **HBT** and **84** and mixtures with copper.
- 7.23 Infrared spectra of the decomposition products of **81**, **86**, **83** and **88**.
- 7.A1 Experimental normalized molar percentage of decomposition gases as estimated by mass spectrometry.
- 7.A2 Predicted molar percentage of decomposition gases using the ICT code for 5,5'-azotetrazolate salts.
- 8.1 Formula structures of 5,5'-azobistetrazole (**75**), 5,5'-hydrazinebistetrazole (**95**) and *N,N*-bis(1*H*-tetrazole-5-yl)-amine (**96**).
- 8.2 Molecular structure of carboxyaminoguanidine betaine monohydrate (**CAGh**, **114**).
- 8.3 Monitoring of the oxidation of **112** to the 5,5'-azotetrazolate salt (**117**) by $^{13}\text{C}\{^1\text{H}\}$ NMR in $\text{DMSO-}d_6$.
- 8.4 Solid state ^{15}N NMR of **95**.
- 8.5a Raman panel plot spectra for alkaline earth metal salts of **95**.
- 8.5b IR panel plot spectra for alkaline earth metal salts of **95**.
- 8.6 Hydrogen-bonding around the molecule in the crystal structure of **95**.
- 8.7a Unit cell of **95** showing the layers formed by the tetrazole moieties.
- 8.7b View of the unit cell of **95** along the *c*-axis showing the gaps left by the molecules.
- 8.8 Asymmetric unit of **97** with the labelling scheme.
- 8.9 View of the unit cell of **97** along the *b*-axis showing the hydrogen-bonding.
- 8.10 View of the unit cell of **99** along the *b*-axis showing the formation of non-planar layers connected by hydrogen-bonding.
- 8.11 Hydrogen-bonding in the crystal structure of **99** with the labelling scheme showing the formation of some characteristic graph-sets.
- 8.12 Optimized structures (B3LYP/cc-pVDZ) of HBT^{2-} , HBT^{2-} planar, **95** C_i and **95** C_i .
- 8.13 View of the unit cell of **113** along the *a*-axis showing "planar" parallel layers of anions connected through hydrogen bonds to water molecules.
- 8.14a Simplified coordination around the metal centre in **113**.
- 8.14b Full coordination around the metal centre in **113**.
- 8.15 Hydrogen-bonding around the HBT^{2-} anion in the crystal structure of **112**.
- 8.16a Simplified coordination around the metal centre in **112**.
- 8.16b Full coordination around the metal centre in **112**.
- 8.17a Simplified coordination around the metal centre in **111**.
- 8.17b Full coordination around the metal centre in **111**.
- 8.18 Asymmetric unit of **110** with the labelling scheme.
- 8.19 Hydrogen-bonding around the HBT^{2-} anion in the crystal structure of **110** showing the non-planar tetrazole rings.
- 8.20 Coordination around the Li^+ cations in the crystal structure of **105** and labelling scheme.
- 8.21 Characteristic hydrogen-bonding ring graph-sets in the crystal structure of **105**.
- 8.22 Coordination around the Rb^+ cations (**Rb1**) in the crystal structure of **108** and labelling scheme.

- 8.23** Tetrazolate layers and hydrogen-bonding in the unit cell of **108**.
- 8.24a** Full coordination around one of the Cs⁺ cations (Cs1) in the crystal structure of **109**.
- 8.24b** Simplified coordination around one of the Cs⁺ cations (Cs1) in the crystal structure of **109**.
- 8.25a** Hydrogen-bonding in the unit cell in the crystal structure of **109**.
- 8.25b** **R4,4(17)** hydrogen-bonding network in the crystal structure of **109**.
- 8.26** DSC plot of **95** at a heating rate of 2 °C min⁻¹.
- 8.27** TG curve of **113** showing the DTA curve and the loss of mass for a measurement at $\beta = 5$ °C min⁻¹.
- 8.28** “Flame tests” for alkali metal salts, “fast heating” (top) and “slow heating” (bottom).
- 8.29** Electrostatic potential (ESP) of **95** for the 0.001 electron/bohr³ isosurface.
- 8.30** Electrostatic potential (ESP) for **97** and **98** for the 0.001 electron/bohr³ isosurface.
- 8.31** Steel sleeve (Koenen) test on 15 g of **95** (port diameter: 8 mm).
- 8.32** Smokeless combustion of **95** *vs.* non-smokeless combustion of guanazinium 5,5'-azotetrazolate.
- 8.33** “Flame tests” for ammonium (**99**) and hydrazinium (**100**) salts of **95**, “fast heating” (top) and “slow heating” (bottom).
- 8.34** IR spectra of the decomposition gases of **95** (top) and **GzZT**.
- 8.A1** Raman and IR of **95** indicating the most important bands.
- 8.A2** Optimized structures (B3LYP/cc-pVDZ) of the ZT²⁻ anion (left) and **75** (right).
- 8.A3** Equilibrium between the two possible configurations of the tetrazole rings in alkaline earth salts of 5,5'-hydrazinebistetrazole.
- 8.A4** Coordination to the Sr²⁺ cations in a layer in the crystal structure of **112**.
- 8.A5** View of the unit cell of **111** along the *c*-axis showing the “apparent coplanarity” between tetrazole rings and the contacts to the calcium atoms.
- 8.A6** View of the unit cell of **110** along the *a*-axis showing the contacts to the Mg²⁺ cations.
- 8.A7** View of the unit cell of **105** along the *a*-axis showing the coordination to the Li⁺ cations.
- 8.A8** Electrostatic potential (ESP) of 1,2-dimethylhydrazine bistetrazole for the 0.001 electron/bohr³ isosurface.
- 8.A9** Electrostatic potential (ESP) of both isomers of 1,2-dimethylhydrazine bis(methyl)tetrazole for the 0.001 electron/bohr³ isosurface.
- 8.A10** Molar percentages of the decomposition gases of **95** and **GzZT**.
- 9.1** Pictures of a) **142**, b) **143** and c) **144**.
- 9.2** ¹⁵N NMR of **128**, **129b** and **137** (see X-ray labels).
- 9.3** Asymmetric unit of **128** with the labelling scheme.
- 9.4** View of the double cell C [-1 .. +1] along the *a*-axis showing the formation of dimer pairs in the crystal structure of **128**.
- 9.5** Asymmetric unit of **145** with the labelling scheme.
- 9.6** View of the unit cell of **145** along the *a*-axis.
- 9.7** Asymmetric unit of **129a** with the labelling scheme.
- 9.8** Hydrogen bonding in the crystal structure of **129a** (view along the *c*-axis).

- 9.9 Asymmetric unit of **135** with the labelling scheme.
- 9.10 Ring graph-sets in the crystal structure of **135**.
- 9.11 Asymmetric unit of **138** with the labelling scheme.
- 9.12 Hydrogen-bonding around the anion in the crystal structure of **138**.
- 9.13 Coordination around one of the K⁺ cations in the crystal structure of **132** with labelling scheme.
- 9.14 Packing in the crystal structure of **132**.
- 9.15 Asymmetric unit of **133** with labelling scheme.
- 9.16 Coordination around one of the Rb⁺ cations (Rb1) in the crystal structure of **133**.
- 9.A1 Predicted decomposition gases for **128**, **129a** and **135** using the ICT-code.
- 9.A2 Predicted decomposition gases for **137**, **138**, RDX and TEX using the ICT-code.

LIST OF TABLES

Table

- 1.1 Sensitivity data of common primary explosives and minimal amount to initiate PETN.
- 1.2 Safety data and detonation parameters of common high explosives.
- 2.1 Selected bond and angle geometries for the 5-aminotetrazolium salts
- 2.2 Hydrogen-bonding geometry in the 5-aminotetrazolium salts.
- 2.3 Graph-set matrix for selected hydrogen bonds in **15**.
- 2.4 Graph-set matrix for selected hydrogen bonds in **17**.
- 2.5 Graph-set matrix for selected hydrogen bonds in **19**.
- 2.6 Graph-set matrix for selected hydrogen bonds of one of the three 1MAT ligands in **20**.
- 2.7 Selected coordination geometry around the Ag⁺ cations in **15**, **17** and **19**.
- 2.8 Comparison of initial safety testing results for silver complexes and tetrazolium salts.
- 3.1 Selected interatomic distances and angles for metal salts of 5-nitro-2*H*-tetrazole (**31**).
- 3.2 Medium to strong hydrogen bonds in the crystal structures of compounds **22**, **23** and **28**.
- 3.3 Physico-chemical properties of alkali metal salts of 5-nitro-2*H*-tetrazole.
- 3.4 Physico-chemical properties of alkaline earth metal salts of 5-nitro-2*H*-tetrazole.
- 3.5 Physico-chemical properties, initial safety data and predicted performance of 5-nitro-2*H*-tetrazole (**31**).
- 3.6 Comparison of the energetic properties of compounds **31** and **31b** with RDX.
- 3.A1 Calculated and measured IR and Raman frequencies with tentative assignment for the NT⁻ anion.
- 3.A2 CBS-4M results.
- 3.A3 Literature values for atomic ΔH_f^{298} .
- 3.A4 Enthalpies of the gas-phase species M and enthalpy of sublimation of 5-nitro-2*H*-tetrazole (**31**).
- 3.A5 Solid state energy and enthalpy of formation of 5-nitro-2*H*-tetrazole (**31**).
- 3.B1 Graph-set matrix for selected hydrogen bonds in lithium 5-nitro-2*H*-tetrazolate.
- 3.B2 Graph-set matrix for selected hydrogen bonds in sodium 5-nitro-2*H*-tetrazolate.

- 3.B3** Graph-set matrix for medium to strong hydrogen bonds in the crystal structure of 5-nitro-2*H*-tetrazole.
- 3.B4** Selected coordination geometry around the metal centre in lithium, sodium and potassium 5-nitro-2*H*-tetrazolate.
- 3.B5** Selected coordination geometry around the metal centre in rubidium and cesium 5-nitro-2*H*-tetrazolate salts.
- 3.B6** Selected coordination geometry around the Ca²⁺ cations in calcium 5-nitro-2*H*-tetrazolate.
- 4.1** ¹⁵N NMR shifts, N–H coupling constants and PIS/MIS for **33** and Gz⁺ and MeGz⁺ salts.
- 4.2** Selected bond lengths /Å and angles /deg for **α-GzI (55a)**, **β-GzI (55b)** and **41**.
- 4.3** Selected bond lengths /Å and angles /deg for the MeGz⁺ cation.
- 4.4** Physico-chemical properties of methylguanazinium salts.
- 4.5** Initial safety testing results and predicted (calculated) energetic performance of methylguanazinium salts using the EXPLO5 code.
- 4.A1** Calculated (C₁ point group) and observed (IR and Raman) frequencies (250 cm⁻¹ > ν > 2000 cm⁻¹) with assignment.
- 4.A2** Calculated electronic and zero point energies (MP2/aug-cc-pVDZ).
- 4.A3** Thermodynamic and explosive properties of formulations of **42**, **44** and **47** with ammonium nitrate (AN).
- 4.A4** Thermodynamic and explosive properties of formulations of **45a**, **45b**, **46a** and **46b** with ammonium nitrate (AN).
- 4.A5** Thermodynamic and explosive properties of formulations of **42**, **44** and **47** with ammonium dinitramide (ADN).
- 4.A6** Thermodynamic and explosive properties of formulations of **45a**, **45b**, **46a** and **46b** with ammonium dinitramide (ADN).
- 4.B1** Selected hydrogen bonding and iodine-hydrogen contact parameters for **α-GzI (55a)**.
- 4.B2** Selected hydrogen bonding and iodine-hydrogen contact parameters for **β-GzI (55b)**.
- 4.B3** Selected hydrogen bonding and iodine-hydrogen contact parameters for **41**.
- 4.B4** Selected hydrogen bonds for **42**.
- 4.B5** Selected hydrogen bonds for **43**.
- 4.B6** Selected hydrogen bonds for **44**.
- 4.B7** Selected hydrogen bonds for **45a**.
- 4.B8** Selected hydrogen bonds for **46a**.
- 4.B9** Selected hydrogen bonds for **47**.
- 5.1** ¹⁵N and ¹³C NMR chemical shifts, PIS/MIS values and coupling constants of azolium picrate salts.
- 5.2** Selected bond distances and angles in the azolium cation of picrate salts.
- 5.3** Selected hydrogen bonds for azolium picrate salts.
- 5.4** Graph-set matrix for strong to medium hydrogen bonds in **60**
- 5.5** Graph-set matrix for strong to medium hydrogen bonds in **62**.
- 5.6** Graph-set matrix for strong to medium hydrogen bonds in **63**.

- 5.7 Graph-set matrix for strong to medium hydrogen bonds in **66**.
- 5.8 Graph-set matrix for strong to medium hydrogen bonds in **67**.
- 5.9 Physico-chemical properties of azolium picrate salts.
- 5.10 Initial safety testing results and predicted and calculated energetic performance of azolium picrate salts.
- 5.11 Predicted decomposition gases and heats of explosion of azolium picrate salts and comparison with commonly used high explosives.
- 5.A1 Results of the quantum chemical calculations (MP2/cc-pVDZ).
- 5.A2 Thermodynamic and explosive properties of formulations of azolium picrate salts with ammonium nitrate.
- 5.A3 Thermodynamic and explosive properties of formulations of azolium picrate salts with ammonium dinitramide.
- 6.1 ^{15}N and ^{13}C NMR chemical shifts and protonation/methylation induced shifts.
- 6.2 Selected bond lengths and angles for the methylated 5-aminotetrazole derivatives.
- 6.3 Medium to strong hydrogen bonds for compound **4** and salts of **4** and **69**.
- 6.4 Selected closed-shell interactions for compounds **11**, **71**, **72** and **74**.
- 6.5 Physico-chemical properties of the energetic salts.
- 6.6 Initial safety testing results and predicted energetic performance of the energetic salts.
- 6.7 Predicted decomposition gases and heats of explosion of methylated 5-aminotetrazole derivatives.
- 6.A1 Calculated electronic and zero point energies (MP2/aug-cc-pVDZ).
- 6.A2 Predicted thermochemical data.
- 6.A3 Thermodynamic and explosive properties of formulations of the energetic salts with ammonium nitrate.
- 6.A4 Thermodynamic and explosive properties of formulations of the energetic salts with ammonium dinitramide.
- 7.1 Bond distances (\AA) in the 5,5'-azotetrazole moiety of 5,5'-azotetrazole derivatives.
- 7.2 Bond angles ($^\circ$) in the 5,5'-azotetrazole moiety of 5,5'-azotetrazole derivatives.
- 7.3 Initial safety testing results and predicted energetic performance of 5,5'-azotetrazole derivatives using the EXPLO5 code.
- 7.4 Physico-chemical properties of 5,5'-azotetrazole derivatives.
- 7.A1 Thermodynamic and explosive properties of formulations of 5,5'-azotetrazole derivatives with AN.
- 7.A2 Thermodynamic and explosive properties of formulations of 5,5'-azotetrazole derivatives with ADN.
- 7.A3 Explosive properties of **HBT** and **84** and comparison with common high explosives and formulations with commonly used oxidizers and high explosives.
- 7.A4 Fragmentation degree for the Koenen (steel-sleeve) test.
- 7.A5 Response to thermal shock of **HBT** and **84** and mixtures with AN and ADN.
- 7.A6 Results of the DFT calculations (MP2/aug-cc-pVDZ).
- 7.B1 Hydrogen-bonding geometry in 5,5'-azotetrazole derivatives.

- 8.1** Physico-chemical properties of nitrogen-rich 5,5'-hydrazinebistetrazole derivatives.
- 8.2** Initial safety testing results and calculated energetic performance of nitrogen-rich 5,5'-hydrazinebistetrazole derivatives and comparison with analogous salts of **96** and **75**.
- 8.3** Physico-chemical properties of alkali and alkaline earth metal salts of **95**.
- 8.A1** Calculated (C_1 point group) and observed (IR and Raman) frequencies for **95**.
- 8.A2** Results of the DFT calculations (B3LYP/cc-pVDZ) on **95**.
- 8.A3** Computational results (B3LYP/cc-pVDZ) of bridged bistetrazoles.
- 8.A4** Thermodynamic and explosive properties of 5,5'-hydrazinebistetrazole (**95**).
- 8.A5** Thermodynamic and explosive properties of formulations of nitrogen-rich hydrazinebistetrazolate salts with ammonium nitrate (AN).
- 8.A6** Thermodynamic and explosive properties of formulations of nitrogen-rich hydrazinebistetrazolate salts with ammonium dinitramide (ADN).
- 8.B1** Graph-set matrix for strong hydrogen bonds in **95**.
- 8.B2** Bond distances in 5,5'-hydrazinebistetrazole derivatives.
- 8.B3** Selected bond distances for alkaline earth salts of 5,5'-hydrazinebistetrazole (**95**).
- 8.B4** Bond angles in 5,5'-hydrazinebistetrazole derivatives.
- 8.B5** Selected bond angles for alkaline earth salts of 5,5'-hydrazinebistetrazole (**95**).
- 8.B6** Hydrogen-bonding geometry in 5,5'-hydrazinebistetrazole derivatives.
- 8.B7** Geometry for selected hydrogen bonds for alkaline earth salts of 5,5'-hydrazinebistetrazole (**95**).
- 8.B8** Selected contact distances for the coordination around the Li^+ atoms in **105**.
- 8.B9** Selected contact distances for the coordination around the Rb^+ atoms in **108**.
- 8.B10** Selected contact distances for the coordination around the Cs^+ atoms in **109**.
- 8.B11** Selected bond distances and angles for the coordination around the Mg^{2+} cations in **110**.
- 8.B12** Selected distances and angles for the coordination around the Ca^{2+} cations in **111**.
- 8.B13** Selected distances and angles for the coordination around the Sr^{2+} cations in **112**.
- 8.B14** Selected distances and angles for the coordination around the Ba^{2+} cations in **113**.
- 9.1** Calculated and experimental frequencies with the corresponding intensities (IR) and activities (Raman) and tentative assignment for the $N^+T^+Tz^-$ anion.
- 9.2** Selected bond lengths [\AA] and angles [$^\circ$] for nitrogen-rich 5-nitrotetrazole derivatives.
- 9.3** Hydrogen-bonding geometry in nitrogen-rich 5-nitrotetrazole derivatives.
- 9.4** Selected bond lengths [\AA] and angles [$^\circ$] for **132** and **133**.
- 9.5** Selected bond distances for the coordination around the K^+ cations in **132**.
- 9.6** Hydrogen-bonding geometry in **132** and **133**.
- 9.7** Selected bond distances for the coordination around the Rb^+ cations in **133**.
- 9.8** Physico-chemical properties of nitrogen-rich salts of **129b**.
- 9.9** Physico-chemical properties of **129b** alkali metal salts.
- 9.10** Physico-chemical properties of **129b** transition metal salts.

- 9.11** Initial safety testing results and predicted energetic performance of nitrogen-rich 5-nitrotetrazole derivatives using the EXPLO5 code.
- 9.12** Thermodynamic and explosive properties of formulations of nitrogen-rich salts of **129b** with ammonium nitrate (AN).
- 9.13** Thermodynamic and explosive properties of formulations of nitrogen-rich salts of **129b** with ammonium dinitramide (ADN).
- 9.14** Predicted decomposition gases and heats of explosion of nitrogen-rich 5-nitrotetrazole derivatives and comparison with known high explosives (using the ICT code).
- 9.A1** Calculated electronic and zero point energies (MP2/aug-cc-pVDZ).
- 9.B1** Graph-set matrix for selected hydrogen bonds in **132**.
- 9.B2** Graph-set matrix for selected hydrogen bonds in **133**.
- 9.B3** Selected bond angles for the coordination around the K⁺ cations in **132**.
- 9.B4** Selected bond angles for the coordination around the Rb⁺ cations in **133**.

LIST OF SCHEMES

Scheme

- 2.1** Synthesis of the 5-aminotetrazolium nitrate and perchlorate salts.
- 2.2** Reaction leading to the formation of **19**.
- 3.1** Formula structures of neutral 5-substituted tetrazoles: 5-amino-1*H*-tetrazole (**1**), 5-nitro-2*H*-tetrazole (**31**), 5-nitriminotetrazole (**A**) and 5-azido-1*H*-tetrazole (**B**).
- 3.2** Synthesis of alkali metal salts of 5-nitro-2*H*-tetrazole by Method A.
- 3.3** Synthesis of alkali and alkaline earth metal salts of 5-nitro-2*H*-tetrazole by Method B.
- 3.4** Synthesis of the free acid **5-NTH** (**31**) from **21a**.
- 4.1** Synthesis of **32** and **33** from thiosemicarbazide.
- 4.2** Synthesis of **α-GzI** (**55a**) and **β-GzI** (**55b**) from S-methylthiosemicarbazide hydroiodide (**54**).
- 4.3** Suggested mechanism for the formation of **GzI** (**55**) from S-methylthiosemicarbazide hydroiodide (**54**).
- 4.4** Synthesis of methylguanazinium energetic salts.
- 4.A1** Born-Haber energy cycle for the calculation of the heat of combustion of **45b** and **46b**.
- 5.1** Reaction equation for the synthesis of azolium picrate salts.
- 6.1** Synthesis of energetic salts of 2-methyl-5-aminotetrazole (**4**) and 1,3-dimethyl-5-iminotetrazole (**69**).
- 6.2** Born-Haber energy cycle for calculating the heat of formation of an ionic CHNO compound.
- 7.1** Decomposition of 5,5'-azotetrazolate salts in acid media.
- 7.2** Oxidation of **5-At** (**1**) to **NaZT** (**77**) in basic solution.
- 7.3** Synthesis of the nitrogen-rich 5,5'-azotetrazolate salts.
- 7.4** Synthesis of **91a** and **92**.

8.1 Synthesis of 5,5'-hydrazinebistetrazole derivatives.

9.1 General Born-Haber cycle for the formation of a CHNO-based salt.

9.2 Synthesis of **128**, **129a** and salts of **129b**.

9.3 Synthesis of transition metal (Ag, Cu) salts of **129b**.

CHAPTER I

INTRODUCTION TO EXPLOSIVE MATERIALS

1.1 History of Explosives

Black powder (*gunpowder*) is the oldest explosive composition. Known already by the Chinese in 220 BC it did not arrive to Europe until 1249. Black powder consists of a mixture of potassium nitrate (KNO_3), charcoal (C) and sulfur (S). It was used in small and big guns and hand grenades during the 15th and 16th centuries and until 1870 it was known as the only explosive in coal mining. Several disastrous explosions occurred involving black powder at that time. With the need of more powerful explosives for mining and tunneling construction, the first nitroglycerine (NG) manufacturing plants started to appear in 1863 many of which blew up due to accidental and unreliable initiation of NG. After loosing his brother in one of these explosion, Alfred Nobel invented the first *blasting caps*, which made use of mercury fulminate ($\text{Hg}(\text{CNO})_2$) and improved the initiation characteristics of black powder. In 1866 Nobel absorbed NG in clay (*kieselguhr*) and patented the first dynamite (*gubr dynamite*). Contemporaneously, nitrocellulose (NC), which was later known as *guncotton*, was being developed and also many accidents occurred. Nobel mixed NC and NG producing a gel, which was developed to produce blasting gelatine and in more modern times gave birth to the first smokeless powder (*ballistite*). Although, reports on the first synthesis of ammonium nitrate (AN) date back to 1654 it was not until the 19th century that it was considered for use in explosive compositions as a replacement for KNO_3 in black powder. Also some explosions involving AN occurred, the most famous one in Texas City in 1947.^[1]

Black powder and dynamite had the problem that were not reliable in use and handling, unpredictable, risk of undesired explosions and low performance. The ideal military explosive should be hard to detonate (except for under specific conditions), have a high performance, should be easy to handle, be easy to load in a shell, stable to most climates... Military explosives developed with the intention to replace black powder and the first nitroaromatic explosives appeared.^[1] The first military explosive to be put in service during World War I (WWI) was picric acid, which was initially used as a dye for silk and wool. The compound suffers though of some drawbacks such as its high melting point (i.e., difficult to fill in a shell), formation of toxic compounds, sensitivity and reaction with heavy metal giving very sensitive salts.^[2] Contemporaneously, tetryl was being developed and used as the base charge of *blasting caps*.^[1]

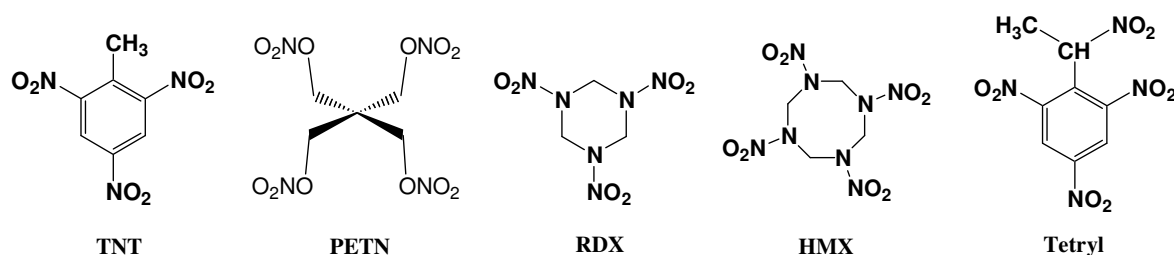


Figure 1.1 Structure of commonly used secondary explosives.

2,4,6-Trinitrotoluene (TNT, Figure 1.1) appeared as an alternative to the use of picric acid during WWI and WWII. The compound shows some improved properties such as lower melting point (81°C), which allows it to be poured in shells, it is cheap and relatively insensitive.^[2] In addition, nitroguanidine (NQ) was used in trench mortar shells at the time. After this, the need for more powerful explosives promoted the development of high explosives based on nitrate esters (e.g., PETN = pentaerythritol tetranitrate) or on nitramine moieties (e.g., RDX = 1,3,5-trinitroperhydro-1,3,5-triazine or HMX = 1,3,5,7-tetranitro-1,3,5,7-tetrazocane, Figure 1.1). The initial problems with the synthesis of PETN due to the non-readily availability of the starting materials added to low chemical stability and high sensitivity of the compound made the use of RDX dominant during WWII, although it was not the main filling in shells and bombs but it was diluted with TNT to reduce the sensitivity.^[1] Such mixtures of RDX + TNT and HMX + TNT were given the name of *hextro* and *octol formulations*, respectively (see section 1.8.2 *Secondary Explosives*).^[2]

1.2 Alternatives to TNT and Cyclic Nitramine-Based Explosives

In the past, high explosives such as RDX, HMX and TNT were considered adequate for all weapon applications. However, the many catastrophic explosions resulting from unintentional initiation of munitions (e.g., by impact or shock) made the above compounds less attractive. In modern ordinance there are strong requirements for explosives having both good thermal stability, impact and shock insensitivity and better performance. However, these requirements are somewhat mutually exclusive. Explosives materials having good thermal stability and impact insensitivity usually exhibit poorer explosive performance and vice versa.^[3]

There are several factors, which affect the energetic performance of a material. One of the critical factors is the energy of the decomposition reaction(s) and the number of moles and molecular weight of the gaseous products.^[4] The velocity at which the explosive wave propagates is another factor of interest. This is proportional to the square of the density. Therefore, as it will be pointed out many times during this work, density also plays an important role since the more moles of an

explosive compound that can be packed into the limited volume of a shell the better. Lastly, a balanced oxygen content and a highly positive heat of formation also contribute to boost the performance although this generally increases the sensitivity of the compound.^[3]

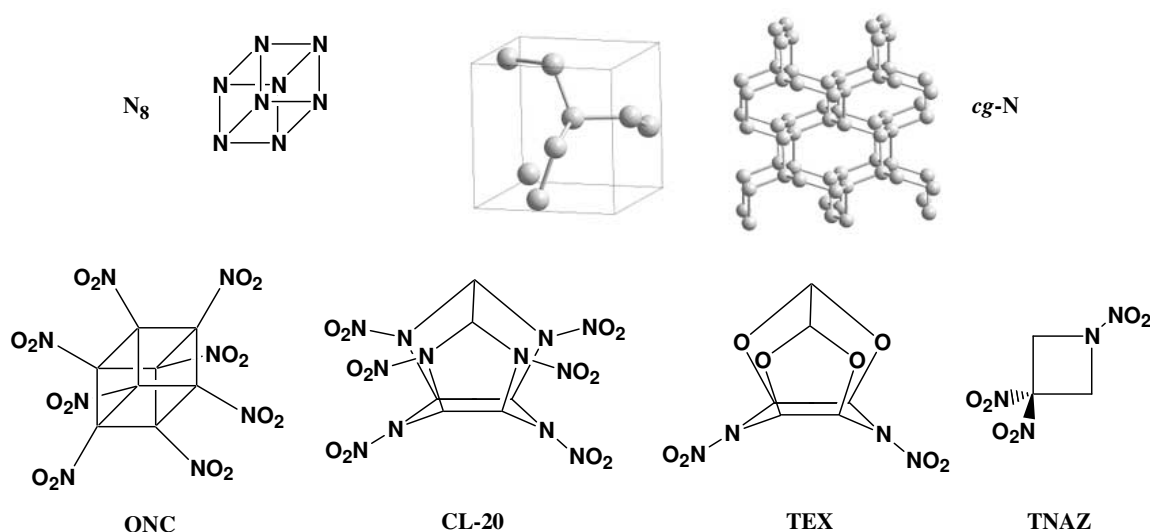


Figure 1.2 Structure of high energy density materials (HEDMs).

In the context above, predictions are useful to identify target molecules with interesting energetic properties^[5,6] and caged structures and bicyclic heterocycles are expected to show the best compromise of stability, oxygen balance, high heat of formation and predicted performance. This sort of materials having a high density are known as HEDMs (High Energy Density Materials). Cyclic compounds exhibit markedly higher (density) values than their acyclic analogues. In addition, the strain inherent to caged structures results in large positive heats of formation. One of the most interesting examples in this regard are cubanes. Cubane itself is kinetically stable decomposing at $>200\text{ }^{\circ}\text{C}$ and has a high positive heat of formation ($\sim 620\text{ kJ mol}^{-1}$).^[7] In addition, highly nitrated cubanes are predicted to be very dense and insensitive to shock.^[8] The main drawback associated with the use of such compounds as high explosives with low sensitivities is that often multistep syntheses are required.^[9,10] In 2000 Zhang et al. reported the synthesis of heptanitrocubane (HpNC) and the long sought octanitrocubane (ONC, $(\text{CNO}_2)_8$)^[8] HpNC is currently easier to make than ONC and is more dense (2.028 g cm^{-3}), which makes it a more powerful explosive. Solid hexanitrobenzene (HNB, $(\text{CNO}_2)_6$)^[11] is an isomer of ONC and counts as one of the most energetic explosives with a heat of formation of 200 kJ mol^{-1} , which is nevertheless much smaller than that of NCO itself (594 kJ mol^{-1})^[10] due to the ring strain, whereas the energy in HNB is lowered by the aromatic stabilization. ONC has been predicted to perform $>20\%$ better than HMX.^[12] The most prominent cubane is octaazacubane (N_8 , Figure 1.2), which has a calculated density of 2.69 g cm^{-3} and the highest calculated detonation velocity (V) for any high explosive known till date ($>15000\text{ m}$

s⁻¹).^[13,14] Recently Eremets et al. reported the synthesis of polymeric nitrogen (*g*-N).^[15] Unfortunately, the compound is only stable at room temperature at a pressure of 42 GPa.

One of the major scientific breakthroughs in the chemistry of caged energetic compounds came with CL-20 (HNIW = 2,4,6,8,10,12-Hexanitrohexaazaisowurtzitan, Figure 1.2), which shows a much easier synthetic approach than cubanes and is stable at room conditions.^[16] Some of the properties of the compound are high density (2.04 g cm⁻³, ϵ -CL-20), high detonation velocity (9380 m s⁻¹), highly positive heat of formation (+410 kJ mol⁻¹) and high thermal stability (T_d = 228 °C). Another attractive feature of the compound is that it shows great compatibility properties with nitramines and nitrate esters, however, its application is limited by its high sensitivity.^[17] Another interesting isowurtzitan derivative is 4,10-dinitro-2,6,8,12-tetraoxa-4,10-diazatetracyclododecane (TEX, Figure 1.2),^[18,19] which emerged with the intention of preparing a high-performing compound with decreased sensitivity. TEX has also many attractive properties such as a high density (1.99 g cm⁻³), excellent thermal stability (T_d >240 °C), V = 8665 m s⁻¹, good compatibility with inert and energetic polymer systems and much less sensitive to friction and impact stimuli than RDX and HMX. Shortly after Archibald et al. reported the synthesis of 1,3,3-trinitro-azetidine (TNAZ),^[20] and Coburn et al. improved the original synthesis.^[21] TNAZ has the advantage that it has a low melting point and a large liquid range making it suitable for casting charges without any energy-diluting binder.^[22] and has been investigated to replace TNT.^[21,23] The compound has a density of 1.84 g cm⁻³, decomposes at >240 °C and is half as impact sensitive as HMX. However, TNAZ is expensive to prepare and slightly volatile.^[24]

1.3 Less Powerful Energetic Materials (LPEMs)

A second area of interest are the so-called less powerful energetic materials (LPEMs). These compounds have the most varied structures. The most classical example of this group is 1,3,5-triamino-2,4,6-trinitrobenzene (TATB, Figure 1.3),^[24] which is based on an aromatic system, but there are newer ones not based on a ring such as 1,1-diamino-2,2-dinitroethene (FOX-7 or DADE).^[25] The low sensitivity of such class of materials is explained in terms of their capability to form hydrogen bridges.^[1] Although so far there has not been many positive results in the field of nano-scaled aluminum particles,^[26] it is believed that the corresponding high-explosive compositions should be more homogeneous and the detonation velocities should be enhanced.

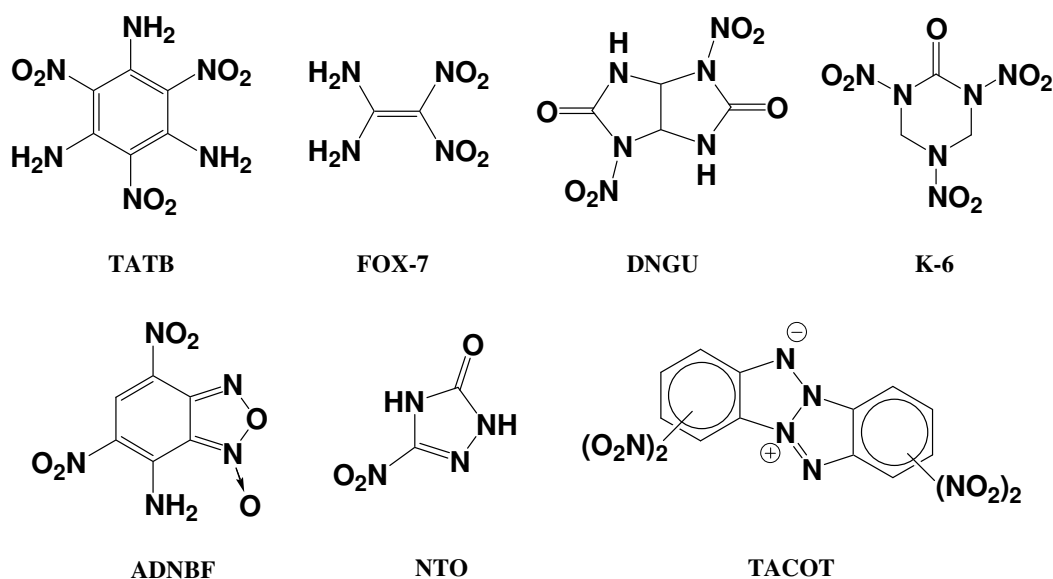


Figure 1.3 Structure of less powerful energetic materials (LPEMs).

The performance of cyclic nitramines (e.g., RDX) can be increased by replacing the methylene groups by carbonyl groups. The result is compounds with higher densities ($>1.9 \text{ g cm}^{-3}$). Whereas the more energetic dinitrourea derivatives suffer of hydrolysis liability, the mono-nitroureas are fairly stable to hydrolysis and insensitive to shock. Some of the most prominent examples of this class of compounds are 1,3,4,6-tetranitroglycouril (TNGU) and 1,4-dinitroglycouril (DNGU),^[17b] with crystal densities of 2.04 and 1.98 g cm^{-3} , respectively. DNGU decomposes in hot water slowly, however, it was studied as an insensitive energetic material that was proposed to replace RDX and TNT.^[27] Other nitroureas with interesting energetic features were produced by Mitchell et al.^[28] The most interesting compound of this study is 2-oxo-1,3,5-trinitro-1,3,5-triazacyclohexane (K-6, Figure 1.3), which is an RDX derivative with a higher density (1.932 g cm^{-3}), decomposition temperature of 205°C and a higher detonation velocity than HMX. In addition, K-6 has better hydrolytic stability than DNGU or TNGU, for example.^[3]

Another area of interest and activity in the recent years has been the replacement of nitro groups by a furoxan ring to achieve an increase in density, detonation velocity, stability and insensitivity. Some furoxan derivatives show promising properties to be used as primary explosives.^[29,30] An example of a secondary explosive belonging to this class of compounds is 7-amino-4,6-dinitrobenzofuroxan (ADNBF), which is under advanced development in the US. The excellent energetic properties of the compound ($\rho = 1.900 \text{ g cm}^{-3}$ and $V = 7900 \text{ m s}^{-1}$)^[31] can be further improved by the introduction of an amino group to form DANBF ($\rho = 1.91 \text{ g cm}^{-3}$ and $V \sim 8050 \text{ m s}^{-1}$), while still being insensitive.^[32] Also in the field of heterocyclic chemistry, energetic materials based on tetrazines show interesting properties for use in propellants or smoke-free pyrotechnic

ingredients because of their low carbon content and high heat of formation. In this regard, Hiskey et al.^[33] prepared (among others) 3,6-bis-(1*H*-1,2,3,4-tetrazole-5-yl-amino)-1,2,4,5-tetrazine), which combines a tetrazine moiety with two 5-amino-1*H*-tetrazole rings and shows a high melting point (264 °C) and high heat of formation (211 kcal mol⁻¹).^[3]

Nitrotriazoles^[34] have received much attention as energetic materials or intermediates for energetic materials. 3-Nitro-1,2,4-triazole-5-one (NTO)^[35] has been widely investigated in main charge warhead fillings for insensitive munitions (IM). The first open synthesis of the compound dates back in 1985^[36] but it had already been developed before in conjunction with HMX in plastic bonded explosives (PBXs).^[37] NTO has a similar detonation velocity than RDX but is less sensitive. Many of its metal salts have found application.^[38] Replacement of the carbonyl group in NTO by an amino group forming 3-amino-5-nitro-1,2,4-triazole (ANTA)^[39] results in interesting properties. The substituent combination of amino and nitro groups results in the formation of inter and intramolecular hydrogen bonding that may stabilize the molecule and increase the density. On the other side, the amino group in ANTA allows the compound to be oxidized to 5,5'-dinitro-3,3'-azobis-(1,2,4-triazole) (DNAzT) by the action of (for example) potassium permanganate, similar to the oxidation of 5-amino-1*H*-tetrazole to sodium 5,5'-azobistetrazolate (see *Chapter VI*). DNAzT is a dense molecule (1.885 g cm⁻³) with a high positive heat of formation (100 kcal mol⁻¹) and together with ANTA, they both offer unique features which are attractive for both explosives and propellants applications.^[3]

Other polyamino-polynitro compounds of interest were prepared by Nissan et al.^[40] and Pagaoria et al.^[41] The first prepared 2,6-diamino-3,5-dinitropyridine-1-oxide (AnPyO), which is a well oxygen-balanced compound (OB = -2.3%), with a density of 1.880 g cm⁻³, decomposes at >340 °C and has an impact sensitivity below that of TNT but with much better performance (7840 m s⁻¹). The latter prepared 2,6-diamino-3,5-dinitropyrazine-1-oxide (LLM-105) a thermally stable compound (*T_d* = 348 °C) with performance and sensitivity values between those of TATB and HMX. This combination of properties make the compound of interest for real world application as a moderate performance insensitive material.^[42] Another novel high explosive is 2,4-dinitroimidazole (2,4-DNI),^[43] which is more expensive to produce than TNT, has lower performance than HMX, less hot detonation products than PETN and is more sensitive than TATB, but it appears to beat them all in terms of a property compromise.^[3]

1.4 Heat Resistant Explosives

The transport of munitions by aircrafts (among others) require heat resistant and thermally stable explosives. Therefore, energetic materials are sought, which are safe and reliable to handle and with improved thermal properties. In this respect, nitroaromatic compound have received special attention. Analysis of the structure of thermally stable compounds indicates that there are (at least) four ways of improving thermal stability: i) introduction of amino groups, ii) condensation with a triazole moiety, iii) formation of salts and iv) introduction of conjugation (e.g., hexanitrostilbene).^[3] When looking at the family of aminated 2,4,6-trinitrobenzenes the increase in the thermal stability is evident when comparing the decomposition temperature of the mono-amino- (MATB), with the 1,3-diamino- (DATB) and with the 1,3,5-triamino-2,4,6-trinitrobenze (TATB, Figure 1.3). DATB is fairly stable ($T_d = 286\text{ }^{\circ}\text{C}$) and has been qualified as a heat resistant explosive, which has found a place in space applications.^[44] On the other side, the strong hydrogen bonds in TATB place the compound first in the list of thermally stable insensitive compounds and the material has been used in military applications and nuclear weapons. However, for civilians applications TATB is too expensive.^[3] It has been shown, that explosives based on heterocycles show the best combination of thermal stability, oxygen balance, heat of formation and performance. For example, 3-picryl-amino-1,2,3-triazole (PATO)^[45] was considered as a potentially useful thermally stable material. PATO is relatively inexpensive, as insensitive as TATB, however it is predicted to have a lower performance. One of the highlights in the field of thermally stable explosives is tetranitrodibenzo-1,3a,4,4a-tetazapentalene (TACOT). In fact, TACOT is a mixture of three isomers, which are used as such and has an unusually high thermal stability ($T_d = 354\text{ }^{\circ}\text{C}$) and shows the highest ignition temperature registered for an energetic compound at $\sim 494\text{ }^{\circ}\text{C}$.^[46]

Having seen the manifold of possibilities that energetic materials have we conclude that whatever impact future technologies might have in the ordinance and designs of rocket motors, explosives (in all its different types) will always play an important role in the field of controlled energy release. The search for the perfect explosive is a never ending task and a challenge for smart chemists.

1.5 Explosives and Explosions

1.5.1 Definitions and Types

An *explosive material* is “a substance or mixture of substances capable to produce gas at such temperature and pressure by chemical reaction as to cause damage to the surroundings”.^[47] However, there are several other definitions,^[48] such as *explosive material* are “substances that are

produced with the intention to be used as explosive materials”. Therefore, fertilizers (e.g., ammonium nitrate) are excluded from the second definition if they are not produced for damage.^[49] The chemical definition says that *explosive materials* are “substances or mixtures thereof, which are capable of releasing large amounts of hot gaseous products over a short period of time when they undergo the intended chemical reaction”.^[47] Almost all reactions of explosive substances proceed exothermally. There are so-called explosophoric groups, which are chemical groups in a molecule that increase its heat of formation and decompose to give gaseous products (e.g., nitro, nitrate, nitrate ester, azide, nitramine...). Also well known are perchlorates and chlorates. These explosophoric groups contain the necessary oxygen for the conversion of explosives into their gaseous products (i.e., NO_x , CO_2 , CO and H_2O). The oxygen balance and the nitrogen content of a molecule are key parameters to identify and explosive compound or mixture.^[50]

Having defined the concept *explosive material*, the next term, which needs defining is *explosion*. Meyer et al.^[22] define *explosion* as “a sudden increase in volume and release of energy in a violent manner, usually with generation of high temperatures and release of gases, causing a pressure wave in the local medium in which it occurs (it is technically different from *detonation*, see section 1.10 *Decomposition of Explosives*). Depending on the nature of the *explosion* we can differentiate between three types:^[1]

- i) *Physical explosions*: they can arise when an explosive material undergoes a rapid physical transformation while being compressed. The classical example is the eruption of a volcano.
- ii) *Chemical explosions*: are the result of a chemical reaction, which occurs over a very short amount of time and is accompanied by the generation of a large amount of heat and (generally) a large amount of gas. This is the type of explosions that are being dealt with in the work described in this thesis.
- iii) *Nuclear explosions*: they are produced by either fusion or fission of atoms and their energies are in the range of 10^6 to 10^9 larger than those of *chemical explosions*. The shock waves are similar in both cases but for *nuclear explosions* they will last longer and will be accompanied by gamma and intense infra-red and ultra-violet radiation.

Depending on their purpose, *explosive materials* (explosives) are divided in three main types: *propellants*, *high explosives* and *pyrotechnics* (Figure 1.4). Whereas the output of *high explosives* is a *detonation*, *propellants* serve to accelerate either rockets, projectiles or missiles and *pyrotechnics* produce

some sort of fire and/or audiovisual effect. This production of fire is based on a redox reaction of inorganic reducing agents and an oxidizer.^[47]

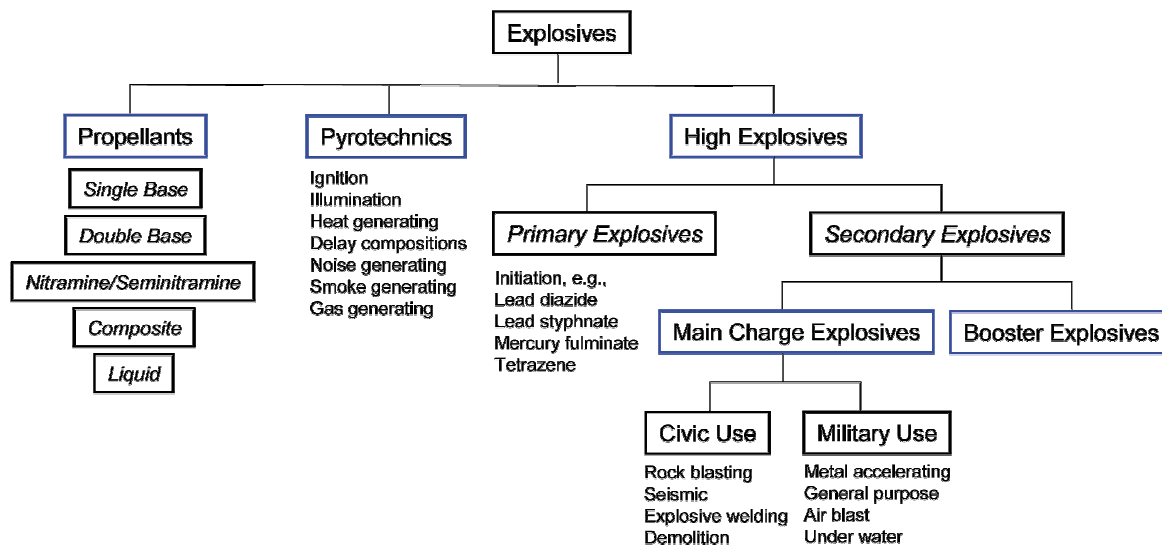


Figure 1.4 Classification of explosives.

1.6 DDT and SDT Transitions

Before moving onto looking at the different types of *explosive materials* there are two concepts, which need to be explained since they play an important role in differentiating one kind of explosive from another. These two concepts are the *deflagration-to-detonation transition* (DDT) and *shock-to-detonation transition* (SDT).

A *detonation reaction* can be initiated by DDT where a *burning reaction* (see section 1.10 *Decomposition of Explosives*) is accelerated to a *deflagration* and by corresponding interference of shock waves further to a *detonation*. The reaction is accelerated to supersonic velocities mainly due to the high energy release and the rate of gas generation, which are both related to the composition of the explosive material. Nitrate esters with neutral or positive oxygen balance, such as nitroglycerine (NG) or pentaerythriol tetranitrate (PETN) are known to have this behavior. In addition, the confinement of a material plays an important role, since this prevents gases from a *burning reaction* from escaping and the pressure builds up.^[5] For example a pile of TNT, which is ignited by a burning match will only burn slowly until all TNT is consumed, however, if the same compound is heated under confinement (e.g., see Koenen test in section 1.13.2 *Standard (BAM) Tests*) the reaction will evolve to a detonation. This is a typical behavior for a main charge explosive. Another way of initiating an explosive charge is based on the impact of a shock wave. This mechanism is known as SDT and the limit of initiation is described by the critical energy (E_c , Eqn. (1)). E_c depends on the density of the

material (ρ_o),^[50a] the shock wave velocity (V) and pressure (P) and the shock impact time (t). For determining this energy so-called gap tests are used where the shock wave pressure for 50% initiation probability is determined.^[22,51]

$$E_c = \frac{P^2 t}{\rho_o V} \quad (1)$$

1.7 Propellants

This type of compounds undergo fast and predictable combustion without detonating and the large volume of hot gas resulting from it is used to propel a projectile (e.g., bullet, missile...) or to drive a turbine in gas generators (e.g., torpedoes).

Propellants can be divided into several classes. Nitrocellulose-based propellants (NC) are the most widely used for gun application. *Single base (SB)*, *double base (DB)*, *triple base (TB)* and *(semi-)nitramine* propellants belong to this group. *SB propellants* consist of $\geq 90\%$ NC, which is gelled by addition of a plasticizer (e.g., dibutylphthalate), which acts also as a surface moderant and coolant, which is important for the favorable burning behavior of a propellant. The energy content (Q value) of such a propellant varies between 3100 and 3700 J g⁻¹.^[1]

DB propellants contain up to 40% nitroglycerine (NG) to increase the energy output. In semi-nitramine propellants this effect is achieved by addition of a high-performing nitramine (e.g., RDX) to the NC matrix. They have Q values of around 4500 J g⁻¹. This explains the faster ageing and the higher flame temperature, which is responsible for the excessive erosion of the gun barrel. In addition, the presence of a muzzle flash can be used to locate the gun.^[1] Some additives such as titanium dioxide or talc can be used to reduce the erosion.^[52] *DB propellants* are found in large caliber cannons, howitzers, ammunitions for pistols and grenade launchers, rockets or missiles...^[53] In *TB propellants* ~50% nitroguanidine (NQ) is added, which results in a reduction of the flame temperature and an increase in the gas volume, which reduces considerably the gun barrel erosion and the muzzle flash found in *DB propellants*. They are found in tank guns or large calibre guns.^[1]

A further group includes propellants, which are based on a synthetic polymer binder system, which can either be inert or energetic. If organic nitramine compounds are added to the polymer, they form the base composition for *nitramine propellants*, whereas when an inorganic oxidizing salt (e.g., perchlorate) is added instead, the composition is called *composite propellant*. The binder can also be energetic (e.g., Glycidyl Azide Polymer (GAP)).^[22] The oxidizers normally found in *composite propellants* are ammonium nitrate (AN) or (mostly used) ammonium perchlorate (AP). The use of AP

produces large amounts of HCl during the burning process,^[54] which results in the formation of a large white cloud, which discloses the position of launching and trajectory of the missile. This is a major problem for tactical missiles. For this reason the addition of HCl-suppressant substances, such as sodium nitrate or magnesium/aluminum alloys is necessary. The main problem associated with the use of AN as an oxidizer are the several crystal modifications the compound has, which could be fatal for the motor. Therefore, the addition of a crystal structure stabilizer (e.g., KNO_3) is necessary. On the other side, the reducing agent used in this sort of propellants is a polymeric fuel such as polymethacrylates or polybutadienes in combination with a metal, normally Al, Zr, Be (very energetic but extremely toxic), B or Mg. They are found in rifles, guns, machine guns, aircraft- and antiaircraft guns, howitzers and rocket propellants.^[53] The NC-based propellants compositions described above all suffer from the risk of accidental initiation by e.g., the event of a fire, impact, shooting... Therefore, insensitive ammunitions have developed for gun propellant applications and special attention has been paid on a new class of *composite propellants* called *low vulnerability ammunition (LOVA)*, which are based on RDX or HMX and are less vulnerable to initiation.^[1] In addition, ammonium dinitramide (ADN) has emerged as a new compound for use in solid rocket propulsion. Some of the most attractive properties of ADN are its high performance, positive oxygen balance (+25.8%), high nitrogen content (45.1%), high enthalpy of formation and relatively low sensitivity.^[22]

Lastly, there are *liquid propellants*, which can be divided into *mono-* and *bi-propellants*. Hydrazine is a typical mono-propellant, which burns with the absence of external oxygen. However, in bi-propellants fuel and oxidizer are stored in separate tanks and they are injected into a combustion chamber where they react and ignite. In this regard, Kerosene or asymmetric dimethylhydrazine are used as fuel, whereas typical oxidizers are nitric acid or N_2O_3 .^[1,55] Liquid propellants are advantageous over solid propellants in that that they are normally cheaper to produce, are less vulnerable to accidental initiation, have a higher energy output per unit volume and a high storage capacity.^[1]

1.8 High Explosives

This type of explosives are classified in *primary* and *secondary explosives*. The first are commonly based on a metal salt. They are used in low quantities in detonators, are initiated by a certain input stimulus (e.g., shock, friction, electricity) detonating and initiate so-called booster explosives, which amplify the detonation and transmit it further to the main charge. Typical booster explosives are TNT, trinitro-2,4,6-phenylmethylnitamine (Tetryl), PETN or (since more recently) RDX. Applications requiring high performances are often based on HMX ($\leq 95\%$) and a binder system

($\geq 5\%$). Blasting explosives, on the other side, can be very heterogeneous. Ammonium nitrate (AN) is commonly used as an oxidizer for a liquid fuel oil (ANFO, see Secondary Explosives section).^[5]

1.8.1 Primary Explosives

The most frequently used *primary explosives* are lead azide, lead styphnate and tetrazolyl guanyltetrazene hydrate (tetracene) (Figure 1.5). In earlier times also mercury fulminate was used. Lead diazide is very sensitive to friction, whereas lead styphnate and tetracene are very sensitive towards electrostatic discharge and impact, respectively.^[22]

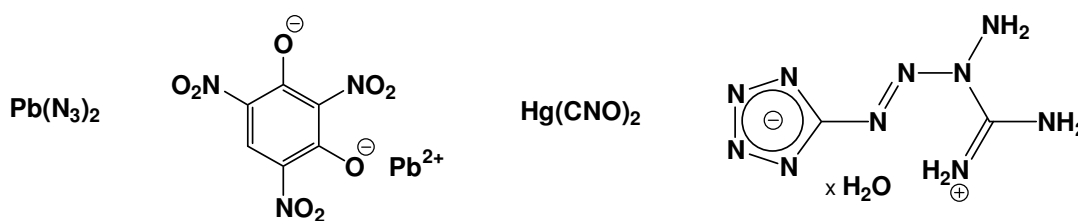


Figure 1.5 Structure of commonly used primary explosives. From left to right: lead diazide, lead styphnate, mercury fulminate and tetracene.

Mercury fulminate ($\text{Hg}(\text{CNO})_2$)^[56] was the most used primary explosive for many years, either by itself or used in a mixture with potassium chlorate (KClO_3). The compound can easily be prepared by reacting mercury metal with nitric acid and ethanol. However there are some drawbacks associated with the compound such as the high toxicity of Hg^{2+} , its short shelf life and its reaction with metals (under moist conditions). Its use was therefore abandoned in many countries and during WWI lead diazide ($\text{Pb}(\text{N}_3)_2$) appeared as a replacement. $\text{Pb}(\text{N}_3)_2$ has also an easy synthesis (reaction between lead(II) nitrate or acetate with sodium azide) and is now the most commonly used *primary explosive* for detonators in combination with lead styphnate, which can be easily initiated by impact, heat and specially sparks.^[2] Table 1.1 contains summarized some sensitivity data of interest for common *primary explosives*.^[22] An example of a new substance, which is devoid of a toxic metal is 1,3,5-triazido-2,4,6-trinitrobenzene (TATNB),^[57] however ageing of the compound results in loss of activity. The replacement of lead by less toxic metals in silver azide or silver fulminate showed compounds with good initiation properties, however their extremely high sensitivity make their use unviable.^[22] A real breakthrough in the field of primary explosives has not been realized yet. *Chapters II and III* will try to address some of the issues in this field.

Primary explosives undergo very rapid *deflagration-to-detonation transition* (DDT) and the shock wave is able to detonate less sensitive explosives. For this reason they are used in initiating devices. Typical

detonation velocities are in the range 3500 to 5500 m s⁻¹. They are very sensitive to friction, impact, electrostatic discharge or high temperature and explode regardless of being confined or not.^[1]

Table 1.1 Sensitivity data of common primary explosives and minimal amount to initiate PETN.

Primary Explosive	Friction (N) ^a	Impact (J) ^b	ESD (mJ) ^c	Initiation (g) ^d
Mercury Fulminate	8	1-2	10	0.17
Lead Azide	0.1-1 (pure)	2.5-4	0.4	0.02
Lead Styphnate	9	2.5-5	1-10	0.55
Tetrazene	7	1	180	Difficult

^aFriction sensitivity; ^bImpact sensitivity; ^cSensitivity to electrical discharge; ^dMinimal amount of primary explosive required to initiate PETN.

Developments in the field of *initiating explosives* lead to the use of *SINOXID* (from the Latin “sine oxide” = without rust)^[22] primer compositions (a mixture of lead styphnate, tetracene and inorganic nitrates), which is characterized by little corrosion and erosion in the gun, good chemical stability and excellent initiating properties.^[58] Due to the high contamination levels reached with the use of lead-based primers, the *SINTOX* (without toxicity) primary composition was developed, which is based on 2-diazo-4,6-dinitrophenole and tetracene. There is also a trend to develop detonators, which do not make use of primary explosives and can be initiated, for example, by a laser beam.^[2]

1.8.2 Secondary Explosives

This class of compounds are difficult to detonate by heat or impact and they generally have higher detonation velocities (5500-9000 m s⁻¹). They are less sensitive than *primary explosives* and can only be initiated by the shock wave produced by the latter when they explode. Examples are TNT, tetryl, picric acid, NC, NG, NQ, RDX, HMX or TATB.^[1]

Table 1.2 shows a summary of some energetic properties of relevance for common high explosives according to reference [22], whereas the structures of the compounds are shown above in Figure 1.1. By looking at the table, the optimization of the main goals (high performance, safety and low vulnerability) seems almost contradictory. Coating or mixing a sensitive energetic compound with a binder system results in desensitization, which influence the vulnerability of the explosive charge. In the case of low melting point explosives, the explosive compound itself can be used as a binder, provided they count with a large liquid range. A typical example is TNT, which is used to dilute high-performing (too) sensitive explosives like RDX (hexogen, hextro formulations) or HMX (octogen, octol formulations). However, cast charges based on TNT do not meet the criteria for insensitive munitions (IM) and alternatives are sought.^[2] In addition to the use of binder, addition of

plasticizers (energetic or not) might be of use because this allows to adjust the mechanical properties of the binder system.

Table 1.2 Safety data and detonation parameters of common high explosives.

Explosive	m.p. (°C) ^a	Impact (J) ^b	Friction (N) ^c	ρ (g cm ⁻³) ^d	P (GPa) ^e	V (m s ⁻¹) ^f
TNT	80.8	15	353	1.654	22.3	6900
PETN	141.3	2	60	1.760	33.5	8400 ^g
RDX	204.0	7.5	120	1.820	34.1	8750 ^b
HMX	275.0	7.4	120	1.900	39.0	9100
Tetryl	129.5	3	353	1.730	26.9	7570 ⁱ

^aMelting point; ^bImpact sensitivity; ^cFriction sensitivity; ^dDensity; ^eDetonation pressure; ^fDetonation velocity; ^gCalculated at a density of 1.700 g cm⁻³; ^bCalculated at a density of 1.760 g cm⁻³; ⁱCalculated at a density of 1.710 g cm⁻³.

Non-military explosives are used mainly for mining, tunnel construction and building demolition and are much more heterogeneous than military explosives. They are normally made of an oxidizer, reducer and a sensitizer in addition to inert components. The oxygen balance of the mixtures are mostly adjusted to neutral or slightly positive in order to diminish the formation of detrimental decomposition gases (e.g., CO or NO_x). Modern formulations are characterized by their insensitive behavior and are made sensitive by the introduction of gas bubbles (i.e., hot-spots). There are many different types of non-military explosives. Some of the most important are *gelatinous explosives*, which consist of blasting oil gelatinized with nitrocellulose (explosive gelatin) with ammonium nitrate as the oxidizer or *Ammonium Nitrate Fuel Oil (ANFO)*, which contain 6% oil, which acts as the fuel and 94% porous ammonium nitrate. Other types are *explosives for underground mining* and *slurry* or *emulsion explosives*.^[59]

1.8.3 Effect of Density in the Velocity of Detonation (V)

In order to achieve the maximum velocity of detonation in high explosives, it is necessary to compact the explosive material to its maximum density (e.g., by pressing, casting...). The limit in the density will be fixed by the density of the explosive crystal. The higher the density of compaction, the higher the detonation velocity. The increase in the detonation velocity by an increase in the compaction density is quantified in Eqn. (2), therefore an increase in the compaction density of ~0.2 g cm⁻³ from $\rho(1)$ to $\rho(2)$, results in an increase of ~700 m s⁻¹ in the detonation velocity (V). Eqn. (3) can be used to calculate the approximate detonation velocity at a density of compaction $\rho(x)$ from the number of moles per gram of gaseous products (n) formed upon detonation and the temperature of detonation (T_d).^[1]

$$V_{\rho(2)} = V_{\rho(1)} + 3500 (\rho(2) - \rho(1)) \quad (2); \quad V_{\rho(x)} = 430(nT_d)^{1/2} + 3500(\rho(x) - 1) \quad (3)$$

As mentioned above, the performance of an explosive compound is of utmost importance and it is quantified by its detonation velocity and by its detonation pressure. Based on bomb calorimetric measurements, the heat of formation of a material can be determined and together with the density of the compound there exists software (e.g., EXPLO5,^[60] CHEETAH^[61]...), which allow to easily predict the detonation parameters (as well as other magnitudes of interest). This software is mostly based on the Kristiakowsky-Wilson (K-W) rules,^[62] which allow to predict the decomposition products formed upon decomposition/explosion of an explosive material. On the other side, most detonation parameters reported in the literature are not based on semiempirical but on purely calculated data. This generally makes use of quantum chemical methods to calculate the electronic energy of the molecule (or ions in the case of ionic compounds), which is in turn used to calculate the heat of formation and the software mentioned above can be used to predict the performance (detonation pressure and velocity) of an explosive compound. A closer explanation of the method used in this work is given in the respective chapters.

On the other side, since many compounds have highly negative oxygen balances it is a well known fact that the heat of explosion and therefore the detonation parameters (e.g., TNT = -74.0%) reach a maximum when this is approximately neutral in the case of commonly used explosives (e.g., TNT, PETN, RDX or HMX). This can be explained by the stoichiometric oxidation of the carbon and the hydrogen in the molecule to carbon dioxide and water, respectively.^[1] Therefore, we also calculated the detonation parameters corresponding to mixtures of the compounds in this work with an oxidizer (i.e., AN or ADN) at a neutral oxygen balance. Again, a detailed explanation will be given in the corresponding chapters.

1.9 Pyrotechnics

Since *pyrotechnics* are not the main scope of this thesis, they will only be explained in passing here. A recent review^[63] will lead the reader to a more detailed discussion on the topic.

Many *pyrotechnic* compositions are based on an oxidizer, a reducing agent (fuel), a binder and several additives to produce a certain effect (e.g., heat, flame, smoke, colored lights, sound...). In addition, pyrotechnic compositions also find use in military explosives such as to delay the initiation of a hand grenade,^[47] as well as in igniter compositions and heat-generating devices.^[1] Another interesting example are flares, which are used to protect aircrafts against the attack of hostile missiles and are based on the generation of heat and light. Typically, such flares are based on Magnesium Teflon and Viton (MTV).^[64] The closest and most fascinating application of light-generating compositions for the non-chemist is possibly fireworks. In such compositions the oxidizer is

generally a nitrate or a perchlorate salt, whereas the fuel is a metal (e.g, alkaline earth metals, Al, Ti...). The color of a firework is due to the frequency of emission of a given metal compound. Generally copper(II) salts (chlorine-free) are used to generate blue colors, sodium for yellow, strontium for red or barium for green flames. When using a perchlorate-based oxidizer the emitting species is generally an excited metal chloride cations (e.g., SrCl^+).^[65]

1.10 Decomposition of Explosives

Depending on the rate of decomposition, we can distinguish between four types of reactions typical for energetic materials:^[47]

- i) *Ageing reactions*: are the slowest of all and characterized by energy loss, change in the mechanical properties.... They can occur at room temperature over several years.
- ii) *Burning reactions*: are several orders of magnitude faster than *ageing reactions* (several meters per second).
- iii) *Deflagration reactions*: are faster in the order of several hundred meters per second.
- iv) *Detonation reactions*: are the fastest of all (several thousand meters per second).

The main factors producing *ageing* of an explosive are temperature, humidity and acid residues. For example diphenylamines are used as stabilizer to catch free NO_x radicals in nitrate esters. A *burning reaction* is started if the temperature is raised above the ignition temperature of the explosive compound. The *burning* process is then a self-sustaining and exothermic redox reaction. Generally the reaction continues in the gas phase under emission of light due to the heat, hot gases and the fine particles, which are being released. *Deflagration* is an intermediate reaction state between *burning* and *detonation*. *Burning* of an energetic material can develop into a *deflagration* when the linear velocity of the reaction achieves the magnitude of the speed of sound in the material. The physical instability of a *deflagration reaction* makes it difficult to control. Depending on the type of explosive, confinement... the reaction can be further accelerated to a *detonation* or slow down to *burning*. In *detonation reactions*, in contrast to *burning* and *deflagration reactions*, which are based on mere heat transfer, the chemical reaction is started by a supersonic shockwave, which travels through the explosive material.^[47]

1.11 Trends in Explosives Research: Azoles and Nitrogen-rich Chemistry

As mentioned above, high-performing safe-to-handle compounds are sought, however it often occurs that high performances and stability are mutually exclusive. In recent years, there has been much research in the field of nitrogen-rich chemistry. In this regard, azoles have become favorite candidates because they are (generally) highly endothermic compounds (due to the many N–N and C–N bonds),^[66] which show relatively high densities (both related to the performance of the materials) and the high nitrogen content in such systems make them attractive from an environmentally point of view, since most of the decomposition products are expected to be (benign) molecular nitrogen, which is in contrast with the formation of relatively large amounts of highly toxic CO and NO_x gases found upon decomposition of some commonly used explosives.^[67] In addition, azole-based energetic materials tend to show good thermal stabilities and are relatively insensitive to classical stimuli.^[68] Therefore, we decided to study the chemistry of azoles and in particular, that of triazoles and tetrazoles and their possibilities as new energetic materials.

Some prominent examples of azole-based energetic materials, which have been developed or have already found use are the above-mentioned 3-nitro-1,2,4-triazole-5-one (NTO)^[25] and 3-picrylamino-1,2,3-triazole (PATO), which are new LPEMs,^[45] or the widely used tetrazole-based *primary explosive* tetracene.^[69] A more recent example of a compound that had been synthesized before^[70] but that has been developed in our group is bis-(triaminoguanidinium) 5,5'-azotetrazolate,^[71] which is currently being produced in the US on a multikilogram scale. Also worth highlighting in this section and in connection with *Chapter III*, is the work from Hiskey and co-workers who prepared “green primaries” based on a new family of 5-nitrotetrazolate salts with a Fe²⁺ cation^[72a] and other metals (Na⁺ and Cu²⁺),^[72b] whereas tetrammine-*cis*-bis(nitro-2H-tetrazolato-N²)cobalt(III) perchlorate (BNCP) has already found application in detonators that are integral to the fire suppression systems for military and commercial aircrafts.^[73] Two reviews about tetrazoles and other nitrogen-rich compounds, that will give the reader the possibility of becoming familiar with the variety of possibilities of this kind of chemistry and with the known compounds, have appeared recently.^[74]

On the other side, the search for solid nitrogen (at room conditions) is still underway.^[75] In addition to the breakthrough study from Eremets et al. about *cg*-N^[15] an important contribution to the field of nitrogen-rich chemistry has been brought by Christie et al. and Östmark et al. They were responsible for the discovery of the homopolyatomic nitrogen species N₅^{+[76]} and N₅^{-[77]} respectively, which add to the homoleptic N₃⁻ (azide) anion reported by Curtius more than a century ago.^[78] Other species such as N₃[·] (radical), N₃⁺ and N₄⁺ have only been observed as free gaseous or matrix-isolated radicals or ions.^[79-81] whereas theoretical studies show that species such as N₄, N₈, N(N₃)₂,

$N(N_3)_3$ and $N(N_3)_4^+$ are vibrationally stable.^[82] Another nitrogen-rich (binary) cation of interest is the triazidocarbenium cation ($C(N_3)_3^+$), also reported by Christie et al.^[83] However, although interesting, most of these species are very labile in combination with energetic ions and therefore its chemistry has been limited to an academic interest, so far. For example, salts containing the N_5^+ cation are only stabilized by (relatively) large (non-energetic) anions such as AsF_6^- , SnF_5^- , SnF_6^- or $B(CF_3)_4^-$.^[76] Therefore, we conclude that azole (and specially tetrazole) chemistry has a great potential for energetic applications.

1.12 Summary of the Ph. D. Thesis

The goals of this work can be gathered together as follows:

- i) Synthesis and full (analytical and spectroscopic) characterization of new and known energetic materials based on azoles.
- ii) Full energetic characterization of the studied compounds: physico-chemical properties, sensitivity, stability and (for nitrogen-rich materials) estimation of performance.
- iii) Design an up-scalable (i.e., safe) syntheses for energetically interesting target molecules that allow to prepare e.g., 5-10 g of the material in the laboratory and send the compounds for further testing.

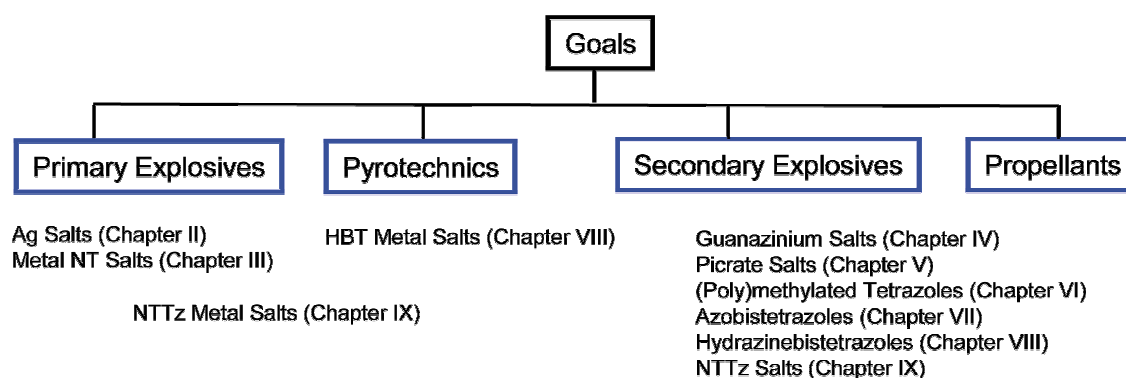


Figure 1.6 Goals of the work on azole-chemistry in regard to the application.

Figure 1.6 shows a classification of the chapters on view of the prospective application of the compounds described in them. As it can be seen some of the application possibilities overlap, specially those concerning possible use of the materials as *secondary explosives* or *propellants*. A short introduction about the scope of each chapter, which highlights and introduces the work to be discussed in the next chapters is given below:

CHAPTER II. The first experimental chapter deals mainly with the synthesis of silver salts with tetrazole ligands, namely 5-amino-1*H*-tetrazole, 1-methyl-5-amino-1*H*-tetrazole and 2-methyl-5-amino-1*H*-tetrazole and nitrate and perchlorate anions. Due to the potential of silver salts as primary explosives, we wanted to propose alternatives to highly sensitive silver azide or silver fulminate based on tetrazolium salts, which combine the excellent initiating properties of silver salts but diminishing the hazard of accidental initiation found in these compounds. In addition, due to our continuous work on tetrazole chemistry we were also interested in comparing the properties (specially energetic) of silver substituted tetrazoles with those of protonated tetrazoles analogues.

CHAPTER III. This is chapter dealing with 5-nitro-2*H*-tetrazole (**5-NTH**) and its metal salts with s-block metals (i.e., alkali and alkaline earth metals). **5-NTH** was reinvestigated and its crystal structure is reported here for the first time. The molecule has the highest density of all compounds described in this work (excepting halogen or metal based compounds) and is the most powerful primary explosive that has been described till date, with detonation parameters perfectly comparable to CL-20 and higher than those of 5-azido-1*H*-tetrazole. The alkali metal salts discussed here complement the silver salts described in the preceding chapter (*Chapter II*). Although the lighter alkali metal salts and the alkaline earth metal salts contain crystal water, the K, Rb and Cs derivatives have characteristics of primary explosives and with devoid of a toxic metal are interesting candidates to be studied as possible less environmentally-malign replacements for lead-containing initiators.

CHAPTER IV describes the chemistry of triazolium salts with classical energetic anions (e.g., nitrate, perchlorate, azide, dinitramide...). 3,4,5-Triamino-1,2,4-triazole (guanazine) is suggested as an alternative to 1,5-diamino-1*H*-tetrazole for the synthesis of energetic materials, due to the larger versatility of possibilities of the first and to the safety issues associated with the preparation of the latter. Since many nitrogen-rich compounds are either thermodynamic or kinetic unstable, a way of stabilizing them consists in the introduction of small alkyl chains (ideally methyl groups).^[84] Quaternization of guanazine with methyl iodide yields the novel methylguanazinium cation, which has been used to generate a new family of energetic compounds including the interesting azide salt, which had not been combined with an azolium cation before our studies. Most of the compounds described here show insensitivity towards impact and friction, while having relatively high performances suggesting their potential as new insensitive materials for energetic applications.

CHAPTER V describes a family of picrate salts with the azolium cations that we have developed during the course of this dissertation. The formation of salt-based materials results in insensitive compounds, which show lower melting points than picric acid and moderate performances approximately in the range between that of TNT and that of NG. With this, many of the drawbacks

associated with the use of picric acid as an explosive compound have been overcome. In addition, the picrate salts studied here are interesting from the historical point of view since they represent the first in-depth study of compounds, which are intermediates between “the first nitroaromatic explosive” (i.e., picric acid) and nitrogen-rich azole chemistry.

CHAPTER VI. The interesting energetic properties of the triazolium salts described in *Chapter IV* are here studied in tetrazolium derivatives, which show a more endothermic character. The energetic properties of salts containing the 2-methyl-5-amino-1*H*-tetrazolium and 1,3-dimethyl-5-amino-1*H*-tetrazolium cations are compared with those of our previous work on energetic salts containing the 1-methyl-5-amino-1*H*-tetrazolium and 1,4-dimethyl-5-amino-1*H*-tetrazolium cations. In this work, all of these cations have been synthesized and considered for the synthesis of energetic salts for the first time. It will be concluded that the substitution pattern changes some of the physico-chemical properties (e.g., thermal stability) without (significantly) affecting the performance of a material and that similar strategies can be used to tune the energetic properties of a compound on view of a suitable application.

CHAPTER VII describes a new family of highly-endothermic 5,5'-azobistetrazole derivatives. The large part of the chapter focuses on salts containing the 5,5'-azotetrazolate anion and azolium cations. In addition, the semicarbazidium salt was also considered as an analogue of our previously reported aminoguanidinium 5,5'-azotetrazolate salt. On the other side, two neutral 5,5'-azobistetrazole derivatives were reinvestigated and energetically characterized for the first time. An alternative procedure to our previously reported synthesis of 2,2'-dimethyl-5,5'-azobistetrazole over silver 5,5'-azotetrazolate is suggested, which does not make use of any highly sensitive intermediate and makes the synthesis of the compound suitable for up-scaling.

CHAPTER VIII. This chapter deals with the chemistry of 5,5'-hydrazinebistetrazole (HBT). Although known for over 100 years, the compounds is studied here for the first time in view of its energetic properties. It is shown that HBT has a great potential for tank and large calibre naval guns due to its high detonation parameters and low sensitivity. Some neutral derivatives of HBT are also discussed. In regard to the high energy inherent to the HBT moiety, we studied salts of HBT with nitrogen-rich cations as potential propellants. On the other side, in view of the interest in metal salts to be used either as primary explosives and/or as a less-toxic alternative to compounds commonly used in pyrotechnic compositions, we decided to study salts of HBT with alkali and alkaline earth metals, which are analogue, and thus complement our previous studies on metal salts of 5,5'-azobistetrazole. Some of the salts oxidize readily to the 5,5'-azobistetrazolate derivatives, which limits their application but however, offer an alternative safer (!!) synthesis of the latter, which does

not make use of highly sensitive barium 5,5'-azotetrazolate. Lastly, interestingly, the alkaline earth metal salts are all stable on air and the strontium salt (SrHBT) could emerge as a new red light emitter in “green” pyrotechnic mixtures.

Chapter IX. The last chapter reports the on-going research and possible future directions to take in tetrazole chemistry. The 5-nitrotetrazolate anion (NT^-), developed during this work and extensively described in *Chapter III*, is combined with a second tetrazole (Tz) ring, yielding the previously unreported 5-(5-nitrotetrazole-2-ylmethyl)-tetrazolate anion (NTTz^-), which is a bridged-bistetrazole, similar to the 5,5'-azotetrazolate anion, described in *Chapter VII*, but with more explosive power due to the nitro group. The synthesis of the free acid NTTzH from ammonium 5-nitrotetrazolate (ANT) is introduced as well as a direct synthesis of anhydrous ANT. Several salts of NTTz were prepared, either with nitrogen-rich cations or with alkali metals, all of which show explosive character when properly stimulated (i.e., impact or friction). Specially worth-mentioning is the high sensitivity of neutral NTTzH to impact, which is in contrast with the low sensitivity to friction, similar to tetryl. Lastly, the aminoguanidinium salt has performance values comparable to PETN but it is much less sensitive and some metal salts (containing Cu) show laser-induction capability.

1.13 Testing of Energetic Materials

In addition to the usual analytical and spectroscopical methods used to characterize organic and inorganic compounds (e.g., NMR, elemental analysis, IR, Raman...), there are other methods, which are more (although not exclusively) specific for the characterization of energetic (organic or inorganic) materials. In this section, methods for determining the thermal stability of the compounds described in the rest of this work as well as the sensitivity properties will be explained in short.

1.13.1 Thermal Stability

Differential scanning calorimetry (DSC) is a very useful technique to assess the thermal stability and heat of transition of explosives (and other compounds) among other variables. The measurement takes place in an insulated furnace, which contains two thermostats (one for the sample and one for the reference). Then a temperature scan is run, which depends on the type of sample and information, which wants to be derived and the difference in heat flow between sample and reference is then recorded by the instrument as a function of the temperature. Normally the furnace is purged by a stream of an inert gas (e.g., nitrogen, argon or helium) but it might also be

useful to flow air or purge oxygen (e.g., to study the oxidative decomposition of a given compound). Normally a positive deflection on the plot corresponds to an exothermic peak (generally a decomposition), whereas an endothermic peak is depicted by a negative deflection and it can correspond to melting, water loss and other processes.^[85] The use of DSC allows to extrapolate a lot of information for energetic substances, for example, in the case of glassy solids the glass transition temperature can be determined by a simple measurement or the energy of activation for the decomposition process can be easily calculated.^[86] Further information about DSC and other thermal analysis methods (e.g., DTA or TGA) can be found in the open literature.^[1]

Lastly, a particular type of DSC method is TSC (Thermal Safety Calorimetry), which enables the analysis of the thermal behavior of chemical substances under non-adiabatic conditions. This analysis can be used to determine critical design parameters such as the long-term stability of a compound or the influence of the surrounding temperature on storage and transport safety. The method enables the prediction of the heat accumulation process and reaction progress for any surrounding temperature profile (isothermal, stepwise, periodic temperature variations, temperature shock and real atmospheric temperature profiles). The experimental approach to TSC analysis is given in the Experimental Section of the corresponding chapters.

1.13.2 Standard (BAM) Tests

In order to release the energy stored in an explosive compound a certain stimulus needs to be applied. There are several stimuli, which can be used to initiate an explosive compound. The classical are impact, friction and electrostatic discharge but also fast heating and others can result in initiation of a compound. More modern techniques such as laser induction, which allow to detonate an energetic compound by irradiating it with a laser beam of a precise frequency are also of interest. In order to be able to quantify the input of a given stimulus that needs to be applied so that an energetic compound releases its stored energy but also to assess the hazards involved with the manipulation of a material (specially in the case of sensitive compounds) standard tests have been developed. In this work, we used so-called standard BAM (BundesAnstalt für Materialprüfung) tests^[48,87] to determine the sensitivity of all compounds to impact and friction.

In the *impact sensitivity test* (drop hammer) a weight (250 g, 1 kg, 2 kg, 5 kg or 10 kg) is dropped from a given height (<100 cm) to two flat, parallel, hardened steel surfaces containing 20-40 mg of the compound to be tested. The lowest energy required to detonate the material is then recorded and this value can be compared to the UN Recommendations on the Transport of Dangerous Goods^[48] to classify the compound in insensitive, less sensitive, sensitive and very sensitive. In the

friction sensitivity test the sample is placed between a ceramic plate and a ceramic pin. The ceramic pin is connected to a lever, onto which several weights can be hung (1-9 kg), corresponding to a force of 5 to 360 N. The sample is then submitted to the friction force between the plate and the pin and the result is evaluated. In the *heat sensitivity test* (e.g., steel sleeve (Koenen) test) the sample is placed in a cylindrical steel thimble (24×75 mm) and this is closed with a screw top with a port diameter between 1 and 20 mm. The thimble is placed in a metallic support and heated with four burners. The result is considered to be an explosion and is therefore described as positive when the thimble is broken in at least three pieces. It is out of the scope of this section to go on an in-depth discussion about the methods used in this work, thus an extensive discussion is omitted here and the reader is recommended to consult more complete literature on the topic.^[22,88]

1.14 Definitions of Interest

In order to avoid confusion and possible misunderstanding it is necessary to define some of the technical words, which will be (more or less) commonly used throughout the chapters to come. This section contains a comprehensive list of such words with the corresponding definitions.^[1,22]

Flame: chemical reaction or reaction product, partly or entirely gaseous, that yields heat and emit light.

Deflagration point: temperature at which a small sample of the explosive, placed in a test tube and externally heated, burst into flame, decomposes rapidly or detonates violently.

Detonator: part of an explosive train, which initiates the detonation of (insensitive) high explosives.

Explosive train: a sequence of combustible and explosive elements arranged in decreasing order of sensitivity. It accomplishes the controlled augmentation of a small impulse into one of a higher energy that acts as the main charge.

Hot spots: increase of the detonation sensibility of explosives by finely dispersed air bubbles.

Energy/Enthalpy of formation: energy which is bound during the formation of a given compound from its constituent elements at constant volume (energy) or at constant pressure (enthalpy).

Heat of explosion: heat liberated during the explosive decomposition of an explosive material, explosive mixture, gunpowder or propellant.

1.15 References

- [1] J. Akhavan in *The Chemistry of Explosives*, 2nd ed. RSC Paperbacks: Cambridge, UK, **2004**.
- [2] J. Mathieu, H. Stucki, *Chimia* **2004**, 58(6), 383-389.
- [3] A. K. Sikder, N. Sikder, *J. Hazard. Mater.* **2004**, A112, 1-15.
- [4] A. L. Kirill, L. Jainchary, E. E. Phillip, K. Nobuhiro, J. Jurgan, P. Eric, G. Richard, *J. Am. Chem. Soc.* **1997**, 119, 9591-9601.
- [5] E. Anderson, *Prog. Astronaut. Aeronaut.* **1993**, 155, 81.
- [6] a) P. B. Kempa, J. Kerth, 32nd Int. Ann. Conf. ICT, Karlsruhe, Germany, **2001**, 147. b) Y. Akutsu, R. Che, M. Tamura, *J. Energ. Mater.* **1993**, 11, 173. c) M. J. Kamlet, H. Hurwitz, *J. Chem. Phys.* **1968**, 23, 3685. d) L. R. Rohstein, R. Peterson, *Propellants, Explos., Pyrotech.* **1979**, 4, 56.
- [7] G. W. Griffin, A. P. Marchand, *Chem. Rev.* **1989**, 89, 997-1000.
- [8] M. X. Zhang, P. E. Eaton, R. Gilardi, *Angew. Chem. Int. Ed.* **2000**, 39(2), 401-404.
- [9] A. P. Marchand, *Tetrahedron* **1988**, 44, 2377-2395.
- [10] P. E. Eaton, M. X. Zhang, R. Gilardi, *Propellants, Explos., Pyrotech.* **2002**, 27, 1-6.
- [11] A. T. Nielson in *Nitrocarbons*, Ed.: VCH-Verlagsgesellschaft, Weinheim, **1995**, 97.
- [12] G. P. Sollot, J. Alster, E. E. Gilbert, *J. Energ. Mater.* **1986**, 4, 5-28.
- [13] N. C. Paul in *Explosives in the Service of Man*, The Royal Society of Chemistry: Cambridge **1997**.
- [14] J. R. Stine, *Mat. Res. Soc. Symp.* **1993**, 296, 3.
- [15] M. I. Eremets, A. G. Gavriluk, I. A. Trojan, D. A. Dzivenko, R. Boehler, *Nature Mater.* **2004**, 3, 558-563.
- [16] A. T. Nielsen, US Dept. of Navy, US 70,631 **1987**.
- [17] a) G. P. Sollott, J. Alster, E. E. Gilbert, O. Sandus, N. Slagg, *J. Energ. Mater.* **1986**, 4, 5. b) J. Boileau, J. M. L. Emeury, J. P. Kehren, US 4,487,938 **1984**. c) A. T. Nielsen, US 5,693,794 **1997**.
- [18] a) V. R. Ramakrishnan, M. Vedachalam, J. M. Boyer, *Heterocycles* **1990**, 3(1), 479. b) J. Hanks, T. Highsmith, A. Sanderson, K. Warner, J. Worthington, *Int. Ann. Conf. ICT*, Karlsruhe, Germany, **2002**, 129.
- [19] K. Karaghiosoff, T. M. Klapötke, A. Michailovski, G. Holl, *Acta Crystallogr. Sect. C* **2002**, 58, o580.
- [20] T. G. Archibald, R. Gilardi, K. Baum, C. George, *J. Org. Chem.* **1990**, 55, 2920.
- [21] M. D. Coburn, M. A. Hiskey, T. G. Archibald, *Waste Manage* **1997**, 17, 143.
- [22] A. Homburg, J. Köhler, R. Meyer in *Explosives*, 6th rev. ed. WILEY-VCH: Weinheim, Germany, **2007**.

- [23] a) K. Dudek, M. Rajic, Z. Zeman, M. Suceska, P. Vavra, *J. Energ. Mater.* **2001**, *19*, 219. b) K. Schmid, D. Kashmieder, *31st Int. Ann. Conf. ICT*, Karlsruhe, Germany, **2000**, 10.
- [24] a) T. Urbanski in *Chemistry and Technology of Explosives*, Pergamon Press: Oxford, **1986**. b) R. D. Schmidt, A. R. Titchell, G. S. Lee, M. D. Coburn, P. F. Pagoria, W. T. Quinlan, R. Thorpe, M. Cates, *31st Int. Ann. Conf. ICT*, Karlsruhe, Germany, **2000**, V37.
- [25] a) N. V. Latypov, J. Bergman, A. Laglet, U. Wellmar, U. Bemm, *Tetrahedron* **1998**, *54*, 11525. b) H. Östmark, H. Bergman, U. Bemm, P. Goede, E. Hogrem, M. Johansson, A. Langlet, N. V. Latypov, A. Petterson, M. L. Petterson, N. Wingborg, C. Vörde, H. Stenmark, L. Karlsson, M. Hinkio, *32nd Int. Ann. Conf. ICT*, Karlsruhe, Germany, **2001**, V26.
- [26] a) P. Brousseau, M. D. Cliff, *32nd Int. Ann. Conf. ICT*, Karlsruhe, Germany, **2001**, V37. b) A. Lefrancois, C. Le Gallic, *32nd Int. Ann. Conf. ICT*, Karlsruhe, Germany, **2001**, V36.
- [27] J. P. Agrawal, *Prog. Energy. Combust.* **1998**, *24*, 1.
- [28] A. R. Mitchell, P. F. Pagoria, C. L. Coon, E. S. Jessop, J. F. Poco, C. M. Tarver, R. D. Breithaupt, G. L. Moody, *Propellants, Explos., Pyrotech.* **1994**, *19*, 232.
- [29] R. J. Spear, W. P. Norris, *Propellants, Explos., Pyrotech.* **1983**, *8*, 85-88.
- [30] W. P. Norris, R. J. Spear, R. W. Read, *Aus. J. Chem.* **1983**, *36*, 297-309.
- [31] A. P. Chafin, S. L. Christaw, R. A. Hollings, A. T. Nielsen, W. P. Norris, *Proceed. ADPA Meeting Compat. Plast. Oth. Mater. Explos., Propellants, Pyroll. Ingrid.*, Long Beachy, CA, **1986**, pp. 122-125.
- [32] A. P. Chafin, R. L. Atkins, US 4,754,040 **1988**.
- [33] a) D. E. Chavez, M. A. Hiskey, *J. Energ. Mater.* **1997**, *17*, 33; b) D. E. Chavez, M. A. Hiskey, *J. Heterocycl. Chem.* **1998**, *35*, 1329; c) D. E. Chavez, M. A. Hiskey, R. D. Gilardi, *Angew. Chem. Int. Ed.* **2000**, *39(10)*, 1791-1793. d) D. E. Chavez, M. A. Hiskey, D. L. Naud, *Propellants, Explos., Pyrotech.* **2004**, *29(4)*, 209-215.
- [34] O. Y. Ang, C. Boren, L. Jiarong, D. Shaun, L. Jianjuan, J. Huiping, *Heterocycles* **1994**, *38*, 1651.
- [35] a) A. Becuwe, A. Deltos, *Proceed. 9th Int. Symp. Detonat. Pval*, Arlington, VA, **1989**, pp. 1008-1013. b) A. R. Basal, V. L. Zbarsky, V. F. Zhilin, *32nd Int. Ann. Conf. ICT*, Karlsruhe, Germany, **2001**, P73.
- [36] a) K. Y. Lee, M. D. Coburn, LA-10302-MS, Los Alamos National Laboratory, NM. b) K. Y. Lee, L. B. Chapman, M. D. Coburn, *J. Energ. Mater.* **1987**, *5*, 27-34.
- [37] A. Becuwe, Fr. Demawde, FR 2,584,066.
- [38] Y. Xi, R. Z. Hu, X. Y. Wang, X. Y. Fu, *Proceed. 17th Int. Pyrotech. Sem.*, Beijing Institute of Technology, Beijing, **1991**, pp. 509-514.
- [39] K. Y. Lee, C. B. Storm, M. A. Hiskey, M. D. Coburn, *J. Energ. Mater.* **1991**, *9*, 415-428.
- [40] R. A. Nissan, S. W. Wilson, Techn. Report China Lake, **1994**, 3-32.

- [41] P. F. Pagoria, T. D. Trans, *Proceed. 33rd Int. Ann. Conf. ICT, Energ. Mater.*, **2002**, 45, 1-16.
- [42] R. D. Chapman, W. S. Wilson, *Thermochim. Acta* **2002**, 384(1-2), 229-243.
- [43] R. L. Simpson, C. L. Coon, M. F. Folts, P. F. Pagoria, LLNL Report, 1-7.
- [44] M. Chaykovskuy, H. G. Adolph, *J. Energ. Mater.* **1990**, 392-414.
- [45] J. Li, C. Boren, O. U. Yuxiang, *Propellants, Explos., Pyrotech.* **1999**, 24, 95.
- [46] R. A. Carboni, J. E. Castle, *J. Am. Chem. Soc.* **1962**, 84, 2453-2454.
- [47] H. Birscher, *Chimia* **2004**, 58(6), 355-362.
- [48] *Manual of Tests and Criteria for the Recommendations on the Transport of Dangerous Goods*, 3rd rev. ed. United Nations, New York and Geneva, **1999**. Impact: Insensitive >40 J, less sensitive ≥ 35 J, sensitive ≥ 4 J, very sensitive ≤ 3 J; friction: Insensitive >360 N, less sensitive = 360 N, sensitive <360 N a. >80 N, very sensitive ≤ 80 N, extreme sensitive ≤ 10 N; According to the UN Recommendations on the Transport of Dangerous Goods (+) indicates: not safe for transport.
- [49] *Bundesgesetz über explosionsgefährliche Stoffe (Sprengstoffgesetz)*, Bern, **1977**.
- [50] a) P. W. Cooper in *Explosives Engineering*, Wiley-VCH: New York, **1997**. b) G. F. Kinney, K. J. Graham in *Explosive Shocks in Air*, Springer-Verlag: New York, **1985**.
- [51] *Explosives, Shock Sensitivity*, Standard Agreement of NATO governments (STANAG) 4488, North Atlantic Treaty Organization, Brussels, **2001**.
- [52] N. Desgardin, C. Perut, *33rd Int. Ann. Conf. ICT*, Karlsruhe, Germany, **2002**, V20.
- [53] P. Folly, P. Mäder, *Chimia* **2004**, 58(6), 374-382.
- [54] P. Naoum, R. Aufschläger, *Z. ges. Schiessw. Sprengstoffw.* **1924**, 19, 121.
- [55] N. Kubota, *J. Pyrotech.* **2000**, 11, 25.
- [56] W. Beck, J. Evers, M. Göbel, G. Oehlinger, T. M. Klapötke, *Z. Anorg. Allg. Chem.* **2007**, 633, 1417-1422. b) W. Beck, T. M. Klapötke, *J. Mol. Struct. (THEOCHEM)* **2008**, 848, 94-97.
- [57] D. Adam, K. Karaghiosoff, T. M. Klapötke, G. Holl, M. Kaiser, *Propellants, Explos., Pyrotech.* **2002**, 27, 7.
- [58] U. Brede, R. Hagel, K. H. Redecker, W. Weuter, *Propellants, Explos., Pyrotech.* **1996**, 21, 113-117.
- [59] O. Ringgenberg, J. Mathieu, *Chimia* **2004**, 58(6), 390-393.
- [60] M. Suceska, *Propellants, Explos., Pyrotech.* **1991**, 16, 197-202.
- [61] L. E. Fried, K. R. Glaesemann, W. M. Howard, P. C. Souers, 2004. *CHEETAH 4.0 User's Manual*, Lawrence Livermore National Laboratory.
- [62] A. A. Kozyro, M. L. Frenkel, A. P. Krasulin, V. V. Simirskii, and G. Ya. Kabo, *Russ. J. Phys. Chem.* **1988**, 62, 897-899.

- [63] T. M. Klapötke, G. Steinhauser, *Angew. Chem. Int. Ed.* **2008**, *47*(18), 3330–3347.
- [64] E. C. Koch, *Propellants, Explos., Pyrotech.* **2001**, *26*, 3.
- [65] B. V. Ingram, *J. Pyrotech.* **2003**, *17*, 1.
- [66] V. A. Strovskii, M. S. Pevzner, T. P. Kofman, I. V. Tselinskii, *Targets Heterocycl. Syst.* **1999**, *3*, 467.
- [67] J. Giles, *Nature* **2004**, *427*, 580–581.
- [68] a) S. V. Levchik, A. I. Balabanovich, O. A. Ivashkevich, A. I. Lesnikovich, P. N. Gaponik, L. Costa, *Thermochim. Acta* **1992**, *207*, 115; b) S. V. Levchik, A. I. Balabanovich, O. A. Ivashkevich, A. I. Lesnikovich, P. N. Gaponik, L. Costa, *Thermochim. Acta* **1993**, *255*, 53; c) A. I. Lesnikovich, O. A. Ivashkevich, S. V. Levchik, A. I. Balabanovich, P. N. Gaponik, A. A. Kulak, *Thermochim. Acta* **2002**, *388*, 233; d) A. Gao, Y. Oyumi, T. B. Brill, *Combust. Flame* **1991**, *83*, 345; e) S. V. Levchik, A. I. Balabanovich, O. A. Ivashkevich, P. N. Gaponik, L. Costa, *Polym. Degrad. Stability* **1995**, *47*, 333.
- [69] a) K. H. Bloss, DE 2,217,780 **1972**. b) K. H. Bloss, DE 2,142,578 **1973**. c) K. Redecker, DE 19,505,568 **1996**. d) H. Gawlick, DE 1,805,358 **1970**.
- [70] M. Tremblay, *Can. J. Chem.* **1965**, *43*(5), 1154–1157.
- [71] A. Hammerl, M. A. Hiskey, G. Holl, T. M. Klapötke, K. Polborn, J. Stierstorfer, J. J. Weigand, *Chem. Mater.* **2005**, *17*(14), 3784–3793.
- [72] a) M. H. V. Huynh, M. D. Coburn, T. J. Meyer, M. Wetzler, *Proc. Natl. Acad. Sci. U. S. A.* **2006**, *103*(27), 10322–10327. b) M. H. V. Huynh, M. A. Hiskey, T. J. Meyer, M. Wetzler, *Proc. Natl. Acad. Sci. U. S. A.* **2006**, *103*(14), 5409–5412.
- [73] A. Y. Zhilin, M. A. Ilyushin, I. V. Tselinskii, A. S. Brykov, *Russ. J. Appl. Chem.* **2001**, *74*(1), 96–99.
- [74] a) R. P. Singh, R. D. Verma, D. T. Meshri, J. M. Shreeve, *Angew. Chem. Int. Ed.* **2006**, *45*, 3584–3601. b) V. A. Ostrovskii, G. I. Koldobskii, R. E. Trifonov, *Tetrazoles*. In *Comprehensive Heterocyclic Chemistry III*, Eds. A. R. Katritzky, C. A. Ramsden, E. F. V. Scriven, R. J. K. Taylor, Elsevier: Oxford, UK, **2008**, *6*, 257–423.
- [75] C. Knapp, J. Passmore, *Angew. Chem. Int. Ed.* **2004**, *43*(37), 4834–4836.
- [76] a) K. O. Christie, W. W. Wilson, J. A. Sheehy, J. A. Boatz, *Angew. Chem. Int. Ed.* **1999**, *38*(13/14), 2004. b) A. Vij, W. W. Wilson, V. Vij, F. S. Tham, V. Jeffrey, K. O. Christie, *J. Am. Chem. Soc.* **2001**, *123*(26), 6308. c) D. A. Dixon, D. Feller, K. O. Christie, W. W. Wislon, A. Vij, H. D. Vij, H. D. B. Brooke, R. M. Olson, M. S. Gordon, *J. Am. Chem. Soc.* **2004**, *126*(3), 834.
- [77] a) A. Hahma, E. Holmber, N. Hore, R. Tryman, S. Wallin, H. Östmark, *33rd Int. Ann. Conf. ICT*, Karlsruhe, Germany, **2002**, *62*, 1. b) A. Vij, J. G. Pavlovich, W. W. Wilson, V. Vij, K. O. Christie, *Angew. Chem. Int. Ed.* **2002**, *41*(16), 3051. c) H. Östmark, S. Wallin, T. Brinck, P. Carlqvist, R. Claidge, E. Hedlun, L. Yudina, *Chem. Phys. Lett.* **2003**, *379*(5,6), 539. d) P. Carlqvist, H. Östmark, T. Brinck, *J. Org. Chem.* **2004**, *69*(9), 3222. e) S. D. Kunikeev, H. S. Taylor, T. Schroer, R. Halges, C. J. B. Jones, K. O. Christie, *Inorg. Chem.* **2006**, *45*, 437–442. f) W. W. Wilson, A. Vij, V. Vij, E. Bernhardt, K. O. Chrsitie, *Chem. Eur. J.* **2003**, *9*, 2840–2844.

- [78] T. Curtius, *Ber. Dtsch. Chem. Ges.* **1890**, 23, 3023.
- [79] J. Wasilewski, *J. Chem. Phys.* **1996**, 105, 10969.
- [80] a) R. Tian, J. C. Facelli, J. Michl, *J. Phys. Chem.* **1988**, 92, 4073. b) J. A. Guthrie, R. C. Chaney, A. J. Cunningham, *J. Chem. Phys.* **1991**, 95, 930.
- [81] a) W. E. Thompson, M. E. Jacox, *J. Chem. Phys.* **1990**, 93, 3856. b) T. Ruchti, T. Speck, J. P. Connelly, E. J. Bieske, H. Linnartz, J. P. Maier, *J. Chem. Phys.* **1996**, 105, 2591.
- [82] a) M. T. Nguyen, T. K. Ha, *Chem. Ber.* **1996**, 129, 1157. b) M. N. Glukhovstev, H. Jiao, P. V. R. Schleyer, *Inorg. Chem.* **1996**, 35, 7124 and references therein.
- [83] M. A. Petrie, J. A. Sheehy, J. A. Boatz, G. Rasul, G. K. S. Prakash, G. A. Olah, K. O. Christie, *J. Am. Chem. Soc.* **1997**, 119, 8802-8808.
- [84] a) J. C. Gálvez Ruiz, G. Holl, K. Karaghiosoff, T. M. Klapötke, K. Löhnwitz, P. Mayer, H. Nöth, K. Polborn, C. J. Rohbogner, M. Suter, J. J. Weigand, *Inorg. Chem.* **2005**, 44(12), 4237-4253. b) J. J. Weigand, Diploma Thesis, Ludwig-Maximilians University Munich, **2002**.
- [85] P. Folly, *Chimia* **2004**, 58(6), 394-400
- [86] a) T. Ozawa, *Bull. Chem. Chem. Soc. Jpn.* **1965**, 38, 1881. b) H. E. Kissinger, *Anal. Chem.* **1957**, 29, 1702.
- [87] a) <http://www.bam.de>. b) T. M. Klapötke, C. M. Rienäcker, *Propellants, Explos., Pyrotech.* **2001**, 26, 43–47.
- [88] J. J. Weigand, *Ph. D. Thesis*, Ludwig-Maximilians University, **2005**.

CHAPTER II

5-AMINOTETRAZOLES AND SILVER-BASED PRIMARIES

2.1 Introduction

As mentioned in the introductory chapter, nitrogen-rich materials and in particular tetrazoles have a great potential for energetic applications.^[1-3] Tetrazole-based energetic materials^[4] tend to have higher (more positive) heats of formation than analogous imidazoles or triazoles^[4,5] and tend to possess high thermal stabilities regardless of their large positive enthalpies of formation.^[6] Therefore, nitrogen rich compounds based on the nitrogen-rich 5-amino-1*H*-tetrazole (5-At, **1**) or 1,5-diamino-1*H*-tetrazole (DAT, **2**) are interesting in relation to the formation of endothermic (or less exothermic) compounds and environmentally friendly decomposition products.

We recently reported the synthesis and characterization of salts of 5-At with nitrate and perchlorate anions.^[7,8] Methylation of 5-At is known to give a separable mixture of 1-methyl- (1MAT, **3**) and 2-methyl-5-amino-1*H*-tetrazole (2MAT, **4**),^[9] and we also studied salts of the compounds with nitrate and perchlorate anions (among others) as prospective insensitive energetic materials with reasonably high performances.^[1g,11,2a] Since, many times highly endothermic compounds turn out to be very sensitive towards classical stimuli (i.e., friction and impact),^[10] the introduction of small alkyl chains (i.e, methyl groups) helps reduce the sensitivity of a material at the same time that increases the thermal stability at the cost of performance. Additionally, the introduction of methyl groups also make interesting compounds accessible. For example, HN_3 is not able to protonate 5-At to form the interesting azide salt, however, quaternization of the tetrazole allows the formation of different tetrazolium azide salts (see also *Chapter VI*).^[1g,11,2a]

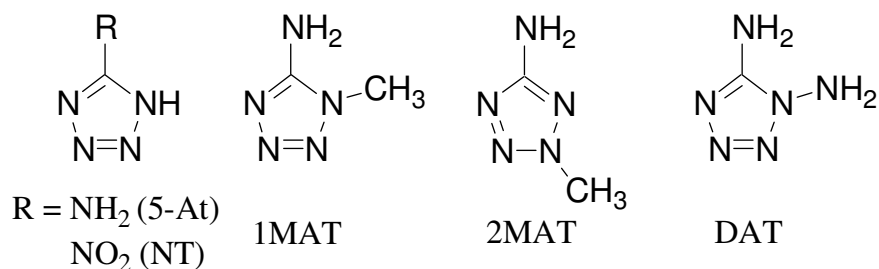


Figure 2.1 Structure of some commonly-used tetrazole-based ligands.

Figure 2.1 shows the structure of some commonly-used tetrazole-based ligands. Most of the literature dealing with tetrazole-based materials concentrates on nitrogen-rich salts like those with cations such as ammonium,^[11] hydrazinium,^[11,12] guanadinium,^[11] aminoguanadinium,^[11] diaminoguanidinium^[11] and triaminoguanidinium,^[11,13] among others^[14] or salts with energetic anions like nitrate, perchlorate, picrate, azide, dinitramide,^[15] 5,5'-azotetrazolate,^[11a,12a,15] or 5-nitrotetrazolate^[3f,16], among others.^[3f,17] On the other side, the description of metal compounds containing a tetrazole moiety is much more elusive in the literature and many compounds are not interesting from the energetic point of view. Compounds of this type that have been reported before include alkali and alkaline-earth metal,^[18] Fe^{2+} ,^[19] $\text{Co}^{2+/3+}$,^[20] Ni^{2+} ,^[16] Cu^{2+} ^[21] and Hg^+ ^[22] salts of 5-nitrotetrazole (NT), salts of 1,5-diamino-1*H*-tetrazole (DAT) with Co^{3+} ,^[23] Ni^{2+} ,^[24a] Cu^{2+} ,^[24] Zn^{2+} and Cd^{2+} ,^[24a] complexes of Mg^{2+} and Ca^{2+} ,^[25a] Cr^{3+} ,^[25b] $\text{Fe}^{2+/3+}$,^[25b] $\text{Co}^{2+/3+}$,^[25c, 25d] Ni^{2+} ,^[25e] Cu^{2+} ,^[25e, 25f] Zn^{2+} ^[25g] and Cd^{2+} ^[25h,25i] with 5-amino-1*H*-tetrazole (5-At) and 1*R*-substituted-5-amino-1*H*-tetrazole transition metals complexes of divalent and trivalent metals (Co^{3+} , Ni^{2+} , Cu^{2+} , Zn^{2+} , Ag^+ and Pd^{2+}) with $\text{R} = \text{Me}$ (1MAT),^[26a] $\text{R} = \text{CH}_2\text{C}(=\text{O})\text{NHNH}_2$,^[26b-d] $\text{R} = \text{CH}=\text{CH}_2$ ^[27a] and $\text{R} = \text{Ph}$.^[27b] Some of them, have either found use or are prospective candidates for use in pyrotechnic mixtures and have other interesting applications such as their use in laser-induced explosives (LIE, e.g., Co complexes).^[25d] LIE explosives are interesting from the initiation point of view since the wave-length of the incident light can be modulated such as to cause explosion of the compound, while this is insensitive to classical stimuli (i.e., shock and friction) and can hence be manipulated easily. However, the mechanism of the induction is not well understood and magnetic measurements combined with crystal structure analysis should help explain this phenomenon allegedly related to the excitement of electrons in *d*-orbitals for transition metals. Unfortunately, apart from some recent work in our group in tetrazole-based alkali metal salts^[18a, 28] and some copper complexes^[1h, 29] there are not many reports dealing with crystal structures in tetrazole-based metal complexes, specially when the cation is a transition metal. To our knowledge, the only examples reported so far are those of $\text{Ni}(\text{NT})_2$,^[16] $\text{Cd}(\text{5-At})_2$,^[25i] $\text{Cu}(\text{DAT})\text{Cl}_2$ ^[24b] and $\text{Co}(\text{NH}_3)_4(\text{1MAT})_2$.^[23a]

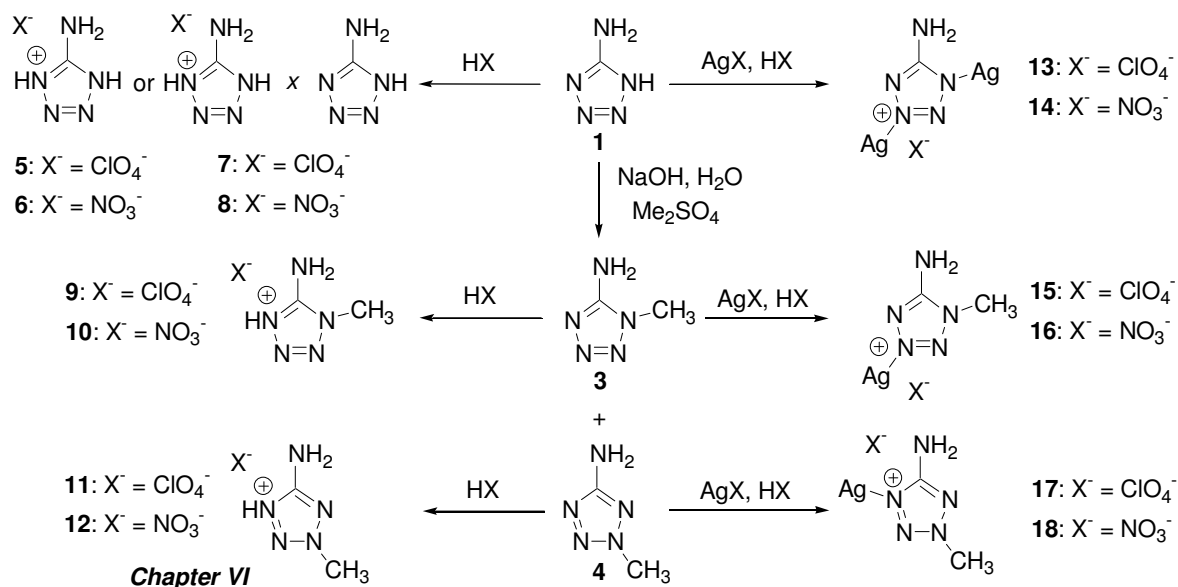
In explosive devices, it is common to construct a so-called “explosive train”,^[30] which is typically made up of an initiator device, a primary and a secondary explosive. One of the problems of primary explosives is their low thermal stability. Silver salts tend to have high decomposition temperatures and are interesting for use as initiators (e.g., silver azide^[31] or silver 5,5'-azotetrazolate^[32]), among others due to the relatively benign character of silver (e.g., table silverware) in comparison to commonly used initiators such as lead diazide ($\text{Pb}(\text{N}_3)_2$). In addition to heavy metal salts, (organic) perchlorate salts are also known to be rather sensitive compounds. In this context, disilver 5-amino-1*H*-tetrazolium perchlorate was patented as a new primary

explosive with excellent thermal stability.^[30] Therefore, in this work, we would like to report the synthesis and full analytical, spectroscopic and energetic characterization of silver salts with different 5-amino-1*H*-tetrazole ligands and perchlorate and nitrate anions as analogous compounds to our previously reported protonated tetrazolium salts and compare the energetic properties of all of them. In addition, we would like to report the crystal structures of three new silver salts with tetrazole-based ligands, which add to the few structural reports on azole-based metal salts and represent the first examples of a silver salt containing an azole ligand, which have been structurally characterized.

2.2 Synthesis

In analogy to our recently reported synthesis of 5-amino-1*H*-tetrazolium nitrate (**5AtNO₃**, **6**),^[7] by protonation of 5-At with nitric acid, we reacted 5-At with perchloric acid. With a large excess of acid we obtained the expected perchlorate salt (**5AtClO₄**, **5**), however, when using 1.2 equivalents of perchloric acid a much more stable adduct (see Energetic Discussion) between **5** and 5-At formed (**5AtClO₄*5At**, **7**) (see Scheme 2.1). All attempts to synthesize the energetically interesting 5-At adduct of **6** (**5AtNO₃*5At**, **8**) either by boiling 5-At with **6** or by reaction of 5-At with different amounts of nitric acid resulted in recovering of the starting materials. Salts of 1MAT and 2MAT (**9-12**) with nitrate and perchlorate anions were synthesized accordingly^[2a,11c] and will be discussed in detail in *Chapter VI*.

In order to synthesize the analogous silver salts of the compounds mentioned above disilver 5-amino-1*H*-tetrazolium perchlorate (**Ag₂AtClO₄**, **13**) was synthesized by reaction of 5-amino-1*H*-tetrazole (5-At) with silver perchlorate in perchloric acid (Scheme 2.1).^[30] After addition of water a highly insoluble white powder of the compound precipitated, which showed a great sensitivity towards shock and friction (primary explosive!!). The interesting explosive properties of the compound prompted us to study other silver salts and we synthesized the nitrate derivative (**Ag₂AtNO₃**, **14**). In order to tune the high sensitivity of these compounds, 5-At was methylated with dimethyl sulphate yielding 1MAT and 2MAT, which were reacted either with silver nitrate or silver perchlorate in the corresponding acid (i.e., nitric or perchloric acid, respectively) yielding a new family of silver salts with methylated tetrazole ligands (**15-18**).



Scheme 2.1 Synthesis of the 5-aminotetrazolium nitrate and perchlorate salts.

Reaction of silver picrate (AgPic) with 1,4-dimethyl-5-amino-1*H*-tetrazolium iodide (1,4DMAT⁺I) to yield the corresponding picrate salt (*Chapter V*), yielded crystals of a by-product, which could be identified as bis-(1,4-dimethyl-5-imino-1*H*-tetrazole)silver picrate (**Ag(DMIT)₂Pic, 19**) (Figure 2.2). Its formation can be explained by the method of preparation of AgPic from picric acid and KOH and subsequent metathesis with silver nitrate. Possibly unreacted KOH deprotonated the 1,4DMAT⁺ cation to form neutral 1,4DMIT (*Chapter III*), which reacted in turn coordinating with the silver picrate formed (Scheme 2.2).

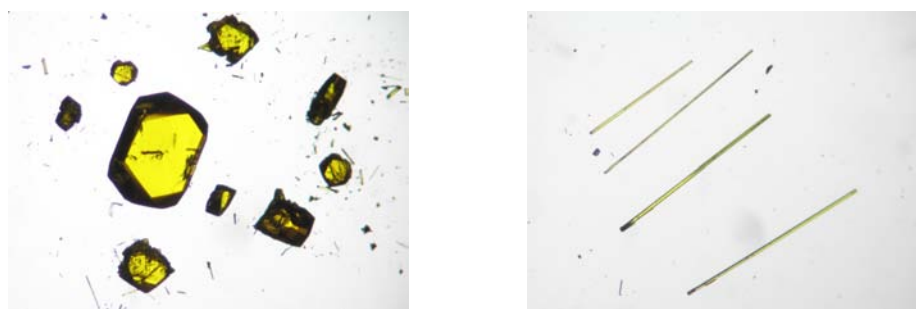
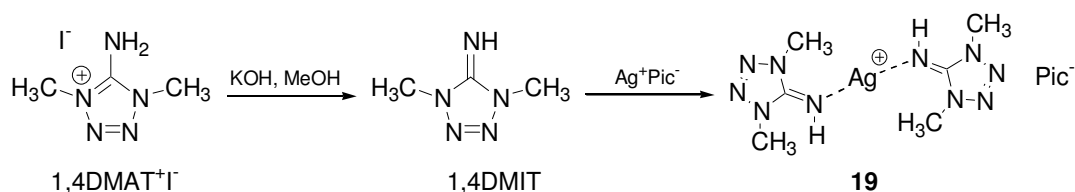


Figure 2.2 Crystals of 1,4-dimethyl-5-amino-1*H*-tetrazolium picrate (left) and of complex **19** (right).



Scheme 2.2 Reaction leading to the formation of **19**.

Lastly, attempted recrystallization to obtain crystals of **16** resulted in the formation of tri-(1-methyl-5-amino-1*H*-tetrazolo) silver nitrate ($\text{Ag}(\text{1MAT})_3\text{NO}_3$, **20**) and silver nitrate. The structure of the compound is discussed below.

2.3 Vibrational and NMR Spectroscopy

All compounds were characterized by IR, Raman and NMR spectroscopy when possible. The highly sensitive perchlorate and nitrate salts **13** and **14** are extremely insoluble compounds in every common solvent. They only dissolve in concentrated acid solutions (e.g., hydrochloric, nitric or perchloric acids) forming the corresponding 5-amino-1*H*-tetrazolium salt (chloride, nitrate and perchlorate) so that the silver cations are no longer coordinating to the tetrazole ring, therefore we omitted any NMR study on these two compounds.

The spectra measured show the characteristic bands of the respective energetic anions (nitrate and perchlorate) for each one of the compounds studied. In the nitrate salts, the anion shows a strong, broad IR (Figure 2.3) absorption centered at $\sim 1385\text{ cm}^{-1}$ and a sharp strong band at $\sim 1040\text{ cm}^{-1}$ (1047 cm^{-1} for **14**) in the Raman (Figure 2.4).^[33] For the silver salts, the perchlorate anion shows a strong stretch with its maximum at $1085\text{--}1090\text{ cm}^{-1}$ in the infrared spectra and strong, sharp bands at $925\text{--}930$ and $460\text{--}465\text{ cm}^{-1}$ in the Raman spectra.^[34] For the perchlorate salts **5** and **7** the anion is observed at $\sim 1088\text{ cm}^{-1}$ (IR) and is shifted to ~ 940 and 457 cm^{-1} (Raman), in respect to the silver compounds.

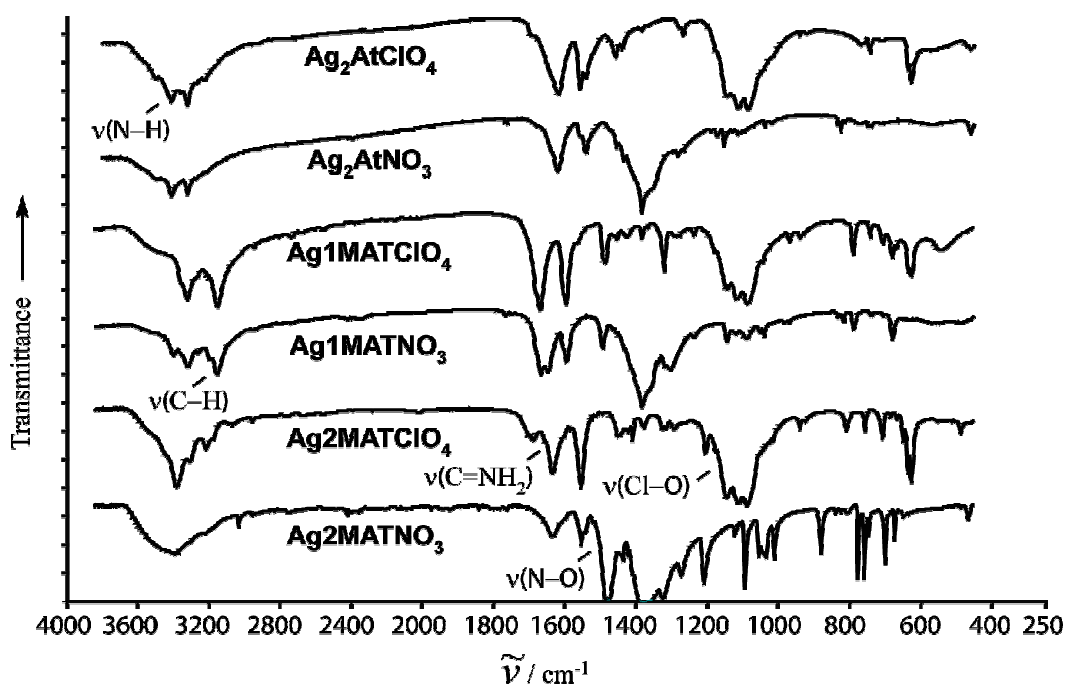


Figure 2.3 Panel plot of the IR spectra of silver complexes.

Apart from the intense bands corresponding to the anion just mentioned above, the IR and Raman spectra of the compounds also contain a set of bands that are characteristic for the cation. Two sharp strong bands at ~ 3415 and ~ 3325 cm^{-1} corresponding to N–H stretching with two smaller shoulders are observed in the IR spectra of **13** and **14**. The rest of the compounds show a much more complicated set of bands in this region with maximum at 3348 and 3420 cm^{-1} (**5** and **7**, respectively), ~ 3325 cm^{-1} (**15** and **16**) and ~ 3390 cm^{-1} (**17** and **18**) in addition to the C–H stretches in the case of the methylated compounds in the range between 2950 and 2060 cm^{-1} . After the anion stretch bands, the strongest absorption is the combined C=NH₂ stretching and the NH₂ deformation modes found at ~ 1620 cm^{-1} for compounds **18** and **17** in the IR spectra and which is shifted to ~ 1635 cm^{-1} (2MAT derivatives) and as high as ~ 1670 cm^{-1} (1MAT derivatives) in the methylated derivatives. This is in agreement with signals at higher energies (~ 1685 cm^{-1}) for **9** and **10**.^[2a] Lastly, the rest of the bands are of lower intensity and can be assigned as follows: 1550-1350 cm^{-1} [ν (tetrazole ring), δ_{as} (CH₃)], ~ 1380 cm^{-1} [δ (CH₃)], 1350-700 cm^{-1} [ν (N–C–N), ν (N–N), γ (CN), δ (tetrazole ring)], <700 cm^{-1} [δ out-of-plane bend (N–H), ω (NH₂)].^[35]

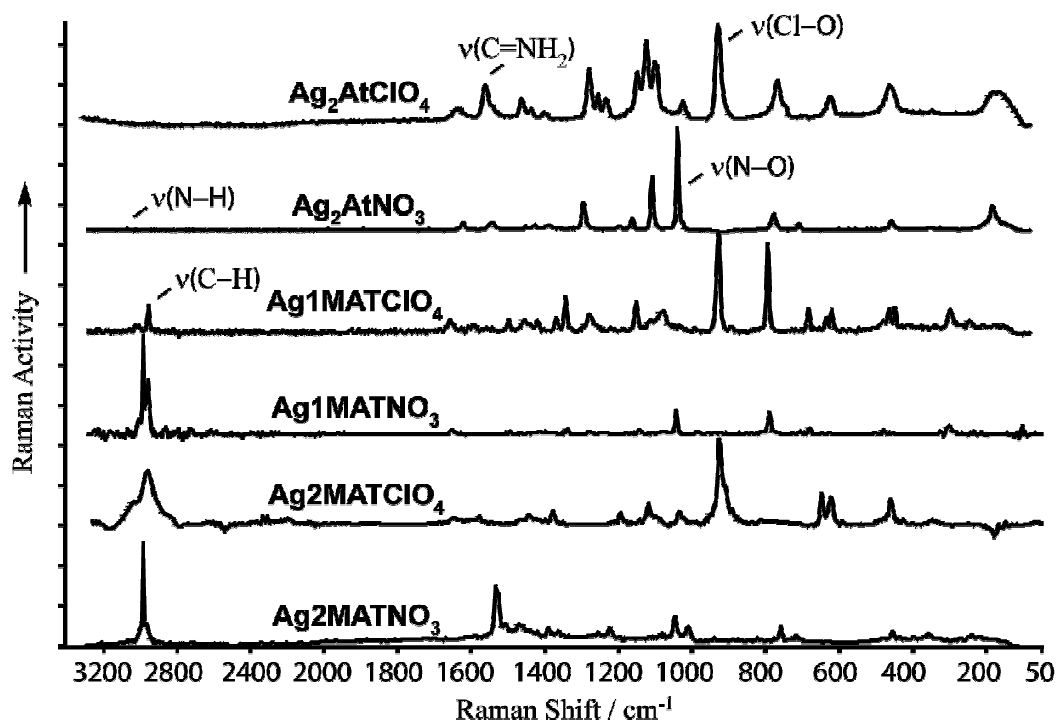


Figure 2.4 Panel plot of the Raman spectra of silver complexes.

On the other side, IR spectroscopy also provides detailed insight into cation structure and interionic interactions including hydrogen-bonding.^[36] A comparison of the IR spectra of the silver salts with those of 5-amino-1*H*-tetrazolium nitrate (**6**) and perchlorate (**5**), shows substantial changes, shifts and sharpening of the ν (N–H) bands observed in **6** and **5** when the ring protons are substituted by silver atoms. For example, perchlorate **5** shows two bands at 3437 and

3348 cm^{-1} , which are shifted to slightly lower wavenumbers ~ 3415 and 3326 cm^{-1} (one only band at $\sim 3400 \text{ cm}^{-1}$ for the methylated derivatives) in the silver salts indicating a weakening (elongation) of the N–H bonds in the exocyclic amino group. In addition to providing information about hydrogen-bonding and N–H bond strengths, IR spectra also indicate other structural differences between silver salts (**13-18**) and their protonated analogues (**5, 6** and **9-12**). For example, the IR spectra of **14** and **13** show a strong band at 1620 and 1617 cm^{-1} and another at 1541 and 1557 cm^{-1} , corresponding to amino group deformation and C=N ring stretch, respectively.^[37,38] In the spectra of salts **6** and **5** a higher energy band corresponding to the coupled amino group deformation and exocyclic C=N stretch is observed at $\sim 1700 \text{ cm}^{-1}$. This observation can be explained nicely by the structural changes expected on substitution of the ring protons by silver atoms, i.e., the exocyclic C=NH₂ bond length should increase (decrease in stretching energy) as observed experimentally (see X-ray discussion).

As mentioned above **13** and **14** were too insoluble in any solvent tried to record an NMR spectrum. As for the rest of the compounds, in the ^1H NMR measured in DMSO- d_6 , the amino group has resonances of ~ 6.0 ppm for the 2MAT derivatives, ~ 7.0 ppm for the 1MAT derivatives and is strongly shifted to low field in the case of **5** and **7**, which only show average signals with the ring NH protons at ~ 11.0 ppm, similarly to **6**^[7] and indicative of the higher acidity of those protons in the latter compounds. The methyl group proton resonances are found at ~ 3.7 and ~ 4.0 ppm for the 1MAT derivatives and the 2MAT derivatives, respectively. In the ^{13}C NMR (as observed in the ^1H NMR) the shifts of the 1MAT derivatives are shifted to higher field in respect to those of the 2MAT derivatives. The methyl group and ring carbon atom shifts are observed at ~ 32.0 and ~ 39.0 ppm and at ~ 156.0 and ~ 167.0 ppm (~ 152.0 ppm for **5** and **7**), respectively. The ^{14}N NMR spectra only shows broad signals associated to the quadrupole moment of the nucleus and the only resonance, which is observed is that of the anion in the nitrate salts at ~ 4 ppm (see Figure 2.5). In comparison with the protonated species, the silver salts **15-18** tend to show resonances to higher field.^[2a]

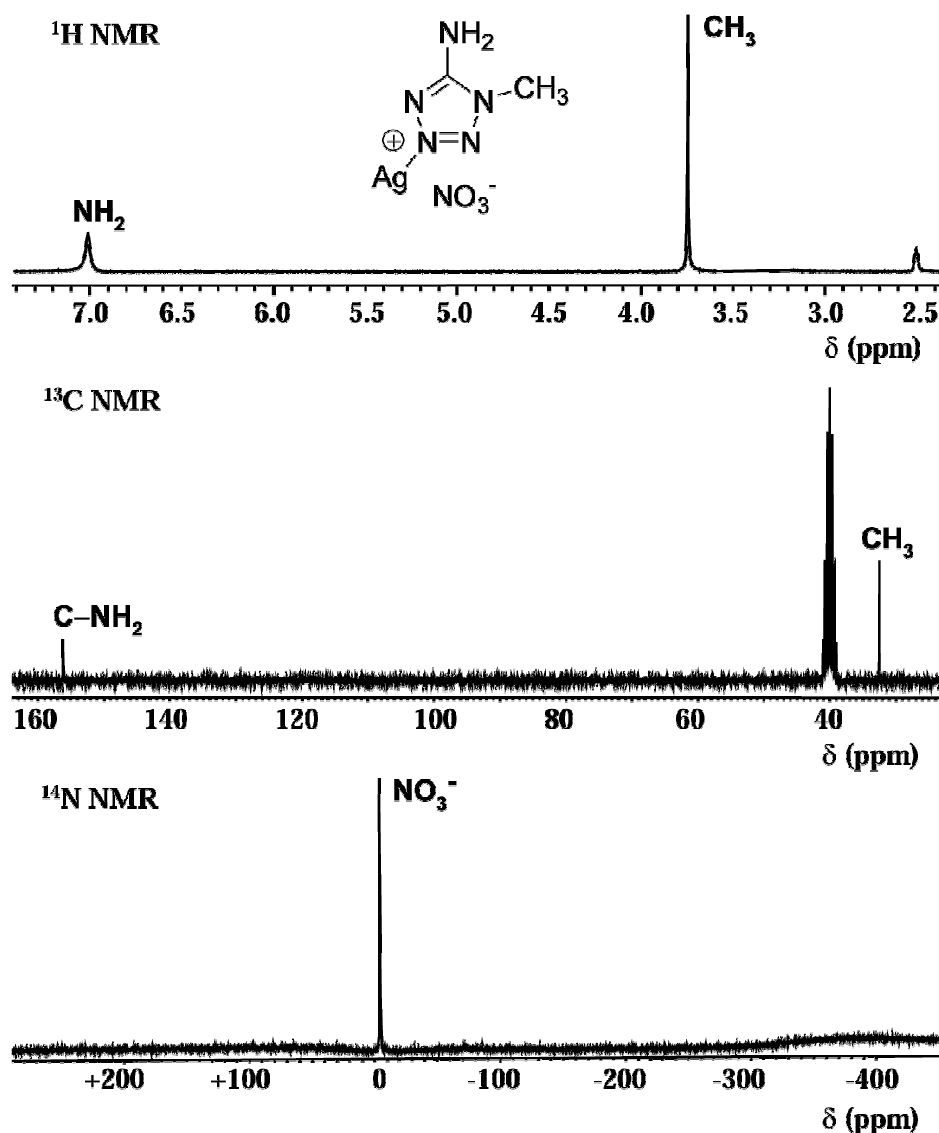


Figure 2.5 ¹H, ¹³C and ¹⁴N NMR spectra of **16** in DMSO-*d*₆.

Figure 2.6 shows the coupled and decoupled ¹⁵N NMR for **5**. The signal at the highest field (-325.1 ppm) can be easily assigned as the amino group nitrogen atom resonance, which couples with the two protons rendering a triplet with ¹*J* = 86.4 Hz, whereas the other two signals can be differentiated by the PIS (proton induced effect),^[2a] which causes a shift to higher field of the resonances of the protonated nitrogen atoms. Thus, the protonated nitrogen atoms N2 and N5 can be identified as the signal at -167.8 ppm, whereas N3 and N4 are found at lower field (-27.0 ppm). In analogy to a proton induced effect, it would also be of interest to examine the effect of the coordination of the silver atoms in the resonances of the ring nitrogen atoms (metal induced effect), unfortunately, the solubility of the silver salts in any solvent tried was again too low to be able to record a ¹⁵N NMR (natural abundance). For the perchlorate salts, the anion is observed at

+1.0 ppm in the ^{35}Cl NMR, as expected. Lastly, all the shifts mentioned above, as well as the PIS values are keeping in with those observed in the protonated derivatives.^[2a,7]

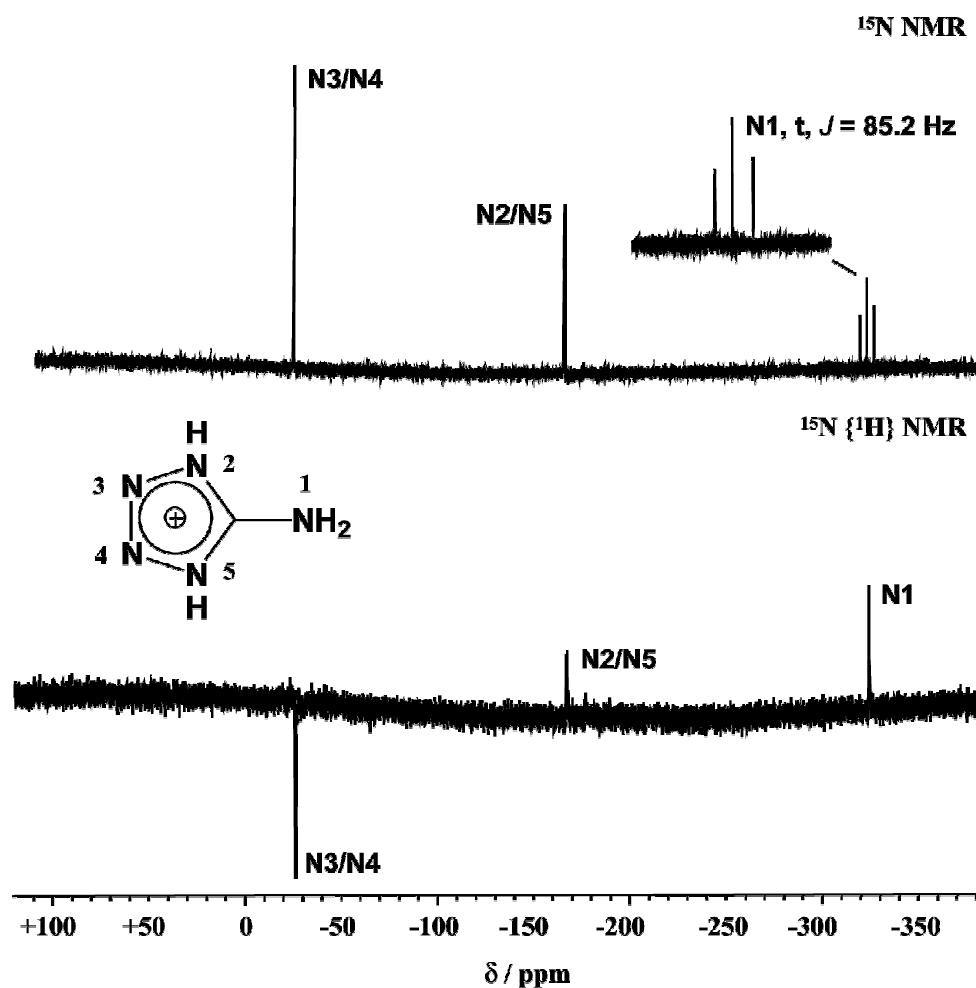


Figure 2.6 ^{15}N NMR of the 5-amino-1H-tetrazolium cation in **5** (**5**) measured in $\text{DMSO}-d_6$.

2.4 Crystal Structures

13, **14** and **18** formed always as powders after recrystallization from several solvents, whereas **16** forms as very fine needles. Therefore any structural characterization of these compounds was not possible and is in consequence omitted from this work. As for the rest of the materials crystals were obtained as described in the experimental section. The X-ray crystallographic data for all compounds were collected on an Oxford Diffraction Xcalibur 3 diffractometer equipped with a CCD detector using graphite-monochromated Mo $\text{K}\alpha$ radiation ($\lambda = 0.71073$ Å). All structures were solved by direct methods (SHELXS-97 and SIR97) and refined by means of full-matrix least-squares procedures using SHELXL-97.^[39,40] All non-hydrogen atoms were refined anisotropically. All hydrogen atoms were located from difference Fourier electron-density maps. For all structures all hydrogen atoms were refined isotropically. Crystallographic data are

summarized in Appendix C. Selected bond lengths and angles are reported in Table 2.1 and hydrogen-bonding geometries in Table 2.2.

As mentioned in the synthesis section, depending on the amount of perchloric acid used to react with 5-At, either the perchlorate salt is obtained or an adduct between the starting material and the product forms. Figure 2.7 shows the asymmetric unit of both compounds with the labeling scheme. The angles and distances for the tetrazolium cations in both compounds are similar and agree with the nitrate salt.^[7] However, the C–N6 and the N8–N9 distances in the second tetrazole ring in the structure of **7** are longer and shorter, respectively than the analogous distances in the tetrazolium cation, in agreement with the published structure of 5-amino-1*H*-tetrazolium monohydrate.^[41]

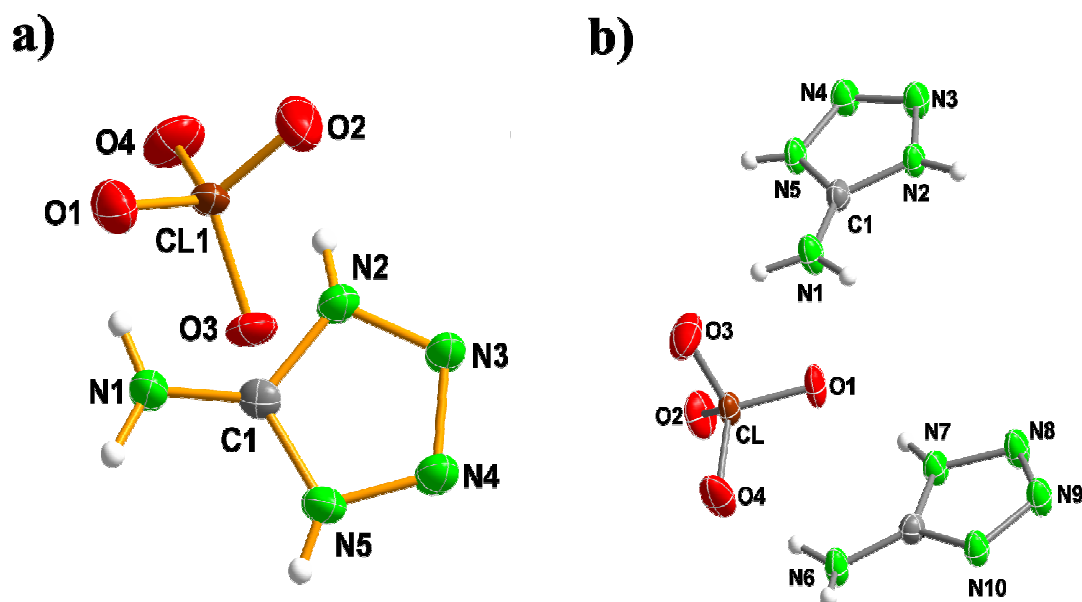


Figure 2.7 Asymmetric unit of a) **5** and b) **7** with the labelling scheme.

The cations in **5** orient very symmetrically forming layers, which in contrast to the nitrate salt^[7] are not planar due to the non-planarity of the perchlorate anion and cut the *a*- and *c*-axis at an angle of $\sim 45^\circ$. Figure 2.8a shows a view of the unit cell of the compound along the *a* axis with a sample of the extensive hydrogen-bonding found in the structure.

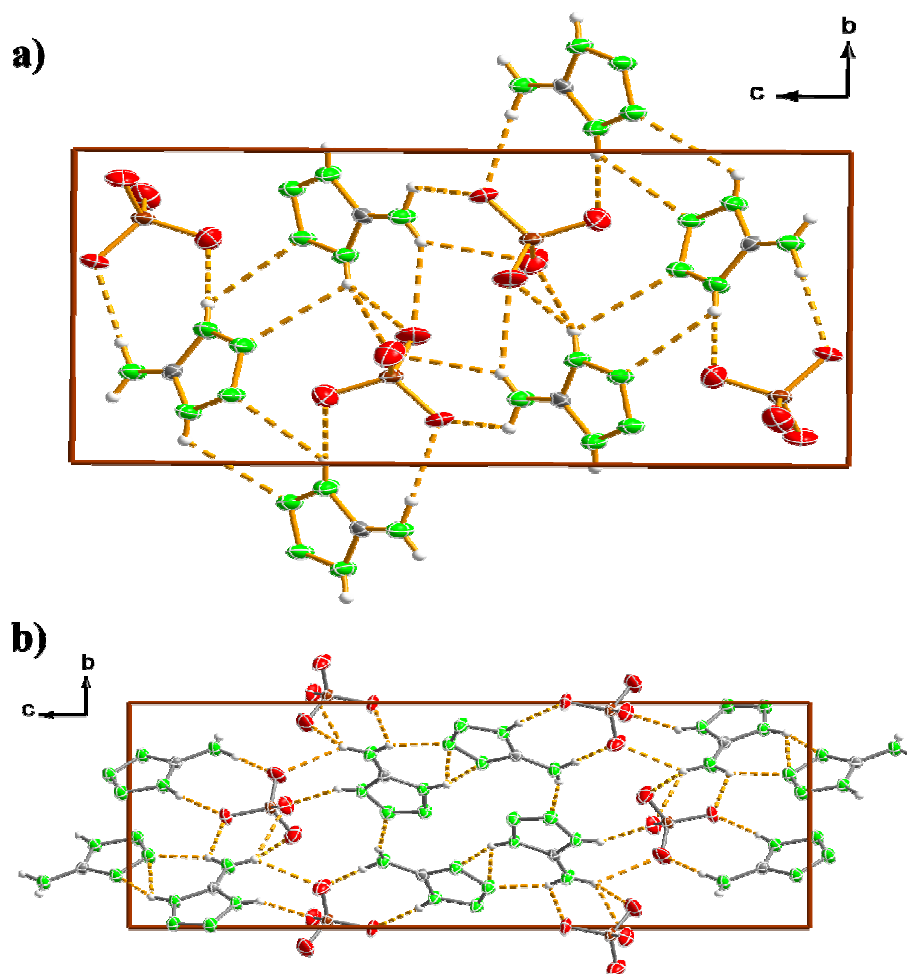


Figure 2.8 Hydrogen-bonding in the unit cell of a) **5** and b) **7**.

The extensive hydrogen-bonding formed is better represented in Figure 2.9 in a view of one layer in the structure and together with the “heavy” perchlorate anion accounts for the high density of the compound at 1.924 g cm^{-3} . Cations and anions alternate along the *b* axis and are connected to each other by the many hydrogen bonds summarized in Table 2.2. The extensive hydrogen-bonding networks are better explained in the formalism of graph-set analysis as introduced by Bernstein et al.^[42] and using the computer program *RPLUTO*.^[43] At the secondary level, the combination of all hydrogen bonds summarized in Table 2.2 yield only a few chain patterns with the descriptor **C2,2(X)** (*X* = 6, 8), whereas the rest of the graph-sets are ring motifs with the following labels: **R1,2(6)**, **R2,2(X)** (*X* = 4, 6, 8), **R4,2(8)** and **R4,4(X)** (*X* = 12, 16), many of which are represented in Figure 2.10. The side-on interaction of a tetrazolium cation with the same oxygen atom of a perchlorate anion gives an **R1,2(6)** graph-set ($\text{N2} \cdots \text{O4}^{\text{i}} = 2.882(3) \text{ \AA}$ and $\text{N1} \cdots \text{O4}^{\text{i}} = 3.017(2) \text{ \AA}$; symmetry code: (i) 1-*x*, 1-*y*, 1-*z*) as found in the structure of 1-methyl-5-amino-1*H*-tetrazolium perchlorate,^[2a] whereas the side-on interaction with two oxygen atoms yields an **R2,2(8)** pattern ($\text{N1} \cdots \text{O3}^{\text{iii}} = 2.931(3) \text{ \AA}$ and $\text{N5} \cdots \text{O1}^{\text{iii}} = 2.942(3) \text{ \AA}$;

symmetry code: (iii) $1-x, -y, 1-z$), which is characteristic for this compound. In addition, the hydrogen bonds formed by the two amino group protons with the anions yield an **R2,2(6)** network ($N1^{\bullet\bullet}O3^{ii} = 3.051(2) \text{ \AA}$ and $N1^{\bullet\bullet}O2^{ii} = 3.054(2) \text{ \AA}$; symmetry code: (ii) $-1+x, y, z$). Lastly, the **R4,4(12)** graph-set (not represented in Figure 2.9 for the sake of simplicity), which is described by the atoms labeled as $N1^i, O3^{iv}, O4^{iv}, N1^{iii}, O2^{ii}$ and $O4^{ii}$ is common for many other perchlorate salts.^[2a,44]

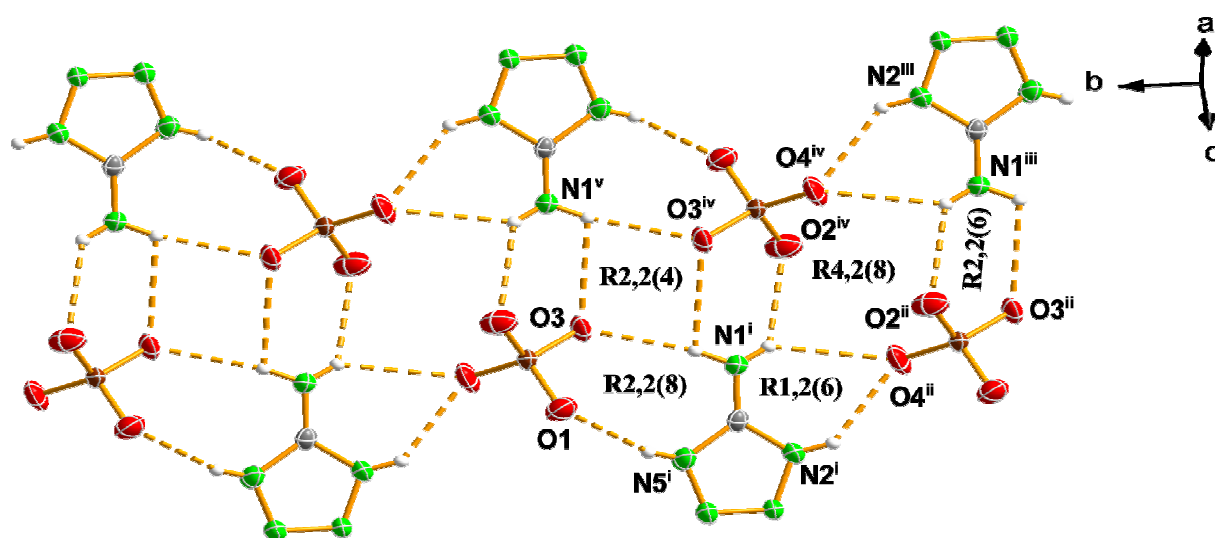


Figure 2.9 Ring graph-sets of interest in the crystal structure of **5**. Symmetry codes: (i) $1-x, -y, 1-z$; (ii) $x, -1+y, z$; (iii) $1+x, -1+y, z$; (iv) $2-x, -y, 1-z$; (v) $1+x, y, z$.

The presence of one molecule of neutral 5-At in the structure of **7** modifies the packing completely. Figure 2.8b shows a representation of the unit cell of the compound with the hydrogen-bonding. The perchlorate anions arrange along the *b*-axis forming smooth waves with large gaps between them ($\sim 6\text{--}11 \text{ \AA}$) occupied by tetrazolium cations and neutral tetrazole molecules. In contrast to **5** where the tetrazolium cations orient forming layers in the same direction, in **7** there exist planar layers of tetrazoles in one direction, which are interrupted by the above-mentioned waves of anions and the following layers of tetrazoles are approximately orthogonal to the first ones and are cut again by the anions so that the following layers are coplanar to the first ones, etc.

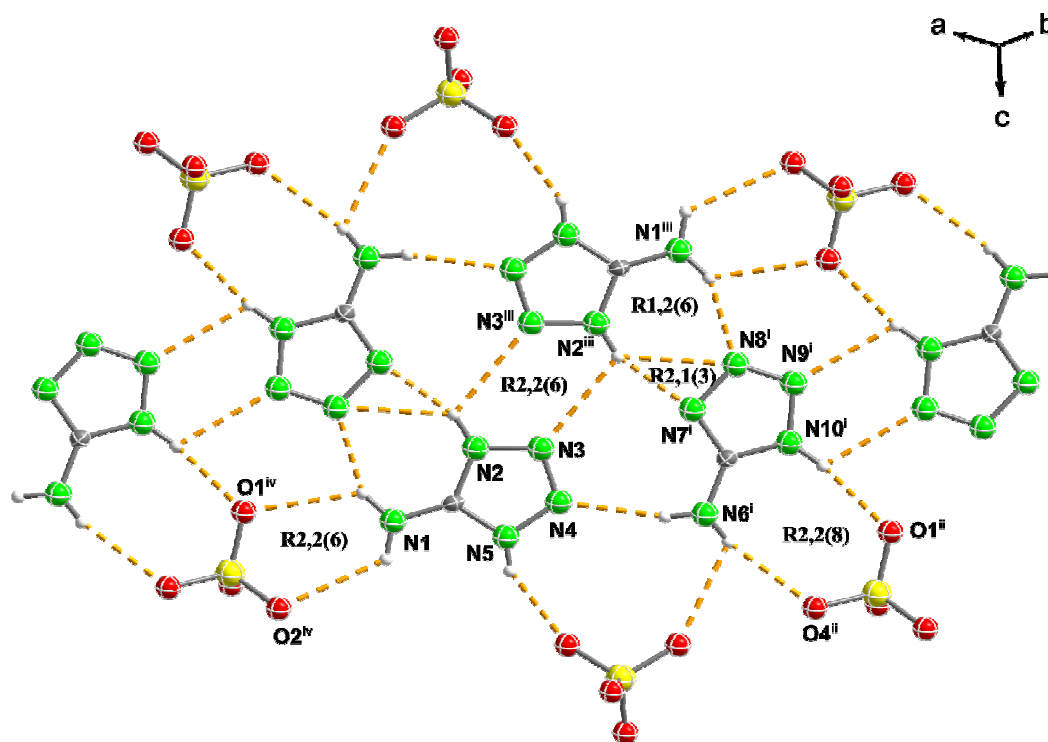
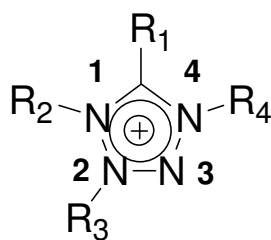


Figure 2.10 Ring graph-sets of interest in the crystal structure of **7**. Symmetry codes: (i) $-1+x, 1+y, z$; (ii) $-1+x, 1+y, z$; (iii) $1-x, 2-y, -z$; (iv) $1+x, y, z$.

Figure 2.10 shows a view of one of the layers of tetrazoles interrupted by lines of anions. The structure contains even more hydrogen bonds (14) than the perchlorate salt described above (**9**), which are at least as strong, however, the non formation of infinite layers as it is the case for **5** makes the compound to be less dense (1.874 g cm^{-3}). An interesting feature about the structure is (as mentioned before) that, in contrast to **5** where cations and anions alternate, here we find large spaces being occupied by the tetrazolium cations and 5-At molecules, which hydrogen-bond to each other and make the structure very stable, which is in turn reflected in the low sensitivity of the compound (see Energetic Discussion). The unitary hydrogen-bonding network is described by the usual **D1,1(2)** dimmeric interactions and an **R2,2(6)** motif formed by two cations, which are linked into dimmer pairs ($\text{N2} \cdots \text{N3}^{\text{ii}} = 3.074(2) \text{ \AA}$; symmetry code: (ii) $1-x, 2-y, -z$). At the secondary level, there are many finite patterns of the form **D1,2(3)**, **D2,1(3)**, **D2,2(X)** ($X = 5-7$), **D3,2(6)** and **D3,3(X)** ($X = 12, 18$), chain motifs with the descriptors **C2,1(4)** and **C2,2(X)** ($X = 6, 8$) and ring graph-sets of the type **R1,2(6)**, **R2,1(3)**, **R2,2(X)** ($X = 6-8$) and **R4,4(X)** ($X = 16, 18, 20$). The other type of **R2,2(6)** networks are described by the head-on interaction of the amino group protons of a cation with a perchlorate anion ($\text{N1} \cdots \text{O1}^{\text{iv}} = 3.129(2) \text{ \AA}$ and $\text{N1} \cdots \text{O2}^{\text{iv}} = 3.146(2) \text{ \AA}$; symmetry code: (iv) $1+x, y, z$) and are analogous to those found in the perchlorate salt discussed above. Lastly, it is also worth mentioning the formation of dimmer pairs, this time between one cation and one neutral tetrazole, which yield the formation of a

R2,1(3) ($N2 \cdots N7^i = 2.819(2)$ Å and $N2 \cdots N8^i = 3.073(2)$ Å; symmetry code: (i) 2-x, 1-y, -z) and an **R1,2(6)** graph-sets. The latter is also formed by the hydrogen bond between N2 and N8ⁱ (see above) and by the one between N1 and N8ⁱ ($N1 \cdots N8^i = 2.861(2)$ Å). Lastly, the same hydrogen bonds forming the two former graph-sets combine yielding a larger **R2,2(7)** motif.

Table 2.1 Selected bond and angle geometries for the 5-aminotetrazolium salts



Parameter	5	7 (5At ⁺)	7 (At)	15	17	19 (A)	19 (B)	20 (A)	20 (B)
R ₁ -C	1.301(5)	1.312(2)	1.342(2)	1.338(6)	1.329(4)	1.286(1)	1.273(1)	1.335(3)	1.333(3)
C-N1	1.333(5)	1.342(2)	1.328(2)	1.344(7)	1.338(4)	1.374(1)	1.358(1)	1.333(3)	1.338(3)
N1-N2	1.353(5)	1.363(2)	1.366(2)	1.360(5)	1.335(4)	1.371(1)	1.351(1)	1.361(3)	1.357(3)
N2-N3	1.266(1)	1.271(2)	1.283(2)	1.295(7)	1.293(4)	1.263(1)	1.282(1)	1.285(3)	1.280(3)
N3-N4	1.352(5)	1.357(2)	1.359(2)	1.356(6)	1.334(4)	1.362(1)	1.360(1)	1.374(3)	1.363(3)
N4-C	1.334(5)	1.341(2)	1.343(2)	1.332(7)	1.352(4)	1.354(1)	1.360(1)	1.335(3)	1.329(3)
N1-R ₂				1.452(9)		1.447(1)	1.452(1)	1.455(3)	1.449(3)
N2-R ₃					1.465(5)		1.457(1)		
N4-R ₄						1.462(1)			
R ₁ -C-N1	128.8(4)	127.9(1)	126.9(1)	124.1(4)	126.2(3)	126.6(1)	127.4(1)	125.7(2)	126.0(2)
C-N1-N2	110.9(4)	109.7(1)	105.4(1)	107.8(4)	102.7(2)	109.4(1)	111.5(1)	108.7(2)	108.3(2)
N1-N2-N3	107.6(3)	108.0(1)	111.9(1)	106.9(4)	114.1(3)	109.0(1)	107.7(2)	107.1(2)	107.0(2)
N2-N3-N4	107.8(3)	108.0(1)	105.6(1)	110.7(4)	106.0(3)	107.9(1)	108.0(1)	110.2(2)	110.6(2)
N4-C-R ₁	128.2(4)	128.0(1)	125.0(1)	106.1(4)	107.1(3)	111.2(1)	110.7(1)	126.3(2)	126.1(2)
N4-C-N1	103.0(3)	104.0(1)	107.9(1)	108.4(4)	110.2(2)	102.6(1)	102.1(1)	108.0(2)	107.9(2)
R ₂ -N1-C				130.2(5)		128.4(2)	130.5(2)	130.5(2)	130.9(2)
R ₂ -N1-N2				121.9(5)		122.2(2)	120.1(2)	120.6(2)	120.8(2)
R ₃ -N2-N1					123.2(3)				
R ₃ -N2-N3					122.7(3)				
R ₄ -N4-N3						127.2(1)	129.1(2)		
R ₄ -N4-C						121.6(1)	120.2(1)		

5: R₁ = NH₂, R₂ = R₄ = H; **7:** R₁ = NH₂, R₂ = H; **15:** R₁ = NH₂, R₂ = CH₃; **17:** R₁ = NH₂, R₃ = CH₃; **19:** R₁ = NH, R₂ = R₄ = CH₃; **20:** R₁ = NH₂, R₂ = CH₃.

15 crystallizes with half a molecule of crystal water in a monoclinic cell (space-group *C2/c*) with *Z* = 8. The coordination around the Ag⁺ atoms is depicted in Figure 2.11a and completed by short interactions in the range ~2.2-2.4 Å to each one of the non-substituted ring nitrogen atoms (N3, N4 and N5) and a longer contact to the water molecule at 2.577(4) Å (3+1). The distances and angles around the cation are summarized in Table 2.7 and agree with those of the rest of the silver salts in this and other studies.^[45]

Table 2.2 Hydrogen-bonding geometry in the 5-aminotetrazolium salts.

D–H...A	D–H (Å)	H...A (Å)	D...A (Å)	D–H...A (°)
5				
N2–H10...O4 ⁱ	0.75(3)	2.27(3)	2.882(3)	139(2)
N1–H7...O4 ⁱ	0.76(2)	2.41(2)	3.017(2)	137(3)
N1–H8...O3 ⁱⁱ	0.82(2)	2.64(2)	3.051(2)	112(2)
N1–H7...O2 ⁱⁱ	0.76(2)	2.47(2)	3.054(2)	135(2)
N1–H8...O3 ⁱⁱⁱ	0.82(3)	2.12(2)	2.931(3)	167(3)
N5–H9...O1 ⁱⁱⁱ	0.72(3)	2.24(2)	2.942(3)	161(3)
N2–H10...O2 ^{iv}	0.745(2)	2.60(3)	3.033(2)	118(2)
N2–H10...N4 ^v	0.75(2)	2.69(2)	3.068(3)	113(2)
N5–H9...N3 ^{vi}	0.72(2)	2.66(2)	3.039(2)	114(2)
7				
N1–H12...O3	0.89(2)	2.51(2)	3.128(2)	127(2)
N6–H61...O4	0.84(2)	2.33(2)	3.132(2)	158(2)
N10–H10...O1	0.89(2)	2.09(2)	2.973(2)	168(2)
N2–H2...N7 ⁱ	0.89(2)	1.97(2)	2.819(2)	159(2)
N2–H2...N8 ⁱ	0.89(2)	2.47(2)	3.073(2)	125(2)
N1–H11...N8 ⁱ	0.90(2)	2.04(2)	2.861(2)	150(2)
N2–H2...N3 ⁱⁱ	0.89(2)	2.64(2)	3.074(2)	111(1)
N10–H10...N9 ⁱⁱⁱ	0.89(2)	2.49(2)	2.949(2)	112(2)
N1–H12...O2 ^{iv}	0.89(2)	2.57(2)	3.146(2)	123(2)
N1–H11...O1 ^{iv}	0.90(2)	2.52(2)	3.129(2)	125(2)
N1–H12...O4 ^v	0.89(2)	2.35(2)	3.063(2)	136(2)
N6–H61...O3 ^{vi}	0.84(2)	2.55(2)	3.008(2)	115(2)
N6–H62...N4 ^{vii}	0.85(2)	2.25(2)	3.072(2)	162(2)
N5–H5...O2 ^{viii}	0.78(2)	2.10(2)	2.816(2)	151(2)
15				
N1–H1A...O3	0.90(6)	2.49(6)	3.360(7)	162(5)
O5–H5...O1	0.77(5)	2.43(6)	3.139(6)	154(6)
N1–H1B...O2 ^{iv}	0.94(6)	1.95(6)	2.871(7)	169(5)
N1–H1A...O2 ^v	0.90(6)	2.27(6)	3.011(7)	140(5)
17				
N1–H1A...O3 ⁱ	0.76(4)	2.23(4)	2.962(4)	161(4)
N1–H1B...O1 ⁱⁱⁱ	0.83(5)	2.32(5)	3.094(4)	157(5)
N1–H1B...O4 ⁱⁱⁱ	0.83(5)	2.62(5)	3.330(5)	145(5)
19				
N6–H7...O2	0.73(6)	2.38(6)	3.074(7)	161(7)
N6–H7...O1	0.73(6)	2.56(6)	3.026(6)	124(6)
N11–H4...O20 ⁱ	0.82(5)	2.37(5)	3.176(6)	168(5)
N11–H4...O10 ⁱ	0.82(5)	2.50(5)	2.995(6)	120(4)
N1–H9...O1 ⁱⁱ	0.74(5)	2.49(5)	3.191(6)	157(6)
N1–H9...O6 ⁱⁱ	0.74(5)	2.55(5)	3.050(7)	126(5)
20				
N1–H35B...N14	0.74(3)	2.54(3)	3.284(3)	174(2)
N6–H33A...N4	0.77(3)	2.69(3)	3.445(3)	166(3)
N11–H31A...N9	0.79(3)	2.61(3)	3.374(3)	163(2)
N1–H35A...O1 ⁱ	0.88(3)	2.22(3)	3.086(3)	166(2)
N1–H35A...O2 ⁱ	0.88(3)	2.49(3)	3.184(3)	136(2)
N6–H33B...O2 ⁱⁱ	0.86(3)	2.21(3)	3.064(3)	171(3)
N6–H33B...O3 ⁱⁱ	0.86(3)	2.53(3)	3.200(3)	135(2)
N11–H31B...O3 ⁱⁱⁱ	0.87(3)	2.20(3)	3.066(3)	172(2)
N11–H31B...O1 ⁱⁱⁱ	0.87(3)	2.57(3)	3.224(3)	132(2)

5: (i) 1-x, 1-y, 1-z; (ii) -1+x, y, z; (iii) 1-x, -y, 1-z; (iv) 2-x, 1-y, 1-z; (v) 1.5-x, 0.5+y, 0.5-z; (vi) 1.5-x, -0.5+y, 0.5-z. **7:** (i) 2-x, 1-y, -z; (ii) 1-x, 2-y, -z; (iii) 1-x, 1-y, -z; (iv) 1+x, y, z; (v) 1.5-x, 0.5+y, 0.5-z; (vi) 1.5-x, -0.5+y, 0.5-z; (vii) 1+x, -1+y, z; (viii) 0.5-x, 0.5+y, 0.5-z. **15:** (iv) 0.5-x, 1.5-y, -z; (v) 0.5+x, 1.5-y, 0.5+z. **17:** (i) 1-x, 0.5+y, 1.5-z; (iii) -x, 0.5+y, 1.5-z. **19:** (i) x, -1+y, z; (ii) 1-x, -y, 1-z. **20:** (i) 2-x, 1-y, 1-z; (ii) 1-x, 2-y, 1-z; (iii) 1-x, 1-y, 2-z.

Table 2.3 Graph-set matrix for selected hydrogen bonds in **15**. First level motifs on-diagonal and second level graph sets off-diagonal.

D–H...A	N1–H1A...O3	O5–H5...O1	N1–H1B...O2 ^{iv}	N1–H1A...O2 ^v
N1–H1A...O3	D1,1(2)			
O5–H5...O1	D2,2(5)	D1,1(2) [D2,2(5)]		
N1–H1B...O2 ^{iv}	R4,4(12)	D2,2(5)	D1,1(2)	
N1–H1A...O2 ^v	R2,1(4)	D2,2(5)	R2,4(8)	D1,1(2)

Symmetry codes for **15**: (iv) 0.5-x, 1.5-y, -z; (v) 0.5+x, 1.5-y, 0.5+z.

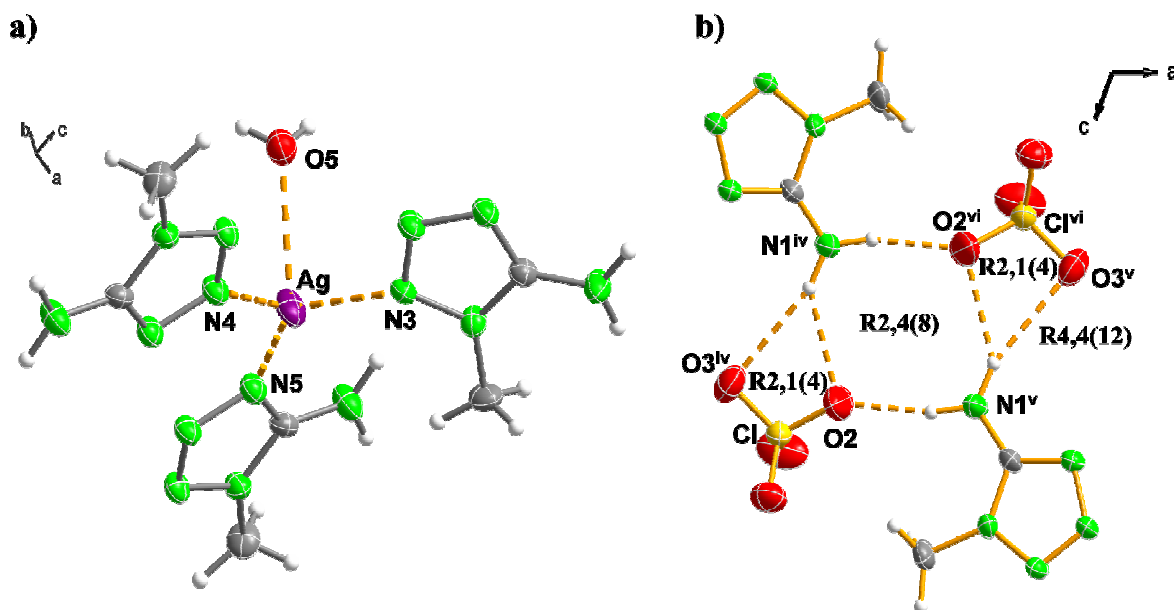


Figure 2.11 a) Full coordination around the Ag⁺ cations and b) Ring graph-sets of interest in the crystal structure of **15** (view along the *b*-axis). Symmetry codes: (iv) -0.5+x, 1.5-y, -0.5+z; (v) 0.5-x, 1.5-y, -z; (vi) -x, y, -0.5-z.

The role of the water molecules in the structure is crucial in determining the packing. Figure 2.12 shows the heteronorborane skeleton, which is the main building block of the structure. This is made out of two Ag⁺ atoms, two times two nitrogen atoms corresponding to two crystallographically related 1MAT ligands and the long-contact described above to O5 of a water molecule, which coordinate two contiguous cations. In addition, the third (non-substituted) nitrogen-atom in the tetrazole ring (N5) connect the heteronorborane units with the shortest contact found in the structure (Ag...N5 = 2.201(5) Å) forming infinite chains through the crystal along a direction, which is approximately parallel to the *c*-axis. The chains, which are positively charged due to the Ag⁺ atoms are separated from the perchlorate anions.

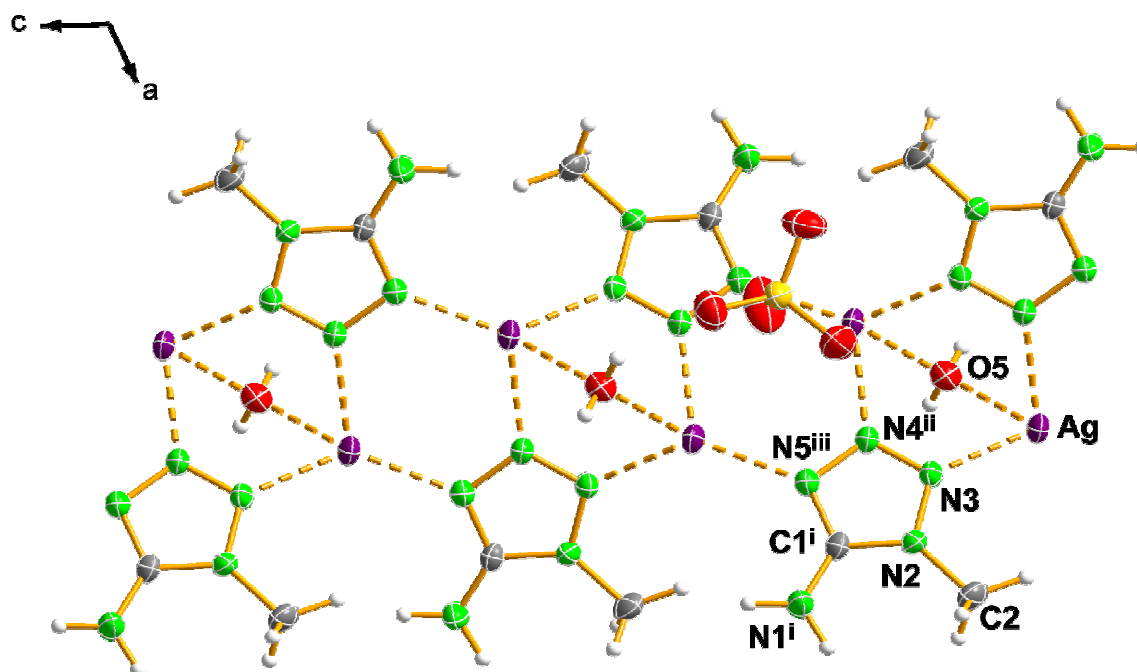


Figure 2.12 Heteronorborane skeleton formed by the coordination of the water molecules to the Ag^+ cations (dotted lines) in the crystal structure of **15** and labelling scheme (symmetry codes: (i) $x, 1-y, 0.5+z$; (ii) $-x, y, 0.5-z$; (iii) $x, 1-y, 0.5+z$).

In Figure 2.13 there is represented a view of a super cell in the crystal structure of **15** showing the loose (non-coordinating) perchlorate anions and a front-view of the structure skeleton along the c -axis with the norborane moieties crossing each other and sharing a common point placed at $\sim 3.7 \text{ \AA}$ of the water molecules. The computer program *RPLUTO*^[43] identifies the four hydrogen bonds summarized in Table 2.2 as forming a primary graph-set of the type $N_1 = \mathbf{D4DD}$, where one of the dimmeric units (**D**) is involved in the formation of a larger one with the label **D2,2(5)** (see Table 2.3). At the secondary level many other dimmeric **D2,2(5)** graph-sets are found together with ring motifs. Graph-sets of the type **R2,1(4)** are formed between one of the hydrogen atoms in the amino group and two oxygen atoms in the anion (Figure 2.11b) whereas the larger **R2,4(8)** and **R4,4(12)** motifs are formed by the interaction of two anions and two cations without including and including the chlorine atoms labelled as Cl and Cl^{vi} , respectively (symmetry code: (vi) $-x, y, -0.5-z$).

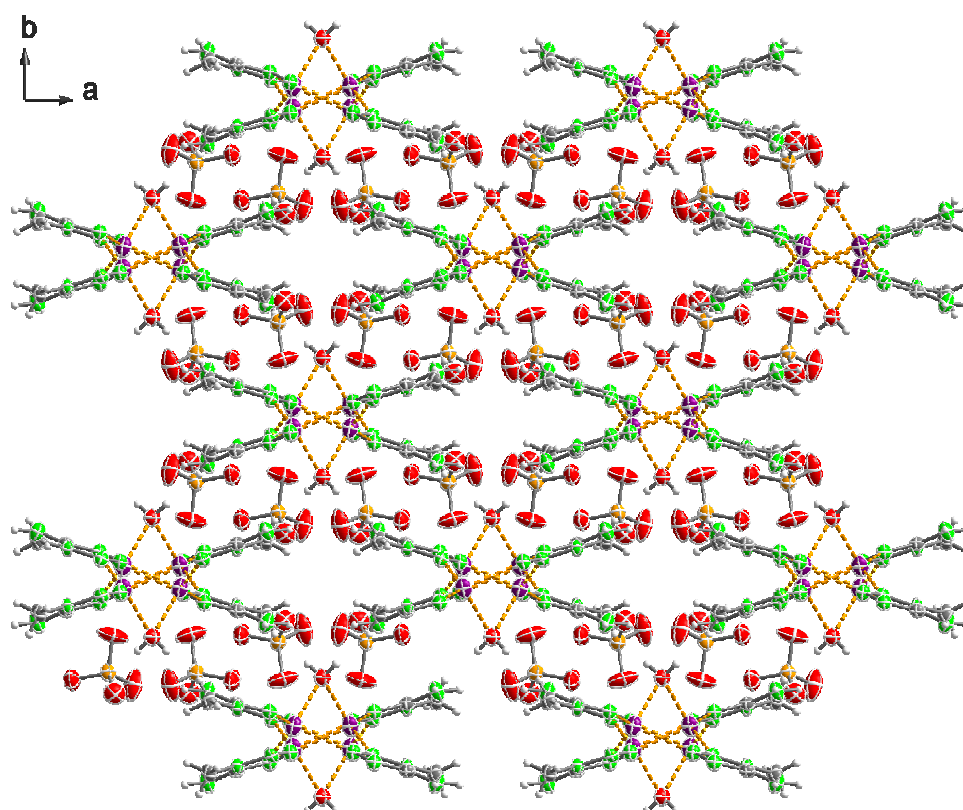


Figure 2.13 View of a supercell along the c -axis in the crystal structure of **15**.

Table 2.4 Graph-set matrix for selected hydrogen bonds in **17**. First level motifs on-diagonal and second level graph-sets off-diagonal.

D–H...A	N1–H1A...O3 ⁱ	N1–H1B...O1 ⁱⁱⁱ	N1–H1B...O4 ⁱⁱⁱ
N1–H1A...O3 ⁱ	D1,1(2)		
N1–H1B...O1 ⁱⁱⁱ	C2,2(6)	D1,1(2)	
N1–H1B...O4 ⁱⁱⁱ	C2,2(6)	R2,1(4)	D1,1(2)

Symmetry codes for **17**: (i) 1-x, 0.5+y, 1.5-z; (iii) -x, 0.5+y, 1.5-z.

Table 2.5 Graph-set matrix for selected hydrogen bonds in **19**. First level motifs on-diagonal and second level graph-sets off-diagonal.

D–H...A	A	B	C	D	E	F
N6–H7...O2 (A)	D1,1(2)					
N6–H7...O1 (B)	R2,1(6)	D1,1(2)				
N11–H4...O20 ⁱ (C)			D1,1(2)			
N11–H4...O10 ⁱ (D)	D2,2(7)	D1,2(3)		D1,1(2)		
N1–H9...O1 ⁱⁱ (E)			R2,1(6)		D1,1(2)	
N1–H9...O6 ⁱⁱ (F)	D2,2(9)	D2,2(7)		R2,1(6)		D1,1(2)

Symmetry codes for **19**: (i) x, -1+y, z; (ii) 1-x, -y, 1-z.

Figure 2.14a shows a view of the asymmetric unit of perchlorate **17**. This, in contrast to **15** crystallizes in the monoclinic space-group $P2_1/c$ with $Z = 4$ but with a very similar crystal density

($\sim 2.4 \text{ g cm}^{-3}$). The lack of crystal water influences the packing strongly. To start with, all atoms in the ligand are crystallographically independent, whereas there are two type of crystallographically related nitrogen atoms in the 1MAT ligand in **15**. More notorious is the type of coordination observed around the Ag^+ atoms (Figure 2.14b), which in this case can be described as 2+3 with $\angle \text{N2} \cdots \text{Ag} \cdots \text{N5}^{\text{ii}} = 159.6(1)^\circ$ (symmetry code: (ii) $1+x, y, z$) formed by two short contacts to tetrazole nitrogen atoms ($\text{Ag} \cdots \text{N} \sim 2.2 \text{ \AA}$) and three longer ones to perchlorate anions in the range $\sim 2.6\text{--}2.8 \text{ \AA}$ (see Table 2.7), whereas in **15** the Ag^+ cations and perchlorate anions were isolated from each other.

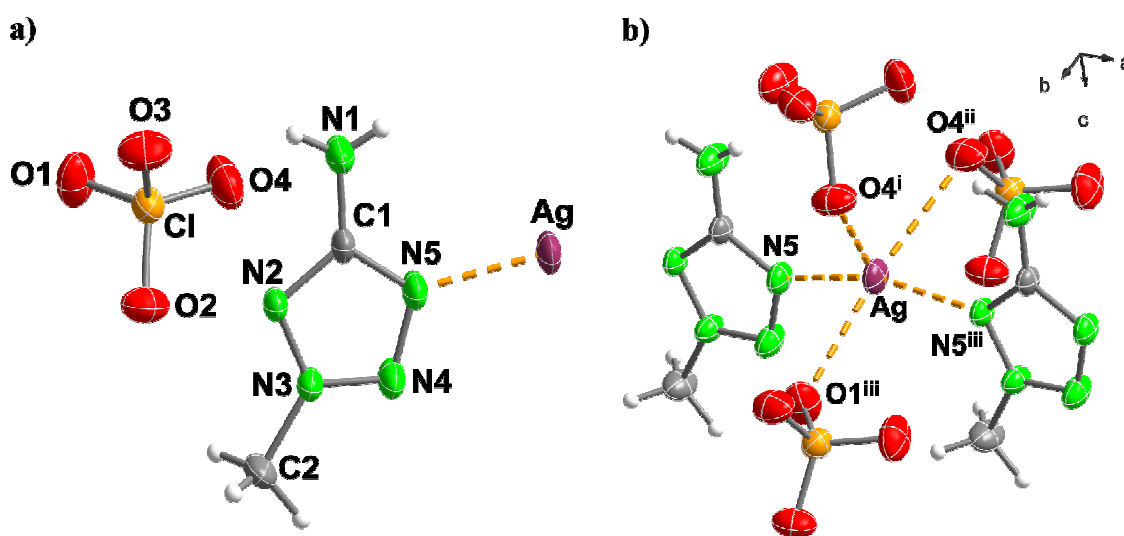


Figure 2.14 a) Asymmetric unit of **17** with the labelling scheme and b) Coordination around the Ag^+ cations in the crystal structure of **17** (symmetry codes: (i) $1-x, 0.5+y, 1.5-z$; (ii) $1+x, y, z$; (iii) $1+x, 1+y, z$).

A view of the unit cell in the structure of the compound is depicted in Figure 2.15, where the 2MAT ligands interact to Ag^+ cations forming infinite chains along the a -axis and the perchlorate anions intervene in the formation of inter-chain interactions to the cations. Lastly, the graph-set analysis of **17**, which only forms three hydrogen bonds is straight-forward. The three finite chains found at the primary level (Table 2.4), combine to form a **R2,1(4)** graph-set similar to that found in **15** and two **C2,2(6)** chain motifs.

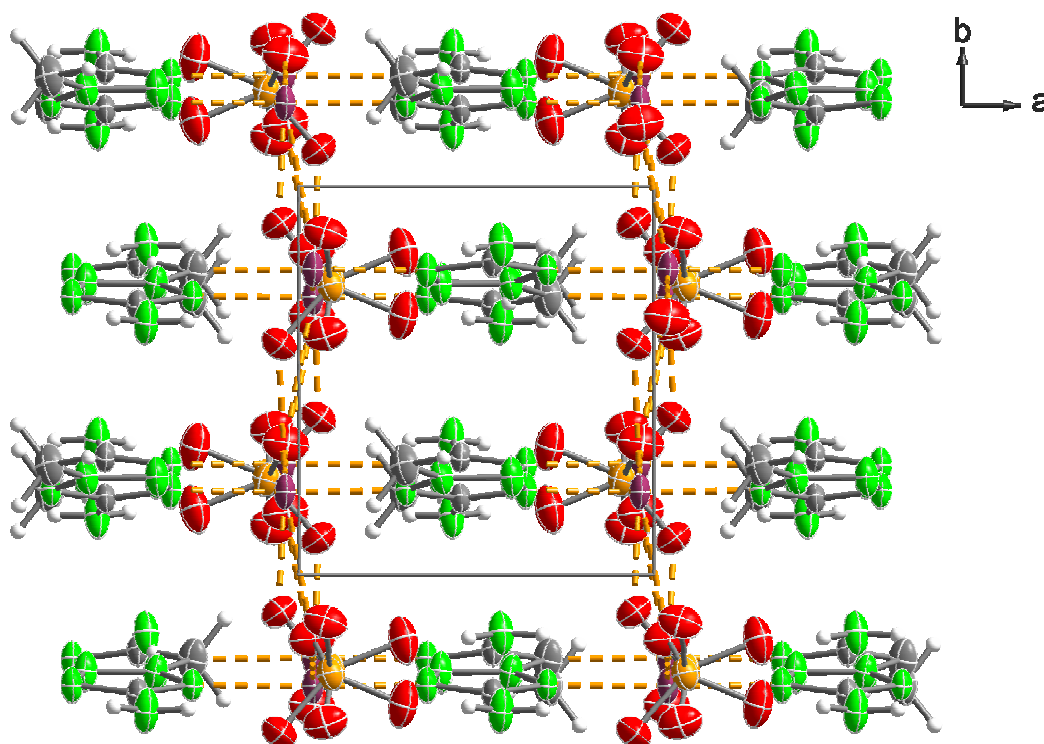


Figure 2.15 View of the unit cell along the c -axis showing the formation of chains along the a -axis in the crystal structure of **17**.

19 formed as yellow needle-like crystals in a triclinic cell (space group $P-1$), with the lowest calculated density of all compounds reported here (1.845 g cm^{-3}). Figure 2.16 shows a view of the asymmetric unit. There exists two types of crystallographically independent and non-interacting **19** moieties, both of which show the simple linear coordination expected for the Ag^+ cations, similarly to salts with the $[\text{Ag}(\text{NH}_3)_2]^+$ cation,^[45a] with $\angle \text{N} \cdots \text{Ag} \cdots \text{N}$ of $169.2(1)$ and $176.4(1)^\circ$ presenting a distorted linear geometry.

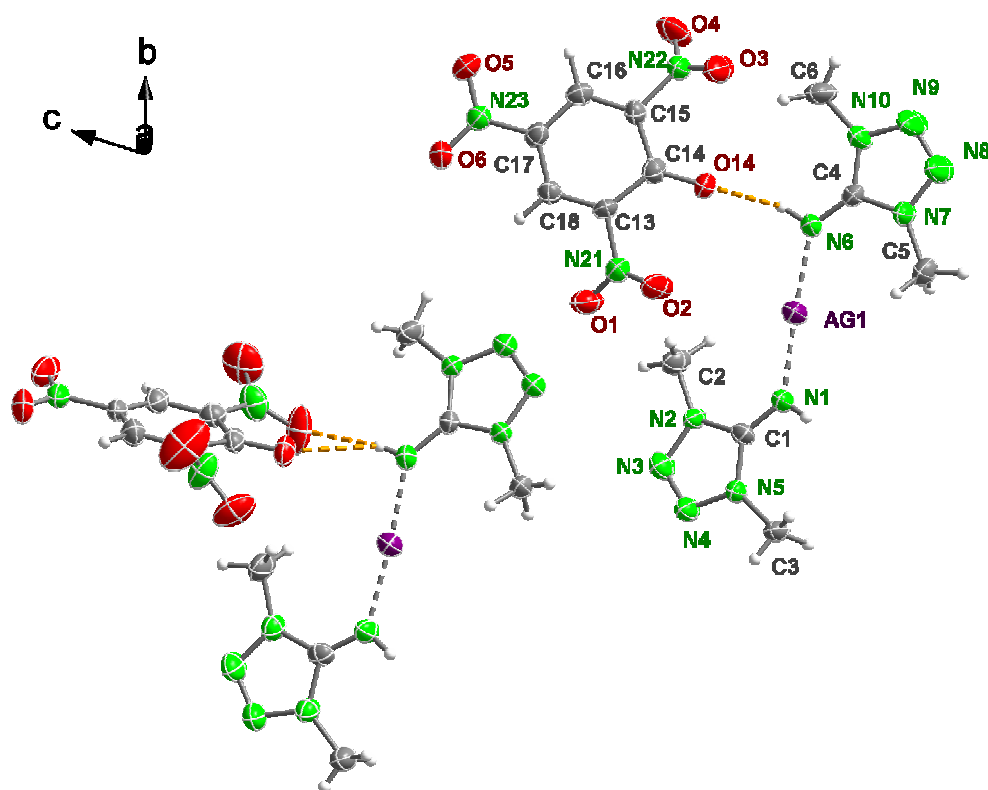


Figure 2.16 View of the asymmetric unit (ASU) of **19** with the labelling scheme showing the coordination to the Ag^+ cations and the hydrogen-bonding to the picrate anion. Only half of the ASU has been labelled for clarity reasons.

The imino-group hydrogen atoms interact with the picrate anions forming a total of three hydrogen bonds (see Table 2.2) with distances between donor (N) and acceptor (O) varying between ~ 3.0 and 3.2 \AA . In addition to classical hydrogen bonds, there exist strong non-classical interactions between C3 and O7 and O8 with distances of $3.263(2)$ and $3.282(2) \text{ \AA}$, respectively similar to the sum of the van der Waals radii ($r_{\text{C}} + r_{\text{O}} = 3.26 \text{ \AA}$),^[46] and as it is common for picrate salts (*Chapter V*). Figure 2.17 represents a view of the unit cell of the compound along the *a*-axis. The $\text{Ag}(\text{DMIT})_2^+$ moieties form interrupted chains approximately parallel to the *b*-axis interacting to anions (*via* the hydrogen bonds described above), which are placed at the vertices of the unit cell and in the center giving place to π -stacking. The formation of up to six different hydrogen bonds in the structure of the compound yields only finite chains at the unitary level (Table 2.5), as commented for the rest of the compounds. At the secondary level only some of them combine to form a small **D1,2(3)** and two larger **D2,2(X)** ($X = 7, 9$) graph-sets. Lastly, the formation of several **R2,1(6)** graph-sets by the interaction of the phenolate oxygen atom and one of the oxygen atoms belonging to a nitro-group at the *ortho* position with the imino-moiety (NH) is common for azolium picrates.^[47]

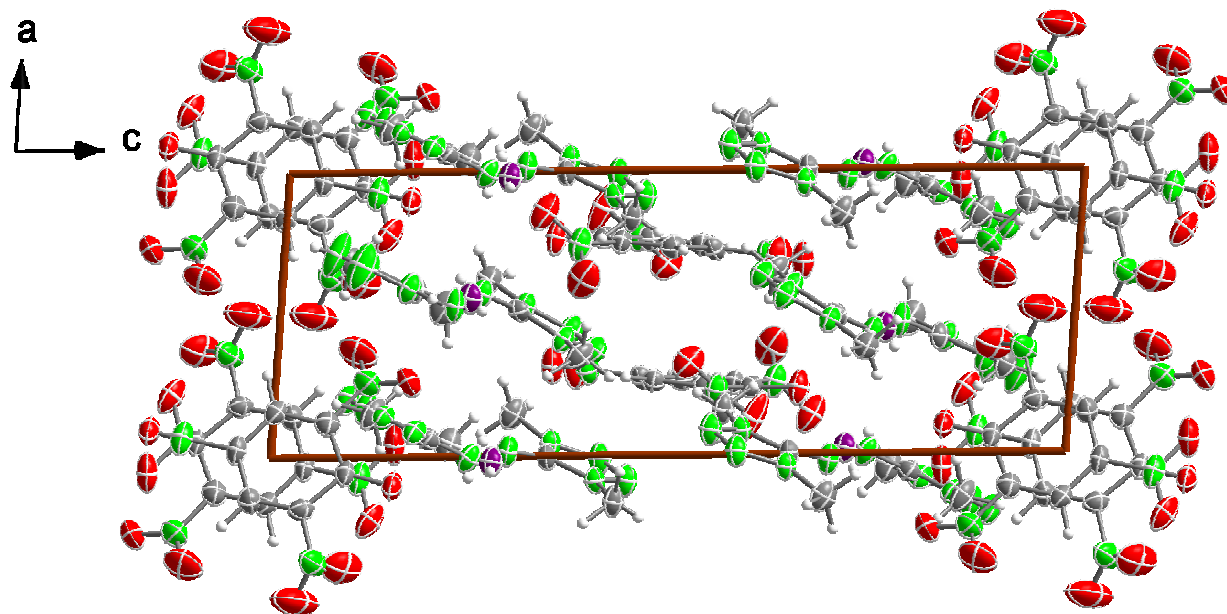


Figure 2.17 View of the unit cell of **19** along the *b*-axis showing the stacks of anions in this direction.

In contrast to the perchlorate salt **15** recrystallization of **16** from water results in rearrangement of the coordination sphere around the Ag^+ cations and more ligands as expected (i.e., three) are found. This results in a lower density in comparison to the other silver salts in this report (1.882 g cm^{-3}). As represented in Figure 2.18, the Ag^+ cations are surrounded by the three 1MAT ligands so that the coordination number in **20** is three forming an slightly distorted *T*-shape geometry. The coordination distances and angles are summarized in Table 2.7. All three distances are very similar ($\sim 2.2 \text{ \AA}$) and comparable to the Ag-N distances in the other complexes described here. On the other side, the angles vary little around the ideal 120° . The nitrate anions do not participate in the coordination but sit on a plane above and with a staggered configuration in respect to the coordination of the Ag^+ cations. The next oxygen atom in the anion is placed further away from the metal center than the sum of the van der Waals radii ($\text{Ag-O1} = 3.359(2) \text{ \AA}$).^[46]

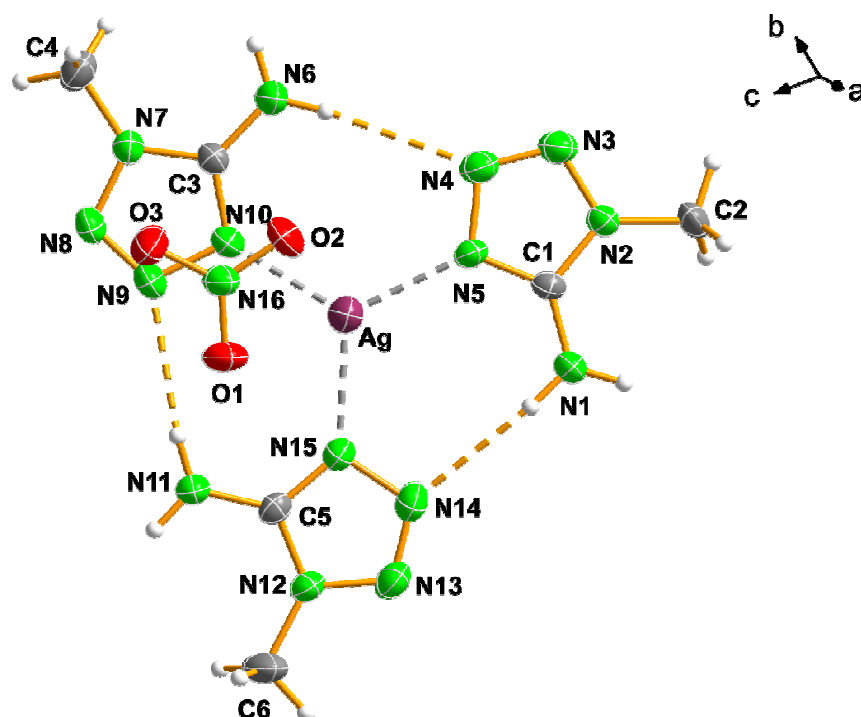


Figure 2.18 View of the asymmetric unit of **20** with the labeling scheme showing the coordination to the Ag^+ cations and the hydrogen-bonding between the 1MAT ligands.

Table 2.6 Graph-set matrix for selected hydrogen bonds of one of the three 1MAT ligands in **20**. First level motifs on-diagonal and second level graph-sets off-diagonal.

D–H...A	N1–H35B...N14	N1–H35A...O1 ⁱ	N1–H35A...O2 ⁱ
N1–H35B...N14	D1,1(2)		
N1–H35A...O1 ⁱ	D2,2(5)	D1,1(2)	
N1–H35A...O2 ⁱ	D1,2(3)	R2,1(4)	D1,1(2)

Symmetry code for **20**: (i) 2-x, 1-y, 1-z.

It is interesting to note that the planarity of all cation, anion and ligand (excepting the hydrogen atoms) results in the coordinating 1MAT ligands to sit on the same plane and these are in turn linked to each other by weak hydrogen bonds in the range 3.25-3.45 Å. This results in the formation of almost perfect layers along a direction, which cuts all (*a*, *b* and *c*) axes at an angle of ~45°. Figure 2.19 shows the hydrogen-bonding in one of these layers, where the $[\text{Ag}(\text{1MAT})_3]^+$ units described above are connected to each other over weak hydrogen bonds to nitrate anions in the range 3.05-3.25 Å. These hydrogen bonds describe several graph-sets of interest, which are identical for all three ligands and are summarized for one of them in Table 2.2. Apart from the usual dimeric interactions (**D1,1(2)**, **D1,2(3)** and **D2,2(5)**) summarized in Table 2.6, it is of note the formation of **R2,1(4)** hydrogen-bonding networks between the nitrogen atoms of the amino groups (donors) and the oxygen atoms in the anions (acceptors). We found this motif to be

common for other ionic compounds containing an $-\text{NO}_2$ moiety, such as dinitramide ($-\text{N}(\text{NO}_2)_2$) and other nitrate salts^[2a,44] as well as for the perchlorate salts (i.e., $-\text{ClO}_2$) described above.

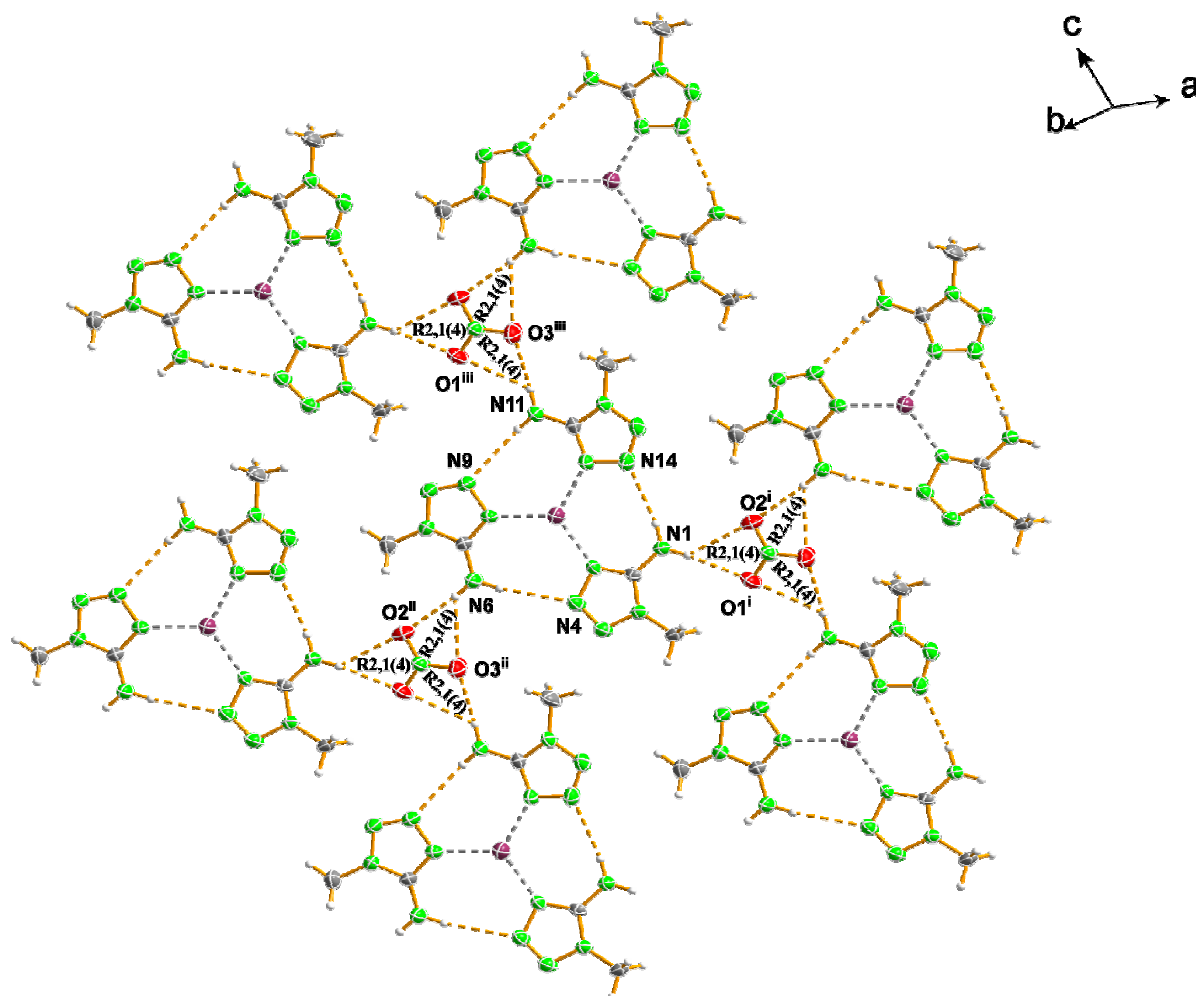


Figure 2.19 Hydrogen-bonding and coordination around the Ag^+ cations in a layer in the crystal structure of **20** (symmetry codes: (i) $2-x, 1-y, 1-z$; (ii) $1-x, 2-y, 1-z$; (iii) $1-x, 1-y, 2-z$).

Table 2.7 Selected coordination geometry around the Ag^+ cations in **15**, **17**, **19** and **20**. Distances in Å and angles in $^\circ$.

15			
Ag–N5	2.201(4)	Ag–N4	2.383(4)
Ag–N3	2.311(4)	Ag–O5	2.577(4)
17			
Ag–N2	2.171(3)	Ag–N5 ⁱⁱ	2.210(3)
Ag–O4 ⁱ	2.596(3)	Ag–O1 ⁱⁱⁱ	2.798(3)
Ag–O4 ⁱⁱ	2.816(3)		

...

...			
19			
Ag1–N1	2.088(4)	Ag2–N6	2.097(5)
Ag1–N16	2.092(5)	Ag2–N11	2.109(4)
20			
Ag–N5	2.186(2)	Ag–N15	2.201(2)
Ag–N10	2.184(2)		
15			
N5–Ag–N3	134.3(1)	N5–Ag–O5	122.8(1)
N5–Ag–N4	121.1(1)	N3–Ag–O5	87.3(1)
N3–Ag–N4	94.1(1)	N4–Ag–O5	82.5(1)
17			
N2–Ag–N5 ⁱⁱ	159.63(1)	N5 ⁱⁱ –Ag–O4 ⁱⁱ	81.3(1)
N2–Ag–O4 ⁱ	106.14(1)	N5 ⁱⁱ –Ag–O1 ⁱⁱⁱ	90.7(1)
N2–Ag–O4 ⁱⁱ	105.0(1)	O4 ⁱⁱ –Ag–O4 ⁱ	93.8(1)
N2–Ag–O1 ⁱⁱⁱ	83.1(1)	O4 ⁱⁱ –Ag–O1 ⁱⁱⁱ	171.8(1)
N5 ⁱⁱ –Ag–O4 ⁱ	92.55(1)	O1 ⁱⁱⁱ –Ag–O4 ⁱ	85.2(1)
19			
N1–Ag1–N16	176.4(2)	N6–Ag2–N11	169.3(2)
20			
N10–Ag–N5	122.1(1)	N5–Ag–N15	118.7(1)
N10–Ag–N15	118.8(1)		

Symmetry codes for **17**: (i) 1-x, 0.5+y, 1.5-z; (ii) 1+x, y, z; (iii) 1+x, 1+y, z.

2.5 Energetic Properties

In order to assess the energetic properties of all materials we experimentally determined the thermal stability (DSC measurement onsets), sensitivity to impact, friction,^[48-50] electrostatic discharge and thermal shock of each compound. The results of these studies are summarized in Table 2.8.

DSC studies on small samples of the energetic silver salts show excellent thermal stabilities above 225 °C. The 1MAT derivatives show additionally distinctive melting points (154 °C for **15** and 182 °C for **16**) and the loss of the half molecule of crystal water in **15** is shown as a broad endothermic peak at 102 °C, similar to the boiling point of water. **17** shows a small melting endotherm (286 °C) shortly before decomposing at 289 °C, whereas **18** decomposes without melting at 259 °C. The disilver salts **13** and **14** (see Figure 2.20) have surprisingly high thermal stabilities (higher than the rest of the compounds in this study) at 319 and 298 °C, respectively (also without melting), so that the trend in the decomposition points correlates well with the type of tetrazole ligand and increases in the order 1MAT < 2MAT < 5At. On the other side, the effect of replacing the two heavy silver atoms in **13** for two (lighter) protons in **5**, translates, as expected in a lower decomposition point (180 °C), this time accompanied by melting only short before decomposition at 176 °C and the formation of the adduct with 5-At (**7**) results in a compound with a similar thermal stability to that of **5** ($T_{\text{dec}} = 173$ °C). To sum things up, the replacement of

hydrogen atoms in compounds **5**, **6**, and **9-12** to form the corresponding silver salts (**13-18**) increases the melting and decomposition points considerably. Additionally, in the case of compounds that melt, perchlorate anion-based salts show larger liquid ranges and for all cases higher decomposition temperatures than the parent nitrate salts. Lastly, the decomposition (and melting) points are keeping in with known heterocycle-based salts^[2a,51] and comparable to the commonly used (but highly toxic) primary explosive lead diazide ($\text{Pb}(\text{N}_3)_2$).

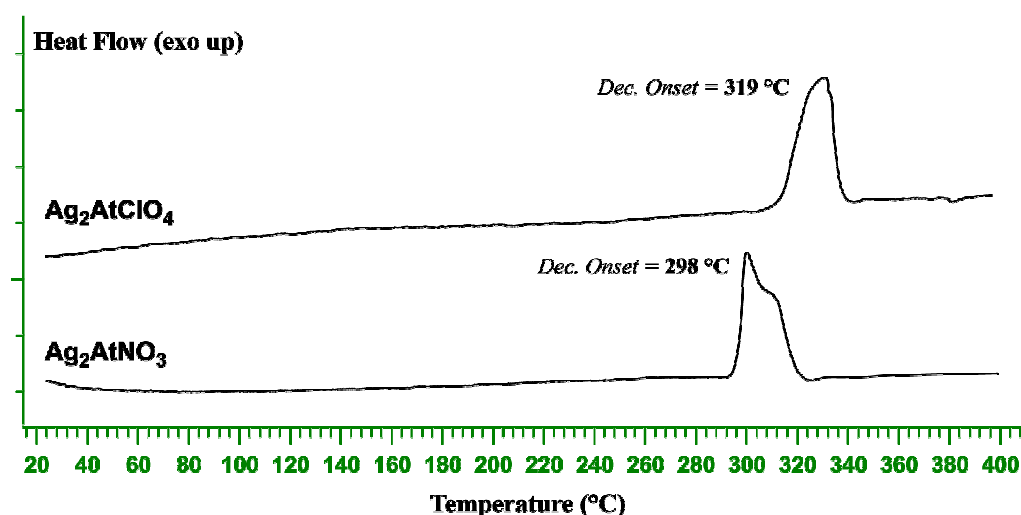


Figure 2.20 DSC thermograms for the disilver derivatives **13** and **14**.

In addition to DSC analysis, the response of each compound to fast thermal shock was tested by placing a small sample of the material in the flame. Again, a trend can be established between perchlorate and nitrate salts. In general, perchlorate salts are more sensitive to fast heating than the corresponding nitrates. For example, in this study there are four perchlorates (**5**, **9**, **11** and **13**), which explode in the flame, whereas the analogous nitrate salts (**6**, **10**, **12** and **14**) either burn or deflagrate. The effect of coordination to a nitrogen-rich ligand in **7**, is also reflected in a less vigorous reaction (deflagration) than **5**. In addition to this, the disilver salts (**13** and **14**) are more reactive (both explode) than the monosilver salts (**15-18**), which both deflagrate in the “flame test”.

Data collected for impact, friction and electrostatic discharge sensitivities are also summarized in Table 2.8. The trend in the sensitivity values obeys that found in the response to fast heating, i.e., the more sensitive the compound the more vigorously it reacts in the “flame test”. In general, the perchlorate salts are very sensitive towards both friction and impact. The only exception to this is the 5-At adduct (**7**), which is stabilized by extensive hydrogen-bonded networks between neutral 5-At and 5-AtH⁺ cations (see X-ray discussion), and shows lower sensitivity values (22 J and 260 N). **5** is a very (impact and friction) sensitive compound (1.5 J and 8 N) and introduction

of a methyl group to form **9** or **11** would be expected to translate into a lower sensitivity. However, it must be taken into consideration that there are many other factors that play a role in determining the sensitivity properties of energetic materials.

Table 2.8 Comparison of initial safety testing results for silver complexes and tetrazolium salts.

Compound [#]	Impact (J)	Friction (N)	ESD (+/-) ^a	T _m (°C) ^b	T _{dec} (°C) ^c	Thermal Shock
5	1.5	8	+	176	180	Explodes
6^d	>30	>360	-	none	173	Deflagrates
7	22	260	-	169	170	Deflagrates
9^e	3	10	+	125	245	Explodes
10^e	>30	>360	-	162	178	Burns
11	1	6	+	125	196	Explodes
12	>30	>360	-	123	161	Burns
13	2	<5	+	none	319	Explodes
14	15	18	+	none	298	Explodes
15	<5	120-360 ^f	-	102 (-H ₂ O), 154	252	Deflagrates
16	10	100-360 ^f	-	182	226	Deflagrates
17	2	<5	+	286	289	Deflagrates
18	20	100-360 ^f	-	none	259	Deflagrates

[#]**5, 6, 9-12, 15** (hemihydrate), **16** and **17** were tested as the crystalline compounds; **7, 13, 14** and **18** were tested as powders; ^aRough sensitivity to electrostatic discharge, + sensitive, - insensitive (using a Tesla coil); ^bmelting or temperature of water loss (**15**) and ^cdecomposition points (from DSC measurements); ^dFrom ref. [7]; ^eFrom ref. [2a]; ^fThe compounds decompose non-explosively in this range.

One factor, which plays a major role in determining the friction and shock sensitivity of a compound is its crystallinity and the shape of the crystals. All **5, 9** and **11** were tested as crystalline compounds, however, whereas **5** forms as very thin platelets, the other two compounds precipitate as large thick crystals. This would explain the unexpectedly high values of the two methylated perchlorate salts in comparison to these of **5**. Replacement of the two tetrazole ring protons in **5** for two silver cations in **13** results in a very insoluble compound (to many effects similar to silver azide), which has a similar impact sensitivity than the proton analogous, which is (regardless of being a powder) more sensitive to friction and explodes already at the minimum setting in the friction test (<5 N). The nitrate salts with ring protons are all insensitive towards shock and friction (>30 J and >360 N), however, the disilver salt (**14**) shows a much higher sensitivity to impact (15 J) similar to secondary explosives such as TNT (15 J) and to friction (18 N).^[52] As for the mono-silver 1MAT and 2MAT nitrate and perchlorate salts, the nitrate salts are impact sensitive compounds with values of 10 J (**16**) and 20 J (**18**), which decompose non-explosively above 100 N in the friction test. On the other side, the perchlorate salts are either sensitive to impact (**15**, <5 J) or very sensitive (**17**, 2 J). This is keeping in with the logic that

hydrated compounds, in this case **15**, tend to be less sensitive to stimuli than anhydrous materials, however, it is surprising that although both **15** and **17** were tested as the crystalline materials and have relatively high impact sensitivity values, in the friction tester **15** decomposes non-explosively in the range 120 to 360 N, whereas **17** already explodes at the lowest setting (<5 N), similarly to powdery **13**. Furthermore, the friction sensitivity values correlate well with the sensitivity towards electrostatic discharge and the very sensitive perchlorate salts **5**, **17** and **13** and the nitrate salt **14**, explode after initiation by the spark of a Tesla coil. Lastly, all results presented in this section are in agreement with previous studies in our group dealing with perchlorate and nitrate salts of tetrazoles (see also *Chapters IV* and *V*).^[11,2a,11c,44]

2.6 Conclusions

A new family of silver substituted tetrazoles with nitrate and perchlorate anions is presented here and compared with the parent proton substituted salts. **5** (**5**) is a very friction sensitive compound with an impact sensitivity higher than that of many primary explosives (e.g., lead diazide), however, we showed it can form a very stable energetic adduct with 5-At, which has decreased sensitivity values. This can be explained by the complex hydrogen-bonded networks between neutral 5-At molecules and 5-AtH⁺ cations found in the crystal structure. Many of the compounds presented here show interesting structural details. For example **15** forms as a hemihydrate and the crystal water tops the vertex of an unexpected heteronorborane-like structure formed by the coordination to the Ag⁺ cations. Lastly, most of the compounds described here have excellent thermal stabilities and can be initiated easily and regardless of the toxicity associated with the perchlorate anion and with silver to a lesser extend (table silverware), they provide a much more environmentally friendly alternative to primary explosives based on either mercury (e.g, mercury fulminate) or lead (e.g, lead azide or styphnate).

2.7 Experimental Section

Caution! *Although we experienced no difficulties with the compounds described here, some of them have sensitivity values, which classify them as primary explosives. Appropriate safety precautions should be taken and larger scale syntheses are not recommended. Laboratories and personnel should be properly grounded, and safety equipment such as Kevlar gloves, leather coats, face shields, and ear plugs are highly recommended.*

General. All chemical reagents and solvents were obtained from Sigma-Aldrich Fine Chemicals Inc. or from the chemical store at the LMU Munich and were used as supplied. 1-Methyl- and 2-methyl-5-amino-1H-tetrazole^[9c] and 1,4-dimethyl-5-amino-1H-tetrazolium iodide^[2a] were synthesized according to previously reported procedures. ¹H and ¹³C NMR spectra were recorded on a JEOL Eclipse 400 instrument in DMSO-*d*₆ at or near 25 °C. The chemical shifts are given relative to tetramethylsilane. Infrared (IR) spectra were recorded on a Perkin-Elmer Spectrum One FT-IR instrument^[53] as KBr pellets at 20 °C. Transmittance values are qualitatively described as “very strong” (vs), “strong” (s), “medium” (m) and “weak” (w). Raman spectra were recorded on a Perkin-Elmer Spectrum 2000R NIR FT-Raman instrument equipped with a Nd:YAG laser (1064 nm). The intensities are reported as percentages of the most intense peak and are given in parentheses. Elemental analyses were performed with a Netsch Simultaneous Thermal Analyzer STA 429. ICP analyses to determine the silver content were performed using an ICP-AES instrument (λ = 328.068). Melting points were determined by differential scanning calorimetry (Linseis DSC PT-10 instrument^[54] calibrated with standard pure indium and zinc). Measurements were in closed aluminum sample pans with a 1 μ m hole in the top for gas release under a nitrogen flow of 20 mL min⁻¹ with an empty identical aluminum sample pan as a reference.

Synthesis of 5-Amino-1H-tetrazolium Perchlorate (5). *Method A:* 5-Amino-1H-tetrazole monohydrate (0.153 g, 1.48 mmol) was suspended in 2 mL water and reacted carefully with a large excess of 70-72% concentrated perchloric acid (0.724 g, 5.05 mmol) to give a colorless solution. The reaction mixture was brought to boiling and refluxed for 5 min. The hot solution was then carefully transferred into a shell and left to stand. Large platelets of the compound suitable for X-ray analysis start to precipitate in the course of several weeks in excellent yield and purity (0.229 g, 83%).

Method B: Alternatively, 5-amino-1H-tetrazolium bromide monohydrate (0.184 g, 1.00 mmol) was reacted with anhydrous silver perchlorate (weighed out in a glove box) (0.207 g, 1.00 mmol) in 15 mL methanol for 2 h. Yellow silver bromide precipitated immediately and the solution (slightly yellow) was filtered and the solvent left to evaporate yielding either directly pure material or material which was pure after recrystallization by diffusing ether into a methanolic solution of the compound (0.155 g, 84%). CH₄N₅O₄Cl (185.53 g mol⁻¹, calc./found): C 6.47 / 6.43, H 2.17 / 2.27, N 37.75 / 37.55; DSC (2 °C min⁻¹, °C): 176 (m.p.), ~180 (dec.); ¹H NMR ([D₆]DMSO, 400.18 MHz, 25°C, TMS) δ /ppm: 9.70 (4H, s, NH/NH₂); ¹³C{¹H} NMR ([D₆]DMSO, 100.63 MHz, 25°C, TMS) δ /ppm: 154.7 (1C, C–NH₂); ¹⁵N NMR (DMSO-*d*₆, 40.55 MHz, 25°C, MeNO₂) δ /ppm: -27.0 (2N, N3/N4), -167.8 (2N, N2/N5), -325.1 (1N, t,

$^1J = 86.4$ Hz, NH_2); ^{35}Cl NMR ($[\text{D}_6]\text{DMSO}$, 39.21 MHz, 25°C, NaCl) δ/ppm : 1.0 (ClO_4); Raman $\tilde{\nu}$ / cm^{-1} (rel. int.): 3279(2) 1706(5) 1592(5) 1449(6) 1381(10) 1299(4) 1100(12) 1066(23) 940(100) 749(48) 629(25) 457(31) 416(27) 138(9); IR $\tilde{\nu}$ / cm^{-1} (KBr, rel. int.): 3348(s) 3186(s) 2076(w) 1701(vs) 1599(w) 1466(w) 1383(w) 1291(m) 1145(s) 1110(vs) 1088(vs) 1014(m) 995(m) 940(w) 869(w) 749(w) 710(m) 670(w) 636(m) 626(m) 540(w) 472(m) 412(w) 400(w) 313(w); m/z (FAB⁺, xenon, 6 keV, m-NBA matrix): 86.1 (100, $[\text{CH}_4\text{N}_5]^+$), 171.1 (35, $[(\text{CH}_3\text{N}_5)_2\text{H}]^+$), 256.0 (9, $[(\text{CH}_3\text{N}_5)_3\text{H}]^+$), 271.1 (5, $[(\text{CH}_3\text{N}_5)_2\text{H}_2\text{ClO}_4]^+$).

Synthesis of 5-Amino-1*H*-tetrazolium Perchlorate 5-Amino-1*H*-tetrazole (7): 5-Amino-1*H*-tetrazole monohydrate (0.165 g, 1.60 mmol) was suspended in 1 mL water and reacted carefully with a small excess of 70-72% concentrated perchloric acid (0.310 g, 2.16 mmol). The insoluble compound dissolved on careful short heating to reflux using a heat-gun giving a clear colorless solution, which was left to cool slowly overnight. Colorless single crystals of the adduct precipitated within 2-3 days (0.118 g, 55%). $\text{C}_2\text{H}_7\text{N}_5\text{O}_4\text{Cl}$ (270.60 g mol⁻¹, calc./found): C 8.88 / 8.54, H 2.61 / 2.65, N 51.76 / 49.69; DSC (2 °C min⁻¹, °C): ~170 (m.p. + dec.); ^1H NMR ($[\text{D}_6]\text{DMSO}$, 400.18 MHz, 25°C, TMS) δ/ppm : 8.04 (7H, s, NH/NH₂); $^{13}\text{C}\{^1\text{H}\}$ NMR ($[\text{D}_6]\text{DMSO}$, 100.63 MHz, 25°C, TMS) δ/ppm : 157.2 (1C, At-NH₂), 154.5 (1C, +HA₂-NH₂); ^{35}Cl NMR ($[\text{D}_6]\text{DMSO}$, 39.21 MHz, 25°C, NaCl) δ/ppm : 1.0 (ClO_4); Raman $\tilde{\nu}$ / cm^{-1} (rel. int.): 3117(3) 3066(3) 1704(4) 1652(7) 1575(9) 1409(17) 1382(27) 1313(6) 1144(13) 1066(74) 937(100) 750(54) 631(21) 457(26) 424(31) 174(31) 128(16); IR $\tilde{\nu}$ / cm^{-1} (KBr, rel. int.): 3420(s) 2976(m) 2378(m) 2346(m) 1701(m) 1650(m) 1452(w) 1384(w) 1298(w) 1121(m) 1087(m) 1047(m) 995(w) 878(w) 710(w) 636(w); m/z (FAB⁺, xenon, 6 keV, m-NBA matrix): 86.1 (100, $[\text{CH}_4\text{N}_5]^+$), 171.1 (63, $[(\text{CH}_3\text{N}_5)_2\text{H}]^+$), 256.0 (14, $[(\text{CH}_3\text{N}_5)_3\text{H}]^+$), 271.1 (7, $[(\text{CH}_3\text{N}_5)_2\text{H}_2\text{ClO}_4]^+$).

Synthesis of Disilver 5-Amino-1*H*-tetrazolium Perchlorate (13): 5-Amino-1*H*-tetrazolium monohydrate (0.196 g, 1.8 mmol) was dissolved in 4 mL concentrated perchloric acid and a solution of silver perchlorate (0.377 g, 1.8 mmol) in 1.5 mL water was added dropwise (cloudiness in the solution was observed as the addition proceeded). The clear solution was stirred for 30 minutes before adding 10 mL water. Immediate precipitation of a white (**highly sensitive!!**) powder was observed and the reaction mixture was stirred for further 15 minutes before filtering the solid by gravity. This was washed five times with water, one time with iso-propanol and one time with ether and left to air-dry overnight. The product was carefully weighed (0.522 g, 73%). $\text{CH}_2\text{N}_5\text{O}_4\text{ClAg}_2$ (399.25 g mol⁻¹, calc./found): C 3.02 / 2.88, H 0.51 / 0.72, N 17.65 / 17.90, Ag 53.89 / 53.70; DSC (5 °C min⁻¹, °C): 319 (dec.); Raman $\tilde{\nu}$ / cm^{-1} (rel. int.): 3332(8) 1637(10) 1562(36) 1464(22) 1437(11) 1403(8) 1281(55) 1256(28) 1235(24) 1150(57) 1125(86) 1102(59) 1026(23) 930(100) 769(40) 625(27) 464(38) 349(10) 166(28); IR $\tilde{\nu}$ / cm^{-1} (KBr, rel. int.): 3414(s) 3326(vs) 3228(m) 2285(w) 1617(s) 1557(s) 1542(s) 1458(m) 1439(w) 1384(w) 1268(w) 1143(s) 1113(vs) 1086(vs) 940(w) 920(w) 768(w) 742(w) 703(w) 636(m) 625(m) 573(w) 460(w) 430(w).

Synthesis of Disilver 5-Amino-1*H*-tetrazolium Nitrate (14): To a suspension of 5-amino-1*H*-tetrazolium monohydrate (0.503 g, 4.9 mmol) in 10 mL concentrated nitric acid was added dropwise a solution of silver nitrate (0.832 g, 4.9 mmol) in 3 mL water. The reaction mixture was stirred for 45

minutes and 10 mL water were added. After a few seconds cloudiness in the solution was observed and after 15 minutes a white powder precipitated, which was filtered off under gravity (**very sensitive compound!!**) and washed thoroughly with isopropanol and ether. The product was left to air-dry on a filter paper (1.423 g, 80%). $\text{CH}_2\text{N}_6\text{O}_3\text{Ag}_2$ (359.83 g mol⁻¹, calc./found): C 3.33 / 3.13, H 0.56 / 0.78, N 23.35 / 23.60, Ag 59.42 / 59.42; DSC (5 °C min⁻¹, °C): 298 (dec.); Raman $\tilde{\nu}$ / cm⁻¹ (rel. int.): 1623(9) 1543(8) 1389(6) 1295(28) 1164(13) 1109(53) 1040(100) 779(16) 710(7) 459(10) 184(25); IR $\tilde{\nu}$ / cm⁻¹ (KBr, rel. int.): 3416(s) 3326(s) 3227(m) 2396(w) 1762(w) 1620(m) 1541(m) 1454(m) 1434(m) 1384(vs) 1282(m) 1189(w) 1173(w) 1153(m) 1113(w) 1038(w) 1021(w) 833(w) 824(w) 816(w) 769(w) 747(w) 567(w) 461(w) 431(w).

Synthesis of Silver 1-Methyl-5-amino-1*H*-tetrazolium Perchlorate Hemihydrate (15): The perchlorate salt was synthesized in analogy to the nitrate derivative from 1-methyl-5-amino-1*H*-tetrazole (0.179 g, 1.8 mmol) in 3 mL concentrated perchloric acid by reaction with a solution of silver perchlorate (0.398 g, 1.9 mmol) in 3 mL water yielding a white powder of pure material (0.342 g, 63%). Recrystallization from hot water afforded single crystals of the compound in high yield. $\text{C}_2\text{H}_6\text{N}_5\text{O}_{4.5}\text{ClAg}$ (315.42 g mol⁻¹, calc./found): C 7.62 / 7.89, H 1.92 / 1.69, N 22.20 / 22.09, Ag 35.20 / 35.58; DSC (5 °C min⁻¹, °C): 102 (-H₂O), 154 (m.p.), 252 (dec.); m/z (FAB⁺, xenon, 6 keV, m-NBA matrix): 206.0 (8, [C₂H₄N₅Ag]) 208.0 (7, [C₂H₆N₅Ag]²⁺), 305.0 (10, [Ag(C₂H₅N₅)₂]⁺); ¹H NMR (DMSO-*d*₆, 400.18 MHz, 25°C, TMS) δ/ppm: 7.02 (2H, s, NH₂), 3.74 (3H, s, CH₃); ¹³C{¹H} NMR (DMSO-*d*₆, 100.63 MHz, 25°C, TMS) δ/ppm: 32.0 (CH₃), 155.6 (C-NH₂); ³⁵Cl NMR (DMSO-*d*₆, 400.18 MHz, 25 °C, NaCl) δ/ppm: +1.0 (ClO₄⁻); Raman $\tilde{\nu}$ / cm⁻¹ (rel. int.): 3014(8) 2956(26) 1658(13) 1595(9) 1499(12) 457(13) 1421(12) 1369(15) 1344(29) 1280(19) 1152(27) 1080(22) 929(89) 795(67) 684(21) 635(14) 622(18) 466(20) 449(20) 300(22) 248(13); IR $\tilde{\nu}$ / cm⁻¹ (KBr, rel. int.): 3326(s) 3155(vs) 2951(m) 2742(w) 1669(vs) 1596(s) 1485(m) 1454(w) 1428(w) 1384(w) 1322(m) 1280(w) 1237(w) 1144(s) 1120(s) 1088(s) 970(w) 940(w) 790(m) 742(w) 707(w) 680(m) 669(w) 636(m) 626(m) 544(m).

Synthesis of Silver 1-Methyl-5-amino-1*H*-tetrazolium Nitrate (16): 1-Methyl-5-amino-1*H*-tetrazole (0.198 g, 2.0 mmol) was solvated in 3 mL concentrated nitric acid and a solution of silver nitrate (0.368 g, 2.2 mmol) in 4 mL water was added causing some cloudiness in the solution. The mixture was stirred for 20 minutes and the formed precipitate was filtered under vacuum, washed with methanol, then with ether and dried under high vacuum yielding an insoluble white powder, which was pure as confirmed by elemental analysis (0.262 g, 48 %). $\text{C}_2\text{H}_5\text{N}_6\text{O}_3\text{Ag}$ (268.97 g mol⁻¹, calc./found): C 8.96 / 8.90, H 1.88 / 2.09, N 31.36 / 31.19, Ag 39.90 / 39.68; DSC (5 °C min⁻¹, °C): 182 (m.p.), 226 (dec.); m/z (FAB⁺, xenon, 6 keV, m-NBA matrix): 206.0 (3, [C₂H₄N₅Ag]) 208.0 (3, [C₂H₆N₅Ag]²⁺), 305.0 (5, [Ag(C₂H₅N₅)₂]⁺); ¹H NMR (DMSO-*d*₆, 400.18 MHz, 25°C, TMS) δ/ppm: 7.01 (2H, s, NH₂), 3.74 (3H, s, CH₃); ¹³C{¹H} NMR (DMSO-*d*₆, 100.63 MHz, 25°C, TMS) δ/ppm: 31.9 (CH₃), 155.7 (C-NH₂); ¹⁴N NMR (DMSO-*d*₆, 40.51 MHz, 25 °C, CH₃NO₂) δ/ppm: -4.3 (1N, NO₃⁻); Raman $\tilde{\nu}$ / cm⁻¹ (rel. int.): 2986(22) 2960(16) 2798(5) 1652(57) 1497(60) 1416(62) 1339(66) 1281(62) 1144(59) 1082(57) 1043(100) 989(42) 791(70) 680(39) 481(31) 304(30); IR $\tilde{\nu}$ / cm⁻¹ (KBr, rel. int.): 3402(m) 3323(s) 3265(m) 2948(w) 2192(m) 3157(s) 2950(w)

2426(w) 2345(w) 1767(w) 1747(w) 1667(s) 1648(s) 1595(s) 1494(m) 1384(vs) 1338(s) 1320(s) 1303(s) 1238(m) 1144(m) 1121(w) 1089(m) 1051(w) 1041(m) 984(w) 833(w) 825(w) 817(w) 788(m) 742(w) 736(w) 707(w) 679(m) 568(w) 483(w).

Synthesis of Silver 2-Methyl-5-amino-1H-tetrazolium Perchlorate (17): Anhydrous silver perchlorate (0.400 g, 1.9 mmol) (weighed in a glove-box) was dissolved in 3 mL water and added to a solution of 2-methyl-5-amino-1H-tetrazole (0.179 g, 1.8 mmol) in 2 mL 70% perchloric acid. After 15 minutes reaction time a white powder precipitated and the reaction mixture was shortly brought to reflux (not all solid dissolved). Single crystals of the title compound formed overnight upon cooling that were filtered, washed thoroughly with acetone and ether and left to air-dry (0.357 g, 65%). $C_2H_5N_5O_4ClAg$ (306.41 g mol⁻¹, calc./found): C 7.87 / 7.79, H 1.65 / 1.91, N 22.96 / 22.75, Cl 11.47 / 11.30, Ag 35.06 / 35.26; DSC (5 °C min⁻¹, °C): 286 (m.p.), 289 (dec.); m/z (FAB⁺, xenon, 6 keV, m-NBA matrix): 206.0 (6, [C₂H₄N₅Ag]) 208.0 (5, [C₂H₆N₅Ag]²⁺), 305.0 (7, [Ag(C₂H₅N₅)₂]⁺); ¹H NMR (DMSO-*d*₆, 400.18 MHz, 25°C, TMS) δ/ppm: 6.1 (2H, s, NH₂), 4.1 (3H, s, CH₃); ¹³C{¹H} NMR (DMSO-*d*₆, 100.63 MHz, 25°C, TMS) δ/ppm: 39.0 (CH₃), 166.9 (C-NH₂); ³⁵Cl NMR (DMSO-*d*₆, 400.18 MHz, 25 °C, NaCl) δ/ppm: +1.0 (ClO₄⁻); Raman $\tilde{\nu}$ / cm⁻¹ (rel. int.): 3246(20) 3223(20) 2962(69) 1647(24) 1578(25) 1444(27) 1378(31) 1196(28) 1169(20) 1119(38) 1036(30) 963(24) 926(100) 892(33) 812(22) 675(18) 649(47) 623(44) 594(21) 461(42) 429(22) 348(22) 250(19) 167(18) 150(20); IR $\tilde{\nu}$ / cm⁻¹ (KBr, rel. int.): 3386(s) 3309(s) 3220(m) 3073(w) 2960(w) 2676(w) 2021(w) 1688(m) 1635(s) 1584(w) 1554(s) 1452(m) 1422(w) 1409(m) 1377(w) 1326(w) 1292(w) 1205(m) 1145(vs) 1112(vs) 1089(vs) 941(w) 809(w) 757(w) 707(m) 684(w) 668(w) 649(m) 636(s) 626(s) 488(w).

Synthesis of Silver 2-Methyl-5-amino-1H-tetrazolium Nitrate (18): 2-Methyl-5-amino-1H-tetrazole (0.198 g, 2.0 mmol) was dissolved in 2 mL 65% nitric acid and a solution of silver nitrate (0.385 g, 2.3 mmol) in 3 mL water was added dropwise causing cloudiness in the solution. The cloudy solution was stirred for 15 minutes at room temperature causing precipitation of a white powder and it was shortly brought to reflux. Lastly, 3 mL water were added to the reaction mixture at room temperature and this was left to stand. The powder that precipitated overnight was filtered, washed thoroughly with acetone and ether and left to air-dry (0.333 g, 62%). $C_2H_5N_6O_3Ag$ (268.97 g mol⁻¹, calc./found): C 8.96 / 8.97, H 1.88 / 1.89, N 31.36 / 31.09, Ag 39.90 / 39.65; DSC (5 °C min⁻¹, °C): 259 (m.p. + dec.); m/z (FAB⁺, xenon, 6 keV, m-NBA matrix): 206.0 (3, [C₂H₄N₅Ag]) 208.0 (3, [C₂H₆N₅Ag]²⁺), 305.0 (4, [Ag(C₂H₅N₅)₂]⁺); ¹H NMR (DMSO-*d*₆, 400.18 MHz, 25°C, TMS) δ/ppm: 6.0 (2H, s, NH₂), 4.0 (3H, s, CH₃); ¹³C{¹H} NMR (DMSO-*d*₆, 100.63 MHz, 25°C, TMS) δ/ppm: 38.8 (CH₃), 166.9 (C-NH₂); ¹⁴N NMR (DMSO-*d*₆, 40.51 MHz, 25 °C, CH₃NO₂) δ/ppm: -4.1 (1N, NO₃⁻); Raman $\tilde{\nu}$ / cm⁻¹ (rel. int.): 3215(4) 3045(6) 2987(100) 2921(6) 1590(11) 1533(58) 1526(51) 1509(22) 1471(22) 1423(15) 1391(18) 1363(15) 1256(13) 1225(18) 1082(12) 1047(89) 1011(19) 941(8) 875(7) 824(8) 760(19) 718(11) 455(14) 439(9) 399(9) 359(13) 275(8) 241(11); IR $\tilde{\nu}$ / cm⁻¹ (KBr, rel. int.): 3395(s) 3034(m) 2957(w) 2426(w) 1921(w) 1842(w) 1762(w) 1636(m) 1554(m) 1484(vs) 1436(m) 1423(m) 1384(vs) 1324(vs) 1273(s) 1210(s) 1122(m) 1094(vs) 1054(s) 1036(s) 1011(s) 881(s) 839(w) 808(w) 776(s) 760(s) 748(m) 701(s) 674(m) 649(w) 468(w).

Synthesis of Bis-(1,4-dimethyl-5-iminotetrazole) Silver Picrate (19): Picric acid (0.229 g, 1.00 mmol) was dissolved in 5 mL methanol and reacted with neat potassium hydroxide (0.056 g, 1.00 mmol) producing the precipitation of a bright orange solid. The reaction mixture was stirred for 30 min. at room temperature and then reacted with a small excess of anhydrous silver perchlorate, weighed in a glove-box (0.249 g, 1.20 mmol). Immediate precipitation of brown (**highly sensitive!!**) silver picrate took place and the reaction mixture was stirred for further 1 h under the exclusion of light. After this time, the insoluble solid was filtered carefully and washed with water to eliminate the excess of AgClO_4 and with methanol. The methanol wet silver picrate was transferred carefully into a plastic beaker, suspended in 10 mL methanol and reacted with a solution of 1,4-dimethyl-5-aminotetrazolium iodide (0.193 g, 0.80 mmol) in 5 mL methanol with immediate precipitation of yellow silver iodide. The reaction mixture was stirred for 30 min under the exclusion of light and the silver iodide was filtered, washed with methanol and discarded. The filtrate was left to slowly evaporate yielding two types of yellow single crystals, namely, bright yellow prismatic single crystals, which were identified as 1,4-dimethyl-5-aminotetrazolium picrate and light yellow needle-like crystals, which were identified as the title compound. The crystals of **19** (formed as a by-product) were mechanically separated and analyzed (0.012 g, 5%). $\text{C}_{12}\text{H}_{16}\text{N}_{13}\text{O}_7\text{Ag}$ (562.21 g mol⁻¹, calc./found): C 25.63 / 25.77, H 2.87 / 2.94, N 32.39 / 32.25; m/z (FAB⁺, xenon, 6 keV, m-NBA matrix): 334.0 (12, $[\text{Ag}(\text{C}_3\text{H}_7\text{N}_5)_2]^+$); m/z (FAB⁻, xenon, 6 keV, m-NBA matrix): 228.0 (51, $[\text{C}_6\text{H}_2\text{N}_3\text{O}_7]^-$); ¹H NMR (DMSO-*d*₆, 400.18 MHz, 25°C, TMS) δ/ppm: 8.58 (2H, s, H-aromat), 3.74 (12H, s, CH₃), 3.36 (2H, br, NH); ¹³C{¹H} NMR (DMSO-*d*₆, 100.63 MHz, 25°C, TMS) δ/ppm: 160.9 (1C, C1), 149.9 (2C, C-NH), 141.8 (2C, C2), 125.2 (2C, C3), 124.4 (1C, C4), 33.0 (4C, CH₃); ¹⁴N NMR (DMSO-*d*₆, 40.55 MHz, 25 °C, MeNO₂) δ/ppm: -12 (3N, NO₂); Raman $\tilde{\nu}$ / cm⁻¹ (rel. int.): 3312(2) 3078(16) 2999(3) 2927(15) 1566(41) 1515(17) 1481(21) 1366(27) 1343(100) 1304(36) 1290(66) 1161(18) 1086(18) 940(21) 905(11) 823(31) 783(11) 700(14) 591(8) 337(20) 300(4) 169(14); IR $\tilde{\nu}$ / cm⁻¹ (KBr, rel. int.): 3320(s) 3070(m) 2922(m) 1645(vs) 1630(s) 1449(m) 1395(s) 1364(m) 1174(w) 1053(w) 1061(m) 1049(m) 1030(m) 975(w) 712(w) 690(w) 578(w).

2.8 References

- [1] a) H.-G. Ang, W. Fraenk, K. Karaghiosoff, T. M. Klapötke, H. Nöth, J. Sprott, M. Suter, M. Vogt, M. Warchhold, *Z. Anorg. Allg. Chem.* **2002**, 628, 2901–2906. b) K. Karaghiosoff, T. M. Klapötke, A. Michailovski, H. Nöth, M. Suter, *Propellants, Explos., Pyrotech.* **2003**, 28(1), 1–6. c) J. Geith, T. M. Klapötke, J. Weigand, G. Holl, *Propellants, Explos., Pyrotech.* **2004**, 29, 3–8. d) T. M. Klapötke, P. Mayer, A. Schulz, J. J. Weigand, *Propellants, Explos., Pyrotech.* **2004**, 29, 325–332. e) T. M. Klapötke, P. Mayer, J. J. Weigand, G. Holl, *Propellants, Explos., Pyrotech.* **2005**, 30(1), 17–26. f) T. M. Klapötke, P. Mayer, A. Schulz, J. J. Weigand, *J. Am. Chem. Soc.* **2005**, 127, 2032–2033. g) J. C. Gálvez-Ruiz, G. Holl, K. Karaghiosoff, T. M. Klapötke, K. Löhnwitz, P. Mayer, H. Nöth, K. Polborn, C. J. Rohbogner, M. Suter, J. J. Weigand, *Inorg. Chem.* **2005**, 44(12), 4237–4253. h) M. Friedrich, J. C. Gálvez-Ruiz, T. M. Klapötke, P. Mayer, B. Weber, J. J. Weigand, *Inorg. Chem.* **2005**, 44(22), 8044–8052. i) M. Göbel, T. M. Klapötke, *Z. Anorg. Allg. Chem.*, in press. j) T. M. Klapötke, C. Miró Sabaté, *Chem. Mater.*, **2008**, 20(11), 3629–3637. k) T. M. Klapötke, C. Miró Sabaté, *Z. Anorg. Allg. Chem.*, **2007**, 633, 2671–2677. l) C. Darwich, T. M. Klapötke, C. Miró Sabaté, *Chem. Eur. J.* **2008**, in press.
- [2] a) K. Karaghiosoff, T. M. Klapötke, P. Mayer, C. Miró Sabaté, A. Penger, J. M. Welch, *Inorg. Chem.* **2008**, 47, 1007–1019. b) A. Hammerl, G. Holl, T. M. Klapötke, P. Mayer, H. Nöth, H. Piotrowski, M. Warchhold, *Eur. J. Inorg. Chem.* **2002**, 4, 834–845. c) A. Hammerl, *Ph. D. Thesis*, Ludwig-Maximilians Universität München, **2001**. d) J. J. Weigand, *Ph. D. Thesis*, Ludwig-Maximilians Universität München, **2005**. e) J. M. Welch, *Ph. D. Thesis*, Ludwig-Maximilians Universität München, **2008**.
- [3] a) T. M. Klapötke, P. Mayer, C. Miró Sabaté, A. Penger, J. M. Welch, *233rd ACS National Meeting*, Chicago, IL, United States, 25–29 March, **2007**. b) T. M. Klapötke, C. Miró Sabaté, *New Trends in Research of Energetic Materials, Proceedings of the 10th Seminar*, Pardubice, Czech Republic, 25–27 April, **2007**. c) T. M. Klapötke, C. Miró Sabaté, *Chem. Mater.*, **2008**, 20(5), 1750–1763. d) H. Xue, Y. Gao, B. Twamley, J. M. Shreeve, *Inorg. Chem.* **2005**, 44(14), 5068–5072. e) T. M. Klapötke, K. Karaghiosoff, P. Mayer, A. Penger, J. M. Welch, *Propellants, Explos., Pyrotech.* **2006**, 31(3), 188–195. f) H. Xue, H. Gao, B. Twamley, J. M. Shreeve, *Chem. Mater.* **2007**, 19(7), 1731–1739. g) A. Hammerl, G. Holl, M. Kaiser, T. M. Klapötke, P. Mayer, H. Nöth, H. Piotrowski, M. Warchhold, *Eur. J. Inorg. Chem.* **2002**, 4, 834–845. h) A. Hammerl, G. Holl, T. M. Klapötke, P. Mayer, H. Nöth, H. Piotrowski, M. T. Suter, *Z. Naturforsch.* **2001**, B56(9), 857–870. i) A. Hammerl, T. M. Klapötke, H. Nöth, M. Warchhold, G. Holl, M. Kaiser, U. Ticmanis, *Inorg. Chem.* **2001**, 40(14), 3570–3575. j) K. A. Clark, T. M. Klapötke, *230th ACS National Meeting*, Washington, DC, United States, 28 Aug–1 Sept, **2005**.
- [4] V. A. Ostrovskii, M. S. Pevzner, T. P. Kofman, I. V. Tselinskii, *Targets Heterocycl. Syst.* **1999**, 3, 467.
- [5] R. C. West, S. M. Selby, *Handbook of Chemistry and Physics*, 48th ed.; The Chemical Rubber Co.; Cleveland, OH, 1967–1968; D22-D51.
- [6] a) S. V. Levchik, A. I. Balabanovich, O. A. Ivashkevich, A. I. Lesnikovich, P. N. Gaponik, L. Costa, *Thermochim. Acta* **1992**, 207, 115; b) S. V. Levchik, A. I. Balabanovich, O. A. Ivashkevich, A. I. Lesnikovich,

P. N. Gaponik, L. Costa, *Thermochim. Acta* **1993**, 255, 53; c) A. I. Lesnikovich, O. A. Ivashkevich, S. V. Levchik, A. I. Balabanovich, P. N. Gaponik, A. A. Kulak, *Thermochim. Acta* **2002**, 388, 233; d) A. Gao, Y. Oyumi, T. B. Brill, *Combust. Flame* **1991**, 83, 345; e) S. V. Levchik, A. I. Balabanovich, O. A. Ivashkevich, P. N. Gaponik, L. Costa, *Polym. Degrad. Stability* **1995**, 47, 333.

[7] M. von Denffer, T. M. Klapötke, G. Kramer, G. Spieß, J. M. Welch, G. Heeb *Propellants, Explos., Pyrotech.* **2005**, 30(3), 191–195.

[8] T. M. Klapötke, C. Miró Sabaté, J. Stierstorfer, *Z. Allg. Anorg. Chem.* **2008**, submitted.

[9] a) R. J. Spear, *Aust. J. Chem.*, **1984**, 37, 2453–2468. b) C. Stadler, J. Daub, J. Koehler, R. W. Saalfrank, V. Coropceanu, V. Schuenemann, C. Ober, A. X. Trautwein, S. F. Parker, M. Poyraz, T. Inomata, R. D. Cannon, *J. Chem. Soc., Dalton Trans.* **2001**, 22, 3373–3383. c) R. A. Henry, W. G. Finnegan, E. Lieber, *J. Am. Chem. Soc.*, **1954**, 76, 2894–2898.

[10] a) A. Hammerl, T. M. Klapötke, P. Mayer, J. J. Weigand, G. Holl, *Propellants, Explos., Pyrotech.* **2005**, 30(1), 17–26. b) J. Stierstorfer, T. M. Klapötke, A. Hammerl, R. D. Chapman, *Z. Anorg. Allg. Chem.*, **2008**, 634, 1051–1057.

[11] a) A. Hammerl, M. A. Hiskey, G. Holl, T. M. Klapötke, K. Polborn, J. Stierstorfer, J. J. Weigand, *Chem. Mater.* **2005**, 17(4), 3784–3793. b) T. M. Klapötke, P. Mayer, K. Polborn, J. M. Welch, *New Trends in Research of Energetic Materials, Proceedings of the 9th Seminar, Pardubice, Czech Republic*, Apr. 19–21 2006, 631–640. c) T. M. Klapötke, P. Mayer, C. Miró Sabaté, J. M. Welch, N. Wiegand, *Inorg. Chem.* **2008**, in press.

[12] a) G. Holl, J. J. Weigand, Ger. Offen. 20051006 (2005). b) A. Hammerl, G. Holl, M. Kaiser, T. M. Klapötke, H. Piotrowski, *Z. Anorg. Allg. Chem.* **2003**, 629(12–13), 2117–2121.

[13] L. Y. Lee, M. M. Stinecipher, U.S. 5256792 (1993).

[14] a) K. E. Gutowski, R. D. Rogers, D. A. Dixon, *J. Phys. Chem. B.* **2007**, 111(18), 4788–4800. b) T. Nakamura, M. Shoji, K. Okada, N. Mayama, A. Yoshikawa, Jpn. Kokai Tokkyo Koho, JP 2006073308 (2006). c) R. Wang, C. M. Jin, B. Twamley, J. M. Shreeve, *Inorg. Chem.* **2006**, 45, 6396–6403. d) A. Hammerl, G. Holl, M. Kaiser, T. M. Klapötke, P. Mayer, H. Piotrowski, M. Vogt, *Z. Naturforsch. B.* **2001**, 56(9), 847–856.

[15] a) M. Göbel, K. Karaghiosoff, T. M. Klapötke, C. Miró, J. M. Welch, *New Trends in Research of Energetic Materials, Proceedings of the 9th Seminar, Pardubice, Czech Republic*, Apr. 19–21 2006, 202–213. b) H. Xue, B. Twamley, J. M. Shreeve, *Eur. J. Inorg. Chem.* **2006**, 2959–2965. c) Y. Gao, H. Gao, C. Piekarski, J. M. Shreeve, *Eur. J. Inorg. Chem.* **2007**, 4965–4972.

[16] J. Charalambous, G. C. Georgious and K. Henrick, *Acta Crystallogr.*, **1987**, C43, 659–661.

[17] (a) C. Ye, J. C. Xiao, B. Twamley, J. M. Shreeve, *Chem. Commun.* **2005**, 21, 2750–2752. (b) R. Wang, H. Gao, C. Ye, B. Twamley, J. M. Shreeve, *Inorg. Chem.* **2007**, 46, 932–938. (d) Z. Zeng, H. Gao, B. Twamley, J. M. Shreeve, *J. Mater. Chem.* **2007**, 17, 3819–3826 (e) H. Gao, Z. Zeng, B. Twamley, J. M.

Shreeve, *Chem. Eur. J.* **2008**, *14*, 1282–1290 (f) Y. Huang, H. Gao, B. Twamley, J. M. Shreeve, *Inorg. Chem.* **2007**, 2025–2030.

[18] a) T. M. Klapötke, C. Miró Sabaté, J. M. Welch, *J. Chem. Soc. Dalton Trans.* **2008**, submitted. b) R. J. Spear, P. P. Elischer, *Austr. J. Chem.* **1982**, *35*(1), 1–13. c) X. C. Xhao, X. Heming, Y. Shulin, *Chem. Phys.* **1992**, *250*(3), 243–248. d) R. Hagel, U. Bley, Ger. Offen. DE 10221044 (2002). e) L. R. Bates, *13th Proceed. Symp. Explos. Pyrotech.* **1986**.

[19] a) A. V. Sachivko, V. P. Tverdokhlebov, I. V. Tselinskii, *Zh. Org. Khim.* **1986**, *22*(1), 206–211. b) M. H. V. Huynh, M. D. Coburn, T. J. Meyer, M. Wetzler *Proc. Natl. Acad. Sci. U. S. A.*, **2006**, *103*(27), 10322–10327.

[20] a) A. Y. Zhilin, M. A. Ilyushin, I. V. Tselinskii, A. S. Brykov, *Russ. J. Appl. Chem.* **2001**, *74*(1), 99–102. b) A. Y. Zhilin, M. A. Ilyushin, I. V. Tselinskii, *Khim. Fiz.* **2002**, *21*(8), 54–57.

[21] a) M. H. V. Huynh, M. A. Hiskey, T. J. Meyer, M. Wetzler, *Proceed. Nat. Acad. Sci. U. S. A.* **2006**, *103*(14), 5409–5412. b) M. A. Hiskey, M. H. V. Huynh, U.S. Pat. Appl. Publ. 030715 (2006). c) L. R. Bates, J. M. Jenkins, U.S. 4094879 (1978).

[22] W. H. Gilligan, M. J. Kamlet, U. S. NTIS, AD Rep. A036086 (1976).

[23] a) A. V. Smirnov, M. A. Ilyushin, I. V. Tselinskii, *Russ. J. Appl. Chem.* **2004**, *77*(5), 794–796. b) A. Y. Zhilin, M. A. Ilyushin, I. V. Tselinskii, A. S. Kozlov, I. S. Lisker, *Russ. J. Appl. Chem.* **2003** *76*(4), 572–576. c) A. Y. Zhilin, M. A. Ilyushin, I. V. Tselinskii, A. S. Kozlov, N. E. Kuzmina, *Russ. J. Appl. Chem.* **2002**, *75*(11), 1849–1851.

[24] a) L. G. Lavrenova, V. P. Karavai, S. V. Larionov, V. N. Ikorskii, L. A. Sheludyakova, *Zh. Neorgan. Khim.* **1988**, *33*(10), 2583–2586. b) P. N. Gaponik, S. V. Voitekhovich, A. S. Lyakhov, V. E. Matulis, O. A. Ivashkevich, M. Quesada, J. Reedijk, *Inorg. Chim. Acta* **2005**, *358*(8), 2549–2557.

[25] a) M. Murotani, H. Mura, M. Takeda, H. Shibafuchi, Eur. Pat. Appl. (1995). b) A. Jr. Katzakian, H. Cheung, C. E. Grix, D. C. McGehee, PCT Int. Appl. WO 9825868 (1998). c) S. Jin, Q. Song, *Hanneng Cailiao* **2003**, *11*(1), 55–56. d) A. Y. Zhilin, M. A. Ilyushin, I. V. Tselinskii, A. S. Brykov, *Russ. J. Appl. Chem.* **2001**, *74*(1), 96–99. e) M. Gabryszewski, *Pol. J. Chem.* **1993**, *67*(11), 2081–2084. f) J. R. J. Sorenson, *J. Med. Chem.* **1976**, *19*(1), 135–148. g) C. E. Vaughan, P. H. Wierenga, G. F. Holland, PCT Int. Appl. WO 2006138733 (2006). h) J. G. Zhang, T. L. Zhang, K. B. Yu, *Huaxue Xuebao* **2001**, *59*(1), 84–90. i) X. He, C. Z. Lu, D. Q. Yuan, *Inorg. Chem.* **2006**, *45*(15), 5760–5766.

[26] a) A. V. Smirnov, M. A. Ilyushin, I. V. Tselinsky, *Proceed. 3rd Autumn Sem. Propell. Explos. Pyrotech.* Chengdu, China, Oct. 5–8, 1999, 5–9. b) T. S. Konkova, Y. N. Matyushin, A. Vorobev, V. P. Sinditskii, M. D. Dutov, A. E. Fogelzang, *36th Int. Ann. Conf. ICT – Energ. Mater.* 2005, 93/1–93/13. c) T. S. Konkova, Y. N. Matyushin, A. B. Vorobev, V. P. Sinditskii, M. D. Dutov, *35th Int. Ann. Conf. ICT – Energ. Mater.* 2004 96/1–96/13. d) X. Zhou, Jpn. Kokai Tokyo Koho JP 2000297078 (2000).

- [27] a) V. N. Kizhnyaev, V. A. Kruglova, *Zh. Priklad. Khim.* **1992**, 65(8), 1879–1884. b) J. R. J. Sorenson, *J. Med. Chem.* **1976**, 19(1), 135–148.
- [28] a) V. Ernst, T. M. Klapötke, J. Stierstorfer, *Z. Anorg. Allg. Chem.* **2007**, 633, 879–887. b) T. M. Klapötke, H. Radies, J. Stierstorfer, *Z. Naturforsch.* **2007**, 62b, 1343–1352.
- [29] a) T. M. Klapötke, P. Mayer, K. Polborn, J. Stierstorfer, J. J. Weigand, *New Trends in Research of Energetic Materials, Proceedings of the 9th Seminar*, Pardubice, Czech Republic, 19–21 April, **2006**, 641–651. b) G. Geisberger, T. M. Klapötke, J. Stierstorfer, *Eur. J. Inorg. Chem.* **2007**, 4743–4750. c) T. M. Klapötke, P. Mayer, K. Polborn, J. Stierstorfer, J. J. Weigand, *New Trends in Research of Energetic Materials, Proceedings of the 10th Seminar*, Pardubice, Czech Republic, 19–21 April, **2006**.
- [30] C. T. Rittenhouse, US 3663553 (1972).
- [31] a) J. N. Maycock, V. R. P. Verneker, C. S. Jr. Gorzynski, *Spectrochim. Acta A* **1967**, 23(11), 2849–2853. b) S. Zeman, M. Dimun, S. Truchlik, V. Kabatova, *Thermochim. Acta* **1984**, 80(1), 137–141.
- [32] a) J. Duguet, US 4566921 (1986). b) A. Hammerl, G. Holl, T. M. Klapötke, P. Mayer, H. Nöth, H. Piotrowski, M. Warchhold, *Eur. J. Inorg. Chem.* **2002**, 4, 834–845. c) T. M. Klapötke, C. Miró Sabaté, *Chem. Mater.* **2008**, 20(5), 1750–1763.
- [33] a) K. Williamson, P. Li, J. P. Devlin, *J. Chem. Phys.* **1968**, 48, 3891–3896. b) J. R. Fernandes, S. Ganguly, C. N. R. Rao, *Spectrochim. Acta* **1979**, 35A, 1013–1020.
- [34] a) H. Cohn, *J. Chem. Soc.* **1952**, 4282 – 4284. b) O. Redlich, E. K. Holt, J. Biegeleisen, *J. Am. Chem. Soc.* **1944**, 55, 13–16.
- [35] N. B. Colthup, L. H. Daly, S. E. Wiberley, *Introduction to Infrared and Raman Spectroscopy*, Academic Press: Boston, **1990**.
- [36] G. A. Jeffrey, *An Introduction to Hydrogen Bonding*, Oxford Univ. Press: New York, **1997**.
- [37] A. Bigotto, R. Klingendath, *Spectrochim. Acta.* **1990**, 46A, 1683–1692.
- [38] S. V. Levchik, A. I. Balabanovich, O. A. Ivashkevich, A. I. Lesnikovich, P. N. Gaponik, L. Costa, *Thermochim. Acta.* **1993**, 225, 53–65.
- [39] Programs for Crystal Structure Analysis (Release 97-2). Sheldrick, G.M., Institut für Anorganische Chemie der Universität, Tammanstrasse 4, D-3400 Göttingen, Germany, **1998**.
- [40] A. Altomare, M. C. Burla, M. Camalli, G. L. Cascarano, C. Giacovazzo, A. Guagliardi, A. G. G. Moliterni, G. Polidori, R. Spagna, *J. Appl. Crystallogr.* **1999**, 32, 115–119.
- [41] D. D. Bray, J. G. White, *Acta Crystallogr.* **1979**, B35, 3089–3091.
- [42] J. Bernstein, R. E. Davis, L. Shimoni, N. Chang, *Angew. Chem. Int. Ed. Engl.* **1995**, 34(15), 1555–1573.
- [43] <http://www.ccdc.cam.ac.uk/support/documentation/rpluto/TOC.html>.

[44] T. M. Klapötke, C. Miró Sabaté, A. Penger, M. Rusan, J. M. Welch, **2008**, manuscript in preparation.

[45] a) S. L. Zheng, A. Volkov, C. L. Nygren, P. Coppens, *Chem. Eur. J.* **2007**, *13*(30), 8583–8590. b) A. P. Purdy, R. Gilardi, J. Luther, R. J. Butcher, *Polyhedron* **2007**, *26*(14), 3930–3938. c) M. L. Simms, J. L. Atwood, D. A. Zatko, *Chem. Commun.* **1973**, *2*, 46–47.

[46] N. Wiberg, *Holleman-Wiberg, Lehrbuch der Anorganischen Chemie*; Walther de Gruyter: Berlin, **2007**.

[47] a) C. Darwich, T. M. Klapötke, C. Miró Sabaté, *Propellants, Explos., Pyrotech.* **2007**, in press. b) T. M. Klapötke, C. Miró Sabaté, *Chem. Matter.* **2008**, manuscript in preparation. c) T. M. Klapötke, C. Miró Sabaté, *Z. Anorg. Allg. Chem.* **2008**, *634*, 1017–1024.

[48] Impact: Insensitive >40 J, less sensitive ≥ 35 J, sensitive ≥ 4 J, very sensitive ≤ 3 J; friction: Insensitive >360 N, less sensitive = 360 N, sensitive <360 N a. >80 N, very sensitive ≤ 80 N, extreme sensitive ≤ 10 N; According to the UN Recommendations on the Transport of Dangerous Goods (+) indicates: not safe for transport.

[49] <http://www.bam.de>.

[50] T. M. Klapötke, C. M. Rienäcker, *Propellants, Explos., Pyrotech.* **2001**, *26*, 43–47.

[51] a) H. Xue, Y. Gao, B. Twamley, J. M. Shreeve, *Inorg. Chem.* **2005**, *44*(14), 5068–5072. b) T. M. Klapötke, K. Karaghiosoff, P. Mayer, A. Penger, J. M. Welch, *Propellants, Explos., Pyrotech.* **2006**, *31*(3), 188–195. c) H. Xue, H. Gao, B. Twamley, J. M. Shreeve, *Chem. Mater.* **2007**, *19*(7), 1731–1739.

[52] J. Köhler, R. Meyer, *Explosivstoffe*, 9th ed.; Wiley-VCH: Weinheim, Germany, 1998.

[53] <http://www.perkinelmer.com>.

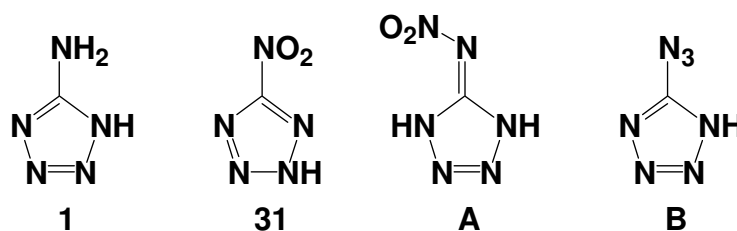
[54] http://www.linseis.net/html_en/thermal/dsc/dsc_pt10.php.

CHAPTER III

5-NITRO-2*H*-TETRAZOLE PRIMARIES

3.1 Introduction

The interesting energetic properties of tetrazole-based energetic materials have been mainly investigated in view of the properties of such compounds for use as propellants and/or secondary explosives^[1,2] and it has only been until recent times that metal salts with 5-substituted tetrazole ligands have been studied as prospective primary explosives.^[3,4] Primary explosives are energetic materials in which detonation is easily initiated by a physical or electrical stimulus. Typical detonation velocities for this class of compounds are in the range 3500-5500 m s⁻¹, much lower than those of secondary explosives (5500-9000 m s⁻¹).^[5] The detonation shockwave generated by a primary explosive is typically used to initiate a larger amount of a less sensitive explosive material (secondary explosive). Therefore, primary explosives are used in small quantities in a wide range of explosive applications. Lead azide and styphnate (often mixed with a variety of other energetic agents) are the most commonly used primary explosives. The harmful effects of lead on human health and the environment are well known and efforts are underway throughout the energetic materials community to develop new primary explosive materials and formulations free of toxic heavy metals and perchlorates. More extensive background information and details concerning some recent work in this area are presented in the introduction of reference [4] and in *Chapter I*.



Scheme 3.1 Formula structures of neutral 5-substituted tetrazoles: 5-amino-1*H*-tetrazole (**1**), 5-nitro-2*H*-tetrazole (**31**), 5-nitriminotetrazole (**A**) and 5-azido-1*H*-tetrazole (**B**).

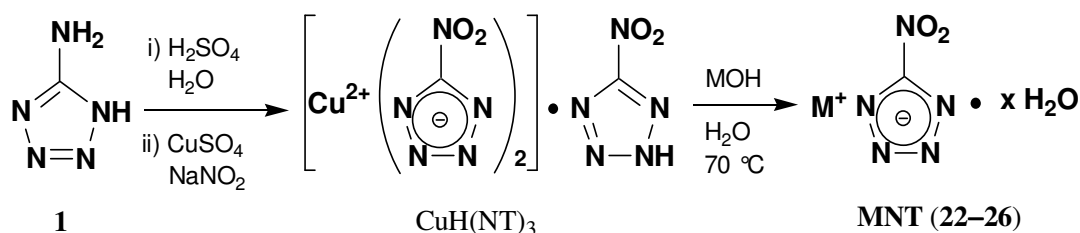
Hiskey and coworkers^[4] investigated several coordination (iron and copper) complexes of 5-nitrotetrazole (**31**, Scheme 3.1) as potential replacements for lead-based primaries. We have recently investigated some nitrogen rich salts of the same anion^[6] and were, in light of the promising properties of the transition metal complexes of **31**, interested to see if the simple s-

block (i.e., alkali and alkaline earth) metal salts might also show some desirable properties. In addition, many heterocycle-based salts of **31** have been investigated recently by several groups.^[7-12]

Sodium 5-nitrotetrazolate dihydrate was first synthesized by von Herz starting from 5-amino-1*H*-tetrazole (**1**) by treating the insoluble acid copper salt of 5-nitrotetrazole formed by the diazotation of 5-amino-(1*H*)-tetrazole in the presence of excess nitrite and copper in aqueous solution with excess sodium hydroxide.^[13] The sodium salt has subsequently served as the source of the 5-nitrotetrazole moiety in a large number of studies^[13-19] but has never been structurally characterized. In addition, although many heavy metal salts of 5-nitrotetrazole have been thoroughly investigated, none of the other alkali metal and the alkaline earth metal salts of 5-nitrotetrazole appear to have been particularly well investigated.^[14-16,19-23] Therefore, we decided to undertake the synthesis and full characterization (i.e., analytical, spectroscopic and energetic) of s-block metal salts of 5-nitrotetrazole as prospective environmentally-friendly replacements for service lead azide. In addition, we determined the crystal structure of the free acid **31** and evaluated its explosive properties.

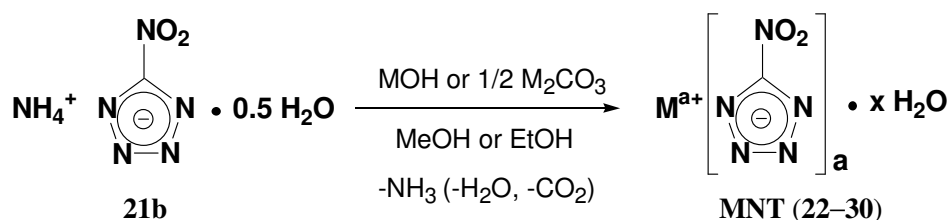
3.2 Synthesis

The alkali metal salts **22–26** were synthesized by two different methods both starting from commercially available 5-amino-1*H*-tetrazole (5-At, **1**). Initially, the sodium salt (**NaNT**, **23**) was synthesized by an improved literature procedure.^[24] 5-At was diazotated with *in situ* generated nitrous acid in the presence of copper(II) sulfate giving a slime of the highly sensitive turquoise copper salt (CuH(NT)₃). This needs to be isolated and washed thoroughly with diluted sulfuric acid in order to achieve maximum purity in the product. Digestion of the highly insoluble copper salt with sodium hydroxide yielded (after filtration of black copper(II) oxide) **23** as slightly green crystals (see 3.8 *Experimental Section*). This method (Method A) could be extrapolated in order to obtain the rest of the alkali metal salts in this study according to Scheme 3.2. **22** and **23** formed as the tri- and dihydrated species, respectively, whereas the rest of the alkali metal salts did not incorporate crystal water and are thus very sensitive materials (see section 3.5 *Energetic Properties*).



Scheme 3.2 Synthesis of alkali metal salts of 5-nitro-2*H*-tetrazole by Method A (M = Li (**22**, x = 3), Na (**23**, x = 2), K (**24**, x = 0), Rb (**25**, x = 0) and Cs (**26**, x = 0)).

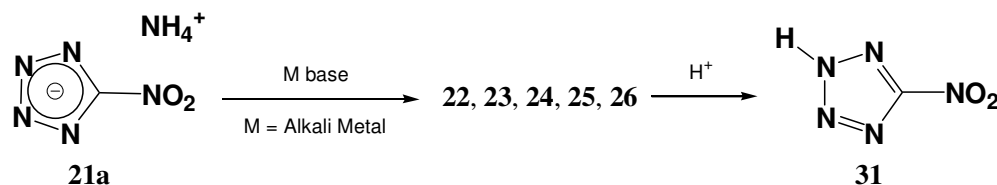
On the other side, in order to make the synthesis of the alkali metal salts more available for up-scaling an alternative procedure (Method B), which avoids having to isolate the highly sensitive copper(II) salt, was sought and ammonium 5-nitro-2*H*-tetrazolate hemihydrate (**ANTh**, **21b**) was deprotonated by a suitable metal hydroxide or carbonate in alcoholic or aqueous solution with concomitant formation of ammonia and/or carbon dioxide, yielding the desired NT salt (Scheme 3.3). This method presents a clear advantage to the one above in terms of safety in the following two points: (i) it does not require the isolation of any highly sensitive intermediate and (ii) the product has many times a greenish color (copper(II) impurities), which makes it extremely sensitive. In addition, this method is also suitable for the synthesis of the alkaline earth metal salts, which can not be prepared by Method A due to the highly insolubility of the alkaline earth metal hydroxides and/or carbonates. Compounds **27–30** are, in analogy to **22** and **23**, obtained as polyhydrates.



Scheme 3.3 Synthesis of alkali and alkaline earth metal salts of 5-nitro-2*H*-tetrazole by Method B (M = Li (**22**, a = 1, x = 3), Na (**23**, a = 1, x = 2), K (**24**, a = 1, x = 0), Rb (**25**, a = 1, x = 0), Cs (**26**, a = 1, x = 0), Mg (**27**, a = 2, x = 6), Ca (**28**, a = 2, x = 6), Sr (**29**, a = 2, x = 5) and Ba (**30**, a = 2, x = 5)).

In addition to having interesting energetic properties, the alkali metal salts of 5-nitro-2*H*-tetrazole (**31**) are also good intermediates for the synthesis of the free acid **31**. The procedure developed in this work starts off anhydrous ammonium 5-nitro-2*H*-tetrazolate (**21a**). Treatment with an equivalent amount of a suitable alkali metal salts base (hydroxide, carbonate or

bicarbonate) using water or alcohol as the solvent yields the intermediate alkali metal salt (**22–26**), which can be reprotonated using sulfuric or hydrochloric acid to form the free acid **31** (Scheme 3.4), which can in turn be extracted with ether. Care must be taken in the isolation process since the compound draws water on time, therefore all operations in air (e.g., determination of the sensitivity towards friction or shock) ought to be carried out quickly. Additionally, drying of the compound requires high-vacuum and due to the high sensitivity of the material (see section 3.5 *Energetic Properties*) special care must be taken when using (*Schlenk*) glass vessels.



Scheme 3.4 Synthesis of the free acid **5-NTH (31)** from **21a**.

Lastly, the alkali and alkaline earth metal salts of 5-nitro-2*H*-tetrazole (**31**) as well as **31** itself are readily soluble in common polar solvents such as water, alcohol, acetone or acetonitrile, soluble in hot THF and insoluble in apolar or less polar solvents such as pentane, ether, dichloromethane or chloroform.

3.3 NMR and Vibrational Spectroscopy

All metal salts of 5-nitro-2*H*-tetrazole (**31**) and **31** were characterized by their NMR (^1H , ^{13}C and ^{14}N) and vibrational (IR and Raman) spectra. In addition, the ^{15}N NMR spectra of the NT^- anion in compound **23** and of neutral **31** were also measured. The ^1H NMR spectra in $\text{DMSO}-d_6$ of the hydrated compounds **22** and **23** and the alkaline earth metal salts show a broad signal for the crystal water at $\delta \sim 3.5$ ppm, which is at high field in respect to the ring proton in neutral **31** ($\delta = 6.29$ ppm). The alkali metal salts **24**, **25** and **26** do not contain any hydrogen atoms and therefore we omitted the corresponding measurements. In the ^{13}C NMR the resonances for the ring carbon atoms are found at $\delta \sim 169$ ppm in the metal salts, similarly to the free acid **31** ($\delta = 168.4$ ppm) and are shifted to low field in respect to that of metal salts of 5-amino-1*H*-tetrazole^[25] and to high field compared to that of metal salts containing the 5,5'-azotetrazolate anion,^[26] keeping in with nitrogen-rich salts with the same anion.^[6] The high symmetry in the anion allows to distinguish the three expected ^{14}N NMR resonances. They are observed at $\delta \sim +20$ (N2, N3), -20 (NO_2) and -60 (N1, N4) ppm and are broad ($\nu_{1/2} \sim 420, 60$ and 400 Hz, respectively). As expected, the ^{15}N NMR resonances of **23** ($\delta = +14, -25$ and -66 ppm) are in agreement with those of the ^{14}N NMR

spectrum but much sharper. Figure 3.1 shows the ^{15}N NMR spectrum of the free acid **31**. The protonation induced shifts (PIS) are useful to identify the protonation site as well as to assign the resonances of the nitrogen atoms. Comparison of the resonances observed for the NT^+ anion in the sodium salt (**23**) with those of the free acid **31** shows notorious shifts. The nitrogen atoms labeled as N2 and N3 (see Figure 3.1 for labeling scheme), which are equivalent due to fast exchange in the NMR of **31** in solution, show the largest (positive) PIS values, indicative of protonation taking place on these two nitrogen atoms as observed (in the solid state) in the crystal structure of the compound (see X-ray discussion). The rest of the PIS are small in value and negative. Lastly, the fast exchange of the ring proton in **31** results in broadening of the resonance corresponding to the protonated nitrogen atom (N2/N3).

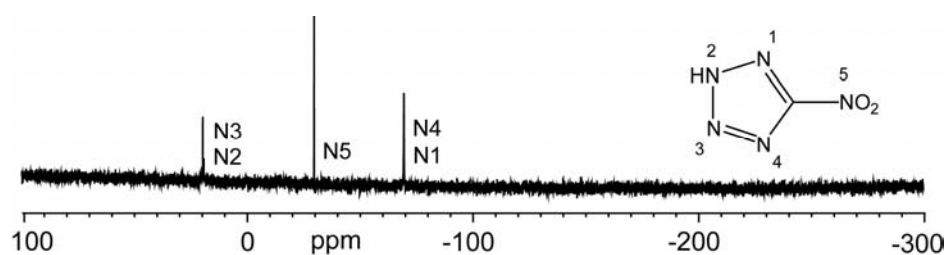


Figure 3.1 Proton decoupled ^{15}N NMR spectrum of the free acid **31** (in $\text{DMSO}-d_6$). δ (ppm): N1/N4 = -69.6 [-3.4], N2/N3 = 19.6 [5.2] and N5 = -29.8 [-4.5]; PIS in respect to **23** in [] brackets.

Table 3.A1 contains tabulated the most significant IR and Raman frequencies with the corresponding assignment by comparison with the calculated values.^[6] The IR and Raman spectra of the alkaline earth salts are shown in Figure 3.2 for illustration purposes. The Raman spectra of all metal salts of 5-nitro-2*H*-tetrazole are dominated by three bands at *ca.* 1420, 1060 and 1030 cm^{-1} corresponding to the coupled (in phase) NO_2 and N1–C–N4 stretching, N1–C–N4 deformation and NO_2 stretching and to the asymmetric ring deformation modes, respectively, observed as one strong and two medium bands at *ca.* 1420, 1050 and 1025 cm^{-1} in the IR spectra. In addition, the IR spectra are dominated by the nitro-group asymmetric stretching (~ 1540 cm^{-1}), nitro-group and N1–C–N4 (out of phase) symmetric stretching (~ 1320 cm^{-1}) and the nitro-group and N1–C–N4 (in phase) deformation (~ 840 cm^{-1}) modes.

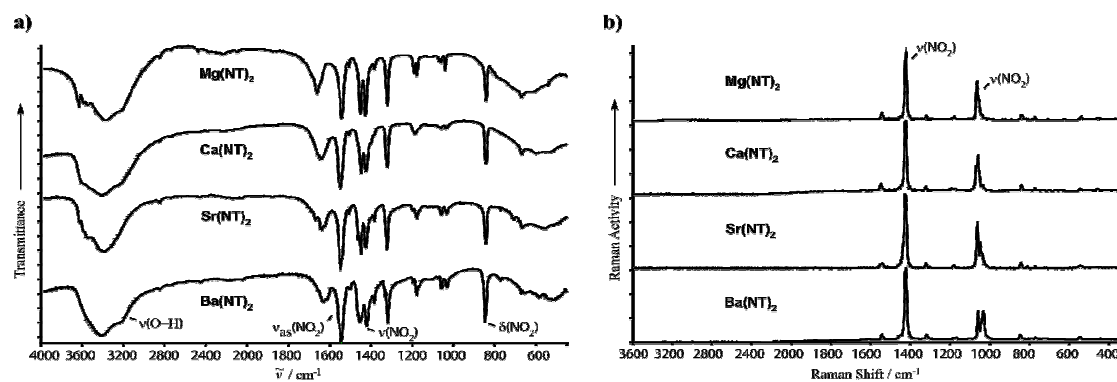


Figure 3.2 Panel plot of the IR (a) and Raman (b) spectra of alkaline earth metal salts of 5-nitro-2*H*-tetrazole (**31**).

3.4 Molecular Structures

Crystals of the metal salts were obtained as described in the *3.8 Experimental Section*. The X-ray crystallographic data for **23** and **24** were collected on an Enraf-Nonius Kappa CCD diffractometer. Data sets for the rest of the materials studied here were collected on an Oxford Diffraction Xcalibur 3 diffractometer equipped with a CCD detector. All data were collected using graphite-monochromated Mo K α radiation ($\lambda = 0.71073$ Å). All structures were solved by direct methods (SHELXS-97 and SIR97) and refined by means of full-matrix least-squares procedures using SHELXL-97.^[27] All non-hydrogen atoms were refined anisotropically. All hydrogen atoms were located from difference Fourier electron-density maps and refined isotropically. Crystallographic data and structure determination details are presented in *Appendix C*. Selected interatomic distances and angles are shown in Table 3.1 and the hydrogen-bonding geometries are summarized in Table 3.2. Additionally, the graph-set analysis results are to be found in *Appendix B* (Tables 3.B1, 3.B2 and 3.B3). Lastly, the coordination geometries around the metal center are tabulated in Tables 3.B4 to 3.B6.

Table 3.1 Selected interatomic distances and angles for metal salts of 5-nitro-2*H*-tetrazole (**31**).

Distances (Å)	22	23	24	25	26	28 (A)	28 (B)	31 (A)	31 (B)
O1–N5	1.229(1)	1.239(2)	1.224(2)	1.221(6)	1.225(3)	1.236(2)	1.214(2)	1.229(3)	1.227(3)
N5–O2	1.222(1)	1.215(2)	1.229(2)	1.234(6)	1.231(3)	1.218(2)	1.231(2)	1.221(3)	1.215(3)
N5–C	1.444(1)	1.439(2)	1.439(2)	1.453(9)	1.449(3)	1.440(2)	1.439(3)	1.440(4)	1.450(4)
C–N1	1.324(1)	1.324(2)	1.321(2)	1.334(8)	1.321(3)	1.317(2)	1.322(3)	1.319(4)	1.310(4)
C–N4	1.320(1)	1.326(2)	1.320(2)	1.323(9)	1.319(3)	1.322(2)	1.318(3)	1.323(4)	1.319(4)
N1–N2	1.342(1)	1.339(2)	1.338(2)	1.344(7)	1.343(3)	1.332(2)	1.339(2)	1.318(3)	1.322(3)
N2–N3	1.325(1)	1.324(2)	1.326(2)	1.353(9)	1.336(3)	1.331(2)	1.322(2)	1.324(4)	1.318(3)
N3–N4	1.345(1)	1.338(2)	1.333(2)	1.331(6)	1.345(4)	1.336(2)	1.337(2)	1.333(4)	1.336(4)

...

...									
Angles (°)	22	23	24	25	26	28 (A)	28 (B)	31 (A)	31 (B)
O1–N5–O2	125.3(1)	124.8(2)	124.5(1)	124.4(5)	123.9(2)	117.5(2)	116.1(2)	125.5(3)	126.0(3)
O1–N5–C	116.4(1)	116.5(2)	117.9(1)	119.0(5)	117.9(2)	124.5(2)	125.4(2)	117.9(3)	117.2(3)
O2–N5–C	118.2(1)	118.5(2)	117.6(1)	116.6(5)	118.1(2)	117.9(1)	118.3(2)	116.6(3)	116.7(3)
N4–C–N1	114.5(1)	114.5(2)	114.9(1)	115.4(6)	116.1(3)	115.0(2)	114.3(2)	114.5(3)	115.8(3)
N4–C–N5	122.5(1)	123.1(2)	122.5(1)	123.1(6)	121.7(2)	123.3(2)	121.9(2)	122.1(3)	121.9(3)
N1–C–N5	122.9(1)	122.3(2)	122.4(1)	121.4(6)	122.3(2)	121.6(2)	123.7(2)	123.2(3)	122.3(3)
N2–N3–N4	109.4(1)	109.8(1)	110.0(1)	109.2(5)	110.0(2)	109.8(1)	108.7(2)	105.7(2)	105.5(2)
C–N1–N2	103.0(1)	103.0(1)	102.8(1)	102.2(5)	102.5(2)	103.1(1)	102.6(2)	100.1(3)	99.0(3)
N3–N2–N1	109.6(1)	109.6(1)	109.3(1)	109.8(5)	109.3(2)	109.4(1)	110.3(2)	114.7(3)	115.4(3)
C–N4–N3	103.2(1)	102.9(1)	102.7(1)	103.4(5)	102.1(2)	102.5(1)	103.8(2)	105.0(2)	104.3(3)

23 is the only alkali metal salt of 5-nitro-2*H*-tetrazole that crystallizes in a triclinic cell (space group *P*–1), whereas the rest of the salts have monoclinic cells in a variety of space groups: *P*2₁/*c* (**22** and **24**), *C*1*c* (**25**) and *C*2*c* (**26**). Interestingly, the volume of the unit cell of the potassium salt (**24**) is smaller than that of the lithium salt (**22**), which is understandable due to the presence of three crystal water molecules in the structure of the latter, which makes the cell parameter *a* ~1.6 times larger than that of **24**, whereas *b* and *c* are only slightly longer for the potassium salt, as expected due to the larger radius of potassium in comparison to lithium. Interestingly, only the sodium and potassium salts (**23** and **24**) form one type of approximately planar layers, whereas for the remainder of the compounds there always exists two layers of anions along different directions. Lastly, the coordination numbers^[28] and contact distances around the metal cations are in agreement with previously published comparable compounds.^[25]

Table 3.2 Medium to strong hydrogen bonds in the crystal structures of compounds **22**, **23** and **28**.

D–H...A	D–H (Å)	H...A (Å)	D...A (Å)	D–H...A (°)
22 ^a				
O4–H1...N4	0.83(2)	1.98(2)	2.789(2)	165(1)
O5–H5...N3	0.83(2)	2.14(2)	2.905(1)	152(2)
O3–H3...N2 ⁱ	0.83(1)	2.08(2)	2.855(2)	155(2)
O5–H6...O3 ⁱ	0.92(1)	1.86(2)	2.748(2)	160(2)
O3–H4...O4 ^{iv}	0.84(2)	1.92(1)	2.761(2)	175(2)
O4–H2...O5 ^v	0.90(2)	1.87(1)	2.772(2)	178(2)
O5–H6...O1 ^{vi}	0.92(2)	2.59(2)	3.042(2)	111(2)
23 ^b				
O4–H1...O3	0.81(1)	2.02(1)	2.803(2)	165(4)
O4–H1...N4 ⁱⁱⁱ	0.82(1)	2.11(1)	2.930(2)	176(4)
O3–H1...N3 ^v	0.82(1)	2.07(1)	2.875(2)	167(4)
O3–H1...O4 ^{vi}	0.81(1)	2.15(3)	2.803(2)	138(4)

...

...

28 ^c				
O5–H61•••N7 ⁱ	0.84(4)	2.06(4)	2.888(3)	169(3)
O6–H61•••N4 ⁱⁱ	0.81(4)	2.06(4)	2.830(3)	157(3)
O6–H62•••N2 ⁱⁱⁱ	0.80(4)	1.98(4)	2.783(3)	178(4)
O5–H62•••N9	0.87(4)	2.10(4)	2.937(3)	163(3)
O5–H62•••N10	0.87(4)	2.67(4)	3.322(3)	133(3)
O7–H71•••N10	0.88(4)	1.92(4)	2.795(3)	170(3)
O7–H72•••N3 ⁱⁱ	0.81(4)	2.06(4)	2.860(3)	170(4)
O8–H81•••N8 ^{iv}	0.88(4)	1.97(4)	2.846(3)	178(4)
O8–H82•••O4	0.81(5)	2.45(4)	3.021(3)	128(3)
O8–H82•••O7 ^v	0.81(5)	2.49(4)	3.171(3)	142(4)
O9–H91•••N5 ^v	0.92(4)	2.04(4)	2.941(3)	167(3)
O9–H92•••O3	0.75(3)	2.21(3)	2.938(3)	162(3)
O20–H201•••N10 ^{vi}	0.82(4)	2.47(4)	3.295(3)	177(4)
O20–H202•••O6 ^{vi}	0.92(5)	1.90(5)	2.821(3)	176(4)
31 ^d				
N2–H1•••N4	0.97(4)	1.88(4)	2.837(4)	171.(3)
N7–H2•••O3 ⁱ	0.85(4)	2.22(4)	3.015(4)	158.(3)
N7–H2•••N3 ⁱⁱ	0.85(4)	2.53(4)	3.057(4)	121.(3)

Symmetry codes for **22**: (i) 2-x, -y, 1-z; (iv) x, 0.5-y, 0.5+y; (v) 2-x, -y, -z; (vi) 2-x, -0.5+y, 0.5-z; ^b**23**: (iii) 1-x, -y, 2-z; (v) x, y, -1+z; (vi) 1+x, y, z; ^c**28**: (i) -0.5+x, 1.5-y, 1+z; (ii) 1-x, 2-y, -0.5+z; (iii) -x, 2-y, -0.5+z; (iv) -0.5+x, 1.5-y, z; (v) -1+x, y, z; (vi) x, y, 1+z; ^d**31**: (i) -x, 0.5+y, -z; (ii) 1-x, 0.5+y, 1-z.

As suggested by the high similarity of the IR and Raman spectra of the metal salts (see discussion above), the 5-nitro-2*H*-tetrazolate anions are, within the limits of structure determination precision, nearly identical (Table 3.1). Furthermore, the anion has the same geometry as the one identified in previous structure determinations of 5-nitro-2*H*-tetrazolate anion-containing salts.^[6,9,22,23] The tetrazole ring bond lengths (~1.33 Å) are all very similar and comparable to other 5-substituted tetrazolate anions with electron-withdrawing substituents^[29] although slightly shorter than those of 5-substituted tetrazolate anions with electron donating substituents.^[25] In addition, the nitro-group, with torsion angles N1–C–N5–O2 between 2 and 5°, is essentially coplanar to the ring. A detailed description of the structures of the compounds follows below.

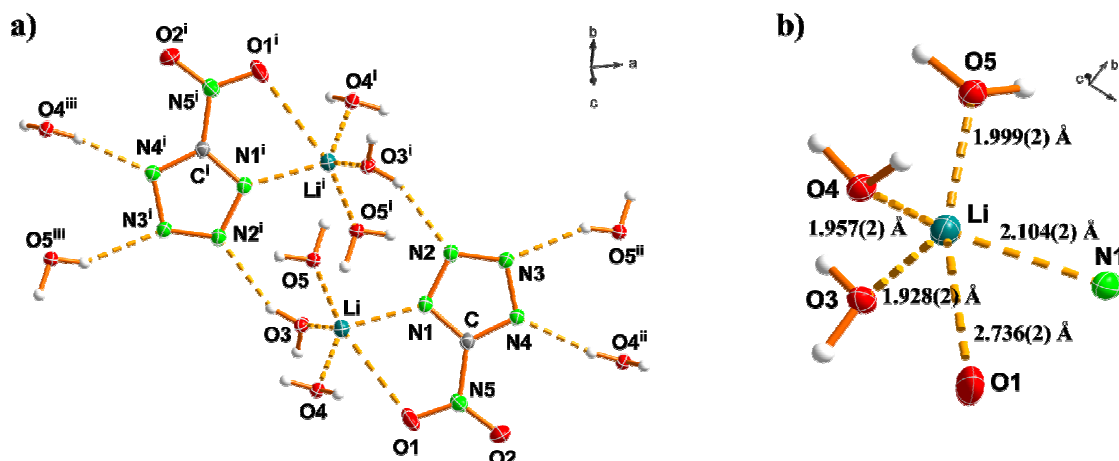


Figure 3.3 a) Full coordination around the Li⁺ cations and b) simplified coordination around the Li⁺ cations in the crystal structure of LiNT (**22**). Symmetry codes: (i) 2-*x*, -*y*, 1-*z*; (ii) -1+*x*, *y*, *z*; (iii) 3-*x*, -*y*, 1-*z*.

22 crystallizes with three water molecules in the asymmetric unit (Figure 3.3) with the lowest calculated density of all metal salts studied here ($\rho_{\text{calc}} = 1.608 \text{ g cm}^{-3}$). The coordination number around the lithium atoms is five forming a distorted square pyramid and is being completed by contacts with the three water molecules and to the anion, which chelates the metal center by using one of the oxygen atoms on the nitro-group and one of the tetrazole ring nitrogen atoms. Table 3.B4 shows the distances and angles of this pyramid. The distances at the base are *ca.* 2.0 Å (Li–O), except for the slightly longer Li–N contact (Li–N1 = 2.105(2) Å), whereas O1 from the nitro-group, found at the axial position, coordinates more loosely to the lithium cation at 2.736(2) Å. Every 5-nitro-2*H*-tetrazolate anion coordinates one single lithium atom (by using O1 and N1). The rest of the ring nitrogen atoms are involved in hydrogen bonding with the water molecules forming a total of three hydrogen bonds (Table 3.2) with distances between donor and acceptor in the range ~2.8–2.9 Å. O2 does not interact significantly neither with lithium centers (through coordination) nor to water molecules (through hydrogen bonding). Two consecutive pyramids with coplanar anions (Figure 3.3) are linked by a hydrogen bond between two of the basal oxygen atoms (O5 \cdots O3ⁱ = 2.748(2) Å; symmetry code: (i) 2-*x*, -*y*, 1-*z*), forming the shortest hydrogen bond in the structure. Figure 3.4 shows a view of the unit cell of **22** along the *a*-axis with selected represented hydrogen bonding. Two pyramids including 5-nitro-2*H*-tetrazolate anions on parallel planes, are connected by two hydrogen bonds between two water molecules (O4 \cdots O5^v = O4^v \cdots O5 = 2.772(2) Å; symmetry code: (v) 2-*x*, -*y*, -*z*).

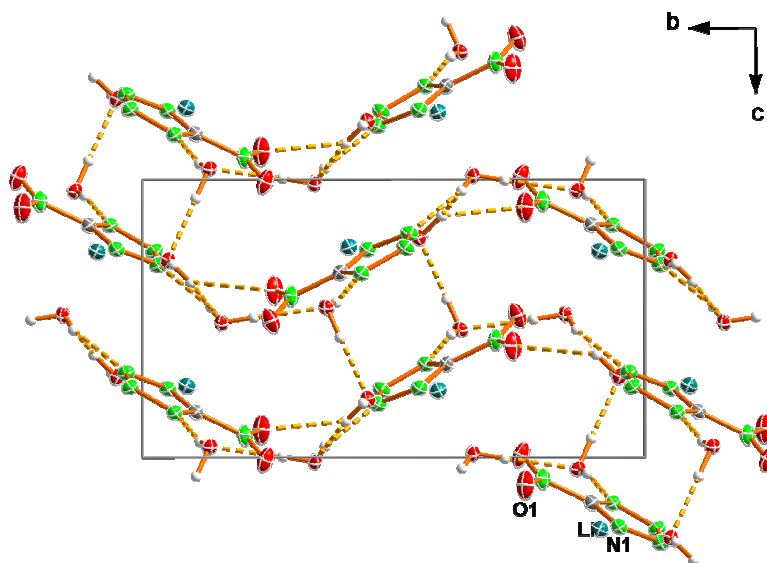


Figure 3.4 View of the unit cell of **LiNT (22)** along the *a*-axis with the hydrogen bonding (dotted lines). Symmetry code: (v) 2-*x*, -*y*, -*z*.

Using the graph-set formalism introduced by Bernstein et al.^[30] and the computer program *RPLUTO*^[31] the hydrogen bonding networks can easily be identified. Table 3.B1 shows tabulated the graph-sets formed by the hydrogen bonds in the structure of **22**. Only dimer interactions are found. At the primary level six finite **D1,1(2)** graph-sets are identified by the program, whereas at the secondary level these combine to yield larger finite patterns of the form **D2,2(X)** with *X* = 4 and 5.

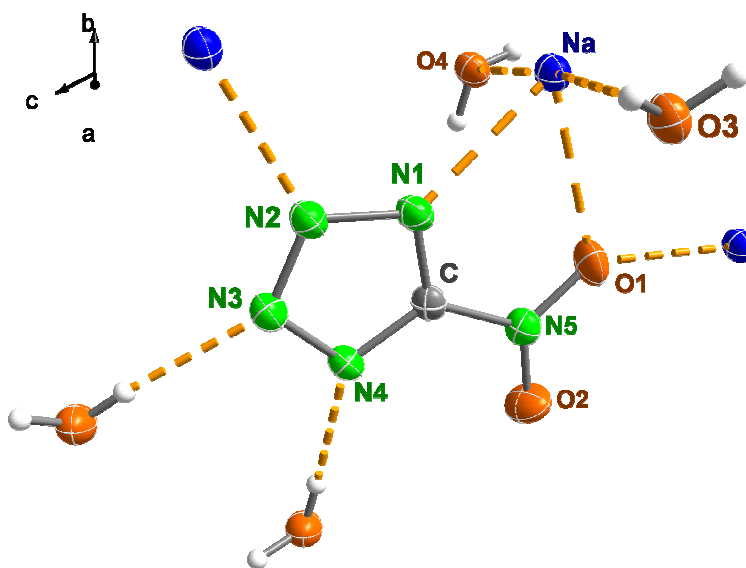


Figure 3.5 View of the packing around the anion in the crystal structure of **NaNT (23)** with the numbering scheme.

Every 5-nitro-2*H*-tetrazolate anion in the crystal structure of **23** is coordinated to two sodium cations (Figure 3.5): once as a single contact with O1, which coordinates to the two metal centers at the same time ($\text{O1-Na} = 2.641(2) \text{ \AA}$ and $\text{O1-Na}^{\text{i}} = 2.470(1) \text{ \AA}$; symmetry code: (i) $1-x, -y, 1-z$) and once as a chelate through N1 and again O1 with $\text{N1-Na} = 2.467(2) \text{ \AA}$. In the unit cell (Figure 3.A1) there are layers of anions, which are linked together by coordination to the metal centre and hydrogen bonds to water molecules (see Table 3.2). The spaces between anions layers are large and accommodate water molecules, which form hydrogen bonds to other water molecules placed on the anions layers ($\text{O}\cdots\text{O} \sim 2.80 \text{ \AA}$). In addition, the water molecules form two other hydrogen bonds to 5-nitro-2*H*-tetrazolate anions with distances between donor (oxygen) and acceptor (nitrogen) atoms of $\text{O4}\cdots\text{N4}^{\text{iii}} = 2.930(2) \text{ \AA}$ and $\text{O3}\cdots\text{N3}^{\text{v}} = 2.875(2) \text{ \AA}$ (symmetry codes: (iii) $1-x, -y, 2-z$; (v) $x, y, -1+z$). Again, using graph-set nomenclature is useful to identify the type of hydrogen bonds found in the structure (see Table 3.B2). In analogy to **22**, **23** forms only **D1,1(2)** (four in total) interactions at the unitary level, which interact to form **D2,2(X)** patterns ($X = 4$ and 5) and, in addition, one less common **R2,2(4)** ring motif (both at the secondary level).

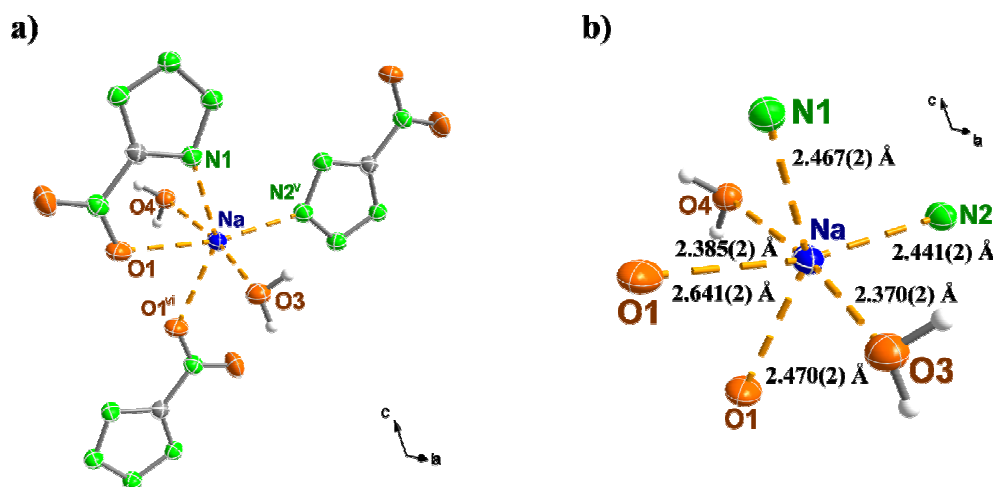


Figure 3.6 a) Full coordination around the Na^+ cations and b) simplified coordination around the Na^+ cations in the crystal structure of **NaNT** (**23**). Symmetry codes: (v) $x, y, -1+z$; (vi) $1+x, y, z$.

As represented in Figure 3.6, every sodium cation forms a distorted octahedron by coordinating to four oxygen and two nitrogen atoms. On the equatorial plane there are found the two water molecules, which strongly coordinate to the metal ($\text{O3-Na} = 2.370(2)$ and $\text{O4-Na} = 2.385(2) \text{ \AA}$) and two contacts with two anions (one through the oxygen and the other through the nitrogen atoms). The axial positions are occupied by a nitrogen atom (N2^v) corresponding to a 5-nitro-2*H*-tetrazolate anion and an oxygen atom (O1) corresponding to an anion, which chelates the metal centre (one time on an equatorial and one time on an axial position). The angle along

the axial axis is $164.4(1)^\circ$ quite apart from the ideal 180° angle expected for a perfect octahedron. On the equatorial plane the angles have values in the range ~ 80 – 100° , relatively close to the ideal 90° .

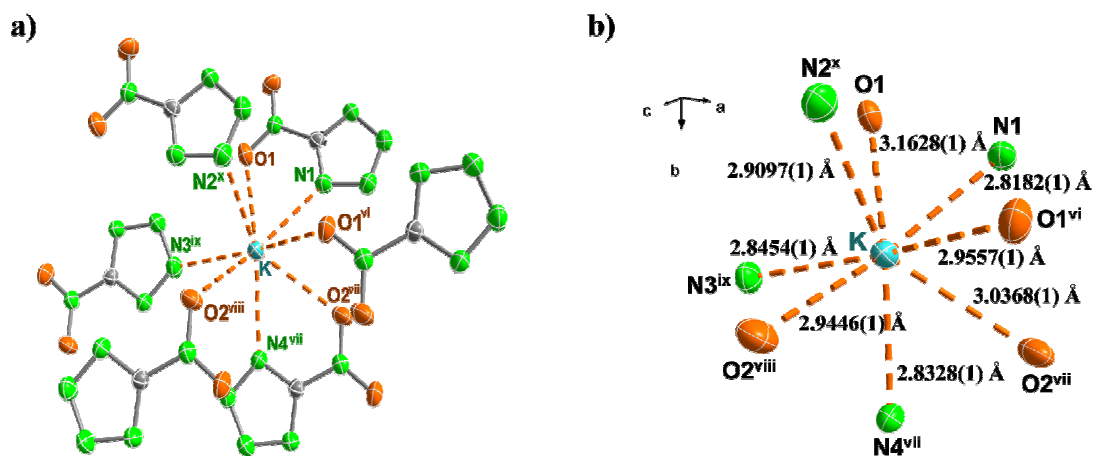


Figure 3.7 a) Full coordination around the K^+ cations and b) simplified coordination around the K^+ cations in the crystal structure of **KNT** (**24**). Symmetry codes: (vi) $x, 0.5-y, -0.5+z$; (vii) $1-x, 0.5+y, 0.5-z$; (viii) $-x, 0.5+y, 0.5-z$; (ix) $-1+x, 0.5-y, 0.5+z$; (x) $-1+x, y, z$.

Potassium 5-nitro-2*H*-tetrazolate (**24**) is the first compound of the series that does not contain crystal water and is, thus, a very sensitive material (see section 3.5 *Energetic Properties*). As shown in Figure 3.A2, apart from N5, every nitrogen and oxygen atoms are coordinated to (at least) one cation. As already discussed for **22** and **23**, N1 and O1 chelate the metal centre with a short N1–K = 2.8182(1) Å and a long O1–K = 3.1628(1) Å distances, which are the shortest and the longest contacts to the potassium cation found in the structure, respectively. **24** crystallizes in wavy layers (Figure 3.A3) where every cation is surrounded by three 5-nitro-2*H*-tetrazolate anions (of the same layer) coordinating through the nitrogen atoms with an average distance (N–K) of *ca.* 2.83 Å. The full coordination sphere around the potassium atoms is however completed by a total of eight contacts (Figure 3.7), two of which are through chelation and the remaining four are normal monodentate interactions, forming a distorted square antiprism. The distances to the center of the antiprism are summarized in Table 3.B4 and vary between 2.8 and 2.9 Å (N–K) and between 2.9 and 3.2 Å (O–K). In comparison to compound **23**, which shows average N–Na and O–Na distances of *ca.* 2.45 and 2.50 Å, respectively, the contacts between potassium cations and nitrogen and oxygen atoms are much looser than the analogous interactions in the sodium salt, possibly due to the higher ionic character of the former. However, although the contacts between anions and cations are relatively long, the heavier atomic weight of potassium (in comparison to sodium) and the efficient packing due to the formation of layers (with short

interlayer distances) account for the larger density of **24** with a value of 2.033 g cm^{-3} ($\rho_{\text{calc}}(\mathbf{23}) = 1.731 \text{ g cm}^{-3}$). Figure 3.8 shows a view of the unit cell of the compound along the *a*-axis. The potassium atoms lay, alternatively, above and below the plane formed by the anions. The nitro-groups are pointed face-on and cations and anions are arranged in such a way that form zig-zag chains along the *b*-axis with a short interchain distance of $\text{K}-\text{O1}^{\text{vi}} = 2.956(1) \text{ \AA}$ (symmetry code: (vi) $x, 0.5-y, -0.5+z$).

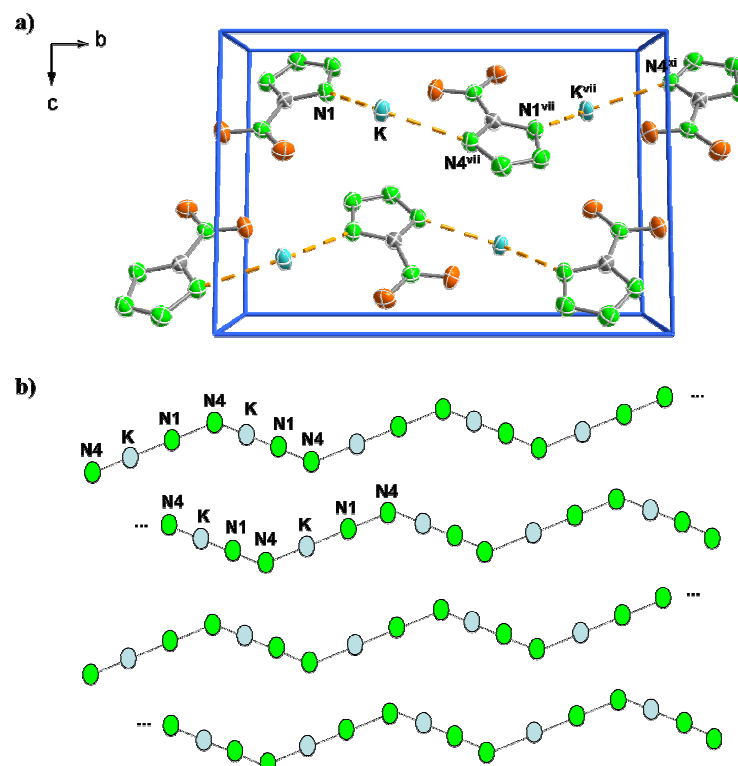


Figure 3.8 a) View of the unit cell of **KNT** (**24**) along the *a*-axis showing the contacts between the K^+ cations and the nitrogen atoms in the anion and b) Schematic representation of the zig-zag chains formed along the *b*-axis (symmetry codes: (vii) $1-x, 0.5+y, 0.5-z$; (xi) $x, 1+y, z$).

In contrast to **24**, not all atoms (N and O) of the anions in the structure of the rubidium derivative **25** (Figure 3.A4) form links to a cation (N5 and N3ⁱ are the exception; symmetry code: (i) $x, 1-y, -0.5+z$). The fact that N3ⁱ does not participate in the coordination does not allow the formation of the hexagons depicted by the coordination to the metal centre found in **26** (see discussion below). Together with the cesium salt, both compounds have the largest coordination number (CN = 10) of the compounds discussed here, as expected from the larger size of the metal centers. The coordination around one of the rubidium cations is depicted in Figure 3.9. In contrast to **22**, **23** and **24** and in analogy to **26**, the rubidium cations coordinate more strongly to

the oxygen than to the nitrogen atoms. The O–Rb distances vary (generally) between 2.9 and 3.0 Å, whereas the N–Rb are slightly longer at 3.0–3.1 Å (see Table 3.B5). However, there exists two longer contacts (Rb–O2^{vi} and Rb–N3^{ix}, symmetry codes: (vi) $-0.5+x, 0.5+y, z$; (ix) $x, -1+y, z$) with a distance of *ca.* 3.5 Å.

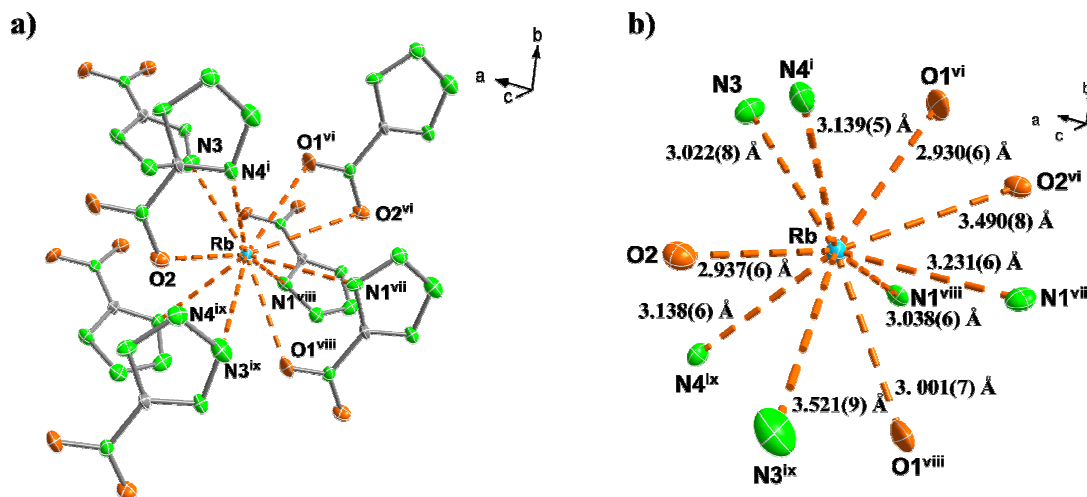


Figure 3.9 a) Full coordination around the Rb⁺ cations and b) simplified coordination around the Rb⁺ cations in the crystal structure of **RbNT** (**25**). Symmetry codes: (i) $x, 1-y, -0.5+z$; (vi) $-0.5+x, 0.5+y, z$; (vii) $-0.5+x, 0.5-y, -0.5+z$; (viii) $-0.5+x, -0.5+y, z$; (ix) $x, -1+y, z$.

Figure 3.10 shows a view of the unit cell of the compound representing the stacks of anions along the *b*-axis, connected among them by coordination to the cations. The two crystallographically independent 5-nitro-2*H*-tetrazolate anions found in the structure form layers, which cut each other at an angle of *ca.* 70°.

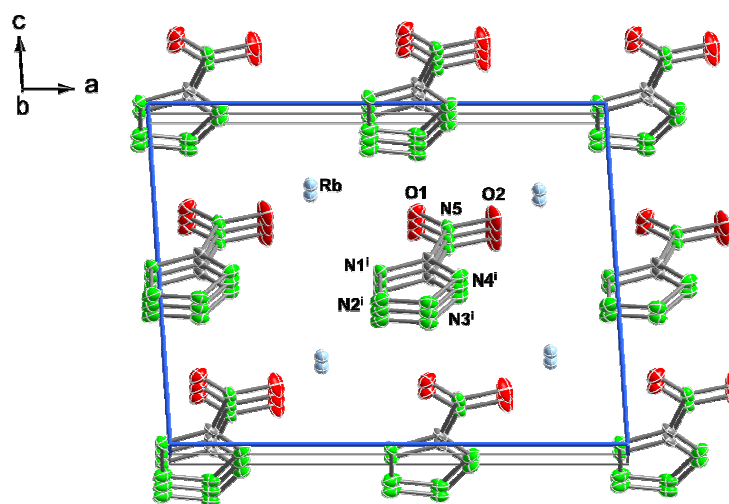


Figure 3.10 View of the unit cell of **RbNT** (**25**) along the *b*-axis showing the stacks of anions. Symmetry code: (i) $x, 1-y, -0.5+z$.

Figure 3.A5 shows the coordination around the anion in the crystal structure of **26**. In analogy to the rubidium salt (**25**) all nitrogen atoms but N5 (as usual) and in this case N4 also, are involved in coordination to (at least) one cation, which sits on a different level to that of the tetrazolate ring. The coordination number around the cesium cations (Table 3.B5) is ten and is represented in Figure 3.11. The O–Cs distances vary between 3.1 and 3.4 Å, whereas the N–Cs are slightly longer at 3.2–3.6 Å. This longest distances (among all compounds in this study) puts into perspective the already predictable highest ionic character of the molecule. The shortest contacts in the structure are Cs–N3 = 3.204(2) and Cs–O1 = 3.112(2) Å.

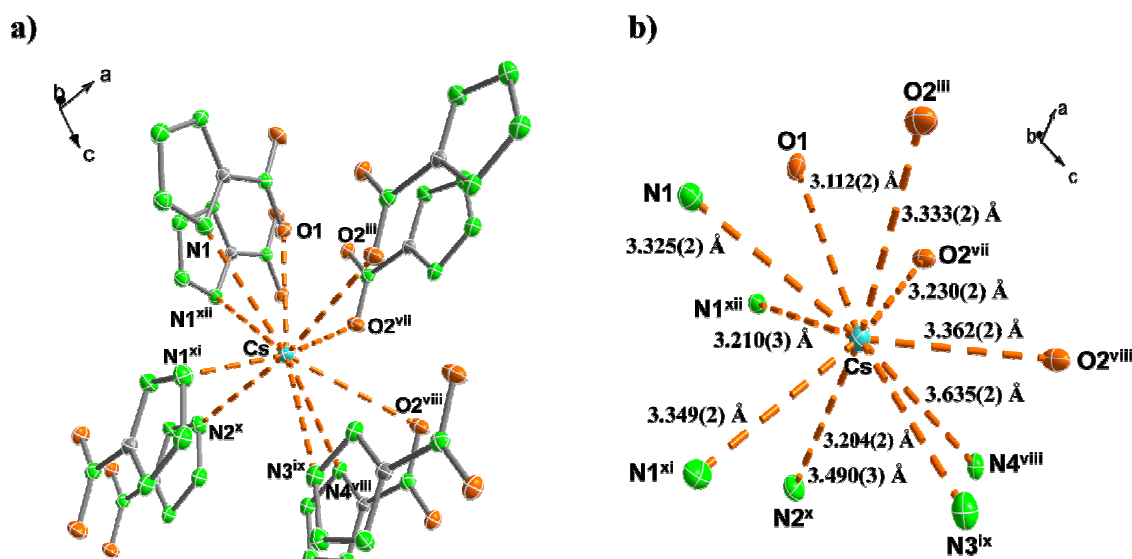


Figure 3.11 a) Full coordination around the Cs⁺ cations and b) simplified coordination around the Cs⁺ cations in the crystal structure of CsNT (**26**). Symmetry codes: (iii) 0.5-x, -0.5+y, 0.5-z; (vii) 0.5-x, 0.5+y, 0.5-z; (viii) x, 2-y, 0.5+z; (ix) x, 3-y, 0.5+z; (x) -x, 2-y, 1-z; (xi) x, 1+y, z; (xii) -x, y, 0.5-z.

An interesting feature about the structure of compound **26** arises when taking a look at the coordination of two contiguous metal atoms to two 5-nitro-2*H*-tetrazolate anions placed on the same plane (Figure 3.12): the pattern described between the two metal centers and the two anions corresponds to a distorted hexagon where the vertices are occupied by Cs, N2, N3, Cs^x, N3^x and N4^x (symmetry code: (x) -x, 2-y, 1-z). The coordination number around the metal center in these “layers” is three forming a distorted *T*-shape with angles N3^x–Cs–O1 = 161.40(6), N3^x–Cs–N2 = 95.39(7) and N2–Cs–O1 = 102.89(6)°. Every cesium atom coordinates to three different 5-nitro-2*H*-tetrazolate anions two of which are coplanar (the ones coordinating through the nitrogen atom) and the third one is approximately orthogonal to the other two (coordinating through the oxygen atom). There is, thus, two types of 5-nitro-2*H*-tetrazolate anions, which form layers among them at an angle of *ca.* 80°.

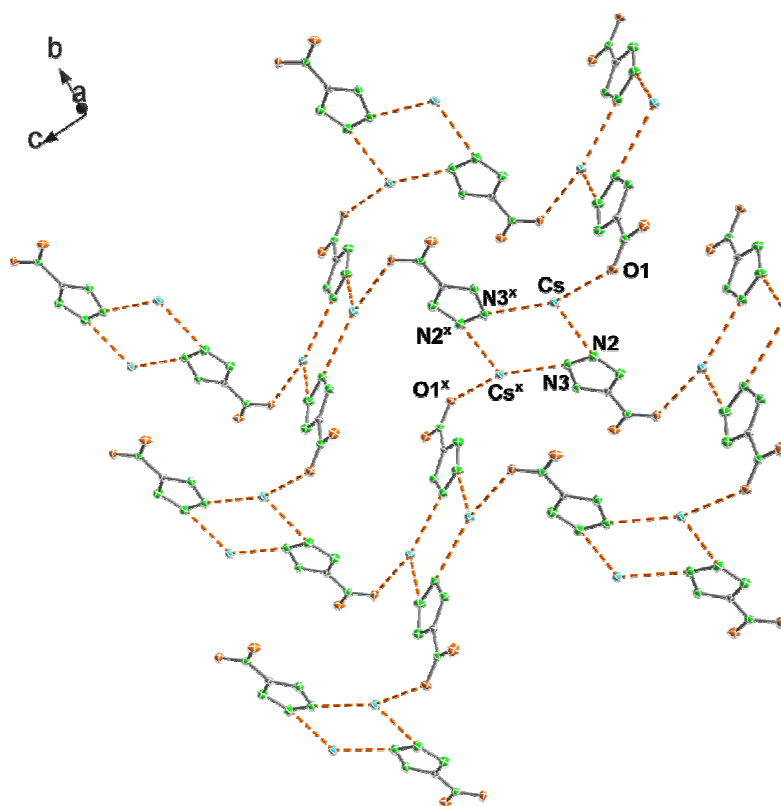


Figure 3.12 View of a supercell in the crystal structure of **CsNT** (**26**) along the *a*-axis showing the contacts between the anions and the Cs⁺ cations (not all contacts have been drawn).

The calcium salt (**28**) crystallizes as a hexahydrate with all six water around the coordination sphere of the metal atom and the seventh vacancy being occupied by one of the two anions forming a distorted pentagonal bipyramid (Figure 3.13). The coordination number around the metal center (CN = 7) is in agreement with a reported average value of 7.31 in calcium salts.^[28] Both NT[−] anions are crystallographically independent with just one of the anions coordinating to the metal center through one of the two nitro-group oxygen atoms (Ca1–O1 = 2.554(1) Å) whereas the other one is loose and the next Ca²⁺ cation is placed at a distance of 4.266(2) Å (Ca1–N10). The coordinating anion occupies one of the axial position forming an angle with the other oxygen atom in the axial position of O1–Ca1–O8 = 153.66(5)°. The water molecules are closely bound to the metal with Ca–O distances varying between 2.352(2) and 2.418(2) Å. The short contacts to the water molecules are in agreement with the high temperature of water loss observed in the DSC measurements (see section 3.5 *Energetic Properties*).

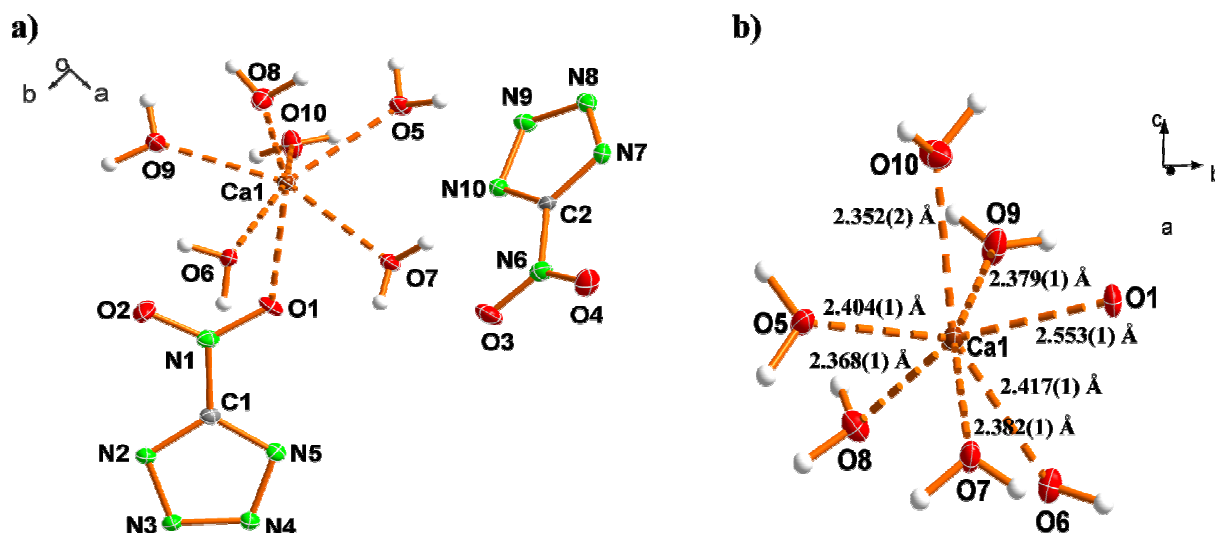


Figure 3.13 a) Asymmetric unit of **CaNT** (**28**) with the labeling scheme and b) simplified coordination around the Ca²⁺ cation.

The unit cell of **28** is represented in Figure 3.14. The *b*-axis is outstandingly long at 32.575(1) Å and there is extensive strong hydrogen bonding formed by the water molecules (Table 3.2), with distances between donor and acceptor atoms in the range ~2.8-3.0 Å. The fourteen hydrogen bonds found in the structure and that only describe **D1,1(2)** dimeric patterns at the unitary level, combine to yield mainly finite patterns with the labels **D1,2(3)**, **D2,1(3)** and **D2,2(X)** (X = 4–7) but also some **C2,2(X)** (X = 6, 8) chain networks.

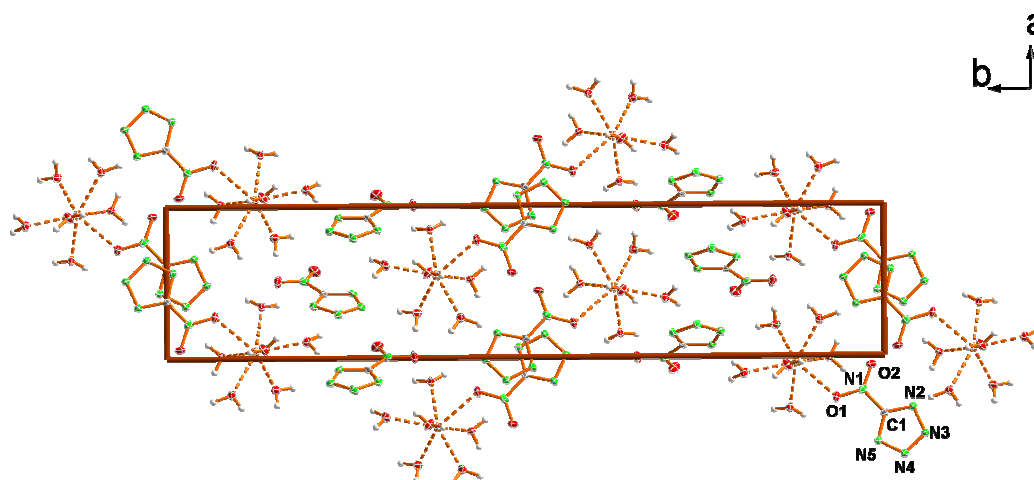


Figure 3.14 View of the unit cell of **CaNT** (**28**) along the *c*-axis (dotted lines depict contacts to the Ca²⁺ cations).

The asymmetric unit of **31** is represented in Figure 3.15 and is constituted of two formula units. Protonation of the NT⁺ anion occurs at N3 (X-ray labels), which is in contrast with 5-amino-^[32] or 5-azidotetrazole.^[33] In Table 3.1 there are summarized the angles and distances of the two 5-nitro-2*H*-tetrazole rings, which, within the limits of error, are not significantly different. The main difference is observed in the twist of the nitro groups in respect to the tetrazole rings. Whereas in one of the two molecules the nitro group is almost coplanar to the ring (O4–N6–C1–N7 = -178.2(3)°), in the other, this is significantly deviated (O2–N1–C1–N2 = -164.9(3)°). So, one of the formula units is similar to metal salts of **31** (this chapter), which show small torsion angles between 2 and 5°,^[3] whereas the other one is more similar to salts of **31** with nitrogen-rich bases (0-10°).^[6] A plausible explanation for this could be that in salts of **31** there is a negative charge, which is delocalized all around the tetrazole ring and over the nitro group, making them virtually coplanar. Proof for this is the relatively longer C1–N1 distances (~1.445(4) Å) in **31**. Therefore one would expect larger torsion angles due to the lack of delocalization in both formula units. The smaller torsion angle for one of the two units can be explained by hydrogen bonding effects (see discussion below).

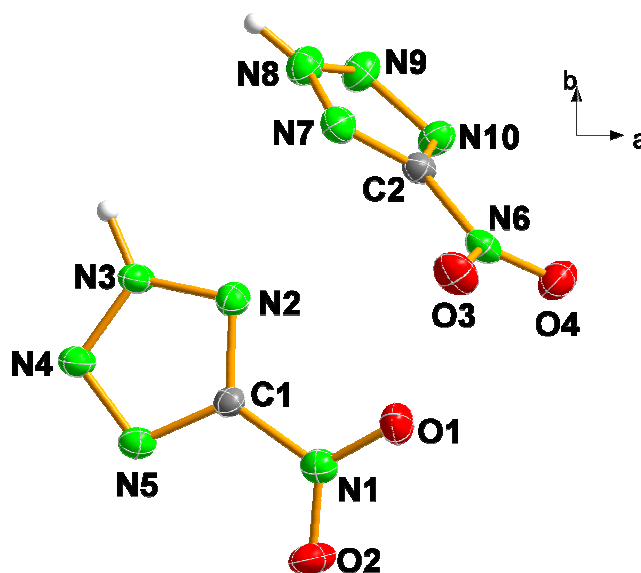


Figure 3.15 Asymmetric unit of 5-NTH (**31**) with the labeling scheme.

Regardless of the expected planarity of **31** the presence of a proton surrounded by many electronegative atoms forces the compound to form hydrogen bonds, which make the structure not to form layers. These hydrogen bonds are formed by the protonated nitrogen atom (N3 or N8) as the donor atom and either tetrazole ring nitrogen atoms or, in one instance, with one of the nitro groups oxygen atoms (O3). A report of the hydrogen bonds found in the structure is given in Table 3.2. The interaction between N8 and O3 ($\text{N8} \cdots \text{O3}^i = 3.015(4)$ Å; symmetry code:

(i) $-x, 0.5+y, -z$ “fixes” the nitro group in such a way that it is coplanar to the tetrazole ring and forms the **C1,1(6)** motifs represented in Figure 3.16 (at the primary level) (Table 3.B3). Similarly, the dimer pairs formed by two crystallographically related rings ($N8 \cdots N4^{ii} = 3.057(4)$ Å; symmetry code: (ii) $1-x, 0.5+y, 1-z$) yield a **C1,1(4)** graph-set. Lastly, the third hydrogen bond found in the structure forms only finite patterns of the type **D1,1(2)** at the primary level, which combine with the other two hydrogen bonds yielding larger dimeric interactions with the label **D3,3(X)** ($X = 7, 9$), at the secondary level. This results in a highly efficient packing as can be deduced from the high density of the compound (1.899 g cm^{-3}).

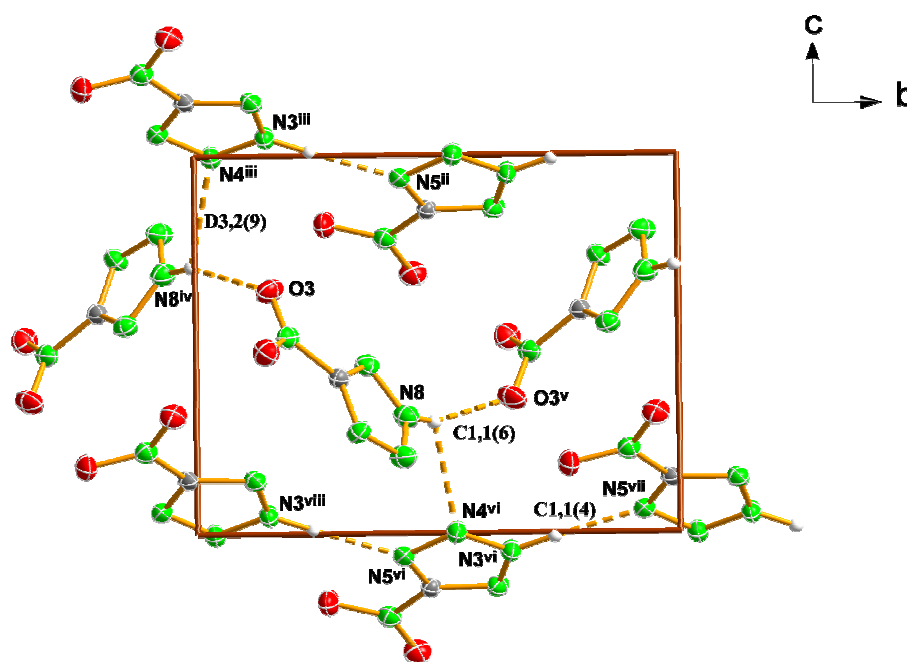


Figure 3.16 View of the unit cell of 5-NTH (**31**) along the a -axis showing the graph-sets in the structure. Symmetry codes: (ii) $1-x, 0.5+y, 1-z$; (iii) $1+x, y, 1+z$; (iv) $1-x, -0.5+y, 1-z$; (v) $2-x, 0.5+y, 1-z$; (vi) $1-x, 0.5+y, -z$; (vii) $x, 1+y, z$; (viii) $1+x, y, z$.

3.5 Energetic properties

A summary of the physico-chemical properties of the metal salts of 5-nitro-2*H*-tetrazole (**31**) and **31** is found in Tables 3.3 to 3.5. For the less sensitive hydrated species (**22**, **23** and alkaline earth metal salts **27-30**), the (constant volume) energy of combustion was determined experimentally using oxygen bomb calorimetry. Additionally, the heats of combustion and formation were back-calculated from the combustion data.

Table 3.3 Physico-chemical properties of alkali metal salts of 5-nitro-2*H*-tetrazole.

	22	23	24	25	26
Formula	CH ₆ N ₅ O ₅ Li	CH ₄ N ₅ O ₄ Na	CN ₅ O ₂ K	CN ₅ O ₂ Rb	CN ₅ O ₂ Cs
MW (g mol ⁻¹)	175.05	173.08	153.16	199.53	246.91
Impact (J) ^a	25	>30	4	1	2
Friction (N) ^a	324	~360	<5	<5	<5
Electrostatics ^b	-	-	+	+	+
Flame	Explodes	Explodes	Explodes	Explodes	Explodes
N (%) ^c	40.0	40.5	45.7	35.1	28.4
N+O (%) ^d	85.7	77.5	66.6	51.2	41.3
Ω (%) ^e	-9.1	-9.2	-10.4	-8.0	-6.5
m.p. (°C) ^f	69 (-H ₂ O)	75 (-H ₂ O)	168	146	158
Dec. (°C) ^g	270	200	195	192	194
ρ (g cm ⁻³) ^h	1.608	1.731	2.033	2.489	2.986
-Δ _c U (cal g ⁻¹) ⁱ	1340(15)	1200(20)	n.m.	n.m.	n.m.
-Δ _c H° (kJ mol ⁻¹) ^j	940(15)	850(20)	n.m.	n.m.	n.m.
-Δ _f H° (kJ mol ⁻¹) ^k	610(55)	360(65)	n.m.	n.m.	n.m.

^a Impact and friction sensitivities determined by standard BAM methods (see references [34-36]); compounds **22** and **24** are semicrystalline solids, whereas **23**, **25** and **26** are crystalline. ^b Rough sensitivity to 20 kV electrostatic discharge (ESD testing): + sensitive, - insensitive from an HF-Vacuum-Tester type VP 24. ^c Nitrogen content. ^d Combined nitrogen and oxygen content. ^e Oxygen balance, calculated according to reference [37]. ^{f,g} Melting and decomposition points (DSC onset) from measurement with β = 2 (**25** and **26**) or 5 (**22-24**) °C min⁻¹. ^h Experimentally determined density (from X-ray). ⁱ Experimental (constant volume) energy of combustion. ^j Experimental molar enthalpy of combustion. ^k Molar enthalpy of formation (n.m. = not measured due to the high sensitivity of the material).

DSC measurements were made on samples of ~1 mg of each material in this study and per duplicate. Figure 3.15 shows typical DSC thermograms for the alkali metal salts, which are representative for all metal salts discussed here. For the hydrated alkali metal salts (**22** and **23**) the crystal water is lost at temperatures of ~70 °C and all alkali metal salts have melting points, which are in the rule quite close to the decomposition temperature. In contrast, the crystal water in the alkaline earth metal salts is more tightly bound and lost at temperatures in the range 100-130 °C (DSC onsets). **22**, **23** and the alkaline earth metal salts only show a highly exothermic decomposition without any melting, whereas **24** shows a small melting endotherm, which can be differentiated from the decomposition (by DSC) and **25** and **26** have distinctive melting points. Apart from **22**, which has a high decomposition temperature at ~270 °C, the rest of the compounds decompose/explode at ~200 °C (alkali metal salts, Table 3.3) and in the range 180–235 °C (alkaline earth metal salts, Table 3.4). The melting and decomposition points of the salts in this study are generally slightly lower than those observed for metal salts of 5-amino-1*H*-tetrazole^[25] and 5,5'-azotetrazole.^[26] Due to the interest in the investigation of tetrazole derivatives and their metal salts as detonators to replace lead diazide,^[38] a comparison of the energetic properties of the 5-nitro-2*H*-tetrazole metal salts described here with those of commonly used primary explosives such as Pb(N₃)₂ and AgN₃ is necessary. Once again, all compounds show

lower melting and decomposition points.^[39] On the other side, neutral 5-nitro-2*H*-tetrazole (**31**) has a low melting point below 100 °C and starts decomposing (highly exothermically) at ~130 °C (DSC onset) showing a similar behavior to 5-azido-1*H*-tetrazole (**B**, Scheme 3.1).^[33] In addition to DSC analysis, all compounds were tested by placing a small sample (~0.5-1 mg) of compound in the flame. In the case of the metal salts this resulted in a loud explosion (both Pb(N₃)₂ and AgN₃ explode under similar conditions) whereas neutral **31** deflagrated.

Table 3.4 Physico-chemical properties of alkaline earth metal salts of 5-nitro-2*H*-tetrazole.

	21a	27	28	29	30
Formula	C ₃ H ₂ N ₆ O ₂	C ₂ H ₁₂ N ₁₀ O ₁₀ Mg	C ₂ H ₁₂ N ₁₀ O ₁₀ Ca	C ₂ H ₁₀ N ₁₀ O ₉ Sr	C ₂ H ₁₀ N ₁₀ O ₉ Ba
MW (g mol ⁻¹)	154.08	360.48	376.26	405.78	455.49
Impact (J) ^a	1.5	≥40	35	15	2.5-5
Friction (N) ^a	96	240	84	48	<20
Electrostatics ^b	—	—	—	—	—
Flame	Burns	Explodes	Explodes	Explodes	Explodes
N (%) ^c	54.5	38.9	37.2	34.5	30.8
N+O (%) ^d	75.2	83.4	79.7	70.0	62.3
Δ (%) ^e	-24.2	-4.4	-4.2	-3.9	-3.5
m.p. (°C) ^f	— ^b	119 (-H ₂ O)	120 (-H ₂ O)	104 (-H ₂ O)	129 (-H ₂ O)
Dec. (°C) ^g	210 ^b	195	180	210	235

^a Impact and friction sensitivities determined by standard BAM methods (see references [34-36]); compounds **27-30** were tested as powders. ^b Rough sensitivity to 20 kV electrostatic discharge (ESD testing): + sensitive, — insensitive from an HF-Vacuum-Tester type VP 24. ^c Nitrogen content. ^d Combined nitrogen and oxygen content. ^e Oxygen balance, calculated according to reference [37]. ^{f,g} Melting (or temperature of water loss) and decomposition points (DSC onset) from measurement with $\beta = 5\text{ °C min}^{-1}$. ^h From reference [6].

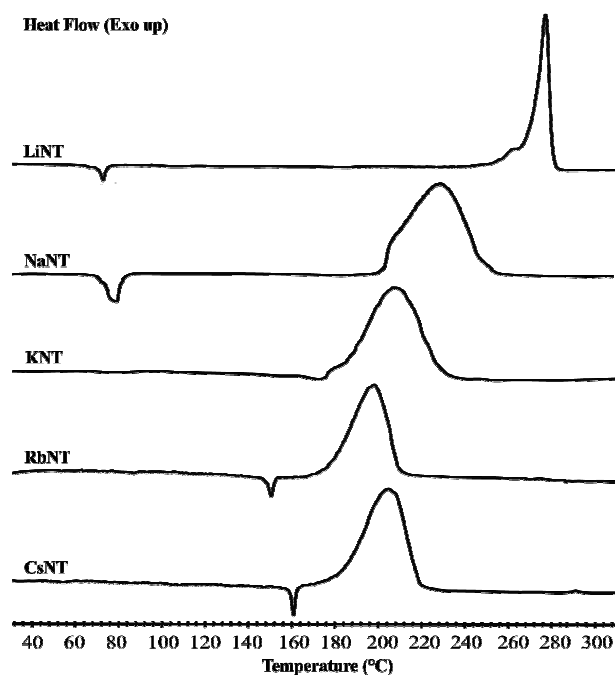
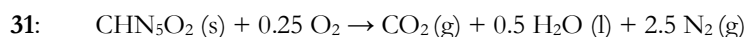
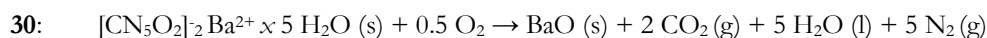
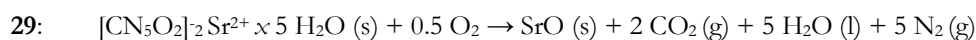
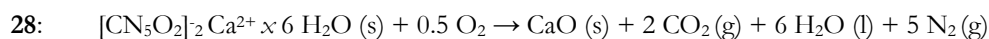
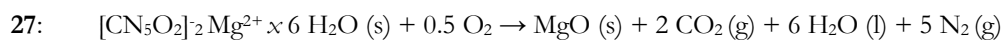
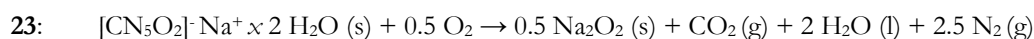
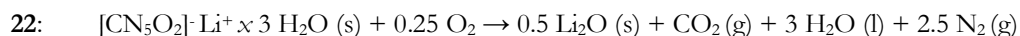


Figure 3.17 DSC plots of alkali metal salts of 5-nitro-2*H*-tetrazole.

Data collected for impact (*i*), friction (*f*) and electrostatic discharge sensitivity testing are summarized in Tables 3.3 and 3.4 for the metal salts and in Table 3.5 for the free acid **31**. The presence of crystal water in compounds **22**, **23** and **27–30** results in less sensitive compounds,^[40] whereas the anhydrous species **24–26** are very sensitive to both friction and shock. All three compounds explode loudly at the minimum setting in the friction tester (<5 N) and have impact sensitivity values in the range 1-5 J, comparable to commonly known primary explosives (e.g. mercury fulminate, *i* = 1 J; lead styphnate, *i* = 4 J).^[39] At this point it is worth mentioning that in contrast to sodium 5-nitro-2*H*-tetrazolate tetrahydrate, the dihydrated species **23** does not lose water spontaneously forming the (expected) highly sensitive anhydrous compound. Several attempts to eliminate the two crystal waters by storage under vacuum over P₄O₁₀ or by heating turned out to be fruitless. Once again, a comparison with the sensitivity values for common explosives is useful to assess the energetic materials in this study. **22**, **23** and **27–30** are less sensitive to impact than the secondary explosive TNT and have a similar value for the friction test (*i* = 15 J, *f* = 355 N).^[39] Salts **24–26**, due to their low initiation barrier, belong to the class known as primary explosive or initiators^[39,41] and have similar sensitivity to both impact and shock as Pb(N₃)₂ (*i* = 3.0-6.5 J, *f* = 0.1-1.0 N for technical grade material).^[39] The trend in the sensitivity values of the alkaline earth metal salts is to increase with the size of the cation. Note the higher sensitivities of the strontium and barium salts (containing five molecules of crystal water) in comparison to the hexahydrates **27** and **28**. In addition, the compounds in this study are significantly more sensitive to friction and impact than nitrogen-rich salts containing the same anion^[6] and than alkali metal salts of **1**^[25] and **A**^[42,43] (see Scheme 3.1) but less sensitive than analogous salts of **B**.^[44,45] The order of sensitivity for alkali salts of 5*R*-substituted tetrazoles is N₃ > NO₂ >> NH–NO₂ > NH₂, which is keeping in with previous studies.^[38a,46] This has been explained in terms of the electron-withdrawing ability of the substituent, which varies in approximately the same order.^[38c,47] Also, each compound was roughly tested for sensitivity to electrostatic discharge by spraying sparks across a small (three to five crystals) sample of material using a tesla coil (ESD testing). All hydrated salts failed to explode under these conditions, whereas compounds **24–26** exploded loudly similarly to Pb(N₃)₂, which is very sensitive to electrostatic discharge (dry as well as wet).

Due to the energetic nature of the compounds in this study, the constant volume energies of combustion ($\Delta_c U$) of the less sensitive hydrated salts (**22**, **23** and the alkaline earth metal compounds **27–30**) were measured using oxygen bomb calorimetry. Measurements for the highly sensitive anhydrous compounds were omitted due to the obvious hazard involved in the preparation of the sample (grinding together with benzoic acid). The standard molar enthalpy of

combustion ($\Delta_c H^\circ$) was calculated from the equation $\Delta_c H^\circ = \Delta_c U + \Delta n RT$ (where Δn is the difference in the number of moles of gases between the products and the reactants). The standard energies of formation of the compounds ($\Delta_f H^\circ$) were back-calculated from the energy of combustion on the basis of their combustion equations (see below), Hess's Law and the known standard heats of formation for Li_2O , Na_2O_2 , MgO , CaO , SrO or BaO , water and carbon dioxide.^[48] The energies of combustion (obtained from sets of four measurements) are much less negative for the alkali metal salts in this study (**22**: -1340(15) and **23**: -1200(20) cal g⁻¹) than for analogous salts of 5-At,^[25] and thus the standard heats of formation (**22**: -610(55) and **23**: -360(65) kJ mol⁻¹) are comparatively more positive (less negative) as expected from the better oxygen balance of the 5-nitro-2*H*-tetrazolate anion in comparison to the 5-amino-1*H*-tetrazolate anion.



Computational Methods. Due to the high sensitivity of neutral **31**, bomb calorimetric measurements could only be performed with small amounts of the material and doubtful combustion data was obtained. Therefore we decided to estimate the thermodynamic data by quantum chemical methods. All calculations were carried out using the Gaussian G03W (revision B.03) program package.^[49] The enthalpies (H) and free energies (G) were calculated using the complete basis set (CBS) method described by Petersson and coworkers in order to obtain very accurate values. The CBS models use the known asymptotic convergence of pair natural orbital expressions to extrapolate from calculations using a finite basis set to the estimated complete basis set limit. CBS-4 begins with a HF/3-21G(d) geometry optimization; the zero point energy is computed at the same level. It then uses a large basis set SCF calculation as a base energy, and a MP2/6-31+G calculation with a CBS extrapolation to correct the energy through second order. A MP4(SDQ)/6-31+(d,p) calculation is used to approximate higher order contributions. In this study we applied the modified CBS-4M method (M referring to the use of minimal population

localization) which is a re-parameterized version of the original CBS-4 method and also includes some additional empirical corrections.^[50,51] The enthalpies of the gas-phase species **M** were computed according to the atomization energy method (Eq. 1)^[52] The results of the calculations are summarized in Tables 3.A2-3.A5 from *Appendix A*.^[53,54] The lattice energies (U_L) and lattice enthalpies (ΔH_L) were calculated from the corresponding molecular volumes according to the equations provided by Jenkins et al.^[55,56] With the calculated lattice enthalpies the gas-phase enthalpies of formation (Table 3.A4) were converted into the solid state (standard conditions) enthalpies of formation (Table 3.A5). These molar standard enthalpies of formation (ΔH_m) were used to calculate the molar solid state energies of formation (ΔU_m) according to Eq. (2).^[39]

$$\Delta_f H^\circ_{(g, M, 298)} = H_{(Molecule, 298)} - \sum H^\circ_{(Atoms, 298)} + \sum \Delta_f H^\circ_{(Atoms, 298)} \quad (1)$$

$$\Delta U_m = \Delta H_m - \Delta n RT \quad (\Delta n \text{ being the change of moles of gaseous components}) \quad (2)$$

Compound **31** is very sensitive towards impact (<1 J) and extremely friction sensitive (<5 N). According to the “UN Recommendations on the transport of dangerous goods”,^[34] compound **31** is classified as “very sensitive” regarding the impact and friction sensitivity values. **31** has a value between that of the primary explosives lead azide (0.1-1.0 N, pure product) and tetrazene (7 N). Lastly, the high sensitivities of the compounds studied here can be attributed not only to the high endothermicity of the $CN_5O_2^-$ anion but also to the only slightly negative oxygen balance, in particular in the case of compound **31**.

Table 3.5 Physico-chemical properties, initial safety data and predicted performance of 5-nitro-2*H*-tetrazole (**31**).

	31		31
Formula	CHN ₅ O ₂	DSC (°C) ^e	98 (mp), 130 (dec)
Molecular Mass (g mol ⁻¹)	115.05	ρ (g cm ⁻³) ^f	1.899
Impact sensitivity (J) ^a	< 1	$\Delta_f H_m^\circ$ (kJ mol ⁻¹) ^g	281
Friction sensitivity (N) ^a	< 5	$\Delta_f U^\circ$ (kJ kg ⁻¹) ^b	+2527
N (%) ^b	60.9	$-\Delta_E U_m^\circ$ (J g ⁻¹) ⁱ	-5744
N + O (%) ^c	88.6	T_E (K) ^j	4804
Ω (%) ^d	-7.0	P (kbar) ^k	390
Thermal Shock	deflagration	D (m/s) ^l	9457
Smokeless	+	Gas vol. [ml g ⁻¹] ^m	779

^a Impact and friction sensitivities determined by standard BAM methods (see references [34-36]); compound **31** was tested as a semicrystalline solid. ^b Nitrogen content. ^c Combined nitrogen and oxygen content. ^d Oxygen balance, calculated according to reference [37]. ^e Melting and decomposition points (DSC onset) from measurement with $\beta = 5^\circ \text{C min}^{-1}$. ^f Experimentally determined density (from X-ray). ^g Calculated molar enthalpy of formation (using the CBS-4M method). ^h Calculated energy of formation. ⁱ Calculated energy of combustion. ^j Temperature of the explosion gases. ^k Detonation pressure. ^l Detonation velocity. ^m Volume of the explosion gases.

In addition to safety considerations, performance of HEDMs is of utmost importance. Using the molecular formula, density (from X-ray) and energy of formation, the EXPLO5 computer code^[58] can be used to calculate the detonation velocity and pressure of CHNO-based explosive materials. The program is based on the chemical equilibrium, steady-state model of detonation. It uses the Becker-Kistiakowsky-Wilson's equation of state (BKW EOS) for gaseous detonation products and Cowan-Fickett's equation of state for solid carbon.^[58-60] The calculation of the equilibrium composition of the detonation products is done by applying modified White, Johnson and Dantzig's free energy minimization technique. The program is designed to enable the calculation of detonation parameters at the CJ point. The BKW equation in the following form was used with the BKWN set of parameters (a, β, κ, θ) as stated below the equations and X_i being the mol fraction of i -th gaseous product, k_i is the molar covolume of the i -th gaseous product.^[58-60] The results of the EXPLO5 calculations for compound **31** are presented in Table 3.5 and in Table 3.6 and Figure 3.18 again with the corresponding values for the isomer 5-nitro-1*H*-tetrazole (**31b**) and for commonly used RDX for comparison purposes.

$$pV / RT = 1 + \kappa e^{\beta x} \quad x = (\kappa \sum X_i k_i) / [V (T + \theta)]^a$$

$$a = 0.5, \beta = 0.176, \kappa = 14.71, \theta = 6620.$$

Table 3.6 Comparison of the energetic properties of compounds **31** and **31b** with RDX.

	31	31b	RDX
$\rho / \text{g cm}^{-3}$	1.899	1.899 ^a	1.820
$\Omega / \%$	-7.0	-7.0	-21.6
$\Delta U / \text{kJ kg}^{-1}$	+2527	+2527	+67
$Q_v / \text{kJ kg}^{-1}$	-5744	-5854	-5902
T_{ex} / K	4804	4870	3986
P / kbar	390	394	299
$D / \text{m s}^{-1}$	9457	9488	8796
$V_0 / \text{L kg}^{-1}$	779	779	932

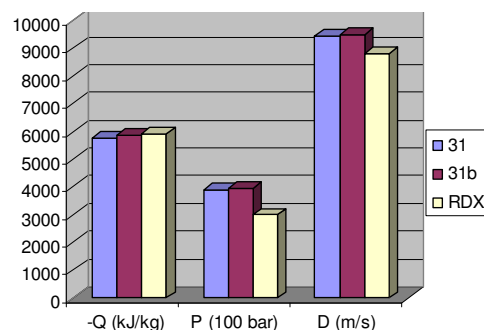


Figure 3.18 Histogram comparing the energetic properties of **31** and **31b** with RDX.

^a density taken to be equal to the isomer **31**. ρ = density, Ω = oxygen balance, Q_v = heat of detonation, T_{ex} = detonation temperature, P = detonation pressure, D = detonation velocity, V_0 = Volume of detonation gases

The physico-chemical properties of **31** are also tabulated in Table 3.5. Compound **31** has a high nitrogen content of ~60% and excellent combined oxygen and nitrogen balances of ~90% and a slightly negative oxygen balance approximately in the range between that of nitroglycol

(C₂H₄N₂O₆, $\Omega = \pm 0.0\%$) and that of nitromethane (CH₃NO₂, $\Omega = -39.3\%$). **31** has an exceptionally high density of 1.899 g cm⁻³ comparable to β -HMX (1.900 g cm⁻³).^[39] As pointed out above, **31** has a highly positive energy of formation of +2527 kJ kg⁻¹ comparable to nitrogen-rich salts with the 5,5'-azotetrazolate anion ([N₄C–N=N–CN₄]²⁻).^[61,62]

Although being very sensitive to impact and friction and thus classifying as a primary explosive in regard to this values, **31** has an astonishingly high calculated detonation velocity of 9457 m s⁻¹, which is comparable to some of the highest performing secondary explosives such as CL-20 (9632 m s⁻¹)^[39] and also higher than the primary explosive 5-azido-1*H*-tetrazole regardless of the lower endothermicity of the –NO₂ group in comparison to the –N₃ substituent.^[33] Here it is necessary to mention that the previous study of Koldobskii and coworkers on compound **31**, reports a density value of 1.73 g cm⁻³,^[17] which is much lower than our calculated value of 1.899 g cm⁻³ and therefore affects strongly the detonation parameters. The detonation pressure of the compound has an accordingly high value (390 kbar), which is slightly higher than that of HMX (382 kbar).^[39] Lastly, the detonation parameters of **31** are higher than those of RDX and comparable to our recently developed triaminoguanidinium dinitramide.^[63]

3.6 Safety Note

While many of the salts of 5-nitro-2*H*-tetrazole described here form as the hydrated species and have relatively low sensitivity towards shock and friction, the potassium (**24**), rubidium (**25**) and cesium (**26**) species form as the anhydrous compounds and are thus extremely sensitive towards the above-mentioned stimuli falling under the category of primary explosives (see *Chapter I*). Furthermore, the copper salt has been reported to be a very sensitive compound in the dry state and explodes violently when submitted to an electric discharge,^[4,64] thus, this ought to never be isolated and ought to always be treated wet (see 3.8 *Experimental Section*). The K⁺ and Rb⁺ salts exploded spontaneously when shaking them gently in an NMR tube (specially the Rb⁺ salt). In one of our late experiences in the laboratory pointing at the synthesis of **23**, we came across a **big explosion!!**: the residue obtained after rotavaporating the water solution to dryness became warm on addition of acetone and detonated catching fire by the light touch of a plastic spatula (see Figure 3.19a). In a similar manner the strontium salt (**29**) exploded spontaneously after loosing the hydrate water by the action of sunlight destroying a 1 cm thick glass shell (see Figure 3.19b).

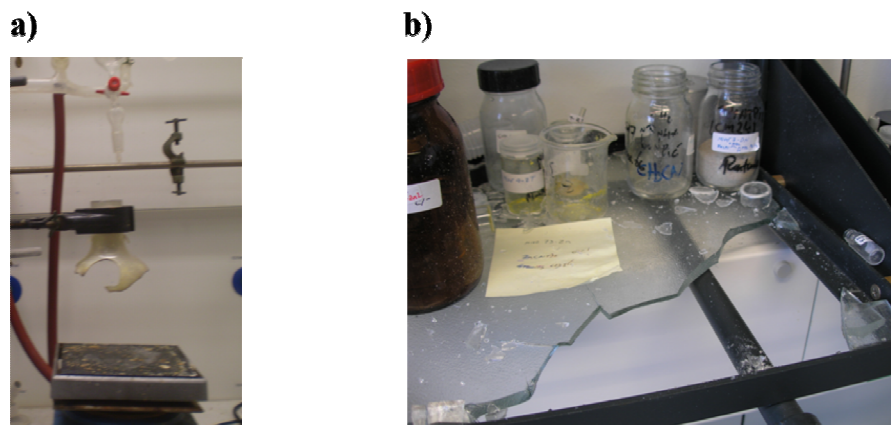


Figure 3.19 a) Result of the explosion of **NaNT** (**23**) after the light touch of a plastic spatula and b) result of the spontaneous explosion of anhydrous **SrNT** (**29**).

3.7 Conclusions

Alkali (**22–26**) and alkaline earth (**27–30**) metal salts with the energetic 5-nitro-2*H*-tetrazolate anion were synthesized by two different methods and fully characterized including X-ray structure analysis. DSC analysis show good thermal stabilities up to (at least) ~200 °C. Standard tests were used to assess the sensitivity of the materials to classical stimuli. The alkaline earth metal salts (**27–30**) and the alkali metal salts with the harder lithium (**22**) and sodium (**23**) cations contain crystal water, which is reflected in the lower sensitivity of the compounds towards shock and friction, whereas the rest of the salts form as the anhydrous species and thus show increased sensitivities but with devoid of a toxic metal (*e.g.* Pb), making them of interest as prospective replacements for commonly used primary explosives. On the other side, protonation of the 5-nitro-2*H*-tetrazolate anion to form the interesting free acid 5-nitro-2*H*-tetrazole (**31**) takes place unequivocally on N2 (NMR labels) both in solution and in the solid state, as proved by NMR and X-ray measurements, respectively. The energetic properties of **31** were assessed by means of standard tests and quantum chemical calculations (CBS-4M), classifying **31** as a primary explosive in regard to its impact and friction sensitivity values and revealing a calculated detonation velocity, which is almost twice as large as that of common primary explosives.

3.8 Experimental Section

Caution! *Tetrazoles and their derivatives are highly endothermic compounds that tend to release their energy after a given stimuli with the possibility of causing serious damage to the surroundings. The use of safety equipment such as leather gloves, face shield, ear plugs and use of Teflon spatulas is mandatory. For obvious safety reasons (see section 3.6 Safety Note), in the case of the anhydrous species the reaction scale should in any case not exceed 250 mg of the product!*



General. All chemical reagents and solvents were obtained from Sigma-Aldrich Fine Inc. or Acros Organics (analytical grade) and were used as supplied. Ammonium 5-nitro-2H-tetrazolate hemihydrate was prepared from 5-amino-1H-tetrazole according to a published procedure in our group.^[6] ¹H, ¹³C, ¹⁴N and ¹⁵N NMR spectra were recorded on a JEOL Eclipse 400 instrument in DMSO-*d*₆ at or near 25 °C. The chemical shifts are given relative to tetramethylsilane (¹H, ¹³C) or nitromethane (¹⁴N, ¹⁵N) as external standards. Infrared (IR) spectra were recorded on a Perkin-Elmer Spectrum One FT-IR^[65] instrument as KBr pellets at 20 °C. Transmittance values are qualitatively described as “very strong” (vs), “strong” (s), “medium” (m) and “weak” (w). Raman spectra were recorded on a Perkin-Elmer Spectrum 2000R NIR FT-Raman instrument equipped with a Nd:YAG laser (1064 nm). The intensities are reported as percentages of the most intense peak and are given in parentheses. CHN elemental analyses for the less sensitive materials were performed with a Netsch Simultaneous Thermal Analyzer STA 429 and a ICP/AAS machine was used to measure the percentage of metal in the metal salts. Mass spectra were measured on a JEOL MStation JMS 700 machine.^[66] Melting points were determined by differential scanning calorimetry (Perkin-Elmer Pyris 6 DSC instrument, calibrated with standard pure indium and zinc). Measurements were performed at a heating rate of 2 or 5 °C min⁻¹ (unless otherwise specified) in closed aluminum sample pans with a 1 μm hole in the top for gas release under a nitrogen flow of 20 mL min⁻¹ with an empty identical aluminum sample pan as a reference.

Bomb Calorimetry. For the calorimetric measurements, a Parr 1356 bomb calorimeter (static jacket) equipped with a Parr 207A oxygen bomb for the combustion of highly energetic materials was used.^[67] A Parr 1755 printer, furnished with the Parr 1356 calorimeter, was used to produce a permanent record of all activities within the calorimeter. The samples (~200 mg each) were carefully mixed with ~800 mg analytical grade benzoic acid and pressed into pellets, which were subsequently burned in a 3.05 MPa atmosphere of pure oxygen. The experimentally determined heats of combustion were obtained as the averages of four single measurements with standard deviations calculated as a measure of experimental uncertainty. The calorimeter was calibrated by the combustion of certified benzoic acid in an oxygen atmosphere at a pressure of 3.05 MPa.

Synthesis of Ammonium 5-nitrotetrazolate (21a): Copper(II) sulfate pentahydrate (11.539 g, 46 mmol) and sodium nitrite (20.948 g, 304 mmol) were loaded into a 250 mL plastic beaker and dissolved in 60 mL distilled water. The mixture was cooled to 0-5 °C by means of an ice bath. Meanwhile, a solution of 5-amino-1H-tetrazole (8.626 g, 101 mmol) and a spatula point of copper (II) sulfate pentahydrate in

140 mL water and concentrated sulphuric acid (5.6 mL, 105 mmol) was prepared, and added to the previous solution drop-wise by means of a dropping-funnel. Addition resulted in vigorous gas evolution accompanied by the formation of a frothy turquoise precipitate of copper(II) 5-nitrotetrazolate. The suspension was stirred at room temperature for 10 min and reacted with neat sodium hydroxide (8.044 g, 200 mmol) for 1 h in a water bath at 70 °C and under vigorous stirring in order to convert the blue copper(II) hydroxide to black-brown copper(II) oxide. The copper(II) oxide was then filtered hot through previously washed celite and the celite was subsequently washed with 80 mL hot water yielding a pale yellow solution. 3.2 mL concentrated sulphuric acid were added to the distillate and this was stirred for 15 min with active charcoal when still warm. The greenish solution was decanted into a 500 mL extraction funnel and acidified by addition of further 3.2 mL concentrated sulphuric acid. The aqueous solution was extracted with ethylacetate (8x75 mL), this was dried over magnesium sulphate, reduced in volume using a rotatory evaporator to ~100 mL and placed in a wash bottle. Ammonia gas was carefully bubbled through the solution for ~2 min resulting in warming of the solvent and the precipitation of a yellow powder. The compound was then filtered, washed with ethylacetate and ether and left to air-dry. The (impure) crude product can be used without further purification. Recrystallization from 15 mL methanol yielded a first crop of the anhydrous compound (3.511 g, 27%) as slightly yellow platelets. A second crop of the material was obtained by slow evaporation of the solvent (2.800 g, 22%). Both crops were pure by elemental analysis and were combined (6.311 g, 49%). C₃H₂N₆O₂ (calc./found): C 23.37 / 23.42, H 1.31 / 1.43, N 54.55 / 54.83

Synthesis of Lithium 5-Nitro-2*H*-tetrazolate Trihydrate (22). *Method A:* **22** was synthesized according to Method A as described for **23** from 1.40 g (20.29 mmol) sodium nitrite, 0.74 g (2.96 mmol) copper(II) sulfate pentahydrate, 0.57 g (6.71 mmol) 5-amino-1*H*-tetrazole and a lithium hydroxide solution in 42% yield (0.49 g).

Method B: Neat lithium hydroxide (0.066 g, 2.76 mmol) was added to a solution of ammonium 5-nitro-2*H*-tetrazolate hemihydrate (0.39 g, 2.76 mmol) in 10 mL (wet) methanol under a stream of nitrogen. The initial suspension turned into a clear solution upon heating, which was stirred over 18 hours at reflux (ammoniac gas was evolved). At this point the solution was filtered hot under vacuum and the solvent was stripped using a rotatory evaporator yielding **22** as the trihydrated species. No further purification was necessary (0.45 g, 93%). Crystals of the compound suitable for X-ray analysis were obtained by dissolving **22** in ethylacetate and letting the solvent to slowly evaporate. DSC (5 °C min⁻¹, °C) ~69 (H₂O loss), ~270 (m.p. + dec.); Found: C, 6.7; H, 3.6; N, 39.7; Li, 4.0. CH₆N₅O₃Li requires C, 6.9; H, 3.5; N, 40.0; Li, 4.0%; Raman $\tilde{\nu}$ /cm⁻¹ 3300-3000(2) 1545(10) 1508(4) 1466(7) 1429(100) 1328(8) 1191(5) 1162(5) 1086(47) 1058(32) 839(6) 776(4) 544(3) 449(3) and 243(3); IR ν_{\max} (KBr)/cm⁻¹ 3341vs, 2867w, 2752w, 2484w, 2087w, 1666m, 1559vs, 1506m, 1468s, 1431s, 1405m, 1384m, 1327s, 1190m, 1161m, 1082w, 1057w, 1040m, 841s, 702s, 662s and 519s; δ_{H} (DMSO-*d*₆, 400.18 MHz, TMS) 3.51 (s, H₂O); δ_{C} (DMSO-*d*₆, 100.63 MHz, TMS) 169.2 (C-NO₂); δ_{14N} (DMSO-*d*₆, 28.89 MHz, TMS) +20 (2 N, $\nu_{\text{1/2}}$ ~430 Hz, N₂/3), -23 (1 N,

$\nu_{1/2}$ ~60 Hz, NO₂), -67 (2 N, $\nu_{1/2}$ ~400 Hz, N1/4); m/z (FAB⁺, xenon, 6 keV, m-NBA matrix) 114 ([NT]⁺, 100%) and 235 ([Li(NT)₂]⁺, 100).

Synthesis of Sodium 5-Nitro-2*H*-tetrazolate Dihydrate (23). *Method A:* 13.70 g (198.6 mmol) sodium nitrite and 7.24 g (29.0 mmol) copper(II) sulfate pentahydrate were dissolved in 40 mL water in a plastic beaker and cooled in a water/ice bath. A solution of 5.60 g (65.8 mmol) 5-amino-1*H*-tetrazole, a spatula tip of copper(II) sulfate pentahydrate and 3.6 mL (68.0 mmol) concentrated sulfuric acid in 80 mL water was added slowly via a dropping funnel under vigorous stirring. The dropping funnel was rinsed with a solution of 2.8 mL (53.0 mmol) concentrated sulfuric acid in 10 mL water. After 30 min. reaction time the precipitated copper(II) 5-nitro-2*H*-tetrazolate 5-nitrotetrazole salt CuH(NT)₃, which is **highly sensitive**, was carefully filtered through a suction filter under water jet vacuum and washed with a solution of 1.6 mL (30.0 mmol) of concentrated sulfuric acid in 32 mL water and thereafter with 32 mL water. The wet cake was carefully transferred to a plastic beaker containing 80 mL water and treated with 20% sodium hydroxide solution until pH >9, as determined by universal indicator paper. The slurry was heated to 70 °C for 1.5 hours and the brown/black precipitate (CuO) was filtrated hot through wet celite. The pH of the yellow filtrate was adjusted with diluted sulfuric acid to 3-4 giving a slightly green solution. Then, the solvent was carefully stripped under vacuum (20 mbar) at 60 °C. The yellow solid residue obtained was subjected to a *Saxhlet* extraction with 50 mL acetone over 3 hours. The slightly yellow acetone solution obtained after the extraction was cooled to -78 °C and the precipitated off-white powder was filtered through a suction filter and washed with diethyl ether yielding 3.51 g of **23**. The rest of the acetone solution was transferred to a plastic beaker and left to evaporate, leaving behind large crystals (suitable for X-ray analysis), which were washed with little cold acetone and thereafter with diethyl ether, yielding further 2.70 g product. Both crops proved to be pure by elemental analysis and that **23** formed as the dihydrated species (combined yield: 6.21 g, 55%).

Method B: **23** was synthesized according to Method B as described for **22** from 0.429 g (3.04 mmol) ammonium 5-nitro-2*H*-tetrazolate hemihydrate and 0.12 g (3.04 mmol) sodium hydroxide in 98% yield (0.52 g). DSC (5 °C min⁻¹, °C) ~75 (H₂O loss), ~200 (dec.); Found: C, 7.1; H, 2.3; N, 40.4; Na, 13.2. CH₄N₅O₄Na requires C, 6.9; H, 2.3; N, 40.5; Na, 13.3%; Raman $\tilde{\nu}$ /cm⁻¹ 3300-2900(2) 1555(12) 1452(7) 1419(100) 1321(6) 1173(4) 1068(62) 1053(24) 842(7) 774(5) 543(4) 456(3) 262(3) 150(4); IR ν_{\max} (KBr)/cm⁻¹ 3417s, 2862w, 2732w, 2468w, 2099w, 1690m, 1548vs, 1508w, 1474m, 1454s, 1421s, 1376w, 1321s, 1193m, 1172m, 1066m, 1041m, 841s, 665m, 602m and 539m; δ_{H} (DMSO-*d*₆, 400.18 MHz, TMS) 3.50 (s, H₂O); δ_{C} (DMSO-*d*₆, 100.63 MHz, TMS) 169.2 (C-NO₂); $\delta_{14\text{N}}$ (DMSO-*d*₆, 28.89 MHz, TMS) +21 (2 N, $\nu_{1/2}$ ~430 Hz, N2/3), -23 (1 N, $\nu_{1/2}$ ~60 Hz, NO₂), -60 (2 N, $\nu_{1/2}$ ~380 Hz, N1/4); $\delta_{15\text{N}}$ (DMSO-*d*₆, 28.89 MHz, TMS) +14 (2 N, s, N2/3), -25 (1 N, s, NO₂), -66 (2 N, s, N1/4); m/z (FAB⁺, xenon, 6 keV, m-NBA matrix) 114 ([NT]⁺, 100%) and 251 ([Na(NT)₂]⁺, 100).

Synthesis of Potassium 5-Nitro-2*H*-tetrazolate (24). *Method A:* **24** was synthesized according to Method A as described for **23** from 1.53 g (22.04 mmol) sodium nitrite, 0.80 g (3.22 mmol) copper(II)

sulfate pentahydrate, 0.62 g (7.30 mmol) 5-amino-1*H*-tetrazole and a potassium hydroxide solution. Before rotavaporating the water solution to dryness the reaction mixture was divided in two fractions, which were treated separately in order to diminish the hazards involved with the isolation of large amounts of the highly sensitive compound (0.53 g, 48%).

Method B: Alternatively, **24** was synthesized according to Method B as described for **22** from 0.22 g (1.59 mmol) ammonium 5-nitro-2*H*-tetrazolate hemihydrate and 0.09 g (1.59 mmol) potassium hydroxide. Due to the high sensitivity of the compound the solvent (methanol) was left to slowly evaporate in a plastic beaker glass (0.24 g, quant. yield). Single crystals of the potassium salt were obtained by slow evaporation of a concentrated solution of the compound in acetone. DSC (5 °C min⁻¹, °C) 168 (m.p.) ~195 (dec.); Found: K, 25.3. CN₅O₂K requires K, 25.5%; Raman $\tilde{\nu}$ /cm⁻¹ 1747(1) 1534(9) 1450(2) 1419(100) 1174(3) 1051(20) 1028(52) 843(6) 774(5) 543(2) 260(1) 150(5); IR ν_{max} (KBr)/cm⁻¹ 2691w, 2411w, 1991w, 1833w, 1586w, 1527s, 1483m, 1441s, 1435s, 1429s, 1404s, 1340w, 1307s, 1163m, 1152w, 1108vs, 1039w, 1020w, 997m, 836s, 757m, 723s, 691s, 668m, 524vs and 457w; δ_{C} (DMSO-*d*₆, 100.63 MHz, TMS) 169.0 (C-NO₂); δ_{I4N} (DMSO-*d*₆, 28.89 MHz, TMS) +20 (2 N, $\nu_{1/2}$ ~430 Hz, N2/3), -21 (1 N, $\nu_{1/2}$ ~60 Hz, NO₂), -66 (2 N, $\nu_{1/2}$ ~400 Hz, N1/4); m/z (FAB⁺, xenon, 6 keV, m-NBA matrix) 114 ([NT]⁺, 100%) and 267 ([K(NT)₂]⁺, 100).

Synthesis of Rubidium 5-Nitro-2*H*-tetrazolate (25). *Method A:* **25** was synthesized according to Method A as described for **23** from 1.31 g (18.87 mmol) sodium nitrite, 0.69 g (2.76 mmol) copper(II) sulfate pentahydrate, 0.53 g (6.25 mmol) 5-amino-1*H*-tetrazole and a rubidium hydroxide solution. Before rotavaporating the water solution to dryness the reaction mixture was divided in two fractions, which were treated separately in order to diminish the hazards involved with the isolation of large amounts of highly sensitive **25** (0.50 g, 41%).

Method B: Ammonium 5-nitro-2*H*-tetrazolate hemihydrate (0.27 g, 1.94 mmol) was dissolved in 10 mL ethanol and reacted with rubidium carbonate (0.22 g, 0.97 mmol) at reflux for 2 days and under exclusion of air. The white insoluble material (rubidium carbonate) was filtered hot and discarded. The product crystallized on slow cooling to room temperature and the yield could be increased by cooling the mother liquors in the fridge. **25** was filtered under gravity and washed with cold ethanol and ether (0.23 g, 59%). Suitable crystals for X-ray crystal structure analysis were obtained from cooling the mother liquors in the fridge. DSC (2 °C min⁻¹, °C) 146 (m.p.), ~192 (dec.); Found: Rb, 42.5. CN₅O₂Rb requires Rb, 42.8%; Raman $\tilde{\nu}$ /cm⁻¹ 1546(7) 1418(100) 1319(4) 1161(3) 1052(42) 1027(34) 842(6) 773(3) 542(3) 253(4) 156(3); IR ν_{max} (KBr)/cm⁻¹ 2854w, 2442w, 2025w, 1546s, 1507w, 1444s, 1417s, 1316s, 1171m, 1159m, 1108w, 1050m, 1025m, 838s, 668m and 528w; δ_{C} (DMSO-*d*₆, 100.63 MHz, TMS) 168.9 (C-NO₂); δ_{I4N} (DMSO-*d*₆, 28.89 MHz, TMS) +20 (2 N, $\nu_{1/2}$ ~430 Hz, N2/3), -22 (1 N, $\nu_{1/2}$ ~50 Hz, NO₂), -64 (2 N, $\nu_{1/2}$ ~400 Hz, N1/4); m/z (FAB⁺, xenon, 6 keV, m-NBA matrix) 114 ([NT]⁺, 100%) and 314 ([Rb(NT)₂]⁺, 100).

Synthesis of Cesium 5-Nitro-2*H*-tetrazolate (26). *Method A:* **26** was synthesized according to Method A as described for **23** from 1.15 g (16.68 mmol) sodium nitrite, 0.61 g (2.44 mmol) copper(II)

sulfate pentahydrate, 0.47 g (5.53 mmol) 5-amino-1*H*-tetrazole and a cesium hydroxide solution. Before rotavaporating the water solution to dryness the reaction mixture was divided in two fractions, which were treated separately in order to diminish the hazards involved with the isolation of large amounts of highly sensitive **26** (0.62 g, 46%).

Method B: Ammonium 5-nitro-2*H*-tetrazolate hemihydrate (0.25 g, 1.77 mmol) was dissolved in 10 mL ethanol before cesium carbonate (0.29 g, 0.88 mmol) was added to it to form a suspension. After 24 hours reaction time at reflux the reaction mixture formed a solution and the insoluble powdery material (cesium carbonate) was filtered when the solution was still hot and discarded. **26** precipitates immediately out of the hot reaction mixture when left to cool slowly to room temperature as feathery crystals, which were used to determine the crystal structure. The solvent was left to evaporate slowly at room temperature and the residue was **CAREFULLY(!)** recrystallized from the minimum amount of hot ethanol (0.38 g, 87%). DSC (2 °C min⁻¹, °C) 158 (m.p.), ~194 (dec.); Found: Cs, 53.6. CN₅O₂Cs requires Cs, 53.8%; Raman $\tilde{\nu}$ /cm⁻¹ 1530(16) 1419(100) 1316(11) 1056(51) 1031(28) 840(13) 733(10) 535(10) 230(9); IR ν_{max} (KBr)/cm⁻¹ 2723w, 2444w, 2055w, 1847w, 1633m, 1528s, 1505m, 1420s, 1384s, 1314s, 1170m, 1151m, 1105m, 1054m, 1030m, 1022w, 876w, 840s, 774w, 730w, 676m, 615w, 559w and 467w; δ_{C} (DMSO-*d*₆, 100.63 MHz, TMS) 168.7 (C-NO₂); δ_{14N} (DMSO-*d*₆, 28.89 MHz, TMS) +21 (2 N, $\nu_{\text{1/2}}$ = 410 Hz, N2/3), -22 (1 N, $\nu_{\text{1/2}}$ = 60 Hz, NO₂), -62 (2 N, $\nu_{\text{1/2}}$ = 380 Hz, N1/4); *m/z* (FAB-, xenon, 6 keV, m-NBA matrix) 114 ([NT]⁺, 100%) and 361 ([Cs(NT)₂]⁺, 100%).

Synthesis of Magnesium 5-Nitro-2*H*-tetrazolate Hexahydrate (27): Ammonium 5-nitro-2*H*-tetrazolate (0.314 g, 2.38 mmol) was dissolved in 10 mL water and reacted with magnesium hydroxide (0.069 g, 1.19 mmol). The reaction mixture was heated to reflux overnight and the initial suspension turned into a clear solution with a small amount of insoluble solid. The solution was filtered hot through a folded paper and the solvent was left to slowly evaporate to dryness in a plastic beaker. After this, the dry solid was carefully scratched out (plastic spatula!) of the beaker and weighed (0.411 g, 96%). The elemental analysis matches with that of the compound containing six molecules of crystal water. C₂H₁₂N₁₀O₁₀Mg (360.48 g mol⁻¹, calc./found): C 6.66 / 6.49, H 3.36 / 3.50, N 38.85 / 38.73; DSC (5 °C min⁻¹, °C): 119 (-H₂O), ~195 (m.p. + dec); *m/z* (FAB-, xenon, 6 keV, m-NBA matrix): 114.0 [NT]⁺; ¹H NMR (DMSO-*d*₆, 400.18 MHz, 25 °C, TMS) δ /ppm: 3.53 (s, H₂O); ¹³C{¹H} NMR (DMSO-*d*₆, 100.63 MHz, 25 °C, TMS) δ /ppm: 168.8 (C-NO₂); ¹⁴N NMR (DMSO-*d*₆, 28.89 MHz, 25 °C, TMS) δ /ppm: +23 (2N, $\nu_{\text{1/2}}$ ~420 Hz, N2/3), -23 (1N, $\nu_{\text{1/2}}$ ~65 Hz, NO₂), -61 (2N, $\nu_{\text{1/2}}$ ~400 Hz, N1/4); Raman $\tilde{\nu}$ / cm⁻¹ (rel. int.): 1545(10) 1424(100) 1321(7) 1179(5) 1066(52) 1057(31) 842(8) 817(2) 775(4) 627(2) 543(5) 455(3) 251(5); IR $\tilde{\nu}$ / cm⁻¹ (KBr, rel. int.): 3633(s) 3588(s) 3546(s) 3379(s) 2852(w) 2739(w) 2476(w) 2242(w) 2104(w) 1873(w) 1662(w) 1543(s) 1507(w) 1452(s) 1427(s) 1384(w) 1321(s) 1189(w) 1178(w) 1070(w) 1060(m) 1040(w) 843(m) 671(m).

Synthesis of Calcium 5-Nitro-2*H*-tetrazolate Hexahydrate (28): Calcium hydroxide (0.072 g, 0.97 mmol) was suspended in 10 mL ethanol and reacted with anhydrous ammonium 5-nitro-2*H*-tetrazolate

(0.257 g, 1.95 mmol). The suspension was reacted overnight at reflux and filtered hot into a plastic beaker. The solvent was left to evaporate and the solid formed was carefully scratched out (plastic spatula!!) onto a piece of paper. No further purification was needed (0.377 g, 93%). $\text{C}_2\text{H}_{12}\text{N}_{10}\text{O}_{10}\text{Ca}$ (376.26 g mol⁻¹, calc./found): C 6.38 / 6.50, H 3.21 / 3.19, N 37.23 / 36.94; DSC (5 °C min⁻¹, °C): 120 (-H₂O), ~180 (m.p. + dec); m/z (FAB-, xenon, 6 keV, m-NBA matrix): 114.0 [NT]⁺; ¹H NMR (DMSO-*d*₆, 400.18 MHz, 25 °C, TMS) δ/ppm: 3.43 (s, H₂O); ¹³C{¹H} NMR (DMSO-*d*₆, 100.63 MHz, 25 °C, TMS) δ/ppm: 169.2 (C-NO₂); ¹⁴N NMR (DMSO-*d*₆, 28.89 MHz, 25 °C, TMS) δ/ppm: +20 (2N, *ν*₂ ~420 Hz, N2/3), -22 (1N, *ν*₂ ~60 Hz, NO₂), -65 (2N, *ν*₂ ~390 Hz, N1/4); Raman $\tilde{\nu}$ / cm⁻¹ (rel. int.): 1550(14) 1426(100) 1323(10) 1195(8) 1070(38) 1062(52) 1038(13) 842(12) 774(8) 547(7) 460(7) 266(8); IR $\tilde{\nu}$ / cm⁻¹ (KBr, rel. int.): 3407(vs) 2480(w) 2237(w) 1643(m) 1549(vs) 1507(w) 1448(s) 1426(s) 1322(s) 1189(w) 1062(w) 1037(w) 842(s) 669(m) 594(m).

Synthesis of Strontium 5-Nitro-2*H*-tetrazolate Pentahydrate (29): A solution of ammonium 5-nitro-2*H*-tetrazolate (0.265 g, 2.01 mmol) in 10 mL ethanol was reacted with strontium hydroxide octahydrate (0.267 g, 1.00 mmol) overnight at reflux of the solvent. The solution was filtered when still hot and the solvent was left to slowly evaporate in a plastic shell leaving behind the solid compound, which was pure by elemental analysis (0.487 g, 95%). $\text{C}_2\text{H}_{10}\text{N}_{10}\text{O}_9\text{Sr}$ (405.78 g mol⁻¹, calc./found): C 5.92 / 6.13, H 2.48 / 2.55, N 34.52 / 34.76; DSC (2 °C min⁻¹, °C): 104 (H₂O loss), ~210 (dec.); m/z (FAB-, xenon, 6 keV, m-NBA matrix): 114.0 [NT]⁺, 429.7 [Sr(NT)₃]⁺; ¹H NMR (DMSO-*d*₆, 400.18 MHz, 25 °C, TMS) δ/ppm: 3.37 (s, H₂O); ¹³C{¹H} NMR (DMSO-*d*₆, 100.63 MHz, 25 °C, TMS) δ/ppm: 169.3 (C-NO₂); ¹⁴N NMR (DMSO-*d*₆, 28.89 MHz, 25 °C, TMS) δ/ppm: +21 (2N, *ν*₂ ~420 Hz, N2/3), -22 (1N, *ν*₂ ~60 Hz, NO₂), -63 (2N, *ν*₂ ~400 Hz, N1/4); Raman $\tilde{\nu}$ / cm⁻¹ (rel. int.): 3400-2800(2) 1554(11) 1432(100) 1325(13) 1064(48) 1039(37) 848(16) 774(4) 551(5) 278(3); IR $\tilde{\nu}$ / cm⁻¹ (KBr, rel. int.): 3421(s) 2856(w) 2465(w) 2067(w) 1883(w) 1630(m) 1548(vs) 1505(m) 1471(s) 1454(s) 1426(s) 1322(s) 1183(m) 1062(m) 1033(w) 846(s) 665(m) 569(s).

Synthesis of Barium 5-Nitro-2*H*-tetrazolate Pentahydrate (30): Barium hydroxide octahydrate (0.167 g, 0.53 mmol) was suspended in 5 mL ethanol and reacted with a solution of ammonium 5-nitro-2*H*-tetrazolate (0.140 g, 1.06 mmol) in 5 mL ethanol by refluxing overnight. After this time the insoluble solid was filtered and discarded and the solution was left to stand yielding the pure compound as a white powder (0.179 g, 93%). $\text{C}_2\text{H}_{10}\text{N}_{10}\text{O}_9\text{Ba}$ (455.49 g mol⁻¹, calc./found): C 5.27 / 5.47, H 2.21 / 2.33, N 30.75 / 30.53; DSC (2 °C min⁻¹, °C): 129, 145 (H₂O loss), ~235 (dec.); m/z (FAB-, xenon, 6 keV, m-NBA matrix): 114.0 [NT]⁺, 479.5 [Ba(NT)₃]⁺; ¹H NMR (DMSO-*d*₆, 400.18 MHz, 25 °C, TMS) δ/ppm: 3.33 (s, H₂O); ¹³C{¹H} NMR (DMSO-*d*₆, 100.63 MHz, 25 °C, TMS) δ/ppm: 168.7 (C-NO₂); ¹⁴N NMR (DMSO-*d*₆, 28.89 MHz, 25 °C, TMS) δ/ppm: +20 (2N, *ν*₂ ~420 Hz, N2/3), -22 (1N, *ν*₂ ~60 Hz, NO₂), -64 (2N, *ν*₂ ~390 Hz, N1/4); Raman $\tilde{\nu}$ / cm⁻¹ (rel. int.): 3300-2900(2) 1544(10) 1425(100) 1322(9) 1173(2) 1061(47) 1038(35) 845(8) 774(6) 546(5) 410(3) 251(3) 147(3); IR $\tilde{\nu}$ / cm⁻¹ (KBr, rel. int.): 3221(vs) 2962(s) 2923(s) 2849(m) 2739(w) 2456(w) 2190(w) 2058(w) 1876(w) 1686(vs) 1629(s) 1546(vs) 1504(m) 1451(s)

1424(s) 1378(m) 1319(s) 1179(s) 1152(m) 1129(m) 1060(s) 1033(m) 951(s) 884(vs) 772(m) 665(m) 638(m) 534(m).

Synthesis of 5-Nitro-2*H*-tetrazole (31): Anhydrous ammonium 5-nitro-2*H*-tetrazolate (0.438 g, 3.316 mmol) and potassium hydroxide (0.186 g, 3.315 mmol) were dissolved in 3.7 mL water. The solution was stirred at reflux until no more ammoniac gas evolved. At this point, the reaction mixture was cooled by means of an ice-bath and cold ~25% sulfuric acid (2 mL) was added dropwise using a plastic syringe. The solution was then extracted with ether (4 x 6 mL) and the ether extracts were combined and washed to remove the excess of acid with water (6 mL). The organic phase was then dried with magnesium sulfate and filtered and the solvent was stripped under high vacuum (~10⁻³ mbar) yielding the pure product as a slightly yellow semicrystalline solid (0.267 g, 72%), which was **carefully** (!) scratched out using a plastic spatula and analyzed. CHN₅O₂ (115.05 g mol⁻¹) should be: C 10.44 / -, H 0.88 / -, N 60.87 / -; DSC (5 °C min⁻¹, °C): 99 (m.p.), >120 (dec.); m/z (FAB⁺, xenon, 6 keV, m-NBA matrix): 113.9 (100, CN₅O₂⁺); ¹H NMR (DMSO-d₆, 400.18 MHz, 25°C, TMS) δ/ppm: 6.29 (1H, NH); ¹³C{¹H} NMR (DMSO-d₆, 100.63 MHz, 25°C, TMS) δ/ppm: 168.4 (1C, C-NO₂); ¹⁴N NMR (DMSO-d₆, 40.55 MHz, 25 °C, MeNO₂) δ/ppm: +14 (2 N, *ν*₂ ~300 Hz, N3/4), -24 (1 N, *ν*₂ ~60 Hz, NO₂), -66 (2 N, *ν*₂ ~320 Hz, N2/5); ¹⁵N NMR (DMSO-d₆, 40.55 MHz, 25 °C, MeNO₂) δ/ppm: +19.6 (2 N, s, N3/N4), -29.8 (1 N, s, NO₂), -69.6 (2 N, s, N2/5); Raman $\tilde{\nu}$ / cm⁻¹ (rel. int.): 3316(2) 3261(2) 1572(14) 1492(9) 1446(100) 1433(90) 1396(15) 1358(7) 1317(13) 1200(13) 1186(14) 1142(30) 1094(42) 1069(13) 1043(11) 1027(26) 837(22) 775(13) 736(4) 592(3) 532(11) 444(22) 256(17) 240(16) 154(6); IR $\tilde{\nu}$ / cm⁻¹ (KBr, rel. int.): 3443(s) 2013(w) 1629(m) 1565(vs) 1443(m) 1401(m) 1320(s) 1262(vw) 1192(w) 1103(w) 1047(m) 1022(m) 840(s) 666(w) 534(vw).

3.9 References

- [1] a) T. M. Klapötke in *Moderne Anorganische Chemie*, E. Riedel (Ed.), 2nd ed., Walter de Gruyter, Berlin/New York, **2003**, 95–100. b) T. M. Klapötke in *High Energy Density Materials*, T. M. Klapötke (Ed.), Springer, Berlin/Heidelberg, **2007**, 85–122.
- [2] a) H. Xue, S. W. Arritt, B. Twamley, J. M. Shreeve, *Inorg. Chem.*, **2004**, *43*, 7972–7977. b) H. Xue, Y. Gao, B. Twamley, J. M. Shreeve, *Chem. Mater.* **2005**, *17*, 191–198. c) Y. Gao, B. Twamley, J. M. Shreeve, *Chem. Eur. J.* **2006**, *12*, 9010–9018. d) J. C. Gálvez-Ruiz, G. Holl, K. Karaghiosoff, T. M. Klapötke, K. Löhnwitz, P. Mayer, H. Nöth, K. Polborn, C. J. Rohbogner, M. Suter, J. J. Weigand, *Inorg. Chem.* **2005**, *44*(12), 4237–4253. e) T. M. Klapötke, C. Miró Sabaté, *Z. Anorg. Allg. Chem.*, **2007**, *633*, 2671–2677. f) C. Darwich, T. M. Klapötke, C. Miró Sabaté, *Chem. Eur. J.*, **2008**, *14*, 5756–5771.
- [3] T. M. Klapötke, C. Miró Sabaté, J. M. Welch, *J. Chem. Soc. Dalton Trans.*, **2008**, submitted.
- [4] a) M. H. V. Huynh, M. D. Coburn, T. J. Meyer, M. Wetzler, *Proc. Natl. Acad. Sci. U. S. A.*, **2006**, *103*(27), 10322–10327. b) M. H. V. Huynh, M. A. Hiskey, T. J. Meyer, M. Wetzler, *Proc. Natl. Acad. Sci. U. S. A.*, **2006**, *103*(14), 5409–5412.
- [5] J. Akhavan in *The Chemistry of Explosives*, 2nd ed. RSC Paperbacks: Cambridge, UK, **2004**.
- [6] T. M. Klapötke, P. Mayer, C. Miró Sabaté, J. M. Welch, N. Wiegand, *Inorg. Chem.*, **2008**, *47*(13), 6014–6027.
- [7] H. Xue, H. Gao, B. Twamley, J. M. Shreeve, *Eur. J. Inorg. Chem.*, **2006**, *15*, 2959–2965.
- [8] C. Darwich, T. M. Klapötke, J. M. Welch, M. Sucasca, *Propellants, Explos., Pyrotech.*, **2007**, *32*, 235–243.
- [9] T. M. Klapötke, K. Karaghiosoff, P. Mayer, A. Penger, J. M. Welch, *Propellants, Explos., Pyrotech.*, **2006**, *31*, 188–195.
- [10] H. Xue, Y. Gao, B. Twamley, J. M. Shreeve, J. M., *Inorg. Chem.*, **2005**, *44*, 5068–5072.
- [11] H. Xue, J. M. Shreeve, *Adv. Mater. (Weinheim, Ger.)*, **2005**, *17*, 2142–2146.
- [12] H. Xue, B. Twamley, J. M. Shreeve, *Inorg. Chem.*, **2005**, *44*, 7009–7013.
- [13] E. von Herz, US Patent 2066954, **1937**.
- [14] P. N. Gaponik, O. A. Ivashkevich, V. A. Krasitskii, A. A. Tuzik, A. I. Lesnikovich, *Russ. J. Org. Chem.*, **2002**, *72*(9), 1457–1464.
- [15] W. H. Gilligan, US Patent 4093623, **1977**.
- [16] W. H. Gilligan, M. J. Kamlet, Report NSWC/WOL/TR 76–146; White Oak Laboratory: Silver Spring, MD, USA, **1976**, 1–15.

- [17] G. I. Koldobskii, D. S. Soldatenko, E. S. Gerasimova, N. R. Khokhryakova, M. Shcherbinin, V. P. Lebedev, V. A. Ostrovskii, *Russ. J. Org. Chem. (Engl. Trans.)*, **1997**, *33*, 1771–1783.
- [18] V. V. Semenov, B. I. Ugrak, S. A. Shevelev, M. I. Kanishchev, A. T. Baryshnikov, A. A. Fainzil'berg, *Russ. Chem. Bull.*, **1991**, *40*, 1658–1666.
- [19] R. J. Spear, P. P. Elischer, *Aust. J. Chem.*, **1982**, *35*(1), 1–13.
- [20] T. M. Becker, J. A. Krause-Bauer, C. L. Homrighausen, M. Orchin, *Polyhedron*, **1999**, *18*(19), 2563–2571.
- [21] J. Charalambous, G. C. Georgiou, K. Henrick, L. R. Bates, M. Healey, *Acta Crystallogr.*, **1987**, *C43*, 659–661.
- [22] X. Jin, M. Shao, H. Huang, J. Wang, Y. Zhu, *Huaxue Tongbao*, **1982**, 336–337.
- [23] B. Morosin, R. G. Dunn, R. Assink, T. M. Massis, J. Fronabarger, E. N. Duesler, *Acta Crystallogr.*, **1997**, *C53*, 1609–1611.
- [24] a) V. A. Ostrovskii, G. I. Koldobskii, *Russ. Khim. Zh.*, **1997**, *41*(2), 84–98. b) Y. L. Peng, C. W. Wong, *Huoyao Jishu*, **1997**, *13*(1), 25–38.
- [25] V. Ernst, T. M. Klapötke, J. Stierstorfer, *Z. Anorg. Allg. Chem.*, **2007**, *633*, 879–887.
- [26] A. Hammerl, G. Holl, T. M. Klapötke, P. Mayer, H. Nöth, H. Piotrowski, M. Warchhold, *Eur. J. Inorg. Chem.*, **2002**, *4*, 834–845.
- [27] a) Oxford Diffraction. ABSPACK, CrysAlis CCD and CrysAlis RED. Versions 1.171. Oxford Diffraction Ltd, Abingdon (England), **2006**. b) Programs for Crystal Structure Analysis (Release 97-2). G. M. Sheldrick, Institut für Anorganische Chemie, Tammanstrasse 4, D-3400 Göttingen, Germany, **1998**. c) A. Altomare, M. C. Burla, M. Camalli, G. L. Cascarano, C. Giacovazzo, A. Guagliardi, A. G. G. Moliterni, G. Polidori, R. Spagna, *J. Appl. Crystallogr.* **1999**, *32*, 115–119.
- [28] I. D. Brown, *Acta Crystallogr.*, **1988**, *B44*, 545–553.
- [29] a) E. O. John, R. D. Willett, B. Scott, R. L. Kirchmeier, J. M. Shreeve, *Inorg. Chem.* **1989**, *28*(5), 893–897. b) S. Bernhardt, M.-J. Crawford, T. M. Klapötke, H. Radies, *Proceedings of the 9th Seminar on New Trends in Research of Energetic Materials*, Pardubice (Czech Republic), **2007**. c) H. P. H. Arp, A. Decken, J. Passmore, D. J. Wood, *Inorg. Chem.*, **2000**, *39*(9), 1840–1848; d) E. J. Graeber, B. Morosin, *Acta Crystallogr.*, **1983**, *C39*, 567–570.
- [30] J. Bernstein, R. E. Davis, L. Shimoni, N.-L. Chang, *Angew. Chem. Int. Ed. Engl.*, **1995**, *34*, 1555–1573.
- [31] http://www.ccdc.cam.ac.uk/free_services/free_downloads.
- [32] D. D. Bray, J. G. White, *Acta Crystallogr., Sect. B* **1979**, *35*, 3089–3091.

- [33] J. Stierstorfer, T. M. Klapötke, A. Hammerl, B. Chapman, *Z. Anorg. Allg. Chem.* **2008**, *634*, 1051–1057.
- [34] Impact: Insensitive >40 J, less sensitive ≥ 35 J, sensitive ≥ 4 J, very sensitive ≤ 3 J; friction: Insensitive >360 N, less sensitive = 360 N, sensitive <360 N a. >80 N, very sensitive ≤ 80 N, extreme sensitive ≤ 10 N; According to the UN Recommendations on the Transport of Dangerous Goods (+) indicates: not safe for transport.
- [35] <http://www.bam.de>
- [36] T. M. Klapötke, C. M. Rienäcker, *Propellants, Explos., Pyrotech.*, **2001**, *26*, 43–47.
- [37] Oxygen balance for a compound with the formula $C_xH_yO_zM_t$: $\Omega(\%) = -1600/MW (2x + y/2 + t - z)$; M = metal and MW = molecular weight.
- [38] a) L. R. Bates, *Proceedings of the 13th Symposium on Explosives and Pyrotechnics*, Waltham Abbey (UK), **1986**; b) M. A. Schroeder, R. A. Henry, Ballistic Research Laboratory Technical Report AD-A 107 288, Aberdeen (US), **1981**; c) C. M. Tarver, T. C. Goodale, M. Cowperthwaite, M. E. Hill, Stanford Research Institute Interim Technical Report AD-A 044 714, California (US), **1977**.
- [39] J. Köhler, R. Mayer in *Explosivstoffe*, ed. Wiley-VCH, Weinheim, Germany, 9th edn., **1998**.
- [40] **23** did not detonate at the maximum setting in the friction test (360 N) but only decomposed.
- [41] http://en.wikipedia.org/wiki/Primary_explosive.
- [42] T. M. Klapötke, H. Radies, J. Stierstorfer, *Z. Naturforsch.*, **2007**, *B62b*, 1343–1352.
- [43] T. M. Klapötke, J. Stierstorfer, *Helv. Chim. Acta*, **2007**, *90*, 2132–2150.
- [44] a) M. J. Leleu, *Cahiers Notes Document.*, **1978**, *92*, 445–449; b) F. D. Marsh, *J. Org. Chem.*, **1972**, *37*(19), 2966–2969.
- [45] A. Hammerl, T. M. Klapötke, H. Nöth, M. Warchhold, G. Holl, *Propellants, Explos., Pyrotech.*, **2003**, *28*(4), 165–173.
- [46] C. Zhao, X. Heming, Y. Shulin, *Chem. Phys.*, **1999**, *250*, 243–248 and references therein.
- [47] G. W. C. Taylor, J. M. Jenkins, *3rd Symposium on Chemical Problems Connected with the Stability of Explosives*, Ystad, **1973**.
- [48] *NIST Chemistry WebBook*, **2003**, www version: <http://webbook.nist.gov/chemistry>.
- [49] Gaussian 03, Revision B0.4, M. J. Frisch, G. W. Trucks, H. B. Schlegel, G. E. Scuseria, M. A. Robb, J. R. Cheeseman, J. A. Montgomery, Jr., T. Vreven, K. N. Kudin, J. C. Burant, J. M. Millam, S. S. Iyengar, J. Tomasi, V. Barone, B. Mennucci, M. Cossi, G. Scalmani, N. Rega, G. A. Petersson, H. Nakatsuji, M. Hada, M. Ehara, K. Toyota, R. Fukuda, J. Hasegawa, M. Ishida, T. Nakajima, Y. Honda, O. Kitao, H. Nakai, M. Klene, X. Li, J. E. Knox, H. P. Hratchian, J. B. Cross, C. Adamo, J. Jaramillo, R. Gomperts, R. E. Stratmann, O. Yazyev, A. J. Austin, R. Cammi, C. Pomelli, J. W. Ochterski, P. Y. Ayala, K. Morokuma, G. A. Voth, P. Salvador, J. J. Dannenberg, V. G. Zakrzewski, S.

Dapprich, A. D. Daniels, M. C. Strain, O. Farkas, D. K. Malick, A. D. Rabuck, K. Raghavachari, J. B. Foresman, J. V. Ortiz, Q. Cui, A. G. Baboul, S. Clifford, J. Cioslowski, B. B. Stefanov, G. Liu, A. Liashenko, P. Piskorz, I. Komaromi, R. L. Martin, D. J. Fox, T. Keith, M. A. Al-Laham, C. Y. Peng, A. Nanayakkara, M. Challacombe, P. M. W. Gill, B. Johnson, W. Chen, M. W. Wong, C. Gonzalez, J. A. Pople, Gaussian, Inc., Pittsburgh PA, **2004**.

[50] J. W. Ochterski, G. A. Petersson, J. A. Montgomery Jr., *J. Chem. Phys.* **1996**, *104*, 2598.

[51] J. A. Montgomery Jr., M. J. Frisch, J. W. Ochterski, G. A. Petersson, *J. Chem. Phys.* **2000**, *112*, 6532.

[52] a) E. F. Byrd, B. M. Rice, *J. Phys. Chem.* **2006**, *110*(3), 1005–1013. (b) B. M. Rice, S. V. Pai, J. Hare, *Combust. Flame* **1999**, *118*(3), 445–458.

[53] L. A. Curtiss, K. Raghavachari, P. C. Redfern, J. A. Pople, *J. Chem. Phys.* **1997**, *106*(3), 1063.

[54] P. J. Linstrom, W. G. Mallard, NIST Chemistry WebBook, NIST Standard Reference Database Number 69, June **2005**, National Institute of Standards and Technology, Gaithersburg MD, 20899.

[55] M. S. Westwell, M. S. Searle, D. J. Wales, D. H. Williams, *J. Am. Chem. Soc.* **1995**, *117*, 5013–5015.

[56] H. D. B. Jenkins, H. K. Roobottom, J. Passmore, L. Glasser, *Inorg. Chem.* **1999**, *38*(16), 3609–3620.

[57] H. D. B. Jenkins, D. Tudela, L. Glasser, *Inorg. Chem.* **2002**, *41*(9), 2364–2367.

[58] M. Sućeska, *Propell. Explos. Pyrotech.* **1991**, *16*, 197–202.

[59] a) M. Sućeska, *Materials Science Forum* **2004**, *465–466*, 325–330. b) M. Sućeska, *Propellants, Explos., Pyrotech.* **1999**, *24*, 280–285.

[60] M. L. Hobbs, M. R. Baer: *Proc. of the 10th Symp. (International) on Detonation*, ONR 33395-12, Boston, MA, July 12–16, **1993**, p. 409.

[61] A. Hammerl, M. A. Hiskey, G. Holl, T. M. Klapötke, K. Polborn, J. Stierstorfer, J. J. Weigand, *Chem. Mater.* **2005**, *17*, 3784.

[62] T. M. Klapötke, C. Miró Sabaté, *Chem. Mater.*, **2008**, *20*(5), 1750–1763.

[63] T. M. Klapötke, J. Stierstorfer, *Phys. Chem. Chem. Phys.* **2008**, ASAP.

[64] *US Pat.*, 4 093 623, **1978**.

[65] <http://www.perkinelmer.com>.

[66] a) <http://www.jeol.com/tabid/96/Default.aspx>; b) <http://www.jeolusa.com/Desktop/Modules/Bring2mind/DMX/Download.aspx?EntryId=331&PortalId=2&DownloadMethod=attachment>; c) <http://www.jeoleuro.com/instr/mass/mass.htm>.

[67] <http://www.parrinst.com>.

CHAPTER IV

1,2,4-TRIAZOLIUM CATION-BASED ENERGETIC SALTS

4.1 Introduction

4.1.1 General

As pointed out earlier, tetrazole-based energetic materials seem to show the best compromise between high heats of formation and good thermal stabilities. On the other hand, however, the presence of one carbon atom in the ring limits the introduction of functionality, whereas triazole-based energetic materials can be much more readily derivatized, for example, to the dinitro,^[1] diamino^[2] or diazido^[3] compounds and the presence of two carbon atoms allows the easy introduction and/or combination of two of the aforementioned highly endothermic functional groups, allowing the formation of compounds with high positive heats of formation (i.e., high performances). Among others, triazolium-based energetic materials have found use as high explosives,^[4] gas generators^[5] and ionic liquids.^[6] The latter may possibly find application in melt-casting explosives.

Child et al.^[7a] were the first to synthesize 3,4,5-triamino-1,2,4-triazole (guanazine, **Gz**, **33**) (Figure 4.1) by refluxing dimethylcyanamide with hydrazine hydrate. Recently, we discovered the potential of **33**, which has a nitrogen content of ~73.6%, for the formation of nitrogen-rich energetic salts with anions such as 5-nitrotetrazolate (**GzNT**, **34**),^[7b] picrate (**GzPic**, **35**) and 5,5'-azotetrazolate (**GzZT**, **36**).^[8] Protonation of the triazole ring, proceeded unambiguously on N2/N3 from the triazole ring, rather than on the N-NH₂ or one of the C-NH₂ groups, as verified by X-ray diffraction studies (see section 4.5 *Molecular Structures*). These are new examples of guanazinium salts, in addition to the already reported dinitramide (**GzDN**, **37**), perchlorate (**GzClO₄**, **38**) and nitrate (**GzNO₃**, **39**) salts by Drake et al.^[9] However, the interesting azide salt (**GzN₃**, **40**) has not been reported so far.

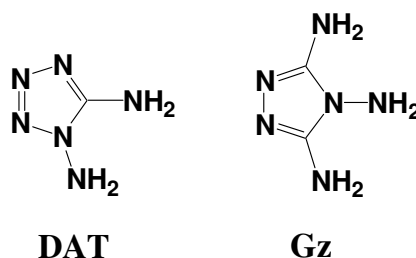


Figure 4.1 Structures of 1,5-diamino-1H-tetrazole (**32**) and 3,4,5-triamino-1,2,4-triazole (**33**).

Our experience in the laboratory indicates that due to the higher acidity of the guanazinium cation (Gz^+) in respect to hydrazoic acid, **40** dissociates readily in solution to **33** and HN_3 . With this in mind, we synthesized **33**^[7] and quaternized it with methyl iodide forming 1-methyl-3,4,5-triamino-1,2,4-triazolium iodide (**MeGzI**, **41**), which had not been described in the literature prior to our studies,^[10] and surprisingly, had not been considered for the synthesis of energetic salts. We report here on the use of **41** as a useful starting material for the synthesis of energetic salts. The presence of the methyl group instead of a proton, should not only allow to obtain the highly endothermic azide compound, but also increase the thermal stability of the new materials, at the same time that having reasonably high nitrogen-contents, necessary for high heats of formations and environmentally-friendly decomposition products. The presence of the three amino-groups should lead to the formation of a significant hydrogen-bonded networks, which should result in high densities. Therefore, we decided to screen salt-based derivatives of methylguanazine with oxidizing anions such as nitrate (**MeGzNO₃**, **43**), perchlorate (**MeGzClO₄**, **44**) and dinitramide (**MeGzDN**, **47**), as well as with nitrogen-rich anions such as azide (**MeGzN₃**, **42**), 5,5'-azotetrazolate (**MeGzZT**, **45**) and 5-nitrotetrazolate (**MeGzNT**, **46**). The combination of the MeG^+ cation with the abovementioned oxidizing anions yields **43**, **44** and **47**, that, with oxygen balances (Ω) between -44 (**47**) and -63% (**43**), have better values than, for example, TNT ($\Omega = -74\%$). The use of azide or 5,5'-azotetrazolate as the counteranion should give compounds with high positive heats of formation due to the nitrogen catenation, whereas the 5-nitrotetrazolate salt, should not only introduce endothermicity but also improve the oxygen balance ($\Omega = -69\%$). However, the prediction of the crystal packing is often troublesome due to the multiplicity of structural possibilities and the lack of directionality of the intermolecular interactions. In consequence, it is important to examine closely the structural details, which may account for packing effects and, in last instance, for the properties of the compounds.

4.1.2 Relationship between 3,4,5-triamino-1,2,4-triazole and 1,5-diamino-1*H*-tetrazole

1,5-Diamino-1*H*-tetrazole (**DAT**, **32**) (Figure 4.1) counts under the nitrogen-richest compounds among organic substances (84.0% N). Much chemistry has been done around this compound in the field of energetic materials.^[11-14] Unfortunately, regardless of the many synthesis described in the literature, they all suffer of several drawbacks. Direct amination of sodium 5-aminotetrazolate with hydroxylamine-*O*-sulfonic acid (**HOSA**, **48**) yields a mixture of the two regioisomers in a very low isolated yield.^[15] The yield can be increased by reaction of thiosemicarbazide (**TScz**, **49**) with lead(II) oxide and sodium azide,^[16] however, this procedure suffers of the formation of large amounts of highly sensitive lead(II) azide as the by-product of the reaction. Recently, Klapötke et

al. reported an improved method to yield the compound starting from diaminoguanidinium chloride (**DAGCl**, **50**),^[11] however, the reaction conditions need to be perfectly well controlled otherwise formation of a metal 5-azido-1*H*-tetrazolate takes place, which makes the procedure extremely hazardous due to the high sensitivity of the compound. Thus, an improved synthesis is still imperative. Recent efforts in our research group have concentrated in using “improved” aminating reagents such as 2,4-dinitro-*O*-phenyloxyphtalimide (**DNPP**, **51**) (Figure 4.2) and research is currently underway.

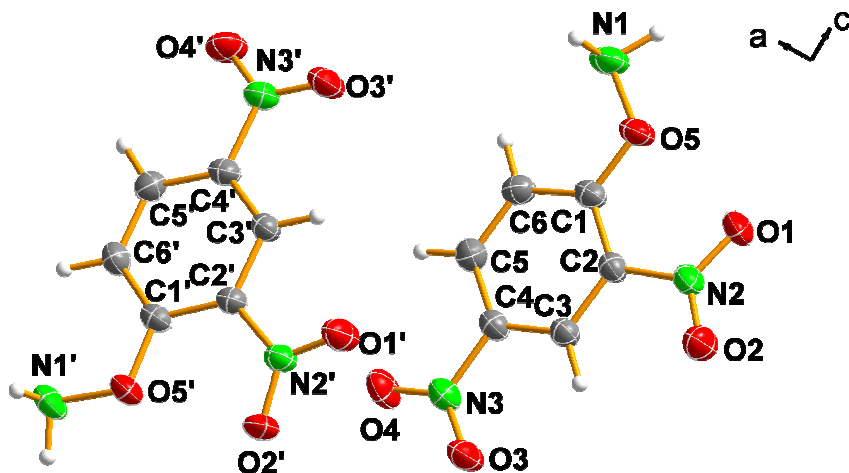
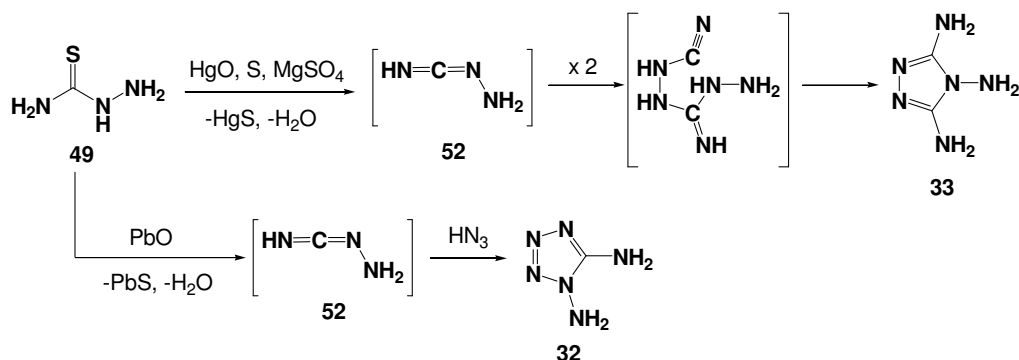


Figure 4.2 Asymmetric unit of 2,4-dinitro-*O*-phenyloxyphtalimide (**51**).

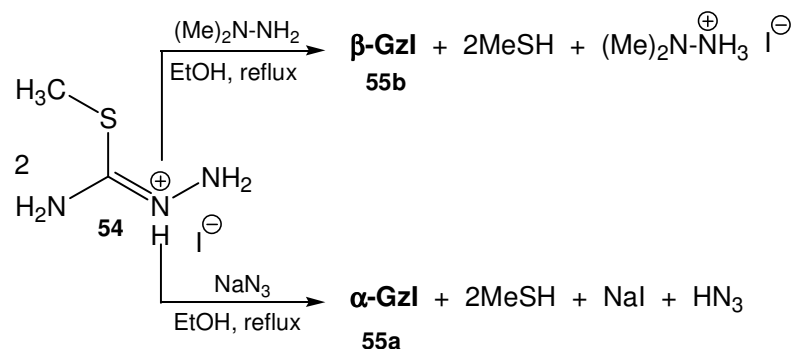
32 and **33** are related to each other in that they can be synthesized by essentially the same reaction. The procedure reported by Gaponik et al. using lead(II) oxide yields **32**, however, when thiosemicarbazide is reacted with mercury(II) oxide, sulfur and magnesium sulphate in dry acetone, diimide (**DI**, **52**) dimerizes to form guanazine according to Scheme 4.1.



Scheme 4.1 Synthesis of **32** and **33** from thiosemicarbazide.

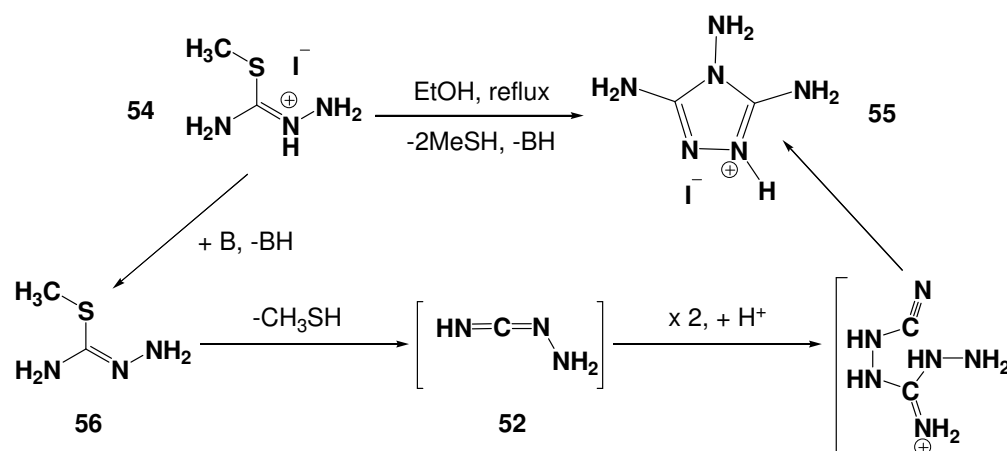
4.2. Synthesis of 3,4,5-triamino-1,2,4-triazolium Halogenides

Because halogenide salts are useful transfer reagents of energetic cations by methathesis reactions (i.e., precipitation of a silver halide), the guanazinium cation (Gz^+) was generated by reaction of dimethylcyanamide with hydrazine hydrate and acid treatment with hydrobromic acid^[8] yielding the bromide salt (**GzBr**, **53**). In analogy to the method using highly toxic HgO (see Scheme 4.1) here we showed that S-methylthiosemicarbazide hydroiodide (**MeTSczI**, **54**) can be deprotonated by weak bases. In the present study, depending on the base and experimental conditions used, two polymorphs of the iodide salt (α and β) were formed, which were distinguished by their molecular structure, vibrational spectra and difference in melting point (measured by DSC). The α phase (α -**GzI**, **55a**) was formed when sodium azide was used as the base in refluxing ethanol (see Scheme 4.2). After recrystallization from the same solvent, **55a** crystallized in a monoclinic crystal system, space-group $C2/c$. When 1,1-dimethylhydrazine was used as the base in ethanol, X-ray analysis revealed a polymorph structure of **55** (β -**GzI**, **55b**) crystallizing in an orthorhombic crystal system, space-group $Aba2$. Further detail about the structure of the compounds are given in the corresponding section. **55b** was alternatively also obtained by treatment of guanazine with hydroiodic acid (see 4.8 *Experimental Section*).



Scheme 4.2 Synthesis of α -**GzI** (**55a**) and β -**GzI** (**55b**) from S-methylthiosemicarbazide hydroiodide (**54**).

Scheme 4.3 shows the suggested mechanism of formation of guanazinium iodide (**55**). B (which denotes a general base or nucleophile) does not act as a nucleophile but as a base, in consequence, methylthiosemicarbazide hydroiodide does not undergo the expected addition reaction but deprotonation by B is instead preferred. The neutral methylthiosemicarbazide (**MeTScz**, **56**) eliminates methylmercaptane forming diimide **52** and reacts with itself in the presence of acid to form an unstable acyclic intermediate that cyclizes readily to form **55** as the only isolated product.

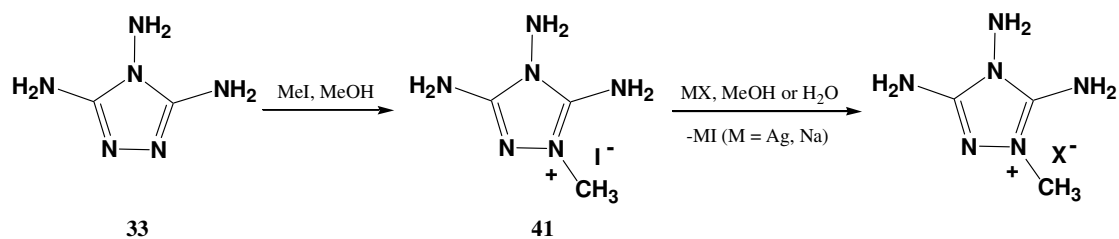


Scheme 4.3 Suggested mechanism for the formation of **55** from S-methylthiosemicarbazide hydroiodide (**54**).

Lastly, as commented at the beginning of this section, the guanazinium halogenide salts described here are useful Gz^+ cation transfer reagents. For example, treatment of either **53** or **55** with picric acid or sodium 5,5'-azotetrazolate pentahydrate yielded the corresponding picrate (**35**) and 5,5'-azotetrazolate (**36**) salts. Further details about the synthesis and properties of these salts are given in the respective chapters (see *Chapter IV* and *Chapter VI*).

4.3 Synthesis of 1-Methyl-3,4,5-triamino-1,2,4-triazolium Energetic Salts

As mentioned in the above paragraph, halogenide salts are excellent “energetic cation” transfer reagents. The synthesis of salts containing the methylguanazinium cation (**42–47**) was accomplished by metathesis of methylguanazinium iodide (**41**),^[10] with one equivalent of a suitable energetic anion transfer reagent (generally a silver salt). In the case of **45** the 5,5'-azotetrazolate transfer reagent used was the sodium salt (Scheme 4.4).^[18] In addition, the dinitramide salt (**47**) was alternatively and more safely prepared by reaction with silver(bispyridine) dinitramide $[\text{Ag}(\text{py})_2(\text{N}_3\text{O}_4)]$.^[17] Lastly, the picrate salt was also prepared and is described in *Chapter V* in detail.



$\text{X} = \text{N}_3$ (**42**), NO_3 (**43**), ClO_4 (**44**), C_2N_{10} (**45**), NT (**46**), $\text{N}(\text{NO}_2)_2$ (**47**)

Scheme 4.4 Synthesis of methylguanazinium energetic salts.

Quaternization of the triazole ring by reaction of guanazine (**33**) with methyl iodide to form the MeGz⁺ cation, allowed us to prepare the azide salt (**42**), which could not be prepared with the Gz⁺ cation, due to the fact that Gz⁺ protonates the azide anion to form guanazine and hydrazoic acid ($pK_a(\text{HN}_3) = 4.7$).^[19] This is in analogy to previous studies in our group on tetrazolium salts (see *Chapter VI*)^[11].

4.4 Vibrational and NMR Spectroscopies

The most intense band in the Raman (Figure 4.3) spectra of the methylguanazinium salts synthesized corresponds to the vibration modes of the anions. They are observed at the following wave-numbers: 1347 cm⁻¹ (azide, $\nu(\text{N}_3)$),^[20] 1049 cm⁻¹ (nitrate, $\nu(\text{NO}_3)$),^[21] 936 and 462 cm⁻¹ (perchlorate, $\nu(\text{ClO}_4)$ and $\delta(\text{ClO}_4)$),^[22] 1373, 1410 and 1488 cm⁻¹ (5,5'-azotetrazolate, $\nu_{\text{sym}}(\text{C}-\text{N}_{\text{azo}})$, $\nu_{\text{as}}(\text{C}-\text{N}_3)$ and $\nu(\text{N}_{\text{azo}}=\text{N}_{\text{azo}})$),^[23] 1069 and 1418 cm⁻¹ (5-nitrotetrazolate, $\nu(\text{N}-\text{N}-\text{C})_{\text{ring}}$ and $\nu(\text{NO}_2)$)^[24] and 1312 cm⁻¹ (dinitramide, $\nu(\text{NO}_2)$).^[25] The bands corresponding to the anions in the IR spectra (Figure 4.4) are observed at similar wave-numbers as in the Raman: 1331 cm⁻¹ (azide), 1046 cm⁻¹ (nitrate), 907 cm⁻¹ (perchlorate), 1385 and 1456 cm⁻¹ (5,5'-azotetrazolate), 1060 and 1419 cm⁻¹ (5-nitrotetrazolate) and 1343 cm⁻¹ (dinitramide). As can be seen in Figure 4.3, the Raman spectrum of the 5,5'-azotetrazolate salt and, to a lesser extent, that of the 5-nitrotetrazolate salt, is dominated by the C–N and N_{azo}=N_{azo} stretching vibrations (**45**) and the nitro group stretching and tetrazole ring deformation modes (**46a**).

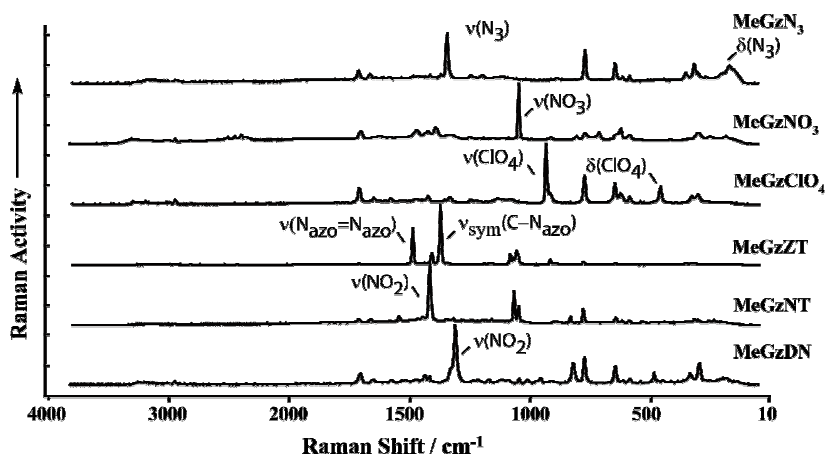


Figure 4.3 Panel plot of the Raman spectra of methylguanazinium energetic salts.

DFT calculations^[26] on neutral guanazine (**33**) were used to facilitate assignment of the bands observed in the vibrational spectra of both guanazinium and methylguanazinium salts. The IR spectra (Figure 4.4) are dominated by the N–H and C–H stretching bands at ~3200–3300 and

3000 cm^{-1} , respectively. These bands have a complex shape depending on the mode of sample preparation and appear at very similar shifts for all salts except for nitrate **43** indicating no significant difference in the strength of the hydrogen-bonding i.e., the suspected extensive hydrogen-bonding due to the large number of hydrogen atoms available to interact with electronegative atoms is not reflected in the IR spectrum. This lack of extensive strong hydrogen-bonding is confirmed (in the solid state) by the X-ray measurements, which show weak hydrogen bonds for all salts and (in solution) by the ^{15}N NMR experiments where a more substantial difference in the shifts caused by differences in hydrogen bonding would be expected (see ^{15}N NMR discussion). The stretching modes of the $(\text{C}-\text{N})_{\text{ring}}$ and $(\text{N}-\text{N})_{\text{ring}}$ are observed as peaks of low intensity at $\nu \sim 1020, 1425, 1533$ and 1580 cm^{-1} (IR).

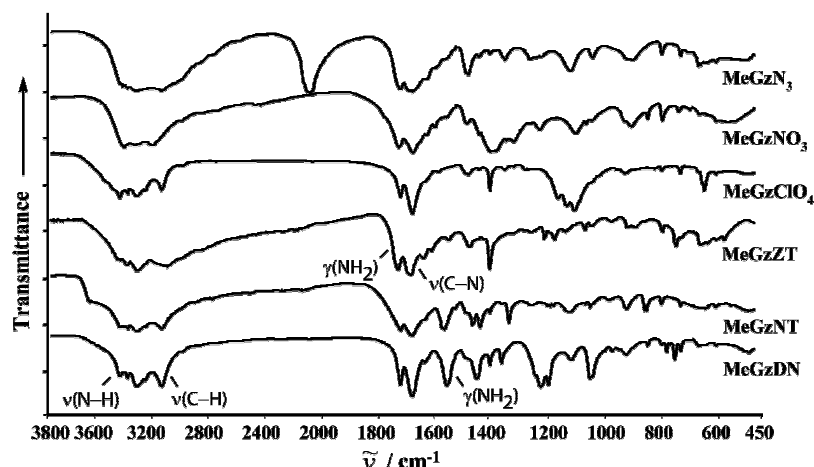


Figure 4.4 Panel plot of the IR spectra of energetic guanazinium salts.

The ^1H NMR spectra of the guanazinium and methylguanazinium salts in $[\text{D}_6]\text{DMSO}$ show three well resolved signals for the amino-group protons for all salts, indicating slow proton exchange in the NMR solvent and measurement scale, at ~ 8.0 (N-bound amino group), 6.5 and 5.7 (C-bound amino groups) ppm, and one sharp peak at 3.4 ppm corresponding to the methyl group resonance in the case of methylguanazinium (MeGz^+) salts. In the case of MeGz^+ salts, the resonances of the amino groups are shifted with respect to neutral **33**^[7b] and Gz^+ salts,^[7-8] which, due to fast proton exchange, show two signals at ~ 7.2 ($\text{N}-\text{NH}_2 + \text{C}-\text{NH}_2$) and ~ 5.5 ppm ($\text{C}-\text{NH}_2$). In the ^{13}C NMR, upon protonation of **33** to form the Gz^+ cation,^[7] there is an upfield shift from 152.1 to ~ 150.5 ppm in the triazolium ring carbon atoms resonances.^[7-10] Similarly, upon methylation the two aromatic carbon atoms become unequivalent and one shows a resonance similar to Gz^+ (~ 151 ppm), whereas the ring-carbon atom closest to the methyl group experiences an upfield shift to ~ 148 ppm. This is a similar effect to that observed in other nitrogen-containing heterocycles upon alkylation or protonation of the heterocyclic ring.^[10,27]

Lastly, the methyl group has a shift of ~ 34 ppm, keeping in with compounds containing an N-methylated azole ring.^[11,27]

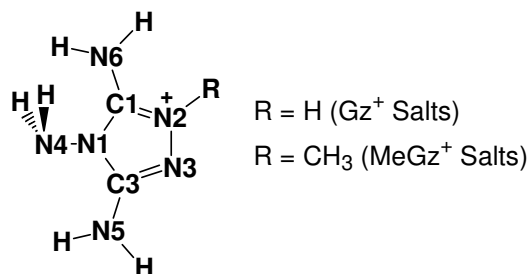


Figure 4.5 NMR labelling scheme.

Table 4.1 ¹⁵N NMR shifts, N–H coupling constants and PIS/MIS for **33** and Gz⁺ and MeGz⁺ salts.^[a]

	N1	N2	N3	N4	N5	N6	C _{ring}
33 ^[b]	-238	-156		-327	-340		152.1
53	-239 [-1]	-203 [-47]		-320 (78) [+7]	-328 (85) [+12]		150.4
55	-239 [-1]	-203 [-47]		-322 (76) [+5]	-329 (88) [+11]		150.5
41	-238 [0]	-163 [-7]	-240 [-2]	-320 (80) [+7]	-322 (71) [+18]	-334 (72) [-6]	150.4, 147.4
42	-239 [-1]	-165 [-9]	-240 [-2]	-322 (75) [+5]	-322 (81) [+18]	-335 (85) [-7]	150.5, 147.6
43	-239 [-1]	-165 [-9]	-240 [-2]	-323 (76) [+4]	-324 (91) [+16]	-336 (87) [-8]	150.5, 147.6
44	-239 [-1]	-165 [-9]	-241 [-3]	-323 (76) [+4]	-324 (91) [+16]	-336 (88) [-8]	150.5, 147.5
45a	-239 [-1]	-165 [-9]	-240 [-2]	-323 (79) [+4]	-323 (89) [+17]	-335 (88) [-7]	150.4, 147.6
46a	-238 [0]	-164 [-8]	-240 [-2]	-322 (76) [+5]	323 (86) [+17]	-335 (88) [-7]	150.8, 147.9
47	-239 [0]	-164 [-8]	-240 [-2]	-322 (76) [+5]	-323 (92) [+17]	-336 (85) [-8]	150.5, 147.5

[a] Shifts (δ) in ppm, coupling constants (J) in Hz in curved brackets () and PIS/MIS in ppm in square brackets []. [b] From reference [7].

In the ¹⁵N NMR of **33** we found again equivalence of the two C–NH₂ nitrogen atoms giving a total of four resonances two of which split in triplets due to the coupling with the protons, with $J = 88.5$ and 75.7 Hz, respectively. A total PIS (proton induced shift) of -47 ppm for N3 from -156 ppm in neutral **33** to -203 ppm in Gz⁺ salts (Table 4.1),^[7b] hints to protonation on this nitrogen atom as seen in the crystal structure and observed in similar compounds (see also *Chapters V* and *VII*).^[7-9] After this, the largest PIS value observed for the other nitrogen atoms is $\sim +10$ ppm for N5, which is the nitrogen closest to the protonation site after N3 (see Figure 4.5 for labeling scheme).

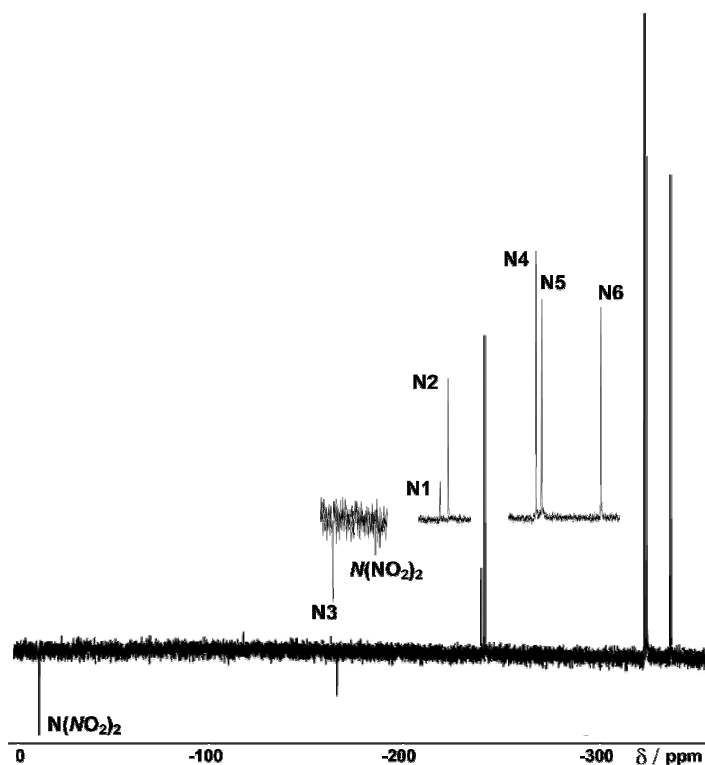


Figure 4.6 $^{15}\text{N}\{^1\text{H}\}$ NMR spectrum of the methylguanazinium cation in **47** measured in $[\text{D}_6]\text{DMSO}$.

On the other side, the ^{15}N NMR spectra of methylguanazinium salts show six signals for the six different nitrogen atoms in the MeGz^+ cation (Figure 4.6). When the spectrum is recorded with broadband decoupling, the resonances of the nitrogen atoms in close proximity to protons are strong and positive.^[8] All nitrogen atoms in the heterocyclic ring have positive signals due to the presence of hydrogen atoms at two bonds (either CH_3 or NH_2) apart from N3, which is at three bonds from the next proton, causing it to have a negative intensity. The resonances of the amino groups nitrogen atoms (at higher field) are well separated from those corresponding to the heterocyclic ring, which appear at lower field, but are very similar. The nitrogen-bound amino group (N4), due to the direct bond to the more electronegative nitrogen atom would be expected to be found at lower field than the carbon-bound nitrogen atoms. The latter two, can be distinguished based on the methylation-induced shift (MIS) caused by the introduction of the methyl group onto guanazine. By comparison with neutral guanazine (Table 4.1), the nitrogen atom closest to the methyl group (N6) would be expected to have the most negative MIS.^[11,27] In this case, the C-NH_2 groups have a MIS of $\sim +17$ ppm (N5) and ~ -7 ppm (N6) and N6 (closest to the methyl group) can be assigned as having the resonance at the highest field. Taking advantage of the MIS observed, the assignment of the alkylated nitrogen atom (N2) is straightforward, whereas the rest of the peaks remain practically unchanged by the methyl group and can be assigned by comparison to neutral guanazine.^[7] The amino group nitrogen atom resonances are

observed at the highest field as three triplets: N4 and N5 overlap (Figure 4.6) whereas N6 has a slightly more negative shift.

The coupling constants ($^1J(^1\text{H}-^{15}\text{N})$) have values of $\sim 75\text{--}80$ Hz (for N4) and $\sim 85\text{--}90$ Hz (for N5 and N6). The shifts mentioned above are in good agreement with iodide salt (**41**)^[10] although the coupling constants to N5 and N6 are slightly larger for the compounds reported here (see Table 4.1). Apart from the cation, the nitrogen atoms belonging to the anion are also observed in the ^{15}N NMR. The dinitramide salt shows one resonance corresponding to the nitro groups at -11.1 ppm ($\text{N}(\text{NO}_2)_2$) and the central nitrogen atom resonates (with low intensity) at -177.8 ppm ($\text{N}(\text{NO}_2)_2$) similarly to other dinitramide salts.^[28] The nitrate nitrogen atom appears as an intense signal at -4.6 ppm, as expected.^[28] In contrast to other compounds with the same anion^[29,23a,30] the 5,5'-azotetrazolate salt was soluble enough in $[\text{D}_6]\text{DMSO}$ to record a ^{15}N NMR (natural abundance) and showed three well resolved signals at $+107.5$ ppm corresponding to the azo-bridge nitrogen atoms and the ring resonances were observed at $+12.4$ (CN_α) and -66.5 (CN_β) ppm, keeping in with the reported values for the solid state NMR of guanazinium 5,5'-azotetrazolate (*Chapter VII*)^[8] and the NMR in solution of the sodium salt.^[23a] Lastly, due to the high symmetry of the azide and 5-nitrotetrazolate anions, their resonances can be readily observed in the ^{14}N NMR spectra as broad signals at -130 (NNN) and -280 (NNN) ppm^[31–32] and at $\sim +20$ (N9/N10), -20 (NO_2) and -60 (N8/N11) ppm,^[33] respectively (see Figure 4.5 for labelling scheme).

4.5 Molecular Structures

Single crystals of the compounds suitable for X-ray diffraction studies were obtained as described in 4.8 *Experimental Section*. Intensity data were collected on an Oxford XCalibur 3 CCD diffractometer equipped with a molybdenum X-ray tube and a highly oriented graphite monochromator. The structures were solved by direct methods using SIR97^[34] and refined by means of full-matrix least-squares procedures using SHELXL-97.^[35] All non-hydrogen atoms were refined anisotropically by full-matrix least-squares methods. Details concerning data collection and refinement are summarized in *Appendix C*. All hydrogen atoms were located from difference Fourier maps and were refined isotropically. CCDC 646967 (**55a**), CCDC 646966 (**55b**), CCDC 650292 (**41**), CCDC 650180 (**42**), CCDC 650177 (**43**), CCDC 650724 (**44**), CCDC 650179 (**45**), CCDC 650725 (**46a**) and CCDC 650178 (**47**) contain the supplementary crystallographic data for all compounds.

Table 4.2 shows selected bond lengths and angles for the iodide salts **55a**, **55b** and **41**. In **55a** and **55b** there are two crystallographically independent cations (only one for **41**) where all distances and angles are essentially the same within experimental error and match nicely the parameters of other known guanazinium salts described in this work (see Figure 4.7).^[7-9] Extensive conjugation all over the aromatic ring is observed but the double bond character is mainly concentrated on N1–C5/N2–C3 of one molecule and N7–C11/N8–C9 of another, with distances between nitrogen and carbon varying from 1.297(2) to 1.328(5) Å ($d_{C-N} = 1.47$ Å, $d_{C=N} = 1.22$ Å).^[26] The C–N bond distances found for the two carbon-bound exocyclic amino groups in all three structures are different, with values varying between 1.319(3) and 1.324(5) Å for C5–N5 and between 1.345(4) and 1.358(2) Å for C3–N3 (1.338(8) and 1.340(7) Å in the case of **41**), and are longer than normal C–N double bonds (1.22 Å) and shorter than normal C–N single bonds (1.47 Å),^[36] which confirms substantial conjugation of the amine lone pairs with the triazole ring.

Table 4.2 Selected bond lengths /Å and angles /deg for **α-GzI (55a)**, **β-GzI (55b)** and **41**.

Distance	41	55a (A)	55b (A)	Distance	55a (B)	55b (B)
C5–N1	1.322(5)	1.316(2)	1.320(4)	N7–C11	1.317(2)	1.328(5)
C5–N5	1.340(5)	1.319(3)	1.324(5)	N7–N8	1.394(2)	1.400(4)
C5–N4	1.356(5)	1.355(2)	1.354(4)	N10–C11	1.355(2)	1.343(3)
N4–N6	1.400(5)	1.398(2)	1.395(4)	N10–C9	1.380(2)	1.378(4)
N4–C3	1.382(5)	1.386(2)	1.399(4)	N10–N12	1.398(2)	1.397(4)
N2–C3	1.315(5)	1.298(2)	1.300(4)	C11–N11	1.319(2)	1.324(5)
N2–N1	1.408(4)	1.392(2)	1.395(4)	N9–C9	1.362(2)	1.338(4)
N3–C3	1.338(6)	1.358(2)	1.345(4)	N8–C9	1.297(2)	1.313(4)
Angle	41	55a (A)	55b (A)	Angle	55a (B)	55b (B)
N2–C3–N3	126.8(4)	127.0(2)	128.6(3)	N8–C9–N9	127.0(1)	126.4(3)
N2–C3–N4	110.9(4)	111.1(1)	110.0(3)	N8–C9–N10	111.50(1)	110.6(3)
N3–C3–N4	122.3(4)	121.8(1)	121.4(3)	N9–C9–N10	121.3(1)	123.0(3)
N1–C5–N5	128.7(4)	129.6(2)	129.3(3)	N7–C11–N11	129.7(2)	128.9(3)
N1–C5–N4	106.9(4)	105.5(2)	105.9(3)	N7–C11–N10	105.6(1)	106.3(3)
N5–C5–N4	124.3(4)	124.8(2)	124.8(3)	N11–C11–N10	124.7(2)	124.8(3)
C5–N1–N2	111.0(3)	112.6(2)	111.9(3)	C3–N4–N6	130.4(1)	129.4(2)
C3–N2–N1	104.1(3)	103.7(1)	104.8(3)	C11–N7–N8	112.4(1)	111.2(3)
C5–N4–C3	107.1(3)	107.1(1)	107.4(3)	C9–N8–N7	103.5(1)	104.0(3)
C5–N4–N6	129.3(3)	122.5(1)	123.1(2)	C11–N10–C9	107.0(1)	107.9(3)
				C11–N10–N12	122.6(1)	122.3(3)
				C9–N10–N12	130.2(1)	129.8(3)

The shorter C5–N5 distances in respect to C3–N3 indicate more delocalization through this bond. This is also reflected in the greater planarity of the C5-bound amino group, which is virtually planar to the guanazinium ring whereas the C3-bound amino group is slightly off the plane (≈ 16 to 26°), and in the hybridization of the amino group nitrogen atoms (N5 is essentially sp^2 hybridized with H6–N5–H7 $\approx 120^\circ$ whereas H2–N3–H3 $< 120^\circ$ shows some contribution of the lone pair to a sp^3 hybridization).

55a crystallizes with 16 molecules per unit cell. One of the amino groups on the cations is essentially planar (Figure 4.7) and protonation takes place on the nitrogen which is closest to this group as already observed in other guanazinium salts.^[7–9] It is precisely this nitrogen atom, which forms a strong intramolecular hydrogen bond with the most off-the-plane amino group, with N5...N6 and N11...N12 distances of 2.860(3) and 2.861(3) Å (see Table 4.B1), respectively, describing an intramolecular **S(5)** motif using graph-set nomenclature.^[37,38]

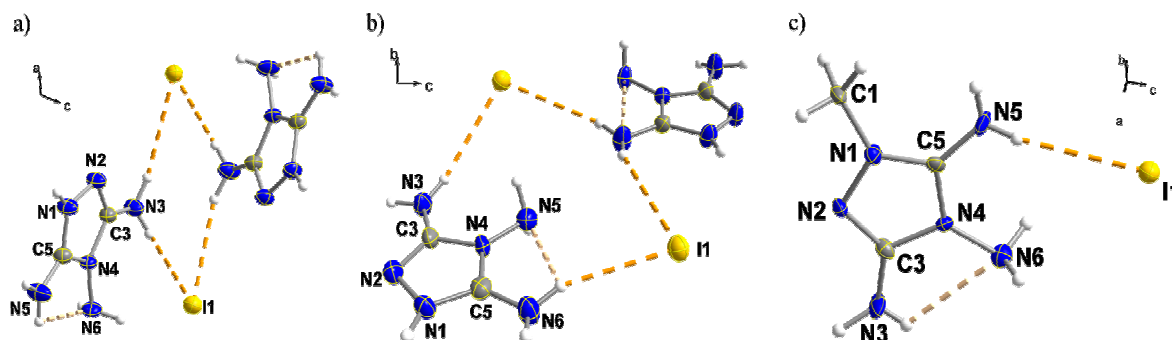


Figure 4.7 Asymmetric unit of a) **α-GzI** (55a), b) **β-GzI** (55b) and c) **41** with numbering scheme.

The guanazinium cations alternate with iodide anions forming layers in two directions, which are approximately perpendicular (Figure 4.8). The iodide anions in one layer interact with hydrogen atoms in a perpendicular layer through two crystallographically independent guanazinium cations with weak contacts between iodine and hydrogen atoms ($\text{H3}\cdots\text{I3}^{\text{iii}} = 2.80(3)$ Å and $\text{H10}\cdots\text{I2}^{\text{vi}} = 2.87(3)$ Å, symmetry codes: (iii) 1-x, -y, 1-z; (vi) 1.5-x, -0.5+y, 1.5-z). Within layers, there exists strong hydrogen-bonding between two crystallographically independent guanazinium cations involving the protonated nitrogen atoms with $\text{N1}\cdots\text{N8}^{\text{i}}$ and $\text{N7}\cdots\text{N2}^{\text{i}}$ distances of 2.873(2) and 2.878(2) Å, respectively (symmetry code: (i) 1.5-x, 0.5-y, 1-z), describing a **R2,2(6)** pattern at the second-level.^[37,38]

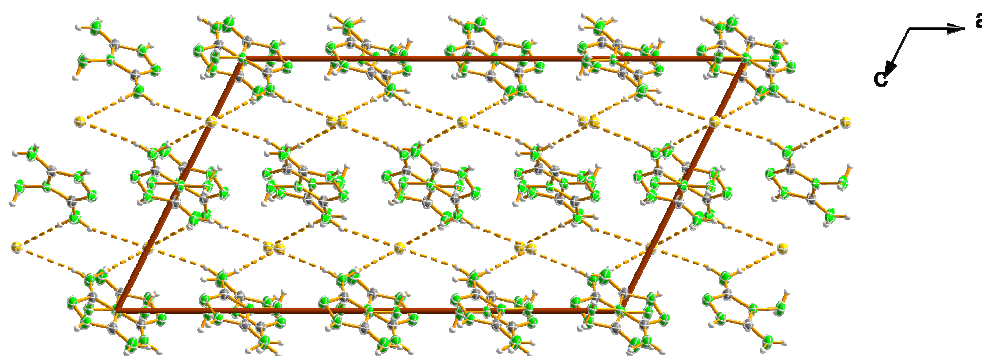


Figure 4.8 Layers in the structure of **α-GzI** (55a) with the contacts between perpendicular layers.

55b is another polymorph of guanazinium iodide (Figure 4.7), which crystallizes in an orthorhombic crystal system with 16 molecules in the unit cell. Similarly to **55a**, one of the amino groups is virtually planar and forms an intramolecular hydrogen bond to the most off-the-plane amino group (see Table 4.B2) with N5...N6 and N11...N12 distances of 2.872(5) and 2.848(5) Å describing the same intramolecular **S(5)** motif as it is typical for 1,2-diamino heterocycles.^[7–9] Again protonation takes place next to the most planar amino-group and these protons form dimer-pairs, which build the already described **R2,2(6)** second-level pattern with N7...N2ⁱ and N1...N8ⁱⁱⁱ (symmetry codes: (i) $x, 0.5+y, 0.5+z$; (iii) $x, -0.5+y, -0.5+z$) distances of 2.831(4) and 2.833(4) Å, which are slightly shorter than for the other polymorph. The contacts between hydrogen and iodine are in this case slightly longer than for **55a** (3.624(4)–3.821(3) Å vs. 3.593(2)–3.770(2) Å).

Figure 4.9 shows a view along the c -axis in the unit cell of **55b**. Two crystallographically independent cations form dimer-pairs which stack with other pairs on the subsequent layer. New dimer-pairs layers are formed, which cross the former at a 90° angle. On a layer, iodide anions occupy the voids between these dimers and interact with hydrogen atoms of the amino group perpendicular to the aromatic ring with H5...I2ⁱⁱ = 2.79(4) Å (symmetry code: (ii) $1-x, 1-y, z$).

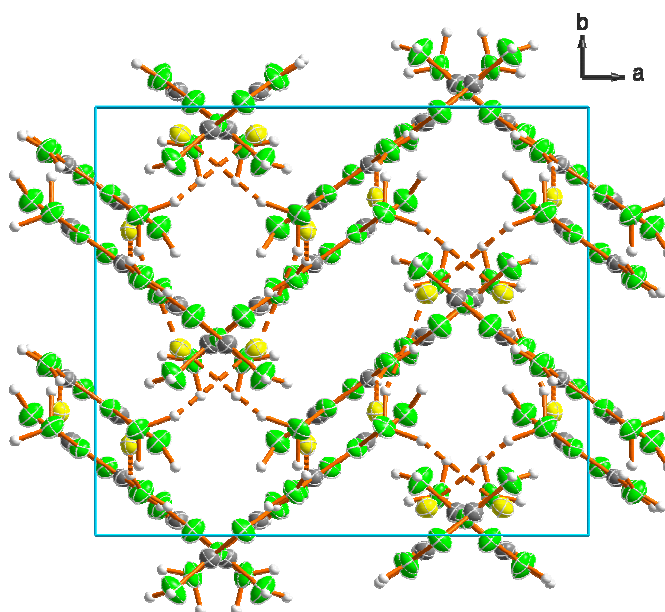


Figure 4.9 View of the unit cell of **β-GzI (55b)** along the c -axis.

41 crystallizes with two molecules in the unit cell. As already discussed for **55a** and **55b**, the two C-amino groups lay on the plane of the ring whereas the N-amino group is approximately perpendicular to it, with the lone pair forming an **S(5)** motif with a N3...N6 distance of 2.872(6) Å (see Figure 4.7 for numbering scheme). In this case, the intramolecular hydrogen bond is

formed between N6 and the C-NH₂ which is furthest from the methyl group (N3) whereas in **55a** and **55b**, this was formed with the C-NH₂ closest to the proton (N5) (see Table 4.B3).

The triazolium cations and iodine atoms alternate with each other forming layers (as in **55a**) with cations and anions laying on the same plane (whereas in **55a** the iodine atoms lay slightly out of the plane described by the heteroaromatic rings). The layers are separated by a distance of ~ 6.5 Å (Figure 4.10a). In one layer, one can see the formation of dimer-pairs between two identical molecules (Figure 4.10b), which are related through an inversion center in the middle of the **R2,2(8)** motif (formed at the second-level) described by N5 and N5ⁱ, with N5...I1ⁱⁱⁱ and N5...I1 distances of 3.607(5) and 3.631(5) Å (symmetry codes: (i) $-x-1, -y+2, -z+1$; (iii) $-x, -y+2, -z+1$) slightly shorter than observed for **55a** and **55b**. The presence of the methyl group instead of a proton diminishes the possibility to form hydrogen bonds and does not allow the formation of the **R2,2(6)** motif observed for the **55** polymorphs, however, the arrangement of the dimer-pairs allows the formation of a new **R2,2(8)** subset at the first-level with a N3...N2^{iv} = 2.983(6) Å (symmetry code: (iv) $-x-1, -y+3, -z+2$; (v) $x-1, y+1, z$).

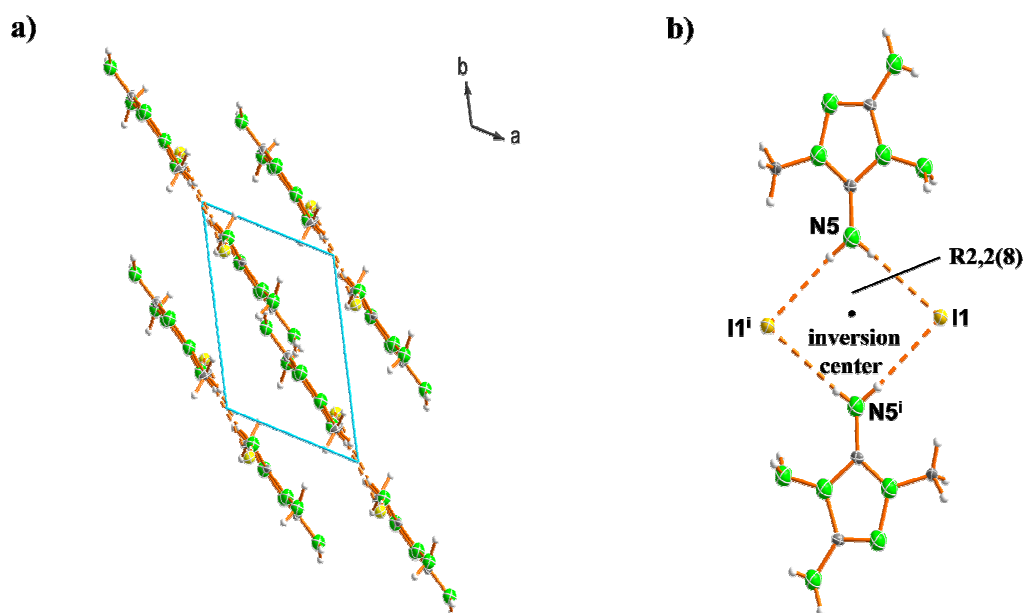


Figure 4.10 a) View of the unit cell of **41** along the c -axis showing the layered structure b) Dimer-pair forming a **R2,2(8)** “hydrogen-bonding” network (symmetry code: (i) $-x-1, -y+2, -z+1$).

Selected bond distances and angles in the methylguanazinium cations of the energetic salts synthesized are shown in Table 4.3. All parameters agree with each other, within experimental error,^[39] and match the data for the structure of the iodide salt (**41**).^[10] The formal exchange of the proton at N2 in guanazinium salts (see also *Chapters V and VII*)^[7,8,10] by a methyl group, shows little variation in the molecular parameters found for the MeGz⁺ cation in comparison to the Gz⁺

cation or neutral guanazine.^[8] The triazolium ring is planar, with the exocyclic nitrogen atoms lying in this plane. The tetrahedral geometry and bond length (N1–N4 \sim 1.40 Å) of the nitrogen-bound (N4) amino group indicates little interaction of the nitrogen lone-pair and the triazolium ring π -system, similar to other triazolium species,^[3,9,11,41] and as predicted by theoretical studies on N-aminoazoles, which led to the conclusion that sp^3 -hybridization for N–NH₂ groups is preferred over sp^2 -hybridization.^[42] On the other hand, the carbon-bound amino groups (N5 and N6) have angles close to 120°, corresponding to a sp^2 -hybridization, and C1–N6 and C3–N5 distances in the range 1.317(4)–1.330(3) and 1.332(3)–1.357(2) Å, respectively. These distances are shorter than C–N single bonds (1.47 Å) and longer than C=N double bonds (1.22 Å),^[36] indicating a more accentuated conjugation of the nitrogen lone-pair with the heteroaromatic ring. In fact, a closer comparison of the C–NH₂ and N–NH₂ (1.393(2)–1.407(3) Å) distances in compounds **42–47** with the C–N and N–N distances in CH₂=NH/CH₃–NH₂ (1.273 and 1.471 Å) and NH=NH/NH₂–NH₂ (1.252 and 1.449 Å), respectively,^[43] further supports this observation and shows the “hydrazine-like” character of the amino group in the 1-position (N4) and the “aniline-like” character of the carbon-bound amino groups (N5 and N6). **42**, **46a** and **47** crystallize in monoclinic systems in the space-group $P2_1/c$ with four molecules in the unit cell (apart from **42**, $Z = 8$) whereas **43**, **44** and **45a** have triclinic cells in the space-group $P-1$, with $Z = 2$. Using graph-set notation^[37] and the computer program *RPLUTO*^[38] the hydrogen bond patterns of interest can be identified and analyzed similarly to described above for **55** and **41**. Common to all structures is the formation of an intramolecular hydrogen bond, which describes an **S(5)** motif at the primary level. The intramolecular hydrogen bond is formed between the C–NH₂ group nearest to the methyl residue (N6, donor) and the N–NH₂ group (N4, acceptor) in the case of **42**, **45a** and **46a**, and between the C–NH₂ group furthest from the methyl residue (N5, donor) and the N–NH₂ group (N4, acceptor) in the case of **43**, **44** and **47**, and has distances of \sim 2.85 Å. In addition, the formation of a hydrogen bond between N5 (donor) of one triazolium cation and N3 (acceptor) of another cation, gives rise to the formation of an **R2,2(8)** motif with N5...N3 \sim 3 Å. The dinitramide salt is the only compound that does not show such a motif (see discussion below).

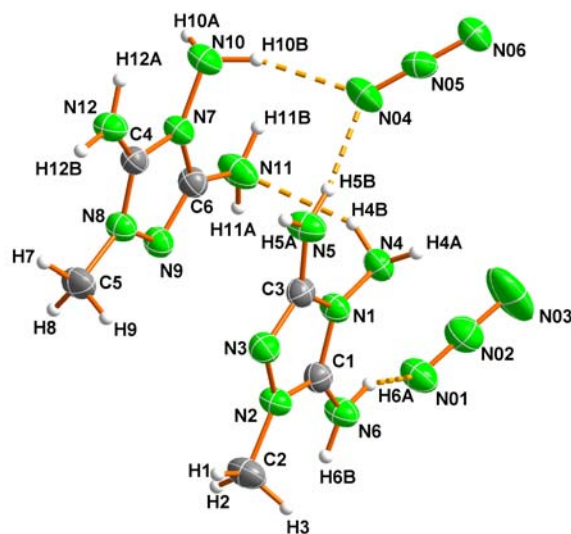


Figure 4.12 Asymmetric unit of **42** showing the numbering scheme (Diamond plot, thermal ellipsoids represent 50% probability).

The asymmetric unit of compound **42** (Figure 4.12) contains two crystallographically independent anions and cations. The cations have very similar geometric parameters between them and with the other salts. Also the azide anions are very similar, essentially linear (N–N–N $\sim 179^\circ$) and symmetrical around the central nitrogen (N02 or N05) with N–N distances of ~ 1.17 Å, typical for N=N double bonds^[44] and similar to other azolium azides.^[31, 41]

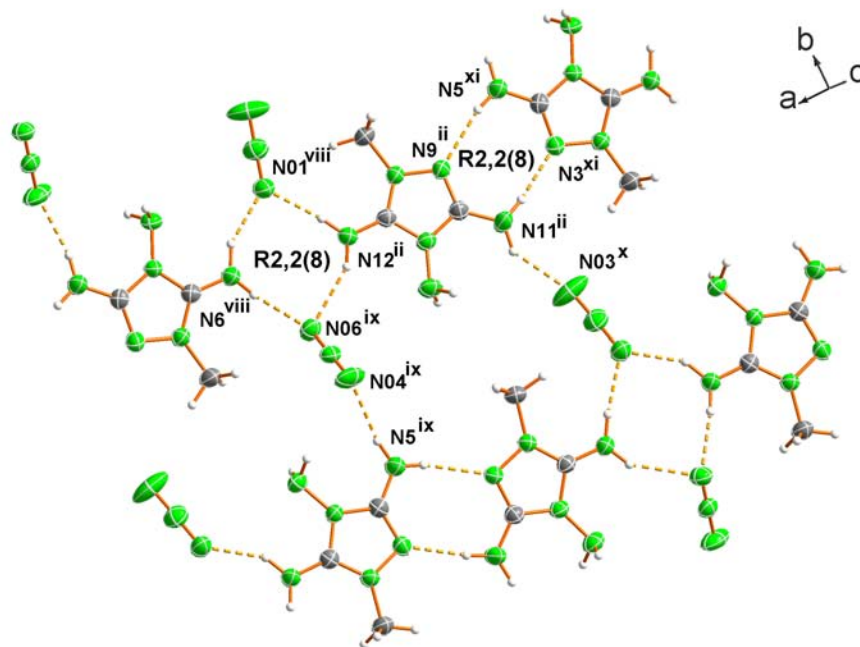


Figure 4.13 Hydrogen-bonding in a layer of **42**. Symmetry codes: (ii) $-x, -y+1, -z+1$; (viii) $1-x, y+1/2, -z+1/2$; (ix) $1+x, y, z$; (x) $x, y, z+1$; (xi) $-x, y+1/2, -z+3/2$.

While the cations arrange forming layers perpendicular to the *ac*-plane, one of the crystallographically independent azide anions lies approximately in this plane (angle between N1, N3 and the *ac*-plane $\sim 15^\circ$) and the other lies crossing these layers at an angle of $\sim 50^\circ$. The more out-of-the-plane azide anion connects three consecutive layers through two hydrogen bonds with the terminal nitrogen atoms ($\text{N4} \cdots \text{N06}^{\text{ii}} = 3.038(4) \text{ \AA}$; $\text{N10} \cdots \text{N04} = 3.028(4) \text{ \AA}$, symmetry code: (ii) $-x, -y+1, -z+1$), whereas the other anion forms a hydrogen bond with the twisted nitrogen-bound amino group in the cation linking layers ($\text{N10} \cdots \text{N03}^{\text{iv}} = 2.994(5) \text{ \AA}$, symmetry code: (iv) $x-1, y, z$). In each layer (Figure 4.13), both azide anions are involved in hydrogen-bonding at the terminal nitrogen atoms ($\text{N6}^{\text{viii}} \cdots \text{N06}^{\text{ix}} = 2.923(3) \text{ \AA}$; $\text{N6} \cdots \text{N01} = 2.893(4) \text{ \AA}$; $\text{N12} \cdots \text{N01}^{\text{iii}} = 2.861(4) \text{ \AA}$; $\text{N12} \cdots \text{N06}^{\text{vi}} = 2.968(4) \text{ \AA}$; $\text{N11} \cdots \text{N03}^{\text{vii}} = 2.815(4) \text{ \AA}$; $\text{N5} \cdots \text{N04} = 2.913(4) \text{ \AA}$; symmetry codes: (iii) $x-1, -y+1/2, z+1/2$; (v) $x, -y+1/2, z+1/2$; (vi) $-x-1, -y+1, -z+1$; (vii) $-x, -y+1, -z$; (viii) $1-x, y+1/2, -z+1/2$; (ix) $1+x, y, z$). One azide anion participates in the formation of four hydrogen bonds (see Table 4.B4), three in a layer and one between layers, whereas the other azide anion forms three hydrogen bonds in a layer and two between layers. The lines of cations are connected by hydrogen-bonding through “azide-bridges” and by direct hydrogen bond interactions between the cations ($\text{N11} \cdots \text{N3}^{\text{i}} = 2.956(4) \text{ \AA}$; $\text{N5} \cdots \text{N9}^{\text{v}} = 3.009(4) \text{ \AA}$; symmetry codes: (i) $x, -y+1/2, z-1/2$; (v) $x, -y+1/2, z+1/2$) forming a two-dimensional network. The side-on interaction of triazole rings, results in the formation of the usual **R2,2(8)** motif. It is interesting also the formation of another **R2,2(8)** subset by the aforementioned “azide-bridged” triazoles, as observed for other azolium azides (see *Chapter VI*).^[27] The formation of extensive strong hydrogen-bonding in a layer and between layers would suggest a high density in the crystal structure of the compound; however, a moderate value of $\sim 1.4 \text{ g cm}^{-3}$ was calculated. This value is similar to that of previously reported 1,4-dimethyl-5-aminotetrazolium azide (**1,4DMATN₃**),^[27] which, due to the presence of the two methyl groups, has many fewer protons available for hydrogen-bonding. The fairly low value indicates that there are many other factors that determine the density of a material in addition to hydrogen bond interactions. The low packing efficiency of **42**, caused by one of the two crystallographically independent azide anions that deviates from the plane formed by the triazolium rings, may explain the similar density value to **1,4DMATN₃**, which forms perfectly planar layers.

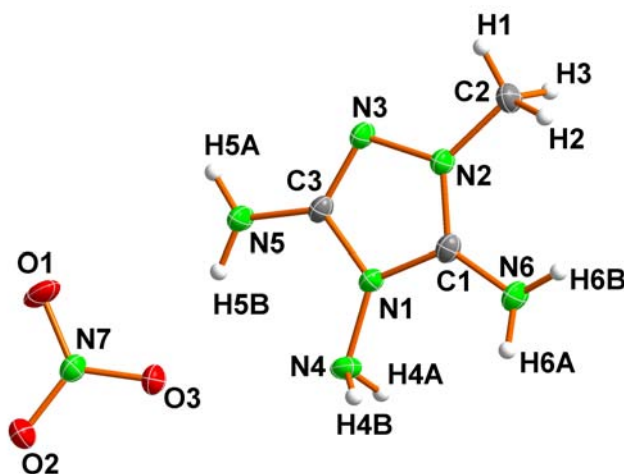


Figure 4.14 Asymmetric unit of **43** showing the numbering scheme (Diamond plot, thermal ellipsoids represent 50% probability).

43 (Figure 4.14) crystallizes in layers, in which the nitrate anion is twisted slightly out of the plane formed by the methylguanazinium cations. The distances between layers are ~ 3.2 Å (measured between the twisted N4H_2 amino group and the nitrate nitrogen atom N7^{ii} from a neighbouring layer, symmetry code: (ii) $1+x, y, z$) and the out-of-the-plane oxygen atom (O3) connects the layers by forming a hydrogen bond with the twisted N4H_2 , with a distance between donor and acceptor ($\text{N4} \cdots \text{O3}^{\text{ii}}$) of $3.026(2)$ Å. In addition, O2 in the nitrate also links the layers by forming a hydrogen bond with the other hydrogen atom on N4 (H4A), with a distance ($\text{N4} \cdots \text{O2}$) of $3.113(2)$ Å.

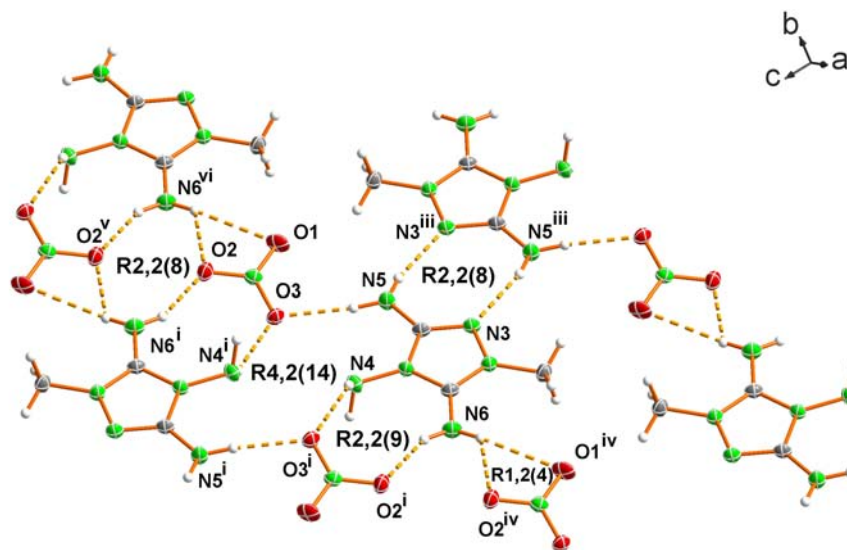


Figure 4.15 View of a layer showing the extensive hydrogen bonding in **43**. Symmetry codes: (i) $1-x, -y, 2-z$; (iii) $1-x, -y, 1-z$; (iv) $2+x, -1+y, z$; (v) $-1-x, 1-y, 2-z$; (vi) $-2+x, 1+y, z$.

Cations and anions alternate forming extensive hydrogen-bonding in a layer as represented in Figure 4.15. Every guanazinium cation is surrounded by three anions and one cation forming strong hydrogen bonds (see Table 4.B5 for hydrogen bonds parameters). The **R2,2(8)** subset is formed by two consecutive guanazinium cations ($N5^{\bullet\bullet\bullet}N3^{\text{iii}} = N5^{\text{iii}}\bullet\bullet\bullet N3 = 3.019(2)$ Å; symmetry code: (iii) 1-x, -y, 1-z) at the primary-level. Many other ring patterns are also formed. The most representative is another **R2,2(8)** subset, which is formed by a strong interaction between two cations and two anions ($N6^{\bullet\bullet\bullet}O2^{\text{i}} = 2.818(2)$ Å, $N6^{\bullet\bullet\bullet}O2^{\text{iv}} = 2.893(3)$ Å, symmetry codes: (i) 1-x, -y, 2-z; (iv) 2+x, -1+y, z), well below the sum of the van der Waals radii ($r_{\text{O}} + r_{\text{N}} = 3.10$ Å)^[45] and a larger **R4,2(14)** motif, again by interaction of two guanazinium cations with two nitrate anions ($N4^{\bullet\bullet\bullet}O3^{\text{ii}} = 3.026(2)$ Å, $N5^{\bullet\bullet\bullet}O3 = 2.911(2)$ Å, symmetry code: (ii) x+1, y, z). Additionally, the **R1,2(4)** ring pattern, common to nitrate salts, is also found with a weak interaction ($N6^{\bullet\bullet\bullet}O1^{\text{iv}} = 3.312(2)$ Å) and a strong one ($N6^{\bullet\bullet\bullet}O2^{\text{iv}} = 2.893(2)$ Å). The parameters corresponding to the anion are as observed for many other nitrate salts^[41,46,47] and will not be further discussed.

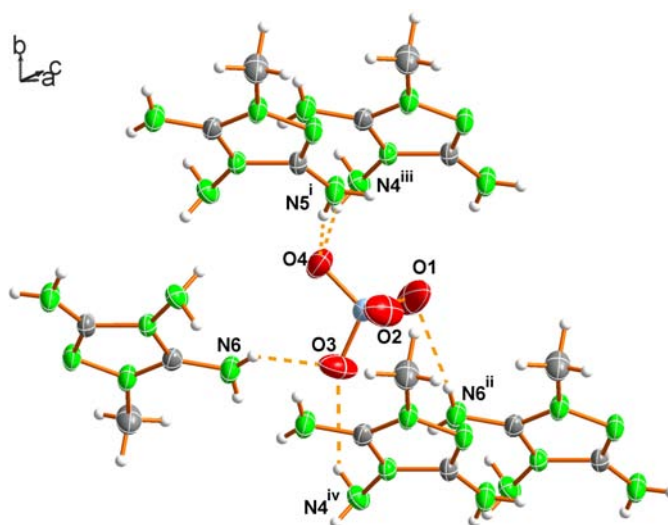


Figure 4.16 Hydrogen bonding around the perchlorate anion in **44**. Symmetry codes: (i) -1-x, 1-y, 1-z; (ii) 1-x, -y, 1-z; (iii) -x, 1-y, 1-z; (iv) -x, -y, 1-z.

The perchlorate anion in **44** is linked to five cations through hydrogen-bonding (Figure 4.16). O3 and O4 form two hydrogen bonds each ($N4^{\text{iv}}\bullet\bullet\bullet O3 = 3.042(3)$ Å, $N6^{\bullet\bullet\bullet}O3 = 2.943(4)$ Å and $N4^{\text{iii}}\bullet\bullet\bullet O4 = 3.111(3)$ Å, $N5^{\text{i}}\bullet\bullet\bullet O4 = 3.198(4)$ Å) whereas O1 forms only one ($N6^{\text{ii}}\bullet\bullet\bullet O1$ 3.055(4) Å) and O2 does not form any (symmetry codes: (i) -1-x, 1-y, 1-z; (ii) 1-x, -y, 1-z; (iii) -x, 1-y, 1-z; (iv) -x, -y, 1-z).

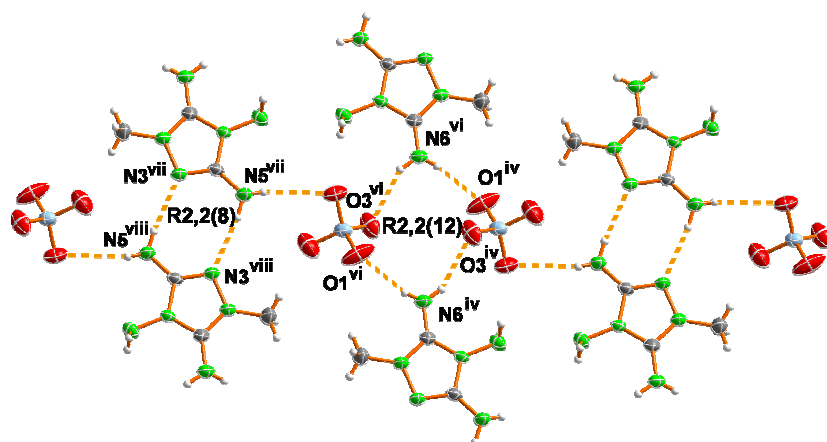


Figure 4.17 View of one of the cations layers in **44**. Symmetry codes: (iv) $-x, -y, 1-z$; (vi) $-x, -y, 1-z; -2-x, 1-y, 1-z$; (viii) $-1-x, 1-y, 1-z$.

Three consecutive layers are connected by hydrogen bonds (Table 4.B6) with the nitrogen-bound amino group, once with O3 and once with O4 of the perchlorate anion ($N4^{vi} \cdots O3$, 3.042(3) Å and $N4^{viii} \cdots O4$, 3.111(3) Å; symmetry codes: (vi) $-x, -y, 1-z$, (viii) $-1-x, 1-y, 1-z$). Figure 4.17 shows one of the layers in the structure. **R2,2(8)** motifs alternate with the much less common **R2,2(12)** subsets. The latter are analogous to the **R2,2(8)** motifs formed by the azide bridges in **42**, only, in this case, the perchlorate anions bridge the two cations through the oxygen atoms ($N6 \cdots O3 = 2.943(4)$ Å, $N6 \cdots O1^{ii} = 3.055(4)$ Å; symmetry code: (ii) $1-x, -y, 1-z$) increasing the size of the hydrogen-bonded ring pattern from 8 (in the azide salt) to 12 (in the perchlorate salt). The perchlorate anion distances and angles are in agreement with other salts of perchloric acid with amines.^[41,46,47]

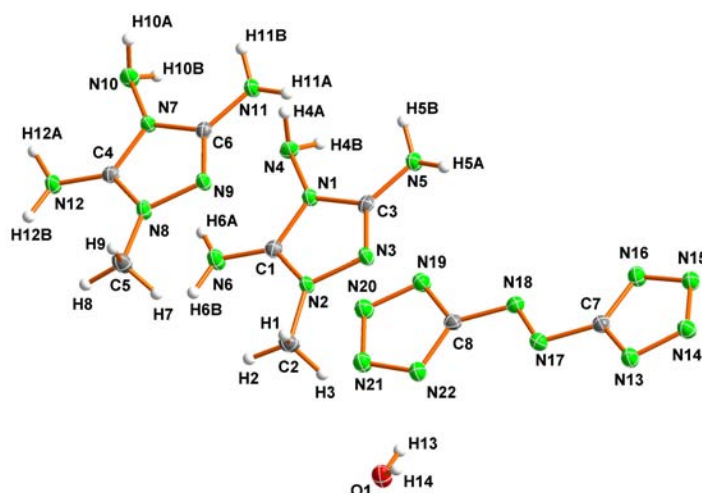


Figure 4.18 Asymmetric unit of **45a** showing the numbering scheme (Diamond plot, thermal ellipsoids represent 50% probability).

The tetrazole rings in the anion of **45a** are not equivalent due to the presence of one molecule of water in the crystal structure (Figure 4.18). The azo bridge distance (N17–N18), with a value of 1.26 Å, is comparable to that observed in metal 5,5'-azotetrazolates^[23a] and hydrazinium 5,5'-azotetrazolate^[48] and longer than the reported bond length of 1.20 Å for bis[hydroxolead(II)] 5,5'-azotetrazolate.^[49] The angles in the anion are all similar to comparable compounds.^[23a,48] The non-planar amino group joins the slightly wavy layers through hydrogen-bonding to the 5,5'-azotetrazolate anions ($\text{N10}\cdots\text{N16}^{\text{ii}} = 3.062(3)$ Å; symmetry code: (ii) 1-x, 1-y, 1-z). The other crystallographically independent cation uses both hydrogen atoms of the most off-the-plane amino group to link to the amino group of a cation of the layer below ($\text{N4}\cdots\text{N5}^{\text{ii}} = 3.191(3)$ Å) and one of the layer above ($\text{N4}\cdots\text{N11} = 3.140(3)$ Å). Furthermore, water molecules build two types of hydrogen bonds of similar strengths (~ 2.93 Å), once to the anion and once to one of the carbon-bound amino groups in the cation.

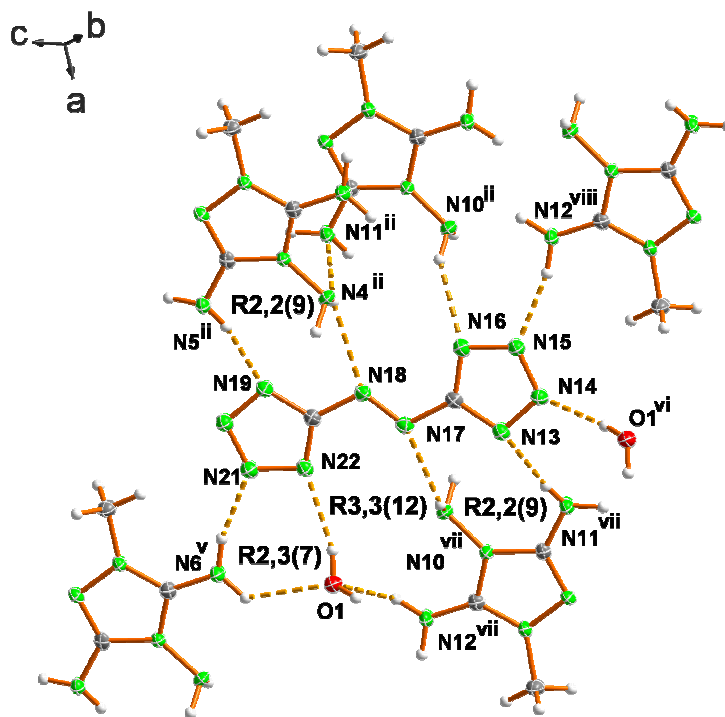


Figure 4.19 Hydrogen-bonding around the 5,5'-azotetrazolate anion in **45a**. Symmetry codes: (i) x, y, 1+z; (ii) 1-x, 1-y, 1-z; (iii) 2-x, 1-y, 1-z; (iv) 1+x, -1+y, 1+z; (v) 2-x, -y, 1-z; (vi) 2-x, 1-y, -z; (vii) x, y, -1+z; (viii) -1+x, 1+y, -1+z.

Figure 4.19 shows the hydrogen-bonding around the anion in **45a** (see Table 4.B7 for distances and angles). Every nitrogen atom in the anion is involved in hydrogen-bonding apart from N20. A total of five guanazinium cations and two water molecules complete the coordination around the anion. Two of the cations form two hydrogen bonds: one to the azo nitrogen atom N17 (N18)

and one to the tetrazole ring nitrogen N13 (N19) atoms with distances between donor and acceptor at $\text{N10}\cdots\text{N17}^i = 3.082(2) \text{ \AA}$ ($\text{N4}\cdots\text{N18}^{ii} = 3.073(3) \text{ \AA}$) and $\text{N11}\cdots\text{N13}^i = 3.034(2) \text{ \AA}$ ($\text{N5}\cdots\text{N19}^{ii} = 2.925(2) \text{ \AA}$, symmetry codes: (i) $x, y, 1+z$; (ii) $1-x, 1-y, 1-z$). Consecutive cations are connected by hydrogen bonds with water molecules ($\text{N6}\cdots\text{O1}^v = 2.862(2) \text{ \AA}$ and $\text{N12}\cdots\text{O1}^i = 2.927(2) \text{ \AA}$; symmetry code: (v) $2-x, -y, 1-z$). The extensive hydrogen-bonding in the structure not only within a layer but also between layers may as well account for the relatively high density of the 5,5'-azotetrazolate salt ($\rho_{\text{calc}} = 1.57 \text{ g cm}^{-3}$) compared to other azolium salts with the same anion, which have densities of $\sim 1.45 \text{ g cm}^{-3}$.^[30,45] Lastly, one **R2,3(7)** and one **R3,3(12)** subsets are formed between one cation, one anion and one molecule of water (i.e., three different hydrogen bonds), thus taking place at the tertiary level.

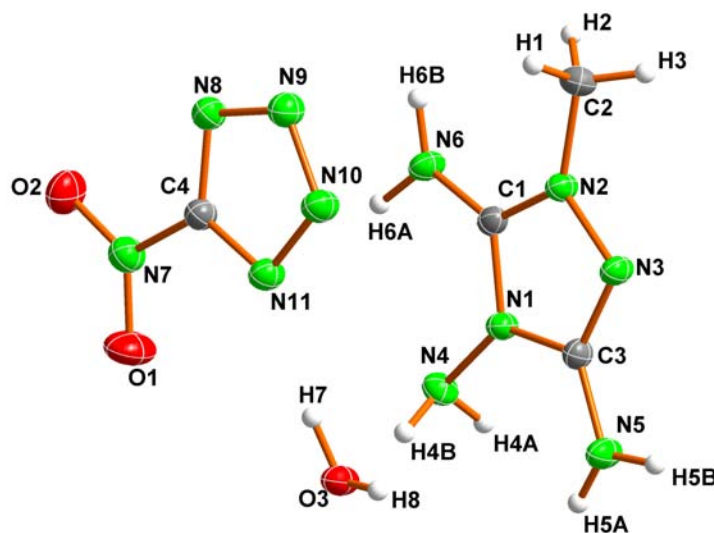


Figure 4.20 Asymmetric unit of **46a** showing the numbering scheme (Diamond plot, thermal ellipsoids represent 50% probability).

46a crystallizes with one water molecule in the unit cell (Figure 4.20) in a layered structure where water molecules link two consecutive layers by hydrogen-bonding to the out-of-plane nitrogen-bound amino group ($\text{N4}\cdots\text{O3} = 2.986(2) \text{ \AA}$). Figure 4.21 shows the hydrogen-bonding in one of these layers. Cations and anions alternate in the b direction. The nitro groups of two 5-nitrotetrazolate anions are oriented head-on, and water molecules connect the anions via one strong and one weak hydrogen bond ($\text{O3}\cdots\text{N11} = 2.808(2) \text{ \AA}$, $\text{O3}\cdots\text{N9}^v = 3.256(2) \text{ \AA}$; symmetry code: (v) $2-x, -0.5+y, 1.5-z$). All nitrogen atoms in the 5-nitrotetrazolate ring are involved in hydrogen-bonding to either one of the aforementioned bridging water molecules or to the carbon-bound amino groups of the cation ($\text{N6}\cdots\text{N10}^i = 2.901(2) \text{ \AA}$; $\text{N5}\cdots\text{N8}^{iv} = 3.125(2) \text{ \AA}$; symmetry codes: (i) $-1+x, y, z$; (iv) $1-x, -0.5+y, 1.5-z$). N5 and N3ⁱⁱ form a **R2,2(8)** motif at the primary level

(N5 \cdots N3ⁱⁱ = 2.977(2) Å; symmetry code: (ii) 2-x, -y, 1-z) and one cation (N6), one anion (N9ⁱ and N10ⁱ) and one water molecule (O3ⁱⁱⁱ) participate in the formation of a **R2,3(7)** subset. Every hydrogen atom of the three amino-groups in the guanazinium moiety also forms hydrogen bonds, which link every cation to two cations, two anions and two water molecules (see Table 4.B8 for distances). N5 (in the cation) and N8^{iv} (in the anion) form a very directional contact with N5–H5A–N8^{iv} = 175°. The tetrazolate anion is, within the limits of error, symmetrical with a symmetry plane, which runs along N7, C4 and cuts in the mid-point of the bond formed by N9 and N10 as reported for salts containing the same anion.^[50,51]

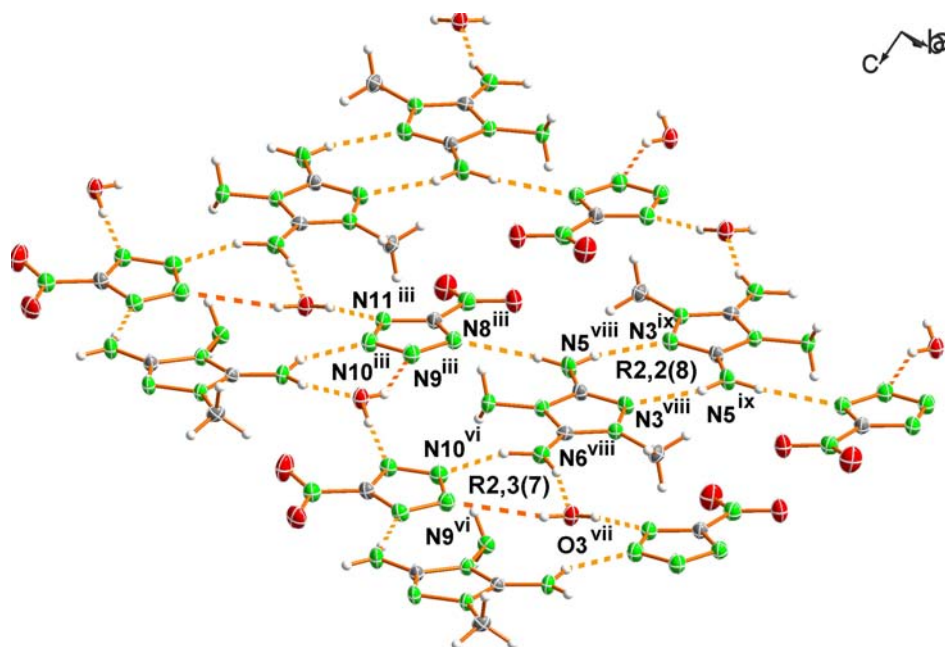


Figure 4.21 View of a layer with the corresponding hydrogen-bonding in **46b**. Symmetry codes: (iii) 1-x, 0.5+y, 1.5-z; (vi) -1+x, 1+y, z; (vii) 1-x, 1.5+y, 1.5-z; (viii) x, 1+y, z; (ix) 2-x, 1-y, 1-z.

The asymmetric unit of **47** is shown in Figure 4.22. The overall geometry of the anion is similar to that observed in comparable dinitramide salts.^[52–54] The two N–N bond lengths are approximately symmetric (~1.38 Å) and shorter than a normal N–N single bond (1.454 Å) though longer than a N=N double bond (1.245 Å).^[36] The N–N–N angle equals to 115.1(2)° as expected. The nitro groups are twisted out of the N–N–N plane (torsion angle O2–N7–N9–O4 = 16.4(2)°) making for the local symmetry of the anion to be C_1 .

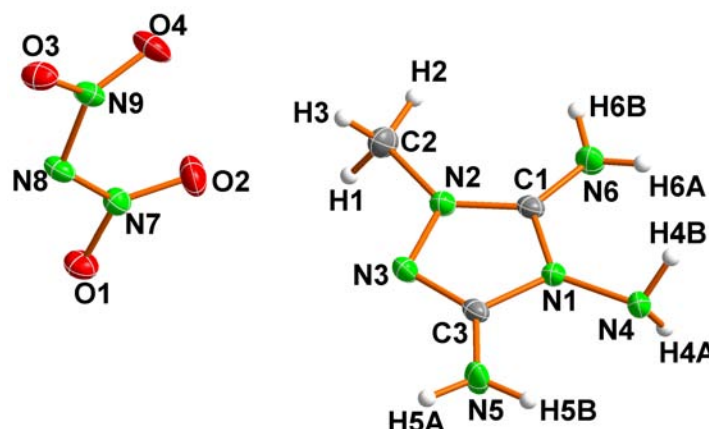


Figure 4.22 Asymmetric unit of **47** showing the numbering scheme (Diamond plot, thermal ellipsoids represent 50% probability).

Figure 4.23 shows a view of the hydrogen-bonding in the crystal structure of **47**. Apart from the aforementioned intramolecular hydrogen bond ($\text{N5} \cdots \text{N4} = 2.841(3) \text{ \AA}$), there are many different strong hydrogen bonds, which make the structure relatively dense ($\rho_{\text{calc}} = 1.656 \text{ g cm}^{-3}$) in comparison to other dinitramide salts.^[27,54] Every guanazinium cation forms up to eight hydrogen bonds, six to the anion and two to another cation. The dinitramide salt is, among the guanazinium salts studied here, the only compound that does not form the common **R2,2(8)** subset described above. N3 interacts via a hydrogen bond with N5^{iii} ($\text{N3} \cdots \text{N5}^{\text{iii}} = 2.966(3) \text{ \AA}$; symmetry code: (iii) $-x, -0.5+y, 0.5-z$), as expected, but there is no interaction between N5 and N3^{iii} .

The lack of formation of this commonly observed motif, might be the result of packing effects in the crystal, which force, in contrast to **41**^[10] and the rest of the compounds studied here, two contiguous cations not to be coplanar. In the anion, O2 and O4 do not participate in hydrogen-bonding whereas O3 forms two hydrogen bonds ($\text{N6} \cdots \text{O3}^{\text{i}} = 3.068(2) \text{ \AA}$ and $\text{N6} \cdots \text{O3}^{\text{iv}} = 2.851(2) \text{ \AA}$; symmetry codes: (i) $x, 1.5-y, 0.5+z$; (iv) $x, 0.5-y, 0.5+z$) and O1 up to three (see Table 4.B9). The central nitrogen atom in the anion also interacts with N4 of the cation ($\text{N4} \cdots \text{N8}^{\text{i}} = 3.041(2) \text{ \AA}$). There are many other hydrogen bond ring patterns, which one would expect for **47**, however, since the compound does not form layers, the formation of hydrogen-bonding around the cation takes place with two anions located at different planes, preventing the formation of, for example, the expected **R1,2(4)** subset (common to compounds containing the NO_2 moiety such as **43**). The only ring pattern observed (**R2,2(9)**) is formed by N4 and N6 (from the cation) and N8^{i} and O3^{i} (from the anion), respectively, with $\text{N4} \cdots \text{N8}^{\text{i}} = 3.041(2) \text{ \AA}$ and $\text{N6} \cdots \text{O3}^{\text{i}} = 3.068(2) \text{ \AA}$.

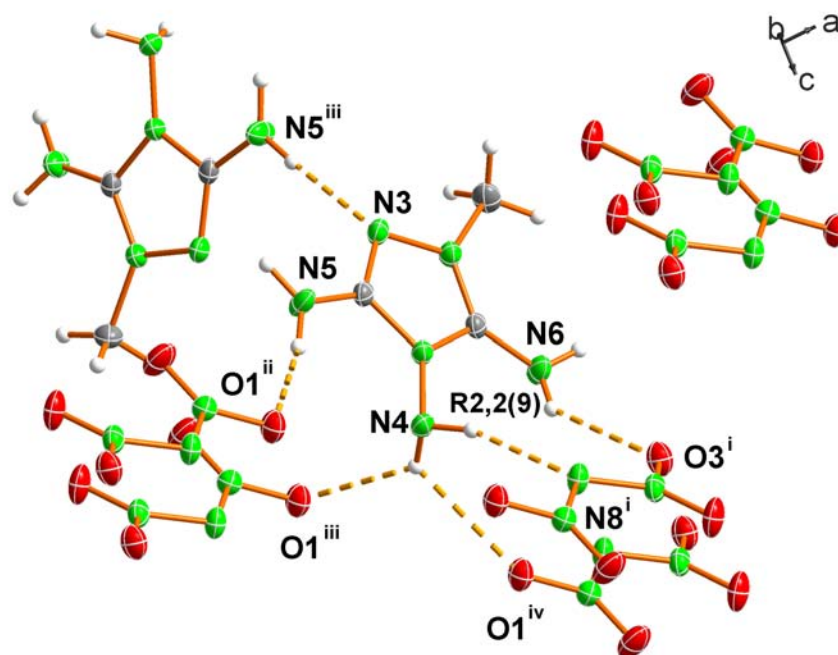


Figure 4.23 Hydrogen-bonding in the structure of 47. Symmetry codes: (i) $x, 1.5-y, 0.5+z$; (ii) $-x, 0.5+y, 0.5-z$; (iii) $-x, -0.5+y, 0.5-z$; (iv) $x, 0.5-y, 0.5+z$.

4.6 Physical and Energetic Properties

The DSC plots of guanazinium iodides (**55a** and **55b**) and methylguanazinium iodide (**41**) were measured at a heating rate of $2^{\circ}\text{C min}^{-1}$ and are shown in Figure 4.24. A small difference in the melting point between **55a** (194°C) and **55b** (190°C) is observed as one would expect from the differences in the molecular packing (see Molecular Structures discussion). The presence of the methyl group in **41** results in an increase in the melting point to 217°C . All three compounds melt with immediate exothermic decomposition just a few degrees above the melting point. In addition, for **41** a second decomposition of lower energy is observed at $\sim 260^{\circ}\text{C}$.

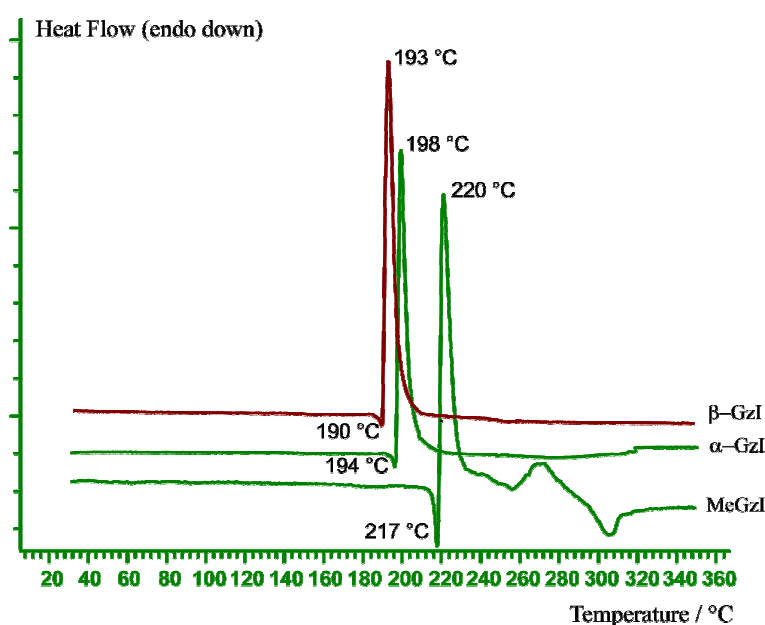
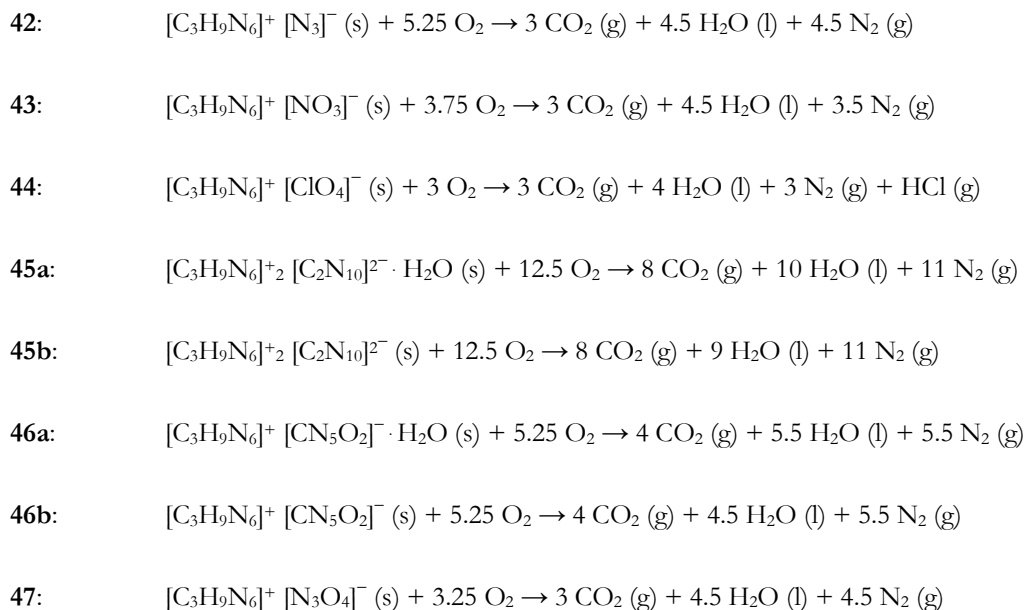


Figure 4.24 DSC plots of α -GzI (**55a**), β -GzI (**55b**) and **41**.

In order to assess the energetic properties of compounds **42–47** the thermal stability (melting and decomposition points from DSC measurements), sensitivity to impact, friction^[55–57] and thermal shock of each salt was experimentally determined. In addition, the constant pressure heats of combustion (ΔH_{comb}) of each salt were calculated from the predicted heats of reaction (ΔH_r) and an approximation of lattice enthalpy using the corresponding combustion equations (see below). Errors in the combustion measurements are estimated at $\sim 5\%$, therefore, disregarding the hydration enthalpy for the monohydrated species is justified. The method used here is explained in detail in *Appendix A*.



DSC studies on small samples of the materials show a family of salts with high thermal stability ($T_{\text{dec}} > 200$ °C, except for **46a** and **47**), possibly attributable to the high thermal stability of the methylguanazinium cation itself and extensive hydrogen-bonding in the solid state. Comparison of the melting points and decomposition temperatures of the iodide salt (**41**)^[10] with the energetic compounds (Table 4.4), clearly illustrates the influence of the different anions, i.e., the melting point follow the order nitrate > perchlorate > azide (> azotetrazolate) > nitrotetrazolate > dinitramide. A similar trend is observed for the decomposition temperatures: perchlorate > nitrate > azide > azotetrazolate > nitrotetrazolate > dinitramide. **42** and **43** melt with concomitant decomposition, whereas **45a** decomposes without melting. On the other hand, **46a** and **47** have decomposition points which are ~30 °C above their melting points and the perchlorate salt (**44**) has the best thermal stability decomposing at >300 °C. Trends in the melting and decomposition temperatures observed are in agreement with our previous report on 1,4-dimethyl-5-aminotetrazolium (1,4DMAT⁺) azide, perchlorate, nitrate and dinitramide salts,^[27] with the exception of the nitrate salt (**43**), which has an expectedly high melting point at 258 °C, much higher than 1,4-dimethyl-5-aminotetrazolium nitrate ($T_{\text{m}} = 181$ °C). This may be due to hydrogen-bonding and packing effects, which are also reflected in the higher density of **43** (1.667 *vs.* 1.523 g cm⁻³) or the nature of the MeG⁺ cation itself, since according to this and previous studies^[7b,8,10a] guanazinium salts tend to have liquid ranges of only a few degrees (if at all). Lastly, the decomposition points are in keeping with known heterocycle-based salts^[27,31] and approximately (except for **47**) in the range between that of RDX (230 °C) and TNT (300 °C).

Table 4.4 Physico-chemical properties of methylguanazinium salts.

	42	43	44	47
Formula	C ₃ H ₉ N ₉	C ₃ H ₉ N ₇ O ₃	C ₃ H ₉ N ₆ O ₄ Cl	C ₃ H ₉ N ₉ O ₄
Mol. Mass (g mol ⁻¹)	171.16	191.15	228.61	235.16
T _m (°C) ^[a]	212	258	247	129
T _d (°C) ^[b]	215	261	310	160
N (%) ^[c]	73.6	51.3	36.8	53.6
N + O (%) ^[d]	73.6	76.4	64.7	80.8
Ω (%) ^[e]	-98.1	-62.8	-42.0	-44.2
ρ (g cm ⁻³) ^[f]	1.399	1.667	1.669	1.657
ΔH _{comb.} / cal g ⁻¹ ^[g]	-4186	-3165	-2873	-2788
ΔU _f ^o / kJ kg ⁻¹ ^[h]	3231	459	2278	1291
ΔH _f ^o / kJ kg ⁻¹ ^[i]	3100	336	2180	1175

	45a	45b	46a	46b
Formula	C ₈ H ₂₀ N ₂₂ O	C ₈ H ₁₈ N ₂₂	C ₄ H ₁₁ N ₁₁ O ₃	C ₄ H ₉ N ₁₁ O ₂
Mol. Mass (g mol ⁻¹)	440.46	422.38	261.24	243.19
T _m (°C) ^[a]	-		162	
T _d (°C) ^[b]	201		196	
N (%) ^[c]	70.0	73.0	59.0	63.4
N + O (%) ^[d]	73.6	73.0	77.4	76.5
Ω (%) ^[e]	-90.8	-94.7	-64.3	-69.1
ρ (g cm ⁻³) ^[f]	1.575	~1.575	1.584	~1.584
ΔH _{comb.} / cal g ⁻¹ ^[g]		-4251		-3321
ΔU _f ^o / kJ kg ⁻¹ ^[h]	4182	4361	2091	2246
ΔH _f ^o / kJ kg ⁻¹ ^[i]	4070	4244	1986	2134

[a] Chemical melting point and [b] Decomposition point (DSC onsets) from measurement with $\beta = 2\text{ }^{\circ}\text{C min}^{-1}$; [c] Nitrogen percentage; [d] Combined nitrogen and oxygen percentages; [e] Oxygen balance according to ref. [58]; [f] Density from X-ray measurements; [g] Calculated constant pressure heat of combustion; [h] Standard heat of formation (back-calculated from ΔH_{comb}); [i] Standard heat of formation.

In addition to DSC analysis, the response of each compound to fast thermal shock was tested by placing a small sample of the material in the flame. Apart from **43** and **45a** that burn normally, the rest deflagrate in the flame (both TNT and RDX explode under similar conditions). From this results it would seem like salts with a high nitrogen content such as **42** and **45a**, or a better (less negative) oxygen balance (**44** and **47**) are more sensitive to fast heating.

Data collected for impact, friction and electrostatic discharge sensitivities are summarized in Table 4.5 together with the calculated (EXPLO5) detonation parameters. Only **44** (25 J) and **47** (20 J) are slightly sensitive to shock whereas the rest of the compounds are insensitive (>40 J). The friction sensitivity values for all materials are also very low (>320 N) except for that of the perchlorate salt (220 N), which can be classified as a sensitive material according to the UN Recommendations on the Transport of Dangerous Goods.^[56] A comparison of these values to

those measured for TNT and RDX is useful to assess the energetic salts in this study. All compounds are less sensitive to impact than TNT (15 J) and RDX (7.4 J), less sensitive to friction than RDX (120 N) and except for **42** (320 N) and **44** (220 N) they are also less sensitive to friction than TNT (355 N).^[62]

Table 4.5 Initial safety testing results and predicted (calculated) energetic performance of methylguanazinium salts using the EXPLO5 code.

	$T_{\text{ex}} / \text{K}^{[a]}$	$V_0 / \text{L kg}^{-1[b]}$	$P / \text{GPa}^{[c]}$	$D / \text{m s}^{-1[d]}$	Impact / J ^[e]	Friction / N ^[e]	Thermal Shock
42	5829	762	27.5	8719	>40	320	Deflagrates
43	3030	843	25.8	8270	>40	>360	Burns
44	-	-	-	-	25	220	Deflagrates
45a	3362	816	28.6	8922	>40	>360	Deflagrates
45b	3242	797	27.7	8834			
46a	3442	829	25.6	8330	>40	>360	Burns
46b	3233	797	23.9	8117			
47	3736	837	27.7	8383	20	360	Deflagrates
TNT	3736	620	20.5	7171	15	355	Explodes
RDX	4334	796	34.0	8885	7.4	120	Explodes

[a] Temperature of the explosion gases; [b] Volume of the explosion gases; [c] Detonation pressure; [d] Detonation velocity; [e] Tests according to BAM methods (see ref. [55–57]).

Table 4.4 also contains the physico-chemical properties of salts **42–47**. The densities range from low ($\rho_{\text{calc}}(\mathbf{42}) = 1.399 \text{ g cm}^{-3}$) to moderate ($\rho_{\text{calc}}(\mathbf{44}) = 1.669 \text{ g cm}^{-3}$) and the predicted constant pressure heats of combustion (ΔH_{comb}) are highly negative. The heats of formation are all positive and tend to decrease with decreasing nitrogen content apart from that of the 5,5'-azotetrazolate salts, which have outstandingly high values (+4100 kJ kg⁻¹) and the perchlorate salt, which regardless of the lowest nitrogen content has a very positive heat of formation (+2180 kJ kg⁻¹). From the experimentally determined densities (X-ray), chemical compositions and energies of formation (back-calculated from the heats of combustion) the detonation pressures and velocities of **42** (8719 m s⁻¹, 27.5 GPa), **43** (8270 m s⁻¹, 25.8 GPa), **45a** (8922 m s⁻¹, 28.6 GPa), **45b** (8834 m s⁻¹, 27.7 GPa), **46a** (8330 m s⁻¹, 25.6 GPa), **46b** (8117 m s⁻¹, 23.9 GPa) and **47** (8383 m s⁻¹, 27.7 GPa) were predicted using the EXPLO5 code.^[63] The following values for the empirical constants in the Becker-Kistiakowsky-Wilson equation of state (BKWN-EOS): $a = 0.5$, $\beta = 0.176$, $\kappa = 14.71$ and $\theta = 6620$, were used. Due to the non-availability of a suitable method for the calculation of detonation parameters of compounds containing atoms others than C, H, N and O, **44** was excluded of this section. At this point it is important to point out that the predicted performances based on theoretical heats of combustion calculated by the above-mentioned method, tend to overestimate the values. In any case, taking into account this systematic overestimation, all

compounds are predicted to outperform TNT (7171 m s^{-1} , 20.5 GPa) and the azide and 5,5'-azotetrazolate salts have predicted values comparable to RDX (8885 m s^{-1} , 34.0 GPa).

Due to the negative oxygen balance of the salts studies here (−42 to −98%) it is of interest to analyze the performance of mixtures of the compounds with an oxidizer such as ammonium nitrate (AN) or ammonium dinitramide (ADN) at an approximately oxygen neutral ratio ($\Delta Q \sim 0\%$) in order to further enhance their performances. The results of the EXPLO5 calculations are summarized in Tables 3.A3–3.A6. Formulations of the compounds with AN show, in general, no increase in the performance and highly negative energies of formation ($\sim -3000 \text{ kJ kg}^{-1}$). On the other side, mixtures with ADN are predicted to have less negative heats of formation (positive values for the 5,5'-azotetrazolate salts) and better performances in all cases in comparison to the stand-alone energetic materials. The latter have high values between 31.3 and 33.7 GPa for the detonation pressures and between 8801 and 9077 m s^{-1} for the detonation velocities, which are similar to the predicted performance of mixtures of RDX and ADN.^[30b]

4.7 Conclusions

Guanazinium halogenide salts have been synthesized and fully characterized by analytical and spectroscopic methods. In addition, the structures of the compounds were determined by X-ray diffraction techniques. Depending on the base used and experimental conditions, **55** was formed in two polymorphic forms (α and β) which can be distinguished by their vibrational spectra, molecular structure and melting/decomposition points. These compounds proved to be useful starting materials for the synthesis of a new family of energetic salts based on the guanazinium cation (*Chapters V and VII*) and on the novel nitrogen-rich methylguanazinium cation. The energetic compounds have been synthesized in high yields and bulk purities and were characterized fully, including X-ray structure analysis. The hydrogen-bonding networks observed in the crystal structures were assessed by means of graph-set analysis. The nitrate and perchlorate anions seem to increase the decomposition points of the compounds whereas the 5-nitrotetrazolate (**46a**) and dinitramide (**47**) salts have lower thermal stabilities. Aside from **47** all materials exhibit excellent thermal stabilities ($>190 \text{ }^{\circ}\text{C}$). All compounds have moderate densities $>1.4 \text{ g cm}^{-3}$, which are, in general, in the range of currently used explosives ($1.6\text{--}1.8 \text{ g cm}^{-3}$) and excellent combined oxygen and nitrogen balances, which are interesting from an environmental point of view. Additionally, all materials can be classified as insensitive or having a low sensitivity to classical stimuli. Formulations with AN are predicted to decrease the detonation parameters whereas ADN increase them substantially. Lastly, the predicted detonation parameters of all

compounds are higher than those of conventionally used TNT and those of the azide (**42**) and 5,5'-azotetrazolate (**45a** and **45b**) salts indicate comparable performances to RDX, which suggest their potential as high-explosives.

4.8 Experimental Section

Caution! Silver azide, silver dinitramide and their derivatives are energetic materials that tend to explode under certain conditions. Although we had no difficulties during the preparation and handling of the compounds described below, they are nevertheless energetic materials and their synthesis should be carried out by experienced personnel. In any case, proper protective measures such as Kevlar gloves, ear protection, safety shoes and plastic spatulas, should be taken at all times especially when working on a large scale (>1 g).

General. All chemical reagents and solvents of analytical grade were obtained from Sigma-Aldrich Inc. and used as supplied. Methylguanazinium iodide,^[10] silver dinitramide and silver(bispyridine) dinitramide,^[17] sodium 5,5'-azotetrazolate pentahydrate^[18] and silver 5-nitrotetrazolate^[64] were prepared according to literature procedures. ¹H, ¹³C, and ¹⁴N/¹⁵N NMR spectra were recorded on a JEOL Eclipse 400 instrument. The spectra were measured in [D₆]DMSO at 25 °C. The chemical shifts are given relative to tetramethylsilane (¹H, ¹³C) or nitromethane (¹⁴N/¹⁵N) as external standards. Coupling constants (*J*) are given in hertz (Hz). Infrared (IR)^[65] spectra were recorded on a Perkin-Elmer Spectrum One FT-IR instrument as KBr pellets at room temperature. Raman spectra were recorded on a Perkin-Elmer Spectrum 2000R NIR FT-Raman instrument equipped with a Nd:YAG laser (1064 nm). The intensities are reported in percentages relative to the most intense peak and are given in parentheses. Elemental analyses were performed with a Netsch Simultaneous Thermal Analyzer STA 429. Melting points were determined by differential scanning calorimetry (Linseis DSC PT-10 instrument, calibrated with standard pure indium and zinc)^[66]. Measurements were performed at a heating rate of $\beta = 2\text{ }^{\circ}\text{C min}^{-1}$ in closed aluminium containers with a hole (1 mm) on the top for gas release with a nitrogen flow of 20 mL min⁻¹. The reference sample was a closed aluminium container.

Bomb Calorimetry. For all calorimetric measurements, a Parr 1356 bomb calorimeter (static jacket) equipped with a Parr 207A oxygen bomb for the combustion of highly energetic materials was used^[67]. A Parr 1755 printer, furnished with the Parr 1356 calorimeter, was used to produce a permanent record of all activities within the calorimeter. The samples (~200 mg each) were carefully mixed with ~800 mg analytical grade benzoic acid and pressed into pellets, which were subsequently burned in a 3.05 MPa atmosphere of pure oxygen. The experimentally determined constant volume energies of combustion were obtained as the average of five single measurements. The calorimeter was calibrated by the combustion of certified benzoic acid in an oxygen atmosphere at a pressure of 3.05 MPa.

Synthesis of 1-Methyl-3,4,5-triamino-1,2,3-triazolium Iodide (41). Guanazine (7.27 g, 63.71 mmol) was refluxed, under a stream of nitrogen, in the presence of an excess of methyl iodide 99% (65 mL, 1.04 mol) in methanol (100 mL). After 40 hours, a yellowish solid was formed, that was filtered out of the solution leading to 13.2 g of crude compound (80.9% yield). The crude product was recrystallized from methanol. C₃H₉N₆I (256.05 g mol⁻¹); C 14.07 (calc. 14.12); H 3.54 (3.61); N 32.82 (33.07); I 49.56 (48.98)%, m. p. (Büchi B-540, uncorrected): 216.9-218.1 °C, DSC (2 °C/min, °C): 217 (m.p.), 220 (dec.), m/z (FAB⁺,

xenon, 6 keV, m-NBA matrix): 129.3 [cation], ^1H NMR (DMSO- d_6 , 400.18 MHz, 25°C, TMS) δ /ppm: 7.96 (2H, s, N(4)H₂), 6.38 (2H, s, N(6)H₂), 5.62 (2H, s, N(5)H₂), 3.39 (3H, s, CH₃), $^{13}\text{C}\{^1\text{H}\}$ NMR (DMSO- d_6 , 100.63 MHz, 25°C, TMS) δ /ppm: 150.4 (1C, C N(5)H₂), 147.4 (1C, C N(6)H₂), 34.6 (1C, CH₃), ^{15}N NMR (DMSO- d_6 , 40.55 MHz, 25°C, MeNO₂) δ /ppm: -334.1 (1N, t, J = 72.1 Hz, N(6)H₂), -321.9 (1N, t, J = 71.4 Hz, N(5)H₂), -319.8 (1N, t, J = 80.3 Hz, N(4)H₂), -239.8 (1N, N(2)), -238.0 (1N, N(1)), -163.3 (1N, N(3)), Raman $\Delta\nu$ / cm^{-1} (rel. int.): 3238(30, $\nu_{\text{N-H}}$) 3123(16, $\nu_{\text{N-H}}$) 2985(12, $\nu_{\text{C-H}}$) 2938(14, $\nu_{\text{C-H}}$) 1700(46, $\nu_{\text{C=N}}$) 1642(13, $\nu_{\text{C=N}}$) 1612(15) 1571(14, $\nu_{\text{N=N}}$) 1529(12) 1472(14) 1427(16) 1338(27) 1133(11) 1098(16) 918(18) 780(100, $\nu_{\text{N(CCN)}}$) 650(52) 619(13) 590(31) 524(15) 338(36) 306(35) 180(17), IR $\Delta\nu$ / cm^{-1} (KBr, rel. int.): 3384(s, $\nu_{\text{N-H}}$) 3257(s, $\nu_{\text{N-H}}$) 3098(s, $\nu_{\text{C-H}}$) 2939(s, $\nu_{\text{C-H}}$) 2824(m, $\nu_{\text{C-H}}$) 1943(w) 1835(w) 1643(s, $\nu_{\text{C=N}}$) 1466(s) 1421(m) 1384(m) 1330(m) 1244(m) 1225(m) 1093(s) 1022(m) 883(s) 775(m, $\nu_{\text{N(CCN)}}$) 708(s) 647(m) 618(m) 586(m).

Synthesis of 1-Methyl-3,4,5-triamino-1,2,3-triazolium Azide (42). Freshly prepared silver azide (0.367 g, 2.45 mmol) was suspended in methanol (10 mL) and **41** (0.424 g, 2.04 mmol) was added with immediate precipitation of yellow silver iodide. The suspension containing an excess of silver azide was filtered after 90 minutes reaction time into ether (80 mL) causing precipitation of a slightly pink product, which was filtered under gravity, washed with ether and recrystallized from ether/methanol yielding single crystals of the compound (0.181 g, 72%). DSC (2 °C min⁻¹, °C): 212 (m.p.), ~215 (dec.); ^1H NMR ([D₆]DMSO, 400.18 MHz, 25°C, TMS) δ /ppm: 8.06 (2H, s, N4H₂), 6.49 (2H, s, N6H₂), 5.68 (2H, s, N5H₂), 3.43 (3H, s, CH₃); $^{13}\text{C}\{^1\text{H}\}$ NMR ([D₆]DMSO, 100.63 MHz, 25°C, TMS) δ /ppm: 150.5 (1C, C–N5H₂), 147.6 (1C, C–N6H₂), 34.2 (1C, CH₃); $^{14}\text{N}\{^1\text{H}\}$ NMR ([D₆]DMSO, 40.55 MHz, 25 °C, MeNO₂) δ /ppm: -132.8 (NNN), -276.9 (NNN); ^{15}N NMR ([D₆]DMSO, 40.55 MHz, 25 °C, MeNO₂) δ /ppm: -134.2 (NNN), -164.8 (1N, N3), -239.0 (1N, N1), -240.5 (1N, N2), -277.9 (NNN), -321.9 (1N, t, J = 74.9 Hz, N4H₂), -322.4 (1N, t, J = 80.5 Hz, N5H₂), -335.4 (1N, t, J = 85.2 Hz, N6H₂); Raman ν / cm^{-1} (rel. int.): 3174(6) 2942(7) 2812(4) 1713(21) 1667(15) 1464(13) 1417(13) 1373(5) 1347(83) 1246(14) 1200(13) 1116(12) 890(8) 775(56) 650(32) 618(11) 590(12) 357(18) 321(31) 273(11) 174(29); IR ν / cm^{-1} (KBr, rel. int.): 3324(s) 3263(s) 3192(s) 3086(s) 2039(s) 1699(s) 1660(s) 1604(m) 1574(m) 1536(w) 1462(m) 1423(w) 1384(w) 1331(w) 1242(w) 1099(m) 1022(w) 881(w) 777(w) 712(w) 649(m) 587(w) 486(w) 348(w); m/z (FAB⁺, xenon, 6 keV, m-NBA matrix): 129.3 (cation); C₃H₉N₉ (calc./found): C 21.05 / 21.10, H 5.30 / 5.31, N 73.65 / 73.41%.

Synthesis of 1-Methyl-3,4,5-triamino-1,2,3-triazolium Nitrate (43). **41** (1.700 g, 6.64 mmol) was reacted, at room temperature, with silver nitrate (1.180 g, 6.95 mmol) in water (30 mL) and the reaction mixture was stirred for 30 minutes. Silver iodide immediately precipitated as a brownish solid, this was filtered and the filtrate was concentrated in vacuo at 60 °C giving pale pink single crystals of the compound upon cooling (0.931 g, 73%). DSC (2 °C min⁻¹, °C): 258 (m.p.), ~261 (dec.); ^1H NMR ([D₆]DMSO, 400.18 MHz, 25°C, TMS) δ /ppm: 7.94 (2H, s, N4H₂), 6.45 (2H, s, N6H₂), 5.69 (2H, s, N5H₂), 3.41 (3H, s,

CH₃); ¹³C{¹H} NMR ([D₆]DMSO, 100.63 MHz, 25°C, TMS) δ/ppm: 150.5 (1C, C–N5H₂), 147.6 (1C, C–N6H₂), 34.2 (1C, CH₃); ¹⁴N{¹H} NMR ([D₆]DMSO, 40.55 MHz, 25°C, MeNO₂) δ/ppm: –4.1 (1N, NO₃); ¹⁵N NMR ([D₆]DMSO, 40.55 MHz, 25 °C, MeNO₂) δ/ppm: –4.6 (NO₃), –164.6 (1N, N3), –238.8 (1N, N1), –240.3 (1N, N2), –322.8 (1N, t, J = 75.8 Hz, N4H₂), –323.7 (1N, t, J = 90.8 Hz, N5H₂), –336.0 (1N, t, J = 87.5 Hz, N6H₂); Raman ν / cm^{–1} (rel. int.): 3214(8) 2953(8) 2402(15) 1703(20) 1652 (2) 1471(23) 1425(20) 1393(26) 1049(100) 916(11) 775(18) 716(19) 627(25) 589(15) 304(18); IR ν / cm^{–1} (KBr, rel. int.): 3349(s) 3278(s) 3150(s) 2948(m) 2424(w) 1704(s) 1656(s) 1578(m) 1538(m) 1465(m) 1423(m) 1383(s) 1327(s) 1301(s) 1209(m) 1082(m) 1046(m) 1024(m) 885(m) 828(m) 775(m) 719(m) 678(w) 586(m) 548(m) 418(m) 350(m) 303(w) 289(w) 279(w); m/z (FAB⁺, xenon, 6 keV, m-NBA matrix): 129.3 (cation); C₃H₉N₇O₃ (calc./found): C 18.85 / 18.73, H 4.75 / 4.85, N 51.29 / 51.25%.

Synthesis of 1-Methyl-3,4,5-triamino-1,2,3-triazolium Perchlorate (44). Anhydrous silver perchlorate was weighed out in a glove box (0.754 g, 3.64 mmol) and dissolved into water (10 mL). Neat **2** (0.931 g, 3.64 mmol) was added portionwise with immediate precipitation of yellow silver iodide. The reaction mixture was stirred at room temperature and under exclusion of light for 1.5 hours, after which time the solution was filtered into a glass shell and left to evaporate overnight yielding pure crystalline **44** (0.831 g, quant. yield). The crystals could be used for diffraction measurements. DSC (2 °C min^{–1}, °C): 247 (m.p.), ~310 (dec.); ¹H NMR ([D₆]DMSO, 400.18 MHz, 25°C, TMS) δ/ppm: 7.92 (2H, s, N4H₂), 6.47 (2H, s, N6H₂), 5.61 (2H, s, N5H₂), 3.41 (3H, s, CH₃); ¹³C{¹H} NMR ([D₆]DMSO, 100.63 MHz, 25°C, TMS) δ/ppm: 150.5 (1C, C–N5H₂), 147.5 (1C, C–N6H₂), 34.2 (1C, CH₃); ¹⁵N NMR ([D₆]DMSO, 40.55 MHz, 25 °C, MeNO₂) δ/ppm: –164.7 (1N, N3), –238.7 (1N, N1), –240.6 (1N, N2), –323.1 (1N, t, J = 75.8 Hz, N4H₂), –324.0 (1N, t, J = 91.2 Hz, N5H₂), –336.2 (1N, t, J = 88.1 Hz, N6H₂); ³⁵Cl NMR ([D₆]DMSO, 39.21 MHz, 25°C, NaCl) δ/ppm: 1.0 (ClO₄); Raman ν / cm^{–1} (rel. int): 3303(4) 2994(3) 2949(7) 2818(2) 1710(27) 1649(11) 1580(10) 1476(9) 1426(14) 1334(13) 1248(8) 1134(10) 936(100) 777(48) 651(34) 629(18) 588(12) 462(29) 332(13) 306(16); IR ν / cm^{–1} (KBr, rel. int.): 3382(s) 3327(s) 3258(s) 3085(s) 1699(s) 1658(vs) 1461(w) 1424(w) 1384(m) 1332(w) 1260(w) 1144(s) 1113(s) 1087(vs) 907(w) 778(w) 712(w) 636(w) 626(m) 587(w) 476(w) 350(w) 321(w) 302(w); m/z (FAB⁺, xenon, 6 keV, m-NBA matrix): 129.1 (cation); C₃H₉N₆O₄Cl (calc./found): C 15.76 / 15.76, H 3.97 / 3.96, N 36.76 / 36.48, Cl 15.51 / 15.40%.

Synthesis of Bis(1-Methyl-3,4,5-triamino-1,2,3-triazolium) 5,5'-Azotetrazolate Monohydrate (45a). **41** (1.025 g, 4.00 mmol) was refluxed with sodium 5,5'-azotetrazolate pentahydrate (0.600 g, 2.00 mmol) in water (20 mL) for 45 minutes. The reaction mixture was left to cool giving a first crop (0.569 g) of the compound. The volume of the orange filtrate was reduced and cooled in a refrigerator yielding slightly orange single crystals of the same product (0.168 g). The total amount of the product obtained as the monohydrate species was 0.737 g (84%). DSC (2 °C min^{–1}, °C): ~90 (H₂O loss), ~198 (dec.); ¹H NMR ([D₆]DMSO, 400.18 MHz, 25°C, TMS) δ/ppm: 8.14 (2H, s, N4H₂), 6.55 (2H, s, N6H₂), 5.79 (2H, s, N5H₂), 3.43 (3H, s, CH₃); ¹³C{¹H} NMR ([D₆]DMSO, 100.63 MHz, 25°C, TMS) δ/ppm: 173.1 (2C,

C–N=N) 150.4 (1C, C–N5H₂), 147.6 (1C, C–N6H₂), 34.2 (1C, CH₃); ¹⁵N NMR ([D₆]DMSO, 40.55 MHz, 25 °C, MeNO₂) δ/ppm: +107.5 (–N=N–), +12.4 (CN_α), –66.5 (CN_β), –164.6 (1N, N3), –239.1 (1N, N1), –240.4 (1N, N2), –322.7 (1N, t, J = 79.1 Hz, N4H₂), –323.2 (1N, t, J = 88.9 Hz, N5H₂), –335.4 (1N, t, J = 87.6 Hz, N6H₂); Raman ν / cm^{–1} (rel. int.): 3188(6) 1710(2) 1615(2) 1488(60) 1410(20) 1373(100) 1348(3) 1160(2) 1088 (6) 1084(18) 1072(11) 1058(23) 919(9) 780(5) 647(2) 594(2) 333(2); IR ν / cm^{–1} (KBr, rel. int.): 3328(s) 3256(s) 3047(s) 2803(m) 1708(s) 1663(s) 1620(m) 1592(m) 1532(w) 1456(w) 1385(m) 1242(w) 1192(w) 1157(w) 1118(w) 1049(w) 1029(w) 957(w) 897(w) 872(w) 774(m) 726(w) 643(m) 587(w) 558(w) 452(w) 360(w) 332(w) 320(w) 296(w) 285(w) 205(w); m/z (FAB⁺, xenon, 6 keV, m-NBA matrix): 129.3 (cation), (FAB[–], xenon, 6 keV, m-NBA matrix): 164.1 (anion); C₈H₂₀N₂₂O (calc./found): C 21.82 / 21.67, H 4.58 / 4.74, N 69.97 / 69.88%.

Synthesis of 1-Methyl-3,4,5-triamino-1,2,3-triazolium 5-Nitrotetrazolate Monohydrate (46a).

Sodium 5-nitrotetrazolate dihydrate (0.286 g, 1.91 mmol) was dissolved in water (3 mL) and a solution of silver nitrate (0.481 g, 2.99 mmol) in water (5 mL) was added dropwise with immediate precipitation of highly explosive white silver 5-nitrotetrazolate. The suspension was stirred for a few minutes and centrifuged. The liquid was decanted and the solid washed one time with water (5 mL) and one time with methanol (5 mL) with subsequent centrifuging. The liquid was decanted in both cases and the silver salt was suspended in methanol (10 mL) before neat **41** (0.417 g, 1.628 mmol) was added portionwise. Silver iodide immediately precipitated and the reaction mixture was stirred for 1.5 hours, after which time the insoluble solid was filtered and the methanol evaporated to dryness giving the crude product, which could be recrystallized by ether diffusion into a saturated methanolic solution of the compound, yielding pure crystalline material, which could be used to measure the crystal structure (0.308 g, 73%). DSC (2 °C min^{–1}, °C): ~85 (H₂O loss), 162 (m.p.), ~196 (dec.); ¹H NMR ([D₆]DMSO, 400.18 MHz, 25°C, TMS) δ/ppm: 7.92 (2H, s, N4H₂), 6.42 (2H, s, N6H₂), 5.62 (2H, s, N5H₂), 3.68 (2H, s, H₂O), 3.37 (3H, s, CH₃); ¹³C{¹H} NMR ([D₆]DMSO, 100.63 MHz, 25°C, TMS) δ/ppm: 168.9 (1C, C–NO₂), 150.8 (1C, C–N5H₂), 147.9 (1C, C–N6H₂), 34.6 (1C, CH₃); ¹⁵N NMR ([D₆]DMSO, 40.55 MHz, 25 °C, MeNO₂) δ/ppm: 18.7 (2N, N9/10), –22.9 (1N, NO₂), –62.5 (2N, N8/11), –164.0 (1N, N3), –238.3 (1N, N1), –239.9 (1N, N2), –321.1 (1N, t, J = 79.98 Hz, N4H₂), –322.2 (1N, t, J = 75.70 Hz, N5H₂), –335.4 (1N, t, J = 87.70 Hz, N6H₂); Raman ν / cm^{–1} (rel. int.): 3138(3) 2959(4) 1712(10) 1662(10) 1546(15) 1447(14) 1418(100) 1320(11) 1184(9) 1162(10) 1068(57) 1051(31) 900(6) 836(13) 782(26) 647(13) 623(7) 591(7) 538(6) 321(10) 260(7) 239(8); IR ν / cm^{–1} (KBr, rel. int.): 3379(s) 3327(s) 3255(s) 3089(s) 2730(w) 2464(w) 2092(w) 1700(s) 1657(s) 1545(s) 1444(s) 1419(s) 1384(m) 1343(w) 1317(m) 1241(w) 1173(w) 1161(w) 1101(m) 1060(w) 1050(w) 1031(w) 963(w) 903(w) 839(w) 832(w) 780(w) 712(w) 625(w) 588(w) 472(w); m/z (FAB⁺, xenon, 6 keV, m-NBA matrix): 129.1 (cation), (FAB[–], xenon, 6 keV, m-NBA matrix): 114.0 (anion); C₄H₁₁N₁₁O₃ (calc./found): C 18.39 / 18.29, H 4.24 / 4.28, N 58.99 / 58.82%.

Synthesis of 1-Methyl-3,4,5-triamino-1,2,3-triazolium Dinitramide (47). *Method A:* A fresh hot solution of silver dinitramide (0.446 g, 3.04 mmol) in methanol (50 mL) was added into a solution of **41**

(0.632 g, 3.04 mmol) in methanol (5 mL) at room temperature. Immediate precipitation of yellow silver iodide was observed and the reaction mixture was stirred for further 45 minutes under exclusion of light. The crude product was precipitated by addition of ether (300 mL) and recrystallized by ether diffusion into a concentrated methanolic solution. The overall yield over two steps is 42% (0.301 g).

Method B: Alternatively, **47** was synthesized in a safer way as follows: Silver dinitramide bispyridine (0.277 g, 1.05 mmol) was dissolved in methanol (5 mL) and neat **41** (0.218 g, 1.05 mmol) was added causing precipitation of yellow silver iodide. The suspension was stirred for 1 hour under exclusion of light and the yellow residue was filtered. Ether (60 mL) was added to the filtrate causing precipitation of a white solid, which was filtered under vacuum. The crude product could be purified by allowing ether to slowly diffuse into a saturated solution of the compound overnight yielding single crystals of the compound (0.147 g, 75%). DSC (2 °C min⁻¹, °C): 129 (m.p.), ~160 (dec.); ¹H NMR ([D₆]DMSO, 400.18 MHz, 25°C, TMS) δ/ppm: 7.93 (2H, s, N4H₂), 6.47 (2H, s, N6H₂), 5.62 (2H, s, N5H₂), 3.41 (3H, s, CH₃); ¹³C{¹H} NMR ([D₆]DMSO, 100.63 MHz, 25°C, TMS) δ/ppm: 150.5 (1C, C–N5H₂), 147.5 (1C, C–N6H₂), 34.2 (1C, CH₃); ¹⁴N{¹H} NMR ([D₆]DMSO, 40.55 MHz, 25°C, MeNO₂) δ/ppm: –10.1 (2N, N(NO₂)₂); ¹⁵N NMR ([D₆]DMSO, 40.55 MHz, 25 °C, MeNO₂) δ/ppm: –11.1 (N(NO₂)₂), –164.5 (1N, N3), –177.8 (N(NO₂)₂), –238.8 (1N, N1), –240.5 (1N, N2), –322.5 (1N, t, J = 76.5 Hz, N4H₂), –323.5 (1N, t, J = 91.9 Hz, N5H₂), –335.9 (1N, t, J = 84.8 Hz, N6H₂); Raman ν / cm⁻¹ (rel. int.): 3200(6) 2954(7) 1706(20) 1649(10) 1577(9) 1473(10) 1437(18) 1421(15) 1312(100) 1220(10) 1090(3) 1174(10) 1118(10) 1047(11) 1014(9) 959(12) 911(7) 823(37) 777(48) 649(31) 588(11) 545(7) 488(21) 452(8) 338(20) 300(37) 192(13); IR ν / cm⁻¹ (KBr, rel. int.): 3381(m) 3327(m) 3258(s) 3086(s) 1699(m) 1658(vs) 1613(w) 1537(m) 1431(m) 1384(w) 1343(w) 1205(s) 1178(s) 1097(w) 1032(m) 953(vw) 905(vw) 828(vw) 778(w) 761(w) 732(w) 712(w) 648(w) 587(w) 470(w); m/z (FAB⁺, xenon, 6 keV, m-NBA matrix): 129.3 (cation); C₃H₉N₉O₄ (calc./found): C 15.32 / 15.21, H 3.86 / 3.77, N 53.61 / 53.88%.

Synthesis of 3,4,5-Triamino-1,2,3-triazolium Bromide (53). A mixture of 72 g (~ 1 mole) of dimethylcyanamide 97% and 50 g (~ 1 mole) of hydrazine hydrate 98% was refluxed for 24 hours. The resulting solid mass obtained on cooling was treated with an excess of a concentrated solution of 48% hydrobromic acid in MeOH. A white solid precipitated, that was filtered off and washed with a saturated solution of sodium carbonate in cold water. Finally, this was recrystallized from water yielding 68 g (70%) of 3,4,5-triamino-1,2,4-triazolium bromide. DSC (2 °C min⁻¹, °C): 269 (m.p.), ~270 (dec.); ¹H NMR ([D₆]DMSO, 400.18 MHz, 25°C, TMS) δ/ppm: 7.20 (broad s, 4H, -NH₂), 5.91 (broad s, 2H, -NH₂); ¹³C{¹H} NMR ([D₆]DMSO, 100.63 MHz, 25°C, TMS) δ/ppm: 150.4 (C-3,5); ¹⁵N NMR ([D₆]DMSO, 40.55 MHz, 25 °C, MeNO₂) δ/ppm: –202.6 (2N, N-1,2), –239.0 (1N, N4), –320.2 (1N, t, J = 75.7 Hz, N(3)H₂), –328.4 (2N, t, J = 85.0 Hz, N(4)H₂); Raman ν / cm⁻¹ (rel. int.): 3238(7), 3162(7), 1699(11), 1671(19), 1451(12), 1381(10), 1315(12), 806(25), 774(100), 631(18), 343(13), 327(18), 181(11); IR ν / cm⁻¹ (KBr, rel. int.): 3306m, 3242w, 3114s, 1702s, 1659s, 1621s, 1527m, 1451m, 1381w, 1152w, 1017m, 920s,

799w, 769w, 692s; m/z (FAB⁺, xenon, 6 keV, m-NBA matrix): 115.0 (cation); Elemental Analysis (C₂H₇N₆Br): calcd., found / %: C 12.32, 12.29; N 43.09, 43.29; H 3.62, 3.60; Br 40.97, 41.05.

Synthesis of α -3,4,5-Triamino-1,2,3-triazolium Iodide (55a). A mixture of S-methylthiosemicarbazide hydroiodide (4.60 g, 19.73 mmol) and sodium azide (1.96 g, 30.18 mmol) in 80 mL ethanol was refluxed overnight under nitrogen until no more methylmercaptane was evolved. The reaction mixture was left to cool, and the precipitated sodium iodide and excess sodium azide were filtered off and discarded leaving an orange filtrate, which was decolorized by refluxing twice in the presence of decolorizing charcoal. After filtration, while still hot, the colorless solution was left to cool yielding a first crop of the product. The volume of the filtrate was reduced and cooled in the fridge leaving a second crop of pure material which was combined with the first one (1.44 g, 60 %). Suitable crystals for XRD were grown by diffusing ether into an ethanolic solution of the product. C₂H₇N₆I (242.02 g mol⁻¹); C 9.93 (calc. 9.71); H 2.91 (2.74); N 34.72 (34.61); I 52.43 (52.03)%, m. p. (Büchi B-540, uncorrected): 193.6-195.1 °C, DSC (2 °C/min, °C): 194 (m.p.), 198 (dec.), m/z (FAB⁺, xenon, 6 keV, m-NBA matrix): 115 [cation], ¹H NMR (DMSO-d₆, 400.18 MHz, 25°C, TMS) δ /ppm: 7.00 (2H, s, N(3)H₂), 5.56 (4H, s, N(4)H₂), ¹³C{¹H} NMR (DMSO-d₆, 100.63 MHz, 25°C, TMS) δ /ppm: 150.5 (2C, C N(4)H₂), ¹⁵N NMR (DMSO-d₆, 40.55 MHz, 25°C, MeNO₂) δ /ppm: -329.5 (2N, t, J = 88.5 Hz, N(4)H₂), -321.9 (1N, t, J = 75.7 Hz, N(3)H₂), -238.8 (1N, N(1)), -202.7 (2N, N(2)), Raman $\Delta\nu$ / cm⁻¹ (rel. int.): 3253(18, ν_{N-H}) 1696(15, $\nu_{C=N}$) 1659(14, $\nu_{C=N}$) 1545(20, $\nu_{N=N}$) 1437(9) 1295(16) 1049(18, $\nu_{N=N}$) 951(9) 800(23) 760(100, $\nu_{N(CCN)}$) 625(14) 575(14) 312(41) 179(15), IR $\Delta\nu$ / cm⁻¹ (KBr, rel. int.): 3397(s, ν_{N-H}) 3283(s, ν_{N-H}) 2020(w) 1697(s, $\nu_{C=N}$) 1646(s, $\nu_{C=N}$) 1384(w) 1332(w) 1298(w) 1129(w) 1101(w) 1006(w, $\nu_{N=N}$) 976(w) 888(m) 788(w) 761(m, $\nu_{N(CCN)}$) 713(m) 614(w) 580(w).

Synthesis of β -3,4,5-Triamino-1,2,3-triazolium Iodide (55b). *Method A:* S-Methylthiosemicarbazide hydroiodide (9.20 g, 39.48 mmol) was dissolved in 120 mL ethanol under nitrogen and 3.0 mL of 1,1-dimethylhydrazine (39.48 mmol) were added in one portion. The reaction mixture was refluxed for three hours and left to cool giving an slightly orange solution. Hydroiodic acid was added till the solution turned colorless and a white solid precipitated, which was filtered off and dried. The solvent was stripped at 40 °C and 50 mbar under nitrogen and the crude was recrystallized from a small amount of ethanol yielding a second crop of a slightly orange crystalline solid. These crystals were used to measure the X-ray structure revealing a new polymorph form of **55** (6.12 g, 63%).

Method B: Guanazine (1.52 g, 13.32 mmol) was reacted with an excess of hydroiodic acid 57% (5 mL, 37.90 mmol) in methanol (20 mL). The mixture was stirred for 15 minutes while maintained in an ice bath, then treated with ether to precipitate the iodide salt formed. After filtration, 1.54 g of off-white solid were obtained (45% yield). The crude compound was recrystallized from methanol and a DSC measurement was run on the colorless crystals showing the same melting point as the compound obtained by *Method A*. C₂H₇N₆I (242.02 g mol⁻¹); C 9.93 (calc. 9.81); H 2.91 (2.77); N 34.72 (34.41); I 52.43 (52.01)%, m. p. (Büchi B-540, uncorrected): 189.6-191.1 °C, DSC (2 °C/min, °C): 190 (m.p.), 193 (dec.), Raman $\Delta\nu$ / cm⁻¹ (rel.

int.): 3283(31) 1707(25) 1637(12) 1559(23) 1438(10) 1321(25) 1295(22) 1131(13) 1018(12) 895(11) 799(22)
766(100) 628(24) 560(24) 329(20) 309(51) 264(15) 197(16), IR $\Delta\nu$ / cm^{-1} (KBr, rel. int.): 3311(s) 3243(s)
1699(s) 1666(s) 1436(w) 1309(m) 1295(m) 1129(w) 1020(m) 916(m) 803(w) 702(m) 621(w).

4.9 References

- [1] a) X.-J. Wang, S.-Y. Jia, B.-Z. Wang, P. Lian, C. Zhou, *Hanneng Cailiao* **2006**, *14*(6), 439–445. b) K. Y. Lee, C. B. Storm, M. A. Hiskey, M. D. Coburn, *J. Energ. Mater.* **1991**, *9*(5), 415–428.
- [2] a) H. G. O. Becker, V. Eisenschmidt, K. Wehner, DD 19670415, **1967**. b) W. P. Norris, R. A. Henry, *J. Org. Chem.* **1964**, *29*(3), 650–660.
- [3] H. Xue, Y. Gao, B. Twamley, J. M. Shreeve, *Chem. Mater.* **2005**, *17*(1), 191–198.
- [4] H. Xue, B. Twamley, J. M. Shreeve, *J. Mater. Chem.* **2005**, *15*(34), 3459–3465.
- [5] G. K. Williams, S. P. Burns, I. B. Mishra, WO 2005035466, **2005**.
- [6] A. R. Katritzky, S. Singh, K. Kirichenko, J. D. Holbrey, M. Smiglak, W. M. Reichert, R. D. Rogers, *Chem. Commun.* **2005**, *7*, 868–870.
- [7] a) R. G. Child, *J. Heterocycl. Chem.* **1965**, *2*(1), 98–99. b) C. Darwich, T. M. Klapötke, M. Sucasca, J. M. Welch, *Propellants, Explos., Pyrotech.* **2007**, *32*(3), 235–243.
- [8] C. Darwich, Klapötke, C. Miró Sabaté, *Propellants, Explos., Pyrotech.* **2007**, in press.
- [9] a) G. W. Drake, T. W. Hawkins, L. A. Hall, J. A. Boatz, A. J. Brand, *Propellants, Explos., Pyrotech.* **2005**, *30*(5), 329–337. b) G. W. Drake, US 6509473, **2003**.
- [10] C. Darwich, K. Karagiosoff, T. M. Klapötke, C. Miró Sabaté, *Z. Anorg. Allg. Chem.* **2008**, *634*, 61–68.
- [11] J. C. Gálvez-Ruiz, G. Holl, K. Karaghisoff, T. M. Klapötke, K. Löhnwitz, P. Mayer, H. Nöth, K. Polborn, C. J. Rohbogner, M. Suter, J. J. Weigand, *Inorg. Chem.* **2005**, *44*(12), 4237–4253.
- [12] T. M. Klapötke, C. Miró Sabaté, J. M. Welch, *Z. Anorg. Allg. Chem.*, **2008**, *634*(5), 857–866.
- [13] Xue, H.; Gao, H.; Twamley, B.; Shreeve, J. M. *Chem. Mater.* **2007**, *19*, 1731–1739.
- [14] V. E. Matulis, A. S. Lyakhov, P. N. Gaponik, S. V. Voitekhovich, O. A. Isashkevich *J. Molec. Str.* **2003**, *649*(3), 309–314.
- [15] Raap, R. *Can. J. Chem* **1969**, *47*(19), 3677.
- [16] (a) Stollé, R.; Netz, H.; Kramer, O.; Rothschild, S.; Erbe, E.; Schick, O. *J. Prakt. Chem.* **1933**, *138*, 1. (b) Gaponik, P. N.; Karavai, V. P. *Khim. Geterotsikl. Soedin.* **1984**, 1388; (c) Willer, R. L.; Henry, R. A. *J. Org. Chem.* **1988**, *53*(22), 5371.
- [17] H.-G. Ang, W. Fraenk, K. Karaghisoff, T. M. Klapötke, P. Mayer, H. Noth, J. Sprott, M. Warchhold, *Z. Anorg. Allg. Chem.* **2002**, *628*(13), 2894–2900.
- [18] a) J. Thiele, *Just. Lieb. Ann. Chem.* **1892**, *270*(1), 54–63. b) J. Thiele, J. T. Marais, *Just. Lieb. Ann. Chem.* **1893**, *273*(2), 144–160. c) J. Thiele, *Chem. Ber.* **1893**, *26*(3), 2645–2646. d) J. Thiele, *Just. Lieb. Ann. Chem.* **1898**, *303*(1), 57–75.
- [19] <http://www.cem.msu.edu/~reusch/VirtualText/acidity2.htm>.

- [20] U. Müller, *Struct. Bond.* **1974**, *14*(1), 141–145.
- [21] a) K. Williamson, P. Li, J. P. Devlin, *J. Chem. Phys.* **1968**, *48*(9), 3891–3896. b) J. R. Fernandes, S. Ganguly, C. N. R. Rao, *Spectrochim. Acta* **1979**, *35A*, 1013–1019.
- [22] a) H. Cohn, *J. Chem. Soc.* **1952**, 4282–4284. b) P. Redlich, J. Holt, T. Biegeleisen, *J. Am. Chem. Soc.* **1944**, *55*, 13–16. c) H. Grothe, H. Willner, *Angew. Chem. Int. Ed. Engl.* **1996**, *108*(7), 816–818.
- [23] a) A. Hammerl, G. Holl, M. Kaiser, T. M. Klapötke, P. Mayer, H. Nöth, H. Piotrowski, M. Warchhold, *Eur. J. Inorg. Chem.* **2002**, *4*, 834–845. b) A. Hammerl, G. Holl, T. M. Klapötke, P. Mayer, H. Nöth, H. Piotrowski, M. T. Suter, *Z. Naturforsch.* **2001**, *B56*(9), 857–870. c) J. Geith, T. M. Klapötke, J. J. Weigand, G. Holl, *Propellants, Explos., Pyrotech.* **2004**, *29*(1), 3–8. d) T. M. Klapötke, P. Mayer, A. Shulz, J. J. Weigand, *Propellants, Explos., Pyrotech.* **2004**, *29*(6), 325–332.
- [24] a) M. Göbel, T. M. Klapötke, P. C. Thumbs, *Proceed. 9th Sem. New Trends Res. Energ. Mater.* (Pardubice, Czech Republic) **2006**, p. 127. b) T. M. Klapötke, P. Mayer, K. Polborn, J. M. Welch, *Proceed. 9th Sem. New Trends Res. Energ. Mater.* (Pardubice, Czech Republic) **2006**, p. 631. c) M. Göbel, K. Karaghiosoff, T. M. Klapötke, C. Miró, J. M. Welch, *Proceed. 9th Sem. New Trends Res. Energ. Mater.* (Pardubice, Czech Republic) **2006**, p. 202.
- [25] K. O. Christe, W. W. Wilson, M. A. Petrie, H. H. Michels, J. C. Bottaro, R. Gilardi, *Inorg. Chem.* **1996**, *35*(17), 5068–5071.
- [26] Gaussian G03W: Gaussian 03, Revision A.1: M. J. Frisch, G. W. Trucks, H. B. Schlegel, G. E. Scuseria, M. A. Robb, J. R. Cheeseman, J. A. Montgomery, T. Jr Vreven, K. N. Kudin, J. C. Burant, J. M. Millam, S. S. Iyengar, J. Tomasi, V. Barone, B. Mennucci, M. Cossi, G. Scalmani, N. Rega, G. A. Petersson, H. Nakatsuji, M. Hada, M. Ehara, K. Toyota, R. Fukuda, J. Hasegawa, M. Ishida, T. Nakajima, Y. Honda, O. Kitao, H. Nakai, M. Klene, X. Li, J. E. Knox, H. P. Hratchian, J. B. Cross, C. Adamo, J. Jaramillo, R. Gomperts, R. E. Stratmann, O. Yazyev, A. J. Austin, R. Cammi, C. Pomelli, J. W. Ochterski, P. Y. Ayala, K. Morokuma, G. A. Voth, P. Salvador, J. J. Dannenberg, V. G. Zakrzewski, S. Dapprich, A. D. Daniels, M. C. Strain, O. Farkas, D. K. Malick, A. D. Rabuck, K. Raghavachari, J. B. Foresman, J. V. Ortiz, Q. Cui, A. G. Baboul, S. Clifford, J. Cioslowski, B. B. Stefanov, G. Liu, A. Liashenko, P. Piskorz, I. Komaromi, R. L. Martin, D. J. Fox, T. Keith, M. A. Al-Laham, C. Y. Peng, A. Nanayakkara, M. Challacombe, P. M. W. Gill, B. Johnson, W. Chen, M. W. Wong, C. Gonzalez, J. A. Pople, Gaussian, Inc. Pittsburgh PA, **2003**.
- [27] K. Karaghiosoff, T. M. Klapötke, P. Mayer, C. Miró Sabaté, A. Penger, J. M. Welch, *Inorg. Chem.* **2008**, *47*, 1007–1019.
- [28] H.-G. Ang, W. Fraenk, K. Karaghiosoff, T. M. Klapötke, H. Nöth, J. Sprott, M. Suter, M. Vogt, M. Warchhold, *Z. Anorg. Allg. Chem.* **2002**, *628*(13), 2901–2906.
- [29] A. Hammerl, M. A. Hiskey, G. Holl, T. M. Klapötke, K. Polborn, J. Stierstorfer, J. J. Weigand, *Chem. Mater.* **2005**, *17*(14), 3784–3793.

- [30] a) T. M. Klapötke, C. Miró Sabaté, *Proceed. ICT Symp. Insens. Energ. Mater.* (Pfinztal, Germany) **2007**.
b) T. M. Klapötke, C. Miró Sabaté, *C. Chem. Mater.* **2008**, 20(5), 1750-1763.
- [31] A. Hammerl, T. M. Klapötke, H. Piotrowski, G. Holl, M. Kaiser, *Propellants, Explos., Pyrotech.* **2001**, 26(4), 161–164.
- [32] A. Hammerl, G. Holl, K. Hubler, M. Kaiser, T. M. Klapötke, P. Mayer, *Eur. J. Inorg. Chem.* **2001**, 3, 755–760.
- [33] T. M. Klapötke, C. Miró Sabaté, *Proceed. 9th Sem. New Trends Res. Energ. Mater.* (Pardubice, Czech Republic) **2007**, p. 191.
- [34] A. Altomare, M. C. Burla, M. Camalli, G. L. Cascarano, C. Giacovazzo, A. Gagliardi, A. G. G. Moliterni, G. Polidori, R. Spagna, *J. Appl. Crystallogr.* **1999**, 32(1), 115–119.
- [35] M. Sheldrick, SHELXL-97, Program for Crystal Structure Refinement, Universität Göttingen, **1997**.
- [36] A. F. Holleman, E. Wiberg, N. Wiberg in *Lehrbuch der Anorganischen Chemie*, 101st ed., Walter de Gruyter, Berlin, Germany, 1995.
- [37] J. Bernstein, R. E. Davis, L. Shimon, N. L. Chang, *Angew. Chem. Int. Ed. Eng.* **1995**, 34(15), 1555–1573.
- [38] RPLUTO, Cambridge Crystallographic Data Centre, Cambridge, UK, **2000**, <http://www.ccdc.cam.ac.uk/support/documentation/rpluto/TOC.html>.
- [39] G. Drake, T. Hawkins, *Ionic Liquids Workshop*, Tampa, FL, March **2004**.
- [40] Y. Huang, H. Gao, B. Twamley, J. M. Shreeve, *Eur. J. Inorg. Chem.* **2007**, 14, 2025–2030.
- [41] a) N. V. Podberezskaya, N. V. Pervukhina, V. P. Doronina, *Zh. Strukt. Khim.* **1991**, 32, 34–39. b) C. Ye, J.-C. Xiao, B. Twamley, J. M. Shreeve, *Chem. Commun.* **2005**, 21, 2750–2752.
- [42] a) C. Foces-Foces, F. H. Cano, R. M. Claramunt, D. Sanz, J. Catalan, F. Fabero, A. Fruchier, J. Elguero, *J. Chem. Soc. Perkin Trans. 2* **1990**, 2, 237–244. b) R. M. Claramunt, D. Sanz, J. Catalan, F. Fabero, N. A. Garcia, C. Foces-Foces, A. L. Llamas-Saiz, J. Elguero, *J. Chem. Soc. Perkin Trans. 2* **1993**, 9, 1687–1699.
- [43] M. D. Harmony, V. W. Laurie, R. L. Kuczkowski, R. H. Schwedeman, D. A. Ramsay, F. L. Lovas, W. J. Lafferty, A. G. Maki, *J. Phys. Chem. Ref. Data* **1979**, 8(3), 619–721.
- [44] In *Vol. C.: International Tables for X-ray Crystallography*, Kluwer Academic Publisher, Dordrecht, **1992**.
- [45] A. Bondi, *J. Phys. Chem.* **1964**, 68(3), 441–451.
- [46] a) S. Asath Bahadur, R. K. Rajaram, M. Nethaki, *Acta Crystallogr.* **1991**, C47(7), 1420–1423. b) A. Wojtczak, M. Jaskólski, Z. Kosturkiewicz, *Acta Crystallogr.* **1988**, C44(10), 1779–1981.
- [47] a) M. Alfonso, Y. Wang, H. Stoeckli-Evans, *Acta Crystallogr.* **2001**, C57(10), 1184–1188. b) S.-C. Shao, D.-R. Zhu, X.-H. Zhu, X.-Z. You, R. S. Shanmuga H.-K. Fun, *Acta Crystallogr.* **1999**, C55(9), 1412–1413.

- [48] A. Hammerl, T. M. Klapötke, H. Nöth, M. Warchhold, H. Holl, M. Kaiser, *Inorg. Chem.* **2001**, *40*(14), 3570–3575.
- [49] M. A. Pierce-Butler, *Acta Crystallogr.* **1982**, *B38*(10), 2681–2683.
- [50] a) H. Xue, Y. Gao, B. Twamley, J. M. Shreeve, *Inorg. Chem.* **2005**, *44*(14), 5068–5072. b) T. M. Klapötke, K. Karaghiosoff, P. Mayer, A. Penger, J. M. Welch, *Propellants, Explos., Pyrotech.* **2006**, *31*(3), 188–195. c) H. Xue, H. Gao, B. Twamley, J. M. Shreeve, *Chem. Mater.* **2007**, *19*(7), 1731–1739.
- [51] T. M. Klapötke, P. Mayer, C. Miró, A. Penger, J. M. Welch, *Abstr. Pap. 233rd ACS Nat. Meet.* (Chigaco, USA) **2007**.
- [52] M. E. Sitzman, R. Gilardi, R. J. Butcher, W. M. Koppes, A. G. Stern, J. S. Trasher, N. J. Trivedi, Z.-Y. Yang, *Inorg. Chem.* **2000**, *39*(4), 843–850.
- [53] A. Martin, A. A. Pinkerton, R. D. Gilardi, J. C. Botarro, *Acta Crystallogr.* **1997**, *B53*(3), 504–512.
- [54] T. M. Klapötke, P. Mayer, A. Schulz, J. J. Weigand, *J. Amer. Chem. Soc.* **2005**, *127*(7), 2032–2033.
- [55] T. M. Klapötke, C. M. Rienäcker, *Propellants, Explos., Pyrotech.* **2001**, *26*(1), 43–47.
- [56] Tests methods according to the UN Recommendation on the Transport of Dangerous Goods, Manual of Tests and Criteria, 4th rev. ed.; United Nations Publications: New York, **2003**.
- [57] Reichel & Partner GmbH, <http://www.reichel-partner.de>.
- [58] Calculation of the oxygen balance: $\Omega(\%) = (\text{O} - 2\text{C} - \text{H}/2 - x\text{AO}) 1600/\text{M}$; M = molecular mass.
- [59] L. Glasser, H. D. B. Jenkins, D. Tudela, *Inorg. Chem.* **2002**, *41*, 2364–2367.
- [60] T. M. Klapötke, P. Mayer, C. Miró Sabaté, J. M. Welch, N. Wiegand, *Inorg. Chem.* **2008**, accepted.
- [61] H. Gao, C. Ye, C. M. Piekarski, J. M. Shreeve, *J. Phys. Chem.* **2007**, *C111*(28), 10718–10731.
- [62] J. Koehler, R. Meyer in *Explosivstoffe*, 9th ed.; Wiley-VCH, Weinheim, **1998**.
- [63] a) M. Sućeska, *Mater. Sci. For.*, **2004**, p. 465. b) M. Sućeska, *Propellants, Explos., Pyrotech.* **1991**, *16*, 197–202. c) M. Sućeska, *Propellants, Explos., Pyrotech.* **1999**, *24*, 280–285.
- [64] L. R. Bates, J. M. Jenkins, US 4094879, **1978**.
- [65] <http://www.perkinelmer.com>.
- [66] http://www.linseis.net/html_en/thermal/dsc/dsc_pt10.php.
- [67] <http://www.parrinst.com>.

CHAPTER V

TRIAZOLIUM AND TETRAZOLIUM PICRATE SALTS

5.1 Introduction

Methylation of 5-amino-1*H*-tetrazole (5-At) in basic media by the action of methyl iodide or methyl sulphate is known to give a separable mixture of two isomers, namely 1-methyl-5-amino-1*H*-tetrazole (1MAT, major product) and 2-methyl-5-amino-1*H*-tetrazole (2MAT, minor product).¹ Recently, we reported the selective methylation of 1MAT with methyl iodide at reflux from acetonitrile to yield 1,4-dimethyl-5-amino-1*H*-tetrazolium iodide (**14DMATI**, **57**).² Our most recent results on the chemistry of tetrazoles showed that both 1MAT and the 14DMAT⁺ cation are valuable intermediates for the synthesis of high energy density materials (HEDMs) in combination with energetic anions such as nitrate, perchlorate, azide or dinitramide.³ Protonation/methylation of the tetrazole ring can occur either at the tetrazole nitrogen atoms or at the exocyclic amino group, so that many tautomeric forms are feasible.^{4,5} ¹⁵N NMR spectroscopy⁶ and more conclusively, in the solid state, X-ray structure determination allows to easily assign the reaction (protonation/methylation) site.

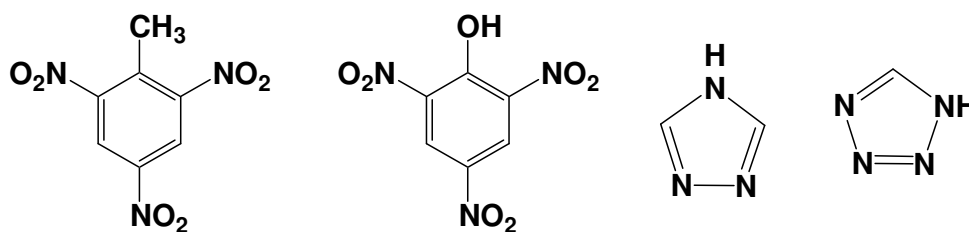


Figure 5.1 From left to right: formula structures of TNT, picric acid, 1,2,4-triazole and 1*H*-tetrazole.

The search for new and/or modified energetic materials, which show the desired properties for use as pyrotechnics, propellants or high explosives is a continuing challenge. As mentioned in the introductory section, classical explosives such as TNT (trinitrotoluene) or RDX (cyclotrimethylenetrinitramine) derive their energy from the oxidation of the carbon backbone^{7,8} whereas nitrogen-rich high energy density materials (HEDMs) owe their energies to their high positive heats of formation.^{2,9-12} The explosive yield of TNT is considered one of the standard measures of strength of bombs and other explosives.¹³ The compound has a relatively high detonation velocity and a high decomposition point.¹⁴ The high thermal stability of aromatic nitro-

compounds is attractive for military applications. On the other side, formal replacement of the methyl by a hydroxyl group in the parent picric acid (PicH, **58**) results in improved detonation parameters in comparison to TNT.¹⁴ However, picric acid is more sensitive to classical stimuli (i.e., impact and friction) than TNT and accidents have occurred in the past. For example, picric acid is known to react with the surrounding metals (e.g., in a shell-casing) yielding very sensitive compounds. Salt-formation is known not only to stabilize the materials through the formation of hydrogen-bonded networks, but such compounds also tend to possess lower vapor pressures and higher densities than their atomically similar non-ionic derivatives. Whereas reports describing energetic nitrate, perchlorate or azide salts are becoming more common, reports on energetic picrate salts are much more elusive in the literature. Recently, Shreeve et al. introduced a new family of mono and bridged azolium picrate salts with prospective use as energetic materials,¹⁵ however, many of the compounds (e.g., 5-amino-1*H*-tetrazolium picrate) were not studied in detail from the energetic point of view. In addition to the latter work, there exist some structural reports of tetrazolium picrate salts^{15–17} but energetic data is scarce. Salts of picric acid, either with nitrogen-rich anions (e.g., ammonium or guanadinium) or with heavy metals (e.g., lead) have interesting properties for use as explosives in military charges and as an active component in initiating mixtures, respectively.

Therefore, we decided to undertake an in-depth study of the energetic properties of picrate salts with triazolium and tetrazolium cations as intermediates between commonly used nitroaromatic energetic materials and (nitrogen-rich) azole chemistry (Figure 5.1). The nitrogen-rich azolium cation should contribute positively to the heats of formation and to enhanced densities. Lastly, due to the negative oxygen balance of the picrates salts studied here, the energetic properties of mixtures of the materials with an oxidizer such as ammonium nitrate or ammonium dinitramide were calculated in order to study the suitability of the mixtures as high explosives and/or propellants.

5.2 Synthesis

The synthesis and crystal structure of 1-methyl-5-amino-1*H*-tetrazolium picrate (**1MATPic**, **60**) were reported during the course of our study by Lyakhov et al.,¹⁷ which synthesized the compound by protonation of 1MAT with picric acid in ethanol. However, a full description of the synthesis is not given and the compound was characterized (in addition to crystal structure determination) only by melting point and ¹H NMR spectroscopy. We found more advantageous to synthesize **60** by the equimolar reaction of 1MAT and picric acid (**58**) using boiling water as the solvent (Scheme 5.1). This method was also applied for the synthesis of some other picrate

salts with the following cations: 5-amino-1*H*-tetrazolium (**5AtPic**, **59**),¹⁵ 2-methyl-5-amino-1*H*-tetrazolium (**2MATPic**, **61**), 1,5-diamino-1*H*-tetrazolium (**DATPic**, **64**)¹⁶ and 3,4,5-triamino-1,2,4-triazolium or guanazinium (**GzPic**, **66**).

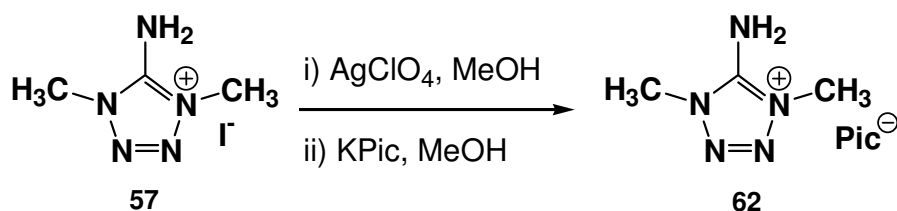
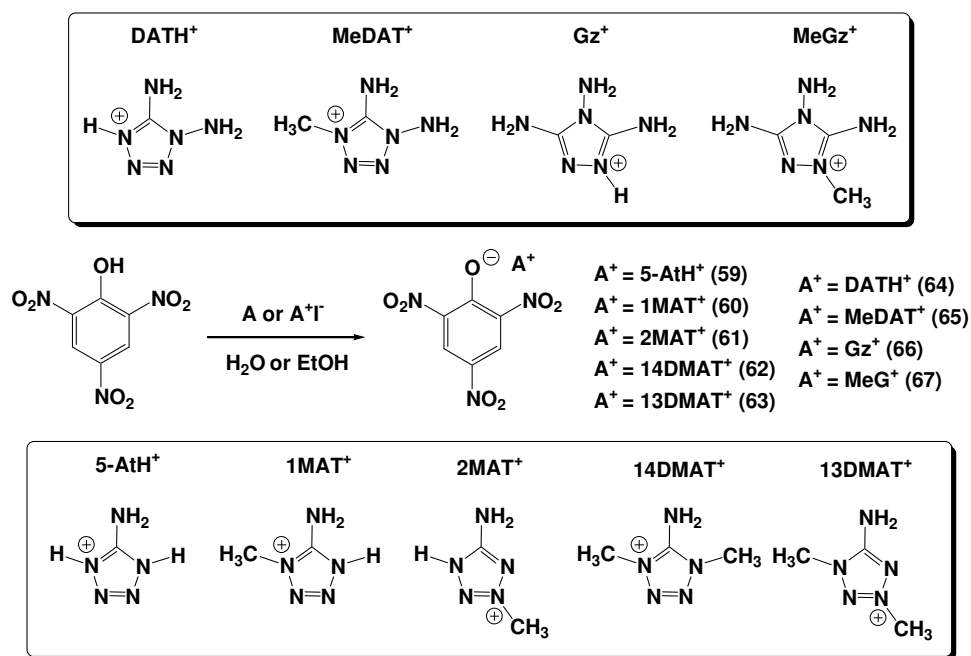


Figure 5.2 Synthesis of **62** (Method 1, Pic = Picrate).

On the other side, the synthesis of 1,4-dimethyl-5-amino-1*H*-tetrazolium picrate (**14DMATPic**, **62**) was reported in 1954 by Henry et al.¹⁸ by the reaction of the free base (1,4-dimethyl-5-imino-1*H*-tetrazole, **14DMIT**) with picric acid (**58**), however, the compound was (again) only poorly characterized. In our study, **62** was initially synthesized by metathesis of 1,4-dimethyl-5-amino-1*H*-tetrazolium perchlorate³ and potassium picrate in methanol (Figure 5.1). Later on, we found out a more convenient synthesis of **62** by direct reaction of the iodide salt (**57**) with picric acid and took advantage of this method to synthesize picrate salts with the following cations: 1,3-dimethyl-5-amino-1*H*-tetrazolium (**13DMATPic**, **63**), 1,5-diamino-4-methyl-1*H*-tetrazolium (**MeDATPic**, **65**) and methylguanazinium (**MeGzPic**, **67**), by reaction of a suitable iodide salt with picric acid.



Scheme 5.1 Reaction equation for the synthesis of azolium picrate salts.

5.3 Vibrational Spectroscopy

All azolium picrate salts were characterized by IR and Raman spectroscopies. Figures 5.3 and 5.4 show and overlap of the corresponding IR and Raman spectra for selected azolium picrate salts. Both IR and Raman spectra are strongly dominated by the bands of the picrate anion. The asymmetric nitro-group N–O stretching is observed as an intense band at 1565 (**59**), 1566 (**60**), 1562 (**61**), 1556 (**62**), 1561 (**63**), 1563 (**64** and **65**), 1541 (**66**) and 1554 (**67**) cm^{-1} in the IR spectra and is inactive in the Raman. The symmetric N–O stretching is observed in both IR and Raman spectra of compounds **59-67**. The differences between starting material (picric acid) and its salts are specially to be found in the Raman spectra due to the splitting of the N–O stretch in many other peaks of high intensity and with maximum for the compounds at the following wave numbers: 1267 (**59**), 1268 (**60**), 1261 (**61**), 1263 (**62**), 1269 (**63**), 1271 (**64**), 1269 (**65**), 1267 (**66**) and 1274 (**67**) cm^{-1} (IR) and 1296 (**59**), 1319 (**60**), 1346 (**61**), 1320 (**62**), 1298 (**63**), 1348 (**64**), 1334 (**65**), 1316 (**66**), 1299 (**67**) cm^{-1} (Raman), respectively. The splitting of the N–O stretches in the Raman spectra of some of the azolium compounds can be seen in Figure 5.4.

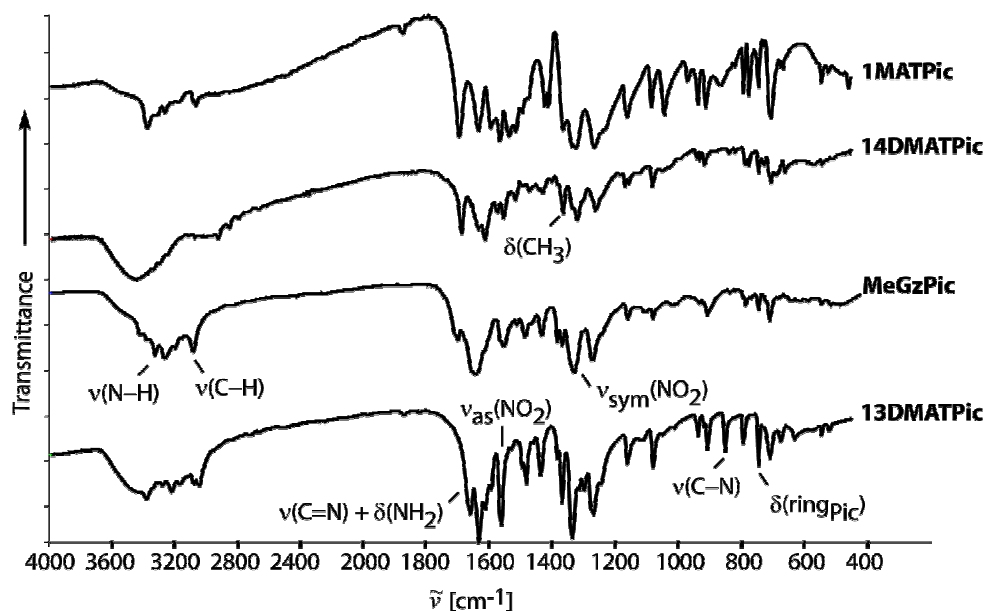


Figure 5.3 IR spectra of selected azolium picrate salts (KBr pellets, 3 scans).

In addition, the IR spectra shows ring deformation modes for the anion at $\sim 745 \text{ cm}^{-1}$. As for the cations, these show broad bands in the range 3400-3100 [$\nu(\text{N-H})$] and 3000-2850 [$\nu(\text{C-H})$] cm^{-1} , in the IR spectra (these bands are of very little intensity in the Raman spectra due to the strong reflections of the nitro-groups). The IR spectra shows bands of strong to very strong intensity in the range between 1659 (**63**) and 1722 (**64**) cm^{-1} , corresponding to the simultaneous elongation and

deformation of the C–NH₂ and NH₂ bonds, respectively. The larger wavenumbers for **64** (1722 cm⁻¹) and **65** (1711 cm⁻¹) in comparison to the rest of the materials, indicates stronger C–N bonds (i.e., more double-bond character) in the exo carbon bound amino group, keeping in with structural reports on salts containing the cations 5-At⁺,¹² 1MAT⁺,^{3,15} 2MAT⁺,¹⁹ 14DMAT⁺,³ 13DMAT⁺,^{19,20} DAT⁺,^{5,6} MeDAT⁺,^{6,21} Gz⁺,^{22,23} and MeGz⁺,^{23,24} which show longer C–NH₂ distances. Lastly, many other bands of lower intensity are also present in both IR and Raman spectra of the salts and can be assigned as follows: 1550-1350 cm⁻¹ [ν (tetrazole ring), δ_{as} (CH₃), δ (N–H)], 1380 cm⁻¹ [δ (CH₃)], 1350-700 cm⁻¹ [ν (N1–C1–N4), ν (N–N), χ (CN), δ (tetrazole ring)], <700 cm⁻¹ [δ out-of-plane bend(N–H) ω (NH₂)].^{3,25}

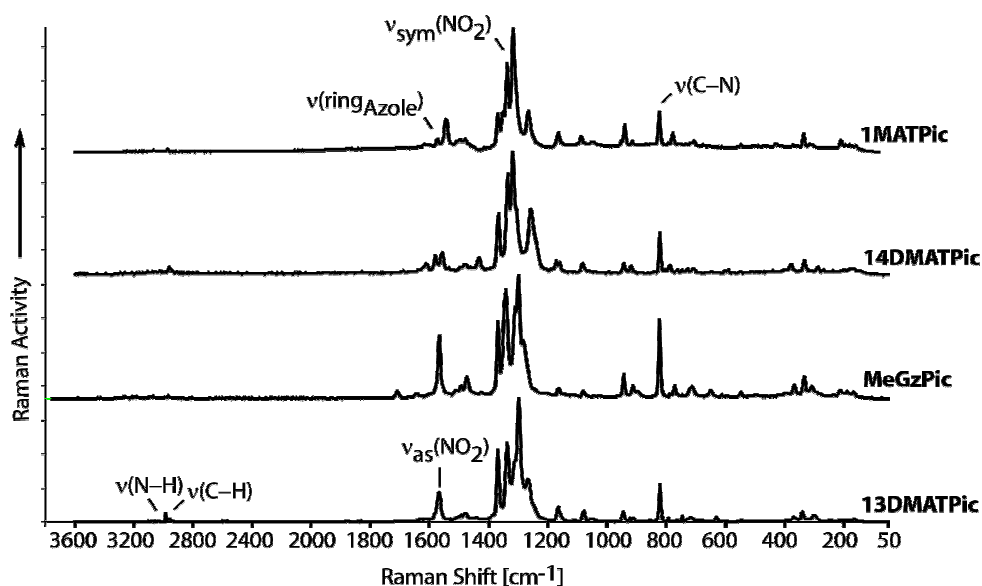


Figure 5.4 Raman spectra of selected azolium picrate salts (400 mW, 50 scans).

5.4 NMR spectroscopy

The ¹H NMR of all azolium picrate salts shows a sharp resonance at ~8.6 ppm corresponding to the aromatic protons in the anion. The N1 methyl group protons (see Figure 5.7 for NMR labels) show similar shifts for all cations in the range between 3.5-3.9 ppm, whereas the N3 methyl group protons in **61** and **63** are shifted to lower field (δ = 4.1 and 4.3 ppm, respectively). The different nature and acidity of the amino groups protons in the picrate salts synthesized in this study can be observed in the ¹H NMR spectra. Whereas the NH and NH₂ group resonances in **60** are observed as one only signal at 5.6 ppm due to the fast exchange in DMSO-d₆, the three different amino groups in **67** give three well resolved resonances (Figure 5.5), which are found at

lower field (see Experimental part). **59**, **62** and **65** have all very acidic protons as suggested by signals above ~ 9.0 ppm, whereas the rest of the compounds show (in general) averaged NH and NH_2 resonances at higher field.

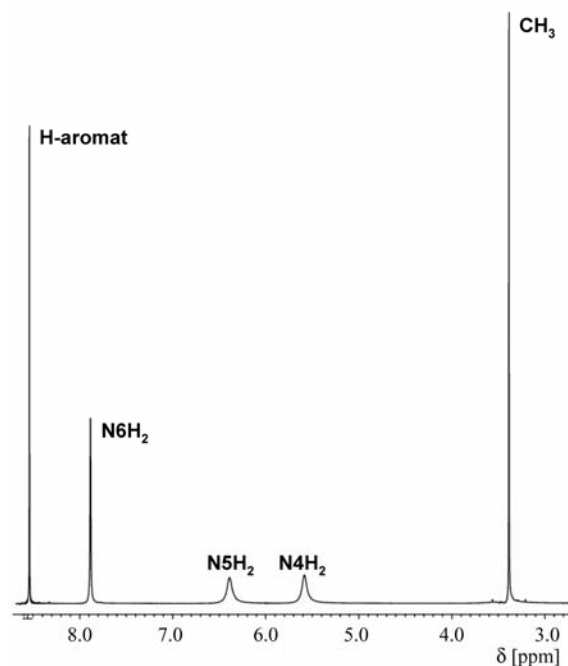


Figure 5.5 ^1H NMR spectrum of picrate salt **67** in DMSO-d_6 .

Figure 5.6 shows the ^{13}C NMR spectrum of **61**. It is interesting to note that the formation of picrate salts results in a strong shift of the resonance of the carbon atom with the NMR label C4 to high field (~ 125 ppm) in respect to picric acid, and this signal almost overlaps with that of the non-substituted carbon atoms (C3). This gives proof for the formation of the picrate salts. Apart from the resonances for the aromatic carbon atoms in the anion in the range ~ 125 -160 ppm (see Experimental part),²⁶ the ^{13}C NMR spectra of the azolium picrate salts show the expected resonances for the cation. In analogy to the ^1H NMR spectra, the N3-substituted (NMR labels) compounds (**61** and **63**) have resonances for the ring carbon atoms (167.1 and 157.8 ppm, respectively), which are at lower field than those of the rest of the compounds, whereas the 1,4-disubstituted tetrazolium salts **62** and **65** and the triazolium salts **66** and **67** have the highest field shifts for this carbon atom (between 147 and 151 ppm). The resonances for the methyl group carbon atoms vary within a relatively large range. First of all one must differentiate between the resonances of the N1 and those of the N3 methyl groups. In the rule, the N3- CH_3 resonances are to be found at lower field (38.8 ppm for **61** and 42.6 ppm for **63**) and overlap with the solvent in the case of **61** (see Figure 5.6), whereas the N1-bound carbon atoms have shifts in the range ~ 32 -34

ppm with the exception of **65**, which shows a high field resonance at 39.6 ppm. The ^1H and ^{13}C NMR resonances are in the ranges described in previous reports of our group for salts containing the same cations (see also *Chapters III, IV, VI and VII*).^{3,6,12,20,22,24}

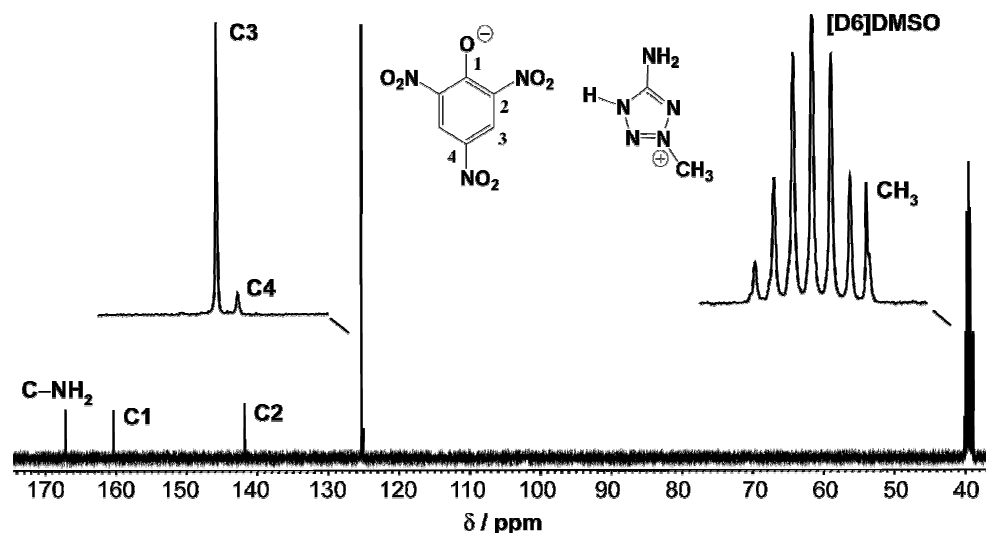


Figure 5.6 ^{13}C NMR spectrum of **61** in $[\text{D}_6]\text{DMSO}$ with the assignments.

The ^{15}N NMR spectra of ~ 0.2 M solutions of the azolium picrate salts in $[\text{D}_6]\text{DMSO}$ show the resonances for the two picrate anion nitro-groups at ~ 12 and ~ 15 ppm. These resonance coalesce in one and can already be observed in the ^{14}N NMR spectra at ~ 12 ppm, whereas the signals for the nitrogen atoms in the cation are broad. In addition to providing a quick method to uniquely identify the picrate salts synthesized, protonation (PIS) and methylation (MIS) induced shifts can be used to obtain information about the structure and interionic interactions in solution. The PIS and MIS shifts for the azolium salts described here can be calculated as the difference in ^{15}N NMR shifts between analogous nitrogen signals in neutral 5-At, 1MAT, 2MAT, DAT and Gz and the compounds. PIS and MIS values have shown to be useful in determining unequivocally the site of protonation/methylation for several heterocyclic compounds.^{27,28} Table 5.1 contains tabulated the ^{15}N NMR (and some ^{13}C NMR) shifts for all salts in this study and those of the corresponding neutral materials, for comparison purposes with the calculated PIS/MIS effect in brackets.

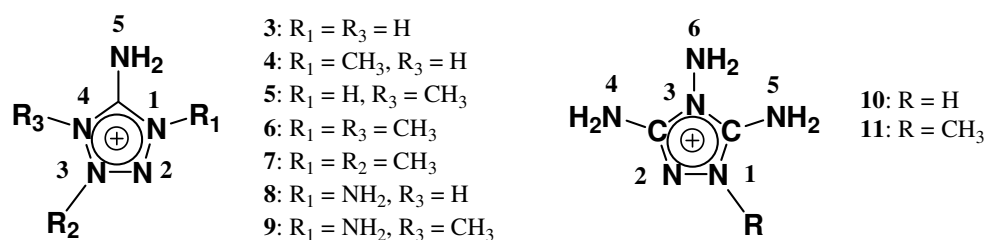


Figure 5.7 NMR labeling scheme for the triazolium and tetrazolium cations.

Table 5.1 ^{15}N and ^{13}C NMR chemical shifts (ppm), PIS/MIS values (ppm) and coupling constants (J) for the azolium picrate salts studied.

Compound ^{a, b, c}	N1	N2	N3	N4	N5	N6	C–NH ₂
5-At	-137.1	-13.1	-13.1	-137.1	-338.9	-	157.2
59	-168.1 (-31.0)	-27.4 (-14.3)	-27.4 (-14.3)	-168.1 (-31.0)	-326.2 (12.7) ¹ J 86.9	-	155.0
1MAT	-185.3	-23.3	-2.0	-92.9	-339.4	-	156.4
60	-184.2 (1.1) ² J 1.9	-24.0 (-0.7) ³ J 1.6	-12.9 (-10.9) ³ J 1.9	-129.3 (-36.4)	-331.1 (8.3)	-	155.1
62	-182.9 (2.4)	-29.3 (-6.0) ³ J 1.9	-29.3 (-27.3) ³ J 1.9	-182.9 (-90.2)	-320.0 (18.2)	-	148.3
2MAT	-116.1	-6.2	-83.0	-116.1	-339.3	-	167.7
61	-114.4 (1.7)	-9.0 (-2.8) ³ J 1.4	-89.2 (-6.2)	-114.9 (1.2)	-339.1 (0.2)	-	167.1
63	-180.2 (-64.1)	-31.6 (-24.4) ³ J 2.3	-108.5 (-24.5)	-110.3 (5.8)	-325.6 (14.7) ¹ J 89.6	-	157.8
DAT	-167.0	-5.5	-20.8	-97.5	-338.3	-315.2	155.0
64	-165.6 (1.4)	-20.9 (-15.4)	-35.8 (-15.0)	-173.8 (-76.3)	-330.2 (8.1)	-320.1 (-4.9)	153.1
65	-168.1 (-1.1) ² J 1.8	-24.2 (-18.7)	-36.0 (-15.2) ³ J 2.0	-186.9 (-89.4) ² J 2.0	-323.8 (14.5)	-312.1 (3.1) ¹ J 75.9	147.4
Gz	-156.0	-156.0	-238.1	-340.2	-340.2	-326.4	152.1
66	-177.1 (-21.1)	-177.1 (-21.1)	-238.9 (-0.8)	-330.2 (10.0)	-330.2 (10.0)	-323.4 (3.0)	150.4
67	-239.8 (-83.8)	-163.8 (-7.8)	-238.3 (-0.2)	-323.0 (17.2) ¹ J 90.9	-335.2 (-5.0) ¹ J 89.7	-322.1 (4.3) ¹ J 82.4	150.7, 147.7

^a PIS/MIS values in curved brackets and coupling constants in Hz. ^b All shifts were measured with respect to CH_3NO_2 internal standard; negative shifts are upfield from CH_3NO_2 . ^c in $[\text{D}_6]\text{-DMSO}$.

Protonation of 5-At to yield the corresponding picrate salt (**59**) is accompanied by a shift (PIS) in the resonance of all nitrogen atoms (Table 5.1), which is more notorious in the case of the protonated nitrogen atom (either N1 or N4) keeping in with the report on the crystal structure of the compound.¹⁶ In a similar way, the reaction of 1MAT with picric acid to yield **60** results in small PIS values in the range between -10.9 and +8.3 ppm for nitrogen atoms N1, N2, N3 and N5 and a markedly larger value (-36.4 ppm) for N4, indicative of protonation of this nitrogen atom, as also confirmed by the crystal structure of the compound.¹⁵ Formal methylation, rather than protonation, of 1MAT to form **62**, results in MIS values between -27.3 (N3) and +18.2 (N5) ppm for all nitrogen atoms apart from the methylated one (N4), which is shifted -90.2 ppm in respect to the analogous nitrogen atom in 1MAT. Unexpectedly, the formation of **61** does not go accompanied by large shifts in the resonances of the nitrogen atoms. Preliminary results concerning the crystal

structure of salts containing the 2MAT⁺⁺ cation,¹⁹ showed protonation to take place on N1, however, NMR studies do not conclusively support this observation and the expected protonated nitrogen atom (N1) shows the largest positive (small) PIS in comparison to neutral 2MAT. A plausible explanation for this might be related with the relatively low basicity of 2MAT in the NMR solvent ([D6]-DMSO). Whereas, reaction of picric acid with 2MAT proceeds readily in water forming **61** (see 5.10 *Experimental Section*), we observed that in less polar solvents (e.g. ethanol, CH₃CN or acetone and possibly [D6]-DMSO) picric acid (**58**) and 2MAT are recovered. Therefore, we conclude that the small PIS values observed for the ¹⁵N NMR of the compound are due to the deprotonation of **61** to form 2MAT and picric acid in the solvent used and during the large time scale of the ¹⁵N NMR measurement (in contrast to ¹H and ¹³C NMR). The MIS values for picrate salt **63** are lower than for the majority of the compounds described here and vary between -24.5 (N4) and +14.7 (N5) ppm, and the methylated nitrogen atom (N1) has the largest (negative) shift of all tetrazolium salts with a value of -64.1 ppm. Lastly, the diaminated salts **64** and **65** show PIS and MIS values of -76.3 and -89.4 ppm for the protonated (**64**) and methylated (**65**) nitrogen atoms, respectively by comparison with DAT and comparison of the shifts of neutral Gz with those of the triazolium salts **66** and **67** also shows relatively small MIS values between -0.2 and +10.0 ppm, for the non-methylated nitrogen atoms, whereas N1 has the largest negative shift (PIS = -21.1 ppm for **66** and MIS = -83.8 ppm for **67**).

For the tetrazolium salts **59**, **60**, **62**, **64** and **65** the nitrogen atoms with the labels N2 and N3 have ¹⁵N NMR resonances to lower field (less negative) below -36 ppm. The other two tetrazolium salts (**61** and **63**) are an exception to these low field shifts and the resonances for the methylated nitrogen atom (N3) are observed at -89.2 and -108.5 ppm, respectively due to the MIS effect. The amino group nitrogen atoms (N5) are easily identified by their resonances at the highest field (between -310 and -340 ppm). For the diaminated tetrazolium (**64** and **65**) and triazolium (**66** and **67**) salts, the two amino group resonances (three in the case of the triazolium salts) can be differentiated by the larger inductive effect of nitrogen over carbon, which shifts the N-NH₂ group resonances to lower field than the C-NH₂ resonances. Finally, for the tetrazolium salts, N1 and N4 resonate in the middle of the negative region between ~-110 and ~-190 ppm, and can be distinguished by the larger PIS/MIS effect on the methylated nitrogen atom, i.e., more negative shift.

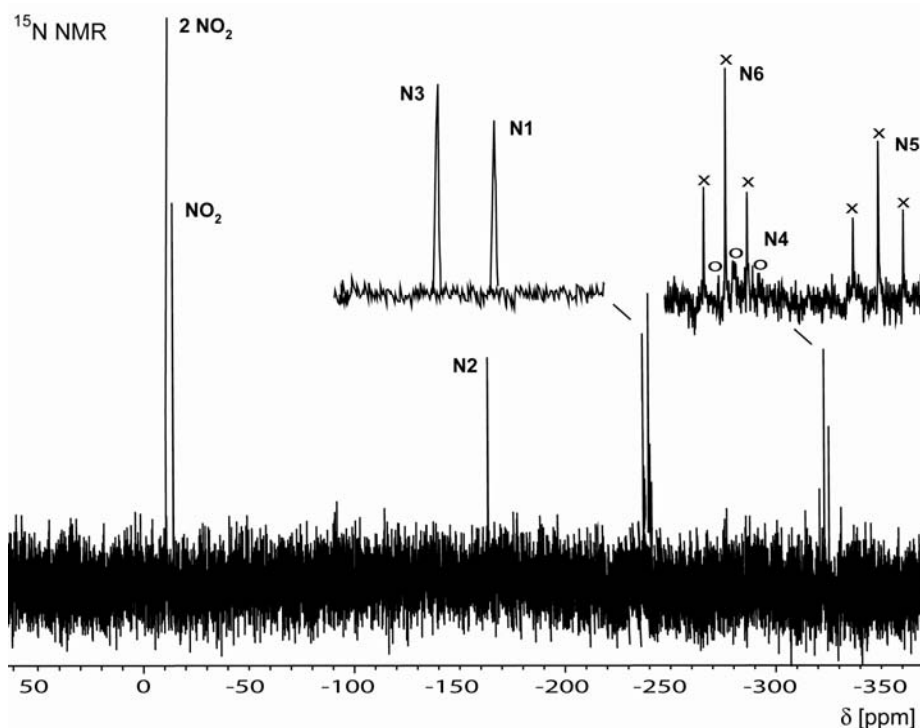


Figure 5.8 Coupled ^{15}N NMR spectrum of **67** in DMSO-d_6 showing the N–H couplings at one bond (see 5.10 *Experimental Section* for values on shifts and coupling constants).

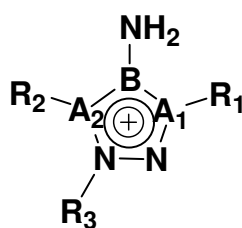
Figure 5.8 shows the coupled ^{15}N NMR spectrum for the triazolium salt **67**. The three amino groups (N4, N5 and N6) have very similar resonances (N4 and N6 overlap for **67**), between -322 and -335 ppm, comparable to the remainder of the compounds. The amino group-bound nitrogen atom (N3) has a very similar shift to that of the methylated nitrogen atom (N1) at ~ -239 ppm and more negative than that of the other triazole-ring nitrogen atom (N2, $\delta = -163.8$ ppm). This is in contrast to **66** where the PIS effect on N1 is smaller than the MIS on N1 in **67** and the two signals have distinctive resonances (N1 = -177.1 and N3 = -338.9 ppm). Lastly, for all compounds the observed coupling constants (2J and 3J) to the methyl-group protons take values, which are in general in the range between 1.5 and 2.5 Hz, whereas those to the amino group protons are much larger ($^1J \sim 90$ Hz). These coupling constants are in good agreement with typical values for 1J , 2J and $^3J(^1\text{H}-^{15}\text{N})$.²⁹

5.5 Molecular Structures

Crystals of the azolium picrate salts were obtained from slow cooling of a concentrated solution of the compounds in hot water. The X-ray crystallographic data for **60**, **62** and **66** were collected on an Enraf-Nonius Kappa CCD diffractometer. Data sets for **63** and **67** were collected

on an Oxford Diffraction Xcalibur 3 diffractometer equipped with a CCD detector.³⁰ All data were collected using graphite-monochromated Mo K α radiation ($\lambda = 0.71073$ Å). No absorption corrections were applied to data sets collected for any of the compounds. All structures were solved by direct methods (SHELXS-97 and SIR97)^{31,32} and refined by means of full-matrix least-squares procedures using SHELXL-97. Crystallographic data are summarized in Table 5.C1. Selected bond lengths and angles are reported in Table 5.2 and hydrogen-bonding geometries in Table 5.3. All non-hydrogen atoms were refined anisotropically. For all compounds all hydrogen atoms were located from difference Fourier electron-density maps and refined isotropically.

Table 5.2 Selected bond distances and angles in the azolium cation of picrate salts.^a



Distances (Å)	60	62	63	66	67
B–N	1.316(2)	1.315(2)	1.324(3)	1.394(3)	1.407(3)
B–A ₁	1.336(1)	1.337(2)	1.356(3)	1.355(3)	1.382(3)
B–A ₂	1.366(1)	1.371(2)	1.339(3)	1.387(3)	1.353(3)
A ₁ –R ₁	1.452(2)	1.459(3)	1.461(3)	1.322(3)	1.345(4)
A ₁ –N	1.357(2)	1.364(2)	1.337(2)	1.326(3)	1.311(3)
N–N	1.271(2)	1.273(3)	1.289(2)	1.400(2)	1.408(3)
N–R ₃			1.463(3)		1.450(3)
N–A ₂	1.335(2)	1.340(2)	1.340(2)	1.305(3)	1.316(3)
A ₂ –R ₂		1.458(3)		1.357(3)	1.323(4)
Angles (°)	60	62	63	66	67
N–B–A ₁	128.1(1)	127.9(2)	124.8(2)	122.5(2)	131.4(2)
N–B–A ₂	127.1(1)	127.3(2)	126.6(2)	130.1(2)	121.0(2)
A ₂ –B–A ₁	104.6(1)	104.8(2)	108.6(2)	107.3(2)	107.6(2)
B–A ₁ –R ₁	128.9(1)	128.8(2)	128.9(2)	125.2(2)	122.8(3)
N–A ₁ –R ₁	121.7(1)	121.2(2)	121.1(2)	128.9(2)	126.6(3)
B–A ₁ –N	109.4(1)	109.5(2)	109.9(2)	106.0(2)	110.5(2)
A ₁ –N–N	107.9(1)	107.8(2)	102.7(2)	111.8(2)	104.1(2)
N–N–R ₃			121.2(2)		119.1(2)
R ₃ –N–A ₂			122.2(2)		128.7(2)
N–A ₂ –R ₂		121.7(2)		126.9(2)	128.7(3)
N–A ₂ –B	109.8(1)	109.5(2)	102.1(2)	110.9(2)	106.5(2)
N–N–A ₂	108.1(1)	108.2(2)	116.6(2)	104.0(2)	111.3(2)
B–A ₂ –R ₂		128.6(2)		122.1(2)	124.8(3)

^a **60**: B = C1, A₁ = N2, A₂ = N5, R₁ = C2; **62**: B = C1, A₁ = N2, A₂ = N5, R₁ = C2, R₂ = C3; **63**: B = C1, A₁ = N2, A₂ = N5, R₁ = C2, R₃ = C3; **66**: B = N4, A₁ = C3, A₂ = C4, R₁ = N3, R₂ = N5. **67**: B = N2, A₁ = C3, A₂ = C1, R₁ = N6, R₂ = N3, R₃ = C2.

Table 5.3 Selected hydrogen bonds for azolium picrate salts (distances in Å, angles in °).

D–H...A	D–H	H...A	D–H...A	D–H–A
60^a				
N1–H1A...O2 ⁱ	0.92(2)	2.14(2)	3.035(2)	163(2)
N1–H1B...O1 ⁱⁱ	0.88(2)	2.35(2)	3.019(2)	132(2)
N1–H1B...O2 ⁱⁱ	0.88(2)	2.52(2)	3.199(2)	134(2)
N5–H5...O1 ⁱⁱ	0.94(2)	1.82(2)	2.618(1)	134(2)
N5–H5...O7 ⁱⁱ	0.94(2)	2.16(2)	2.896(2)	140(2)
62^b				
N1–H1A...O1	1.00(2)	1.76(2)	2.747(2)	170(2)
N1–H1A...O2	1.00(2)	2.45(2)	2.970(2)	112(1)
N1–H1B...O3 ⁱ	0.87(3)	2.05(3)	2.894(2)	163(2)
63^c				
N1–H1A...O3 ⁱ	0.90(3)	2.20(3)	3.019(3)	151(2)
N1–H1B...O1 ⁱⁱ	0.88(3)	1.95(3)	2.686(2)	140(2)
66^d				
N1–H5...O4	0.86(3)	2.57(3)	3.157(3)	126(3)
N3–H1...N1	0.88(3)	2.49(3)	2.867(3)	107(2)
N3–H1...O7 ⁱⁱ	0.89(3)	2.24(3)	3.072(3)	154(2)
N4–H7...O1 ⁱⁱ	0.90(3)	1.92(3)	2.653(2)	137(2)
N4–H7...O2 ⁱⁱ	0.90(3)	2.25(3)	3.014(2)	142(2)
N5–H3...N6 ⁱⁱ	0.90(3)	2.12(3)	2.993(3)	162(3)
N1–H6...O5 ⁱⁱⁱ	0.86(3)	2.26(3)	3.034(3)	150(2)
N3–H1...O6 ^{iv}	0.88(3)	2.27(3)	3.136(3)	168(3)
67^e				
N3–H3A...N1	0.80(3)	2.52(3)	2.834(4)	105(2)
N3–H3A...O3	0.80(3)	2.26(3)	2.779(3)	123(3)
N3–H3B...O5 ⁱ	0.89(4)	2.15(4)	3.018(4)	165(3)
N6–H6A...O1 ⁱⁱ	0.86(4)	2.11(4)	2.944(3)	163(3)
N6–H6A...O7 ⁱⁱ	0.86(4)	2.56(4)	3.118(3)	124(3)
N1–H1B...O1 ⁱⁱ	0.84(4)	2.12(4)	2.924(4)	160(3)
N1–H1B...O2 ⁱⁱ	0.84(4)	2.34(3)	2.834(4)	118(3)
N6–H6B...N5 ⁱⁱⁱ	0.93(4)	2.18(4)	3.062(4)	158(3)

Symmetry codes for **60**: (i) 1+x, 1+y, z; (ii) -x, 1-y, 2-z. **62**: (i) 1-x, 0.5+y, 0.5-z. **63**: (i) 1-x, 2-y, -z; (ii) x, 2.5-y, 0.5+z.^d**66**: (ii) 1+x, y, 1+z; (iii) 1+x, y, z; (iv) 2-x, -y, 1-z. **67**: (i) 1-x, 0.5+y, 0.5-z; (ii) 1-x, 2-y, 1-z; (iii) 2-x, 4-y, 1-z.

The crystal structure of **60** was reported during the course of our research on azolium picrate salts,¹⁵ thus, only the features in the structure not described before are highlighted (i.e., graph-sets). The rest of the picrate salts have been crystallographically characterized for the first time in this work and a detailed description of their molecular structures and packing follows. Since the picrate anion is well established, its structure will not be discussed in detail here.

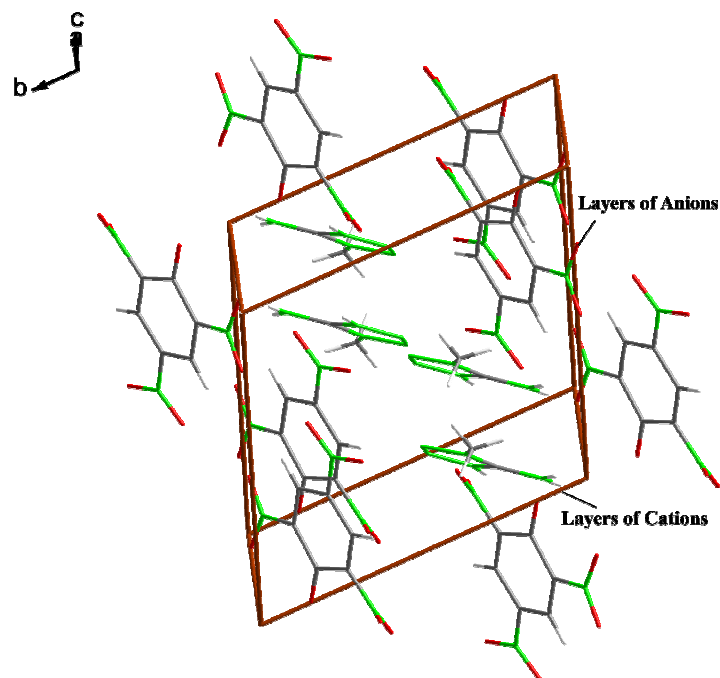


Figure 5.9 Layers of cations and anions in the unit cell of **60** (view along the *a*-axis).

Among the picrate salts studied here, **60** is the only one that crystallizes in a triclinic cell in the space-group *P*-1, whereas the rest of the compounds have monoclinic cells in the space-group *P*₂₁/*c*. In the structure of **60** polymeric chains are formed along the *a* axis with simple van der Waals interactions between chains. Although cations and anions do not pack in a layered structure (Figure 5.9), there exists coplanarity among cations and anions. Since the performance of a material is a function (among other properties) of its density and this is governed by the molecular structure and hydrogen-bonding, it is of interest to take a closer look at the hydrogen-bonding motifs formed in the crystal structure. The formalism of graph-set introduced by Bernstein et al.³³ and the program *RPLUTO*³⁴ are useful to assign and describe patterns in the hydrogen-bonding. The five hydrogen bonds tabulated in Table 5.3 could be identified by the program as forming common finite interactions of the type **D1,1(2)** at the primary level (see Table 5.4). These dimmeric interactions combine at the secondary level to form exclusively ring graph-sets of variable sizes going from the small **R2,2(4)** to the large **R4,4(26)** graph-sets. Some of the most characteristic patterns are depicted in Figure 5.10. For example, the phenolate oxygen atom interacts (together with one of the *o*-NO₂ oxygen atoms) with two of the cation hydrogen atoms forming one very strong (N5...O1ⁱⁱ = 2.618(1) Å) and three medium (N1...O1ⁱⁱ, N1...O2ⁱⁱ and N5...O7ⁱⁱ = 2.9-3.2 Å; symmetry code: (ii) -x, 1-y, 2-z) hydrogen bonds, which describe two **R2,1(6)** motifs. A similar pattern is also formed by the cation, where in this case it forms two interactions using two different hydrogen atoms and thus takes the label **R1,2(6)**. Lastly, two symmetrically generated cations and anions are linked together by interactions to the amino-groups protons yielding a larger **R2,4(8)**

ring graph-set. The latter is identical to the patterns found in compounds containing the 14DMAT⁺ cation and analogous to the **R4,4(12)** motif found in the perchlorate salt.³

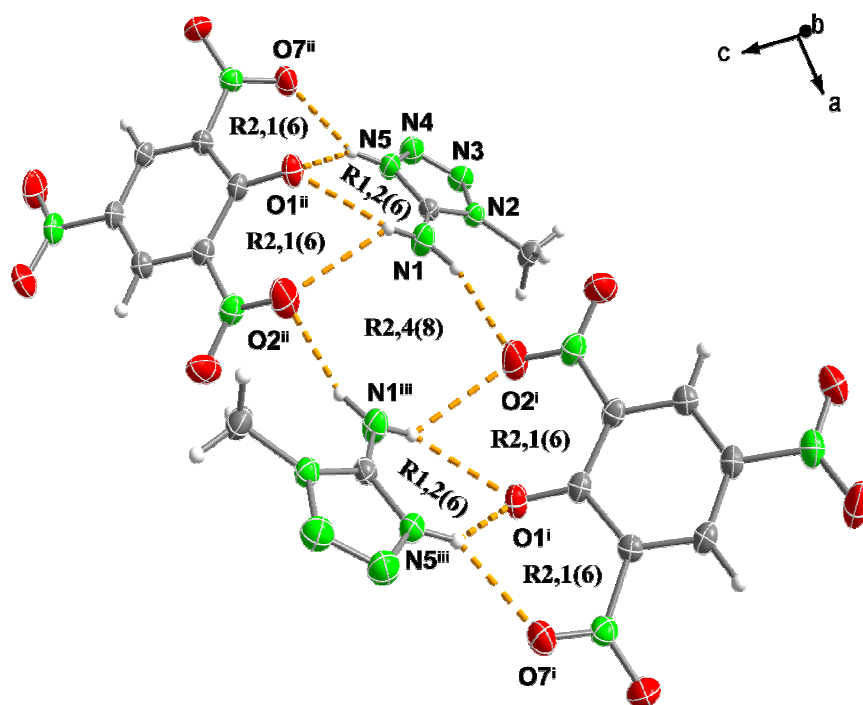


Figure 5.10 Hydrogen-bonding in the crystal structure of picrate salt **60** showing some characteristic ring graph-sets (symmetry codes: (i) $1+x, 1+y, z$; (ii) $-x, 1-y, 2-z$; (iii) $1-x, 2-y, 2-z$).

Table 5.4 Graph-set matrix for strong to medium hydrogen bonds in **60**. First level motifs on-diagonal and second level graph-sets off-diagonal.

H bond	N1–H1A...O2 ⁱ	N1–H1B...O1 ⁱⁱ	N1–H1B...O2 ⁱⁱ	N5–H5...O1 ⁱⁱ	N5–H5...O7 ⁱⁱ
N1–H1A...O2 ⁱ	D1,1(2)				
N1–H1B...O1 ⁱⁱ	R4,4(16)	D1,1(2)			
N1–H1B...O2 ⁱⁱ	R2,4(8)	R2,2(4)	D1,1(2)		
N5–H5...O1 ⁱⁱ	R4,4(20)	R1,2(6)	R2,4(12)	D1,1(2)	
N5–H5...O7 ⁱⁱ	R4,4(24)	R2,2(10)	R4,4(26)	R2,1(6)	D1,1(2)

Symmetry codes: (i) $1+x, 1+y, z$; (ii) $-x, 1-y, 2-z$.

In contrast to **60** where the amino group protons are approximately coplanar to the tetrazole ring, in the structure of **62** these are bent out of the plane ($\text{H1B–N1–C1–N2} = 165(1)^\circ$). The formal exchange of a proton in **60** for a methyl-group in **62** results in a less efficient packing as represented in Figure 5.11 and reflected in a decrease in the density from 1.716 to 1.639 g cm⁻³. In addition, less hydrogen bonds are formed (5 vs. 3).

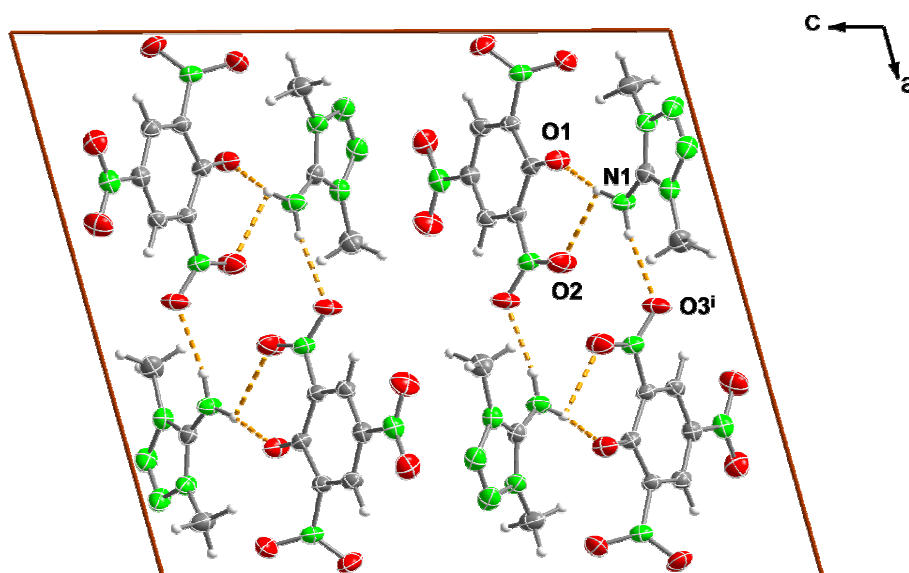


Figure 5.11 View of the unit cell of picrate salt **62** along the *b*-axis showing the hydrogen-bonding (dotted lines, symmetry code: (i) 1-x, 0.5+y, 0.5-z).

Once again, the phenolate anion participates in the formation of an **R2,1(6)** graph-set and the N5-bound methyl-group forms a non-classical hydrogen bond to O7 ($C3 \cdots O7 = 3.401(3)$ Å). As can be seen in Figure 5.12 the orientation of the ions does not allow the formation of the **R2,4(8)** pattern mentioned above for **60**, but one of the cations interacts *via* N1 to two picrate anions ($N1 \cdots O1 = 2.747(2)$ and $N1 \cdots O3^i = 2.894(2)$ Å; symmetry code: (i) 1-x, 0.5+y, 0.5-z), which in turn form a hydrogen bond to two crystallographically related cations ($N1^i$ and $N1^{ii}$; symmetry code: (ii) 1-x, -0.5+y, 0.5-z). This is in contrast with the iodide,² azide and perchlorate salts and in analogy to the dinitramide compound.³ Lastly, two chain graph-sets of the type **C2,2(X)** (X = 6, 8) are found at the secondary level (Table 5.5).

Table 5.5 Graph-set matrix for strong to medium hydrogen bonds in **62**. First level motifs on-diagonal and second level graph-sets off-diagonal.

H bond	N1–H1A \cdots O1	N1–H1A \cdots O2	N1–H1B \cdots O3 ⁱ
N1–H1A \cdots O1	D1,1(2)		
N1–H1A \cdots O2	R2,1(6)	D1,1(2)	
N1–H1B \cdots O3 ⁱ	C2,2(8)	C2,2(6)	D1,1(2)

Symmetry codes: (i) 1-x, 0.5+y, 0.5-z.

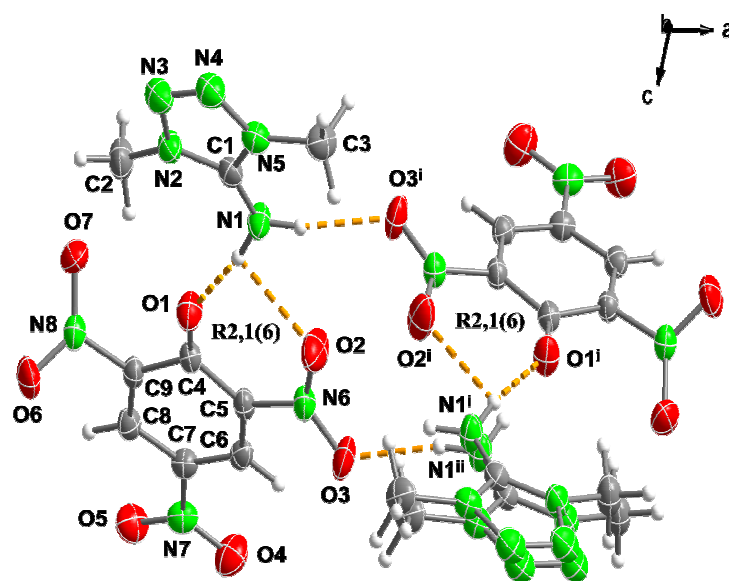


Figure 5.12 Hydrogen-bonding in the crystal structure of **62** showing some characteristic ring graph-sets (symmetry codes: (i) $1-x, 0.5+y, 0.5-z$; (ii) $1-x, -0.5+y, 0.5-z$).

63 (Figure 5.13) is the “asymmetric” isomer of **62**. Both compounds crystallize in the same monoclinic space group ($P2_1/c$) and have very similar cell parameters (see *Appendix C*) and almost identical unit cell volumes ($\sim 1390 \text{ \AA}^3$). A view along the *b* axis of the unit cell of **62** (Figure 5.11) and **63** (Figure 5.14) make the similarities in the structure in both compounds obvious. Only one medium ($\text{N1} \cdots \text{O3}^{\text{i}} = 3.019(3) \text{ \AA}$) and one strong ($\text{N1} \cdots \text{O1}^{\text{ii}} = 2.686(2) \text{ \AA}$) hydrogen bonds are formed (symmetry codes: (i) $1-x, 2-y, -z$; (ii) $x, 2.5-y, 0.5+z$). Alike **62**, two cations and two anions are connected *via* hydrogen bonds (Table 5.3) and again the two picrate anions are linked once to the same cation and once to two crystallographically related cations.

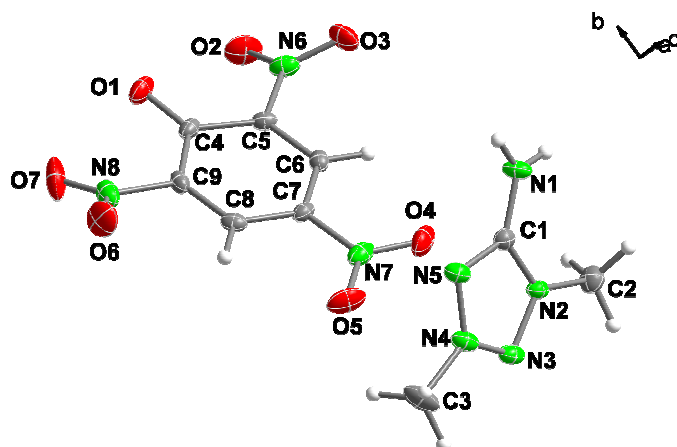


Figure 5.13 Asymmetric unit of picrate salt **63** with the labeling scheme.

In **63** the arrangement of the anions does not allow the formation of the **R2,1(6)** graph-set described for **62** and only a chain **C2,2(8)** motif involving both hydrogen bonds is found (Table 5.6) instead of the expected **R2,2(16)** pattern that would form if the cations and anions that interact were to lay in the same plane. This lack of efficiency in the packing is reflected in the lower density values ($\sim 1.64 \text{ g cm}^{-3}$) of both compounds in respect to the other salts reported here.

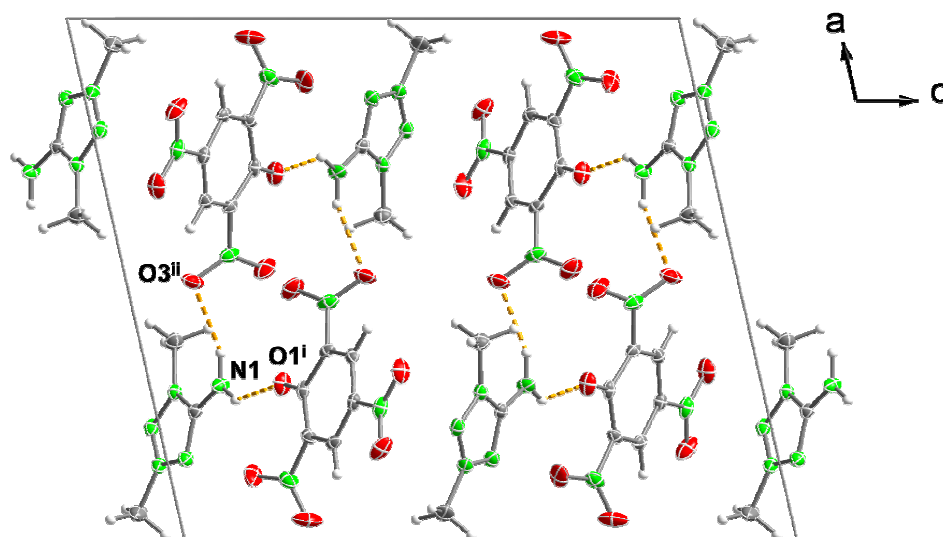


Figure 5.14 View of the unit cell of picrate salt **63** along the *b*-axis showing the hydrogen-bonding (dotted lines, symmetry codes: (i) 1-*x*, 2-*y*, -*z*; (ii) *x*, 2.5-*y*, 0.5+*z*).

Table 5.6 Graph-set matrix for strong to medium hydrogen bonds in **63**. First level motifs on-diagonal and second level graph-sets off-diagonal.

H bond	N1–H1A...O3 ⁱ	N1–H1B...O1 ⁱⁱ
N1–H1A...O3 ⁱ	D1,1(2)	
N1–H1B...O1 ⁱⁱ	C2,2(8)	D1,1(2)

Symmetry codes: (i) 1-*x*, 2-*y*, -*z*; (ii) *x*, 2.5-*y*, 0.5+*z*.

For the guanazinium salt (**66**), the rings of the cation and anion form two planes defining an angle of 8.2° (Figure 5.15) and the packing in the unit cell consists of discrete dimmeric ionic pairs stacking (Figure 5.16). As for the bond distances in the cation, comparison with neutral guanazine (Gz)^{22a} shows that the N4–N5 and N1–N2 distances are both shorter while C1–N4 and C2–N5 are both longer. The angles C2–N5–N4 and C1–N4–N5, which are identical in neutral Gz,^{22a} are significantly different in the picrate salt which is in good agreement with other triaminotriazolium salts.^{22,35}

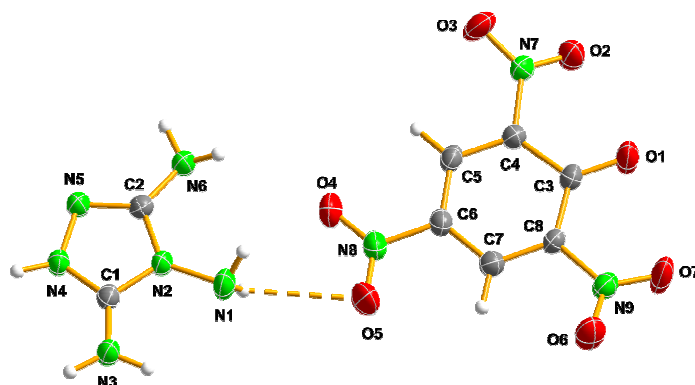


Figure 5.15 Molecular structure of **66** in the crystalline state. Displacement ellipsoids are shown at the 50% probability level.

Protonation occurs at the position crystallographically labelled as N4 on the triazole ring and the N1 amino group protons adopt a configuration similar to that found in the 5-nitrotetrazolate,^{22a} perchlorate and dinitramide salts³⁵ but opposite to the same protons in the nitrate salt³⁵ where they are facing away from N6. This is keeping in with methylguanazinium salts (see *Chapter IV*).²⁴ Many types of strong hydrogen bonds (Table 5.3) are observed in the molecular structure of **66**, which account for its high thermal stability and low sensitivity (see section 5.6 *Energetic Properties*). The two ions are linked by strong hydrogen bonds: $N4 \cdots O1^{ii} = 2.653(2) \text{ \AA}$, $N4 \cdots O2^{ii} = 3.014(2) \text{ \AA}$, $N1 \cdots O5^{iii} = 3.034(3) \text{ \AA}$, $N3 \cdots O6^{iv} = 3.136(3) \text{ \AA}$ and $N1 \cdots O4 = 3.157(3) \text{ \AA}$ (symmetry codes: (ii) $1+x, y, 1+z$; (iii) $1+x, y, z$; (iv) $2-x, -y, 1-z$).

Table 5.7 Graph-set matrix for strong to medium hydrogen bonds in **66**. First level motifs on-diagonal and second level graph sets off-diagonal.

H-Bond	A	B	C	D	E	F	G	H
N6–H3 \cdots N5 ⁱⁱ (A)	R2,2(8)							
N3–H2 \cdots O1 ⁱⁱ (B)	D3,3(14) [R2,2(8)]	D1,1(2)						
N3–H2 \cdots O6 ⁱⁱ (C)	D3,3(14) [R2,2(8)]	R2,1(6)	D1,1(2)					
N4–H7 \cdots O1 ⁱⁱ (D)	D3,3(11) [R2,2(8)]	R1,2(6)	R2,2(10)	D1,1(2)				
N4–H7 \cdots O2 ⁱⁱ (E)	D3,3(11) [R2,2(8)]	R2,2(10)	R2,2(12)	R2,1(6)	D1,1(2)			
N1–H6 \cdots O5 ⁱⁱⁱ (F)	D3,3(13) [R2,2(8)]	C2,2(13)	C2,2(13)	C2,2(13)	C2,2(13)	D1,1(2)		
N3–H1 \cdots O6 ^{iv} (G)	D3,3(14) [R2,2(8)]	R4,4(16)	R4,4(12)	R4,4(20)	R4,4(24)	R4,4(26)	D1,1(2)	
N1–H5 \cdots O4 (H)	D3,3(13) [R2,2(8)]	C2,2(13)	C2,2(13)	C2,2(13)	C2,2(13)	C2,2(6)	R4,4(26)	D1,1(2)

Symmetry codes: (ii) $1+x, y, 1+z$; (iii) $1+x, y, z$; (iv) $2-x, -y, 1-z$.

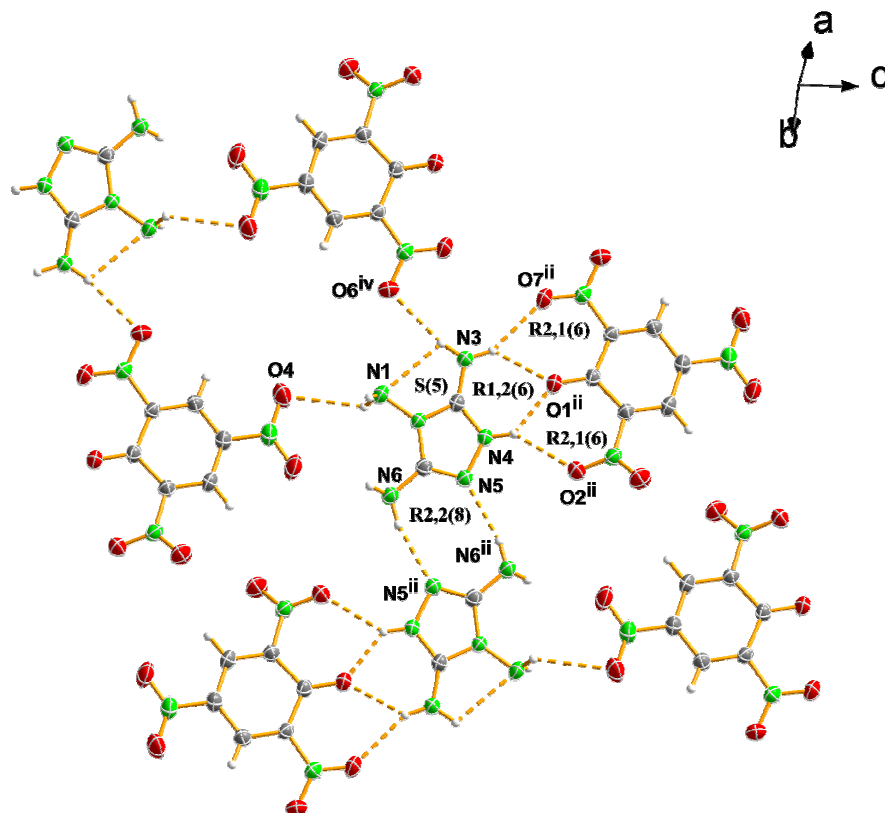


Figure 5.16 Primary and secondary graph-sets of interest in **66**.

The unitary hydrogen-bonding network of **66** is described by several **D1,1(2)** dimmeric patterns, one **R2,2(8)** ring network and one **S(5)** intramolecular graph-set.^{33,34} The intramolecular **S(5)** motif is formed by a proton of the C–NH₂ group, which is planar with the triaminotriazolium ring, and the N–NH₂ lone pair (Figure 5.16). The third amino group of two triazolium cations, which does not participate in this **S(5)** motif, forms a **R2,2(8)** ring graph-set at the first level. At the second level, this hydrogen bond formed by N6 (donor) and N5 (acceptor) combines with all the other hydrogen-bonds in the structure to build different **R2,2(8)** motifs (Table 5.7). The phenolate oxygen (O1) together with both nitro-groups builds two **R2,1(6)** and one **R1,2(6)** subsets and two larger ones denoted as **R2,2(10)** and **R4,4(16)**.

It is interesting to note the presence of non-classical C...O hydrogen-bonds between two coplanar and crystallographically equivalent picrate anions describing a **R2,2(10)** network at the primary-level. The existence of such interactions is proven by the following: i) the directionality of the nitro-group pointing with an oxygen atom (O3) to the proton, ii) a relatively short distance between proton and acceptor at O3...H1' = 2.61(2) Å (the sum of the van der Waals radii $r_O + r_H = 2.7$ Å)¹¹ and iii) the formation of a **R2,2(10)** subset in the structure of other known azolium picrates.¹²⁻¹⁴

Comparison of the crystal structures of **59**,¹² **60**,¹⁴ **64**¹³ and **66** reveals a **R2,2(10)** pattern in the graph-set analysis for all compounds. The C–H distances in all structures are relatively similar. More conspicuous are the changes in the H···O and donor-acceptor distances (C···O), which are much shorter in the case of **66** (H···O = 2.61(2) Å and C···O = 3.442(3) Å). In the case of **59** and **64** two of the nitro groups are approximately coplanar with the phenyl ring and the third group is slightly off-the-plane whereas the observed situation is somewhat different for **66** and **60** where we find an approximately coplanar, a slightly off-the-plane and a much more off-the-plane nitro-group (the torsion angles in the case of **66** are 5.9(3), 11.9(3) and 25.8(3)°). In contrast with the other three picrates where the **R2,2(10)** pattern is described by interaction with an oxygen on a nitro-group coplanar with the ring, in this case it is precisely the most off-the-plane nitro-group, which forms this interaction. This interaction with the off-the-plane nitro-group considerably deviates the C–H–O angle from the ideal 180°, regardless of the strong directionality of the interaction (C–H–O = 147.7(2)°). The interaction with the “on-the-plane” nitro-groups in the case of **59**, **64** and **60** is reflected in a C–H–O angle much closer to the ideal 180° (165.4(7), 175.8(2) and 176.4(1)°, respectively).

In **67** the picrate anion shows two essentially planar nitro groups whereas the third one is clearly out-of-the-plane formed by the aromatic ring with a torsion angle (C4–C9–N9–O7) of ~38°. It is precisely this out-of-the-plane nitro group, which participates in the formation of a non-classical hydrogen bond with the methyl group in the methylguanazinium cation (C2···O7^{iv} = 3.259(4) Å; symmetry code: (iv) 1+x, 1+y, z) with H1···O7^{iv} = 2.54(5) Å (sum of the van der Waals radii $r_O + r_H$ = 2.70 Å),³⁶ as already observed for other picrate salts.^{5,16,17} As represented in Figure 5.17 cations and anions alternate in the *a*-direction, whereas there exists π -stacks of anions and cations along the *b*-axis connected by extensive hydrogen-bonding. The presence of three amino groups in the cation is reflected in the larger number of hydrogen bonds formed in comparison to the other picrate salts described in this report (Table 5.3).

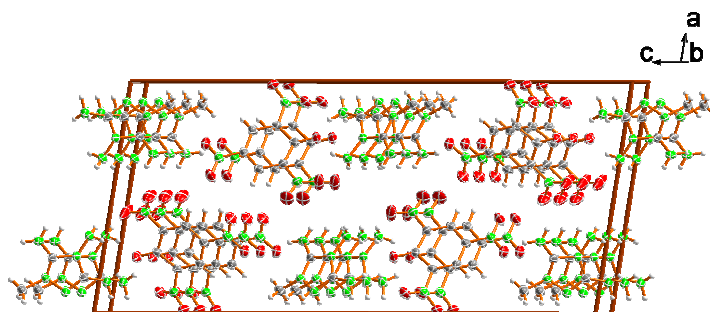


Figure 5.17 View of the unit cell of picrate salt **67** showing the stacks of cations and anions along the *b*-axis.

In addition to the non-classical C \cdots O hydrogen bond, every cation is implied in the formation of eight other hydrogen bonds (Figure 5.18), two of which are to another cation yielding an **R2,2(8)** subset at the primary level (N6 \cdots N5ⁱⁱⁱ = 3.062(4) Å; symmetry code: (iii) 2-x, 4-y, 1-z). Also at the primary level, an **S(5)** motif (N3 \cdots N1 = 2.834(4) Å) is found, which is in analogy with **66** and is common for other 1,2-diaminosubstituted azoles.^{6,23,24} The rest of the hydrogen bonds are to three crystallographically related anions. It is interesting to note that one of these anions alone forms up to four different medium-to-strong hydrogen bonds to the same triazolium cation (N1 \cdots O1ⁱⁱ = 2.924(4), N1 \cdots O2ⁱⁱ = 2.834(4), N6 \cdots O1ⁱⁱ = 2.944(3) and N6 \cdots O7ⁱⁱ = 3.118(3) Å; symmetry code: (ii) 1-x, 2-y, 1-z), describing two **R2,1(6)** subsets (similarly to **60**) and one **R1,2(7)** motif by interaction of the penholate oxygen atom (O1ⁱⁱ) with the nitrogen atoms labelled as N1 and N6 at the same time. Lastly, apart from the above-mentioned graph-set there exist (among others) many ring patterns of the type **R4,4(X)** (X = 18, 22, 24, 28) and infinite hydrogen-bonded chains, which take the label **C2,2(X)** (X = 10, 13, 14, 15) (see Table 5.8).

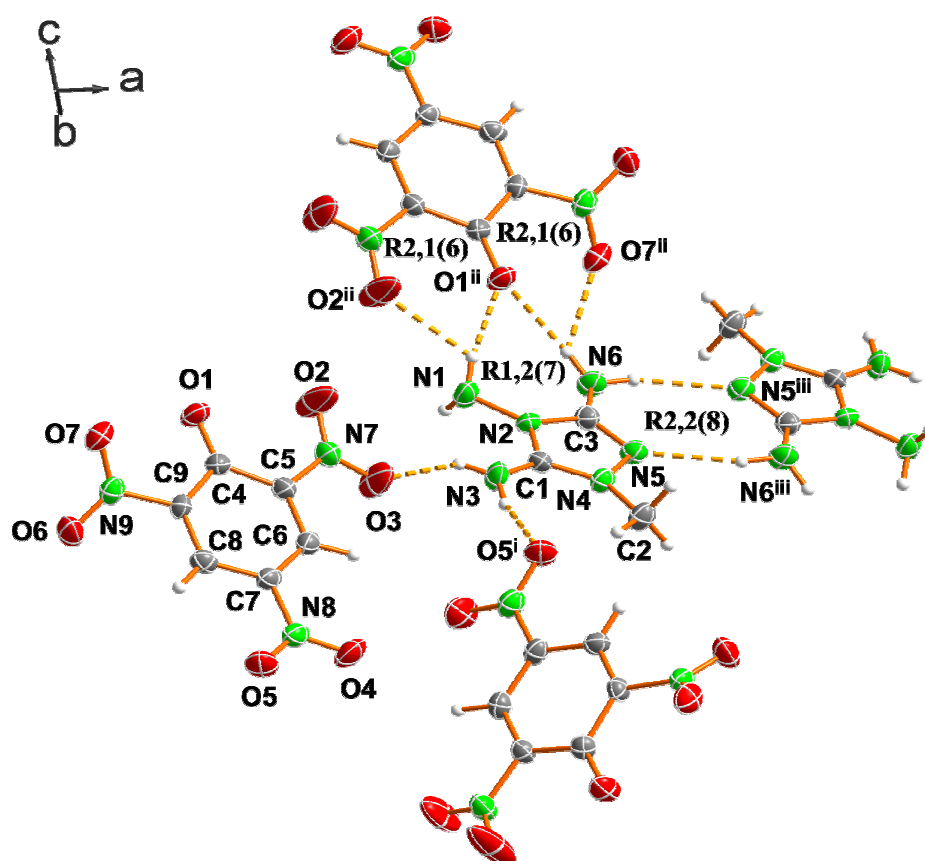


Figure 5.18 Hydrogen-bonding in the crystal structure of **67** showing some characteristic ring graph-sets (symmetry codes: (i) 1-x, 0.5+y, 0.5-z; (ii) 1-x, 2-y, 1-z; (iii) 2-x, 4-y, 1-z).

Table 5.8 Graph-set matrix for strong to medium hydrogen bonds in **67**. First level motifs on-diagonal and second level graph-sets off-diagonal.

H bond	A	B	C	D	E	F	G	H
N3–H3A•••N1 (A)	S1,1(5)							
N3–H3A•••O3 (B)		D1,1(2)						
N3–H3B•••O5 ⁱ (C)		C2,2(10)	D1,1(2)					
N6–H6A•••O1 ⁱⁱ (D)		R4,4(24)	C2,2(14)	D1,1(2)				
N6–H6A•••O7 ⁱⁱ (E)		R4,4(28)	C2,2(14)	R2,1(6)	D1,1(2)			
N1–H1B•••O1 ⁱⁱ (F)		R4,4(22)	C2,2(13)	R1,2(7)	R2,2(11)	D1,1(2)		
N1–H1B•••O2 ⁱⁱ (G)		R4,4(18)	C2,2(13)	R2,2(11)	R2,2(13)	R2,1(6)	D1,1(2)	
N6–H6B•••N5 ⁱⁱⁱ (H)		C2,2(13)	C2,2(14)	C2,2(13)	C2,2(15)	C2,2(14)	C2,2(15)	R2,2(8)

Symmetry codes: (i) 1-x, 0.5+y, 0.5-z; (ii) 1-x, 2-y, 1-z; (iii) 2-x, 4-y, 1-z.

5.6 Energetic Properties

Computational Methods. All quantum chemical calculations were carried out with the Gaussian03W software package.³⁷ Electronic energies for all cations and the picrate anion were calculated using Møller-Plesset perturbation theory truncated at the second order (MP2)³⁸ and were used unscaled. The structures of the cations and anion were optimized based on the single-crystal structures using the correlation consistent polarized double-zeta basis set cc-pVDZ.^{39,40} All of the optimized structures were characterized to be true minima on the potential energy surface without imaginary frequencies.

Based on Born-Haber energy cycles⁴¹ the heat of formation (ΔH_f°) of an ionic salt can be calculated from the heats of formation of cation and anion and the lattice energy (ΔH_L) using Equation (1). The lattice energy can, in turn, be calculated using Jenkins' Equation (2)⁴² from the lattice potential energy (U_{TOT}) and n_x and n_y , which are indexes for the ions X_a^+ and Y_b^- , and are equal to 3 for monoatomic ions, 5 for polyatomic ions and 6 for nonlinear polyatomic ions. Lastly, the lattice potential energies can be readily derived from the density of the material (ρ) in g cm⁻³, the chemical formula mass (M) in g, and the coefficients γ (kJ mol⁻¹ cm⁻¹) and δ (kJ mol⁻¹) that take their values from the literature⁴² according to Equation (3).

$$\Delta H_f^\circ (\text{ionic salt, 25 }^\circ\text{C}) = \Delta H_f^\circ (\text{cation, 25 }^\circ\text{C}) + \Delta H_f^\circ (\text{anion, 25 }^\circ\text{C}) - \Delta H_L \quad (1)$$

$$\Delta H_L = U_{\text{TOT}} + [a(n_x/2 - 2) + b(n_y/2 - 2)]RT \quad (2)$$

$$U_{\text{TOT}} = \gamma(\delta/M)^{1/3} + \delta \quad (3)$$

In order to assess the energetic properties of the azolium picrate salts the thermal stability (DSC measurements), sensitivity to friction, impact, electrostatic discharge and thermal shock of each salt was experimentally determined. For each salt the constant volume energy of combustion

was determined experimentally using oxygen bomb calorimetry and also predicted on the basis of calculated electronic energies (see Computational Methods section and Table 5.A1) and an estimation of lattice enthalpy^{42,43}. Prediction of thermochemical properties of energetic materials using similar methods has been described before.⁴⁴ Using the experimental combustion data, the energies of formation were calculated and used in conjunction with the densities (either calculated from the X-ray measurements or experimentally determined using a picnometer) and the molecular formulas to calculate the detonation pressure and velocity using the EXPLO5 computer code.⁴⁵

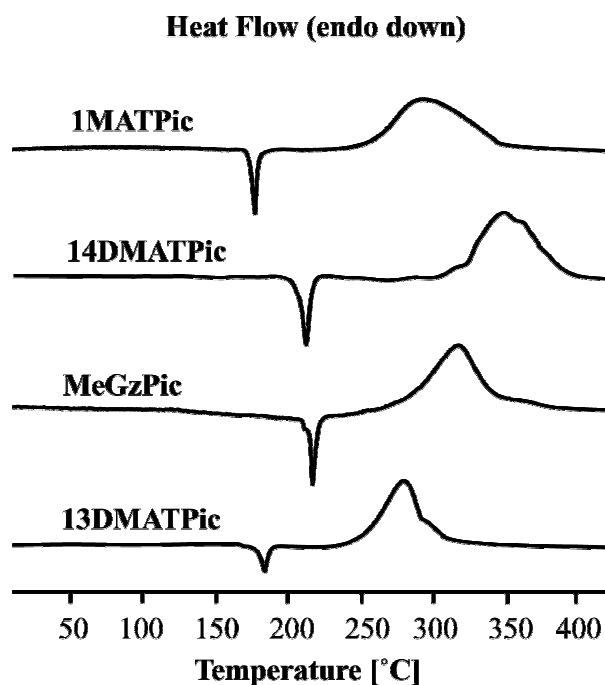


Figure 5.19 Differential scanning calorimetry (DSC) plots for selected azolium picrate salts.

Figure 5.19 shows typical DSC curves for some of the picrates salts described here. DSC measurements on a small sample of each salt in this study show distinctive melting point for the methylated derivatives (**60-63** and **67**) between 175 and 210 °C, well apart from their decomposition temperatures (all of them above 250 °C). **60** melts at 175 °C, whereas the replacement of one of the protons in the compound by a methyl group in **62**, results in an increase of the melting point to 210 °C, as observed for other salts with the 1MAT⁺ and 14DMAT⁺ cations.³ **67** shows a defined melting point at 207 °C, which is in contrast to non-methylated guanazinium salts, which generally melt with concomitant decomposition,^{22,23} whereas the isomer of **62** (**63**), as expected due to the asymmetric substitution pattern that makes the packing in the solid-state less effective, has a lower melting point similar to the monomethylated

picrate salt **60** ($T_m = 180\text{ }^{\circ}\text{C}$). All compounds have excellent (very similar) thermal stabilities above $250\text{ }^{\circ}\text{C}$. The liquid-ranges (differences between melting and decomposition points) of **60**, **62**, **67** and **63** are ~ 95 , ~ 59 , ~ 43 and $\sim 98\text{ }^{\circ}\text{C}$, respectively, making **60** and **63** of prospective interest as new energetic compounds for use in melt-casting explosives. On the other side, the non-methylated compounds (**59**, **64** and **66**), have either narrow liquid ranges (e.g., **59** $\sim 30^{\circ}\text{C}$) or melt with concomitant decomposition. Apart from **59** and **64**, which decompose slowly at temperatures above $170\text{ }^{\circ}\text{C}$, the rest of the materials have excellent thermal stabilities to as high as $278\text{ }^{\circ}\text{C}$ (**63**). The trend in the decomposition (and melting) points, is, in general, to increase with the number of carbon atoms, however, the guanazinium salts, with three amino groups readily form extensive hydrogen-bonding (see X-ray discussion), which increases its thermal stability. In comparison to commonly used high explosives the azolium picrate salts here have melting points, which are in the rule between that of TNT ($81\text{ }^{\circ}\text{C}$) and that of RDX ($204\text{ }^{\circ}\text{C}$)¹⁴ and the decomposition points are generally comparable to RDX ($230\text{ }^{\circ}\text{C}$). In addition to DSC analysis the response of the compound to fast heating in the flame of a Bunsen burner was also tested. In all cases the picrate salts burned nicely and in the case of the more energetic 5At^+ , DAT^+ and Gz^+ salts the compounds burned notoriously faster, as might be expected from the higher detonation parameters of the compounds (see discussion below). This is a similar response to that observed in high explosives such as TNT or picric acid. From these “flame test” observations it would seem like the azolium picrates composed of a higher percentage of nitrogen were more sensitive to thermal shock.

Table 5.9 Physico-chemical properties of azolium picrate salts.

	59	60	61	62	63
Formula	$\text{C}_7\text{H}_6\text{N}_8\text{O}_7$	$\text{C}_8\text{H}_8\text{N}_8\text{O}_7$	$\text{C}_8\text{H}_8\text{N}_8\text{O}_7$	$\text{C}_9\text{H}_{10}\text{N}_8\text{O}_7$	$\text{C}_9\text{H}_{10}\text{N}_8\text{O}_7$
Mol. Mass (g mol^{-1})	314.17	328.05	328.05	342.25	342.25
T_m ($^{\circ}\text{C}$) ^a	148	175	161	210	180
T_d ($^{\circ}\text{C}$) ^b	>175	270	242	269	278
N (%) ^c	35.7	34.1	34.1	32.7	32.7
$N + O$ (%) ^d	71.3	68.3	68.3	65.5	65.4
Ω (%) ^e	-50.9	-63.4	-63.4	-74.8	-74.8
ρ (g cm^3) ^f	1.840	1.716	1.711 ^g	1.639	1.636
$\Delta_c U$ / $\text{cal g}^{-1} \& j$	-2650(10) [-2899]	-3000(35) [-3251]	-2990(20) [- 3236]	-3320(30) [-3572]	-3310(25) [-3558]
ΔU_f° / $\text{kJ kg}^{-1} h, j$	-320(30) [718]	-440(145) [609]	-460(80) [549]	-540(130) [506]	-580(100) [448]
ΔH_f° / $\text{kJ kg}^{-1} i, j$	-410(30) [635]	-520(145) [522]	-550(80) [463]	-630(130) [416]	-670(100) [357]

...

...

	64	65	66	67
Formula	C ₇ H ₇ N ₉ O ₇	C ₈ H ₉ N ₉ O ₇	C ₈ H ₉ N ₉ O ₇	C ₉ H ₁₁ N ₉ O ₇
Mol. Mass (g mol ⁻¹)	329.19	343.21	343.20	357.24
T _m (°C) ^a	170	148	-	207
T _d (°C) ^b	174	154	269	250
N (%) ^c	38.3	36.7	36.7	35.3
N + O (%) ^d	72.3	69.3	69.3	66.6
Ω (%) ^e	-51.0	-62.9	-62.9	-73.9
ρ (g cm ³) ^f	1.756	1.688 ^k	1.746	1.685
Δ _c U / cal g ⁻¹ g ⁱ	-2780(10)	-3100(10)	-3000(30)	-3310(15)
	[-2936]	[-3267]	[-3179]	[-3486]
ΔU _f ^o / kJ kg ⁻¹ ^{h,j}	330(50)	160(40)	-250(130)	-370(60)
	[962]	[838]	[470]	[369]
ΔH _f ^o / kJ kg ⁻¹ ^{i,j}	240(50)	65(40)	-350(130)	-470(60)
	[875]	[748]	[380]	[276]

^aChemical melting point and ^bDecomposition point (DSC onsets) from measurement with $\beta = 5$ °C min⁻¹; ^cNitrogen percentage; ^dCombined nitrogen and oxygen percentages; ^eOxygen balance according to ref. 46; ^fDensity from X-ray measurements; ^gCalculated constant pressure heat of combustion; ^hStandard heat of formation (back-calculated from ΔH_{comb}); ⁱStandard heat of formation; ^jUncertainties in () brackets and calculated (from MP2 electronic energies) values in [] brackets. ^kExperimental density from picnometer measurements.

Data collected for friction, impact and electrostatic discharge sensitivity testing are summarized in Table 5.10. None of the compounds exploded under the drop hammer (impact sensitivity >40 J) and they were also not sensitive towards friction at the maximum setting of a BAM tester (friction sensitivity >360 N).⁴⁷⁻⁴⁹ These observations are interesting since picric acid itself is more sensitive to both impact and friction¹⁴ and puts into perspective the potential of azolim picrate salts as insensitive energetic materials regardless of their higher (less negative) heats of formation in comparison to picric acid. Additionally, each salt was also roughly tested for sensitivity to electrostatic discharge by spraying sparks across a small sample of the material using a Tesla coil (electrostatic discharge from an HF-Vacuum-Tester type VP 24). None of the compound turned out to be sensitive to an electrostatic discharge of ~20 kV, similarly to TNT. Lastly, all of the compounds in this study can be classified as insensitive according to the UN Recommendations on the Transport of Dangerous Goods as described in ref. 47.

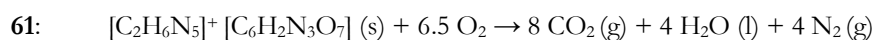
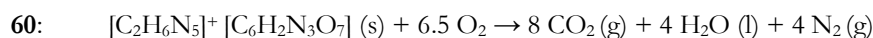
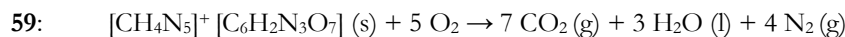
Table 5.10 Initial safety testing results and predicted and calculated^a energetic performance of azolium picrate salts using the EXPLO5 code.

	T_{ex} (K) ^b	V_0 (L kg ⁻¹) ^c	P (GPa) ^d	D (m s ⁻¹) ^e	Impact (J) ^f	Friction (N) ^f	ESD (+/-) ^g	Thermal Shock
59	3395 [3978]	665 [674]	25.6 [30.1]	7795 [8308]	>40	>360	-	Burns Fast
60	3205 [3745]	672 [681]	21.2 [24.5]	7343 [7755]	>40	>360	-	Burns
61	3168 [3718]	672 [681]	20.4 [24.2]	7213 [7722]	>40	>360	-	Burns
62	3005 [3555]	675 [682]	17.8 [21.2]	6876 [7384]	>40	>360	-	Burns
63	2986 [3501]	674 [682]	17.6 [20.4]	6846 [7252]	>40	>360	-	Burns
64	3663 [4011]	694 [699]	25.4 [27.8]	7864 [8143]	>40	>360	-	Burns Fast
65	3429 [3755]	694 [700]	22.1 [23.7]	7492 [7682]	>40	>360	-	Burns
66	3201 [3580]	688 [693]	22.5 [25.0]	7495 [7808]	>40	>360	-	Burns Fast
67	3029 [3403]	688 [693]	19.8 [22.1]	7162 [7486]	>40	>360	-	Burns

^aCalculated values in square [] brackets; ^bTemperature of the explosion gases; ^cVolume of the explosion gases;

^dDetonation pressure; ^eDetonation velocity; ^fTests according to BAM methods (see ref. 47-49); ^gRough sensitivity to 20 kV electrostatic discharge (ESD), + sensitive, - insensitive from an HF-Vacuum-Tester type VP 24.

Apart from sensitivity issues, performance of energetic materials is also of critical importance. The EXPLO5 computer code⁴⁵ can be used to predict the performance of CHNO-based energetic compounds. Therefore, the energies of formation of the azolium picrate salts in this study were back-calculated from their heats of combustion on the basis of their combustion equations (see below) using Hess's Law and the known standard heats formation for water and carbon dioxide⁵⁰ and a correction for change in gas volume during combustion. No corrections for the non-ideal formation of nitric acid (typically ~5% of the nitrogen content reacts to form HNO₃) were made. The EXPLO5 code, using the following values for the empirical constants in the Becker-Kistiakowsky-Wilson equation of state (BKWN-EOS): $\alpha = 0.5$, $\beta = 0.176$, $\kappa = 14.71$ and $\theta = 6620$, was used. Due to the reasonably large standard deviations of experimental combustion measurements, the enthalpies of combustion for each material were predicted on the basis of published methods, using calculated electronic energies and an approximation of lattice enthalpy,^{42,43} in order to validate the experimentally determined values.



- 62:** $[\text{C}_3\text{H}_8\text{N}_5]^+ [\text{C}_6\text{H}_2\text{N}_3\text{O}_7]^- (\text{s}) + 8 \text{O}_2 \rightarrow 9 \text{CO}_2 (\text{g}) + 5 \text{H}_2\text{O} (\text{l}) + 4 \text{N}_2 (\text{g})$
- 63:** $[\text{C}_3\text{H}_8\text{N}_5]^+ [\text{C}_6\text{H}_2\text{N}_3\text{O}_7]^- (\text{s}) + 8 \text{O}_2 \rightarrow 9 \text{CO}_2 (\text{g}) + 5 \text{H}_2\text{O} (\text{l}) + 4 \text{N}_2 (\text{g})$
- 64:** $[\text{CH}_5\text{N}_6]^+ [\text{C}_6\text{H}_2\text{N}_3\text{O}_7]^- (\text{s}) + 5.25 \text{O}_2 \rightarrow 7 \text{CO}_2 (\text{g}) + 3.5 \text{H}_2\text{O} (\text{l}) + 4.5 \text{N}_2 (\text{g})$
- 65:** $[\text{C}_2\text{H}_7\text{N}_6]^+ [\text{C}_6\text{H}_2\text{N}_3\text{O}_7]^- (\text{s}) + 6.75 \text{O}_2 \rightarrow 8 \text{CO}_2 (\text{g}) + 4.5 \text{H}_2\text{O} (\text{l}) + 4.5 \text{N}_2 (\text{g})$
- 66:** $[\text{C}_2\text{H}_7\text{N}_6]^+ [\text{C}_6\text{H}_2\text{N}_3\text{O}_7]^- (\text{s}) + 6.75 \text{O}_2 \rightarrow 8 \text{CO}_2 (\text{g}) + 4.5 \text{H}_2\text{O} (\text{l}) + 4.5 \text{N}_2 (\text{g})$
- 67:** $[\text{C}_3\text{H}_9\text{N}_6]^+ [\text{C}_6\text{H}_2\text{N}_3\text{O}_7]^- (\text{s}) + 8.25 \text{O}_2 \rightarrow 9 \text{CO}_2 (\text{g}) + 5.5 \text{H}_2\text{O} (\text{l}) + 4.5 \text{N}_2 (\text{g})$

The experimental constant volume energies of combustion ($\Delta_c U_{(\text{exp})}$) of all azolium picrate salts were determined using oxygen bomb calorimetry to be -2650(10) cal g⁻¹ (**59**), -3000(35) cal g⁻¹ (**60**), -2990(20) cal g⁻¹ (**61**), -3320(30) cal g⁻¹ (**62**), -3310(25) cal g⁻¹ (**63**), -2780(10) cal g⁻¹ (**64**), -3125(10) cal g⁻¹ (**65**), -3160(30) cal g⁻¹ (**66**) and -3310(15) cal g⁻¹ (**67**). Because of the experimental uncertainties obtained in these measurements, their validity was checked by way of quantum chemical calculation (MP2) of electronic energies and an approximation of lattice enthalpy. Keeping in mind that calculated values tend to systematically overestimate the experimental ones, the predicted constant volume energies of combustion ($\Delta_c U_{(\text{pred})}$) calculated by this method are in close agreement with the experimental values. The overestimation in the values for the energies of formation is, in general, comparable to previous reports of our group⁵¹ and keeping in with other compounds with low possibility to form hydrogen bonds.^{52,53} The larger disagreement is found for the non-methylated salts **59**, **64** and **66**, which form more hydrogen bonds and are due to the low capacity of the method to account for “strong” hydrogen-bonding. Accordingly, the calculated heats (or energies) of formation have all more positive (or less negative) values than the heats of formation back-calculated from the heats of combustion. The experimental values vary all within a relatively narrow range and are slightly negative (e.g., $\Delta_c U_{(\text{exp})}$ (**63**) = -670(100) kJ kg⁻¹) or slightly positive (e.g., $\Delta_c U_{(\text{exp})}$ (**64**) = +240(50) kJ kg⁻¹). The density values vary between moderate (ρ (**63**) = 1.636 g cm⁻³) and high (ρ (**59**) = 1.840 g cm⁻³) and are approximately in the range of commonly used high explosives (e.g., ρ (**TNT**) = 1.654 g cm⁻³ or ρ (**RDX**) = 1.800 g cm⁻³).

From the experimentally determined (picnometer) or calculated (X-ray) density, chemical composition and energies of formation (back calculated from the heats of combustion) the detonation pressures and velocities of **59** (7795 m s⁻¹, 25.6 GPa), **60** (7343 m s⁻¹, 21.2 GPa), **61** (7213 m s⁻¹, 20.4 GPa), **62** (6876 m s⁻¹, 17.8 GPa), **63** (6846 m s⁻¹, 17.6 GPa), **64** (7864 m s⁻¹, 25.4 GPa), **65** (7492 m s⁻¹, 22.1 GPa), **66** (7495 m s⁻¹, 22.5 GPa) and **67** (7162 m s⁻¹, 19.8 GPa) were predicted using

the EXPLO5 code. These values are in the rule higher than those calculated for TNT (at $\rho = 1.60 \text{ g cm}^{-3}$: 7073 m s^{-1} , 19.4 GPa) and in some instances also higher than those of picric acid itself (at $\rho = 1.70 \text{ g cm}^{-3}$: 7185 m s^{-1} , 20.1 GPa)⁴⁵ and fit nicely with the computed ones from (MP2) electronic energies taking into consideration the systematic overestimation of the latter method. In comparison with other azolium salts for which predicted performance data is reported, the azolium picrate salts in this study are predicted to outperform methylated aminotetrazolium salts (6200 m s^{-1} , 15.5 GPa)² and some of them have performances comparable to substituted triazolium salts ($7500\text{-}7900 \text{ m s}^{-1}$, $20\text{-}25 \text{ GPa}$).^{22a,41,44}

A closer look into the heats of formation and detonation parameters (“experimental” or computed) of the azolium picrates studied here clearly illustrates the influence of the cation in these values and allows to draw conclusions about what sort of cations are best suited to achieve a desired result. **59** has an experimental negative heat of formation of $-410(30) \text{ kJ kg}^{-1}$ and substitution of a proton in the ring by a methyl group in **60** and **61** results in an increase in the exothermicity of the compounds ($<-520 \text{ kJ kg}^{-1}$). A second methyl group in the isomeric **62** and **63** results in further decrease in the heats of formation ($<-630 \text{ kJ kg}^{-1}$). However, exchange of a proton in the ring of **59** by an amino group (**64**) yields an endothermic compound ($+240(50) \text{ kJ kg}^{-1}$) and quaternization of the ring to form **65** decreases again the heat of formation ($65(40) \text{ kJ kg}^{-1}$). On the other side, although triazoles are in the rule less endothermic compounds than tetrazoles (1,2,4-triazole ($\Delta_f H_{cryst}^\circ = 26.1 \text{ kcal mol}^{-1}$) in comparison to 5-*H*-tetrazole ($\Delta_f H_{cryst}^\circ = 56.7 \text{ kcal mol}^{-1}$),⁵⁴ the three amino groups in the guanazinium salts **66** and **67** make the compounds more endothermic than the analogous tetrazolium salts with equal number of carbon atoms reported here. The effect of the cation in the heats of formation is accordingly observed in the detonation parameters. The most endothermic compound (**64**) has the highest calculated values, whereas the negative heat of formation of **59** is compensated by its surprisingly high density (1.840 g cm^{-3}) and the salt has the second highest detonation velocity of the picrate salts described here, whereas the rest of the compounds have accordingly higher performances the higher their density.

All compound have high combined oxygen and nitrogen contents ($>65\%$) and the calculated oxygen balances range from -50 to -75% which are comparable to that of picric acid (-43%) or TNT (-74%) and only slightly more negative than RDX (-22%). Due to the negative oxygen balances of the azolium picrates salts in this work, it is of interest to study the performances of mixtures of the compounds with an oxidizer. Therefore, the EXPLO5 code was used to predict the performance of mixtures of the picrate salts with ammonium nitrate (AN) and ammonium

dinitramide (ADN) at an approximately neutral oxygen balance in order to further increase the performance in respect to the stand-alone compounds. The results of the calculations are summarized in Tables 5.A2 and 5.A3. Formulations with AN are predicted to have highly negative heats of formation below -3200 kJ kg^{-1} but better detonation velocities than the stand-alone compounds in the range 8000 to 8200 m s^{-1} . On the other side, mixtures with ADN as the oxidizer are predicted to have less negative heats of formation between -700 and -1100 kJ kg^{-1} and much higher detonation parameters (8700 - 8900 m s^{-1} and 31.0 - 33.0 GPa).

Lastly, it is important to point out that all performance values reported in the literature are based exclusively on predicted heats of combustion using electronic energies as discussed above. This method tends to systematically overestimate the heats of combustion and the resulting performance values and therefore exaggerated. This overestimation is higher, the higher the possibility of a compound to form extensive hydrogen-bonding. However, on the other side, experimentally determined heats of formation tend to be underestimated and performance predictions thereof should thus be underestimated.

5.7 Long Term Stabilities of **1MATPic (60)** and **13DMATPic (63)**

Long term stability tests are also useful to assess the shelf-life of energetic compounds. A description of the results obtained from the thermal stability tests follows below. The long-term stabilities of **60** and **63**, which show a larger liquid range (see above), were measured. Figure 5.20 shows the thermal safety calorimetry (TSC) curves. At a temperature $\sim 50 \text{ }^{\circ}\text{C}$ below the decomposition point, compound **60** shows an slightly exothermic peak after a few hours and after the test (2 days) a black residue is formed indicating low stability of the material in the molten phase. On the other side, the presence of the extra methyl-group in **63**, results in a material with better long-term stability than **60**. The TSC curve for this salt looks identical to that of the oven and after the measurement the initial yellow color of the sample is maintained. In the praxis this translates in shelf-lives (at room temperature) of at least 15 years for **63**, which is a basic requisite for further investigation.

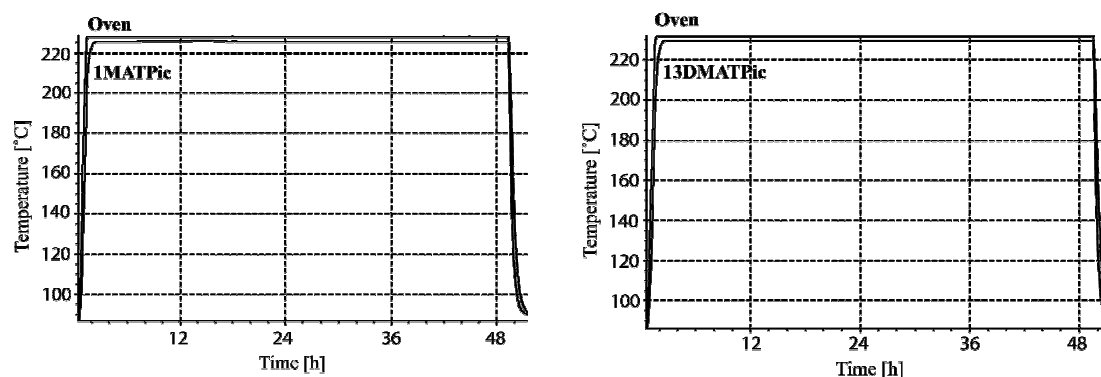


Figure 5.20 Thermal safety calorimetry (TSC) plots for **60** (left) and **63** (right).

5.8 Decomposition Gases

Using the experimentally determined heat of formation (back-calculated from the heats of combustion), the density (from X-ray) and the molecular formula the ICT code⁵⁵ was used to predict the heats of explosion as well as the decomposition gases formed upon explosion/decomposition of the azolium picrate salts in this work. The results of the calculations are summarized in Table 5.11, which also contains the predicted data for TNT and picric acid for comparison purposes.

Table 5.11 Predicted decomposition gases and heats of explosion of azolium picrate salts and comparison with commonly used high explosives (using the ICT code).^a

Compnd.	CO ₂	H ₂ O	N ₂	CO	H ₂	NH ₃	CH ₄	HCN ^b	C	ΔH _{ex} / cal g ^{-1 c}
59	269.7	163.1	353.4	26.7	0.2	3.7	0.2	-	182.1	1117
60	199.2	202.9	335.9	27.9	0.5	6.4	0.8	0.3	225.6	1093
61	199.1	202.8	335.9	28.1	0.5	6.5	0.8	0.3	225.5	1085
62	141.5	235.1	318.9	26.8	0.8	10.1	2.0	0.4	263.9	1066
63	141.5	234.9	318.8	26.9	0.8	10.1	2.1	0.4	263.8	1056
64	227.7	179.5	378.5	26.1	0.3	5.0	0.4	0.3	181.5	1245
65	165.2	215.5	360.3	25.6	0.6	8.3	1.0	0.3	222.9	1226
66	165.1	216.9	360.3	23.3	0.4	8.1	0.8	0.3	224.0	1265
67	113.5	245.8	342.2	21.7	0.8	12.7	1.9	0.4	260.6	1081
TNT	318.1	184.8	182.2	47.0	0.6	3.2	1.2	-	262.0	1350
Pic. acid	495.9	113.5	182.3	47.5	0.2	1.1	0.2	-	158.5	1272

^aThe amount of gases formed at 298 K is given in grams of gas per kilogram of energetic compound; ^bNo HCN formation was predicted for **59**, TNT and picric acid; ^cHeat of explosion.

As might be expected from a nitrogen-rich cation, nitrogen gas is predicted to be the major decomposition product (~315-375 g kg⁻¹) for the azolium picrates salts and it is expected to form in amounts almost twice as high as those predicted for classical nitroaromatic explosives (i.e., TNT and picric acid). The amounts of carbon soot are also relatively high due to the picrate anion but still much lower than TNT (262 g kg⁻¹) and in the case of the nitrogen richer **59** and **64**

salts only slightly higher than picric acid (~182 vs. 158.5%). The major decomposition product expected from the explosion of classical nitroaromatics is anticipated to be CO₂, which is in agreement with the fact that classical explosives derive their energy mostly from the oxidation of their carbon backbone, and is also expected to form in relatively (although much smaller) amounts for **59** and **64** (269.7 and 227.7 g kg⁻¹, respectively). Water (gas) is expected to be generated in a higher ratio for the carbon-rich azolium salts and in larger amounts than for neutral nitroaromatics. In addition, only small amounts of CO are foreseen by the code (20-30 g kg⁻¹) and there is expected to be little nitrogen that goes into the formation of NH₃ (3-13 g kg⁻¹) and negligible amounts of CH₄ (<2.1 g kg⁻¹) and HCN (<0.4 g kg⁻¹) formed. Lastly, the heats of explosion have all values above 1000 cal g⁻¹, are higher for the endothermic compounds **64**, **65** and **66** (>1200 cal g⁻¹) and comparable to TNT and picric acid.

5.9 Conclusions

We have successfully synthesized and fully characterized (analytically and spectroscopically) a new family of picrate salts with triazolium and tetrazolium cations. A full description of the ¹⁵N NMR shifts and PIS/MIS values is given, which helps to determine unequivocally the protonation/methylation site without need of expensive equipment. When suitable, the crystal structure of the compound was determined by X-ray diffraction techniques and a complete description of the hydrogen-bonding patterns in the structure is given on the basis of graph-set analysis. Energetic testing on the sensitivity of the compounds towards impact and friction revealed insensitive picrate salts ($i > 40$ J, $f > 360$ N), which is in contrast with picric acid. DSC analysis showed highly thermally stable compounds (e.g., $T_d(\mathbf{63}) = 278$ °C) with melting points relatively close to the decomposition temperatures. Bomb calorimetry measurements were used to determine the heats of formation of all materials and the results were verified by means of MP2 electronic energy calculations. Calculation of the detonation parameters using the EXPLO5 code predicted performance values higher than those of TNT and in many cases comparable or higher than picric acid. The ICT-code predicted decomposition gases for azolium picrate salts anticipate larger amounts of environmentally friendly nitrogen gas with less carbon soot residue. Lastly, the compounds described here are interesting examples of intermediates between classical nitroaromatic explosives and nitrogen-rich chemistry and might be of interest as prospective insensitive energetic compounds with moderate performances.

5.10 Experimental Section

Caution Note! *Although we had no difficulties handling the picrate salts described here, they are nevertheless energetic materials and their explosive properties are not well established. Picric acid is sold as a water suspension and tends to detonate under certain conditions. It is recommended the synthesis to be carried out only by expert personnel, wearing protective gear, using conductive equipment and on a small scale.*

General. All chemical reagents and solvents were obtained from Sigma-Aldrich Inc. or Acros Organics (analytical grade) and were used as supplied. 1-Methyl- and 2-methyl-5-amino-1*H*-tetrazole,¹ 1,4-dimethyl-5-amino-1*H*-tetrazolium iodide,² 1,3-dimethyl-5-amino-1*H*-tetrazolium iodide,²⁰ 1,5-diamino-1*H*-tetrazole,⁵⁶ 1,5-diamino-4-methyl-1*H*-tetrazolium iodide,⁶ guanazine^{22a} and methylguanazinium iodide²³ were prepared according to previously published procedures. In addition, 5-amino-1*H*-tetrazolium picrate¹⁶ and 1,5-diamino-1*H*-tetrazolium picrate⁵⁶ were synthesized by modified literature procedures as given below. ¹H, ¹³C, and ¹⁵N NMR spectra were recorded on a JEOL Eclipse 400 instrument in DMSO-*d*₆ at or near 25 °C. The chemical shifts are given relative to tetramethylsilane (¹H, ¹³C) or nitromethane (¹⁵N) as external standards and coupling constants are given in Hertz (Hz). Infrared (IR) spectra were recorded on a Perkin-Elmer Spectrum One FT-IR instrument as KBr pellets at 20 °C.⁵⁷ Transmittance values are qualitatively described as “very strong” (vs), “strong” (s), “medium” (m) and “weak” (w). Raman spectra were recorded on a Perkin-Elmer Spectrum 2000R NIR FT-Raman instrument equipped with a Nd:YAG laser (1064 nm). The intensities are reported as percentages of the most intense peak and are given in parentheses. Elemental analyses were performed with a Netsch Simultaneous Thermal Analyzer STA 429. Melting points were determined by differential scanning calorimetry (Linseis DSC PT-10 instrument⁵⁸ calibrated with standard pure indium and zinc). Measurements were performed at a heating rate of 5 °C min⁻¹ in closed aluminum sample pans with a 1 μm hole in the top for gas release under a nitrogen flow of 20 mL min⁻¹ with an empty identical aluminum sample pan as a reference.

Long Therm Stability Tests

The long term stabilities were performed with a Systag FlexyTSC (thermal safety calorimetry)⁵⁹ in combination with a RADEX V5 oven and the SysGraph software. The tests were run on a ~500 mg sample (**60**) and a ~200 mg sample 50% diluted in sand (**63**) in glass test-vessels at atmospheric pressure. The substances were tempered at ~50 °C below their decomposition temperature for 48 hours.

Bomb Calorimetry

For the calorimetric measurements of the picrate salts, a Parr 1356 bomb calorimeter (static jacket) equipped with a Parr 207A oxygen bomb for the combustion of highly energetic materials was used.⁶⁰ A Parr 1755 printer, furnished with the Parr 1356 calorimeter, was used to produce a permanent record of all activities within the calorimeter. The samples (~200 mg each) were carefully mixed with ~800 mg analytical grade benzoic acid and carefully pressed into pellets, which were subsequently burned in a 3.05 MPa

atmosphere of pure oxygen. The experimentally determined constant volume energies of combustion ($\Delta_c U_{(\text{exp.})}$) were obtained as the averages of five single measurements with standard deviations calculated as a measure of experimental uncertainty. The calorimeter was calibrated by the combustion of certified benzoic acid in an oxygen atmosphere at a pressure of 3.05 MPa.

Synthesis of 5-Amino-1*H*-tetrazolium Picrate (59). Picric acid (1.035 g, 4.52 mmol) was dissolved in 60 mL methanol giving a bright yellow solution and was reacted with neat anhydrous 5-amino-1*H*-tetrazole (0.372 g, 4.38 mmol) at 60 °C for 32 h. At this point the solvent was stripped using a rotatory evaporator at 40 °C and 100 mbar giving a yellow oil, which became solid under high vacuum (10^{-3} mbar). The crude product was recrystallized from 8 mL of a methanol/dichloromethane mixture (1:2) and the pure compound precipitated as a crystalline solid on cooling overnight (0.723 g). The solvent was then stripped again and the crude compound recrystallized a second time using the same solvent. The crystalline compound, which precipitated from the cold solution (0.381 g) was pure by elemental analysis and was combined with the first fraction (1.104 g, 80%).

$\text{C}_7\text{H}_6\text{N}_8\text{O}_7$ (314.17 g/mol), calcd.: C 26.76, H 1.92, N 35.67%; found: C 26.76, H 2.08, N 35.72%; m.p. (uncorrected): 147.2-148.5 °C; DSC (5 °C/min, °C): 148 (m.p.), >175 (non-explos. dec.); m/z (FAB⁺, xenon, 6 keV, m-NBA matrix): 73.1 (72), 86.1 (100, $[\text{CH}_4\text{N}_5]^+$), 171.2 (18, $[(\text{CH}_3\text{N}_5)_2\text{H}]^+$), 207.2 (9), 221.2 (7), 239.2 (29), 327.1 (4); (FAB, xenon, 6 keV, m-NBA matrix): 212.0 (31, $[\text{C}_6\text{H}_2\text{N}_3\text{O}_6]^-$), 228.0 (100, $[\text{C}_6\text{H}_2\text{N}_3\text{O}_7]^-$), 313.0 (17), 381.0 (3); ^1H NMR (DMSO- d_6 , 400.18 MHz, 25 °C, TMS) δ /ppm: 10.13 (4H, broad, NH/NH₂), 8.56 (2H, s, H-aromat.); $^{13}\text{C}\{^1\text{H}\}$ NMR (DMSO- d_6 , 100.63 MHz, 25 °C, TMS) δ /ppm: 160.6 (1C, C1), 155.0 (C-NH₂), 141.8 (2C, C2), 125.3 (2C, C3), 124.8 (1C, C4); ^{14}N NMR (DMSO- d_6 , 28.92 MHz, 25 °C, MeNO₂) δ /ppm: -12 ($\Delta\nu_{1/2}$ = 170 Hz, NO₂); ^{15}N NMR (DMSO- d_6 , 40.55 MHz, 25 °C, MeNO₂) δ /ppm: -12.0 (2N, NAO₂), -15.2 (1N, NBO₂), -27.4 (2N, N2/N3), -168.1 (2N, N1/N4), -326.2 (1N, t, 1J = 86.9 Hz, N5); Raman $\tilde{\nu}$ / cm^{-1} (rel. int.): 3030(3) 1559(35) 1488(16) 1366(32) 1324(81) 1296(100) 1164(21) 1090(28) 945(17) 913(7) 828(35) 750(18) 417(9) 344(20); IR $\tilde{\nu}$ / cm^{-1} (KBr, rel. int.): 3382(s) 3250(m) 3078(m) 1706(vs) 1636(vs) 1580(m) 1565(s) 1484(m) 1432(m) 1364(m) 1336(vs) 1317(s) 1267(s) 1159(m) 1079(m) 1055(m) 1027(m) 992(w) 944(w) 925(w) 911(w) 830(w) 791(w) 745(m) 716(w) 703(w) 625(w) 547(w).

Synthesis of 1-Methyl-5-amino-1*H*-tetrazolium Picrate (60). A solution of 1-methyl-5-amino-1*H*-tetrazole (0.179 g, 1.8 mmol) in 2 mL hot water was added to a solution of picric acid (0.398 g, 1.7 mmol) in 3 mL hot water. The mixture was boiled together for a few minutes and let to cool slowly to room temperature. Yellow prismatic crystals of **60** precipitated immediately. The crystals were filtered and washed with cold acetone and ether. A second crop could be obtained from cooling the mother liquors in the fridge overnight and filtering cold. This was treated as described above. Both (combined) crops were pure by elemental analysis (0.521 g, 91%). The reaction can be easily scaled up to yield ~5.0 g of **60**, without significantly affecting the yield or the purity of the material.

$C_8N_8H_8O_7$ (328.20 g/mol), calcd.: C 29.3, H 2.5, N 34.1%; found: C 29.4, H 2.5, N 34.4%; m.p. (uncorrected): 174.0-175.4 °C; DSC (5 °C/min, °C): 175 (m.p.), ~270 (non-explos. dec.); m/z (FAB⁺, xenon, 6 keV, m-NBA matrix): 100.1 (100, $[C_2H_6N_3]^+$), (FAB⁻, xenon, 6 keV, m-NBA matrix): 228.0 $[C_6H_2N_3O_7^-]$; ¹H NMR (DMSO-d₆, 400.18 MHz, 25 °C, TMS) δ/ppm: 8.6 (2H, s, H-aromat.), 5.6 (3H, broad, NH/NH₂) 3.7 (3H, s, CH₃); ¹³C{¹H} NMR (DMSO-d₆, 100.63 MHz, 25 °C, TMS) δ/ppm: 160.6 (1C, C1), 155.1 (1C, C-NH₂), 141.8 (2C, C2), 125.2 (2C, C3), 124.6 (1C, C4), 31.7 (1C, CH₃); ¹⁵N NMR (DMSO-d₆, 40.55 MHz, 25 °C, MeNO₂) δ/ppm: -11.7 (2N, NAO₂), -12.9 (1N, N3), -14.9 (1N, NBO₂), -24.0 (1N, q, ³J = 1.6 Hz, N2), -129.3 (1N, N4), -184.2 (1N, q, ²J = 1.9 Hz, N1), -331.3 (1N, N5); Raman $\tilde{\nu}$ / cm⁻¹ (rel. int.): 3070(1) 2974(2) 1707(3) 1616(6) 1603(6) 1572(10) 1545(26) 1497(10) 1479(10) 1369 (31) 1353(32) 1338(71) 1319(100) 1267(32) 1165(15) 1087(12) 1049(8) 941(22) 916(8) 824(32) 794(7) 778(15) 758(6) 707(9) 676(5) 548(5) 463(5) 429(6) 373(5) 336(14) 315(6) 209(9) 179(5) 161(5); IR $\tilde{\nu}$ / cm⁻¹ (KBr, rel. int.): 3380(m) 3263(w) 3160(w) 3085(w) 3067(w) 2926(w) 1872(w) 1744(w) 1697(s) 1667(w) 1634(s) 1596(m) 1567(s) 1537(m) 1517(w) 1496(w) 1476(w) 1425(m) 1414(m) 1367(s) 1337(s) 1269(s) 1164(m) 1086(m) 1046(m) 971(w) 939(m) 914(m) 867(w) 821(w) 794(m) 777(m) 746(m) 731(w) 706(s) 676(w) 669(w) 547(w) 526(w) 502(w) 461(w).

Synthesis of 2-Methyl-5-amino-1*H*-tetrazolium Picrate (61). 2-Methyl-5-amino-1*H*-tetrazole (0.220 g, 2.2 mmol) was dissolved in 5 mL water and added to a solution of picric acid (0.512 g, 2.2 mmol) in 5 mL of the same solvent at 60 °C. The reaction mixture was brought to boiling and reacted for 2 hours at this temperature. After this time, the solvent was stripped using a rotatory evaporator and the crude product recrystallized from a minimum amount of hot water. The product precipitated as a dark yellow powder, which was filtered under vacuum and washed with little cold ethanol and then ether. The dry compound was pure by elemental analysis (0.502 g, 75%).

$C_8N_8H_8O_7$ (328.20 g/mol), calcd.: C 29.28, H 2.46, N 34.14%; found: C 29.22, H 2.51, N 33.81%; m.p. (uncorrected): 161.6-163.4 °C; DSC (5 °C/min, °C): 161 (m.p.), 242 (non-explos. dec.); m/z (FAB⁺, xenon, 6 keV, m-NBA matrix): 100.1 (100, $[C_2H_6N_3]^+$), 115.1 (18), 253.2 (15); (FAB⁻, xenon, 6 keV, m-NBA matrix): 212.0 (39, $[C_6H_2N_3O_6^-]$), 228.0 (100, $[C_6H_2N_3O_7^-]$), 381.0 (6); ¹H NMR (DMSO-d₆, 400.18 MHz, 25 °C, TMS) δ/ppm: 8.60 (2H, s, H-aromat.), 5.43 (3H, broad, NH/NH₂) 4.07 (3H, s, CH₃); ¹³C{¹H} NMR (DMSO-d₆, 100.63 MHz, 25 °C, TMS) δ/ppm: 167.1 (1C, C-NH₂), 160.5 (1C, C1), 141.8 (2C, C2), 125.2 (2C, C3), 124.7 (1C, C4), 38.8 (1C, CH₃); ¹⁵N NMR (DMSO-d₆, 40.55 MHz, 25 °C, MeNO₂) δ/ppm: -9.0 (1N, q, J = 1.4 Hz, N2), -11.9 (2N, NAO₂), -15.1 (1N, NBO₂), -89.2 (1N, s, N3) - 114.4 (1N, s, N1 or N4), -114.9 (1N, s, N4 or N1), -339.1 (1N, s, N5H₂); Raman $\tilde{\nu}$ / cm⁻¹ (rel. int.): 3107(2) 2961(3) 1633(7) 1612(7) 1562(12) 1530(15) 1346(100) 1279(26) 1178(21) 1087(4) 942(13) 832(25) 649(5) 401(7) 350(9) 329(11) 208(8); IR $\tilde{\nu}$ / cm⁻¹ (KBr, rel. int.): 3373(m) 3302(m) 3214(m) 3104(m) 2958(w) 2923(w) 1630(s) 1607(s) 1572(w) 1562(m) 1548(s) 1527(s) 1502(m) 1468(w) 1440(m) 1428(s) 1409(m) 1391(w) 1339(s) 1313(s) 1261(s) 1204(m) 1177(m) 1148(m) 1086(s) 1016(m) 941(w) 918(s) 832(w) 808(w) 783(m) 763(s) 701(s) 647(s).

Synthesis of 1,4-Dimethyl-5-amino-1*H*-tetrazolium Picrate (62). *Method A:* A fresh solution of 1,4-dimethyl-5-amino-1*H*-tetrazolium perchlorate prepared from reacting over 1 hour 1,4-dimethyl-5-amino-1*H*-tetrazolium iodide (0.845 g, 3.5 mmol) with silver perchlorate (0.730 g, 3.5 mmol) in 15 mL methanol was added (after filtering yellow silver iodide) to a suspension of orangey potassium picrate, prepared from stirring during 30 min. a mixture of picric acid (0.803 g, 3.5 mmol) and potassium hydroxide (0.197 g, 3.5 mmol) in 15 mL methanol. The reaction mixture was stirred under reflux for 3 hours. After this time, yellowish potassium perchlorate was filtered hot and the reaction mixture left to cool to room temperature. **62** precipitated immediately as a yellow solid. The solvent was left to evaporate overnight yielding yellow material (0.894 g, 75%).

Method B: Alternatively, 1,4-dimethyl-5-amino-1*H*-tetrazolium iodide (1.691 g, 7.0 mmol) was dissolved in 15 ml water (at room temperature) and added to a solution of picric acid (1.605 g, 7.0 mmol) in 15 mL hot water (~70 °C). Compound **62** precipitated immediately and the suspension was stirred for 30 minutes at ~70 °C and boiled for 1 hour forming a solution. The pure compound reprecipitated upon cooling to room temperature (1.712 g, 72%).

C₉H₁₀N₈O₇ (342.25 g/mol), calcd.: C 31.6, H 3.0, N 32.7%; found: C 31.7, H 2.8, N 33.0%; m.p. (uncorrected): 207.2-208.9 °C; DSC (5 °C/min, °C): 210 (m.p.), ~269 (non-explos. dec.); m/z (FAB⁺, xenon, 6 keV, m-NBA matrix): 114.1 [C₃H₈N₅]⁺, (FAB⁺, xenon, 6 keV, m-NBA matrix): 228.0 [C₆H₂N₃O₇]; ¹H NMR (DMSO-d₆, 400.18 MHz, 25 °C, TMS) δ/ppm: 9.1 (2H, broad, NH₂), 8.6 (2H, s, H-aromat.), 3.9 (6H, s, CH₃); ¹³C{¹H} NMR (DMSO-d₆, 100.63 MHz, 25 °C, TMS) δ/ppm: 160.6 (1C, C1), 148.3 (C-NH₂), 141.6 (2C, C2), 125.0 (2C, C3), 124.0 (1C, C4), 33.8 (2C, CH₃); ¹⁵N NMR (DMSO-d₆, 40.55 MHz, 25 °C, MeNO₂) δ/ppm: -11.1 (2N, NAO₂), -14.5 (1N, NBO₂), -29.3 (2N, q, ³J = 1.9 Hz, N2/3), -183.0 (2N, q, ²J = 1.5 Hz, N1/4), -319.6 (N5); Raman $\tilde{\nu}$ / cm⁻¹ (rel. int.): 3074(1) 2962(4) 1689(1) 1611(7) 1580(14) 1556(14) 1535(4) 1479(7) 1433(12) 1368(45) 1336(74) 1319(100) 1306(44) 1257(52) 1172(11) 1161(8) 1083(8) 944(7) 933(3) 919(6) 843(1) 822(30) 787(6) 764(2) 747(2) 729(3) 708(2) 644(2) 591(2) 546(1) 510(1) 439(1) 378(7) 335(8) 288(4) 169(3); IR $\tilde{\nu}$ / cm⁻¹ (KBr, rel. int.): 3445(s) 3072(w) 3025(w) 2923(w) 2853(w) 2795(w) 2663(w) 1833(w) 1688(s) 1657(w) 1635(s) 1613(s) 1575(w) 1555(m) 1517(w) 1491(w) 1475(w) 1430(w) 1400(w) 1366(s) 1321(s) 1263(m) 1170(m) 1159(w) 1122(w) 1082(m) 994(w) 943(w) 931(w) 916(m) 840(w) 821(w) 789(m) 777(m) 745(m) 729(w) 707(m) 690(m) 662(w) 575(w) 544(w).

Synthesis of 1,3-Dimethyl-5-amino-1*H*-tetrazolium Picrate (63). 1,3-Dimethyl-5-amino-1*H*-tetrazolium iodide (0.487 g, 2.0 mmol) and picric acid (0.454 g, 2.0 mmol) were dissolved in 5 mL hot water and heated at 100 °C for 15 minutes. Yellow crystals of **63** precipitated upon slow cooling (~3 hours) and were filtered at room temperature. After washing with a small amount of cold water, the product was left to air-dry yielding pure material (0.601 g, 87%).

C₉H₁₀N₈O₇ (342.20 g/mol), calcd.: C 31.6, H 2.9, N 32.7%; found: C 31.5, H 2.9, N 32.6%; DSC (5 °C/min, °C): 180.0 (m.p.), ~278 (dec.); m/z (FAB⁺, xenon, 6 keV, m-NBA matrix): 114.1 [C₃H₈N₅]⁺; (FAB⁺, xenon, 6

keV, m-NBA matrix): 228.0 [C₆H₂N₃O₇]; ¹H NMR (DMSO-d₆, 400.18 MHz, 25°C, TMS) δ/ppm: 8.5 (2H, s, H-aromat.), 8.2 (2H, broad, NH₂), 4.3 (3H, s, N3-CH₃), 3.9 (3H, s, N1-CH₃); ¹³C{¹H} NMR (DMSO-d₆, 100.63 MHz, 26.1°C, TMS) δ/ppm: 160.9 (1C, C1), 158.2 (1C, C-NH₂), 141.7 (2C, C2); 125.4 (1C, C3), 124.7 (1C, C4), 42.6 (1C, N3-CH₃), 34.2 (1C, N1-CH₃); ¹⁴N NMR (DMSO-d₆, 40.55 MHz, 25 °C, MeNO₂) δ/ppm: -11.1 (3N, NAO₂/NBO₂); ¹⁵N{¹H} NMR (DMSO-d₆, 40.55 MHz, 25°C, MeNO₂) δ/ppm: -11.0 (2N, NAO₂), -14.4 (1N, NBO₂), -31.6 (1N, N3), -108.5 (1N, N2), -110.3 (1N, N1), -180.2 (1N, N4), -325.6 (1N, NH₂); ¹⁵N NMR (DMSO-d₆, 40.55 MHz, 25°C, MeNO₂) δ/ppm: -11.0 (2N, NAO₂), -14.5 (1N, NBO₂), -31.9 (1N, q, ³J = 2.3 Hz, N3), -108.6 (1N, N2), -110.2 (1N, N1), -180.8 (1N, N4), -326.4 (1N, t, ¹J = 89.6 Hz, NH₂); Raman $\tilde{\nu}$ / cm⁻¹ (rel. int.): 2958(2) 1567(23) 1479(6) 1414(3) 1369(58) 1338(63) 1298(100) 1268(34) 1166(11) 1080(8) 946(8) 912(3) 821(29) 792(2) 746(4) 719(3) 631(4) 369(3) 340(7) 300(5) 165(2); IR $\tilde{\nu}$ / cm⁻¹ (KBr, rel. int.): 3383(m) 3307(m) 3278(m) 3221(m) 3172(m) 3078(m) 3045(m) 2721(vw) 2659(vw) 2526(vw) 2313(vw) 2244(vw) 1869(vw) 1820(vw) 1659(s) 1633(vs) 1614(s) 1594(m) 1561(s) 1530(vw) 1509(vw) 1496(w) 1484(w) 1463(vw) 1438(w) 1384(w) 1369(m) 1336(vs) 1316(m) 1299(m) 1269(s) 1248(m) 1163(m) 1120(w) 1080(m) 1014(vw) 937(w) 920(vw) 908(w) 852(w) 795(w) 745(m) 710(w) 676(w) 632(w) 546(w) 522(vw).

Synthesis of 1,5-Diamino-1*H*-tetrazolium Picrate (64). 1,5-Diamino-1*H*-tetrazole (0.500 g, 5.00 mmol) was added to a solution containing an equivalent amount of picric acid (1.146 g, 5.00 mmol) in 60 mL ethanol forming a bright yellow suspension. The reaction mixture was stirred for 20 h at 70 °C and left to cool slowly. Yellow crystals of the product started to separate after short time and were filtered and washed with ether yielding a first crop of the compound (0.889 g). The filtrate was rotavaporated to dryness and the crude product was recrystallized from 20 mL ethanol giving a second crop, which was combined with the first one (1.269 g, 77%). No further purification was necessary.

C₇H₇N₉O₇ (329.19 g/mol), calcd.: C 25.54, H 2.14, N 38.29%; found: C 25.27, H 2.12, N 38.42%; m.p. (uncorrected): 169.1-170.4 °C; DSC (5 °C/min, °C): 170 (m.p.), 174 (dec.) ~250 (dec.); m/z (FAB⁺, xenon, 6 keV, m-NBA matrix): 101.1 (30, [CH₅N₆]⁺), 167.1 (7), 254.2 (12); (FAB⁻, xenon, 6 keV, m-NBA matrix): 211.9 (28, [C₆H₂N₃O₆]⁻), 227.9 (92, [C₆H₂N₃O₇]⁻), 253.0 (7), 380.9 (8); ¹H NMR (DMSO-d₆, 400.18 MHz, 25 °C, TMS) δ/ppm: 8.59 (2H, s, H-aromat.), 8.00 (5H, broad, NH/NH₂); ¹³C{¹H} NMR (DMSO-d₆, 100.63 MHz, 25 °C, TMS) δ/ppm: 160.7 (1C, C1), 153.1 (1C, C-NH₂), 142.0 (2C, C2), 125.5 (2C, C3), 125.2 (1C, C4); ¹⁴N NMR (DMSO-d₆, 28.92 MHz, 25 °C, MeNO₂) δ/ppm: -12 (Δν_{1/2} = 180 Hz, NO₂); ¹⁵N NMR (DMSO-d₆, 40.55 MHz, 25 °C, MeNO₂) δ/ppm: -11.7 (2N, NAO₂), -14.8 (1N, NBO₂), -20.9 (1N, N2), -35.8 (1N, N3), -165.6 (1N, N1), -173.8 (1N, N4), -320.1 (1N, N6H₂), -330.2 (1N, N5); Raman $\tilde{\nu}$ / cm⁻¹ (rel. int.): 3017(2) 1549(28) 1482(11) 1369(53) 1355(41) 1334(83) 1348(100) 1270(72) 1166(18) 1087(15) 950(12) 940(23) 915(7) 823(54) 780(12) 716(5) 335(18) 309(11) 212(9); IR $\tilde{\nu}$ / cm⁻¹ (KBr, rel. int.): 3385(s) 3307(m) 3257(m) 3069(m) 1876(w) 1722(vs) 1634(s) 1612(s) 1581(s) 1563(s) 1536(s) 1482(s) 1429(s) 1366(s) 1334(vs) 1271(vs) 1165(s) 1127(m) 1085(s) 997(m) 940(m) 913(m) 869(s) 794(m) 779(w) 749(w) 707(s) 691(m) 660(w) 518(m) 479(m).

Synthesis of 1,5-Diamino-4-methyl-1*H*-tetrazolium Picrate (65). Picric acid (0.899 g, 3.93 mmol) was dissolved in 15 mL boiling water and reacted with a solution of 1,5-diamino-4-methyl-1*H*-tetrazolium iodide (0.950 g, 3.93 mmol) in 7 mL water at room temperature. The reaction mixture was stirred for 25 min. and left to cool overnight. Large crystals of picric acid (0.323 g) precipitated upon cooling and were filtered and kept for another reaction. Filtration resulted in cloudiness in the solution and eventual precipitation of a yellow powder, which was filtered and left to air-dry. The compound was identified as the desired product and no further purification was necessary (0.692 g, 51%).

C₈H₉N₉O₇ (343.21 g/mol), calcd.: C 28.00, H 2.64, N 36.73%; found: C 27.79, H 2.51, N 36.23%; DSC (5 °C/min, °C): 148 (m.p.), 154 (dec.); m/z (FAB⁺, xenon, 6 keV, m-NBA matrix): 115.1 (100, [C₂H₇N₆]⁺), 268.2 (14), 421.2 (2); (FAB⁻, xenon, 6 keV, m-NBA matrix): 212.0 (18, [C₆H₂N₃O₆]⁻), 227.9 (100, [C₆H₂N₃O₇]⁻), 381.0 (6); ¹H NMR (DMSO-d₆, 400.18 MHz, 25 °C, TMS) δ/ppm: 8.97 (2H, broad, N-NH₂); 8.57 (2H, s, H-aromat.), 7.02 (2H, broad, C-NH₂), 3.84 (3H, s, CH₃); ¹³C{¹H} NMR (DMSO-d₆, 100.63 MHz, 25 °C, TMS) δ/ppm: 160.7 (1C, C1), 147.4 (1C, C-NH₂), 141.8 (2C, C2), 125.1 (2C, C3), 124.1 (1C, C4), 39.6 (1C, CH₃); ¹⁴N NMR (DMSO-d₆, 28.92 MHz, 25 °C, MeNO₂) δ/ppm: -14 (Δ*v*_{1/2} = 175 Hz, NO₂); ¹⁵N NMR (DMSO-d₆, 40.55 MHz, 25 °C, MeNO₂) δ/ppm: -11.8 (2N, NAO₂), -14.5 (1N, NBO₂), -24.2 (1N, N2), -36.0 (1N, q, ³*J* = 2.0 Hz, N3), -168.1 (1N, t, ²*J* = 1.8 Hz, N1), -186.9 (1N, q, ²*J* = 2.0 Hz, N4), -312.1 (1N, t, ¹*J* = 75.9 Hz, N6H₂), -323.8 (1N, N5H₂); Raman $\tilde{\nu}$ / cm⁻¹ (rel. int.): 3425(2) 3076(3) 2966(3) 1607(7) 1568(22) 1547(21) 1487(11) 1433(12) 1372(41) 1337(100) 1316(67) 1300(42) 1270(47) 1163(20) 1085(7) 944(15) 920(6) 888(4) 825(51) 794(15) 766(5) 719(7) 602(6) 545(5) 399(7) 368(10) 331(18) 287(8) 202(11); IR $\tilde{\nu}$ / cm⁻¹ (KBr, rel. int.): 3357(s) 3236(s) 3188(s) 3118(s) 3048(s) 1866(vw) 1711(s) 1634(s) 1612(s) 1563(s) 1544(s) 1495(s) 1484(m) 1431(m) 1368(s) 1334(vs) 1269(vs) 1162(m) 1082(m) 1037(w) 1006(vw) 964(w) 936(w) 913(m) 839(vw) 795(w) 788(w) 751(w) 746(w) 710(m) 664(vw) 635(vw) 574(w) 547(w) 527(vw).

Synthesis of 3,4,5-Triamino-1,2,4-triazolium Picrate (66). *Method A:* To an aqueous solution of 0.57 g (5.0 mmol) of 3,4,5-triamino-1,2,4-triazole was added 1.15 g of picric acid (1 wt.% in H₂O from Aldrich dried over 2 days at 60°C in the oven). This mixture was stirred and boiled for 30 minutes. The solvent volume was then reduced and allowed to cool yielding 1.48 g (~86%) of yellow crystals suitable for X-ray structure determination.

Method B: 3,4,5-Triamino-1,2,4-triazolium bromide (0.867 g, 4.45 mmol) was dissolved in 25 mL water and reacted with neat picric acid (1.018 g, 4.44 mmol) producing immediate precipitation of the product. The reaction mixture was stirred at reflux for 1 h and left to cool. The product was then filtered, washed with little water and ethanol and left to air-dry. The compound was obtained as a yellow powder and no further purification was necessary (1.326 g, 87%).

C₈H₉N₉O₇ (343.21 g/mol): calcd., found / %: C 28.00, 28.10; N 36.73, 36.46; H 2.64, 2.85; DSC (2 °C/min, °C): ~269 (dec.); m/z (FAB⁺, xenon, 6 keV, m-NBA matrix): 115.1 [C₂H₇N₆]⁺, (FAB⁻, xenon, 6

keV, m-NBA matrix): 228.1 [C₆H₂N₃O₇]; ¹H NMR ([D₆]DMSO, 400.18 MHz, 25 °C, TMS) δ/ppm: 8.60 (2H, s, H-aromat.), 7.03 (4H, broad, N-NH₂), 5.56 (2H, broad, C-NH₂); ¹³C{¹H} NMR ([D₆]DMSO, 100.63 MHz, 25 °C, TMS) δ/ppm: 161.2 (1C, C1), 150.5 (1C, C-NH₂), 142.2 (2C, C2), 125.7 (2C, C3), 124.7 (1C, C4); ¹⁵N NMR (DMSO-d₆, 40.55 MHz, 25 °C, MeNO₂) δ/ppm: 3.2 (1N, -NO₂), -10.8 (2N, -NO₂), -177.1 (2N, N-1,2), -238.9 (1N, N4), -323.4 (1N, NH₂), -330.2 (2N, NH₂); Raman $\tilde{\nu}$ / cm⁻¹ (rel. int.): 3301(5), 1568(30), 1559(34), 1370(69), 1340(69), 1316(100), 1300(88), 1277(40), 944(23), 826(71), 308(11); IR $\tilde{\nu}$ / cm⁻¹ (KBr, rel. int.): 3401(w) 3174(m) 1706(m) 1639(m) 1541(m) 1430(w) 1329(s) 1267(s) 1156(w) 908(w) 786(s) 712(m).

Synthesis of 1-Methyl-3,4,5-Triamino-1,2,4-triazolium Picrate (67). Methylguanazinium iodide (0.280 g, 1.1 mmol), dissolved in a small amount of water, was added to a solution of picric acid (0.251 g, 1.1 mmol) in hot water (total volume ~5 mL). Immediate precipitation of a yellow powder was observed and the reaction mixture was brought to reflux for 10 minutes after which time the heating was switched off and the reaction mixture was left to cool slowly in the water bath. Yellow crystals of **67** separated from the yellow solution after a short time. The compound was filtered at room temperature, washed with THF and ether and dried under vacuum. No further purification was necessary (0.359 g, 93%).

C₉H₁₁N₉O₇ (353.24 g/mol), calcd.: C 30.2, H 3.1, N 35.3%; found: C 30.2, H 3.0, N 35.4%; DSC (2 °C/min, °C): 207 (m.p.), ~250 (dec.); m/z (FAB⁺, xenon, 6 keV, m-NBA matrix): 129.1 [C₃H₉N₆]⁺, (FAB⁺, xenon, 6 keV, m-NBA matrix): 228.1 [C₆H₂N₃O₇]; ¹H NMR (DMSO-d₆, 400.18 MHz, 25°C, TMS) δ/ppm: 8.57 (2H, s, H-aromat.), 7.91 (2H, broad, N₆H₂), 6.42 (2H, broad, N₅H₂), 5.62 (2H, broad, N₄H₂), 3.45 (3H, s, CH₃); ¹³C{¹H} NMR (DMSO-d₆, 100.63 MHz, 25°C, TMS) δ/ppm: 161.2 (1C, C1), 150.7 (1C, C-N₄H₂), 147.7 (1C, C-N₅H₂), 141.8 (2C, C2), 124.8 (2C, C3), 125.5 (1C, C4), 34.4 (1C, CH₃); ¹⁵N NMR (DMSO-d₆, 40.55 MHz, 25 °C, MeNO₂) δ/ppm: -11.1 (2N, NAO₂), -14.5 (1N, NBO₂), -163.8 (1N, N2), -238.3 (1N, N3), -239.8 (1N, N1), -322.1 (1N, t, ¹J = 82.4 Hz, N₆H₂), -323.0 (1N, t, ¹J = 90.9 Hz, N₄H₂), -335.2 (1N, t, ¹J = 89.7 Hz, N₅H₂); Raman $\tilde{\nu}$ / cm⁻¹ (rel. int.): 3199(1) 2966(1) 1710(5) 1642(3) 1567(51) 1493(10) 1474(17) 1427(5) 1368(62) 1342(88) 1311(73) 1299(100) 1283(46) 1165(8) 1082(5) 945(19) 913(10) 822(63) 787(3) 772(10) 745(1) 713(9) 650(6) 612(2) 589(2) 548(4) 496(3) 367(10) 334(17) 309(9) 212(6) 188(5) 167(5); IR $\tilde{\nu}$ / cm⁻¹ (KBr, rel. int.): 3380(m) 3327(m) 3264(m) 3200(m) 3086(m) 1698(m) 1646(s) 1554(m) 1513(w) 1488(m) 1434(m) 1384(m) 1369(m) 1331(s) 1274(s) 1163(w) 1105(w) 1080(w) 1018(w) 932(w) 909(w) 838(w) 786(w) 745(w) 711(w) 642(w) 615(w) 588(w) 546(w) 518(w).

5.11 References

- [1] R. A. Henry, W. G. Finnegan, *J. Am. Chem. Soc.* **1954**, 76, 923-924.
- [2] T. M. Klapötke, K. Karaghiosoff, P. Mayer, A. Penger, J. Welch, *Propellants, Explos., Pyrotech.* **2006**, 31(3), 188-195.
- [3] K. Karaghiosoff, T. M. Klapötke, P. Mayer, C. Miró Sabaté, A. Penger, J. M. Welch, *Inorg. Chem.* **2008**, 47, 1007-1019.
- [4] V. N. Naumenko, A. O. Koren, P. N. Gaponik, *Magn. Reson. Chem.* **1992**, 30, 558.
- [5] V. E. Matulis, A. S. Lyakhov, P. N. Gaponik, S. V. Voitekhovich, O. A. Ivashkevich, *J. Molec. Struct.*, **2003**, 649, 309-314.
- [6] J. C. Gálvez-Ruiz, G. Holl, K. Karaghiosoff, T. M. Klapötke, K. Löhnwitz, P. Mayer, H. Nöth, K. Polborn, C. J. Rohbogner, M. Suter, J. J. Weigand, *Inorg. Chem.* **2005**, 44(12), 4237-4253.
- [7] H. Feuer, A. T. Nielsen in *Nitro Compounds*; VCH, New York, Weinheim, Cambridge, **1990**.
- [8] A. T. Nielsen in *Nitrocarbons*; VCH, New York, Weinheim, Cambridge, **1995**.
- [9] D. E. Chavez, M. A. Hiskey, R. D. Gilardi, *Angew. Chem. Int. Ed.* **2000**, 39, 1791.
- [10] A. Hammerl, T. M. Klapötke, H. Nöth, M. Warchhold, G. Holl, M. Kaiser, *Inorg. Chem.* **2001**, 40, 3570-3575.
- [11] T. M. Klapötke, P. Mayer, A. Shulz, J. J. Weigand, *J. Am. Chem. Soc.* **2005**, 127, 2032-2033.
- [12] M. von Denffer, G. Heeb, T. M. Klapötke, G. Kramer, G. Spiess, J. M. Welch, *Propellants, Explos., Pyrotech.* **2005**, 30(3), 191-195.
- [13] <http://en.wikipedia.org/wiki/Trinitrotoluene>, checked in December 2007.
- [14] J. Köhler, R. Meyer, *Explosivstoffe*, 7. Aufl., Wiley-VCH, Weinheim, **1991**.
- [15] A. S. Lyakhov, S. V. Voitekhovich, L. S. Ivashkevich, P. N. Gaponik, *Acta. Cryst.* **2005**, E61, o3645-o3647.
- [16] C. M. Jin, C. Ye, C. Piekarski, B. Twamley, J. M. Shreeve, *Eur. J. Inorg. Chem.*, **2005**, 3760-3767
- [17] (a) P. N. Gaponik, V. P. Karavai, *Chem. Heterocycl. Compd.* **1984**, 20(12), 1388-1391. (b) V. E. Matulis, A. S. Lyakhov, P. N. Gaponik, S. V. Voitekhovich, O. A. Ivashkevich, *J. Mol. Struct.* **2003**, 649, 309-314.
- [18] R. A. Henry, W. G. Finnegan, E. Lieber, *J. Am. Chem. Soc.* **1954**, 76(11), 2894-2898.
- [19] T. M. Klapötke, C. Miró Sabaté, unpublished results.
- [20] T. M. Klapötke, C. Miró Sabaté, M. Rusan, *Z. Allg. Anorg. Chem.* **2008**, 634(4), 688-695.
- [21] T. M. Klapötke, C. Miró Sabaté, J. M. Welch, *Z. Anorg. Allg. Chem.*, **2008**, 634(5), 857-866.

- [22] (a) C. Darwich, T. M. Klapötke, M. Sucasca, J. M. Welch, *Propellants, Explos., Pyrotech.* **2007**, in press.
(b) C. Darwich, T. M. Klapötke, C. Miró Sabaté, *Propellants, Explos., Pyrotech.*, **2008**, in press.
- [23] C. Darwich, T. M. Klapötke, C. Miró Sabaté, *Z. Allg. Anorg. Chem.*, **2008**, *634*(4), 61-68.
- [24] C. Darwich, T. M. Klapötke, C. Miró Sabaté, *Chem. Eur. J.*, **2008**, accepted.
- [25] N. B. Colthup, L. H. Daly, S. E. Wiberley, *Introduction to Infrared and Raman Spectroscopy*; Academic Press: Boston, 1990.
- [26] E. Pretsch, P. Bühlmann, C. Affolter, A. Herrera, R. Martínez, *Determinación Estructural de Compuestos Orgánicos*, Springer-Verlag Ibérica: Barcelona, Spain, 2001.
- [27] A. Garrone, R. Fruttero, C. Tironi, A. Gasco *J. Chem. Soc., Perkin Trans. 2* **1989**, *12*, 1941-1945.
- [28] J. C. Gálvez-Ruiz, G. Holl, K. Karaghiosoff, T. M. Klapötke, K. Löhnwitz, P. Mayer, H. Nöth, K. Polborn, C. J. Rohbogner, M. Suter, J. J. Weigand, *Inorg. Chem.* **2005**, *44*(14), 5192-5201.
- [29] G. J. Martin, M. L. Martin, J.-P. Gouesnard, *¹⁵N NMR Spectroscopy*; Springer: Berlin, Germany, 1981.
- [30] <http://www.oxford-diffraction.com>.
- [31] *Programs for Crystal Structure Analysis (Release 97-2)*. Sheldrick, G.M., Institut für Anorganische Chemie der Universität, Tammanstrasse 4, D-3400 Göttingen, Germany, 1998.
- [32] A. Altomare, M. C. Burla, M. Camalli, G. L. Cascarano, C. Giacovazzo, A. Guagliardi, A. G. G. Moliterni, G. Polidori, R. Spagna, *J. Appl. Crystallogr.* **1999**, *32*, 115-119.
- [33] J. Bernstein, R. E. Davis, L. Shimon, N. Chang, *Angew. Chem. Int. Ed. Engl.* **1995**, *34*(15), 1555-1573.
- [34] <http://www.ccdc.cam.ac.uk/support/documentation/rpluto/TOC.html>.
- [35] a) G. W. Drake, T. W. Hawkins, L. A. Hall, J. A. Boatz, A. J. Brand, *Propellants, Explos., Pyrotech.* **2005**, *30*(5), 329-337. b) G. W. Drake, US 6509473, **2003**.
- [36] A. F. Holleman, E. Wiberg, N. Wiberg in *Lehrbuch der Anorganischen Chemie*, 101 Auflage, (Eds.: Walter de Gruyter), Berlin, Germany, 1995.
- [37] M. J. Frisch, G. W. Trucks, H. B. Schlegel, G. E. Scuseria, M. A. Robb, J. R. Cheeseman, J. A. Montgomery, Jr. T. Vreven, K. N. Kudin, J. C. Burant, J. M. Millam, S. S. Iyengar, J. Tomasi, V. Barone, B. Mennucci, M. Cossi, G. Scalmani, N. Rega, G. A. Petersson, H. Nakatsuji, M. Hada, M. Ehara, K. Toyota, R. Fukuda, J. Hasegawa, M. Ishida, T. Nakajima, Y. Honda, O. Kitao, H. Nakai, M. Klene, X. Li, J. E. Knox, H. P. Hratchian, J. B. Cross, C. Adamo, J. Jaramillo, R. Gomperts, R. E. Stratmann, O. Yazyev, A. J. Austin, R. Cammi, C. Pomelli, J. W. Ochterski, P. Y. Ayala, K. Morokuma, G. A. Voth, P. Salvador, J. J. Dannenberg, V. G. Zakrzewski, S. Dapprich, A. D. Daniels, M. C. Strain, O. Farkas, D. K. Malick, A. D. Rabuck, K. Raghavachari, J. B. Foresman, J. V. Ortiz, Q. Cui, A. G. Baboul, S. Clifford, J. Cioslowski, B. B. Stefanov, G. Liu, A. Liashenko, P. Piskorz, I. Komaromi, R. L. Martin, D. J. Fox, T. Keith, M. A. Al-Laham, C. Y. Peng, A. Nanayakkara, M. Challacombe, P. M. W. Gill, B. Johnson, W. Chen, M. W. Wong, C. González, J. A. Pople, *Gaussian 03, Revision C.02*, Gaussian, Inc.: Wallingford, CT, 2004.

- [38] J. A. Pople, R. Seeger, R. Krishnan, *Int. J. Quant. Chem.* **1977**, *11*, 149-163.
- [39] A. K. Rick, T. H. Dunning, J. H. Robert, *J. Chem. Phys.* **1992**, *96*(9), 6796-6806.
- [40] A. P. Kirk, E. W. David, T. H. Dunning, *J. Chem. Phys.* **1994**, *100*(10), 7410-7415.
- [41] H. Xue, H. Gao, B. Twamley, J. M. Shreeve, *Chem. Mater.* **2007**, *19*, 1731-1739.
- [42] H. D. B. Jenkins, D. Tudela, L. Glasser, *Inorg. Chem.* **2002**, *41*(9), 2364-2367.
- [43] H. D. B. Jenkins, H. K. Roobottom, J. Passmore, L. Glasser, *Inorg. Chem.* **1999**, *38*(16), 3609-3620.
- [44] H. Gao, C. Ye, C. M. Piekarski, J. M. Shreeve, *J. Phys. Chem. C* **2007**, *111*(28), 10718-10731.
- [45] M. Sucasca, *Propellants, Explos., Pyrotech.* **1991**, *16*(4), 197-202.
- [46] Calculation of the oxygen balance: $\Omega(\%) = (\text{O} - 2\text{C} - \text{H}/2 - x\text{AO}) 1600/\text{M}$; M = molecular mass.
- [47] Impact: Insensitive >40 J, less sensitive ≥ 35 J, sensitive ≥ 4 J, very sensitive ≤ 3 J; friction: Insensitive >360 N, less sensitive = 360 N, sensitive <360 N a. >80 N, very sensitive ≤ 80 N, extreme sensitive ≤ 10 N; According to the UN Recommendations on the Transport of Dangerous Goods (+) indicates: not safe for transport.
- [48] <http://www.bam.de>.
- [49] T. M. Klapötke, C. M. Rienäcker, *Propellants, Explos., Pyrotech.* **2001**, *26*, 43-47.
- [50] NIST Chemistry WebBook, NIST Standard Reference Database Number 69 - March, **2003** Release, www version: <http://webbook.nist.gov/chemistry>.
- [51] T. M. Klapötke, P. Mayer, C. Miró Sabaté, J. M. Welch, N. Wiegand, *Inorg. Chem.*, **2008**, accepted.
- [52] K. E. Gutowski, R. D. Rogers, D. A. Dixon, *J. Phys. Chem. B*, **2007**, *111*, 4788-4800.
- [53] C. Ye, J. M. Shreeve *J. Chem. Eng. Data*, **2008**, *53*(2), 520-524.
- [54] Ostrovskii, V. A.; Pevzner, M. S.; Kofman, T. P.; Tselinskii, I. V. *Targets Heterocycl. Syst.* **1999**, *3*, 467.
- [55] (a) ICT-Thermodynamic Code, v. 1.0, Fraunhofer-Institut für Chemische Technologie (ICT): Pfinztal, Germany, 1988-2000. (b) R. Webb, M. van Rooijen, *Proceedings of the 29th International Pyrotechnics Seminar*, 2002, 823-828. (c) H. Bathelt, F. Volk, *27th International Annual Conference of ICT*, 1996, *92*, 1-16.
- [56] P. N. Gaponik, V. P. Karavai, *Chem. Heterocycl. Compd.* **1984**, *20*(12), 1388-1391.
- [57] <http://www.perkinelmer.com>.
- [58] http://www.linseis.net/html_en/thermal/dsc/dsc_pt10.php.
- [59] <http://www.systag.ch>.
- [60] <http://www.parrinst.com>.

CHAPTER VI

METHYLATED 5-AMINOTETRAZOLE DERIVATIVES

6.1 Introduction

One of the general goals of modern energetic materials development is the synthesis of materials with acceptable performances and very low sensitivities to physical stimuli. Unfortunately, the performance and sensitivity properties of an explosive material are linked both to each other and to general physical and chemical properties of that material. In order to counteract the correlation of high performance (high detonation pressure and velocity) with high sensitivity to impact, friction and shock systems such as 1,1-diamino-2,2-dinitroethene (FOX-7)^[1] or 1,3,5-triamino-2,4,6-trinitrobenzene,^[2] which form extensive hydrogen bonding networks in the solid state are the state of the art. Hydrogen bonded networks (especially between amino and nitro groups) like those formed in FOX-7 and TATB help to stabilize the material substantially without dramatically reducing energetic performance.

On the other side, ionic energetic materials based on azoles (in particular aminotetrazoles, Figure 6.1) and other nitrogen-rich compounds are also known to form strong hydrogen bonding networks and thus show remarkable stability and considerable insensitivity to physical stimuli as well as good performance.^[3-7] With these properties in mind, aminotetrazole based compounds have long been of interest as potential energetic materials. We recently studied a family of simple energetic salts based on the major mono-methylation product of 5-amino-1*H*-tetrazole (**1**), 1-methyl-5-aminotetrazole (**3**). In that study, **3** was protonated with strong mineral acids (perchloric and nitric) and also quaternized with methyl iodide yielding, after metathesis reactions, a series of salts based on 1,4-dimethyl-5-iminotetrazole (**68**).^[8]

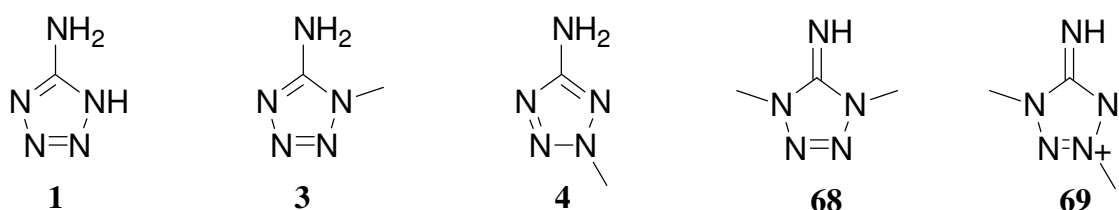


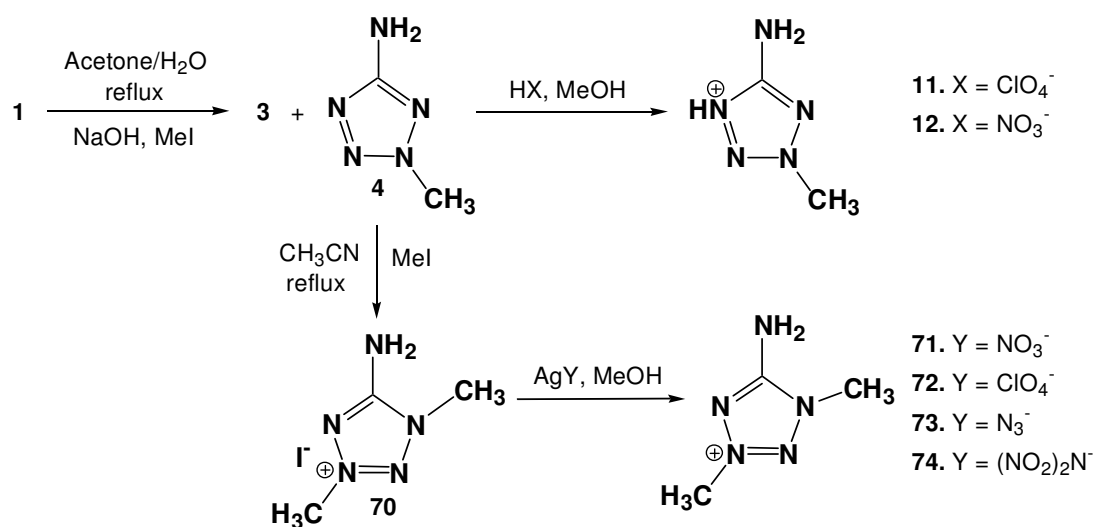
Figure 6.1 Structural formula of 5-aminotetrazoles.

Initially, we ignored salts of 2-methyl-5-aminotetrazole (**4**) and those of 1,3-dimethyl-5-iminotetrazole (**69**) since **4** is only formed as a minor product (10–20% depending on conditions)

of the above mentioned methylation of **1**.^[9] However, given the current interest in ionic liquid based energetic systems and the low symmetry of the cation of **69** (an important criteria for potential ionic liquid formation) we have investigated the structure and properties of the family of ionic energetic salts based on **4** and **69** in hopes of developing a second family of new low sensitivity materials and potentially new liquid ionic energetic materials.

6.2 Synthesis

As introduced in the previous section, **4** was obtained by methylation of the sodium salt of 5-aminotetrazole (**1**) with dimethyl sulfate as described in the literature,^[9] as the minor isomer together with **3** (major isomer). After separation of the two isomers by fractional crystallization and extraction, pure **4** was reacted with a strong acid (either nitric or perchloric acid) to generate the corresponding energetic nitrate (**12**) and perchlorate (**11**) salts. Similarly to our previous work on energetic salts of **3**,^[8] every attempt to generate the energetically interesting azide salt was in vain.^[8,10] On the other side, methylation of **4** with methyl iodide using acetonitrile as the solvent resulted in the regioselective methylation of **4** yielding iodide salt **70**,^[11] which was used as the starting material for the synthesis of energetic salts of **69** with nitrate (**71**), perchlorate (**72**), azide (**73**) and dinitramide (**74**) anions. The general method (illustrated in Scheme 6.1) works through the metathesis reaction between iodide **70** and a suitable “energetic anion transfer reagent”, generally a silver salt (see 6.10 *Experimental Section*).



Scheme 6.1 Synthesis of energetic salts of 2-methyl-5-aminotetrazole (**4**) and 1,3-dimethyl-5-aminotetrazole (**69**).

Most of the compounds were obtained in excellent yields and purities and crystalline materials formed when diffusing diethyl ether into a saturated alcoholic solution of the salts. Lastly, all

compounds described here are readily soluble in polar solvents such as methanol, ethanol, water, DMF, DMSO or acetonitrile and insoluble or little soluble in less polar or apolar solvents such as THF, DCM, diethyl ether or pentane.

6.3 Vibrational Spectroscopy

The salts of **4** and **69**, generated as described above, were qualitatively identified by vibrational spectroscopy (IR and Raman). The spectra (both IR and Raman) of **4** are in perfect agreement with those reported in the literature.^[12] The spectrum of each compound showed the characteristic bands of the relevant energetic anion (nitrate, perchlorate, azide or dinitramide) and set of bands corresponding to the cation. The nitrate anion, NO_3^- , shows a strong (or very strong) IR absorption centered at 1384 cm^{-1} (both **12** and **71**) and a sharp band at $\sim 1045\text{ cm}^{-1}$ in the Raman spectrum.^[13] Compound **12** shows a broad IR signal of medium intensity with maxima at 1308 cm^{-1} , which is masked by the absorptions of the cation in salt **71**. Salts of the perchlorate anion, ClO_4^- , show a strong or very strong broad stretch with its maximum at $\sim 1090\text{ cm}^{-1}$ in the IR spectra and strong, sharp bands at ~ 930 and 465 cm^{-1} in the Raman spectra.^[14] The asymmetric stretch of the anion in compound **73** is observed as a strong absorption at 2042 cm^{-1} , whereas the symmetric stretch is weak in intensity and found at 1297 cm^{-1} in the IR spectrum. In the Raman spectrum only the symmetric stretch is observed as a strong band at 1301 cm^{-1} , as it is usual for ionic azides.^[15] In contrast to the azide salt of **68** the absence of the asymmetric stretch in the Raman spectrum of azide salt **73** indicates that only weak interactions between cation and anion are present. The dinitramide anion, $\text{N}(\text{NO}_2)_2^-$, in salt **74** has medium to very strong absorptions at $1515, 1430, 1384, 1186$ and 1011 cm^{-1} in the IR spectrum and strong bands in the Raman spectrum at 1324 and 825 cm^{-1} .^[16] On the other side, the bands corresponding to the cation can be assigned as follows: $3500\text{--}3100\text{ cm}^{-1}$ [$\nu(\text{N-H})$], $3000\text{--}2850\text{ cm}^{-1}$ [$\nu(\text{C-H})$], $\sim 1660\text{ cm}^{-1}$ [$\nu(\text{C5=N5}) + \delta(\text{N5H}_2)$], $1550\text{--}1350\text{ cm}^{-1}$ [$\nu(\text{tetrazole ring}), \delta_{\text{as}}(\text{CH}_3), \delta(\text{N4-H})$], $\sim 1380\text{ cm}^{-1}$ [$\delta(\text{CH}_3)$], $1350\text{--}700\text{ cm}^{-1}$ [$\nu(\text{N1-C1-N4}), \nu(\text{N-N}), \nu(\text{CN}), \delta(\text{tetrazole ring})$] and $<700\text{ cm}^{-1}$ [δ out-of-plane bend (N-H), $\omega(\text{N5H}_2)$].^[8,17]

In addition to allowing quick, qualitative identification of materials, vibrational spectroscopy also provides insight into structural features, specifically of the cation and hydrogen bonding found in each material studied. Of particular interest are the vibrations corresponding to N-H stretches and deformations and the coupled C5=N5 stretching and N5H₂ deformation modes. These bands are sensitive indicators of hydrogen bond strength and the geometry of the

exocyclic amino group. The neutral parent compounds **3** and **4** show slightly different energies for the above mentioned vibrations. The N5–H stretching modes are observed at slightly higher energies for **4** and the C5=N5 stretching and N5H₂ deformation vibrations at slightly lower energy, indicating weaker hydrogen bonding and a weaker (longer) C5=N5 bond in **4** as compared to **3**. This relationship is also observed in the N5–H stretches and deformations and the coupled C5=N5 stretching and N5H₂ deformation modes in the ionic species based on **68** and **69**, pointing to less C5=N5 double bond character in the cations based on **4** and weaker hydrogen bonding interactions between the cations and anions in salts of **4** and **69** as opposed to the stronger interactions observed for salts of **3** and **68**.

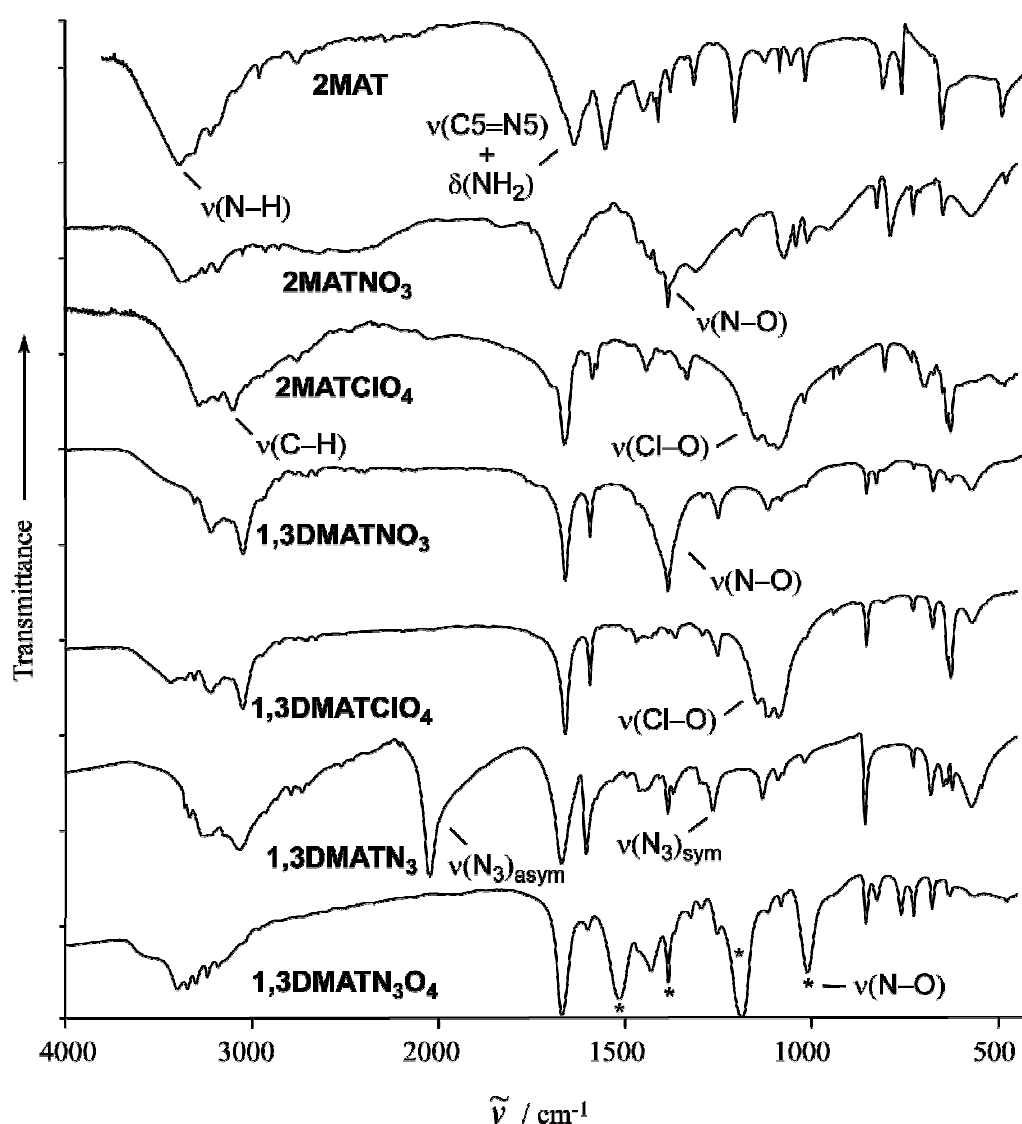


Figure 6.2 Panel plot of the IR spectra of energetic salts of 2-methyl-5-aminotetrazole (**4**) and 1,3-dimethyl-5-iminotetrazole (**69**).

Within the series of salts based on **3** and **68**, on the basis of IR spectroscopy (Figure 6.2), we observed a trend in hydrogen bond strength dependent on the anion used. In the case of the compounds in the current study, the nitrate salt **12** does show stronger hydrogen bonding (presence of a broad absorption centered at $\sim 2400\text{ cm}^{-1}$) than the perchlorate salt **11** (no absorptions are observed in the range $2800\text{--}1800\text{ cm}^{-1}$) as is expected and as was the case for salts based on **3**. However, in contrast to the IR spectra of salts based on **68**, the spectra of salts based on **69** (compounds **70–74**) show no such trend. Compounds **70–74** all have, aside from bands attributed to the anions, nearly identical IR and Raman spectra. This indicates not only that hydrogen bonding is not particularly pronounced in any one compound in this series but also that the cations are expected to be very nearly structurally identical (for further details see section 6.5 *Molecular Structures*). The relatively weak hydrogen bonding in salts of **69** as compared to salts of **68** may be clarified by differences in cation acidity.

6.4 NMR Spectroscopy

Each compound studied in this work was fully characterized by multinuclear (^1H , ^{13}C , ^{15}N and when applicable ^{35}Cl) NMR spectroscopy. The chemical shifts recorded for all nuclei as well as 1J , 2J and 3J ($^1\text{H}\text{--}^{15}\text{N}$) coupling constants are reported in the experimental section. In the case of **4**, all recorded signals and $^1J(^1\text{H}\text{--}^{15}\text{N})$ couplings are in very good agreement with previous studies in our group and the ^1H and ^{13}C resonances are observed as expected.^[8,10,18]

The ^1H NMR spectra of all compounds measured in $[\text{D}_6]\text{-DMSO}$ show two or three resonances for the protons in the cation of **4** and **69**, respectively. The sharp peaks of the methyl group protons occur at $\delta \sim 4.0$ ppm (salts of **4**) and at $\delta \sim 4.2$ and 3.9 ppm (salts of **69**). A broadened peak corresponding to the protons of the amino group occurs at above $\delta = 8.0$ ppm for all compounds. In the ^{13}C NMR the tetrazole carbon signal of the cation is found at $\delta \sim 167.0$ ppm for the salts of **4** and is shifted to high field in the salts of **69** ($\delta \sim 158.3$ ppm). Similarly to observed in the ^1H NMR spectra, the signals corresponding to the methyl groups in compounds **11** and **12** ($\delta \sim 40.0$ ppm) are found at high field in respect to the N3-CH_3 carbon atom resonance ($\delta \sim 43.0$ ppm) and to low field in respect to the N1-CH_3 carbon atom resonance ($\delta \sim 34.4$ ppm). In the ^{15}N NMR spectra of all compounds five resonances (all in the negative range) can be observed as a consequence of low symmetry, that may be assigned to the cations of **4** and **69** (see Figure 6.3 and 6.10 *Experimental Section*). In general, every nitrogen atom in the cation of **69** shows coupling to protons. The amino group nitrogen atom couples at one bond to its protons with $^1J \sim 90.0$ Hz. The nitrogen atoms N1 and N3 couple at two bonds and N2 and N4 at three bonds to

the methyl groups hydrogen atoms with coupling constants which vary between ~ 1.9 and 2.7 Hz. In addition, the resonances corresponding to the anion are also observed. Compounds **3** and **12** show a peak at $\delta \sim -5$ ppm in the ^{15}N NMR spectra corresponding to the nitrogen atom of the nitrate anion. In the ^{15}N NMR spectra of the azide salt **73** two further resonances at $\delta \sim -135$ and -285 ppm can be observed corresponding to the nitrogen atoms of the azide anion, similar to the ^{14}N NMR resonances. The dinitramide salt **74** shows additional signals at $\delta \sim -11$ ppm and -57 ppm corresponding to the nitro group nitrogen atoms and the bridging nitrogen atom in the anion, respectively. Lastly, the perchlorate anion chlorine atom of salts **11** and **72** shows a resonance at $\delta \sim 1.0$ ppm in the ^{35}Cl NMR spectra of the compounds.

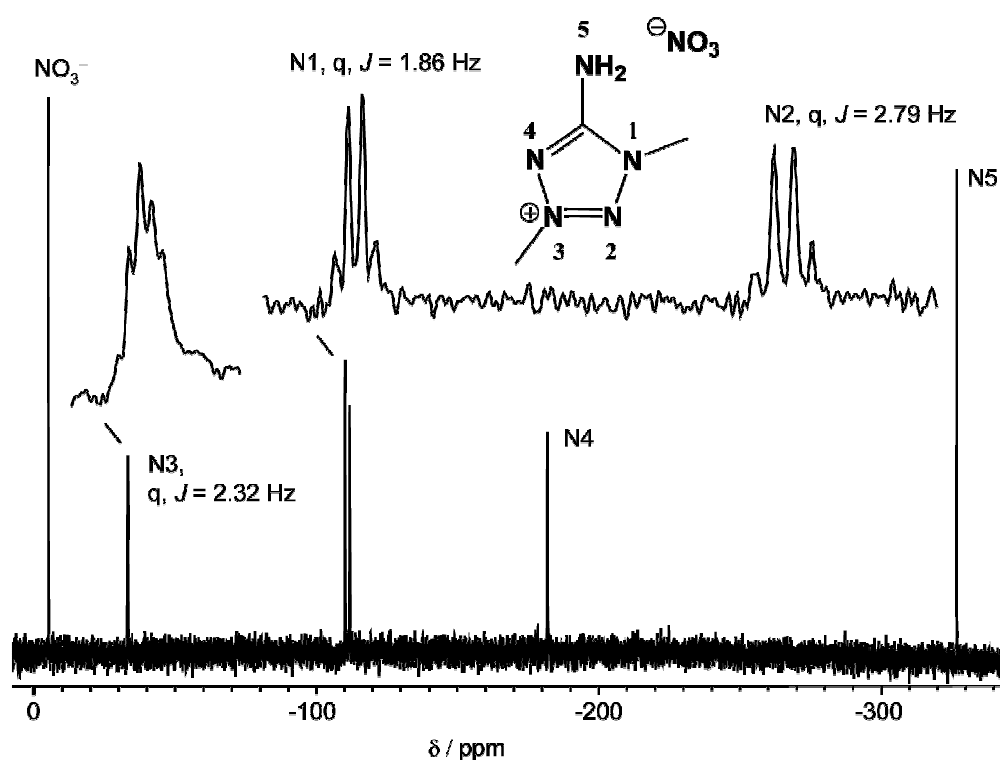


Figure 6.3 ^{15}N NMR spectrum of the 1,3-dimethyl-5-aminotetrazolium cation in compound **71**, measured in $[\text{D}_6]\text{-DMSO}$.

In addition to providing a quick method to uniquely identify the compounds synthesized and help with the assignment of the resonances, protonation (**11** and **12**, PIS) and methylation (**70–74**, MIS) induced shifts (calculated as the difference in ^{15}N NMR shifts between analogous nitrogen signals in neutral **4** and salts of **4** and **69**)^[10] can be used to derive information about the structure in solution and hydrogen bonding (interionic interactions).^[8,10,19] As was the case for the nitrate and perchlorate salts of **3**, the PIS data for **11** and **12** show the most significant shifts occurring at N4 , indicating that protonation in solution occurs primarily at N4 . However, the shifts

themselves are quite small in comparison to those observed for other ring-protonated heterocyclic salts, which seems to indicate that in DMSO solution **11** and **12** exist primarily as **4** and nitric and perchloric acid, respectively. The dissociation of the salts in solution seems to corroborate the IR spectroscopic observation that interionic interactions are weaker for salts of **4** than they are for salts of **3**. The N1 (N4 in salts of **4**) resonance shows an MIS of approximately -97 relative to N4 of **4**. The observed resonances and MIS values observed and calculated for all salts of **69** except for **73** are all very nearly equal within the tolerances of the measurement. **73** shows the strongest cation-anion interactions and thus the least positive (or most negative) MIS values as would be expected, since the resonances observed for the cation in **73** should tend toward the values observed for **69**. The remaining MIS data simply indicate a great deal of similarity in interaction strength between the cation and the different anions in solution.

Table 6.1 ^{15}N and ^{13}C NMR chemical shifts (ppm) and protonation (PIS)/methylation (MIS) induced shifts in [D6]-DMSO.^[a]

	N1 (N4)	N2 (N3)	N3 (N2)	N4 (N1)	N5	C _{ring}
3	-185	-23.2	2.2	-92.7	-338.2	156.4
3a ^[b]	-184.0 (1.0)	-24 (-0.8)	-13.5 (-15.7)	-129.7 (-37)	-331.4 (6.8)	153.6
3b ^[b]	-183.8 (1.2)	-24.3 (-1.1)	-17.4 (-19.6)	-139.1 (-46.4)	-329.5 (8.7)	155.2
68a ^[b]	-182.9 (2.1)	-29.9 (-6.7)	-29.9 (-32.1)	-182.9 (-90.2)	-318 (20.2)	149.1
68b ^[b]	-182.8 (2.2)	-29.5 (-6.3)	-29.5 (-31.7)	-182.8 (-90.1)	-320.4 (17.8)	148.9
68c ^[b]	-182.9 (2.1)	-29.5 (-6.3)	-29.5 (-31.7)	-182.9 (-90.2)	-320 (18.2)	148.5
68d ^[b]	-185.8 (-0.8)	-30.7 (-7.5)	-30.7 (-32.9)	-185.8 (-93.1)	-307.2 (31.0)	148.8
68e ^[b]	-182.7 (2.3)	-29.4 (-6.2)	-29.4 (-31.6)	-182.7 (-90.0)	-320.1 (18.1)	148.5
4	-115.6	-115.7	-6.5	-83.3	-339.7	167.7
11	-113.4 (2.2)	-114.2 (1.5)	-8.8 (-2.3)	-90.0 (-6.7)	-340.1 (-0.4)	166.8
12	-114.4 (1.2)	-114.9 (0.8)	-6.9 (-0.4)	-84.4 (-1.1)	-339.5 (0.2)	167.2
70	-109.0 (6.6)	-111.3 (4.4)	-31.8 (-25.3)	-180.6 (-97.3)	-324.4 (15.3)	157.8
71	-109.6 (6.0)	-111.1 (4.6)	-32.6 (-26.1)	-181.2 (-97.9)	-326.0 (13.7)	158.6
72	-109.3 (6.3)	-111.3 (4.4)	-31.4 (-24.9)	-180.3 (-97.0)	-327.2 (12.5)	158.1
73	-113.2 (2.4)	-113.4 (2.3)	-33.1 (-26.6)	-189.0 (-105.7)	-327.6 (12.1)	158.1
74	-109.4 (6.2)	-111.2 (4.5)	-33.3 (-26.8)	-181.1 (-97.8)	-326.8 (12.9)	158.6

[a] PIS and MIS shifts in parentheses. [b] From ref. [8], **3a**: 1-methyl-5-aminotetrazolium nitrate, **3b**: 1-methyl-5-aminotetrazolium perchlorate, **68a**: 1,4-dimethyl-5-aminotetrazolium iodide, **68b**: 1,4-dimethyl-5-aminotetrazolium nitrate, **68c**: 1,4-dimethyl-5-aminotetrazolium perchlorate, **68d**: 1,4-dimethyl-5-aminotetrazolium azide and **68e**: 1,4-dimethyl-5-aminotetrazolium dinitramide.

6.5 Molecular Structures

The structures of all salts of **4** and **69** and that of the neutral parent compound **4** were determined by X-ray diffraction. Crystals were grown as summarized in 6.10 *Experimental Section*. Crystallographic data and structure determination details are presented in *Appendix C*. Selected

interatomic distances and angles are shown in Table 6.2 and hydrogen bond parameters are tabulated in Table 6.3. The X-ray crystallographic data for **12** were collected on an Enraf-Nonius Kappa CCD diffractometer. Data sets for the rest of compounds were collected on an Oxford Diffraction Xcalibur 3 diffractometer equipped with a CCD detector. All data were collected using graphite-monochromated Mo K α radiation ($\lambda = 0.71073$ Å). No absorption corrections was applied to the data set collected for **12**. A multi-scan numerical absorption correction was applied to data collected for the remainder of the compounds in this study using the ABSPACK^[20] software supplied by Oxford Diffraction. All structures were solved by direct methods (SIR92)^[21] and refined by means of full-matrix least-squares procedures using SHELXL-97^[22] implemented in the WingGX software package^[23] and the structures were finally checked using PLATON.^[24] All non-hydrogen atoms were refined anisotropically. For all compounds all hydrogen atoms were located from difference Fourier electron-density maps and refined isotropically.

Table 6.2 Selected bond lengths (Å) and angles (°) for the methylated 5-aminotetrazole derivatives.

	4	11	12	70	71	72	73	74
C2–N2	1.463(4)	1.454(2)	1.464(3)	1.461(3)	1.461(2)	1.456(2)	1.457(2)	1.458(2)
C5–N1	1.333(3)	1.325(2)	1.343(2)	1.358(3)	1.357(2)	1.356(2)	1.358(2)	1.354(1)
C5–N4	1.341(3)	1.344(2)	1.353(3)	1.340(3)	1.339(2)	1.331(2)	1.337(2)	1.333(2)
C5–N5	1.354(3)	1.312(2)	1.322(3)	1.335(3)	1.322(2)	1.325(2)	1.325(2)	1.327(2)
N1–N2	1.334(3)	1.334(2)	1.339(2)	1.342(2)	1.335(2)	1.339(2)	1.332(2)	1.334(1)
N2–N3	1.304(3)	1.277(2)	1.290(2)	1.295(2)	1.290(2)	1.287(2)	1.289(2)	1.286(1)
N3–N4	1.331(3)	1.323(2)	1.330(2)	1.346(2)	1.334(2)	1.343(2)	1.340(2)	1.342(1)
C1–N1				1.468(3)	1.456(2)	1.451(2)	1.460(2)	1.456(2)
N3–N2–N1	114.9(2)	115.9(1)	116.4(2)	102.8(2)	102.9(1)	103.1(1)	103.0(1)	102.9(1)
N2–N3–N4	105.6(2)	102.7(1)	103.0(2)	116.3(2)	116.5(1)	116.2(1)	116.3(1)	116.4(1)
N3–N4–C5	106.0(2)	110.6(1)	110.0(2)	102.2(2)	102.3(1)	102.2(1)	102.3(1)	101.9(1)
N4–C5–N5	123.6(2)	125.7(1)	124.8(2)	125.5(2)	126.1(1)	126.3(2)	126.4(2)	126.7(1)
N1–C5–N4	112.8(2)	107.7(1)	108.4(2)	108.7(2)	108.3(1)	108.9(1)	108.4(1)	109.0(1)
N1–C5–N5	123.6(2)	126.4(1)	126.7(2)	125.7(2)	125.4(1)	124.7(2)	125.1(2)	124.2(1)
C5–N1–N2	100.6(2)	102.6(1)	102.0(2)	109.8(2)	109.8(1)	109.4(1)	109.9(1)	109.5(1)
N1–N2–C2	123.1(3)	122.2(1)	122.1(2)	121.6(2)	121.1(1)	122.4(2)	121.0(1)	121.6(1)
N3–N2–C2	122.0(3)	121.8(1)	121.4(2)	121.9(2)	122.2(2)	121.3(1)	122.5(1)	121.8(1)
N2–N1–C1				120.5(2)	121.2(1)	121.5(1)	120.2(1)	121.9(1)
C5–N1–C1				129.4(2)	128.9(1)	129.0(1)	129.7(2)	128.5(1)

The crystal structure of the neutral compound **4** was determined by Bryden in 1956.^[25] Therefore, only the details of the improved structure measured here, which are of interest are discussed. The bond lengths for the rest of the materials in the tetrazole ring vary between ~1.28 and 1.35 Å (Table 6.2) and fit in the range between N–N single bonds (1.45 Å) and N=N double bonds (1.25 Å). Also the ring C–N distances between ~1.31 and 1.36 Å lie within the expected values for C–N single and C=N double bonds.^[26]

Compound **4** crystallizes in layers, which are perfectly planar without taking into consideration the sp^3 hybridized methyl group. The layers are separated by ~ 3.5 Å and there exists no significant interactions between them. However, within layers there exists lines of molecules, which run parallel to the a axis and where the molecules of **4** are linked together by hydrogen bonds ($N5 \cdots N4^i = 3.045(4)$ Å and $N5 \cdots N1^{ii} = 3.090(4)$ Å; symmetry codes: (i) $0.5+x, y, 0.5-z$; (ii) $-0.5+x, y, 0.5-z$) describing ring patterns of the form **R2,2(8)** and (of less note) chain graph-sets of the type **C1,1(4)** and **C2,2(6)** (Figure 6.4).

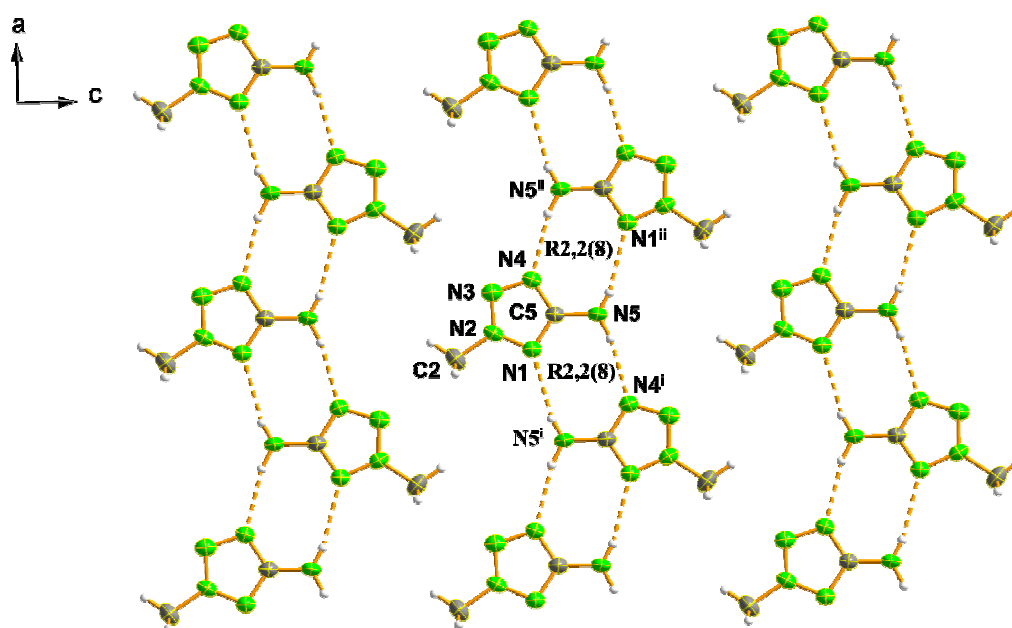


Figure 6.4 Hydrogen bonding in a layer in the crystal structure of compound **4**. Symmetry codes: (i) $0.5+x, y, 0.5-z$; (ii) $-0.5+x, y, 0.5-z$.

Generally and in contrast to salts of **3** and **68**, which form either strong three dimensional hydrogen bond networks or hydrogen bonded dimers of cations and anions, salts of **4** and **69** form either planar or wave-shaped layers within which cations and anions are joined by hydrogen bonding interactions. Also, although the densities of salts of **4** and **69** seem to be, somewhat unexpectedly, similar to or slightly higher than those of analogous salts of **3** and **68**, the hydrogen bonding found in salts of **4** and **69** seems to be generally weaker than that in salts of **3** and **68**. Further inspection of several of the structures in this study (and in previous work) points to a secondary set of closed-shell interactions between the cations and anions which may be responsible for the higher than expected densities found for salts of **4** and **69**. Lastly, the cation methyl groups in several salts of **69** appear, from electron density maps, to be disordered, a circumstance which was not observed for salts of **68**. In addition to disorder in the methyl

groups, the dinitramide anion in **74** also appears to suffer from both static and dynamic disorder. Further discussion of the disorder found in this work and its treatment follows below. All of these factors seem to indicate a change in the dominant type of interionic interactions from directional hydrogen bonding (in salts of **3** and **68**) to less directional electrostatic interactions (in salts of **4** and **69**).

Table 6.3 Medium to strong hydrogen bonds for compound **4** and salts of **4** and **69**.

D–H•••A	D–H (Å)	H•••A (Å)	D•••A (Å)	D–H•••A (°)
4				
N5–H5A•••N4 ⁱ	0.88(3)	2.18(3)	3.045(4)	167(2)
N5–H5B•••N1 ⁱⁱ	0.79(2)	2.31(3)	3.090(4)	166(2)
11				
N4–H4•••N1 ⁱ	0.76(3)	2.43(3)	3.076(2)	144(2)
N4–H4•••O4 ⁱⁱ	0.76(3)	2.46(3)	3.013(2)	131(2)
N5–H5A•••O3 ⁱⁱⁱ	0.79(2)	2.27(2)	3.056(2)	179(2)
N5–H5A•••O1 ⁱⁱⁱ	0.79(2)	2.56(2)	3.053(2)	121(2)
N5–H5B•••O3 ^{iv}	0.76(2)	2.17(2)	2.918(2)	166(2)
12				
N5–H5A•••O1	0.82(3)	2.24(3)	2.983(3)	151(2)
N5–H5B•••O1 ⁱ	0.92(3)	2.11(3)	3.025(3)	176(2)
N5–H5B•••O3 ⁱ	0.92(3)	2.48(3)	3.048(2)	120(2)
N4–H4•••O3 ⁱⁱ	0.92(3)	1.76(3)	2.670(2)	174(3)
N4–H4•••O2 ⁱⁱ	0.92(3)	2.60(3)	3.258(3)	130(2)
71				
N5–H5A•••O3 ⁱ	0.86(2)	2.06(1)	2.925(1)	175(1)
N5–H5B•••O1 ⁱⁱ	0.81(2)	2.08(2)	2.862(1)	161(1)
72				
N5–H5A•••O1 ⁱ	0.82(2)	2.25(2)	3.051(2)	167(2)
N5–H5A•••O2 ⁱ	0.82(2)	2.64(2)	3.052(2)	112(2)
N5–H5B•••O2 ⁱⁱ	0.83(2)	2.12(2)	2.946(2)	176(2)
73				
N5–H5B•••N6 ⁱ	0.83(3)	2.10(3)	2.919(3)	172(3)
N5–H5A•••N8 ⁱⁱ	0.88(3)	2.04(3)	2.921(3)	176(3)
74				
N5–H5B•••O1 ⁱ	0.83(3)	2.14(3)	2.952(3)	166(2)
N5–H5B•••O3 ⁱ	0.83(3)	2.34(2)	2.930(3)	126(2)
N5–H5A•••O4 ⁱⁱ	0.88(2)	2.06(2)	2.908(2)	162(2)

Symmetry codes for **4**: (i) 0.5+x, y, 0.5–z; (ii) –0.5+x, y, 0.5–z; **11**: (i) –1+x, y, z; (ii) –x, –0.5+y, 0.5–z; (iii) 1–x, –y, –z; (iv) –x, –y, –z; **12**: (i) 0.5–x, –0.5+y, 1.5–z; (ii) x, –1+y, z; **71**: (i) x, 0.5–y, –0.5+z; (ii) –x, –y, –z; **72**: (i) –1+x, y, z; (ii) –x, –y, 1–z; **73**: (i) –0.5+x, 0.5–y, –0.5+z; (ii) 1–x, –y, –z; **74**: (i) 1–x, 1–y, 1–z; (ii) x, 0.5–y, 0.5+z.

Also, generally speaking, the cations in this study (2-methyl-5-aminotetrazolium and 1,3-dimethyl-5-aminotetrazolium) are all nearly geometrically identical within the limits of structure determination precision (see Table 6.2) and are also in perfect agreement with the structures determined by Bryden^[25] and us.^[11] The geometry of the protonated (in **11** and **12**) and methylated (in **70–74**) cations also show an extremely strong geometric similarity to the neutral parent compound **4**. A slight shortening of the C5–N5 and N2–N3 bonds are observed and a slight

lengthening of the C5–N4 (for salts of **4**) and C5–N1 (for salts of **5**) bonds is also apparent. Differences in bond lengths found in **4** and those found in salts of **4** and **5** are as might be expected for the increased electronic demand of an extra proton or methyl group. The cation structures observed are also, aside from methyl group substitution patterns and the resulting lower symmetry, surprisingly similar to those of salts of **3** and **68**.

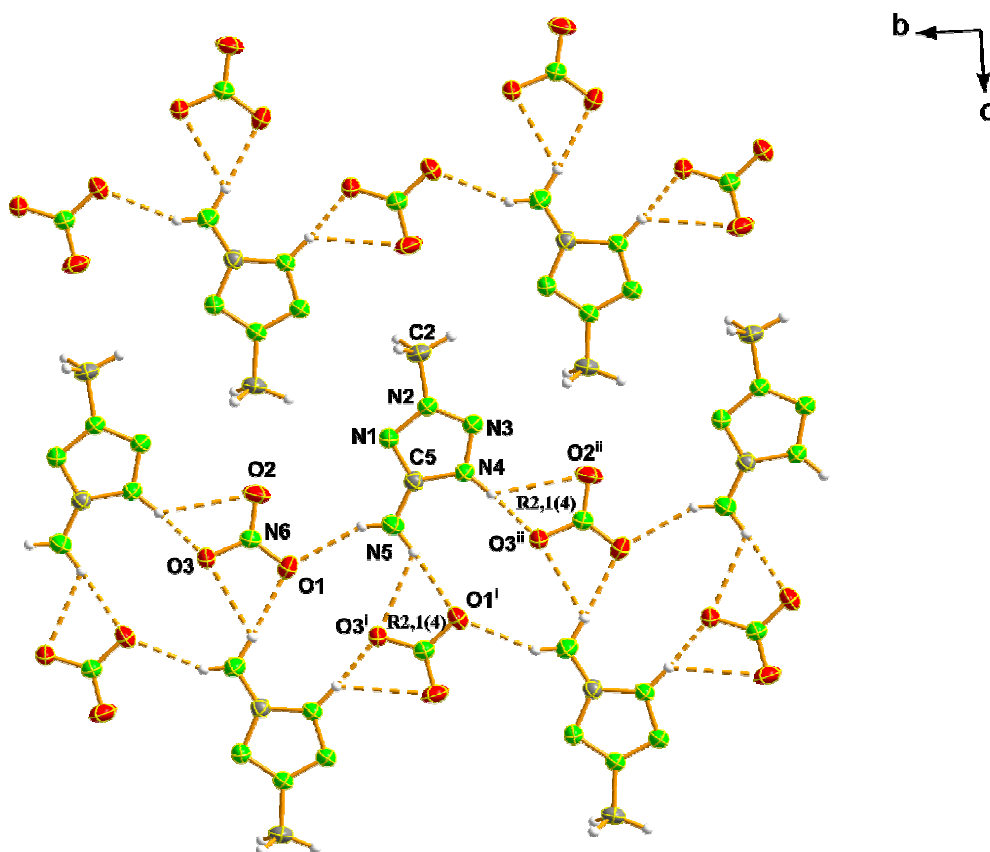


Figure 6.5 Hydrogen bonding in a layer of nitrate salt **12**. Symmetry codes: (i) $0.5-x, -0.5+y, 1.5-z$; (ii) $x, -1+y, z$.

As stated above, the strength and extent of the hydrogen bonding networks observed in salts of **4** and **5** seem to be less than that found for salts of **3** and **68**. Specifically, both compounds **11** and **12** form only five hydrogen bonds each (see Table 6.3 and Figures 6.5 and 6.6) as opposed to the seven hydrogen bonds formed in analogous salts of **3**. Since **12** crystallizes in a layer structure, hydrogen bonding in **12** only occurs between cations and anions lying in the same plane. In addition, cations and anions form hydrogen-bonded bands within each plane, between which only non-polar interactions between the methyl groups are observed. Non-dimeric hydrogen bond patterns are observed only at the secondary level and are mainly of the chain variety with the designators **C1,2(X)** ($X = 4, 6$) and **C2,2(X)** ($X = 6-8$). Each nitrate anion also chelates two protons (see Figure 6.5 for details) forming **R2,1(4)** ring systems. The five hydrogen bonds in **11**

form a three dimensional network composed mainly of common hydrogen bond patterns such as **C1,1(4)**, **C1,2(4)**, **C2,2(8)**, **D3,2(7)** and **D3,3(11)**. Of note are the chain patterns observed at the primary level formed by the $N4 \cdots N1^i$ hydrogen bond (symmetry code: (i) $-1+x, y, z$), which connects only the cations in the structure along the *a* axis and the **R2,1(4)** ring patterns, which are comparable to those formed in the nitrate salt **12**. The two latter networks are represented in Figure 6.6.

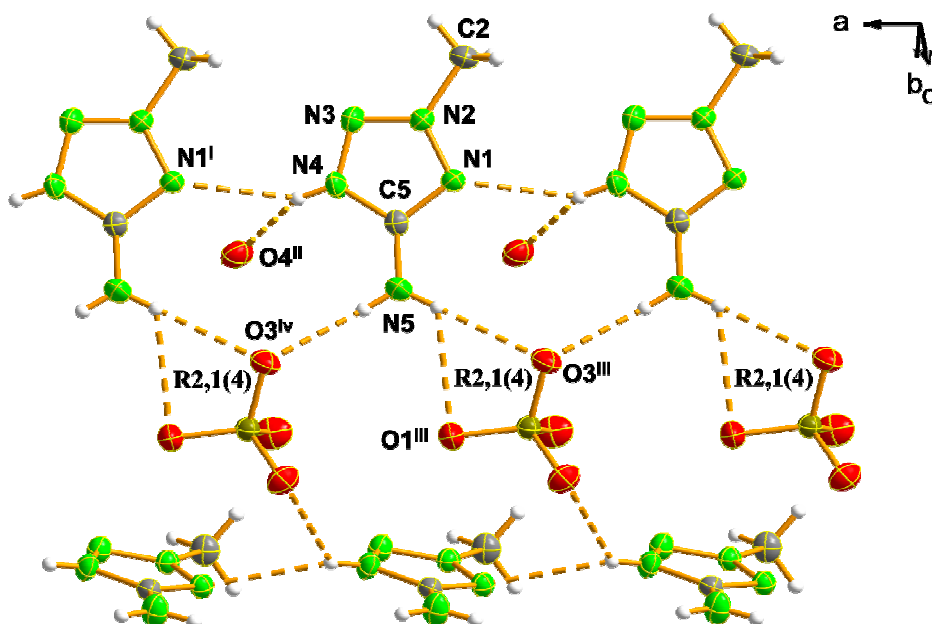


Figure 6.6 Section of the hydrogen bonding in the crystal structure of perchlorate salt **11**. Some of the perchlorate anion atoms have been omitted for simplicity purposes. Symmetry codes: (i) $-1+x, y, z$; (ii) $-x, -0.5+y, 0.5-z$; (iii) $1-x, -y, -z$; (iv) $-x, -y, -z$.

The salts of **5** show very similar number of hydrogen bonds to those found in analogous salts of **68** (see Table 6.3 and Figures 6.8–6.11). The hydrogen bond patterns formed in salts of **69** are generally quite simple due to the small number of interactions observed. For **70**, **71** and **72** similar hydrogen bonded chains of cations and anions **C1,2(4)**,^[11] **C2,2(6)** (Figure 6.8) and **C2,2(6)** (Figure 6.9), respectively, are observed. The relationship between the structures of **70** and **71** seems, on account space group and unit cell similarities, to extend beyond hydrogen bond patterns to overall packing. Both **70** and **71** crystallize in the orthorhombic space group *Pbca* forming very similar zig-zag arrangements of hydrogen bonded chains of cations and anions as shown in Figure 6.7.

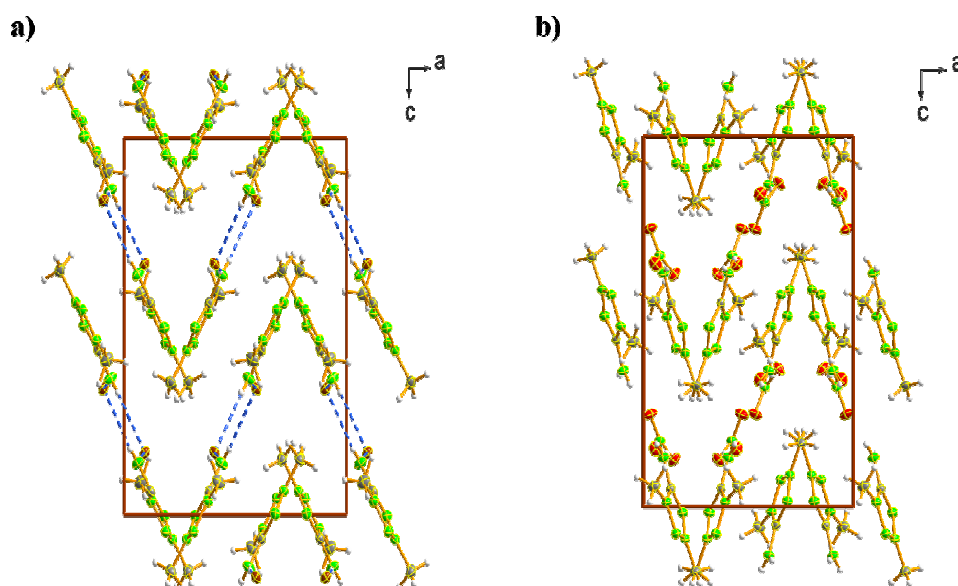


Figure 6.7 View of the unit cells of iodide salt **70** (a) and nitrate salt **71** (b) along the *b* axis showing the formation of zig-zag chains. The hydrogen bonds in the unit cell of **71** have been omitted for simplicity purposes.

In both structures the crystallographic *b* axis are quite similar (see *Appendix C*) which seems to result from the fact that the hydrogen bonded chains of cations and anions run in the *b* direction. As can be seen in Figure 6.7, the angle between neighboring chains is slightly higher in **70** ($\sim 70^\circ$) than in **71** ($\sim 50^\circ$). This difference can be explained due to the spherical iodide anions in contrast to the planar nitrate anions. This structural difference has the greatest effect on the crystallographic *a* axis and a lesser effect on the *c* axis as shown by the lattice parameters listed in *Appendix C*. In Figure 6.8a the hydrogen bonding between the cation and the nitrate anion is shown (Table 6.3). The hydrogen bonds formed by the two hydrogen atoms on N1 and the oxygen atom of the nitrate anion are similar in length ($\text{N1}\cdots\text{O3}^{\text{i}} = 2.925(1) \text{ \AA}$ and $\text{N1}\cdots\text{O1}^{\text{ii}} = 2.862(1) \text{ \AA}$; symmetry codes: (i) $x, 0.5-y, -0.5+z$; (ii) $-x, -y, -z$) and show two **D1,1(2)** dimeric interactions and the **C2,2(6)** chain motif mentioned above that includes the amino group ($-\text{NH}_2$) of the cation and an $-\text{NO}_2$ moiety of the anion. From the lateral view (Figure 6.8b) the formation of wave-like layers along the *b* axis can be seen.

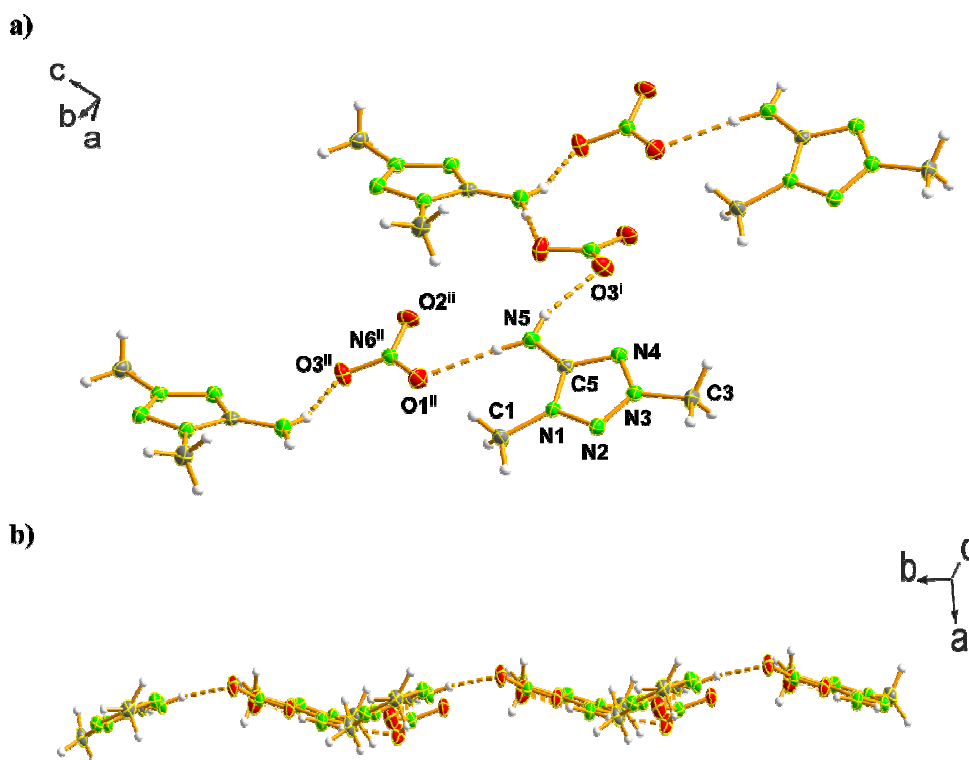


Figure 6.8 a) **C2,2(6)** chain networks in the crystal structure of nitrate salt **71** and b) lateral view of one of the waved-layers formed along the *b* axis. Symmetry codes: (i) $x, 0.5-y, -0.5+z$; (ii) $-x, -y, -z$.

The planar cation and the tetrahedral perchlorate anion in compound **72** interact forming cation-anion dimers joined by an **R4,4(12)** pattern identical to those formed in the analogous salt of **68** (Figure 6.9). This (large) ring graph-set is formed by the superposition of two smaller ring patterns with the labels **R2,1(4)** and **R4,4(8)**. In analogy to the other two salts of **69** described above, infinite zig-zag chains are formed, this time along the *c* axis. Lastly, there exist no hydrogen bonding between chains but only weak covalent interactions.

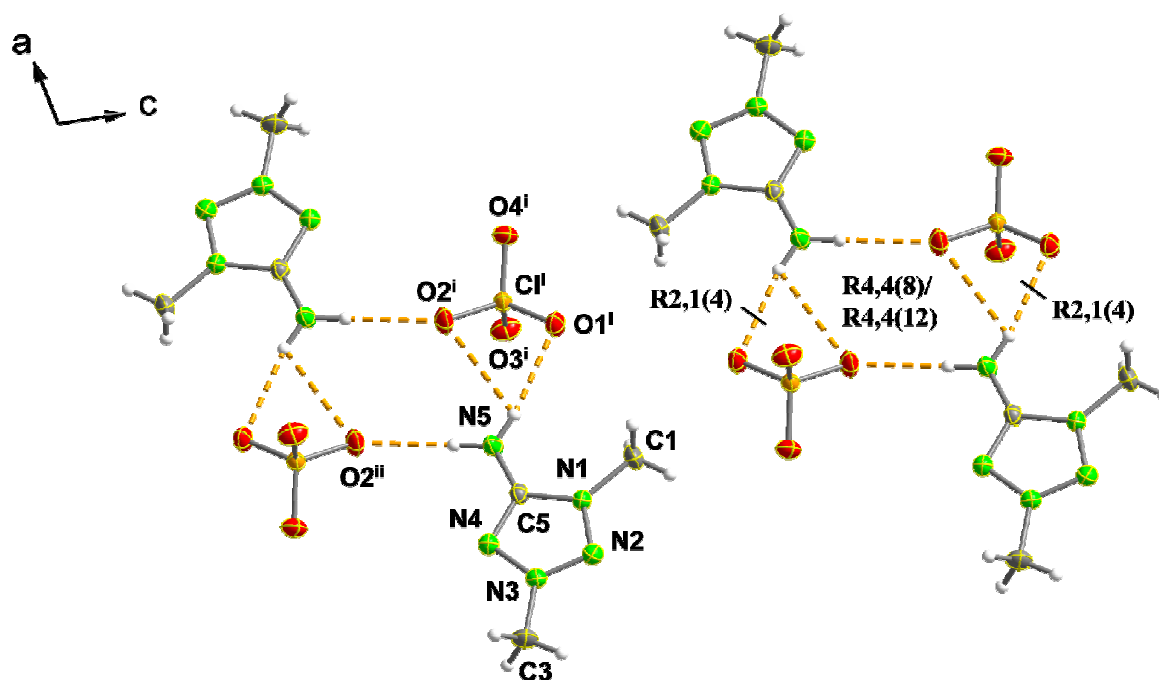


Figure 6.9 Formation of ring graph-sets in the crystal structure of perchlorate salt **72**. Symmetry codes: (i) $-1+x, y, z$; (ii) $-x, -y, 1-z$.

Compound **73** is formed by the planar 1,3-dimethyl-5-aminotetrazolium cation and a linear azide anion ($N6-N7-N8 = 179.7(2)^\circ$). **73**, with different unit cell parameters and symmetry, however does not show the strong similarities discussed above between **70** and **71**. A view along the b axis in the structure of the compound shows wave-like chains of alternating cations and anions forming layers (Figure 6.10a). Among these layers there are no hydrogen bonds. The hydrogen bonding in such a layer is depicted in Figure 6.10b. There exist two **D1,1(2)** dimeric interactions and a **C2,2(6)** chain motif, which goes from one of the protons on N5 to $N8^{ii}$. The hydrogen bond length between the atoms N5 and $N6^i$ ($N5 \cdots N6^i = 2.919(3)$ Å; symmetry code: (i) $-0.5+x, 0.5-y, -0.5+z$) is very similar to that between the atoms N5 and $N8^{ii}$ ($N5 \cdots N8^{ii} = 2.921(3)$ Å; symmetry code: (ii) $1-x, -y, -z$).

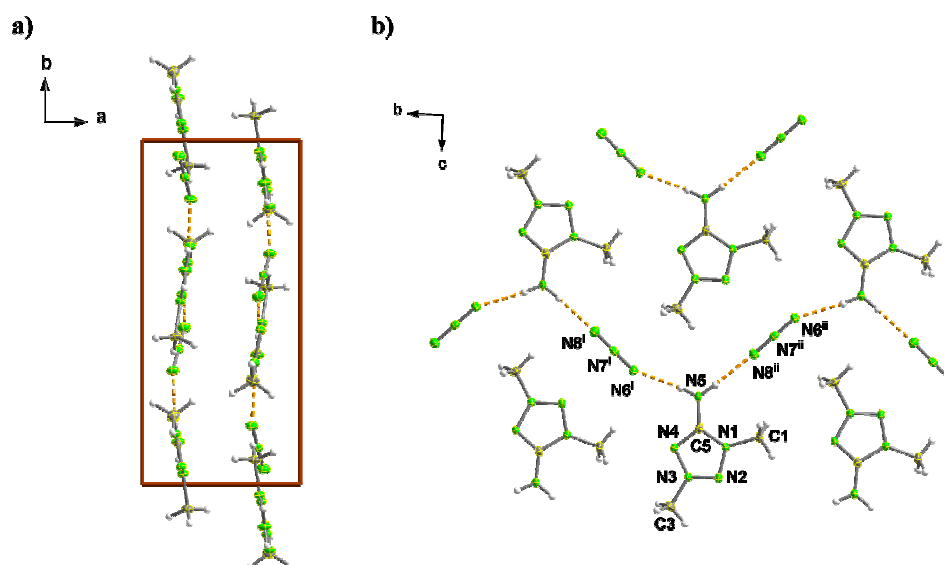


Figure 6.10 a) Waves of anions and cations in the unit cell of azide salt **73** along the b axis and b) view of the hydrogen bonding in a layer (dotted lines). Symmetry codes: (i) $-0.5+x, 0.5-y, -0.5+z$; (ii) $1-x, -y, -z$.

The anions in this study (iodide, nitrate, perchlorate, azide and dinitramide) are structurally well characterized and aside from the dinitramide anion in **74**, show no unusual structural features. From the X-ray structure of **74**, the dinitramide appears to suffer of both considerable static and dynamic disorder, conditions not previously observed in structures involving the dinitramide anion.^[8,18,27] The presence of disorder is not particularly surprising, given that the interactions between the delocalized cation and anion in **74** should not be particularly strong (as indicated by the very low melting point of **74**). Therefore, static disorder results from the lack of single energetically preferred arrangement of cations and anions and dynamic disorder from the lack of strong directional interactions between O2 and O3 of the dinitramide anion and the cation. Although a complete analysis of the hydrogen bond patterns found in **74** is difficult on account of the disordered anion, it is apparent that **74** forms the same helical hydrogen bonded chains of cations and anions as was observed in the dinitramide salt of **68** (Figure 6.11).^[8] The planar cation and the pyramidal dinitramide anion interact forming three strong hydrogen bonds with different lengths ($N5\cdots O1^i = 2.952(3)$ Å, $N5\cdots O3^i = 2.930(3)$ Å and $N5\cdots O4^{ii} = 2.908(2)$ Å; symmetry codes: (i) $1-x, 1-y, 1-z$; (ii) $x, 0.5-y, 0.5+z$). The $N5H_2$ group forms two hydrogen bonds with the oxygen atoms labelled as $O1^i$ and $O3^i$ resulting in an **R2,1(6)** ring graph-set. Furthermore, three **D1,1(2)** dimeric interactions, one **C2,2(6)** and one **C2,2(8)** chain patterns occur. The cations and anions form layers, which alternate and there exist hydrogen bonds between and within these layers.

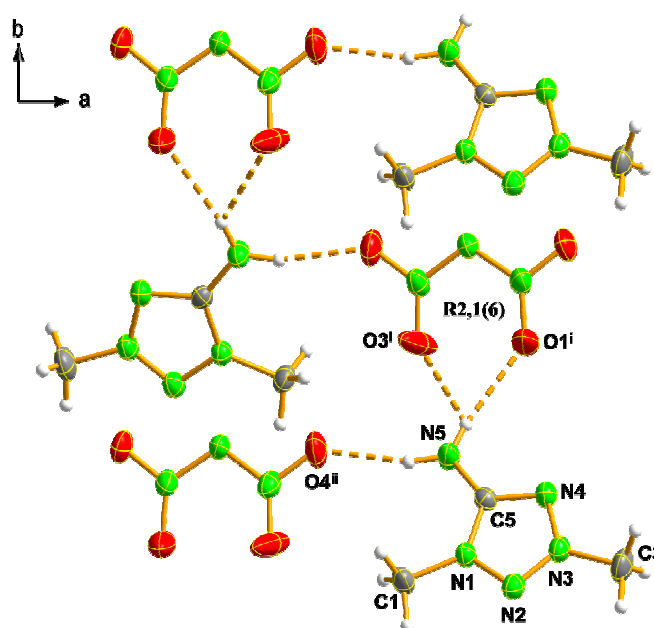


Figure 6.11 Hydrogen bonding in the crystal structure of dinitramide salt **74**. Symmetry codes: (i) $1-x$, $1-y$, $1-z$; (ii) x , $0.5-y$, $0.5+z$.

Table 6.4 Selected closed-shell interactions for compounds **11**, **71**, **72** and **74** (in Å).

11			
N3•••O4	3.098(2)	N1•••O4 ⁱ	3.196(2)
N4•••O3	3.186(2)	N2•••O2 ⁱ	3.091(2)
N1•••O1 ⁱ	3.278(2)	N4•••O1 ⁱ	3.285(2)
N1•••O2 ⁱ	3.194(2)		
71			
N1•••O3 ⁱ	3.021(1)	N4•••O3 ⁱⁱⁱ	3.230(2)
N2•••O2 ⁱⁱ	3.267(2)		
72			
N1•••O4	3.081(2)	N1•••O4 ⁱ	3.230(2)
N2•••O2	3.160(2)	N2•••O4 ⁱ	3.051(2)
N3•••O2	3.003(2)	N3•••O4 ⁱ	3.085(2)
N1•••O3 ⁱ	3.076(2)	N5•••O3 ⁱ	3.160(2)
74			
N3•••O4 ⁱ	3.209(1)	N2•••O4 ⁱⁱ	3.132(2)
N4•••O4 ⁱ	3.253(1)	N3•••O4 ⁱⁱ	3.037(2)

Symmetry codes for **11**: (i) $1-x$, $-0.5+y$, $0.5-z$; **71**: (i) $0.5-x$, $-0.5+y$, z ; (ii) $-x$, $1-y$, $1-z$; (iii) x , $-1+y$, z ; **72**: (i) $-x$, $-0.5+y$, $0.5-z$; **74**: (i) $1-x$, $1-y$, $1-z$; (ii) $1-x$, $0.5+y$, $0.5-z$.

The above observations concerning hydrogen bonding seem to suggest weaker interionic interactions in salts of **4** and **69** as opposed to those observed in salts of **2** and **68**. However, the densities of the salts of **4** and **69** are generally similar to or higher than those of salts of **3** and **68** suggesting some other form of cation-anion interaction. Further inspection of the structures indicates the presence of additional cation-anion interactions in compounds **11**, **71**, **72** and **74**.

These interactions appear to be similar in nature to the closed-shell interactions^[28] that we already identified previously between a dinitramide anion and a quaternized tetrazolium cation.^[27] Such interactions may have similar strengths to hydrogen bonds, which may explain the discrepancies between the observed cation-anion interaction strengths and densities. The close contacts (within or near the sum of the van der Waals radii) between the cations and anions found in **11**, **71**, **72** and **74** are tabulated in Table 6.4.

6.6 Energetic Properties

The thermal stability (melting and decomposition points from DSC measurements) and sensitivity to friction, impact, electrostatic discharge and thermal shock of each energetic salt studied was experimentally determined (Tables 6.5 and 6.6). The friction sensitivity tests were carried out according to STANAG 4489,^[29] which was modified with the instructions^[30] for using a BAM (Bundesanstalt für Materialforschung)^[31] drop hammer. The friction sensitivity tests were carried out according to STANAG 4487.^[32] Additionally, the constant volume energy of combustion of each material was determined experimentally using oxygen bomb calorimetry and also predicted on the basis of calculated electronic energies (see section 6.7 *Computational Methods* and Table 6.A1) and an estimation of lattice enthalpy^[33,34] (Table 6.A2) as described previously.^[35]

Table 6.5 Physico-chemical properties of the energetic salts.

	11	12	71	72	73	74
Formula	C ₂ H ₆ N ₅ O ₄ Cl	C ₂ H ₆ N ₆ O ₃	C ₃ H ₈ N ₆ O ₃	C ₃ H ₈ N ₅ O ₄ Cl	C ₃ H ₈ N ₈	C ₃ H ₈ N ₈ O ₄
Mol. Mass (g mol ⁻¹)	199.57	162.11	176.15	213.59	156.17	220.17
T _m (°C) [a]	125	123	150	132	171	58
T _d (°C) [b]	196	161	199	285	282	168
N (%) [c]	35.1	51.8	47.7	32.8	71.8	50.9
N + O (%) [d]	67.1	81.4	74.9	62.8	71.8	80.0
Ω (%) [e]	-20.0	-39.5	-63.6	-41.2	-102.5	-43.6
ρ (g cm ⁻³) [f]	1.844	1.620	1.569	1.631	1.479	1.575
ΔU _{comb.} / cal g ⁻¹ [g,h]	-2250(40) [-2346]	-2620(20) [-2587]	-3250(35) [-3271]	-2735(40) [-2937]	-4430(35) [-4377]	-2750(35) [-2848]
ΔU _f ^o / kJ kg ⁻¹ [h,i]	3765(160) [2752]	950(90) [794]	520(150) [612]	2610(170) [2518]	3670(155) [3560]	1060(150) [1474]
ΔH _f ^o / kJ kg ⁻¹ [h,i]	3670(160) [2666]	810(90) [680]	380(150) [493]	2505(170) [2425]	3480(155) [3433]	930(150) [1362]

[a] Chemical melting point and [b] decomposition point (DSC onsets) from measurement with $\beta = 5$ °C min⁻¹; [c] Nitrogen percentage; [d] Combined nitrogen and oxygen contents; [e] Oxygen balance according to ref. [36]; [f] Density from X-ray measurements; [g] Experimentally determined (oxygen bomb calorimetry) constant volume energy of combustion; [h] Uncertainty in brackets () and calculated values (from electronic energies) in [] square brackets; [i] Experimentally determined (back-calculated from ΔU_{comb.}) standard energy of formation; [j] Experimentally determined standard enthalpy of formation.

DSC measurements on samples of ~1 mg of each energetic compound in this study (**11**, **12** and **71–74**) show a wide range of melting points from 58° C (**74**) to 171° C (**73**) and decomposition points between 161° C (**12**) and 285° C (**72**) (Table 6.5). As might be expected for a lower symmetry cation, salts of **4** and **69** generally have slightly lower melting points than analogous salts of **3** and **68**.^[8] In comparison to commonly used explosives like TNT and RDX, **74** melts at a temperature lower than TNT (81 °C) and belongs to the class of compounds known as ionic liquids (m.p. <100 °C), whereas the remaining compounds have higher melting points than TNT and lower than RDX (204 °C).^[37] Compounds **11**, **12**, **71** and **74** decompose at lower temperatures than RDX (230 °C), whereas salts **72** and **73** decompose at a higher temperature than RDX slightly below the decomposition point of TNT (300 °C). In addition to DSC analysis, all compounds were tested by placing a small sample (~0.5–1.0 mg) of compound in the flame (Figure 6.12). In the case of the very sensitive perchlorate salt **11** the sample exploded. For **72–74** deflagration (rapid combustion accompanied by a hissing sound) without explosion was observed and the nitrate derivatives **12** and **71** simply burn normally. From these “flame test” observations it can be derived that the compounds in this study composed of a higher percentage of nitrogen or containing a highly oxidant anion (e.g., perchlorate or dinitramide) were more sensitive to thermal shock as might be expected.

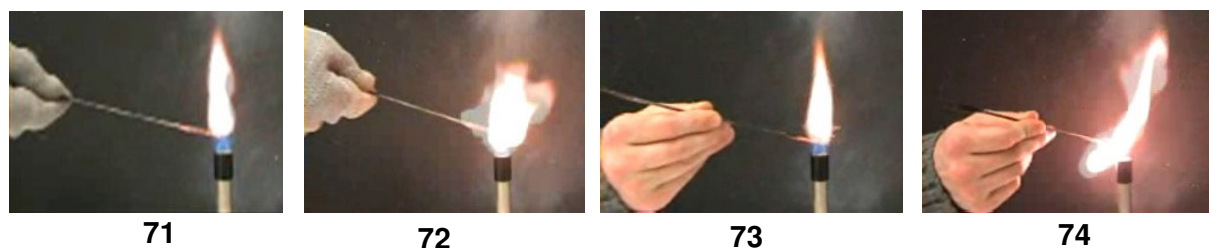


Figure 6.12 “Flame test” of 1,3-dimethyl-5-aminotetrazolium salts **71–74**.

Compounds **11**, **12** and **71–74** are highly endothermic compounds, as expected due to the large number of energetic N–N and C–N bonds,^[38] which show, however, relatively low sensitivities. Data collected for friction, impact and electrostatic discharge sensitivity testing are summarized in Table 6.6. The compounds in this study are slightly less or equally sensitive to physical and electrical stimuli as analogous salts of **3** and **68**. Within the series of salts based on **4** and **69** the trend of increasing sensitivity with decreasingly negative oxygen balance is observed as was the case for the “flame test.” Also, each compound was roughly tested for sensitivity to electrostatic discharge by spraying sparks across a small (3–5 crystals) sample of material using a tesla coil (ESD testing). Apart from the sensitive perchlorate salts **11** and **72**, all compounds failed to explode under these conditions. Once again, a comparison with the properties of TNT and RDX

is useful to assess the energetic salts in this study. The perchlorate-free compounds (**12**, **71**, **73** and **74**) are less sensitive to both friction and impact than TNT (15 J) and RDX (7.4 J),^[37] whereas the perchlorate salts **11** and **72** are quite sensitive to both friction and impact with sensitivities similar to those of primary explosives and very sensitive secondary explosives. All compounds are most likely less sensitive to electrostatic discharge than both TNT and RDX, although this was not unambiguously confirmed by quantitative testing. Lastly, all of the compounds in this study, except for the perchlorate salts **11** and **72**, are safe for transport under the UN Recommendations on the Transport of Dangerous Goods as described in ref. [39].

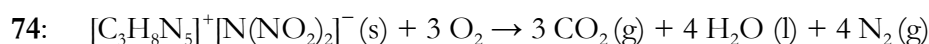
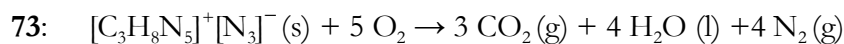
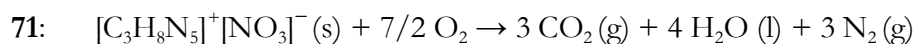
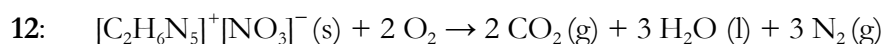
Table 6.6 Initial safety testing results and predicted energetic performance of the energetic salts using the EXPLO5 computer code.

	T_{ex} (K) ^[a]	V_0 (L kg ⁻¹) ^[b]	P_{det} (GPa) ^[c]	D (m s ⁻¹) ^[d]	Impact (J) ^[e]	Friction (N) ^[e]	ESD (+/-) ^[f]	Thermal Shock
11					1	6	+	Explodes
12	3771 [3698]	838 [837]	25.9 [25.5]	8150 [8109]	>30	>360	–	Burns
71	3234 [3277]	826 [826]	22.6 [22.7]	7850 [7864]	>30	>360	–	Burns
72					3.5	24	+	Deflagrates
73	2880 [2837]	835 [834]	23.5 [23.2]	8436 [8393]	>30	>360	–	Deflagrates
74	3769 [3997]	825 [826]	23.7 [25.3]	7869 [8097]	15	>360	–	Deflagrates
TNT	3736	620	20.5	7171	15	355	0.57 J ^[g]	Burns
RDX	4334	795	34.0	8885	7.4	120	0.15 J ^[g]	Burns

[a] Temperature of the explosion gases; [b] Volume of the explosion gases; [c] Detonation pressure; [d] Detonation velocity; [a-d] Experimental values (from bomb calorimetry) and calculated values (from electronic energies) in [] square brackets. [e] Tests according to BAM methods (see refs. [39-41]); [f] Rough sensitivity to electrostatic discharge, + sensitive, – insensitive. [g] From ref. [42].

Since the performance of new energetic materials is also of considerable interest, the EXPLO5 computer code was used to calculate the detonation velocity and pressure of the CHNO explosives in this work on the basis of the molecular formula, density (from X-ray) and energy of formation ($\Delta U^\circ_{\text{f}}$, both experimental and calculated) of each material. Therefore, the energies of formation of **11**, **12** and **71–74** were back-calculated from the constant volume energies of combustion by first converting to standard enthalpies of combustion and then on the basis of the combustion equations (see below), Hess's Law and incorporating the known standard heats formation for water and carbon dioxide^[43] and a correction for change in gas volume during combustion.^[44] No correction was applied for the non-ideal formation of nitric acid (generally ~5% of the nitrogen atoms react to form nitric acid). Due to the reasonably large uncertainty

inherent in experimental combustion measurements of energetic materials, the thermochemical data (ΔU_{comb} , $\Delta U_{\text{f}}^{\circ}$ and $\Delta H_{\text{f}}^{\circ}$) for each compound were predicted on the basis of known methods, utilizing calculated electronic energies and an approximation of lattice enthalpy,^[33,34] in order to validate the experimentally determined values. The results of the thermochemical measurements and calculations are presented in Tables 6.5 and 6.6 in square brackets.



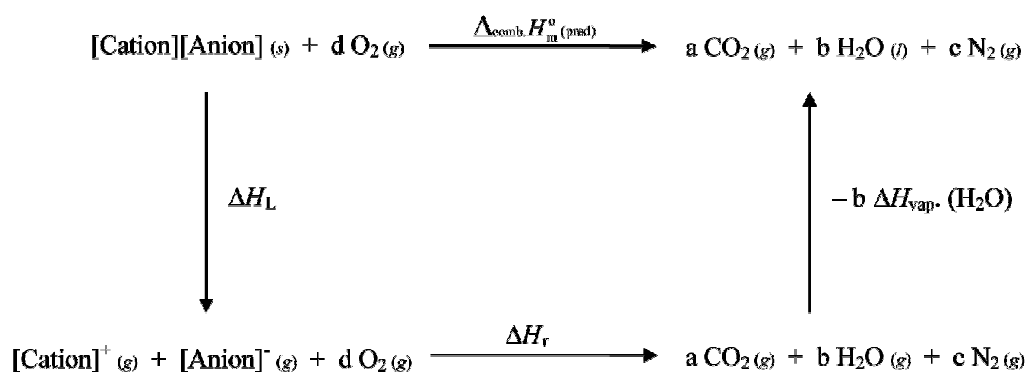
The experimentally determined thermochemical data were then used in conjunction with the EXPLO5 computer code to predict the detonation parameters of each CHNO compound in this study. The program uses the Becker-Kistiakowsky-Wilson equation of state (BKWN-EOS) for gaseous detonation products and Cowan-Fickett's equation of state for solid carbon.^[45,46] The following values for the empirical constants in the BKWN-EOS equation: $\alpha = 0.5$, $\beta = 0.176$, $\kappa = 14.71$ and $\theta = 6620$ were used for all compounds in this study. The results of the calculations are shown in Table 6.6 along with the results of EXPLO5 calculations for TNT and RDX. From these predictions made using the BKWN-EOS parameters given above and the known data for TNT and RDX, it would seem that detonation velocity and most likely pressure as well are slightly overestimated. Taking into account this systematic overestimation, the performance of all compounds assessed in this study is expected to fall between that of TNT (7171 m s⁻¹, 20.5 GPa) and that of RDX (8885 m s⁻¹, 34.0 GPa). The performance of salts of **4** and **69** seem, surprisingly, to exceed that of salts of **3** and **68**. It seems that in spite of the lower symmetry of the cation of **69**, generally slightly higher densities are observed for salts of **69** as compared to salts of **68** leading to higher predicted performances for salts of **69** due to the strong dependence of this property on the density.^[47] The experimentally determined detonation parameters are in excellent agreement with those predicted on the basis of electronic energies (see section 6.7 *Computational Methods*). The nitrogen-rich azide salt **73** has the highest performance of all materials in this

study (8436 m s^{-1} , 23.5 GPa) regardless of its relatively low density (1.479 g cm^{-3}) and it is yet insensitive to impact and friction. The nitrate salt **12** is relatively well oxygen balanced ($\Omega = -39.5\%$) comparable to that of RDX ($\Omega = -21.6\%$) and shows a reasonably high performance (8150 m s^{-1} , 25.9 GPa) greater than that of nitrogen-rich salts with the 5,5'-azotetrazolate anion ($[\text{C}_2\text{N}_{10}]^{2-}$).^[7a,48]

It is known that the performance of a material reaches its maximum value when the oxygen balance is approximately neutral. Due to the generally highly negative oxygen balance of the CHNO compounds **12**, **71**, **73** and **74**, we calculated the detonation parameters of mixtures of the compounds with an oxidizer, namely, ammonium nitrate (AN) and ammonium dinitramide (ADN) in order to further increase the performance in comparison to the stand-alone energetic materials. The results of the calculations are summarized in *Appendix A* (Tables 6.A3 and 6.A4). AN slightly increases the detonation parameters of the compounds ($\sim 8200\text{--}8300 \text{ m s}^{-1}$ and $\sim 26 \text{ GPa}$), whereas ADN is predicted to increase the performance much more notoriously ($\sim 8700\text{--}8900 \text{ m s}^{-1}$ and $\sim 31\text{--}32 \text{ GPa}$).

6.7 Computational Methods

All quantum chemical calculations were carried out with the Gaussian 03W software package.^[49] Electronic energies for all anions and the 2-methyl-5-aminotetrazolium and 1,3-dimethyl-5-aminotetrazolium cations were calculated using Møller-Plesset perturbation theory truncated at the second order (MP2)^[50] and were used unscaled. The results of the MP2 electronic energy calculations are tabulated in *Appendix A* Table 6.A1. For all atoms in all calculations, the correlation consistent polarized valence double-zeta basis set cc-pVDZ was used.^[51,52]



Scheme 6.2 Born-Haber energy cycle for calculating the heat of formation of an ionic CHNO compound.

Based on the Born-Haber cycle shown in Scheme 6.2,^[53] the heat of formation of an ionic compound can be simplified by subtracting the lattice energy of the salt (ΔH_L) from the sum of the heats of formation of cation and anion (at standard conditions) according to Eq. 1. ΔH_L (kJ mol⁻¹) can be predicted using Jenkins' equation (Eq. 2),^[33] where n_x and n_y depend on the nature of cation and anion, respectively, and have a value of 6 for nonlinear polyatomic ions. The potential energy (U_{POT} in kJ mol⁻¹) can be readily calculated from the density of the material (ρ) in g cm⁻³, the chemical formula mass (M) in g and the coefficients γ (kJ mol⁻¹ cm⁻¹) and δ (kJ mol⁻¹) that take their values from the literature^[33] according to Eq. 3.

$$\Delta H_f^\circ (\text{ionic compound, 298 K}) = \sum \Delta H_f^\circ (\text{cation, 298 K}) + \sum \Delta H_f^\circ (\text{anion, 298 K}) - \Delta H_L \quad (1)$$

$$\Delta H_L = U_{\text{POT}} + [a(n_x/2 - 2) + b(n_y/2 - 2)]RT \quad (2)$$

$$U_{\text{POT}} = \gamma(\delta/M)^{1/3} + \delta \quad (3)$$

6.8 Decomposition Gases

The ICT thermodynamic code^[54] can be used to predict the gaseous products formed upon decomposition and/or explosion of an energetic compound as well as its heat of explosion. Using the experimentally determined heats of formation (back-calculated from the heats of combustion), the density (from X-ray) and the molecular formula, the explosion products and corresponding heats of explosion were calculated for all energetic compounds in this work. The results are tabulated in Table 6.7 together with analogous calculations for commonly used high explosives.

Compounds **11**, **12** and **71–74** have (generally) high nitrogen contents varying in the range ~35–72% and thus, the major decomposition product predicted by the code is molecular nitrogen. The amounts of nitrogen gas formed add up to 545.2 g kg⁻¹ for the nitrogen-richer azide salt **73** and decrease accordingly with the lower nitrogen content for the rest of the compounds. Apart from the CHN compound **73**, which cannot be oxidized to form water, for the remainder of the compounds this is expected to be the second major decomposition product (~210–280 g kg⁻¹). As expected, the higher oxygen content of the perchlorate salts **11** and **72** anticipates relatively large amounts of carbon being oxidized to carbon dioxide. Due to the negative oxygen content of the compounds studied here (~–20 to –100%) not all the carbon atoms can be oxidized and carbon soot is expected to form in amounts larger than for RDX but lower than for TNT. On the other side, excepting compound **73**, the rest of the compounds have predicted heats of explosion higher

than that of TNT and perchlorate salts **11** and **72** are foreseen to show better values than RDX. This can be explained by the high density and high endothermicity of the compounds due to the perchlorate anion. Unfortunately, relatively large amounts of (toxic) hydrochloric acid are anticipated by the code, which might limit its use. The formation of a small cloud of hydrochloric acid was already observable in the “flame test” of compound **72** (see Figure 6.12). In any case, the formation of large amounts of environmentally benign nitrogen gas for the rest of the materials is in clear advantage in respect to classical energetic compounds and together with the properties summarized above might as well make the materials prospective candidates for future application as high explosive compounds, gas generators or components in propellants or propellant charges.^[55-58]

Table 6.7 Predicted decomposition gases and heats of explosion of methylated 5-aminotetrazole derivatives and comparison with known high explosives (using the ICT code).^[a]

Compnd.	CO ₂	H ₂ O	N ₂	CO	H ₂	NH ₃	CH ₄ / HCl ^[b]	HCN	C	$\Delta H_{\text{ex}} /$ cal g ⁻¹ ^[c]
11	167.7	213.2	345.6	16.0	0.2	6.3	182.7	0.3	67.4	2164
12	54.8	281.2	495.8	11.0	0.7	27.0	1.3	0.6	127.2	1391
71	18.4	286.7	427.7	7.6	1.5	59.6	6.1	0.8	191.3	1253
72	80.5	260.7	315.0	16.5	0.7	15.3	1.5/170.7	0.4	138.3	1876
73 ^[d]	—	—	545.2	—	3.7	208.8	42.9	1.2	198.1	1004
74	55.7	273.4	486.7	12.5	0.8	26.6	1.8	0.6	141.4	1395
TNT ^[d]	318.1	184.8	182.2	47.0	0.6	3.2	1.2	—	262.0	1350
RDX ^[d]	292.6	232.8	373.9	21.5	0.2	5.1	—	0.3	72.7	1593

[a] The amount of gases formed at 298 K is given in grams of gas per kilogram of energetic compound; [b] CH₄ for compounds **12** and **71–74** and HCl for compounds **11** and **72**; [c] Heat of explosion; [d] — = gas not predicted by the code.

6.9 Conclusions

We have synthesized a family of energetic salts based on the new 2-methyl- and 1,3-dimethyl-5-aminotetrazolium cations and nitrate, perchlorate, azide and dinitramide anions, which are analogous to our previously reported salts of **3** and **68**. The new compounds were fully characterized including determination of their solid state structure. Insight into the structure of the compounds in solution was gained by means of ¹⁵N NMR measurements, which also give insight into the high acidity of the cations of **4** and **69**. The crystal structures are discussed making use of the graph-set formalism and show, in general, weak interactions between cations and anions, as already anticipated by analysis of the vibrational spectra. Nevertheless, the compounds show, in the rule, density values, which are slightly higher than those of salts of **3** and **68** regardless of the asymmetric substitution pattern in the cation of **69**. This better efficiency in packing can be

explained by closed-shell interactions, which are similar in strength to hydrogen bonds and contribute to the unexpectedly larger detonation parameters of salts of **4** and **69** in comparison to salts of **3** and **68**, while having similar sensitivity values. The asymmetric substitution pattern of the cation of **69** results in slightly lower decomposition temperatures and a drop in the melting points. Interestingly, the dinitramide salt **74** melts at 58 °C and thus classifies as an ionic liquid with a high performance, whereas the azide salt **73** has a detonation velocity perfectly comparable to commonly used high performing high explosives such as PETN or RDX in addition to a large liquid range (>100 °C) and it has the advantage that it is neither impact nor friction sensitive. As expected from the high nitrogen content of the compounds large amounts of nitrogen are predicted by the ICT code, which makes the compounds (excepting the perchlorate salts **11** and **72**) attractive for environmentally friendly energetic materials. Lastly, the relatively high performance of the remainder of the compounds, together with excellent combined oxygen and nitrogen contents and low sensitivities make the materials and in particular compounds **73** and **74** very attractive as prospective candidates for future application.

6.10 Experimental Section

Caution: *Although we experienced no difficulties with the compounds described here, silver azide, dinitramides, aminotetrazoles and their derivatives are energetic materials and tend to explode under certain conditions. Appropriate safety precautions should be taken, especially when these compounds are prepared on a larger scale. Laboratories and personnel should be properly grounded and safety equipment such as Kevlar gloves, leather coats, face shields and ear plugs are highly recommended.*

General. All chemical reagents and solvents were obtained from Sigma-Aldrich Inc. or Acros Organics (analytical grade) and were used as supplied. Silver azide and silver bis-pyridine dinitramide ¹² were prepared according to known procedures. ¹H, ¹³C and ¹⁵N NMR spectra were recorded on a JEOL Eclipse 400 instrument in [D₆]-DMSO at or near 25 °C. The chemical shifts are given relative to tetramethylsilane (¹H and ¹³C), nitromethane (¹⁴N and ¹⁵N) or sodium chloride (³⁵Cl) as external standards and coupling constants are given in Hertz (Hz). Infrared (IR) spectra were recorded on a Perkin-Elmer Spectrum One FT-IR instrument^[59] as KBr pellets at 20 °C. Transmittance values are qualitatively described as “very strong” (vs), “strong” (s), “medium” (m) and “weak” (w). Raman spectra were recorded on a Perkin-Elmer Spectrum 2000R NIR FT-Raman instrument equipped with a Nd:YAG laser (1064 nm). The intensities are reported as percentages of the most intense peak and are given in parentheses. Elemental analyses were performed with a Netsch Simultaneous Thermal Analyzer STA 429. Melting points were determined by differential scanning calorimetry (Linseis DSC PT-10 instrument, calibrated with standard pure indium and zinc).^[60] Measurements were performed at a heating rate of 5 °C min⁻¹ in closed aluminum sample pans with a 1 µm hole in the top for gas release under a nitrogen flow of 20 mL min⁻¹ with an empty identical aluminum sample pan as a reference.

Bomb Calorimetry. For all calorimetric measurements a Parr 1356 bomb calorimeter (static jacket) equipped with a Parr 207A oxygen bomb for the combustion of highly energetic materials was used.^[61] A Parr 1755 printer, furnished with the Parr 1356 calorimeter, was used to produce a permanent record of all activities within the calorimeter. The samples (~200 mg each) were carefully mixed with ~800 mg analytical grade benzoic acid and pressed into pellets, which were subsequently burned in a 3.05 MPa atmosphere of pure oxygen. The experimentally determined heats of combustion were obtained as the averages of five single measurements with standard deviations calculated as a measure of experimental uncertainty. The calorimeter was calibrated by the combustion of certified benzoic acid in an oxygen atmosphere at a pressure of 3.05 MPa.

Synthesis of 2-methyl-5-aminotetrazole (4). Crystalline material was obtained by slow cooling of a saturated benzene-hexane solution as described previously.^[9] Crystals for X-ray structure determination were obtained by vacuum sublimation. C₂H₅N₅ (calc./found): C 24.24 / 24.19, H 5.08 / 4.82, N 70.67 / 70.60; DSC (5 °C min⁻¹, °C, onset): 102 (m.p.); m/z (EI⁺, 70 eV, >5%): 113(8), 99(8) [M⁺], 71(13), 57(7), 43(24), 42(45), 28(35), 18(100), 15(18). ¹H NMR ([D₆]-DMSO, 400.18 MHz, TMS) δ/ppm: 5.92 (s, 2H, -NH₂), 4.06 (s, 3H, N-CH₃); ¹³C{¹H} NMR ([D₆]-DMSO, 100.52 MHz, TMS) δ/ppm: 167.7 (C_{arom}), 39.4

(N-CH₃); ¹⁵N{¹H} NMR ([D₆]-DMSO, 40.51 MHz, MeNO₂) δ/ppm: -6.5 (1N, N₃), -83.3 (1N, N₄), -115.6 (1N, N₁), -115.7 (1N, N₂), -339.7 (1N, NH₂); Raman $\tilde{\nu}$ /cm⁻¹ (rel. int.): 3213(19), 3025(21), 2960(90), 1646(18), 1544(53), 1449(26), 1375(76), 1314(17), 1200(40), 1127(17), 1084(85), 1056(30), 1016(73), 805(17), 649(100), 473(48), 319(42), 159(37); IR $\tilde{\nu}$ /cm⁻¹ (KBr, rel. int.): 3385(s), 3307(s), 3217(s), 3083(w), 2959(w), 2758(w), 1635(s), 1553(s), 1448(m), 1420(w), 1409(m), 1376(m), 1314(m), 1204(s), 1124(w), 1084(w), 1054(w), 1015(m), 808(m), 757(m), 649(s), 488(m).

Synthesis of 2-methyl-5-aminotetrazolium perchlorate (11). **4** (0.25 g, 2.52 mmol) was dissolved in the minimum amount of 72% concentrated perchloric acid. The reaction mixture was layered with ether and stored in the fridge overnight yielding colorless plates of the product, which were filtered, washed with ether and let to air-dry. No further purification was necessary. Single crystals of the compound suitable for X-ray analysis were obtained by ether diffusion into a concentrated methanolic solution (0.39 g, 77%). C₂H₆N₆O₃ (calc./found): C 12.02 / 12.04, H 3.05 / 3.03, N 35.12 / 35.09; DSC (5 °C min⁻¹, °C, onset): 125 (m.p.), 196 (dec.t.); m/z (FAB⁺, xenon, 6 keV, m-NBA matrix): 100.0 [Cation]⁺; ¹H NMR ([D₆]-DMSO, 400.18 MHz, TMS) δ/ppm: 8.67 (s, 2H, NH₂), 7.51 (s, 1H, NH), 3.97 (s, 3H, CH₃); ¹³C{¹H} NMR ([D₆]-DMSO, 100.63 MHz, TMS) δ/ppm: 166.8 (1C, C-ring), 40.7 (1C, CH₃); ¹⁵N NMR ([D₆]-DMSO, 40.55 MHz, MeNO₂) δ/ppm: -8.8 (1N, q, J = 1.33 Hz, N₃), -90.0 (1N, s, N₄) -113.4 (1N, s, N₁), -114.2 (1N, s, N₂), -340.1 (1N, s, NH₂); Raman $\tilde{\nu}$ / cm⁻¹ (rel. int.): 3198(5) 3046(8) 2972(22) 1686(7) 1492(7) 1442(22) 1411(13) 1385(19) 1182(9) 1091(21) 1024(27) 926(100) 803(14) 651(25) 637(21) 623(16) 479(19) 468(20) 453(22) 321(19) 224(9); IR $\tilde{\nu}$ / cm⁻¹ (KBr, rel. int.): 3287(s) 3254(s) 3183(s) 3097(s) 3025(m) 2756(m) 2480(w) 2351(w) 2319(w) 2139(w) 2030(w) 1661(vs) 1586(m) 1575(w) 1442(w) 1408(w) 1391(w) 1333(w) 1180(m) 1145(s) 1109(vs) 1089(vs) 1018(m) 940(w) 923(w) 803(w) 732(w) 696(m) 672(w) 647(m) 637(m) 626(s) 481(w).

Synthesis of 2-methyl-5-aminotetrazolium nitrate (12). 0.100 g (1.0 mmol) of solid crystalline **4** were dissolved in a minimum of concentrated (65 %) nitric acid. The clear, colorless reaction mixture was stirred until all **4** had dissolved. The solution was then cooled to 4 °C overnight resulting in the formation of clear colorless crystals suitable for X-ray analysis, which were filtered off cold and washed until dry and acid free with diethyl ether. No further purification was necessary (0.073 g, 73%). C₂H₆N₆O₃ (calc./found): C 14.81 / 14.70, H 3.73 / 3.68, N 51.84 / 51.26; DSC (5 °C min⁻¹, °C, onset): 123.2 (m.p.), 161.4 (dec.t.); m/z (FAB⁺, xenon, 6 keV, m-NBA matrix): 100.0 [2MAT]⁺; ¹H NMR ([D₆]-DMSO, 400.18 MHz, TMS) δ/ppm: 8.50 (s, 3H, NH + NH₂), 4.01 (s, 3H, CH₃); ¹³C{¹H} NMR ([D₆]-DMSO, 100.63 MHz, TMS) δ/ppm: 167.2 (1C, C-ring), 38.9 (1C, CH₃); ¹⁴N{¹H} NMR ([D₆]-DMSO, 40.55 MHz, MeNO₂) δ/ppm: -14 (1N, NO₃⁻), -111 (2N, N₁/N₂); ¹⁵N NMR ([D₆]-DMSO, 40.55 MHz, MeNO₂) δ/ppm: -6.9 (1N, q, J = 1.30 Hz, N₃), -15.1 (1N, s, NO₃⁻), -84.4 (1N, s, N₄) -114.4 (1N, s, N₁), -114.9 (1N, s, N₂), -339.5 (1N, s, NH₂); Raman $\tilde{\nu}$ /cm⁻¹ (rel. int.): 3192(3), 3049(11), 3039(9), 2968(30), 1663(9), 1437(21), 1383(27), 1297(5), 1189(11), 1086(18), 1043(100), 1010(18), 789(15), 728(11), 713(9), 649(33), 480(14), 321(23), 212(9), 141(22); IR $\tilde{\nu}$ /cm⁻¹ (KBr, rel. int.): 3383(m), 3249(m), 3184(m), 3049(w),

2925(w), 2853(w), 2637(w), 2426(w), 1677(s), 1430(m), 1384(s), 1308(m), 1187(w), 1073(m), 1041(m), 1010(m), 953(w), 823(m), 787(m), 726(m), 647(m), 575(m), 478(w).

Synthesis of 1,3-Dimethyl-5-aminotetrazolium Iodide (70). To a solution of **4** (9.04 g, 91.26 mmol) in acetonitrile (60 ml) methyl iodide (25.92 g, 182.62 mmol) was added and the reaction mixture was heated at 80 °C for about 24 hours under a nitrogen atmosphere. After cooling (1 day), the product that precipitated was filtered and washed with ether until white. Further precipitation was yielded by adding more ether (100 ml) to the filtrate. The brown solid that separated was treated like and combined with the first crop. This procedure can be repeated several times yielding pure product (19.58 g, 89%). $C_3H_8N_5I$ (calc./found): C 14.95 / 14.99, H 3.35 / 3.26, N 29.06 / 29.04, I 52.65 / 50.18; DSC (5 °C min⁻¹, °C, onset): 180.6 (m.p.), ~220 (dec.t.); m/z (FAB⁺, xenon, 6 keV, m-NBA matrix): 114.2 [Cation]⁺; ¹H NMR ([D₆]-DMSO, 400.18 MHz, TMS) δ/ppm: 8.25 (s, 2H, NH₂), 4.34 (s, 3H, C₃H₃), 3.91 (s, 3H, C₂H₃); ¹³C{¹H} NMR ([D₆]-DMSO, 100.52 MHz, TMS) δ/ppm: 157.81 (1C, C1-NH₂), 39.70 (1C, C₃H₃), 34.09 (1C, C₂H₃); ¹⁵N NMR ([D₆]-DMSO, 40.51 MHz, MeNO₂) δ/ppm: -31.87 (q, 1N, ²J = 2.32 Hz, N₄), -108.99 (q, 1N, ³J = 2.31 Hz, N₃), -111.35 (q, 1N, ²J = 2.75 Hz, N₂), -180.62 (q, 1N, ³J = 1.87 Hz, N₅), -324.42 (t, 1N, ¹J = 90.09 Hz, NH₂); Raman $\tilde{\nu}$ /cm⁻¹ (rel. int.): 3256(11), 3171(12), 3111(32), 3023(55), 2995(59), 2942(100), 2869(8), 2813(11), 2776(5), 2758(4), 2633(3), 2513(2), 1648(22), 1580(27), 1526(10), 1496(18), 1466(25), 1438(44), 1412(60), 1394(38), 1366(15), 1319(8), 1287(11), 1252(37), 1118(14), 1078(21), 1066(21), 1016(14), 894(3), 851(75), 728(6), 675(28), 662(9), 632(73), 587(7), 530(24), 489(10), 445(6), 325(69), 290(17), 231(22), 192(11); IR $\tilde{\nu}$ /cm⁻¹ (KBr, rel. int.): 3261(s), 3166(s), 3104(vs), 3021(m), 2994(m), 2939(m), 2695(w), 2636(w), 2495(w), 2427(w), 2174(w), 2105(w), 1972(w), 1905(w), 1864(w), 1659(vs), 1581(s), 1464(m), 1435(m), 1414(m), 1363(m), 1287(m), 1251(m), 1118(m), 1081(m), 1054(m), 1015(m), 850(m), 783(w), 720(m), 674(m), 627(w), 585(w), 494(m).

Synthesis of 1,3-Dimethyl-5-aminotetrazolium Nitrate (71). A solution of silver nitrate (0.60 g, 3.53 mmol) in methanol (5 ml) was added under stirring to a solution of **70** (0.85 g, 3.53 mmol) in methanol (10 ml). Under exclusion of light the solution was stirred at room temperature for 50 min. and then filtered. After evaporating the solvent the slightly brown residue was dissolved in the minimum amount of methanol and crystallised overnight in an ether chamber. The colourless precipitate was then filtered under vacuum and dried on air (0.52 g, 79%). $C_3H_8N_6O_3$ (calc./found): C 20.46 / 20.38, H 4.58 / 4.48, N 47.71 / 47.66; DSC (5 °C min⁻¹, °C, onset): 150.1 (m.p.), 198.5 (dec.t.); m/z (FAB⁺, xenon, 6 keV, m-NBA matrix): 114.2 [Cation]⁺; ¹H NMR ([D₆]-DMSO, 399.78 MHz, TMS) δ/ppm: 8.27 (s, 2H, NH₂), 4.30 (s, 3H, C₃H₃), 3.87 (s, 3H, C₂H₃); ¹³C{¹H} NMR ([D₆]-DMSO, 100.52 MHz, TMS) δ/ppm: 158.60 (1C, C1-NH₂), 43.04 (1C, C₃H₃), 34.64 (1C, C₂H₃); ¹⁴N NMR ([D₆]-DMSO, 28.88 MHz, MeNO₂) δ/ppm: 3.82 (1N, NO₃⁻); ¹⁵N NMR ([D₆]-DMSO, 40.51 MHz, MeNO₂) δ/ppm: -4.54 (s, 1N, NO₃), -32.63 (q, 1N, ²J = 2.32 Hz, N₄), -109.61 (q, 1N, ³J = 1.86 Hz, N₃), -111.08 (q, 1N, ²J = 2.79 Hz, N₂), -181.18 (m, 1N, N₅), -326.05 (s, 1N, ¹J = 89.5 Hz, NH₂); Raman $\tilde{\nu}$ /cm⁻¹ (rel. int.): 3028(7), 2994(5), 2965(29), 1660(5), 1593(5), 1444(10), 1415(18), 1294(5), 1257(12), 1126(5), 1077(13), 1049(100), 1014(7), 852(17), 714(11), 678(9), 632(19), 534(5), 363(4), 328(15), 300(6), 236(7), 207(6), 105(1), 85(1); IR $\tilde{\nu}$ /cm⁻¹

(KBr, rel. int.): 3307(w), 3217(m), 3045(m), 2767(w), 2703(w), 2657(w), 2499(w), 2426(w), 2395(w), 2184(w), 2122(w), 1659(s), 1593(m), 1384(vs), 1289(w), 1250(m), 1116(m), 1081(w), 1014(w), 851(w), 825(w), 725(w), 674(w), 627(w), 569(w), 365(w), 332(w).

Synthesis of 1,3-Dimethyl-5-aminotetrazolium Perchlorate (72). To a solution of **70** (2.37 g, 9.83 mmol) in methanol (20 ml) a solution of silver perchlorate (2.04 g, 9.84 mmol) in methanol (20 ml) was added and stirred under light exclusion for 1 hour. The precipitated silver iodide was then filtered and washed with methanol. After removing the solvent, the colourless residue was dissolved in a small amount of methanol and recrystallised overnight in an ether chamber. After filtering the colourless solid, this was dried on air (1.63 g, 78%). $C_3H_8N_5O_4Cl$ (calc./found): C 16.89 / 16.91, H 3.78 / 3.86, N 32.86 / 32.72, Cl 16.41 / 17.73; DSC (5 °C min⁻¹, °C, onset): 132.3 (m.p.), 285.1 (dec.t.); m/z (FAB⁺, xenon, 6 keV, m-NBA matrix): 114.2 [Cation]⁺; ¹H NMR ([D6]-DMSO, 499.78 MHz, TMS) δ/ppm: 8.23 (s, 2H, NH₂), 4.30 (s, 3H, C3H₃), 3.87 (s, 3H, C2H₃); ¹³C{¹H} NMR ([D6]-DMSO, 100.52 MHz, TMS) δ/ppm: 158.09 (1C, C1–NH₂), 42.54 (1C, C3H₃), 34.18 (1C, C2H₃); ³⁵Cl NMR ([D6]-DMSO, 39.21 MHz, NaCl) δ/ppm: 1.01 (ClO₄); ¹⁵N{¹H} NMR ([D6]-DMSO, 40.55 MHz, MeNO₂) δ/ppm: –31.43 (1N, N4), –108.71 (1N, N3), –110.76 (1N, N2), –180.26 (1N, N5), –327.01 (1N, NH₂); ¹⁵N NMR ([D6]-DMSO, 40.51 MHz, MeNO₂) δ/ppm: –32.04 (q, 1N, ²J = 2.79 Hz, N4), –109.32 (q, 1N, ³J = 1.86, N3), –111.30 (q, 1N, ²J = 2.79 Hz, N2), –180.84 (q, 1N, ³J = 1.86 Hz, N5), –327.18 (t, 1N, ¹J = 89.51 Hz, NH₂); Raman $\tilde{\nu}$ /cm⁻¹ (rel. int.): 3427(1), 3238(2), 3053(10), 3025(11), 2966(46), 2818(2), 1666(9), 1595(4), 1500(6), 1442(13), 1416(29), 1396(9), 1294(5), 1261(15), 1118(8), 1076(12), 1015(6), 936(100), 854(21), 820(2), 680(11), 634(33), 529(4), 464(22), 318(21), 290(8), 238(10), 194(4), 84(1); IR $\tilde{\nu}$ /cm⁻¹ (KBr, rel. int.): 3434(m), 3308(m), 3220(m), 3217(m), 3047(s), 2946(m), 2840(w), 2767(w), 2704(w), 2657(w), 2501(w), 2439(vw), 2184(w), 2122(w), 2024(w), 1923(w), 1864(w), 1666(vs), 1593(s), 1566(w), 1497(w), 1468(m), 1430(m), 1384(w), 1363(m), 1290(m), 1251(m), 1144(s), 1120(s), 1088(s), 1013(m), 940(w), 852(m), 726(w), 674(w), 626(m), 568(w).

Synthesis of 1,3-Dimethyl-5-aminotetrazolium Azide (73). To a suspension of freshly prepared silver azide (1.50 g, 10.01 mmol) in methanol (50 ml) **70** (2.13 g, 8.85 mmol) was added. The reaction mixture was stirred under exclusion of light at room temperature for ~1.5 hours and then filtered. After the solvent was evaporated the colourless solid was dried under high vacuum (1.11 g, 81%). $C_3H_8N_8$ (calc./found): C 23.06 / 23.04, H 5.16 / 4.94, N 71.77 / 71.47; DSC (5 °C min⁻¹, °C, onset): 170.8 (m.p.), ~282 (dec.t.); m.p. 171.3 °C–172.7 °C (Büchi, uncorrected); m/z (FAB⁺, xenon, 6 keV, m-NBA matrix): 114.1 [Cation]⁺; ¹H NMR ([D6]-DMSO, 399.78 MHz, TMS) δ/ppm: 8.47 (s, 2H, NH₂), 4.30 (s, 3H, C3H₃), 3.88 (s, 3H, C2H₃); ¹³C{¹H} NMR ([D6]-DMSO, 100.52 MHz, TMS) δ/ppm: 158.15 (1C, C1–NH₂), 42.49 (1C, C3H₃), 34.13 (1C, C2H₃); ¹⁴N NMR ([D6]-DMSO, 28.88 MHz, MeNO₂) δ/ppm: –133 (1N, N–N–N, N₃⁻), –277 (2N, N–N–N, N₃⁻); ¹⁵N NMR ([D6]-DMSO, 40.51 MHz, MeNO₂) δ/ppm: –33.14 (q, 1N, ²J = 2.60 Hz, N4), –113.22 (q, 1N, ³J = 2.53, N3), –113.40 (q, 1N, ²J = 2.91 Hz, N2), –135.15 (1N, N–N–N, N₃⁻), –188.99 (q, 1N, ³J = 1.97 Hz, N5), –285 (2N, N–N–N, N₃⁻), –327.57 (t, 1N, ¹J = 86.25 Hz, NH₂); Raman $\tilde{\nu}$ /cm⁻¹ (rel. int.): 3038(9), 2957(36), 2809(2), 1664(10), 1609(4), 1500(5),

1436(10), 1412(7), 1388(9), 1341(62), 1301(5), 1266(12), 1135(5), 1076(16), 1019(4), 858(26), 814(2), 727(2), 681(7), 639(33), 624(5), 599(2), 544(12), 439(2), 341(13), 293(12), 236(8), 158(8), 123(2); IR $\tilde{\nu}$ /cm⁻¹ (KBr, rel. int.): 3359(m), 3334(m), 3253(m), 3067(s), 2926(m), 2790(m), 2731(m), 2519(w), 2461(w), 2206(vw), 2054(vs), 2042(vs), 1669(s), 1604(s), 1536(w), 1495(w), 1460(w), 1446(w), 1385(m), 1370(m), 1317(vw), 1297(w), 1264(m), 1131(m), 1089(m), 1075(m), 1018(w), 856(m), 727(m), 680(m), 645(w), 636(w), 622(w), 571(m), 543(m).

Synthesis of 1,3-Dimethyl-5-aminotetrazolium Dinitramide (74). *Method 1:* To a suspension of silver-bis-pyridine dinitramide (1.60 g, 4.30 mmol) in methanol (15 ml) **70** (1.04 g, 4.33 mmol) was added. Under exclusion of light the suspension was stirred at room temperature for 2 hours and then filtered. After removing the solvent under vacuum the colourless crude solid was dissolved in a small amount of methanol and crystallised overnight in an ether chamber. Since no precipitation was observed the sample was left to evaporate and an oily green-yellow liquor formed. Crystallisation was induced by scratching with a glass stirrer on the sides of the glass vessel. The colourless solid was then scratched out, filtered and washed with ethyl ether (0.70 g, 73.37%).

Method 2: In the first synthesis step the nitrate salt (**6**) was generated by addition of **8** (5.08 g, 21.08 mmol) to a solution of silver nitrate (3.54 g, 20.87 mmol) in methanol (80 ml) followed by stirring at room temperature for about 2 hours. After filtration, the solvent was evaporated and the colourless residue was dissolved in a minimum amount of methanol and diethyl ether was allowed to diffuse into the methanol solution overnight yielding clear colourless quadrangular crystals, which were identified as 1,3-dimethyl-5-aminotetrazolium nitrate by measuring the melting point (150.8 °C–152.9 °C). In the second step **9** (0.96 g, 5.45 mmol) was dissolved in ethanol (40 ml) and potassium dinitramide (0.79 g, 5.46 mmol) was added. The reaction mixture was heated at 80 °C for 4 hours and then filtered hot. After evaporating the solvent the yellow oily residue was dried under high vacuum yielding an oil. Crystallisation was induced by scratching with a glass stirrer on the sides of the flask yielding a slightly yellow product (1.12 g, 93%). C₃H₈N₈O₄ (calc./found): C 16.37 / 16.20, H 3.66 / 3.70, N 50.90 / 50.83; DSC (5 °C min⁻¹, °C, onset): 57.9 (m.p.), 168.4 (dec.t.); m/z (FAB⁺, xenon, 6 keV, m-NBA matrix): 114.1 [Cation]⁺, (FAB⁻, xenon, 6 keV, m-NBA matrix): 106.0 [Anion]⁻; ¹H NMR ([D₆]-DMSO, 399.78 MHz, TMS) δ /ppm: 8.21 (s, 2H, NH₂), 4.24 (s, 3H, N4–C3H₃), 3.86 (s, 3H, N2–C2H₃); ¹³C{¹H} NMR ([D₆]-DMSO, 100.52 MHz, TMS) δ /ppm: 158.58 (1C, C1–NH₂), 42.93 (1C, C3H₃), 34.57 (1C, C2H₃); ¹⁴N NMR ([D₆]-DMSO, 28.88 MHz, MeNO₂) δ /ppm: –10 (2N, NO₂) ¹⁵N{¹H} NMR ([D₆]-DMSO, 40.51 MHz, MeNO₂) δ /ppm: –11.28 (2N, NO₂), –32.24 (1N, N4), –57.24 (1N, N(NO₂)₂), –109.38 (1N, N3), –111.12 (1N, N2), –181.02 (1N, N5), –326.81 (1N, NH₂); ¹⁵N NMR ([D₆]-DMSO, 40.51 MHz, MeNO₂) δ /ppm: –11.29 (s, 2N, NO₂), –32.29 (1N, N4), –57.22 (1N, N(NO₂)₂), –109.43 (q, 1N, ³J = 1.86 Hz, N3), –111.18 (q, 1N, ²J = 2.79 Hz, N2), –181.06 (1N, N5), –326.79 (s, 1N, NH₂); Raman $\tilde{\nu}$ /cm⁻¹ (rel. int.): 3238(5), 3169(5), 3144(5), 3053(11), 3032(12), 2964(28), 2829(5), 2676(5), 2563(7), 2510(8), 2467(8), 2434(8), 2336(8), 2294(8), 2283(8), 2245(8), 2204(9), 2184(8), 2156(9), 2135(9), 2060(9), 1870(14), 1820(15), 1700(15), 1670(22), 1602(16), 1561(16), 1519(25), 1496(25), 1457(28), 1439(31), 1421(27), 1394(25), 1324(100), 1254(22), 1176(16),

1115(13), 1082(20), 1052(19), 1019(14), 964(13), 946(14), 856(29), 825(28), 761(7), 706(5), 680(11), 632(37), 531(5), 480(26), 418(5), 388(4), 325(16), 300(16), 246(10), 203(7); IR $\tilde{\nu}$ / cm^{-1} (KBr, rel. int.): 3399(m), 3345(m), 3301(m), 3239(m), 3182(m), 1668(s), 1600(w), 1515(s), 1430(m), 1384(m), 1324(w), 1295(w), 1253(w), 1186(vs), 1117(w), 1082(w), 1011(m), 854(m), 824(w), 760(m), 726(m), 676(w), 629(w), 564(w), 478(w).

6.11 References

- [1] U. Bemm, H. Ostmark, *Acta Crystallogr.* **1998**, *C54*, 1997–1999.
- [2] H. H. Cady, A. C. Larson, *Acta Crystallogr.* **1965**, *18*, 485–496.
- [3] a) C. Ye, J. Xiao, B. Twamley, J. M. Shreeve, *Chem. Comm.* **2005**, *21*, 2750–2752. b) R. P. Singh, R. D. Verma, D. T. Meshri, J. M. Shreeve, *Angew. Chem. Int. Ed.* **2006**, *45*, 3584–3601, references therein.
- [4] a) Y. Huang, H. Gao, B. Twamley, J. M. Shreeve, *Eur. J. Inorg. Chem.* **2007**, *14*, 2025–2030. b) H. Xue, H. Gao, B. Twamley, J. M. Shreeve, *Eur. J. Inorg. Chem.* **2006**, *15*, 2959–2965. c) H. Xue, Y. Gao, B. Twamley, J. M. Shreeve, *Chem. Mater.* **2005**, *17*(1), 191–198. d) H. Xue, B. Twamley, J. M. Shreeve, *J. Mater. Chem.* **2005**, *15*(34), 3459–3465.
- [5] a) Y. Gao, C. Ye, B. Twamley, J. M. Shreeve, *Chem. Eur. J.* **2006**, *12*, 9010–9018. b) H. Gao, R. Wang, B. Twamley, M. A. Hiskey, J. M. Shreeve, *Chem. Commun.* **2006**, 4007–4009. c) R. Wang, H. Gao, C. Ye, J. M. Shreeve, *Chem. Mater.* **2007**, *19*(2), 144–152. d) R. Wang, H. Gao, C. Ye, B. Twamley, J. M. Shreeve, *Inorg. Chem.* **2007**, *46*, 932–938. e) H. Gao, C. Ye, O. D. Gupta, J.-C. Xiao, M. A. Hiskey, B. Twamley, J. M. Shreeve, *Chem. Eur. J.* **2007**, *13*, 3853–3860. f) Y. Guo, H. Gao, B. Twamley, J. M. Shreeve, *Adv. Mater.* **2007**, *19*, 2884–2888.
- [6] a) Z. Zeng, H. Gao, B. Twamley, J. M. Shreeve, *J. Mater. Chem.* **2007**, *17*, 3819–3826. b) C. Ye, H. Gao, J. M. Shreeve, *J. Fluor. Chem.* **2007**, *128*, 1410–1415. c) C. Ye, G. L. Gard, R. W. Winter, R. G. Syvret, B. Twamley, J. M. Shreeve, *Org. Lett.* **2007**, *19*(9), 3841–3844. d) C. Ye, H. Gao, B. Twamley, J. M. Shreeve, *N. J. Chem.* **2007**, *32*, 317–322. e) H. Gao, Z. Zeng, B. Twamley, J. M. Shreeve, *Chem. Eur. J.* **2008**, *14*, 1282–1290. f) H. Gao, Y. Huang, B. Twamley, C. Ye, J. M. Shreeve, *Chem. Sus. Chem.* **2008**, *2*, 222–227. g) H. Gao, Y. Huang, C. Ye, B. Twamley, J. M. Shreeve, *Chem. Eur. J.* **2008**, *14*, 5596–5603. h) Y. Huang, H. Gao, B. Twamley, J. M. Shreeve, *Eur. J. Inorg. Chem.* **2008**, 2560–2568. i) Y.-H. Joo, B. Twamley, S. Garg, J. M. Shreeve, *Angew. Chem. Int. Ed.* **2008**, ASAP.
- [7] a) A. Hammerl, M. A. Hiskey, G. Holl, T. M. Klapötke, K. Polborn, J. Stierstorfer, J. J. Weigand, *Chem. Mater.* **2005**, *17*(14), 3784–3793. b) J. Geith, T. M. Klapötke, J. J. Weigand, G. Holl, *Propellants, Explos., Pyrotech.* **2004**, *29*(1), 3–8. c) M. von Denffer, T. M. Klapötke, G. Kramer, G. Spiess, J. M. Welch, G. Heeb, *Propellants, Explos., Pyrotech.* **2005**, *30*(3), 191–195.
- [8] K. Karaghiosoff, T. M. Klapötke, P. Mayer, C. Miró Sabaté, A. Penger, J. M. Welch, *Inorg. Chem.* **2008**, *47*, 1007–1019.
- [9] R. A. Henry, W. G. Finnegan, E. Lieber, *J. Am. Chem. Soc.* **1954**, *76*, 2894–2898.
- [10] J. C. Gálvez-Ruiz, G. Holl, K. Karaghiosoff, T. M. Klapötke, K. Löhnwitz, P. Mayer, H. Nöth, K. Polborn, C. J. Rohbogner, M. Suter, J. J. Weigand, *Inorg. Chem.* **2005**, *44*, 4237–4253.
- [11] T. M. Klapötke, C. Miró Sabaté, M. Rusan, *Z. Anorg. Allg. Chem.* **2008**, *634*(4), 688–695.
- [12] A. Bigotto, R. Klingendrath, *Spectrochim. Acta* **1990**, *46A*(12), 1683–1692.

- [13] a) K. Williamson, P. Li, J. P. Devlin, *J. Chem. Phys.* **1968**, *48*(9), 3891–3896. b) J. R. Fernandes, S. Ganguly, C. N. R. Rao, *Spectrochim. Acta* **1979**, *35A*, 1013–1019.
- [14] a) H. Cohn, *J. Chem. Soc.* **1952**, 4282–4284. b) P. Redlich, J. Holt, T. Biegeleisen, *J. Am. Chem. Soc.* **1944**, *55*, 13–16. c) H. Grothe, H. Willner, *Angew. Chem. Int. Ed. Engl.* **1996**, *108*(7), 816–818.
- [15] U. Müller, *Struct. Bond.* **1974**, *14*(1), 141–145.
- [16] K. O. Christe, W. W. Wilson, M. A. Petrie, H. H. Michels, J. C. Bottaro, R. Gilardi, *Inorg. Chem.* **1996**, *35*(17), 5068–5071.
- [17] N. B. Colthup, L. H. Daly, S. E. Wiberley, *Introduction to Infrared, Raman Spectroscopy*; Academic Press: Boston, 1990.
- [18] C. Darwich, T. M. Klapötke, C. Miró Sabaté, *Chem. Eur. J.* **2008**, *14*, 5756–5771.
- [19] a) C. Darwich, K. Karaghiosoff, T. M. Klapötke, C. Miró Sabaté, *Z. Anorg. Allg. Chem.* **2008**, *634*, 61–68. b) A. Garrone, R. Fruttero, C. Tironi, A. Gasco, *J. Chem. Soc., Perkin Trans. 2* **1989**, *12*, 1941–1945.
- [20] Oxford Diffraction. ABSPACK, CrysAlis CCD, CrysAlis RED. Versions 1.171. Oxford Diffraction Ltd, Abingdon, Oxfordshire, England, 2006.
- [21] *SIR-92, A Program for Crystal Structure Solution*: A. Altomare, G. Cascarano, C. Giacovazzo, A. Guagliardi, *J. Appl. Crystallogr.* **1993**, *26*, 343.
- [22] G. M. Sheldrick, *SHELXL-97, Program for the Refinement of Crystal Structures*, University of Göttingen, Germany, **1997**.
- [23] *WinGX Suite for Small Molecule Single-Crystal Crystallography*: L. J. Farrugia, *J. Appl. Crystallogr.* **1999**, *32*, 837–838.
- [24] A. L. Spek, *PLATON, A Multipurpose Crystallographic Tool*, Utrecht University, Utrecht, The Netherlands, **1999**.
- [25] J. H. Bryden, *Acta Crystallogr.* **1956**, *9*, 874–878.
- [26] N–N values, N=N values from: *International Tables for X-ray Crystallography*, Kluwer Academic Publishers, Dordrecht, The Netherlands, **1992**, vol. C.
- [27] T. M. Klapötke, P. Mayer, A. Schulz, J. J. Weigand, *J. Am. Chem. Soc.* **2005**, *127*, 2032–2033.
- [28] A. H. Pakiari, K. Eskandari, *THEOCHEM* **2007**, *806*(1–3), 1–7.
- [29] *NATO Standardization Agreement (STANAG) on Explosives, Impact Sensitivity Tests*, No. 4489, 1st ed., Sept. 17, **1999**.
- [30] *WIWEB-Standardarbeitsanweisung 4–5.1.02, Ermittlung der Explosionsgefährlichkeit, hier der Schlagempfindlichkeit mit dem Fallhammer*, Nov. 8, **2002**.
- [31] <http://www.bam.de>.

- [32] NATO Standardization Agreement (STANAG) on Explosives, Friction Sensitivity Tests, No. 4487, 1st ed., Aug. 22, **2002**.
- [33] H. D. B. Jenkins, D. Tudela, L. Glasser, *Inorg. Chem.* **2002**, *41*, 2364–2367.
- [34] H. D. B. Jenkins, H. K. Roobottom, J. Passmore, L. Glasser, *Inorg. Chem.* **1999**, *38*, 3609–3620.
- [35] H. Gao, C. Ye, C. M. Piekarski, J. M. Shreeve, *J. Phys. Chem.* **2007**, *C111*, 10718–10731.
- [36] Calculation of the oxygen balance: $\Omega(\%) = (\text{O} - 2\text{C} - \text{H}/2 - x\text{AO}) 1600/\text{M}$; M = molecular mass.
- [37] J. Koehler, R. Meyer, *Explosivstoffe*, 9th ed.; Wiley-VCH, Weinheim, **1998**.
- [38] M. A. Hiskey, D. E. Chavez, D. L. Naud, S. F. Son, H. L. Berghout, C. A. Bolme, *Proc. Int. Pyrotech. Semin.* **2000**, *27*, 3–14.
- [39] Tests methods according to the UN Recommendation on the Transport of Dangerous Goods, Manual of Tests, Criteria, 4th rev. ed.; United Nations Publications: New York, **2003**.
- [40] T. M. Klapötke, C. M. Rienäcker, *Propellants, Explos., Pyrotech.* **2001**, *26(1)*, 43–47.
- [41] <http://www.reichel-partner.de>.
- [42] a) S. Zeman, V. Pelikán, J. Majzlík, *C. Eur. J. Energ. Mater.* **2006**, *3(3)*, 45–51. b) D. Skinner, D. Olson, A. Block-Bolten, *Propellants Explos. Pyrotech.* **1997**, *23*, 34–42.
- [43] <http://webbook.nist.gov>.
- [44] T. M. Klapötke, P. Mayer, C. Miró Sabaté, J. M. Welch, N. Wiegand, *Inorg. Chem.* **2008**, *47(13)*, 6014–6027.
- [45] a) *Calculation of Detonation Parameters by EXPLO5 Computer Program*, M. Sucasca, *Mater. Science Forum* **2004**, *465–466*, 325–330; b) M. Sucasca, *Propellants Explos. Pyrotech.* **1991**, *16*, 197–202; c) M. Sucasca, *Propellants Explos. Pyrotech.* **1999**, *24*, 280–285.
- [46] M. L. Hobbs, M. R. Baer, *Calibration of the BKW-EOS with a Large Product Species Data Base, Measured CJ Properties*, Proceedings of the 10th International Symposium on Detonation, ONR 33395–12, Boston, MA, July 12–16, **1993**, p. 409.
- [47] J. Akhavan, *The Chemistry of Explosives*, 2nd ed. RSC Paperbacks: Cambridge, UK, **2004**.
- [48] T. M. Klapötke, C. Miró Sabaté, *Chem. Mater.* **2008**, *20(5)*, 1750–1763.
- [49] Gaussian G03W: Gaussian 03, Revision A.1: M. J. Frisch, G. W. Trucks, H. B. Schlegel, G. E. Scuseria, M. A. Robb, J. R. Cheeseman, J. A. Montgomery, T. Jr Vreven, K. N. Kudin, J. C. Burant, J. M. Millam, S. S. Iyengar, J. Tomasi, V. Barone, B. Mennucci, M. Cossi, G. Scalmani, N. Rega, G. A. Petersson, H. Nakatsuji, M. Hada, M. Ehara, K. Toyota, R. Fukuda, J. Hasegawa, M. Ishida, T. Nakajima, Y. Honda, O. Kitao, H. Nakai, M. Klene, X. Li, J. E. Knox, H. P. Hratchian, J. B. Cross, C. Adamo, J. Jaramillo, R. Gomperts, R. E. Stratmann, O. Yazyev, A. J. Austin, R. Cammi, C. Pomelli, J. W. Ochterski, P. Y. Ayala, K. Morokuma, G. A. Voth, P. Salvador, J. J. Dannenberg, V. G. Zakrzewski, S. Dapprich, A.

D. Daniels, M. C. Strain, O. Farkas, D. K. Malick, A. D. Rabuck, K. Raghavachari, J. B. Foresman, J. V. Ortiz, Q. Cui, A. G. Baboul, S. Clifford, J. Cioslowski, B. B. Stefanov, G. Liu, A. Liashenko, P. Piskorz, I. Komaromi, R. L. Martin, D. J. Fox, T. Keith, M. A. Al-Laham, C. Y. Peng, A. Nanayakkara, M. Challacombe, P. M. W. Gill, B. Johnson, W. Chen, M. W. Wong, C. Gonzalez, J. A. Pople, Gaussian, Inc. Pittsburgh PA, **2003**.

[50] J. A. Pople, R. Seeger, R. Krishnan, *Int. J. Quantum Chem., Symp.* **1977**, *11*, 149–163.

[51] A. K. Rick, T. H. Dunning, J. H. Robert, *J. Chem. Phys.* **1992**, *96*, 6796–6806.

[52] A. P. Kirk, E. W. David, T. H. Dunning, *J. Chem. Phys.* **1994**, *100*, 7410–7415.

[53] H. Xue, H. Gao, B. Twamley, J. M. Shreeve, *Chem. Mater.* **2007**, *19*, 1731–1739.

[54] a) ICT-Thermodynamic Code, v. 1.0, Fraunhofer-Institut für Chemische Technologie (ICT): Pfinztal, Germany, 1988–2000. b) R. Webb, M. van Rooijen, *Proceedings of the 29th International Pyrotechnics Seminar*, 2002, 823–828. c) H. Bathelt, F. Volk, *27th International Annual Conference of ICT*, 1996, *92*, 1–16.

[55] Y. N. Matyushin, T. S. Kon'kova, A. B. Vorob'ev, Y. A. Lebedev, *36th International Annual Conference of ICT* **2005**, *92/* 1–92/9.

[56] a) T. M. Klapötke, J. Stierstorfer, *Chem. Sus. Chem.* **2008**, submitted; b) T. M. Klapötke, J. Stierstorfer, *New Trends in Research of Energetic Materials*, Proceedings of the 11th Seminar, Pardubice, Czech Republic, **2008**, *2*, 810–831.

[57] N. Wingborg, N. V. Latypov, *Propellants Explos. Pyrotech.* **2003**, *28*, 314–318.

[58] H. R. Blomquist, US 6004410, **1999**.

[59] <http://www.perkinelmer.com>.

[60] http://www.linseis.net/html_en/thermal/dsc/dsc_pt10.php.

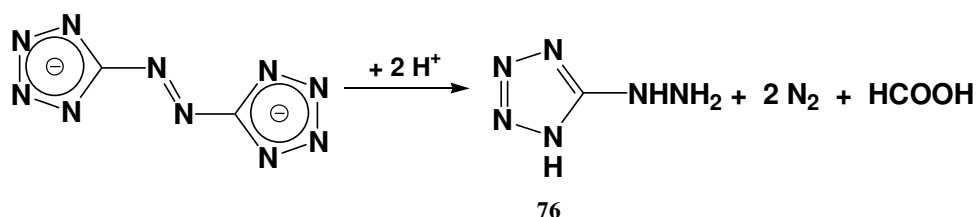
[61] <http://www.parrinst.com>.

CHAPTER VII

5,5'-AZOTETRAZOLE DERIVATIVES

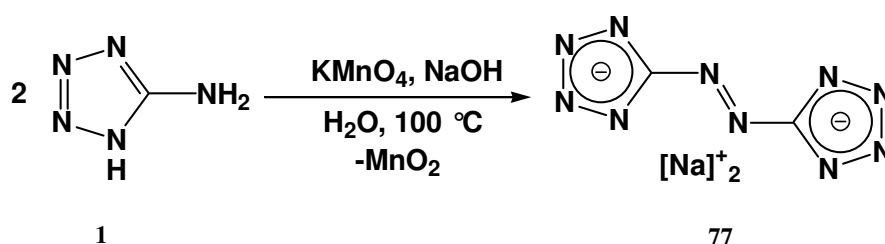
7.1 Introduction

5,5'-Azotetrazole (**H₂ZT**, **75**) is an azo compound with an extremely high nitrogen content (84.3%), making it of interest for the synthesis of highly energetic materials if it were more chemically stable. The compound was described by Thiele^[1] more than a century ago to readily decompose at room temperature evolving nitrogen to yield 5-hydrazino-1*H*-tetrazole (**5-HyTz**, **76**) and formic acid (Scheme 7.1). The instability of the compound was confirmed in our group and 5,5'-azotetrazole was shown to be stable only at temperatures below -30 °C in methanol solution as a methanol adduct in the solid state, as shown by crystal structure determination.^[2]



Scheme 7.1 Decomposition of 5,5'-azotetrazolate salts in acid media.

Due to its high nitrogen content, high heat of formation and readily availability there has been increasing recent interest in the synthesis of energetic salts based on the 5,5'-azotetrazolate anion. The cations of choice thus far have been those of easily-protonated nitrogen bases such as ammonium,^[3] hydrazinium,^[4] guanidinium, aminoguanidinium, diaminoguanidinium or triaminoguanidinium^[5] giving rise to compounds with high nitrogen contents. The most readily available 5,5'-azotetrazolate anion source is the sodium salt (**NaZT**, **77**),^[1d] which can be synthesized by oxidizing 5-amino-1*H*-tetrazole (**5-At**, **1**) with potassium permanganate in sodium hydroxide solution (Scheme 7.2) and is the starting material for a wide family of metal salts (M= Li, K, Rb, Cs, Mg, Ca, Sr, Ba, Al, Y, La, Ce, Nd and Gd).^[2]



Scheme 7.2 Oxidation of **5-At** (**1**) to **NaZT** (**77**) in basic solution.

Many 5,5′-azotetrazolate salts have found practical application: several salts with nitrogen bases (e.g. guanidinium, aminoguanidinium, triaminoguanidinium and hydrazinium) have been used in gas generators for airbags as well as in fire extinguishing systems,^[3,4] heavy metal salts of 5,5′-azotetrazolate (e.g., $[\text{Pb}(\text{OH})]^+$) have been used as initiators,^[6] other 5,5′-azotetrazoles have been used as additives in solid rocket propellants,^[7] etc.

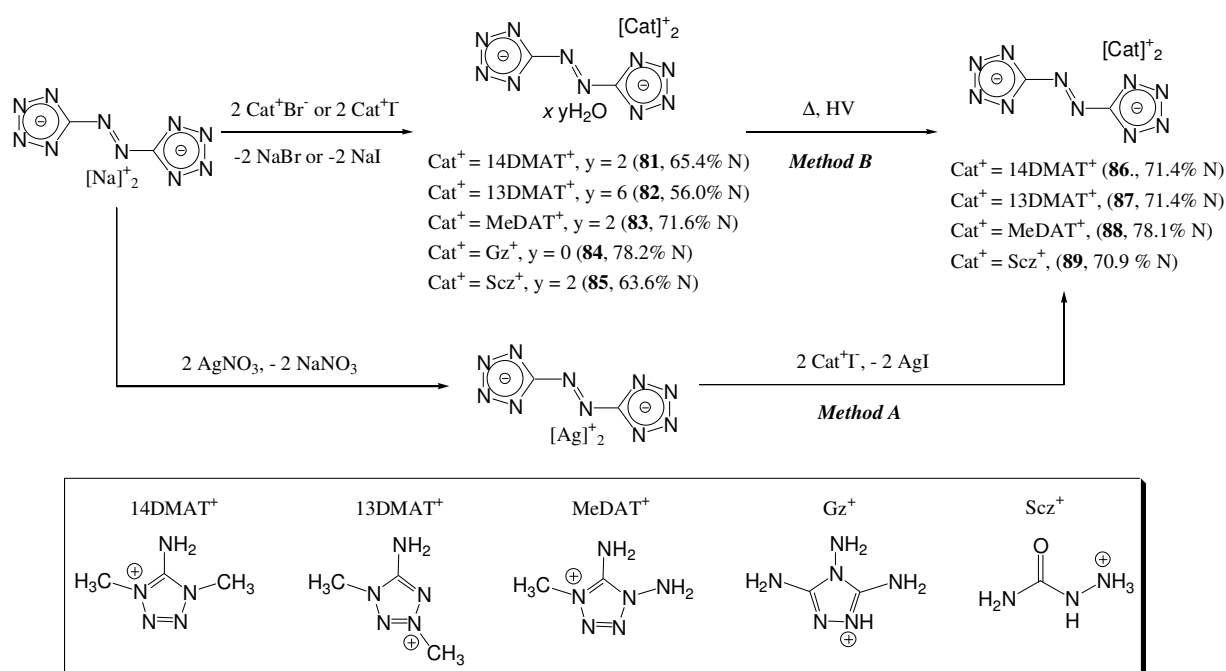
Excluding this work, there are only three tetrazolium 5,5′-azotetrazolates described in the literature so far. 1,4,5-trimethyltetrazolium 5,5′-azotetrazolate (**TMeATZT**, **78**) synthesized by Shreeve et al.^[8] has a high positive heat of formation of $+1547 \text{ kJ kg}^{-1}$. The nitrogen-rich 5-amino-1*H*-tetrazolium (**5-AtZT**, **79**) and 1,5-diaminotetrazolium (**DATZT**, **80**) 5,5′-azotetrazolate were also claimed to have been synthesized by Tremblay and coworkers^[9] by metathesis of potassium 5,5′-azotetrazolate with the corresponding tetrazolium chloride in water. However, repetition of these syntheses by the literature procedure failed and gas evolution followed by decoloration of the yellow solution was observed.

Due to the high endothermicity of 5,5′-azotetrazole derivatives, we synthesized compounds containing the 5,5′-azotetrazolate anion with azolium-based cations, which have high nitrogen contents and highly positive energies of formation. In addition, the semicarbazidium salt (with and without crystal water) was also synthesized due to the obvious similarities in the chemical structure of the cation with that in the “widely used” aminoguanidinium salt (see above). Lastly, we suggest an improved synthesis for two neutral 5,5′-azotetrazole derivatives, which should make the production of the compounds suitable for up-scaling to multigram quantities.

7.2.1 Synthesis of 5,5′-Azotetrazolate Salts

As it is usual for 5,5′-azotetrazolate salts when the synthesis is carried out in aqueous solution, the compounds incorporate crystal water in the structure.^[1,4] The 1,4-dimethyl-5-aminotetrazolium (**14DMATZTh**, **81**), 1,3-dimethyl-5-aminotetrazolium (**13DMATZTh**, **82**), 1,5-diamino-4-methyltetrazolium (**MeDATZTh**, **83**) and semicarbazidium (**SczZTh**, **85**) 5,5′-azotetrazolate salts could be obtained by recrystallization from water of equimolar amounts of sodium 5,5′-azotetrazolate pentahydrate and a suitable halogenide salt either as the dihydrated or as the hexahydrated species (Scheme 7.3). On cooling, **81** and **82** precipitated as a yellow solid (Figure 7.1), whereas **83** and **85** formed as orange and dark orange/brown crystals, all of them in yields $>70\%$. The 3,4,5-triamino-1,2,4-triazolium (guanazinium) salt (**GzZT**, **84**) was prepared in an analogous way by using either the bromide or iodide salts. The compound formed immediately as a (in hot water) highly insoluble yellow powder and unexpectedly, regardless of

the great possibility to form hydrogen-bonding due to the presence of the three amino groups, did not incorporate crystal water. The anhydrous compounds **1,4DMATZT** (**86**), **1,3DMATZT** (**87**), **MeDATZT** (**88**), and **SczZT** (**89**) were synthesized in moderate yield by a metathesis reaction between highly sensitive silver 5,5'-azotetrazolate (**AgZT**, **90**), generated from **77** and silver nitrate, and the corresponding halogenide salt in dry methanol. Alternatively, the crystal water in the hydrated compounds could be completely removed by heating to temperatures around 80 °C (40 °C for **85**, due to the ease of decomposition) for several days under high vacuum, yielding the anhydrous species in quantitative isolated yields and providing a much more efficient and safer method for their syntheses on a larger scale.

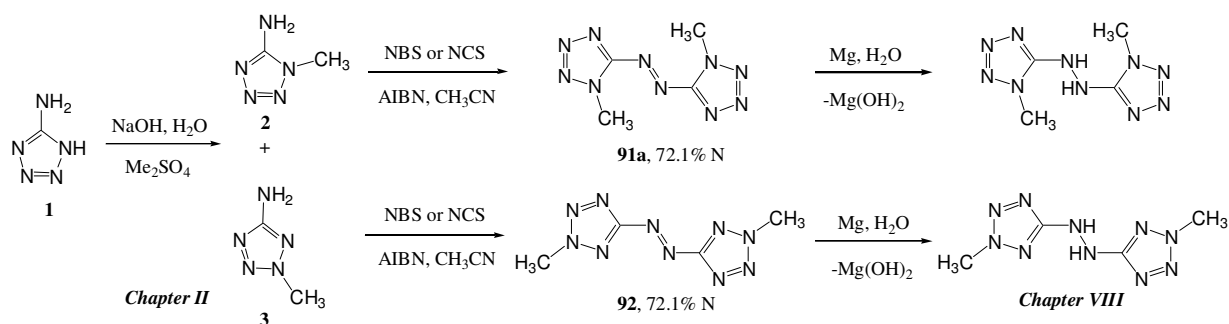


Scheme 7.3 Synthesis of the nitrogen-rich 5,5'-azotetrazolate salts.

Apart from **84**, which is highly insoluble in most classical solvents and only dissolves in DMSO or DMF, the rest of the compounds are insoluble in acetone and apolar solvents and moderately soluble in water or alcohol. Lastly, all compounds are stable solids at room conditions and apart from **85** and **89**, which decompose in a variety of polar solvents (e.g., H₂O, DMSO, DMF...), also stable in their solutions.

7.2.2 Synthesis of Neutral 5,5′-Azotetrazoles

Although 1,1′-dimethyl- (1,1DMZT, **91a**) and 2,2′-dimethyl-5,5′-azotetrazole (2,2DMZT, **92**) had been reported in the literature before our studies,^[10] the former had not been fully characterized and the energetic characterization of both materials is unreported. In addition, reduction of the azo-bridge in azotetrazolate salts using magnesium is known to proceed readily,^[11] however, the energetically interesting hydrazine derivatives of **91a** and **92** (Scheme 7.4) are not described in the literature. Therefore, we were interested in i) completing the characterization of **91a**, ii) study the energetic properties of both compounds and iii) use the energetic azo-bridged compounds **91a** and **92** as starting materials or intermediates for the synthesis of other energetic (hydrazino-bridged) neutral azoles, namely, 1,1′-dimethyl- (1,1DMHBT) and 2,2′-dimethyl-5,5′-hydrazinobistetrazole (2,2DMHBT, see Chapter VIII).

Scheme 7.4 Synthesis of **91a** and **92**.

91a was synthesized by a modified literature procedure using NBS^[10] and a catalytic amount of AIBN in acetonitrile (Scheme 7.4). Alternatively, NCS can be used as a cheaper oxidizer without significant loss in the yield of the reaction. The use of AIBN is imperative otherwise the reaction does not go to completion. Other oxidizers such as NaOCl, Br₂ or Cl₂ can also be used but they are not recommended because they require much longer reaction times. The synthesis using NCS or NBS could be extrapolated for the preparation of the isomer **92**, which supposes a clear advantage for up-scaling in comparison to the known procedure, which reacts highly sensitive silver 5,5′-azotetrazolate with methyl iodide,^[2a] at the same time that increases the yield from 34 to 61%.



Figure 7.1 Pictures of 5,5'-azotetrazole derivatives: **14DMATZTh** (**81**), **1,1DMZT** (**91a**) and **2,2DMZT** (**92**).

Lastly, **91a** forms as an orange crystalline solid whereas **92** is obtained as yellow crystals (Figure 7.1) and both compounds show similar solubility properties: they are little soluble in water at RT, insoluble in ether and readily soluble in acetonitrile, alcohol, hot water, acetone, ethylacetate, DMSO, DMF, chloroform and dichloromethane.

7.3 Vibrational and NMR Spectroscopy

Intense signals in the Raman spectra of salts **81–89** corresponding to the symmetric C–N_{azo} stretching ($\sim 1380\text{ cm}^{-1}$) and the stretching mode of the azo group ($\sim 1480\text{ cm}^{-1}$) obscure the bands corresponding to the cation as shown in Figure 7.2a for some of the compounds in this study. These bands are closer in the Raman spectra of the neutral compounds **91a** and **92** ($\sim 1400\text{ cm}^{-1}$ and $\sim 1460\text{ cm}^{-1}$). The Raman spectra of salts **81–89** have (with the exception of that of **84**) nearly identical shapes, and only slight differences in vibrational energies are observed (see Experimental Section). The CH₃ stretches for the 5,5'-azotetrazolate salts are, as mentioned above, obscured by the peaks corresponding to the anion, however, in the neutral compounds **91a** and **92** they constitute some of the most intense signals. The formation of the azolium 5,5'-azotetrazolate compounds is easily confirmed by comparing the Raman spectra of the reaction products with those of the starting materials. The two bands centered at ~ 1060 and $\sim 1090\text{ cm}^{-1}$ for **81–89** are shifted in respect to the sodium salt (1068 and 1099 cm^{-1}) and have exchanged their relative intensities. The IR spectra of all compounds show the characteristic bands of the 5,5'-azotetrazole moiety for the asymmetric C–N₃ ($\sim 1400\text{ cm}^{-1}$) and the asymmetric C–N₂ ($\sim 730\text{ cm}^{-1}$) stretching modes. However, the most intense peak in the IR spectra can be assigned to the stretching mode in the cation (compounds **81–89**) between the tetrazole carbon and the exocyclic imino nitrogen atoms ($\sim 1715\text{ cm}^{-1}$ [$\nu(\text{C}=\text{N})$]). The IR and Raman spectra also contain other sets of bands of lower intensity that can be assigned to the cations: $3400\text{--}3100\text{ cm}^{-1}$ [$\nu(\text{N-H})$], $3000\text{--}2850\text{ cm}^{-1}$ [$\nu(\text{C-H})$], $1680\text{--}1550$ [$\delta(\text{NH}_2)$, $\delta(\text{NH}_2)$], $1550\text{--}1350\text{ cm}^{-1}$ [$\nu(\text{tetrazole ring})$, $\delta_{\text{as}}(\text{CH}_3)$],

$\sim 1380\text{ cm}^{-1}$ [$\delta(\text{CH}_3)$], $1350\text{--}700\text{ cm}^{-1}$ [$\nu(\text{N--C--N})$, $\nu(\text{N--N})$, $\nu(\text{CN})$, $\delta(\text{tetrazole ring})$], $<700\text{ cm}^{-1}$ [δ out-of-plane bend (N--H), $\omega(\text{NH}_2)$].^[12–14]

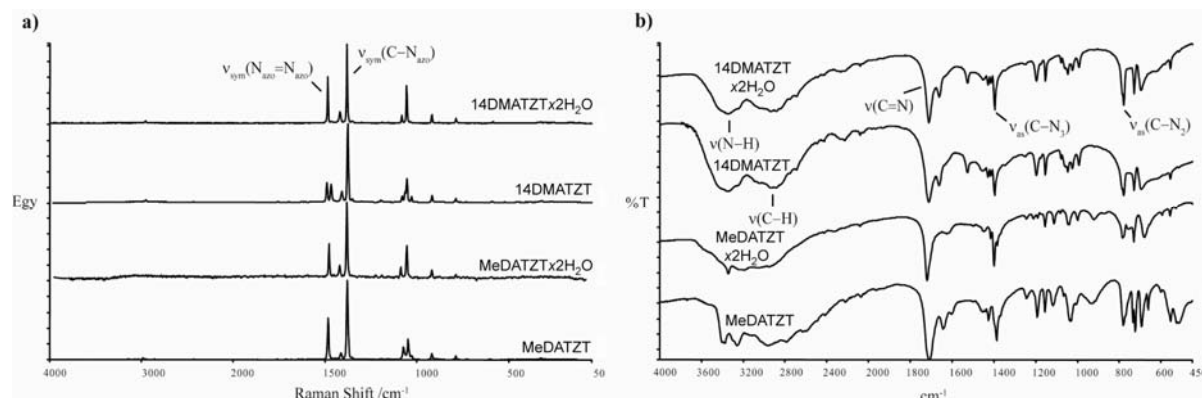


Figure 7.2 a) Raman and b) IR spectra of selected 5,5'-azotetrazolate salts.

The IR spectra (Figure 7.2b) also provide insight into the cation structure (**81–89**) and hydrogen-bonding.^[15] The free base of **81** and **86** (1,4-dimethyl-5-imino-1*H*-tetrazole) shows one only sharp band at 3314 cm^{-1} ^[16a] corresponding to the N11–H stretching, which upon formation of the 5,5'-azotetrazolate salts **81** and **86** splits in two sets of broad bands centred at ~ 3345 and $\sim 3210\text{ cm}^{-1}$, indicative of the formation of NH_2 group extensive hydrogen-bonding as confirmed by the crystal structures. The most intense peak in the IR spectrum of 1,4-dimethyl-5-imino-1*H*-tetrazole corresponds to the C3=N11H stretching vibration (1649 cm^{-1}), which is shifted to significantly higher energies in **81** (1713 cm^{-1}) and **86** (1714 cm^{-1}), indicating variations in the C3=N11 distances between $1,4\text{DMAT}^+$ and 1,4-dimethyl-5-imino-1*H*-tetrazole and proving again the existence of strong hydrogen-bonding. In analogy to **81** and **86**, the IR spectrum of the free base of **83** and **88** (1-amino-4-methyl-5-imino-1*H*-tetrazole) shows a sharp band at 3281 cm^{-1} ^[16b] which is split into two centered at ~ 3360 and $\sim 3225\text{ cm}^{-1}$. The C3=N11H stretching of the free base 1-amino-4-methyl-5-imino-1*H*-tetrazole (1670 cm^{-1}) is once again shifted to higher energies in **83** (1721 cm^{-1}) and **88** (1709 cm^{-1}). A similar observation can be made for the 1,3-dimethyl-5-aminotetrazolium salts **82** and **87**, the semicarbazidium salts **85** and **89**, as well as for the guanazinium salt (**84**), however, the changes observed when comparing the IR spectra of the latter compound with that of neutral guanazine are much more notorious and reflected in the high density value for the compound (see X-ray structure discussion for **84**).

In the ^1H NMR in $\text{DMSO-}d_6$ the signals corresponding to the methyl groups (**81–83** and **86–88**) are found just below 4.0 ppm apart from the C_3H_3 group in **82** and **87**, which resonates at ~ 4.4 ppm. There seems to be fast exchange in the NMR solvent so that the crystal water is seen as one only broad signal together with the amino group resonances. The 1-amino and 5-amino groups in the case of the MeDAT^{++} derivatives (**83** and **88**) also suffer from fast exchange and are

shifted to higher field in comparison to the 5-amino group in the DMAT⁺ salts (~7.0 vs. ~8.5 ppm) and to lower field in comparison to the Gz⁺ salt (6.5 and 5.5 ppm). In the ¹³C NMR, the shifts are very similar to the starting materials. Resonances for the two 5,5'-azotetrazolate carbon atoms are found at ~173 ppm and the azole sp²-hybridized carbon atoms resonate at ~148 ppm (**81**, **83**, **86** and **88**), ~150 ppm (**84**) and ~158 ppm (**82**, **85**, **87** and **89**). For the methalyted compounds, the methyl groups appear at lower field in the case of the diaminated salts **83** and **88** (~34.5 ppm) in comparison to the dimethylated species **81** and **86** (~32.0 ppm), whereas for the asymmetrically substituted compounds **82** and **87** one of the methyl carbon atoms is very deshielded and resonates at ~42.5 ppm and the other appears at markedly higher field (~34.2 ppm).

The quadrupolar broadening found in the ¹⁴N NMR does not allow the differentiation of any signal from the base line and all compounds were not soluble enough in any solvent to record a ¹⁵N NMR (natural abundance). Figure 7.3 shows the ¹⁵N NMR spectrum of compound **81** in the solid state. The resonances for the cation are sharp and split due to differences in the interactions in the crystal structure (see Crystal Structures section). They are centered at -317.1 (-NH₂), -180.0 (N-CH₃) and -28.8 (-N=N-) ppm in agreement with the ¹⁵N NMR in DMSO-*d*₆ solution of other compounds containing the same cation,^[13] whereas the lack of protons on the 5,5'-azotetrazolate anion make the corresponding signals rather broad and low in intensity. Alike the cation, the anion in **81** also shows three resonances corresponding to the azo bridge nitrogen (+89.5 ppm), the ring α-nitrogen (+0.4 ppm) and the ring β-nitrogen (-71.2 ppm) atoms.^[2] The solid state ¹⁵N NMR spectrum of **83** shows even broader signals corresponding to the 5,5'-azotetrazolate anion resonances and just the cation shifts can be easily identified. They occur at -317.0 (C-NH₂), -308.9 (N-NH₂), -180.8 (N-CH₃), -170.7 (N-NH₂), -58.7 (N13) and -47.2 (N14) ppm keeping in with other MeDAT⁺ salts.^[12] For the 1,3-dimethyl-5-aminotetrazolium salts all efforts to measure an spectrum both in solution and in the solid state resulted in vain due to the low solubility of the compound (NMR in solution) and to the structure of the cation (solid state), respectively.

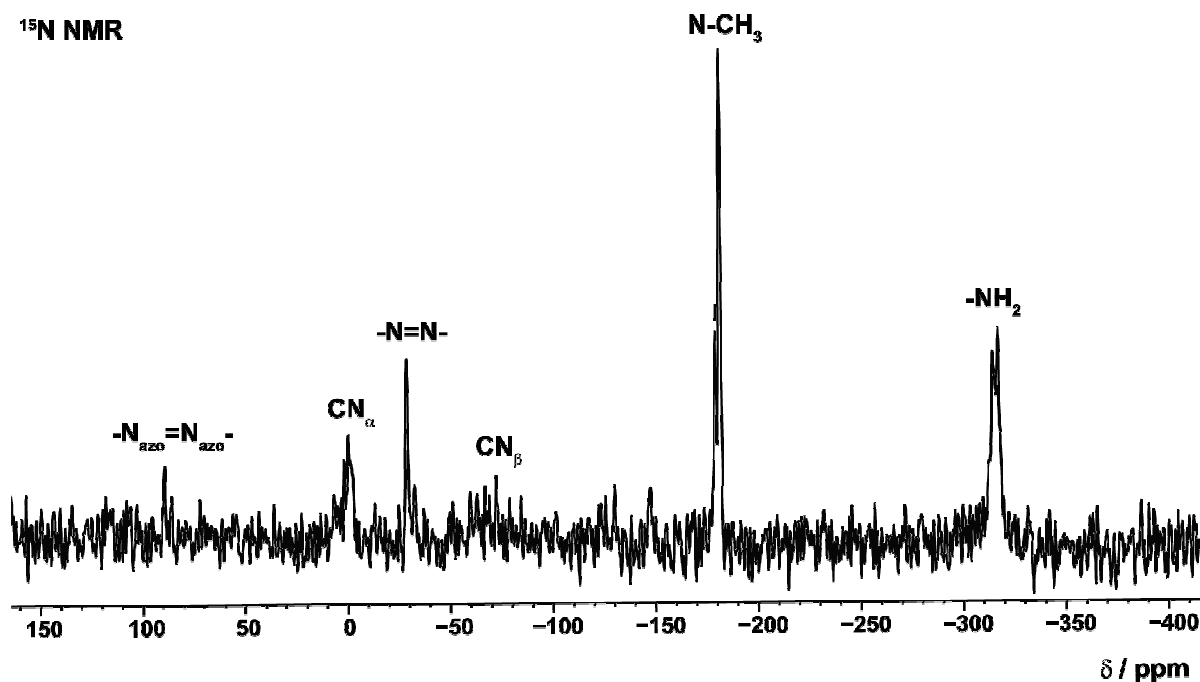


Figure 7.3 Solid state ^{15}N NMR spectrum of **81**.

Interesting is the observation of the disorder found in the crystal structure in the solid state ^{15}N NMR spectrum of **84** (see X-ray structure discussion). Up to fourteen resonances were observed, which can be assigned as follows: 9.4, 4.7, 1.8 and -0.9 ppm (CN_α , two crystallographically independent and disordered sites), -52.3, -63.0, -82.9 and -85.5 ppm (CN_β , two crystallographically independent and disordered sites), -188.9 and -189.2 ppm (N9/N10, crystallographically independent but not disordered), -239.9 ppm (N7) and -318.4, -323.9 and -330.0 ppm ($-\text{NH}_2$ groups). Figure 7.4 shows a schematic representation of the disorder found in this structure.

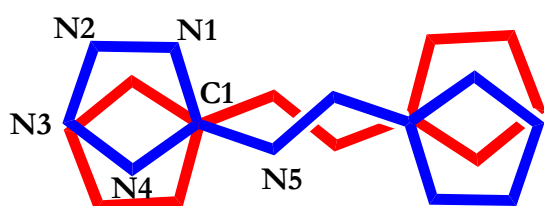


Figure 7.4 Schematic representation of the disorder found in the 5,5'-azotetrazolate anion of **84**.

On the other side, formal alkylation of the ZT^{2-} anion in the 5,5'-azotetrazolate salts to form **91a** and **92**, would be expected to result in five resonances for the nitrogen atoms in the ^{15}N NMR spectra in solution instead of the three expected signals for the ZT^{2-} anion, due to the loss of symmetry caused by the introduction of the methyl groups. Unfortunately, as it is common for 5,5'-azotetrazole derivatives the solubility of **92** in any solvent was too low to record a ^{15}N NMR and no signals were observed in the solid state measurements either. However, **91a** was soluble

enough in DMSO- d_6 yielding the five signals shown in Figure 7.5. In comparison with **77**, which has resonances (in D₂O) at -76.2 (CN_β), +0.6 (CN_α) and +101.8 (N=N)^[2] the electronic changes caused by the lack of a delocalized negative charge in **91a** results in an strong high-field shift for the azo-bridge nitrogen atoms to -1.1 ppm. The two CN_α and the two CN_β nitrogen atoms are no longer equivalent and can be differentiated by the methyl induced effect (MIS, see *Chapter IV*), which causes the methylated nitrogen atom (N1) to be strongly shifted to high field (-272.3 ppm) and N2 (at two bonds from the methyl group) still feels the MIS and is also correspondingly shifted (less strongly) to high field (-123.0 ppm). In addition the two bonds (N1) and three bonds (N2) N–H couplings split the two latter signals in quadruplets with $^2J = 1.94$ Hz and $^3J = 1.55$ Hz, respectively.

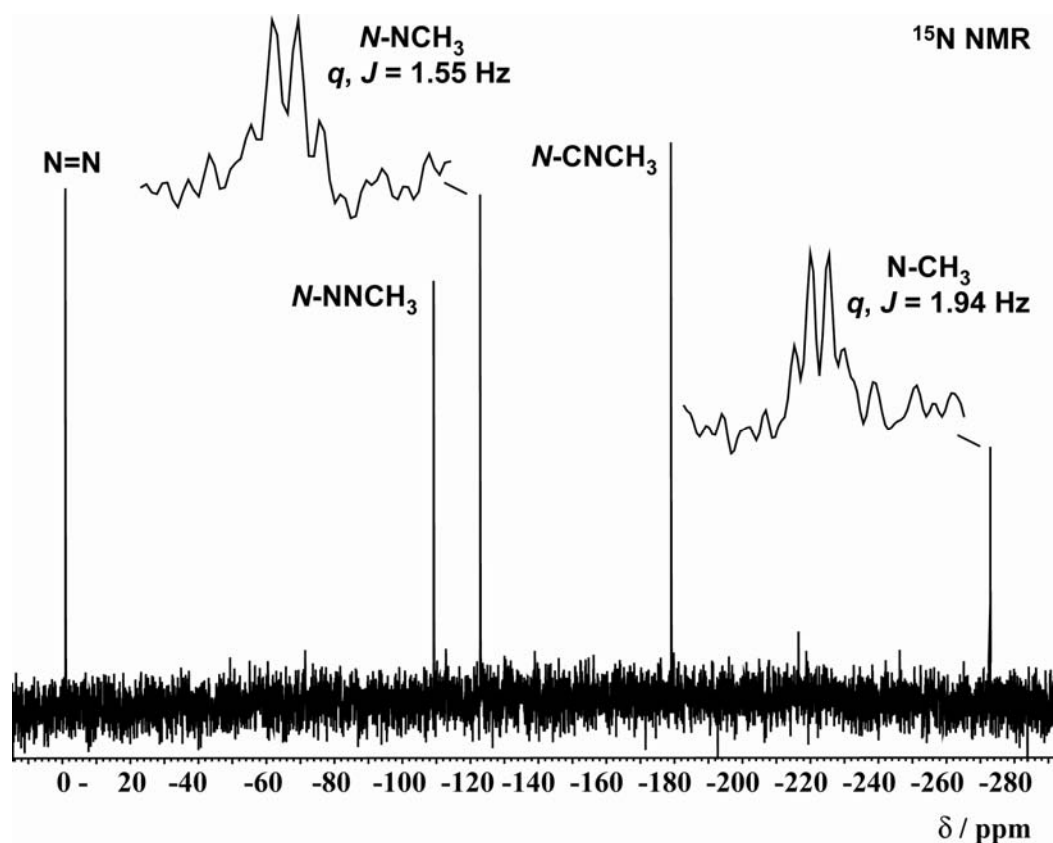


Figure 7.5 ^{15}N NMR spectrum of **91a** in DMSO- d_6 .

7.4 Molecular Structures

Crystals of the 5,5′-azotetrazole derivatives were obtained as described in the experimental section. The X-ray crystallographic data for **81** and **86** were collected on an Enraf-Nonius Kappa CCD diffractometer. Data sets for the rest of compounds were collected on an Oxford Diffraction Xcalibur 3 diffractometer equipped with a CCD detector. All data were collected using graphite-monochromated Mo K α radiation ($\lambda = 0.71073$ Å). No absorption corrections were applied to data sets collected for any of the compounds. All structures were solved by direct methods (SHELXS-97 and SIR97)^[17] and refined by means of full-matrix least-squares procedures using SHELXL-97. All non-hydrogen atoms were refined anisotropically. For all compounds all hydrogen atoms were located from difference Fourier electron-density maps and refined isotropically.

81 and **82** crystallize in the monoclinic system (space group $P2_1/c$ and $P2_1/n$, respectively), whereas the remainder of the compounds have triclinic cells and crystallize in the same space group ($P-1$). **81**, as would be expected from the greater number of molecules in the unit cell ($Z = 4$), has the largest cell volume, whereas **83** and **84** with $Z = 1$ have the smallest. **86** and **88** have very similar cell parameters (both almost identical cell lengths and identical angles) as well as very similar hydrogen-bonding networks (a graph-set analysis of the hydrogen-bonding patterns follows below).

A representation of the asymmetric unit for **88** is omitted from the following discussion due to the fact that the compound crystallizes with the methyl and amino groups disordered. Interatomic distances (Table 7.1) and angles (Table 7.2) for the 5,5′-azotetrazolate anion in the ionic salts (5,5′-azotetrazole moiety for **91a**) are very similar (with the exception of the disordered part in **84**). The N–N distances on the tetrazole rings, between 1.317(3) and 1.345(3) Å, are longer than normal C=N double bonds (1.22 Å) and shorter than normal C–N single bonds (1.47 Å),^[18] implying a certain delocalization throughout the tetrazole ring. The azo-bridge N–N distances between 1.250(2) and 1.265(3) Å are slightly longer than a typical N=N double bond showing the aromatic character of the anion.^[19] Both distances compare nicely with the values measured for the crystal structures of 5,5′-azotetrazolate salts with alkali and alkaline earth metals^{1c} and other salts containing the same anion.^[5,8] Within the uncertainty of the experiment, all parameters agree with the previously reported distances for salts containing the 1,4DMAT⁺^[20,21] and MeDAT⁺^[12,22] cations. The C3–N11 (C6–N17) and N13–N14 (N19–N20) distances in the cation suggest a partial localization of the double bond character in these two bonds making

the imino form a more suitable structure to describe the bonding situation in the solid state structure of the salts described here in agreement with other tetrazolium salts.^[12,13,22]

Table 7.1 Bond distances (Å) in the 5,5'-azotetrazole moiety of 5,5'-azotetrazole derivatives.

Bond	81 ^a	82 ^b	83 ^c	84 ^d	85 ^e	86 ^f	88 ^g	91b ^h
N1–N2	1.336(4)	1.342(2)	1.345(2)	1.326(2)	1.343(3)	1.326(1)	1.333(3)	1.339(2)
N1–C1	1.331(4)	1.337(2)	1.336(2)	1.324(2)	1.336(3)	1.326(1)	1.335(3)	1.337(2)
N2–N3	1.319(4)	1.323(2)	1.321(2)	1.314(2)	1.320(3)	1.325(1)	1.322(3)	1.313(2)
N3–N4	1.347(4)	1.335(2)	1.335(2)	1.334(2)	1.332(3)	1.335(1)	1.336(3)	1.353(2)
N4–C1	1.321(4)	1.328(2)	1.330(2)	1.323(3)	1.332(3)	1.332(1)	1.339(3)	1.323(2)
N5–C1	1.402(4)	1.406(2)	1.411(2)	1.465(6)	1.423(3)	1.417(1)	1.415(3)	1.407(2)
N5–A	1.265(3)	1.256(3)	1.258(2)	1.278(8)	1.233(4)	1.245(1)	1.250(3)	1.258(2)
N6–C2	1.402(4)					1.407(1)	1.399(3)	
C2–N7	1.333(4)					1.325(1)	1.332(3)	
N7–N8	1.334(4)					1.334(1)	1.336(3)	
N8–N9	1.318(4)					1.318(1)	1.324(3)	
N9–N10	1.345(3)					1.341(1)	1.337(3)	
N10–C2	1.323(4)					1.333(1)	1.344(3)	
N6–B						1.265(1)	1.262(3)	

^a**81**: A = N6; ^b**82**: A = N5ⁱ (symmetry code: (i) 0.5-x, -0.5+y, 0.5-z). ^c**83**: A = N5ⁱ (symmetry code: (i) 2-x, -y, 1-z). ^d**84**: A = N5ⁱ (symmetry code: (i) 1+x, y, z). ^e**85**: A = N5ⁱ (symmetry code: (i) 2-x, 1-y, 1-z); ^f**86**: A = N5ⁱ, B = N6ⁱⁱ (symmetry codes: (i) 1-x, 1-y, 1-z; (ii) -1-x, -y, -z); ^g**88**: A = N5ⁱ, B = N6ⁱⁱ (symmetry codes: (i) 1-x, -2-y, 2-z; (ii) 1-x, -1-y, 1-z); ^h**91b**: A = N5ⁱ (symmetry code: (i) 1-x, -y, -z).

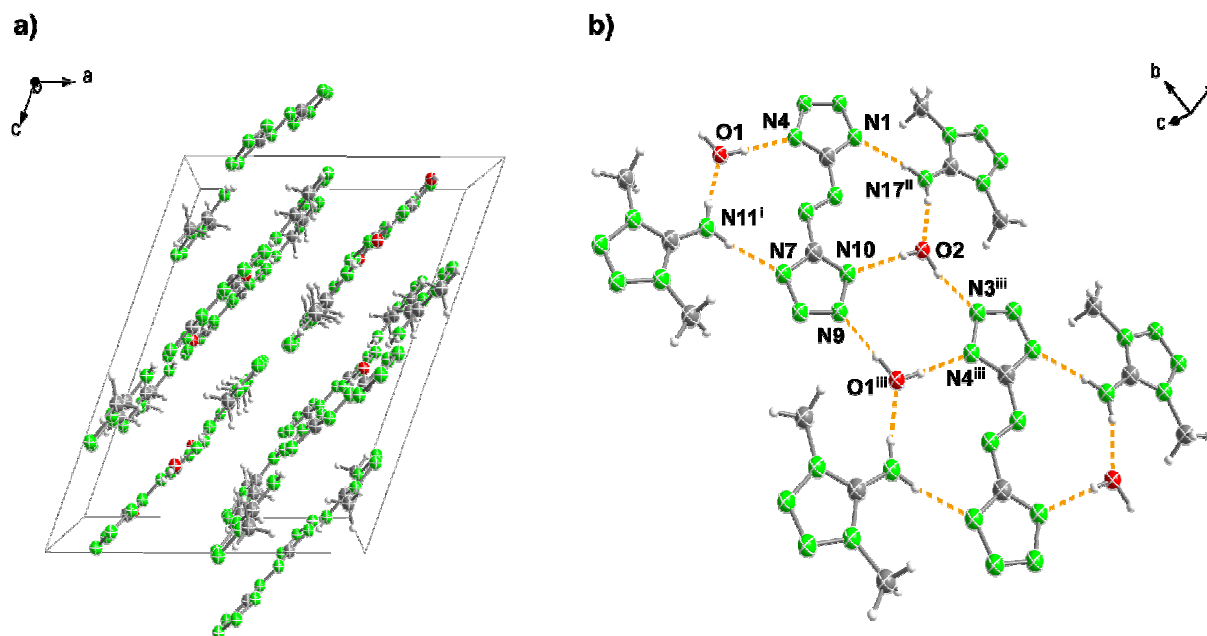


Figure 7.6 View of the unit cell along the b axis (a) and hydrogen-bonding in a layer (b) in the crystal structure of **81** (symmetry codes: (i) x, -0.5-y, 0.5+z; (ii) x, -0.5-y, -0.5+z; (iii) x, -1+y, z).

hydrogen bonds (two as the donor and one as the acceptor). The water molecules have H–O–H angles of 99° in **81** and 103° in **83**. In the case of **81** the asymmetric unit describes a complete formula moiety (two cations, one anion and two water molecules; see Figure 7.8). Four different hydrogen bonds to four water molecules with distances between donor and acceptor atoms (N–H...O) ranging from 2.793(4) to 2.933(4) Å (Table 7.B1) are observed. In addition, there are two hydrogen bond types between water molecules and amino groups with D–A distances of 2.704(4) and 2.740(4) Å. The remaining hydrogen atoms of the amino groups form hydrogen bonds to N1ⁱ and N7ⁱⁱ of the azotetrazolate anion with distances of 2.889(4) and 2.876(4) Å, respectively (symmetry codes: (i) $x, -0.5-y, 0.5+z$; (ii) $x, -0.5-y, -0.5+z$). There are no appreciable contacts between layers, the closest distance is between O2 and N19^{vi} at 3.902(4) Å (symmetry code: (vi) $x, 1.5-y, 0.5+z$). Description of the hydrogen-bonding networks is facilitated by the use of graph-set analysis as reported by Bernstein et al. (unitary = primary = first order, binary = secondary = second order...).^[23] The computer program *RPLUTO*^[24-26] was used to identify unitary and binary graph-sets. The unitary hydrogen-bonding network (N_1) for **81** is made up of eight dimmeric interactions of the type **D1,1(2)**, which connect the anions and the cations, either directly or by means of bridging water molecules, forming a complex hydrogen-bonded structure. At the secondary level, the primary **D1,1(2)** dimmeric interactions combine to form many **D2,2(4)** and **D2,2(9)** graph-sets and the less common **D2,2(5)** and **D2,2(8)** motifs, which extend, for example, from one of the hydrogen atoms on N11ⁱ to one on O2, and from one of the hydrogen atoms on O2 to one on O1, respectively (symmetry code: (i) $x, -0.5-y, 0.5+z$). Two chain motifs defined as **C2,2(10)** including the two hydrogen atoms on O1 or O2 and the azotetrazolate azo-bridge to N9 or N3, respectively are observed.

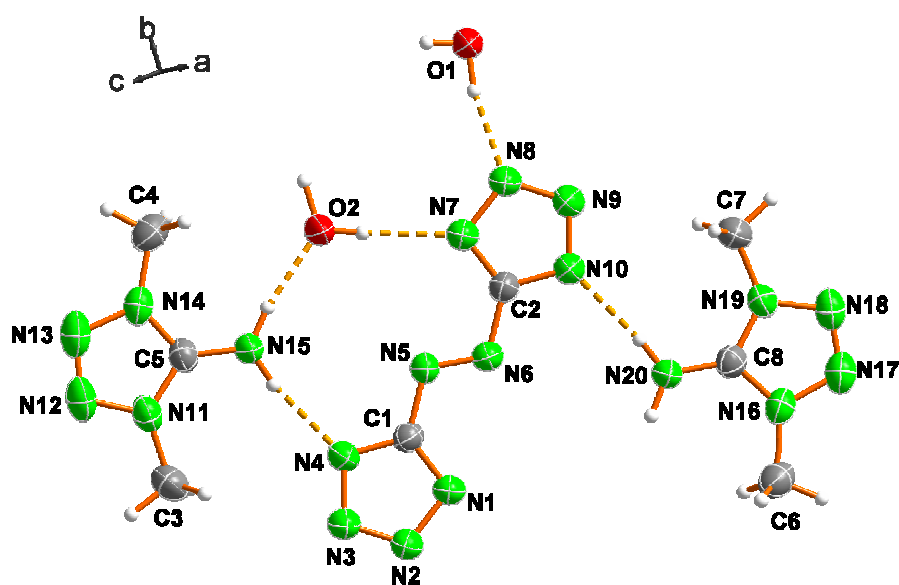


Figure 7.8 Asymmetric unit of **81** with hydrogen-bonding (dotted lines) and the labeling scheme (ellipsoids are represented at the 50% probability).

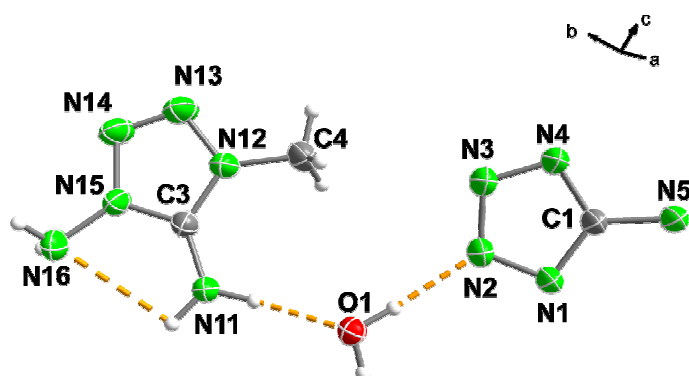


Figure 7.9 Asymmetric unit of **83** showing the N11–N16 intramolecular hydrogen bond and the labeling scheme (ellipsoids are represented at the 50% probability).

In **83** the inversion centre of the space group ($P\bar{1}$) causes both halves of the 5,5′-azotetrazolate anion to be identical (Figure 7.9). The anions form four hydrogen bonds to two different water molecules with distances of 2.806(1) and 2.832(1) Å (Figure 7.7b). N3 and the azo nitrogen N5 do not form any significant hydrogen bond whereas N4 forms a hydrogen bond to the C-bound amino group of the tetrazolium cations with $N11\cdots N4^{\text{xiii}} = 2.892(2)$ Å (symmetry code: (xiii) $-1+x, y, -1+z$). Both tetrazolium cations are also identical due to symmetry. The two cation amino groups have different hybridizations. The C–NH₂ is sp²-hybridized whereas the N–NH₂ is sp³-hybridized with the nitrogen lone pair directed towards the C–NH₂ nitrogen atom yielding an intramolecular hydrogen bond ($N11\cdots N16 = 2.912(1)$ Å). It is this twisted sp³ hybridized amino group, which allows for the formation of hydrogen bonds with one of the anion nitrogen atoms of one layer ($N16\cdots N1^{\text{viii}} = 3.168(1)$ Å; symmetry code: (viii) $1-x, 1-y, -z$) and a water molecule of another layer ($N16\cdots O1^{\text{xv}} = 3.024(1)$ Å; symmetry code: (xv) $-1+x, y, z$) as shown in Figure 7.7a.

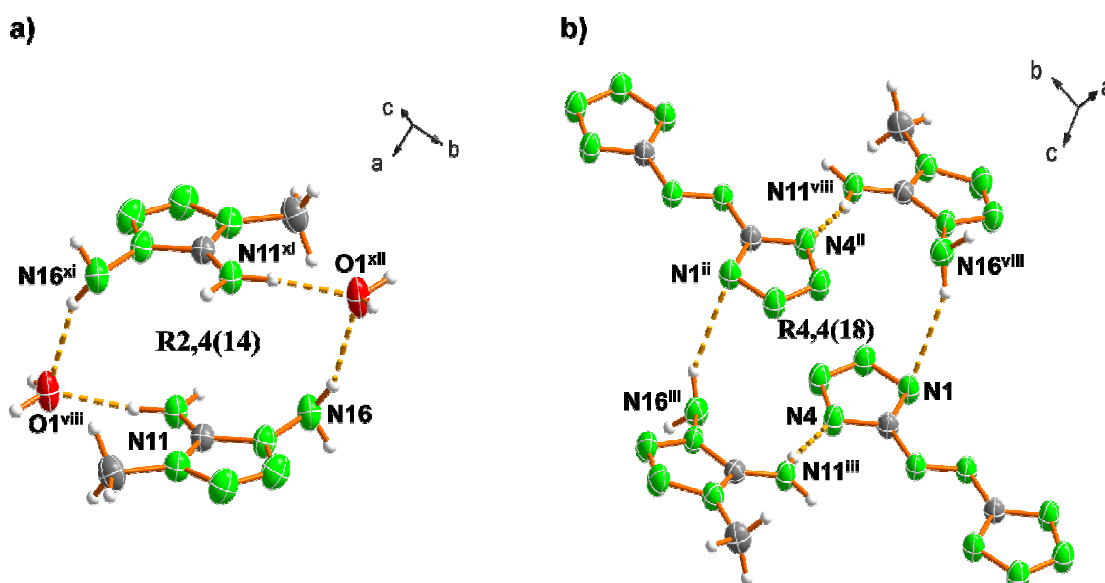


Figure 7.10 View of an **R2,4(14)** (a) and an **R4,4(18)** (b) hydrogen-bonding graph-sets in the crystal structure of **83** (symmetry codes: (ii) $2-x, 1-y, 1-z$; (iii) $1+x, y, 1+z$; (viii) $1-x, 1-y, -z$; (xi) $-x, 1-y, -z$; (xii) $1+x, y, -z$).

Using graph-set nomenclature the primary graph-set for **83** is described by six **D1,1(2)** dimmeric interactions and an intramolecular hydrogen bond between N11 and N16, which takes the label **S(5)**. In analogy to **81** multiple combinations of hydrogen bonds to form **D2,2(4)** and **D2,2(9)** secondary motifs are possible. Once again, the dimmeric **D2,2(5)** (e.g., from N11^{iv} to O1^{vii}, symmetry codes: (iv) 1-x, -y, -z; (vii) 1+x, y, 2+z) and **D2,2(8)** (e.g., from one hydrogen atom on O1ⁱⁱ to one on O1^v, symmetry codes: (ii) 2-x, 1-y, 1-z; (v) x, -1+y, z) graph-sets as well as the **C2,2(10)** chain motif (from one hydrogen atom on O1^{vii} to N1) are found. Additionally, a longer **C2,2(12)** chain starting at N4 and finishing at one of the hydrogen atoms on N16^{iv} is observed. Further similarities in the hydrogen-bonding networks of **81** and **83** are observed. In the case of **83**, symmetry (symmetry code: (i) 2-x, -y, 1-z) allows for the formation of a **R4,4(10)** ring motif at the secondary level, which is analogous to the ring hydrogen-bonded by N9, N10, O2, N3ⁱⁱⁱ, N4ⁱⁱⁱ and O1ⁱⁱⁱ in the crystal structure of **81** (symmetry code: (iii) x, -1+y, z), which involves four different hydrogen bonds and is thus generated at the quaternary level. Lastly, the presence of the twisted N-bound amino group, allows for the formation of interlayer ring patterns of even higher order, namely **R2,4(14)** (Figure 7.10a) and **R4,4(18)** (Figure 7.10b), which are formed along two bridging water molecules or two 5,5'-azotetrazolate anions, respectively.

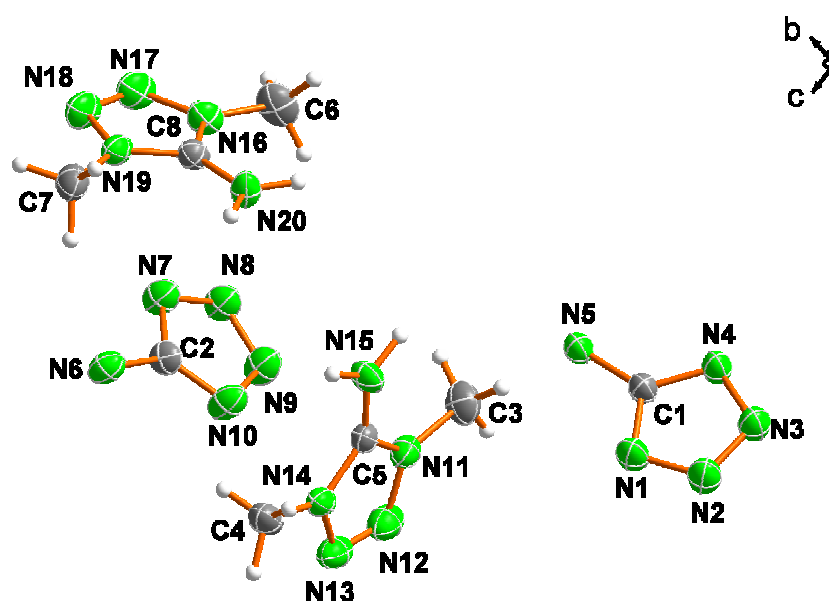


Figure 7.11 Asymmetric unit of **86** with the labeling scheme (view along the *a*-axis, ellipsoids are represented at the 50% probability).

The absence of crystal water in **86** and **88** results in non-layered structures in contrast to the dihydrated species **81** and **83**. In **86** (Figure 7.11) there are two types of azotetrazolate anions, which are symmetric and surrounded by four tetrazolium cations each one forming two different

types of hydrogen bonds to the amino group hydrogen atoms (Figure 7.12). Both anions participate in different hydrogen-bonding. Whereas one of them coordinates face-on to two tetrazolium cations through hydrogen bonds ($\text{N11} \cdots \text{N3} = 2.860(2) \text{ \AA}$ and $\text{N17} \cdots \text{N2}^{\text{iii}} = 2.922(2) \text{ \AA}$; symmetry code: (iii) $1-x, 1-y, 1-z$), the other one interacts side-on ($\text{N11} \cdots \text{N7} = 2.849(2) \text{ \AA}$ and $\text{N17} \cdots \text{N8}^{\text{iii}} = 2.885(2) \text{ \AA}$).

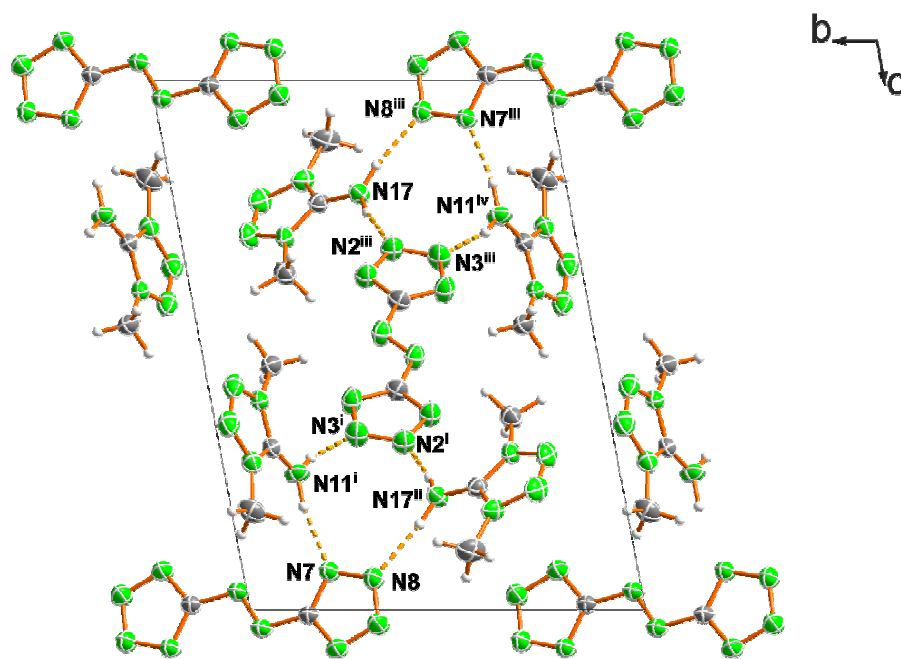


Figure 7.12 Hydrogen-bonding around the azotetrazolate anion in the unit cell of **86** (view along the *a* axis; symmetry codes: (i) $2+x, y, z$; (ii) $3-x, 1-y, 1-z$; (iii) $1-x, 1-y, 1-z$; (iv) $2-x, 1-y, 1-z$).

The absence of crystal water in **86** reduces markedly the number of hydrogen atoms available to interact through dipole-dipole bonds and only half as many hydrogen bonds as in the parent dihydrate **81** are formed (Table 7.B1). The unitary graph-set is described by four **D1,1(2)** dimmeric interactions. These combine at the secondary level to form further dimmeric networks. For example, the usual **D2,2(4)** and **D2,2(9)** graph-sets can be found. Two **D2,2(5)** patterns in which N11^{i} and N17^{ii} of two cations link two azotetrazolate anions (symmetry codes: (i) $2+x, y, z$; (ii) $3-x, 1-y, 1-z$) and the usual **D2,2(8)** pattern described above for **81** and **83** are observed. Both **D2,2(5)** secondary graph-sets combine to form a pseudo-ring network with the nomenclature **R4,4(10)** (similar to **81**), starting at N7 and finishing at N8 (the pseudo-ring term refers to the fact that two secondary networks combine to form a quaternary one, when generally the graph-set analysis is limited to the secondary level). As described for **83**, the formation of this ring-pattern at the quaternary level is due to symmetry reasons. Lastly, four dimmer graph-sets **D2,2(10)** are formed (e.g. starting at one hydrogen atom on N17 and finishing on a hydrogen atom linked to N17^{ii}).

In **88** the most significant changes in the cation distances are observed in the N–NH₂ and the N–CH₃ bond lengths (Figure 7.13). Whereas in **83** there is a noticeable difference between the N–NH₂ (1.383(1) Å) and N–CH₃ (1.455(1) Å) distances, in **88** the bond distances are the result of averaged methyl and amino group positions and are thus very similar (1.449(3) and 1.455(3) Å). Further analysis of the disorder found in 5,5'-azotetrazolate salt **88** is out of the scope of this work and will be omitted.

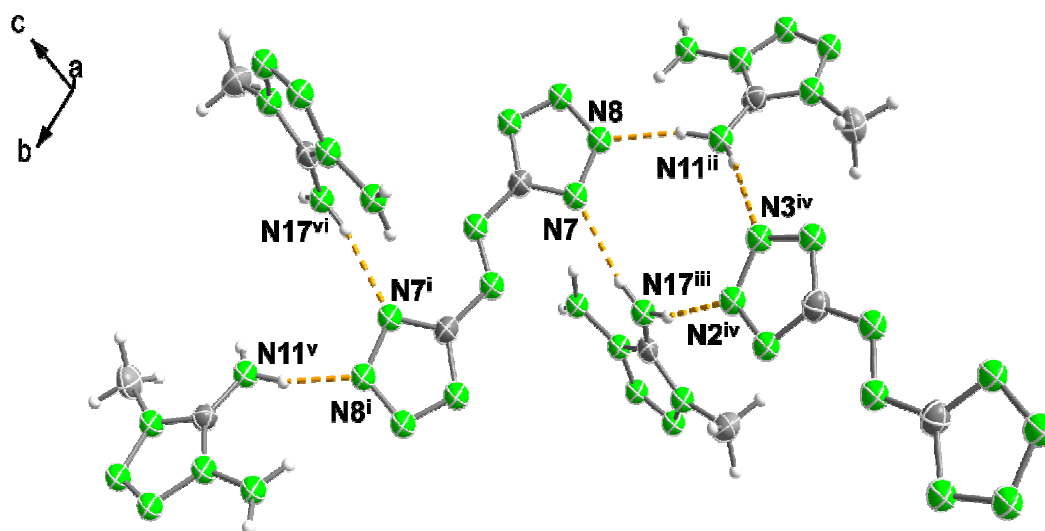


Figure 7.13 Hydrogen-bonding around the anion in the crystal structure of **88** (symmetry codes: (i) $-x+1, -y-1, -z+1$; (ii) $-x, -1-y, -z$; (iii) $-x, -y, -z$; (iv) $-1-x, -1-y, -z$; (v) $-1+x, 2+y, -1+z$; (vi) $-1+x, 1+y, 1+z$).

The disorder found in the crystal structure of **88** does also not allow a complete analysis of the hydrogen-bonding situation. In Figure 7.13 the hydrogen-bonding around the anion is depicted. Every anion is surrounded by four cations with which they interact via hydrogen-bonding. Half of the anion is related to the other half by symmetry and forms one hydrogen bond to each one of the two crystallographically independent cations ($N11 \cdots N3^{vii} = 2.929(3)$ Å and $N17 \cdots N2^{vii} = 2.863(3)$ Å; symmetry code: (vii) $1+x, y, z$), which, in turn, coordinate to the other crystallographically independent half of the anion ($N11 \cdots N8^{viii} = 2.884(3)$ Å and $N17 \cdots N7^{viii} = 2.852(3)$ Å; symmetry code: (viii) $1-x, 1-y, 1-z$). Without taking into consideration the disordered methyl and amino groups, the hydrogen-bonding network is identical to that of **81**. Four primary dipole-dipole dimmeric graph-sets **D1,1(2)** combine to form two **D2,2(4)**, two **D2,2(5)**, one **D2,2(8)**, one **D2,2(9)** and four **D2,2(10)** secondary motifs, exactly as observed for **81**. Lastly, once again, symmetry does not allow for the formation of a secondary graph-set **R4,4(10)**, but this is formed at the quaternary level instead.

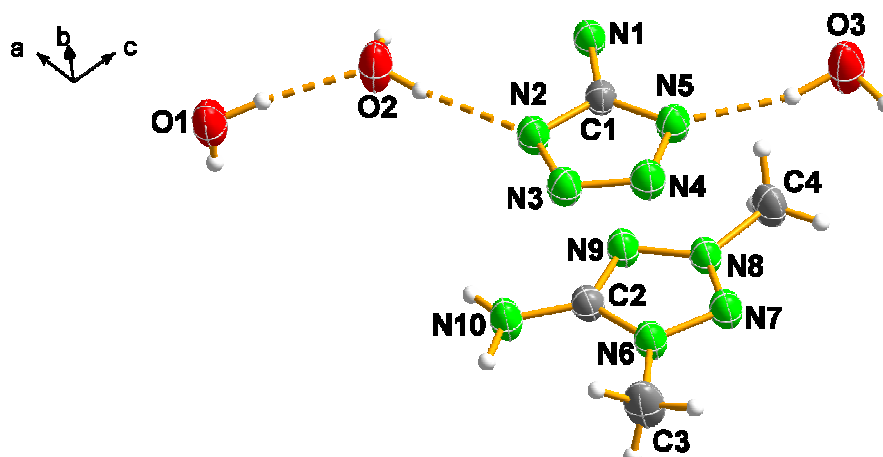


Figure 7.14 Asymmetric unit of 5,5′-azotetrazolate **82** with the labeling scheme (ellipsoids are represented at the 50% probability).

82 crystallizes in a monoclinic cell in the space group $P2_1/n$ with two molecules in the unit cell as the hexahydrate species. (Figure 7.14). Half of the molecule can be generated by symmetry (symmetry code (i) $1-x, 1-y, 1-z$). The molecules pack in the unit cell forming waved layers, which are connected by strong hydrogen bonds formed by two water molecules ($O1 \cdots O2^v = 2.763(3) \text{ \AA}$; symmetry code: (v) $1.5-x, -0.5+y, 0.5-z$). In a layer (Figure 7.15), there exists extensive hydrogen bonding. Every anion forms a hydrogen bond to the cation amino-group ($N10^i \cdots N3 = 2.974(2) \text{ \AA}$, symmetry code: (ii) $0.5-x, 0.5+y, 0.5-z$) and is surrounded by six water molecules to which it forms hydrogen-bonding with distances between donor and acceptor atoms of $\sim 2.9 \text{ \AA}$. All nitrogen atoms in the tetrazole rings are involved in hydrogen-bonding, only the bridging nitrogen atoms do not participate in any significant interaction.

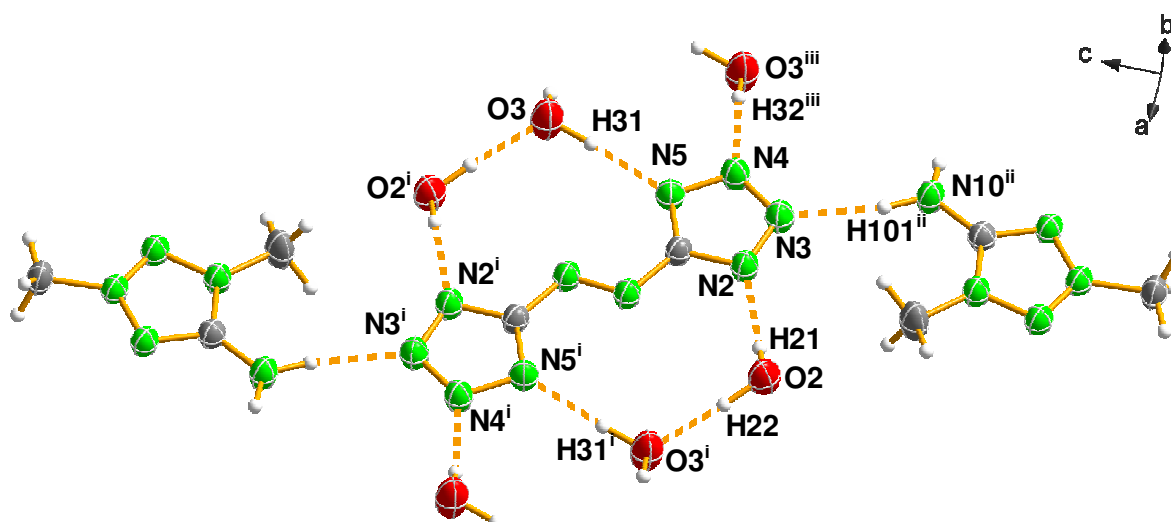


Figure 7.15 Hydrogen-bonding around the anion in the structure of **82** (symmetry codes: (i) $1-x, 1-y, 1-z$; (ii) $0.5-x, 0.5+y, 0.5-z$; (iii) $x, 1-y, 1-z$).

It is interesting to compare the hydrogen-bonding networks formed by **82** with those containing the isomeric 1,4DMAT⁺ cation. *RPLUTO* identifies up to 35 graph-sets formed by the hydrogen bonds summarized in Table 7.B1. At the primary level only dimeric interactions of the type **D1,1(2)** are found, which combine at the secondary level to form mainly other finite patterns with the labels **D2,2(X)** (X = 4, 5, 8-10), however, there also exist some **C1,2(4)** and **C2,2(10)** chain patterns and one **R4,4(10)** network formed by the side-on interaction of two tetrazolate anions over two water molecules ($\text{O3}\cdots\text{N6} = 2.899(2) \text{ \AA}$ and $\text{O3}\cdots\text{N7}^{\text{iii}} = 2.894(2) \text{ \AA}$; symmetry code: (iii) $-x, 1-y, 1-z$). The latter is common for all tetrazolium 5,5'-azotetrazolate salts described here. Lastly, the presence of six molecules of water in the crystal structure makes that most of the hydrogen-bonded networks are formed by more than only two hydrogen bonds rendering the standard graph-set nomenclature insufficient since it just describes patterns, which are formed by one or two different hydrogen bonds, thus at the primary or secondary level. Therefore, an extended graph-set nomenclature for more complex hydrogen-bonding networks would be useful (e.g. to describe the **R3,3(11)** ring network formed at the tertiary level by N2^{i} , O2^{i} , O3 and N5 in Figure 7.15).

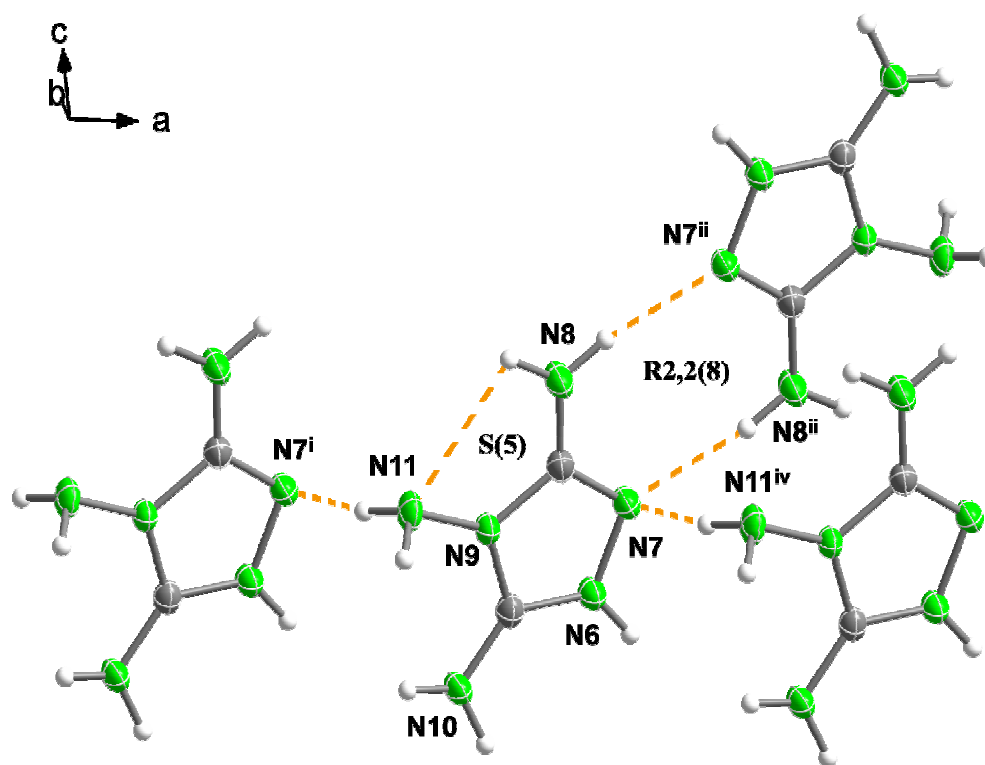


Figure 7.16 Hydrogen-bonding around the guanazinium cation in the crystal structure of **84** (the hydrogen bonds formed with the disordered azotetrazolate anion have been omitted). Symmetry codes: (i) $1+x, y, z$; (ii) $-1-x, 1-y, -z$; (iii) $-1+x, y, z$.

For **84** molecules are arranged in layers, which are parallel planar chains oriented orthogonally to the plane formed by the *a*- and *b*-axes. The triazolium and 5,5'-azotetrazolate rings define two planes with a torsion angle of 12.2°. The geometry of the cation is in good agreement with previous reports^[27,28] and, unlike in the picrate salt (*Chapter V*), the N11 amino-group protons adopt a configuration similar to those in the nitrate derivative^[28] as they are oriented to the side of the protonated nitrogen atom, which is in contrast to the 5-nitrotetrazolate, dinitramide and perchlorate structures.^[27,28] The anion shows a severe disorder in the azo-group, which also affects the tetrazole ring: in each side of the azo-group, there are two overlapping tetrazole rings occupying two plausible positions around C1 (see Figure 7.4). The disorder, common for other 5,5'-azotetrazolate derivatives (e.g., **88** shows the above-mentioned disorder) was also observed in the ¹⁵N solid state NMR spectrum (see NMR discussion above) and explains the anomalies in some of the angles and bond distances for the anion in **84** (Tables 7.1 and 7.2). As for the cation, the N7–N6 and N11–N9 distances are both shorter than in neutral guanazine,^[27] again keeping in with the picrate salt (*Chapter V*).

As mentioned in the introductory section, hydrogen-bonding is an important consideration in the synthesis of new energetic materials since the more extensive it is, the higher the density of a material, which, in turn, increases the performance (detonation parameters) of the same. As expected from the substantial number of electronegative (nitrogen) atoms, readily available to form hydrogen bonds in **84** the compound forms complicated hydrogen-bonded networks, which are difficult to describe due to the disorder found in the 5,5'-azotetrazolate anion. A solution of the disorder is out of the scope of this work, thus a description of the hydrogen-bonding involving the anion is omitted here. However, the cation forms up to five hydrogen bonds (see Figure 7.16) with other cations, one of which is intramolecular (N8•••N11 = 2.837(3) Å). N7 and N11 are involved in a long hydrogen bond between layers (N11•••N7ⁱ = 3.277(2) Å; symmetry code: (i) 1+x, y, z), whereas N7 and N8 link with N8ⁱⁱ and N7ⁱⁱ, respectively forming cation dimer-pairs (N8•••N7ⁱⁱ = 2.981(2) Å; symmetry code: (ii) -1-x, 1-y, -z). Using graph-set nomenclature, the intramolecular hydrogen bond found in the cation can be described as a common^[12-14] **S(5)** motif at the primary level, whereas the dimer-pairs formed by N7 and N8 describe a ring pattern with the label **R2,2(8)** (also at the primary level). The formation of dimer-pairs is common for guanazinium salts.^[12,13] The three amino groups in the cation allow for the formation of a very dense structure ($\rho = 1.708 \text{ g cm}^{-3}$) in comparison to other 5,5'-azotetrazolate salts, which, in the rule, have densities between 1.45-1.55 g cm⁻³ [5,15,16] or at the best, around 1.6 g cm⁻³, in the case of salts with counterions that have possibility to form a significant number of hydrogen bonds such as the triaminoguanidinium cation.^[5,29]

85 crystallizes with two molecules of crystal water and a relatively high density of 1.638 g cm^{-3} similar to guanadinium salts containing the same anion^[5] and higher than tetrazolim 5,5′-azotetrazolate salts.^[30] This high value is explained by the extensive hydrogen-bonding found in the structure. Table 7.B1 contains tabulated the nine hydrogen bonds found in the structure. These hydrogen bonds are between $\text{N}\cdots\text{N}$, $\text{N}\cdots\text{O}$, $\text{O}\cdots\text{N}$ and $\text{O}\cdots\text{O}$ and are strong with distances between donor and acceptor atoms in the range $\sim 2.7\text{--}3.1 \text{ \AA}$, in general well below the sum of the van der Waals radii ($r_{\text{N}} = 1.55 \text{ \AA}$; $r_{\text{O}} = 1.52 \text{ \AA}$).^[31]

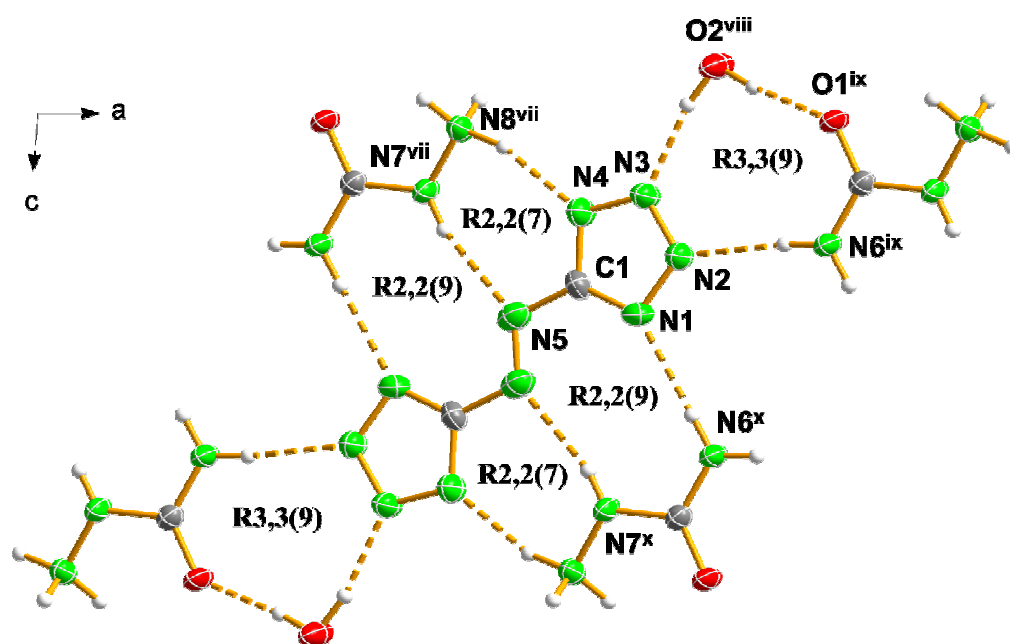


Figure 7.17 Hydrogen-bonding around the 5,5′-azotetrazolate anion in the crystal structure of **85**. Symmetry codes: (vii) $1-x, -y, 1-z$; (viii) $1+x, 1+y, -1+z$; (ix) $3-x, 1-y, 1-z$; (x) $1+x, 1+y, z$.

The compound crystallizes forming layers, which are connected *via* hydrogen bonds to the NH_3^+ moiety in the cation ($\text{N8}\cdots\text{O1}^{\text{v}} = 3.038(4) \text{ \AA}$; symmetry code: (v) $-1+x, y, z$). Figure 7.17 shows the hydrogen-bonding in one of this layers. Every single electronegative atom in the structure is involved in the formation of (at least) one hydrogen bond. The reasonably complex hydrogen-bonding networks can be described in terms of graph-set analysis.^[23,26] At the unitary level (N_1) The program identifies seven of the hydrogen bridges in the structure as describing **D1,1(2)** finite patterns, five of which combine (still at the primary level) to generate larger **D2,2(X)** ($X = 4, 8, 10$) dimmer graph-sets. In addition, the other two hydrogen bonds form a **C1,1(5)** chain and an **R2,2(10)** ring networks. At the secondary level, two hydrogen bonds combine to form dimmeric **D2,2(X)** ($X = 4\text{--}10$), **D2,3(8)**, **D3,3(10)**, chain **C3,3(X)** ($X = 10, 14, 16, 18$), **C2,2(X)** ($X = 9, 10$) and more interestingly ring **R2,2(X)** ($X = 4, 7, 9, 10, 12$) and **R4,4(X)** ($X = 10, 14, 16, 18, 20, 26$) patterns., whereas three hydrogen bonds combine forming

an **R3,3(9)** motif. The **R2,2(7)** and **R2,2(9)** graph-sets are formed both by interaction between one cation and one anion ($N8^{vii} \cdots N4 = 2.864(3) \text{ \AA}$; $N7^{vii} \cdots N5 = 2.998(3) \text{ \AA}$; $N6^x \cdots N1 = 3.000(3) \text{ \AA}$; symmetry codes: (vii) $1-x, -y, 1-z$; (x) $1+x, 1+y, z$) whereas the **R3,3(9)** network is described by one cation, one anion and one molecule of crystal water and they are all represented in Figure 7.17. Figure 7.18 depicts the hydrogen-bonding between cations. The hydrogen bond between layers described above describes a small **R2,2(4)** graph-set, whereas two cations interact yielding a larger **R2,2(10)** ring network at the primary level ($N8 \cdots O1^{iv} = 2.957(3) \text{ \AA}$; symmetry code: (iv) $1-x, -y, 2-z$).

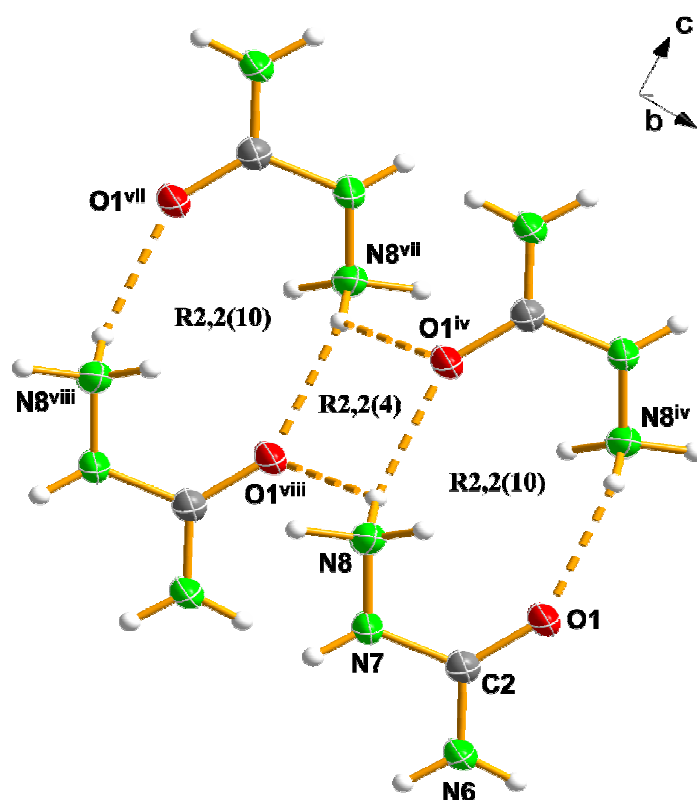


Figure 7.18 Hydrogen-bonding between cations in the crystal structure of **85**. Symmetry codes: (iv) $1-x, -y, 2-z$; (vii) $-x, -y, 2-z$; (viii) $-1+x, y, z$.

After recrystallization from water, **91a** crystallizes in a monoclinic crystal system with four molecules per unit cell as the monohydrated species (**1,1DMZTh**, **91b**). The asymmetric unit of the compounds is represented in Figure 7.19 together with the labeling scheme. The bond distances and angles of the two tetrazole rings are, within the limits of error, identical to those of the 5,5'-azotetrazolate anion found in compounds **81-88**. Half of the molecule can be derived from the other half by symmetry operations (symmetry code: (i) $1-x, -y, -z$) and the bulkiness of the methyl group added to the fact that this prevents N1 from forming hydrogen-bonds with the water molecules does not allow it to form a layered structure.

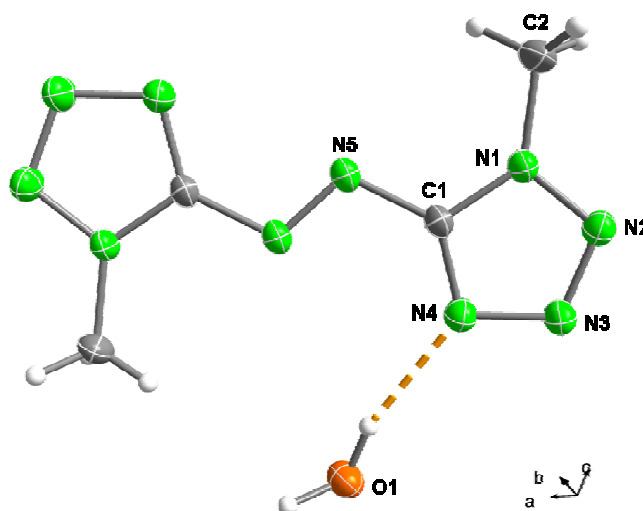


Figure 7.19 Molecular structure of **91b** (half the molecule is generated by symmetry, symmetry code: (i) 1-x, -y, -z); thermal ellipsoids are set at 50 % probability.

Regardless of that, it still does exist planarity within the azotetrazole moieties in one direction and although the water molecules hydrogen atoms stick out of this plane with a torsion angle of $\sim 44.5^\circ$ the hydrogen bonds are still relatively directional ($161.70(2)^\circ$) and short ($O1 \cdots N4 = 2.929(2) \text{ \AA}$). The $O1-H$ distance in the hydrogen bond at $0.923(2) \text{ \AA}$ is relatively long and the distance with the acceptor atom $H \cdots N4 = 2.039(2) \text{ \AA}$ is short making for a relatively efficient packing in terms of density ($\rho_{calc.} = 1.572 \text{ g cm}^{-3}$) in comparison with 5,5′-azotetrazolate salts,^[30,32] which have densities of $\sim 1.4\text{--}1.5 \text{ g cm}^{-3}$ (with the exception of **84**). The second hydrogen bond (formed by a water molecule), equivalent to the one described above by symmetry, links two azotetrazole moieties which forms an angle of $\sim 78.2^\circ$ with one another. In consequence, every azotetrazole molecule is involved in two equivalent hydrogen bonds with two symmetrically equivalent water molecules. Figure 7.20 shows a view of the unit cell along the *b*-axis with the hydrogen bonds to the water molecules. The lack of extensive hydrogen-bonding due to the presence of the two methyl groups allows only the formation of two **D1,1(2)** dimmeric graph-sets, which are generated by symmetry.

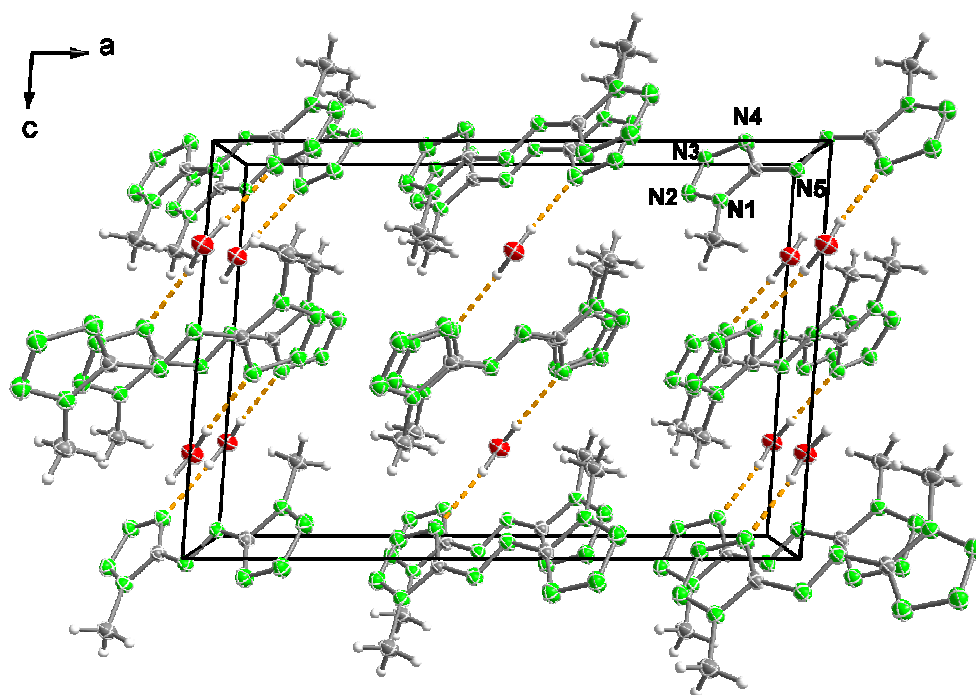


Figure 7.20 Unit cell of **91b** (view along the *b*-axis) showing the hydrogen-bonding (dotted lines).

7.5 Thermal and Energetic Properties

In order to assess the thermal and energetic properties of the 5,5'-azotetrazole derivatives studied here the thermal stability (decomposition points from DSC measurements), as well as the sensitivities to friction, impact, electrostatic discharge and thermal shock of each material were experimentally assessed (Tables 7.3 and 7.4) using standard BAM tests.^[33-35] In addition, for all four CHN(O) salts the constant volume energies of combustion (ΔU_{comb}) were determined experimentally using oxygen bomb calorimetry. The heats and energies of formation were back-calculated from the combustion data and subsequently used in conjunction with the molecular formula and density (from X-ray) to predict the detonation performance parameters (pressure and velocity) for each compound using the EXPLO5 computer code.^[36] Because of the (in some cases) significant experimental uncertainties obtained in the bomb calorimetry measurements, the validity of the values obtained for the detonation parameters was checked by way of quantum chemical calculation (MP2) of electronic energies and an approximation of lattice enthalpy. A detailed explanation of the method used here is given in *Appendix B of Chapter IV*.^[37]

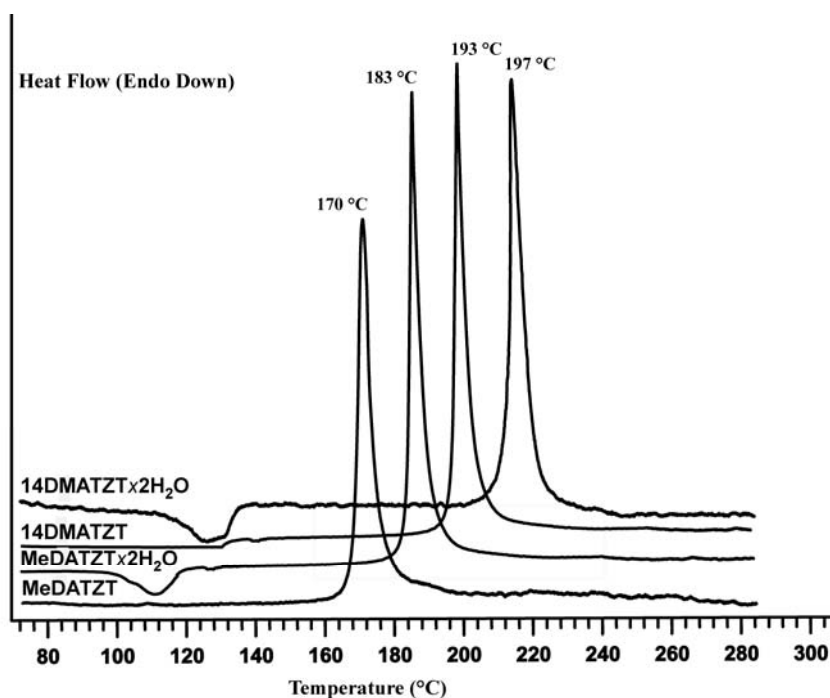


Figure 7.21 DSC plots for selected 5,5'-azotetrazolate salts at a heating rate of $\beta = 5\text{ }^{\circ}\text{C min}^{-1}$.

Slow heating in a DSC apparatus ($\beta = 5\text{ }^{\circ}\text{C min}^{-1}$) of samples of $\sim 1\text{ mg}$ of each energetic material gives rapid decomposition without melting at temperatures above $175\text{ }^{\circ}\text{C}$ for all compounds apart from the semicarbazidium salts **85** and **89**, which melt with concomitant decomposition already at $\sim 120\text{ }^{\circ}\text{C}$ and show a second decomposition step at $\sim 150\text{ }^{\circ}\text{C}$. Figure 7.21 show typical DSC curves for two of the hydrated compounds in this work (**81** and **83**) and for the analogous anhydrous species (**86** and **88**). For the hydrated compounds in addition to the decomposition exotherm, the DSC curves show endotherms at 84 (**81**), 119 (**82**), 92 (**83**) and 96 (**85**) $^{\circ}\text{C}$, respectively, corresponding to the loss of the crystal water. These studies show that the 5,5'-azotetrazolate salts presented here have high thermal stabilities, which most likely can be attributed to the extensive hydrogen-bonding observed in the crystal structures, specially in the case of **84** ($T_{\text{dec}} = 212\text{ }^{\circ}\text{C}$). In addition to DSC analysis, all compounds were tested by placing a small sample ($\sim 0.5 - 1.0\text{ mg}$) of compound in the flame. This resulted in smokeless burning in the case of the semicarbazidium salts **85** and **89**, a vigorous reaction (deflagration) in the case of **81**, **82**, **84**, **87**, **91a** and **92** and (in some instances) explosion for **83**, **88** and **86** (both TNT and RDX explode under similar conditions).

Data collected for friction, impact and electrostatic discharge sensitivity are summarized in Table 7.3. The compounds in this study are significantly less sensitive to friction and impact than ionic salts containing the same cation.^[12,13,22] None of the compounds showed sensitivity towards shock or friction. No detonation was observed in the drop hammer test ($>30\text{ J}$)^[33-35] nor in the friction tester ($>360\text{ N}$). Also no detonation occurred when grinding the compounds in a mortar.

In addition, each compound was roughly tested for sensitivity to electrostatic discharge by spraying sparks across a small sample of material using a tesla coil.

Table 7.3 Initial safety testing results and predicted energetic performance of 5,5'-azotetrazole derivatives using the EXPLO5 code.

	T_{ex} (K) ^a	V_0 (L kg ⁻¹) ^b	P_{det} (GPa) ^c	D (m s ⁻¹) ^d	Impact (J) ^e	Friction (N) ^e	ESD (+/-) ^f	Thermal Shock
81	2987 [3797]	822 [822]	20.2 [25.3]	7820 [8590]	>30	>360	-	Deflagrates
82	3931 [4086]	890 [890]	25.1 [25.8]	8585 [8685]	>30	>360	-	Deflagrates
83	2811 [4115]	842 [843]	22.4 [30.9]	8090 [9174]	>30	>360	-	Explodes
84	2758 [1892]	801 [805]	27.7 [19.9]	8702 [7683]	>30	>360	-	Deflagrates
85	2166 [3862]	879 [879]	20.0 [32.8]	7694 [9258]	>30	>360	-	Burns
86	3046 [3559]	782 [782]	20.0 [22.8]	7803 [8233]	>30	>360	-	Explodes
87	2973 [3530]	783 [783]	19.0 [21.5]	7667 [8089]	>30	>360	-	Deflagrates
88	3323 [3974]	808 [810]	21.1 [23.9]	7977 [8373]	>30	>360	-	Explodes
89	2779 [3587]	836 [836]	23.4 [29.7]	8125 [8886]	>30	>360	-	Burns
91a	3275	735	22.0	7941	>30	>360	-	Deflagrates
92	3422	736	22.5	8017	>30	>360	-	Deflagrates

^aTemperature of the explosion gases; ^bVolume of the explosion gases; ^cDetonation pressure; ^dDetonation velocity; ^eTests according to BAM methods (see refs. [33-35]); ^fRough sensitivity to electrostatic discharge using a Tesla coil (~20 kV), + sensitive, - insensitive. ^gCalculated values in [] brackets (see *Chapter IV* for calculation method).

A comparison with the properties of TNT and RDX is useful to assess the energetic compounds in this study. All materials studied here turned out to be much less sensitive to impact than TNT (15 J) and RDX (7.4 J).^[39] This can be explained by the fact that extensive hydrogen-bonding helps to stabilize a material and is interesting since the density and heat of formation (related to the performance) are favored by strong hydrogen bonds.^[40] Hence, compounds that foreseeably form many hydrogen bonds are of interest as prospective insensitive materials with high performances.^[41,42] In addition, all compounds under study were also less sensitive to friction and electrostatics than either TNT or RDX. Lastly, all materials reported here are safe for transport under the UN Recommendations on the Transport of Dangerous Goods.^[33]

In addition to safety considerations, performance of new high energy density materials is of significant importance. Using the molecular formula, density (from X-ray) and energy of formation (ΔU_f), the EXPLO5 computer code can be used to calculate the detonation velocity and pressure of CHNO-based explosive materials. The following values for the empirical constants in the Becker-Kistiakowsky-Wilson equation of state (BKWN-EOS) were used: $a = 0.5$, $\beta = 0.176$, $\kappa = 14.71$ and $\theta = 6620$. The detonation parameters for all the 5,5'-azotetrazole

derivatives are presented in Table 7.3 and the experimentally determined energies of combustion and back-calculated energies of formation for sets of five individual measurements are tabulated in Table 7.4, together with some other physico-chemical properties of interest.

Table 7.4 Physico-chemical properties of 5,5'-azotetrazole derivatives.

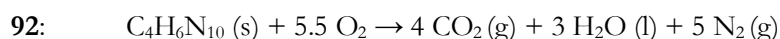
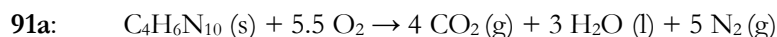
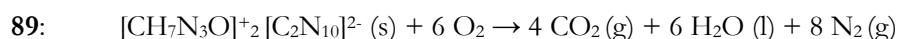
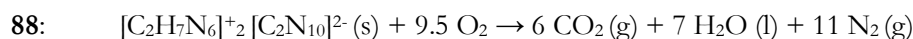
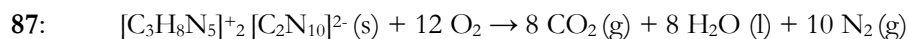
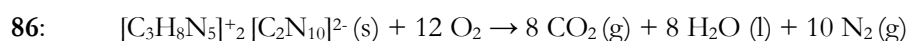
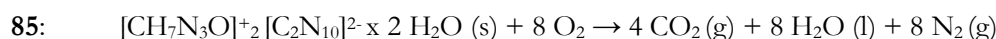
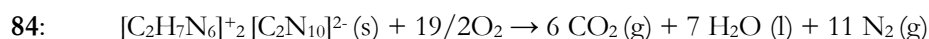
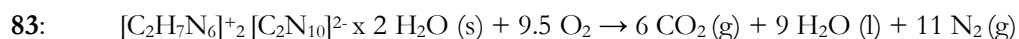
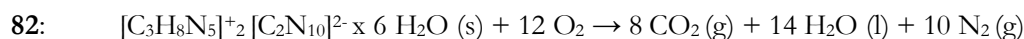
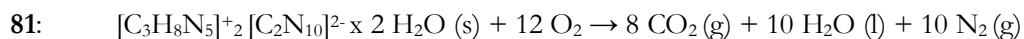
	81	82	83	84	85
Formula	C ₈ H ₂₀ N ₂₀ O ₂	C ₈ H ₂₈ N ₂₀ O ₆	C ₆ H ₁₈ N ₂₂ O ₂	C ₆ H ₁₄ N ₂₂	C ₄ H ₁₆ N ₁₆ O ₄
MW (g mol ⁻¹)	428.44	500.51	430.35	394.33	352.28
T _m (°C) ^a	-	~119	-	-	127
T _d (°C) ^b	197	194.3	183	212	127, 160
N (%) ^d	65.4	56.0	71.6	78.2	63.6
Ω (%) ^e	-89.6	-76.7	-70.6	-77.1	-54.5
ρ (g cm ³) ^f	1.441	1.396	1.546	1.708	1.638
ΔU _{comb.} / cal g ⁻¹ g ^h	-3800(30)	-4190(15)	-3000(10)	-3380(100) [-2775]	-2455(15)
ΔU _f / kJ kg ⁻¹ h ⁱ	+2800(100) [+4528]	+3386(60) [+3781]	+2210(40) [+5057]	+3200(300) [+1442]	-560(60) [+3093]
ΔH _f / kJ kg ⁻¹ h ^j	+2600(100) [+4424]	+3220(60) [+3692]	+2030(40) [+4954]	+3000(300) [+1329]	-730(60) [+2987]

	86	87	88	89	91a	92
Formula	C ₈ H ₁₆ N ₂₀	C ₈ H ₁₆ N ₂₀	C ₆ H ₁₄ N ₂₂	C ₄ H ₁₂ N ₁₆ O ₂	C ₄ H ₆ N ₁₀	C ₄ H ₆ N ₁₀
MW (g mol ⁻¹)	392.35	392.19	394.39	316.25	194.19	194.19
T _m (°C) ^a	-	-	-	121	-	- ^[2]
T _d (°C) ^b	193	193.2	170	121, 145	205	170 ^[2]
N (%) ^d	71.4	71.4	78.1	70.9	72.1	72.1
Ω (%) ^e	-97.8	-97.9	-77.1	-60.7	-90.6	-90.6
ρ (g cm ³) ^f	1.431	1.412	1.427	1.614	1.520 ^[10]	1.515 ^[2]
ΔU _{comb.} / cal g ⁻¹ g ^h	-4000(10) [-4465]	-4158(20) [-4434]	-3400(20) [-3925]	-2865(20) [-3282]	-3950(25)	-4020(20)
ΔU _f / kJ kg ⁻¹ h ⁱ	+3840(30) [+4944]	+3652(86) [4821]	+4110(70) [+5518]	+1700(75) [+3445]	+4110(100)	+4410(70)
ΔH _f / kJ kg ⁻¹ h ^j	+3660(30) [+4831]	+3475(86) [4707]	+3930(70) [+5405]	+1527(75) [+3328]	+4010(100)	+4250(70)

^aChemical melting point and ^bDecomposition point (DSC onsets) from measurement with $\beta = 5$ °C min⁻¹; ^dNitrogen percentage; ^eOxygen balance according to ref. [38]; ^fDensity from X-ray measurements; ^hExperimentally determined (oxygen bomb calorimetry) constant volume energy of combustion; ⁱUncertainty in brackets (); ^jExperimentally determined (back-calculated from ΔU_{comb.}) energy of formation; ^kExperimentally determined enthalpy of formation. ^gCalculated values in [] brackets (see *Chapter IV* for calculation method).

All materials have nitrogen contents between ~56 and 78% and highly negative oxygen balances (Ω) similar to TNT (Ω = -74.0%) between -71 and -98%. The densities, either calculated from the X-ray measurements or determined experimentally using a picnometer, are relatively low (~1.40-1.55 g cm⁻³) except for the semicarbazidium salts **85** and **89** and specially the guanazinium salt **84**, that has an outstandingly high value of $\rho = 1.708$ g cm⁻³ (see X-ray structure discussion). The experimentally determined energies of combustion have highly negative values in the range from -2400 to -4200 cal g⁻¹. The energies of formation (ΔU_f) of salts **81–89** were back-calculated from the energies of combustion on the basis of their combustion equations (see

below), Hess's Law, the known standard heats of formation for water and carbon dioxide^[43] and a correction for change in gas volume during combustion. No corrections for the non-ideal formation of nitric acid (typically ~5% of the nitrogen content reacts to form HNO₃) were made.



The ΔU°_f values for the 5,5'-azotetrazolate salts studied here, with the exception of **85**, are all highly positive and higher in the case of the anhydrous species, as expected. Exchange of a methyl group in **81** and **86** for an amino group in **83** and **88** would be expected to increase the energies of formation, however this is only observed in the case of the anhydrous species **88**. **83** has a relatively low value of $\Delta U^\circ_f = +2200(40) \text{ kJ kg}^{-1}$, which is, however, still higher than that of the 1,4,5-trimethyltetrazolium salt described in the literature,^[8] whereas the anhydrous salts **84**, **86**, **87** and **88** show considerably greater positive heats of formation comparable to bishydrazinium 5,5'-azotetrazolate (**HZT**, **93**) for which $\Delta U^\circ_f = +3700 \text{ kJ kg}^{-1}$. Lastly, the two neutral and isomeric 5,5'-azotetrazole derivatives (**91a** and **92**) are also highly endothermic compounds with nearly identical values within the limits of uncertainty.

The 5,5'-azotetrazolate salts synthesized have detonation velocities (D) that vary within a narrow range and take values around 8000 m s^{-1} for all compounds apart from **84** (Table 7.3), higher than TNT ($D = 7171 \text{ m s}^{-1}$) but lower than RDX ($D = 8885 \text{ m s}^{-1}$). The detonation pressures (P) for the same compounds have values around 21.0 GPa and are also comparable to that of TNT ($P = 20.5 \text{ GPa}$). The higher density value calculated for **84** ($\rho = 1.708 \text{ g cm}^{-3}$) accounts for its highest detonation velocity among all 5,5'-azotetrazole derivatives studied here ($D = 8702 \text{ m s}^{-1}$), comparable to that of RDX but with a much lower sensitivity, making the

compound interesting as a prospective high-performing compound with a reduced sensitivity. On the other side, due to sharing the same sum formula **91a** and **92** have very similar detonation parameters between them and with the salts described above (**91a**: $D = 7941 \text{ m s}^{-1}$, $P = 22.0 \text{ GPa}$ and **92**: $D = 8017 \text{ m s}^{-1}$, $P = 22.5 \text{ GPa}$), similar to some of the 5,5'-azotetrazolate salts in this chapter regardless of the lower nitrogen content and as a consequence of their higher density. Lastly, it must be said that the calculated detonation parameters and heats of formation, predicted using electronic energies (calculated by the MP2 method), tend to be overestimated (see Tables 7.3, 7.4 and 7.A6). This is an important issue since most of the performance parameters discussed in the literature are based on calculations and not on experimental data from calorimetric measurements. The result is overestimations of (at least) ~5% in the detonation velocities, therefore, compounds, which have predicted detonation velocities (using electronic energies) of ~8400 m s^{-1} should have experimental detonation velocities (from calorimetric measurements) of ~8000 m s^{-1} . In general, this fits nicely with the order of magnitude of the error in the detonation velocities of the 5,5'-azotetrazolate salts described here. Thus we conclude that most of the materials discussed in this section are in many cases as high-performing as those described in the literature. This topic will be more accurately addressed in *Chapter VI*.

Due to the negative oxygen balances of the materials studied here, it is of interest to study the performance of mixtures with an oxidizer at a neutral oxygen balance in order to further increase the performance values. Mixtures of the 5,5'-azotetrazole derivatives with AN (Table 7.A1) show, only a slight increase in D for all compounds except for **84** for which the performance of the mixture is predicted to decrease. In any case the values are at least as good as those calculated for TNT formulations with AN ($D = 8086 \text{ m s}^{-1}$ and $P = 25.4 \text{ GPa}$). However, formulations with ADN (Table 7.A2) have a much better predicted performance than the stand-alone energetic compounds with values higher than those calculated for TNT + ADN ($D = 8739 \text{ m s}^{-1}$ and $P = 31.7 \text{ GPa}$) and approaching those of RDX + ADN ($D = 9091 \text{ m s}^{-1}$ and $P = 34.9 \text{ GPa}$). Lastly, combination of **84** with RDX, HMX or CL-20, increases the detonation velocity and pressure, more significantly in formulations with the more dense CL-20 (Table 7.A3).

Apart from the detonation parameters calculated using the EXPLO5 computer-code, another method of assessing the performance of a material in a more practical way is the Koenen (steel-sleeve) test,^[44] in which the sensitivity of a material to intense heat under confinement is tested. **84**, which is (in theory) the most powerful of the compounds reported here, exploded when using port sizes of 10 and 8 mm, resulting in 3 and 4 fragments of the steel-sleeve, respectively (at least 3 fragments are necessary to be able to consider it an explosion), however, many grams of the yellow compound were found on the test bench after the explosion, which means that the

reaction was not complete as can be seen from the smoke in the pictures and a much better performance could potentially be achieved. This is in according to the relatively poor combustion properties of the compound observed in the “flame test” (see discussion below). According to Table 7.A4, which shows a classification of the types of fragments that result after a steel-sleeve test, **84** explodes giving type F fragments (potentially type G, if the explosion would have been complete).

7.6 Long-term Stability and Response to Thermal Shock of **84**

The long-term thermal stability of **84** was measured by thermal safety calorimetry using a Systag FlexyTSC instrument^[45] in combination with a RADEX V5 oven and the SysGraph software. The sample to be measured (~300 mg) was loaded in a glass test-vessel and the tests were conducted at atmospheric pressure at a temperature ~40 °C below the decomposition temperature of the compound for a period of 48 hours. In addition to the pure compound, homogeneous mixtures of the same with copper powder were also tested in order to simulate the conditions in shell-casing found in many propellant applications. A typical Radex plot for **84**, **HBT** (*Chapter VIII*) and mixtures of both compounds with copper is shown in Figure 7.22. Both pure **84** and **84** mixed with copper show no sign of decomposition from the TSC plots or by comparing the color of the samples before and after the test. Therefore they are thermally stable over the measurements, which translates in storage periods of over 50 years at room temperature.

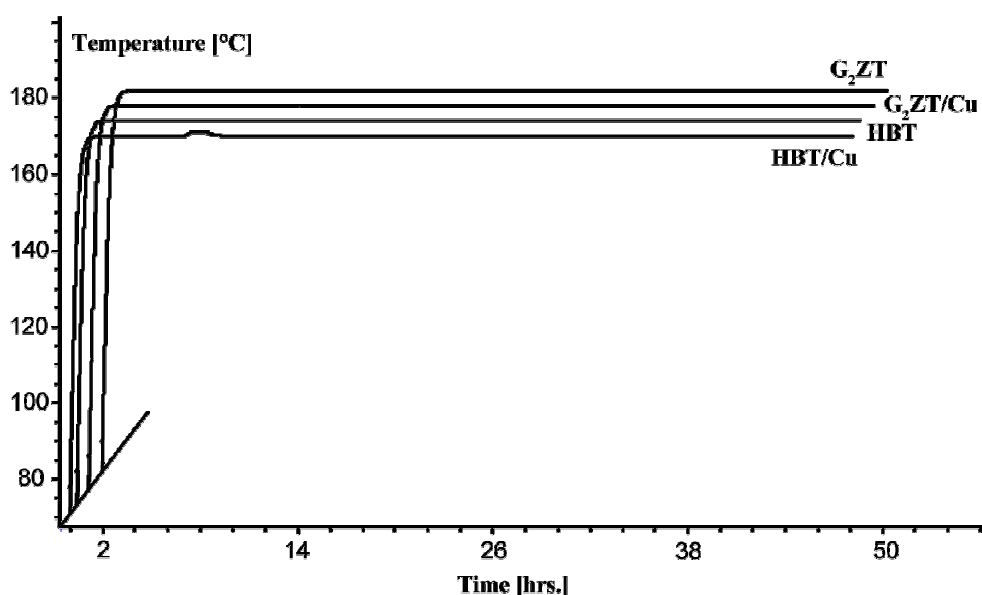


Figure 7.22 Radex plot for the long-term thermal stability of **HBT** (*Chapter VIII*) and **84** and mixtures with copper (Cu).

The response to thermal shock of **84** and its mixtures with ammonium nitrate (AN) and ammonium dinitramide (ADN) in an approximately neutral oxygen balance was assessed by putting the compound in contact with a flame (Table 7.A5). The neat powder deflagrated forming little smoke (see *Chapter VIII*), whereas when the compound was pressed into a pellet and held into a flame, it burned nicely initially but ended producing a relatively dense smoke, which puts into perspective the relatively poor combustion behavior of the compound already mentioned above (see steel sleeve test discussion). Mixtures with an oxidizer (AN or ADN) burned smokeless in both cases, however, the source of heat needs to be continuously applied to achieve complete combustion.

7.7 Decomposition Experiments

The gases formed upon decomposition of the 5,5'-azotetrazole derivatives were measured, with the exception of **85** and **89**, which have a low thermal stability and decompose in solution, making their application questionable. The mass spectra (EI^+) of the decomposition products of the nitrogen-rich salts are, as expected, dominated by a peak at $m/z = 28$ corresponding to the formation of molecular nitrogen (N_2^+). In addition, the following fragments are formed: $m/z = 12$ (C^{4+}), 13 (CH^{3+}), 14 (CH_2^{2+} , N^+), 15 (CH_3^+), 16 (CH_4^+ , NH_2^+), 17 (NH_3^+), 18 (CH_4) and 27 (HCN^+)^[46-48] for all compounds apart from **84** for which the absence of a methyl group does not allow the formation of CH_4 and hydrazine (observed in the IR spectrum) is formed instead. For **81** and **86** a small additional peak at $m/z = 41$ with its corresponding fragmentations, which is assumed to be due to the formation of acetonitrile in the gas phase upon decomposition, is found. On the other hand, for **83** and **88** dimethylamine ($m/z = 44$) forms instead of acetonitrile.

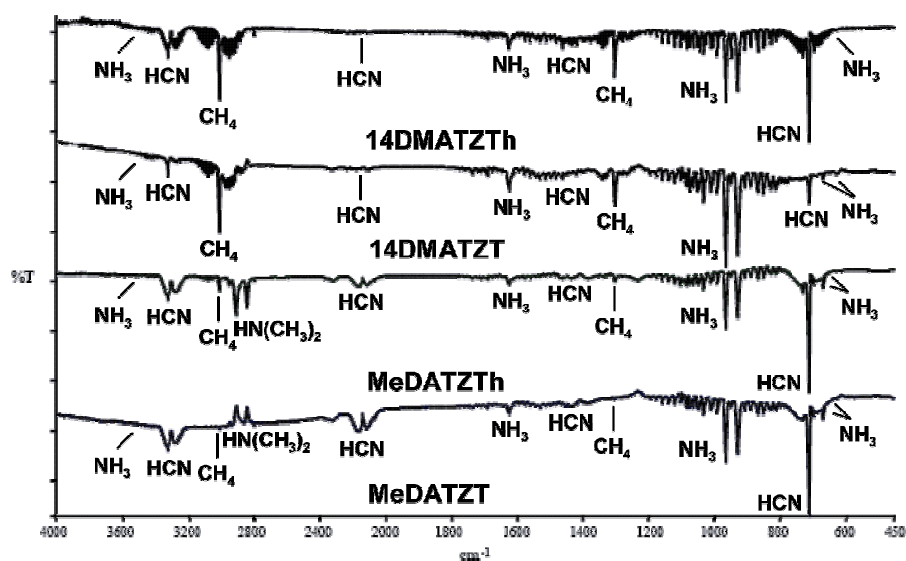


Figure 7.23 Infrared spectra of the decomposition products of **81**, **86**, **83** and **88**.

In addition to mass spectrometry, the decomposition gases were also analyzed by IR spectroscopy. Figure 7.23 shows a representative panel plot for the decomposition products of 5,5'-azotetrazolate salts (**81**, **86**, **83** and **88**). The formation of water and acetonitrile (liquid at room temperature) was not observed in the IR gas measurements due to the presence of these species in the condensed phase. The results are in accordance with the mass spectrometry measurements (Figure 7.A1). Apart from molecular nitrogen, NH_3 , HCN and CH_4 formed on decomposition (also CH_3CN for **81** and **86** and $\text{HN}(\text{CH}_3)_3$ for **83** and **88**). HCN is formed in relatively large amounts as measured from the intensities of the peaks in the EI^+ experiments. For example, in the case of **83** the amount of HCN formed adds to almost 1/3 of the amount of nitrogen gas formed. However, it must be kept in mind that HCN is much more easily ionized than N_2 , and as a consequence the amounts of HCN are expected to be highly overestimated. A closer estimation of the total amount of the gases formed upon decomposition is out of the scope of this work and a more in-depth discussion is therefore omitted.

Furthermore, the predicted decomposition gases were calculated using the ICT code (Figure 7.A2).^[49] As expected, the major gas is predicted to be molecular N_2 and the rest of the gases are very similar for the DMAT^{++} salts on one side and for the MeDAT^{++} salts on the other. The main difference is, as expected, the formation of water, not observed in the experimental measurements due to the presence of the same in the condensed phase. The replacement of a methyl group in the DMAT^{++} salts by an amino group in the MeDAT^{++} salts is anticipated to produce higher amounts of NH_3 and lower amounts of CH_4 , as observed experimentally, although, ammonia forms in smaller amounts than expected. In addition, for compounds **81** and **83**, the program predicts the formation of minute amounts of CO and CO_2 not observed by neither MS nor IR experiments. This is probably due to the fact that the crystal water remains as such after combustion and does not react to oxidize the carbon atoms in the compounds. In theory, relatively high molar amounts of H_2 would be expected from the calculation of the explosion gases of all compounds, however, this could not be observed in the MS due to the low molecular mass of hydrogen, which falls out of the measuring range. According to the ICT code only very small amounts of HCN form upon decomposition when in fact relatively large amounts could be detected by both IR and MS. Lastly, the formation of CH_3CN and $\text{HN}(\text{CH}_3)_2$ were not predicted by the code.

7.8 Conclusions

Convenient syntheses for a new family of nitrogen-rich 5,5'-azotetrazolate salts (**81–89**) and two previously known neutral 5,5'-azotetrazoles (**91a** and **92**) are reported, many of which allow to obtain the materials on a multigram scale using non-hazardous and cheap materials (e.g., the improved synthesis for **92** presented here avoids using highly sensitive silver 5,5'-azotetrazolate). The new compounds were fully characterized by analytical and spectroscopic methods. In addition, their crystal structures in the solid state were determined by diffraction techniques. The hydrogen-bonding networks in all compounds are described in terms of graph-set analysis. All compounds turned out to be insensitive to shock, friction and electrostatic discharge as determined by standard BAM tests and thermally stable to temperatures above 170 °C (DSC onsets), with the exception of the semicarbazidium salts **85** and **89**, which have a limited stability decomposing slowly in solution. In addition, bomb calorimetry measurements allowed the calculation of the detonation parameters (EXPLO5), which were compared with the calculated ones (MP2) of the new salts (**81–89**) revealing high performances in the range between TNT and RDX but with more environmentally-friendly explosion gases, as predicted by the ICT code and measured experimentally. Furthermore, the detonation velocity of **84** approaches that of RDX but its reduced sensitivity makes the compound interesting for application as a new nitrogen-rich material with a high performance and reduced sensitivity for use in propellants or propellants charges. Lastly, three of the compounds described in this chapter have been send to the U.S. Army for further testing and studies.

7.9 Experimental Section

Caution! *Although no problems occurred during the synthesis and handling of the materials studied in this work, silver azotetrazolate, aminotetrazoles and their derivatives are energetic materials and tend to explode under certain conditions. All HEDMs should be treated with respect and appropriate safety precautions should be taken at all times. Laboratories and personnel should be properly grounded and safety equipment such as Kevlar gloves, leather coat, face shield and ear plugs are necessary, in particular when working on a larger scale.*

General Method. All chemicals and solvents (analytical grade) were used as supplied by Sigma-Aldrich Inc. Disodium 5,5'-azotetrazolate pentahydrate^[1d] and 1,4-dimethyl-5-aminotetrazolium^[21] and 1,5-diamino-4-methyltetrazolium^[12] iodides were synthesized according to known procedures. ¹H, and ¹³C NMR spectra were recorded on a JEOL Eclipse 400 instrument in DMSO-*d*₆ at or near 25 °C. The chemical shifts are given relative to tetramethylsilane as external standard. Infrared (IR) spectra were recorded on a Perkin-Elmer Spectrum One FT-IR instrument as KBr pellets at 20 °C. Transmittance values are qualitatively described as “very strong” (vs), “strong” (s), “medium” (m) and “weak” (w). Raman spectra were recorded on a Perkin-Elmer Spectrum 2000R NIR FT-Raman instrument equipped with a Nd:YAG laser (1064 nm). The intensities are reported as percentages of the most intense peak and are given in parentheses. Elemental analyses were performed with a Netsch Simultaneous Thermal Analyzer STA 429. Melting points were determined by differential scanning calorimetry (Linseis DSC PT-10 instrument,^[50] calibrated with standard pure indium and zinc). Measurements were performed at a heating rate of 5 °C min⁻¹ in closed aluminum sample pans with a 1 µm hole in the top for gas release under a nitrogen flow of 20 mL min⁻¹ with an empty identical aluminum sample pan as a reference.

Explosion experiments. For the analysis of the explosion gases of all compounds, a steel bomb (dried at 100 °C for several days) with a volume of 100 mL was loaded with the corresponding salt (~100 mg). One end of the bomb was sealed and the other end was attached to a valve for gas transfer after the explosion had occurred. The bomb was evacuated with a vacuum line (~10⁻³ mbar) and the valve was closed. The explosion and/or decomposition was induced by placing the compound in the bottom of the bomb and heating it directly for 5-10 minutes with a Bunsen burner. The explosion products were allowed to expand in the bomb and after cooling the apparatus was attached to a mass spectrometer (JEOL MStation JMS 700).^[51] The reservoir of the spectrometer was evacuated during 15 minutes prior to opening the valve in the bomb and allowing the decomposition gases to diffuse into the ionization source. The explosion gases were then analyzed by mass spectrometry using electron impact (EI) mode (mass range 1 – 120, 1 scan per second). The same bomb was attached to a previously evacuated IR gas cell (NaCl windows) and the gases were left to slowly diffuse into the cell by shortly opening the valve. The evacuated IR cell was measured as the background and subsequently the IR spectrum of the sample was recorded (5 scans, 4000 – 450 cm⁻¹, resolution = 4.0) on a Perkin-Elmer Spektrum One FT-IR instrument.^[52]

Bomb Calorimetry. For all calorimetric measurements, a Parr 1356 bomb calorimeter (static jacket) equipped with a Parr 207A oxygen bomb for the combustion of highly energetic materials was used.^[53] A Parr 1755 printer, furnished with the Parr 1356 calorimeter, was used to produce a permanent record of all activities within the calorimeter. The samples (~200 mg each) were carefully mixed with ~800 mg analytical grade benzoic acid and pressed into pellets, which were subsequently burned in a 3.05 MPa atmosphere of pure oxygen. The experimentally determined constant volume energies of combustion were obtained as the averages of five single measurements. The calorimeter was calibrated by the combustion of certified benzoic acid in an oxygen atmosphere at a pressure of 3.05 MPa.

Synthesis of 1,4-Dimethyl-5-aminotetrazolium 5,5'-Azotetrazolate Dihydrate (81): Sodium azotetrazolate pentahydrate (5.003 g, 16.7 mmol) was dissolved in 50 mL hot water yielding a clear bright yellow solution and 1,4-dimethyl-5-aminotetrazolium iodide (8.076 g, 33.5 mmol) was added neat in small portions. The reaction mixture was boiled for 1 hour before the oil bath and stirring were switched off. Immediate precipitation of the product was observed as the reaction mixture cooled. The resulting solution was stored in a refrigerator for 2 hours. After this time the yellow powder was filtered and recrystallized from a minimal amount of hot water. After cooling in a refrigerator for 2 further hours the precipitated solid was filtered, washed with 10 mL cold water, 30 mL acetone and 30 mL ether. Lastly, the product was left to air-dry (5.491 g, 79%). Several crystals of the product suitable for X-ray structure analysis could be obtained together with powdery bulk material when the same reaction was conducted in a 1 mmol scale and the mother liquors were kept in the fridge for 1 week. C₈H₂₀N₂₀O₂ (calc./found): C 22.42 / 22.49, H 4.71 / 4.60, N 65.40 / 65.68; DSC (5 °C min⁻¹, °C): 84 (-H₂O), 197 (m.p. + dec.); m/z (FAB⁺, xenon, 6 keV, m-NBA matrix): 114.2 [DMAT]⁺; m/z (FAB⁻, xenon, 6 keV, m-NBA matrix): 165.2 [C₂N₁₀H]⁻; ¹H NMR (DMSO-*d*₆, 400.18 MHz, 25°C, TMS) δ/ppm: 3.8 (CH₃), 8.7 (NH₂, H₂O); ¹³C{¹H} NMR (DMSO-*d*₆, 100.63 MHz, 25°C, TMS) δ/ppm: 31.7 (CH₃), 148.5 (C-NH₂), 173.1 ([N₄C=N=N-CN₄]²⁻); ¹⁵N NMR (solid state, 25°C) δ/ppm: -317.1 (-NH₂), -180.0 (N-CH₃), -71.2 (CN_β), -28.8 (-N=N-), +0.4 (CN_α), +89.5 (-N_{azo}=N_{azo}-); Raman $\tilde{\nu}$ / cm⁻¹ (rel. int.): 2961(3) 1487(58) 1420(14) 1382(100) 1356(3) 1191(1) 1084(10) 1058(47) 921(11) 790(6) 588(2) 328(1); IR $\tilde{\nu}$ / cm⁻¹ (KBr, rel. int.): 3350(s) 2941(s) 2885(s) 2696(m) 2086(w) 1838(w) 1713(vs) 1663(m) 1528(m) 1454(m) 1429(m) 1416(m) 1398(s) 1253(w) 1198(m) 1178(w) 1156(m) 1081(w) 1061(w) 1048(w) 1026(w) 995(w) 922(w) 780(s) 730(m) 698(m) 586(w) 558(w) 517(w).

Decomposition Experiments. MS (EI): *m/z* = 12 (0.2, C⁺), 13 (0.4, CH⁺), 14 (4.8, CH₂²⁺, N⁺), 15 (7.1, CH₃⁺), 16 (8.4, CH₄⁺, NH₂⁺, O²⁺), 17 (2.4, NH₃⁺, OH⁺), 18 (2.7, H₂O⁺), 26 (2.8, CN⁺), 27 (17.5, HCN⁺), 28 (100.0, N₂⁺), 38 (1.4, CCN³⁺), 39 (1.9, CHCN²⁺), 40 (4.5, CH₂CN⁺), 41 (7.2, CH₃CN⁺); IR (Gas): Δ*v* (cm⁻¹) = 3452 (vw, NH₃), 3332 (m, HCN), 3282 (m, HCN), 3083 (m, CH₄), 3011 (s, CH₄), 2951 (m, CH₄), 2166 (vw, HCN), 2102 (vw, HCN), 1621 (w, NH₃), 1430 (vw, HCN), 1381 (vw, HCN), 1302 (s, CH₄), 965 (vs, NH₃), 926 (vs, NH₃), 732 (m, HCN), 713 (vs, HCN), 682 (m, HCN), 629 (vw, NH₃).

Synthesis of 1,3-Dimethyl-5-aminotetrazolium 5,5'-Azotetrazolate Hexahydrate (82): Sodium 5,5'-azotetrazolate pentahydrate (0.61 g, 2.02 mmol) was dissolved in hot water (6 ml) at about 70 °C and 1,3-dimethyl-5-aminotetrazolium iodide (0.97 g, 4.01 mmol) was added to this hot solution. The solution was then heated for 3 hours at 100 °C. After cooling slowly in an oil bath the yellow precipitate was filtered and washed with acetone and ether giving a yellow solid (0.701 g, 69%). $C_8H_{28}N_{20}O_6$ (calc./found): C 19.20 / 19.28, H 5.64 / 5.23, N 55.98 / 56.18; DSC (5 °C/min, °C, onset): ~119 (m.p.), 194.3 (dec.t.); m/z (FAB⁺, xenon, 6 keV, m-NBA matrix): 114.1 [Cation]⁺, (FAB⁻, xenon, 6 keV, m-NBA matrix): 165.1 [Anion][H]⁺; ¹H NMR (DMSO-*d*₆, 399.78 MHz, TMS) δ/ppm: 8.23 (s, 2H, NH₂), 4.48 (s, 3H, C3H₃), 3.98 (s, 12H, H₂O), 3.85 (s, 3H, C2H₃); ¹³C{¹H} NMR (DMSO-*d*₆, 100.52 MHz, TMS) δ/ppm: 173.32 (2C, [N₄C-N=N-CN₄]²⁻), 158.17 (1C, C1-NH₂), 42.58 (1C, C3H₃), 34.24 (1C, C2H₃); Raman Δν/cm⁻¹ (rel. int.): 2957(1), 1488(48), 1420(5), 1386(100), 1358(2), 1197(1), 1162(1), 1099(2), 1082(19), 1065(26), 919(7), 854(2), 626(3), 346(1), 292(1), 239(1); IR Δν/cm⁻¹ (KBr, rel. int.): 3429(m), 3291(m), 3225(m), 3061(m), 2725(vw), 2215(vw), 2075(vw), 1675(s), 1622(m), 1457(w), 1393(m), 1365(w), 1289(w), 1244(w), 1187(vw), 1178(vw), 1154(vw), 1142(vw), 1129(vw), 1074(vw), 1041(vw), 1027(vw), 1019(vw), 853(w), 775(w), 732(w), 674(w), 616(w), 555(w).

Synthesis of 1,5-Diamino-4-methyl-tetrazolium 5,5'-Azotetrazolate Dihydrate (83): Sodium azotetrazolate pentahydrate (0.148 g, 0.5 mmol) was dissolved in 2 mL hot water and 1,5-diamino-4-methyltetrazolium iodide (0.244 g, 1.1 mmol) in 1 mL hot water was added to the bright yellow solution. The reaction mixture was brought to boiling for 10 minutes and subsequently stored in a refrigerator for 1 hour. Once again, the mixture was boiled for 15 minutes and left to slowly crystallize to room temperature in an oil bath and in the fridge for 2 hours yielding orange crystals suitable for X-ray structure analysis (0.153 g, 72%). $C_6H_{18}N_{22}O_2$ (calc./found): C 16.74 / 16.88, H 4.22 / 4.21, N 71.61 / 71.32; DSC (5 °C min⁻¹, °C): 92 (-H₂O), 183 (m.p. + dec.); m/z (FAB⁺, xenon, 6 keV, m-NBA matrix): 115.3 [MeDAT]⁺; m/z (FAB⁻, xenon, 6 keV, m-NBA matrix): 165.2 [C₂N₁₀H]⁻; ¹H NMR (DMSO-*d*₆, 400.18 MHz, 25°C, TMS) δ/ppm: 3.9 (CH₃), 7.2 (NH₂, H₂O); ¹³C{¹H} NMR (DMSO-*d*₆, 100.63 MHz, 25°C, TMS) δ/ppm: 34.5 (CH₃), 147.7 (C-NH₂), 173.2 ([N₄C-N=N-CN₄]²⁻); ¹⁵N NMR (solid state, 25°C) δ/ppm: -317.0 (C-NH₂), -308.9 (N-NH₂), -180.8 (N-CH₃), -170.7 (N-NH₂), -82.1 (CN_β), -58.7 (N13), -47.2 (N14), -0.3 (CN_α), +90.1 (-N_{azo}=N_{azo}-); Raman $\tilde{\nu}$ / cm⁻¹ (rel. int.): 2972(6) 1479(46) 1422(19) 1382(100) 1089(17) 1057(44) 921(12) 790(7) 278(5); IR $\tilde{\nu}$ / cm⁻¹ (KBr, rel. int.): 3345(s) 3193(s) 3063(s) 2958(s) 2087(w) 1721(vs) 1627(w) 1499(w) 1450(w) 1416(m) 1400(s) 1384(m) 1245(w) 1213(w) 1192(w) 1157(w) 1114(w) 1083(w) 1048(w) 1040(w) 1001(w) 923(w) 875(w) 787(m) 756(m) 732(m) 681(m) 597(w) 559(w) 531(w).

Decomposition Experiments. MS (EI): m/z = 12 (0.8, C⁴⁺), 13 (0.3, CH³⁺), 14 (3.8, CH₂²⁺, N⁺), 15 (1.1, CH₃⁺), 16 (3.9, CH₄⁺, NH₂⁺, O²⁺), 17 (4.7, NH₃⁺, OH⁺), 18 (1.5, H₂O⁺), 26 (4.5, CN⁺), 27 (26.1, HCN⁺), 28 (100.0, N₂⁺), 44 (2.3, N(CH₃)₂⁺); IR (Gas): Δν (cm⁻¹) = 3450 (vw, NH₃), 3330 (w, HCN), 3282 (w, HCN), 3083 (w, CH₄), 3012 (w, CH₄), 2918 (vw, CH₄), 2850 (m, HN(CH₃)₂), 2810 (m, HN(CH₃)₂), 2166 (w, HCN), 2102 (w, HCN), 1621 (w, NH₃), 1430 (vw, HCN), 1380 (vw, HCN), 1302 (w, CH₄), 965 (s, NH₃), 926 (s, NH₃), 732 (m, HCN), 713 (vs, HCN), 682 (w, HCN), 667 (w, NH₃), 629 (w, NH₃).

Synthesis of bis(3,4,5-triamino-1,2,4-triazolium) 5,5'-azotetrazolate (84): To an aqueous solution of sodium azotetrazolate pentahydrate (31.01 g, 103.25 mmol) in 150 mL hot water was added 3,4,5-triamino-1,2,4-triazolium bromide (40.185 g, 206.50 mmol) in 100 mL hot water. The mixture was stirred and boiled for 3 hours and the title compound, only slightly soluble in hot water, started to precipitate. After slow cooling to room temperature the yellow solid was filtered, washed with a small amount of cold water and methanol and air-dried (37.24 g, 91.6%). Crystals suitable for X-ray analysis were obtained by recrystallization from water of a small amount of the compound. $C_6H_{14}N_{22}$ (calc./found, %): C 18.28/18.22, H 3.58/3.68, N 78.15/77.95, DSC (5 °C min⁻¹, °C): 212 (m.p. + dec); m. p. (Büchi B-540, uncorrected): 211.3-212.4 °C, ¹H NMR (DMSO-*d*₆, 400.18 MHz, 25°C, TMS) δ/ppm: 6.60 (4H, s, C-NH₂), 5.58 (2H, s, N-NH₂); ¹³C{¹H} NMR (DMSO-*d*₆, 100.63 MHz, 25°C, TMS) δ/ppm: 173.24 (2C, [N₄C-N=N-CN₄]²⁺), 150.31 (2C, C-NH₂); ¹⁵N{¹H}-RAMP CP MAS NMR (DMSO-*d*₆, 50.70 MHz, 25 °C, MeNO₂) δ/ppm: 9.4, 4.7, 1.8 and -0.9 ppm (CN_α), -52.3, -63.0, -82.9 and -85.5 ppm (CN_β), -188.9 and -189.2 ppm (2N, N9/N10), -239.9 ppm (1N, N7), -318.4, -323.9 and -330.0 ppm (-NH₂ groups). Raman $\tilde{\nu}$ / cm⁻¹ (rel. int.): 3275(1), 1491(83), 1418(16), 1382(100), 1074(18), 1060(34), 1047(53), 1031(18), 923(15), 773(12), 360(3). IR $\tilde{\nu}$ / cm⁻¹ (KBr, rel. int.): 3434w, 3178m, 1707m, 1658s, 1613m, 1443w, 1391m, 1102w, 1007w, 879s, 767m, 732s, 580s, 565s.

Decomposition Experiments. MS (EI): *m/z* = 12 (0.6, C⁺), 13 (0.3, CH³⁺), 14 (3.4, CH₂²⁺, N⁺), 15 (0.4, CH₃⁺), 16 (10.0, CH₄⁺, NH₂⁺), 17 (13.6, NH₃⁺), 26 (5.8, CN⁺), 27 (38.0, HCN⁺), 28 (100.0, N₂⁺), 31 (0.1, NH₂NH⁺), 32 (0.2, NH₂NH₂⁺), 38 (0.0, CCN³⁺), 39 (0.0, CHCN²⁺), 40 (0.1, CH₂CN⁺), 41 (0.2, CH₃CN⁺); IR (Gas): Δ*v* (cm⁻¹) = 3450 (w, NH₃), 3333 (s, HCN), 3285 (m, HCN), 2166 (w, HCN), 2102 (w, HCN), 1623 (s, NH₃), 1431 (w, HCN), 1382 (w, HCN), 964 (vs, NH₃), 925 (vs, NH₃), 731 (m, HCN), 714 (vs, HCN), 681 (m, HCN), 667 (w, NH₃), 624 (vw, NH₃).

Synthesis of Semicarbazidium 5,5'-Azotetrazolate Dihydrate (85): Sodium 5,5'-azotetrazolate pentahydrate (1.017 g, 3.39 mmol) was suspended in 10 mL water and the suspension was gently warmed up until all insoluble material had dissolved by means of a heat gun. A solution of semicarbazidium chloride (0.752 g, 6.78 mmol) in 5 mL water at room temperature was added at once and the clear dark orange solution was stirred for two minutes. Crystallization was induced by scratching the sides of the flask with a glass stab and the solution was left to stand overnight yielding brown/orange crystals of the compound. Elemental analysis showed that the compound formed as the dehydrated species and no further purification was necessary (0.578 g, 48%). $C_4H_{16}N_{16}O_4$ (calc./found): C 13.64 / 13.75, H 4.58 / 4.45, N 63.62 / 63.50; DSC (5 °C min⁻¹, °C): 96 (-H₂O), 127 (m.p. + dec.), ~160 (dec.); *m/z* (FAB⁺, xenon, 6 keV, m-NBA matrix): 76.1 (70, cation); *m/z* (FAB⁻, xenon, 6 keV, m-NBA matrix): 165.1 [C₂N₁₀H]⁻; ¹H NMR (DMSO-*d*₆, 400.18 MHz, 25°C, TMS) δ/ppm: 9.48 (3H, s, NH₃⁺), 8.50 (1H, s, NH), 6.57 (2H, s, NH₂), 3.89 (4H, s, H₂O); ¹³C{¹H} NMR (DMSO-*d*₆, 100.63 MHz, 25°C, TMS) δ/ppm: 157.9 (2C, C=O), 173.1 (2C, [N₄C-N=N-CN₄]²⁺); Raman $\tilde{\nu}$ / cm⁻¹ (rel. int.): 1505(60) 1430(17) 1388(100) 1203(3) 1085(15) 1065(60) 1040(14) 925(15) 357(1); IR $\tilde{\nu}$ / cm⁻¹ (KBr, rel. int.): 3348(vs) 3232(vs) 2924(s)

2638(s) 2089(w) 2066(w) 2012(w) 1683(s) 1577(s) 1537(s) 1454(m) 1405(s) 1396(m) 1267(m) 1202(m) 1163(w) 1147(w) 1130(w) 1081(w) 1055(w) 1035(w) 938(w) 767(w) 742(m) 684(w) 666(w) 614(w) 570(w) 528(m).

Synthesis of 1,4-Dimethyl-5-aminotetrazolium 5,5'-Azotetrazolate (86). *Method A:* Four equal portions of sodium azotetrazolate pentahydrate (total 1.003 g, 3.3 mmol) were suspended in 4 x 5 mL water in four separate plastic test-tubes. Silver nitrate (total 1.245 g, 7.3 mmol) was then added in approximately equal amounts to each tube. Immediate precipitation of highly sensitive silver azotetrazolate was observed and the four reaction mixtures were stirred for 15 further minutes to ensure completion of the reaction. The mother liquors were centrifuged and the remaining orange solid was washed 2 times with 5 mL water with subsequent centrifuging. The water was eliminated by washing 2 times with 5 mL dry methanol. The silver salt, wet with methanol, was suspended in 5 mL fresh, dry methanol and 1,4-dimethyl-5-aminotetrazolium iodide (1.590 g, 6.6 mmol) was added in equal portions to the reaction tubes. After 30 minutes reaction time yellow silver iodide was separated by filtration and the four methanol fractions were combined and rotavaporated to dryness yielding yellow amorphous material, which was scratched out of the flask and recrystallized from little hot dry methanol (0.801 g, 62%). Crystals of **86** suitable for X-ray analysis were obtained when the same reaction was carried out in water and the solvent was left to slowly evaporate.

Method B: Alternatively, the water in **81** (1.151 g, 2.7 mmol) could be eliminated quantitatively when this was heated under high-vacuum at 80 °C for 7 days yielding 1.048 g of pure product. C₈H₁₆N₂₀ (calc./found): C 24.48 / 24.42, H 4.11 / 4.04, N 71.41 / 71.30; DSC (5 °C min⁻¹, °C): 193 (m.p. + dec.); m/z (FAB⁺, xenon, 6 keV, m-NBA matrix): 114.2 [DMAT]⁺; m/z (FAB⁻, xenon, 6 keV, m-NBA matrix): 165.2 [C₂N₁₀H]⁻; ¹H NMR (DMSO-*d*₆, 400.18 MHz, 25°C, TMS) δ/ppm: 3.6 (CH₃), 8.5 (NH₂); ¹³C{¹H} NMR (DMSO-*d*₆, 100.63 MHz, 25°C, TMS) δ/ppm: 32.4 (CH₃), 148.8 (C-NH₂), 173.3 ([N₄C-N=N-CN₄]²⁻); Raman $\tilde{\nu}$ / cm⁻¹ (rel. int.): 2951(2) 1490(25) 1468(22) 1410(14) 1378(100) 1353(4) 1197(2) 1082(8) 1066(14) 1057(30) 1031(7) 919(8) 791(5) 325(2) 271(1); IR $\tilde{\nu}$ / cm⁻¹ (KBr, rel. int.): 3341(s) 3049(s) 2937(s) 2887(s) 2696(m) 1714(vs) 1663(m) 1528(m) 1453(m) 1430(m) 1416(m) 1398(s) 1348(w) 1253(w) 1198(m) 1178(w) 1156(m) 1080(w) 1061(w) 1048(m) 1026(w) 995(m) 921(w) 789(s) 780(s) 730(s) 696(s) 586(w) 558(w) 517(w).

Decomposition Experiments. MS (EI): *m/z* = 12 (0.2, C⁴⁺), 13 (0.3, CH³⁺), 14 (4.2, CH₂²⁺, N⁺), 15 (4.0, CH₃⁺), 16 (5.1, CH₄⁺, NH₂⁺), 17 (5.1, NH₃⁺), 26 (0.6, CN⁺), 27 (1.1, HCN⁺), 28 (100.0, N₂⁺), 38 (0.7, CCN³⁺), 39 (1.1, CHCN²⁺), 40 (2.8, CH₂CN⁺), 41 (5.0, CH₃CN⁺); IR (Gas): Δν (cm⁻¹) = 3452 (vw, NH₃), 3334 (w, HCN), 3284 (vw, HCN), 3084 (m, CH₄), 3012 (s, CH₄), 2951 (m, CH₄), 2166 (vw, HCN), 2102 (vw, HCN), 1620 (w, NH₃), 1431 (vw, HCN), 1381 (vw, HCN), 1302 (s, CH₄), 966 (vs, NH₃), 926 (vs, NH₃), 732 (vw, HCN), 713 (w, HCN), 682 (vw, HCN), 668 (w, NH₃), 629 (w, NH₃).

Synthesis of 1,3-Dimethyl-5-aminotetrazolium 5,5'-Azotetrazolate (87): Drying **82** under high vacuum for four days at 80 °C resulted in the formation of the title compound in quantitative yield. C₈H₁₆N₂₀ (calc./found): C 24.49 / 24.35, H 4.11 / 4.16, N 71.40 / 70.27; DSC (5 °C/min, °C, onset): 193.2 (dec.t.); m/z (FAB⁺, xenon, 6 keV, m-NBA matrix): 114.1 [Cation]⁺, (FAB⁻, xenon, 6 keV, m-NBA matrix): 165.1 [Anion]⁻[H]⁺; ¹H NMR (DMSO-d₆, 399.78 MHz, TMS) δ/ppm: 8.40 (s, 2H, NH₂), 4.34 (s, 3H, C3H₃), 3.92 (s, 3H, C2H₃); ¹³C{¹H} NMR (DMSO-d₆, 100.52 MHz, TMS) δ/ppm: 173.34 (2C, [N₄C-N=N-CN₄]²⁻), 158.12 (1C, C1-NH₂), 42.50 (1C, C3H₃), 34.17 (1C, C2H₃); Raman Δν/cm⁻¹ (rel. int.): 2968(2), 1483(57), 1436(2), 1412(6), 1379(100), 1353(3), 1185(1), 1070(11), 1044(41), 1027(7), 918(11), 879(1), 849(2), 629(3), 343(1), 290(1); IR Δν/cm⁻¹ (KBr, rel. int.): 3434(m), 3360(m), 3245(m), 3059(m), 2791(w), 2732(w), 2516(w), 2401(vw), 2206(vw), 2059(vw), 1675(s), 1622(m), 1451(m), 1430(m), 1385(m), 1367(w), 1289(w), 1248(w), 1185(w), 1151(w), 1114(w), 1070(w), 1035(w), 849(m), 773(w), 730(m), 676(w), 628(w), 561(w).

Decomposition Experiments. MS (EI): *m/z* = 12 (0.5, C⁴⁺), 13 (0.5, CH³⁺), 14 (3.3, CH₂²⁺, N⁺), 15 (5.3, CH₃⁺), 16 (6.9, CH₄⁺, NH₂⁺), 17 (2.1, NH₃⁺), 26 (6.6, CN⁺), 27 (30.6, HCN⁺), 28 (100.0, N₂⁺), 38 (0.2, CCN₃⁺), 39 (0.4, CHCN₂⁺), 40 (0.9, CH₂CN⁺), 41 (1.7, CH₃CN⁺); IR (Gas): Δν (cm⁻¹) = 3451 (vw, NH₃), 3332 (m, HCN), 3283 (m, HCN), 3085 (w, CH₄), 3012 (s, CH₄), 2950 (w, CH₄), 2167 (vw, HCN), 2102 (vw, HCN), 1621 (w, NH₃), 1430 (w, HCN), 1382 (vw, HCN), 1300 (m, CH₄), 965 (s, NH₃), 926 (s, NH₃), 731 (s, HCN), 713 (vs, HCN), 684 (m, HCN), 669 (vw, NH₃), 625 (vw, NH₃).

Synthesis of 1,5-Diamino-4-methyl-tetrazolium 5,5'-Azotetrazolate (88). *Method A:* Sodium azotetrazolate pentahydrate (0.522 g, 1.7 mmol) was reacted with silver nitrate (0.311 g, 1.8 mmol) in 5 mL water causing immediate precipitation of orange highly sensitive silver azotetrazolate. The reaction mixture was stirred for 5 minutes and centrifuged. The solvent was decanted off and the silver salt was freed of excess silver nitrate by washing with 5 mL water and subsequently centrifuging. The water was eliminated by washing 2 times with 5 mL dry methanol. The metathesis reaction was carried out in 5 mL dry methanol by addition of neat 1,5-diamino-4-methyltetrazolium iodide (0.300 g, 1.2 mmol) and stirring for 15 minutes. Yellow silver iodide was filtered and the solvent was removed under high vacuum leaving yellow crude product that could be recrystallized by ether diffusion into a small amount of methanol. Yellow crystals suitable for X-ray analysis and powdery material formed overnight (0.312 g, 64%).

Method B: Alternatively the dihydrated species **83** (1.081 g, 2.5 mmol) could be freed from water by heating at 80 °C under high vacuum for 5 days yielding 0.989 g of the product (quantitative yield). C₆H₁₄N₂₂ (calc./found): C 18.26 / 18.26, H 3.58 / 3.59, N 78.15 / 77.34; DSC (5 °C min⁻¹, °C): 170 (m.p. + dec); m/z (FAB⁺, xenon, 6 keV, m-NBA matrix): 115.3 [MeDAT]⁺; m/z (FAB⁻, xenon, 6 keV, m-NBA matrix): 165.2 [C₂N₁₀H]⁻; ¹H NMR (DMSO-d₆, 400.18 MHz, 25°C, TMS) δ/ppm: 3.9 (CH₃), 6.9 (NH₂); ¹³C{¹H} NMR (DMSO-d₆, 100.63 MHz, 25°C, TMS) δ/ppm: 34.9 (CH₃), 147.5 (C-NH₂), 173.3 ([N₄C-N=N-CN₄]²⁻); Raman $\tilde{\nu}$ / cm⁻¹ (rel. int.): 2969(1) 1484(52) 1414(9) 1380(100) 1353(3) 1196(1) 1158(1) 1074(16) 1049(26) 1030(5) 920(7) 790(4) 732(1) 605(1) 328(2); IR $\tilde{\nu}$ / cm⁻¹ (KBr, rel. int.): 3737(s) 3378(s)

3259(s) 2968(s) 2786(s) 2630(m) 2419(m) 2225(w) 1709(vs) 1643(m) 1603(m) 1497(w) 1456(m) 1443(m) 1427(m) 1388(sm) 1245(w) 1193(m) 1157(m) 1119(m) 1067(w) 1039(m) 1031(m) 1008(m) 934(m) 782(m) 736(m) 725(m) 694(m) 663(m) 602(w) 555(m) 527(m) 516(m).

Decomposition Experiments. MS (EI): m/z = 12 (0.4, C⁺), 13 (0.1, CH³⁺), 14 (3.4, CH₂²⁺, N⁺), 15 (0.1, CH₃⁺), 16 (1.1, CH₄⁺, NH₂⁺), 17 (1.4, NH₃⁺), 26 (1.3, CN⁺), 27 (8.3, HCN⁺), 28 (100.0, N₂⁺), 44 (2.7, N(CH₃)₂⁺); IR (Gas): $\Delta\nu$ (cm⁻¹) = 3450 (vw, NH₃), 3330 (w, HCN), 3282 (w, HCN), 3083 (vw, CH₄), 3012 (vw, CH₄), 2951 (vw, CH₄), 2917 (w, HN(CH₃)₂), 2849 (w, HN(CH₃)₂), 2166 (w, HCN), 2103 (w, HCN), 1622 (w, NH₃), 1430 (vw, HCN), 1380 (vw, HCN), 1302 (vw, CH₄), 965 (s, NH₃), 926 (s, NH₃), 732 (m, HCN), 713 (vs, HCN), 682 (m, HCN), 668 (w, NH₃), 629 (w, NH₃).

Synthesis of Semicarbazidium 5,5'-Azotetrazolate (89): The crystal water in **85** could be completely eliminated by heating the compound (0.514 g, 1.58 mmol) at 40 °C under vacuum (10⁻² mbar) over two days yielding **89** in quantitative yield and high purity as a slightly brown powder (0.497 g). C₄H₁₆N₁₆O₄ (calc./found): C 15.18 / 15.28, H 3.82 / 3.87, N 70.87 / 70.57; DSC (5 °C min⁻¹, °C): 121 (m.p. + dec.), ~145 (dec.); m/z (FAB⁺, xenon, 6 keV, m-NBA matrix): 76.1 (100, cation); m/z (FAB⁻, xenon, 6 keV, m-NBA matrix): 165.1 (100, [C₂N₁₀H]⁻); ¹H NMR (DMSO-*d*₆, 400.18 MHz, 25°C, TMS) δ /ppm: 8.50 (1H, s, NH), 8.10 (3H, s, NH₃⁺), 6.36 (2H, s, NH₂); ¹³C{¹H} NMR (DMSO-*d*₆, 100.63 MHz, 25°C, TMS) δ /ppm: 159.3 (2C, C=O), 171.2 (2C, [N₄C-N=N-CN₄]²⁻); Raman $\tilde{\nu}$ / cm⁻¹ (rel. int.): 1500(46) 1422(14) 1380(100) 1189(2) 1156(2) 1079(10) 1049(51) 1033(19) 923(11) 348(1) 190(1); IR $\tilde{\nu}$ / cm⁻¹ (KBr, rel. int.): 3347(vs) 3234(vs) 2926(s) 2681(m) 2091(w) 2066(w) 2011(w) 1683(vs) 1581(vs) 1536(s) 1459(w) 1404(s) 1396(s) 1267(m) 1202(m) 1188(m) 1173(m) 1151(m) 1133(m) 1081(w) 1056(w) 1036(w) 941(w) 876(w) 767(m) 742(m) 685(m) 612(m) 571(m) 529(m) 511(m).

Synthesis of 1,1'-dimethyl-5,5'-azobistetrazole (91a).^[10] 1-Methyl-5-amino-1*H*-tetrazole (6.328 g, 63.86 mmol) and *N*-chlorosuccinimide (8.750 g, 65.52 mmol) were loaded in a 250 mL round-bottom flask and suspended in 80 mL water at room temperature (an slightly brown residue formed at the bottom of the flask). The suspension was slowly heated to boiling and stirred vigorously for 3 hours. After this time, the orange solution formed was left to slowly cool down to room temperature (~4 hours). The orange half crystalline solid that separated was filtered, washed with cold water and ethanol and left to air-dry. The product could be purified by recrystallization from 20 mL hot water and 8 mL ethylacetate (3.719 g, 55%). C₄H₆N₁₀ (calc./found): C 24.73 / 24.80, H 3.11 / 3.31, N 72.15 / 71.88; DSC (5 °C/min, °C): 205 (m.p. + dec.); m/z (DEI⁺, xenon, 6 keV, MeOH + TBME): 194.0 (15, [C₆H₄N₁₀]⁺), 43.0 (100, [Me-N=N-Me]⁺), 28.0 (24, N₂⁺), 15.0 (36, CH₃⁺); ¹H NMR (DMSO-*d*₆, 400.18 MHz, 25°C, TMS) δ /ppm: 4.35 (6H, s, CH₃); ¹³C{¹H} NMR (DMSO-*d*₆, 100.63 MHz, 25°C, TMS) δ /ppm: 160.0 (2C, N₄C-N=N-CN₄), 36.1 (2C, CH₃); ¹⁵N NMR (DMSO-*d*₆, 40.55 MHz, 25 °C, MeNO₂) δ /ppm: -1.1 (2N, N=N), -109.4 (2N, N3), -123.0 (2N, q, *J* = 1.55 Hz, N2), -179.2 (2N, N4), -272.3 (2N, q, *J* = 1.94 Hz, N1); Raman ν / cm⁻¹ (rel. int.): 3044(1) 2986(2) 2963(7) 1508(33) 1474(18) 1461(21) 1428(100) 1412(46) 1279(11) 1269(11) 1225(12) 1202(8) 1190(11) 1102(23) 1047(11) 1003(5) 917(16) 755(1) 711(3) 679(1)

319(2) 242(2) 202(2); IR ν / cm^{-1} (KBr, rel. int.): 3042(w) 2961(w) 2609(w) 2460(w) 2224(w) 2136(w) 1631(m) 1506(m) 1503(m) 1475(s) 1441(s) 1395(m) 1308(w) 1283(m) 1268(m) 1253(w) 1227(w) 1188(s) 1111(w) 1030(m) 987(w) 936(w) 916(w) 806(w) 756(s) 750(s) 722(w) 711(s) 690(s) 668(m) 660(m) 604(w) 553(s) 545(s).

Improved Synthesis of 2,2'-dimethyl-5,5'-azotetrazole (92): Alternative safer synthesis: 2-methyl-5-aminotetrazole (1.697 g, 17.12 mmol) and a catalytic amount of AIBN (0.029g, 0.18 mmol) were dissolved in 40 mL acetonitrile. *N*-chlorosuccinimide (4.573 g, 34.24 mmol) was added portionwise as the neat solid and the reaction mixture was stirred overnight at reflux. The bright orange solution formed was rotavaporated to dryness and the crude material was recrystallized from 50 mL hot water and 6 mL ethylacetate yielding elemental analysis pure material (1.011 g, 61%). $\text{C}_4\text{H}_6\text{N}_{10}$ (calc./found): C 24.73 / 24.85, H 3.12 / 3.22, N 72.15 / 72.41. ^1H NMR (CD_3CN , 400.18 MHz, 25°C, TMS) δ /ppm: 4.51 (6H, s, CH_3); $^{13}\text{C}\{^1\text{H}\}$ NMR (CD_3CN , 100.63 MHz, 25°C, TMS) δ /ppm: 171.3 (2C, $\text{N}_4\text{C-N=N-CN}_4$), 40.4 (2C, CH_3).

7.10 References

- [1] (a) Thiele, J. *Just. Lieb. Ann. Chem.* **1892**, 270, 54-63. (b) Thiele, J.; Marais, J. T. *Just. Lieb. Ann. Chem.* **1893**, 273, 144-160. (c) Thiele, J. *Ber.* **1893**, 26, 2645-2646. (d) Thiele, J. *Just. Lieb. Ann. Chem.* **1898**, 303, 57-75.
- [2] (a) Hammerl, A.; Holl, G.; Klapötke, T. M.; Mayer, P.; Nöth, H.; Piotrowski, H.; Warchhold, M. *Eur. J. Inorg. Chem.* **2002**, 4, 834-845. (b) Hammerl, A. *Ph. D. Thesis*, Ludwig-Maximilians Universität München, **2001**.
- [3] Hiskey, M. A.; Goldman, N.; Stine, J. R. *J. Energ. Mater.* **1998**, 16(2 & 3), 119-127.
- [4] (a) Adam, D.; Holl, G.; Klapötke, T. M. *Heteroat. Chem.* **1999**, 10(7), 548-553. (b) Klapötke, T. M.; Ang, H.-G. *Propellants, Explos., Pyrotech.* **2001**, 26(5), 221-224. (c) Hammerl, A.; Klapötke, T. M.; Nöth, H.; Warchhold, M.; Holl, G.; Kaiser, M.; Ticmanis, U. *Inorg. Chem.* **2001**, 40(14), 3570-3575. (d) Klapötke, T. M.; Mayer, P.; Schulz, A.; Weigand, J. J. *Propellants, Explos., Pyrotech.* **2004**, 29(6), 325-332. (e) Klapötke, T. M.; Holl, G.; Geith, J.; Hammerl, A.; Weigand, J. *New Trends in Research of Energetic Materials, Proceedings of the 7th Seminar*, Pardubice, Czech Republic, 20-22 April, **2004**. (f) Clark, K. A.; Klapötke, T. M. *230th ACS National Meeting*, Washington, DC, United States, 28 Aug-1 Sept, **2005**.
- [5] Hammerl, A.; Hiskey, M. A.; Holl, G.; Klapötke, T. M.; Polborn, K.; Stierstorfer, J.; Weigand, J. J. *Chem. Mater.* **2005**, 17(14), 3784-3793.
- [6] (a) Chaudhri, M. M. *Nature* **1976**, 263, 121-122. (b) Reddy, G. O.; Chatterjee, A. K. *Nature* **1983**, 66, 231-244. (c) Whelan, D. J.; Spear, R. J.; Read, R. W. *Thermochim. Acta*, **1984**, 80, 149-163. (d) Chaudhri M. M. *J. Mater. Sci. Lett.*, **1984**, 3, 565-568.
- [7] (a) Williams, M. M.; McEwan, W. S.; Henry R. A. *J. Phys. Chem.* **1957**, 61, 261-267. (b) Pan, W. *24th International Annual Conference of the ICT*, **1994**, 77.
- [8] (a) Ye, C.; Xiao, J.-C.; Twamley, B.; Shreeve, J. M. *Chem. Comm.* **2005**, 21, 2750-2752. (b) Gao, H.; Ye, C.; Piekarski, C. M.; Shreeve, J. M. *J. Phys. Chem. A* **2007**, 111(28), 10718-10731.
- [9] Tremblay, M. *Can. J. Chem.* **1965**, 43(5), 1154-1157.
- [10] Lyakhov, A. S.; Serebrianskaia, T. V.; Gaponik, P. N.; Voitecovich S. V.; Ivaskevich L. S., *Acta Crystallogr.* **2006**, C62(6), m223-m226.
- [11] (a) T. M. Klapötke, C. Miró Sabaté *Z. Anorg. Allg. Chem.*, **2007**, 633, 2671-2677. (b) Spear, R. J.; Elischer, P. P. *J. Austr. Chem.* **1982**, 35(1), 1-13.
- [12] (a) Gálvez-Ruiz, J. C.; Holl, G.; Karaghiosoff, K.; Klapötke, T. M.; Loehnwitz, K.; Mayer, P.; Nöth, H.; Polborn, K.; Rohbogner, C. J.; Suter, M.; Weigand, J. J. *Inorg. Chem.* **2005**, 44(12), 4237-4253. (b) Gálvez-Ruiz, J. C.; Holl, G.; Karaghiosoff, K.; Klapötke, T. M.; Loehnwitz, K.; Mayer, P.; Nöth, H.; Polborn, K.; Rohbogner, C. J.; Suter, M.; Weigand, J. J. *Inorg. Chem.* **2005**, (Correction), 44(12), 5192-5192.

- [13] Karaghiosoff, K.; Klapötke, T. M.; Mayer, P.; Miró Sabaté, C.; Penger, A.; Welch, J. M. *Inorg. Chem.* **2007**, in press.
- [14] Colthup, N. B.; Daly, L.H.; Wiberley, S. E. *Introduction to Infrared and Raman Spectroscopy*, Academic Press: Boston, USA, **1990**.
- [15] Jeffrey, G. A. *An Introduction to Hydrogen Bonding*, Oxford Univ. Press: New York, **1997**.
- [16] (a) Klapötke, T. M.; Miró Sabaté, C.; Welch, J. M., **2007**, unpublished results. (b) Klapötke, T. M.; Miró Sabaté, C.; Welch, J. M., *Z. Anorg. Allg. Chem.* **2007**, submitted.
- [17] (a) Programs for Crystal Structure Analysis (Release 97-2). Sheldrick, G.M., Institut für Anorganische Chemie der Universität, Tammanstrasse 4, D-3400 Göttingen, Germany, **1998**. (b) Altomare, A.; Burla, M. C.; Camalli, M.; Cascarano, G. L.; Giacovazzo, C.; Guagliardi, A.; Moliterni, A. G. G.; Polidori, G.; Spagna, R. *J. Appl. Crystallogr.* **1999**, *32*, 115-119.
- [18] Holleman, A. F.; Wiberg, E.; Wiberg N. *Lehrbuch der Anorganischen Chemie*, 101 Auflage, Walter de Gruyter: Berlin, Germany, **1995**.
- [19] http://academic.pg.cc.md.us/~ssinex/struc_bond/oxides_of_nitrogen.htm.
- [20] (a) Göbel, M.; Karaghiosoff, K.; Klapötke, T. M.; Miró Sabaté, C.; Welch, J. M. *New Trends in Research of Energetic Materials, Proceedings of the 9th Seminar*, Pardubice, Czech Republic, Apr. 19-21, **2006**. (b) Klapötke, T. M.; Mayer, P.; Miró Sabaté, C.; Penger, A.; Welch, J. M. *233rd ACS National Meeting*, Chicago, IL, United States, 25-29 March, **2007**. (c) Klapötke, T. M.; Miró Sabaté, C. *New Trends in Research of Energetic Materials, Proceedings of the 10th Seminar*, Pardubice, Czech Republic, 25-27 April, **2007**.
- [21] Klapötke, T. M.; Karaghiosoff, K.; Mayer, P.; Penger, A.; Welch J. M. *Propellants, Explos., Pyrotech.* **2006**, *31*(3), 188-195.
- [22] Klapötke, T. M.; Mayer, P.; Schulz, A.; Weigand, J. J. *J. Am. Chem. Soc.* **2005**, *127*(7), 2032-2033.
- [23] Bernstein, J.; Davis, R. E.; Shimon, L.; Chang, N-L. *Angew. Chem. Int. Ed.* **1995**, *34*(15), 1555-1573.
- [24] Motherwell, W. D. S.; Shields, G. P.; Allen, F. H. *Acta Crystallogr.* **2000**, *B56*(3), 466-473.
- [25] Motherwell, W. D. S.; Shields, G. P.; Allen, F. H. *Acta Crystallogr.* **1999**, *B55*(6), 1044-1056.
- [26] <http://www.ccdc.cam.ac.uk/support/documentation/rpluto/TOC.html>.
- [27] C. Darwich, T. M. Klapötke, M. Sućeska J. Welch, *Propellants, Explosives, Pyrotechnics* **2007**, in press.
- [28] G. W. Drake, T. W. Hawkins, L. A. Hall, J. A. Boatz, A. J. Brand, *Propellants, Explosives, Pyrotechnics* **2005**, *30*(5), 329.
- [26] Darwich, C.; Klapötke, T. M.; Miró Sabaté, C. *Propell. Explos. Pyrotech.* **2007**, in press.
- [27] Darwich, C.; Karaghiosoff, K.; Klapötke, T. M.; Miró Sabaté, C. *Z. Anorg. Allg. Chem.* **2008**, *634*, 61-68.

- [28] Gálvez-Ruiz, J. C.; Holl, G.; Karaghiosoff, K.; Klapötke, T. M.; Löhnwitz, K.; Mayer, P.; Nöth, H.; Polborn, K.; Rohbogner, C. J.; Suter, M.; Weigand, J. J. *Inorg. Chem.* **2005**, *44*(12), 4237-4253.
- [29] Ye, C.; Xiao, J.; Twamley, B.; Shreeve, J. M. *Chem. Comm.* **2005**, *21*, 2750-2752.
- [30] T. M. Klapötke, C. Miró Sabaté, *Chem. Mater.*, **2008**, *20*(5), 1750-1763.
- [31] A. Bondi, *Phys. Chem.* **1964**, *68*(3), 441-451.
- [32] (a) Hammerl, A.; Klapötke, T. M.; Nöth, H.; Warchhold, M.; Holl, G.; Kaiser, M.; Ticmanis, U. *Inorg. Chem.* **2001**, *40*(14), 3570-3575. (b) Hammerl, A.; Holl, G.; Kaiser, M.; Klapötke, T. M.; Mayer, P.; Piotrowski, H.; Vogt, M. Z. *Naturforsch.* **2001**, *B56*(9), 847-856.
- [33] Impact: Insensitive >40 J, less sensitive ≥ 35 J, sensitive ≥ 4 J, very sensitive ≤ 3 J; friction: Insensitive >360 N, less sensitive = 360 N, sensitive <360 N a. >80 N, very sensitive ≤ 80 N, extreme sensitive ≤ 10 N; According to the UN Recommendations on the Transport of Dangerous Goods (+) indicates: not safe for transport.
- [34] <http://www.bam.de>.
- [35] Klapötke, T. M.; Rienäcker, C. M. *Propellants, Explos., Pyrotech.* **2001**, *26*, 43.
- [36] Sucasca, M. *Propellants, Explos., Pyrotech.* **1991**, *16*(4), 197-202.
- [37] T. M. Klapötke, P. Mayer, C. Miró Sabaté, J. M. Welch, N. Wiegand, *Inorg. Chem.* **2008**, in press.
- [38] Calculation of the oxygen balance: $\Omega(\%) = (\text{O} - 2\text{C} - \text{H}/2 - x\text{AO}) 1600/\text{M}$; M = molecular mass.
- [39] Koehler, J.; Meyer, R. *Explosinstoffe*, 9th ed., Wiley-VCH: Weinheim, Germany, **1998**.
- [40] Cady, H. H.; Larson, A. C. *Acta Crystallogr.* **1965**, *18*, 485-496.
- [41] Bemm, U.; Östmark, H. *Acta Crystallogr.* **1998**, *C54*, 1997-1999.
- [42] Westwell, M. S.; Searle, M. S.; Wales, D. J.; Williams, D. H. J. *Am. Chem. Soc.* **1995**, *117*, 5013-5015.
- [43] NIST Chemistry WebBook, NIST Standard Reference Database Number 69 - March, **2003** Release, www version: <http://webbook.nist.gov/chemistry>.
- [44] http://www.sms-ink.com/products_koenen.html.
- [45] <http://www.systag.ch>.
- [46] Shimanouchi, T. *Tables of Molecular Vibrational Frequencies Consolidated*, Volume I, National Bureau of Standards 1, **1972**.
- [47] Shimanouchi, T. J. *Phys. Chem.* **1972**, *6*(3), 993-1012.
- [48] Pretsch E.; Bühlmann, P.; Affolter, C.; Herrera, A.; Martínez R. *Determinación Estructural de Compuestos Orgánicos*, Springer-Verlag Ibérica: Barcelona, Spain, **2001**.
- [49] (a) ICT-Thermodynamic Code, version 1.0, Fraunhofer-Institut für Chemische Technologie (ICT): Pfintal/Berghausen, Germany, 1988-2000. (b) Webb, R.; van Rooijen, M.. *Proceedings of the 29th International*

Pyrotechnics Seminar, **2002**, 823-828. (c) Bathelt, H.; Volk, F. *27th International Annual Conference of ICT*, **1996**, 92.1-16.

[50] http://www.linseis.net/html_en/thermal/dsc/dsc_pt10.php.

[51] (a) <http://www.jeol.com/tabid/96/Default.aspx>. (b) <http://www.jeolusa.com/DesktopModules/Bring2mind/DMX/Download.aspx?EntryId=331&PortalId=2&DownloadMethod=attachment>. (c) <http://www.jeoleuro.com/instr/mass/mass.htm>.

[52] <http://www.perkinelmer.com>.

[53] <http://www.parrinst.com>.

[54] Weigand, J. J. *Ph. D. Thesis*, Ludwig-Maximilians Universität München, **2001**.

[55] Gaussian G03W: Gaussian 03, Revision A.1: Frisch, M. J.; Trucks, G. W.; Schlegel, H. B.; Scuseria, G. E.; Robb, M. A.; Cheeseman, J. R.; Montgomery, J. A.; Vreven, Jr. T.; Kudin, K. N.; Burant, J. C.; Millam, J. M.; Iyengar, S. S.; Tomasi, J.; Barone, V.; Mennucci, B.; Cossi, M.; Scalmani, G.; Rega, N.; Petersson, G. A.; Nakatsuji, H.; Hada, M.; Ehara, M.; Toyota, K.; Fukuda, R.; Hasegawa, J.; Ishida, M.; Nakajima, T.; Honda, Y.; Kitao, O.; Nakai, H.; Klene, M.; Li, X.; Knox, J. E.; Hratchian, H. P.; Cross, J. B.; Adamo, C.; Jaramillo, J.; Gomperts, R.; Stratmann, R. E.; Yazyev, O.; Austin, A. J.; Cammi, R.; Pomelli, C.; Ochterski, J. W.; Ayala, P. Y.; Morokuma, K.; Voth, G. A.; Salvador, P.; Dannenberg, J. J.; Zakrzewski, V. G.; Dapprich, S.; Daniels, A. D.; Strain, M. C.; Farkas, O.; Malick, D. K.; Rabuck, A. D.; Raghavachari, K.; Foresman, J. B.; Ortiz, J. V.; Cui, Q.; Baboul, A. G.; Clifford, S.; Cioslowski, J.; Stefanov, B. B.; Liu, G.; Liashenko, A.; Piskorz, P.; Komaromi, I.; Martin, R. L.; Fox, D. J.; Keith, T.; Al-Laham, M. A.; Peng, C. Y.; Nanayakkara, A.; Challacombe, M.; Gill, P. M. W.; Johnson, B.; Chen, W.; Wong, M. W.; Gonzalez, C.; Pople, J. A. *Gaussian, Inc.*, Pittsburgh PA, **2003**.

CHAPTER VIII

5,5′-HYDRAZINEBISTETRAZOLE DERIVATIVES

8.1 Introduction

As discussed in the preceding chapter, bridged bistetrazoles are interesting energetic compounds with high nitrogen contents, large positive heats of formation and relatively high performances, which are nevertheless insensitive to classical stimuli (i.e., impact and friction). Many metal and nitrogen-rich salts with the 5,5′-azotetrazolate anion (ZT^{2-})^[1-3] that have been synthesized in our group make use of highly sensitive barium 5,5′-azotetrazolate (**BaZT**, **94**). Recently, we patented a safer synthesis of the interesting bishydrazinium 5,5′-azotetrazolate salt, which makes the synthesis of this highly endothermic compound ($\Delta U_f^\circ = 3700 \text{ kJ kg}^{-1}$)^[4] non-hazardous for up-scaling.

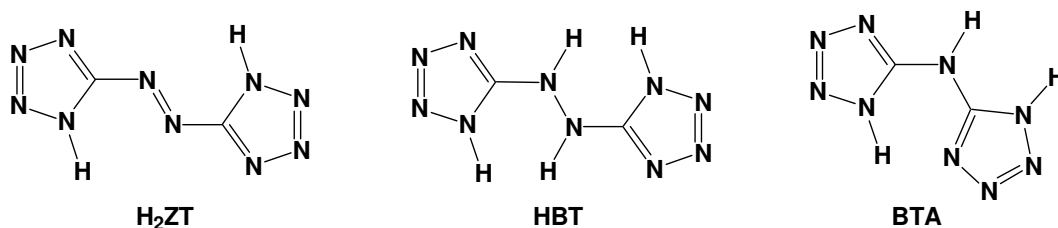


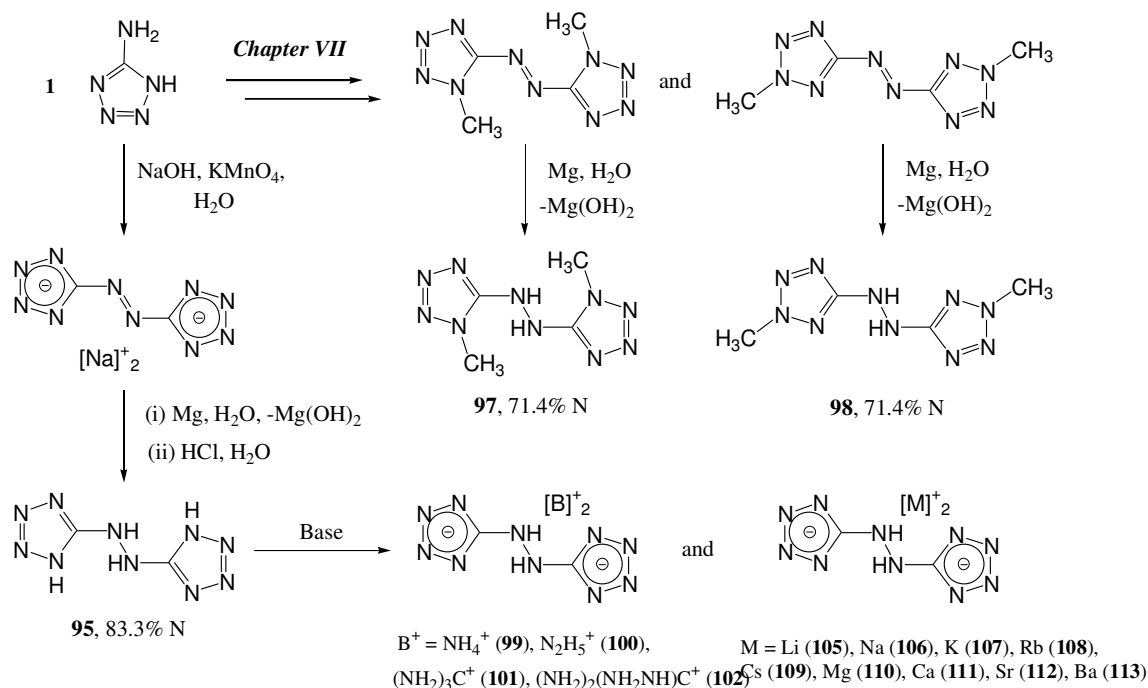
Figure 8.1 Formula structures of 5,5′-azobistetrazole (**H₂ZT**, **75**), 5,5′-hydrazinebistetrazole (**HBT**, **95**) and *N,N*-bis(1*H*-tetrazole-5-yl)-amine (**BTA**, **96**).

The high instability of 5,5′-azobistetrazole (**H₂ZT**, **75**, Figure 8.1)^[5] is in contrast with this of the parent 5,5′-hydrazinebistetrazole (**HBT**, **95**) as proofed by recent work in our group (see discussion below).^[6,7] **95** was first reported more than a century ago by Thiele^[5] and later on was studied by Spears et al. as an energetic sensitizer^[8] However, the compound had hardly been characterized and the energetic properties remained unreported. The energetic properties of metal salts of **75**^[2] and of the parent *N,N*-bis(1*H*-tetrazole-5-yl)-amine (**BTA**, **96**)^[9] have been studied recently. Also recently, we reported the energetic properties of nitrogen-rich salts of **75**,^[3] which were complemented by recent work of Shreeve et al. on similar salts of **96**.^[10] Metal salts of **75** and **96** show, in the rule, great thermal stabilities, whereas the nitrogen-rich salts are high-performing materials. Apart from preliminary results on the synthesis and characterization^[11] and thermal studies of salts of **95**^[11,12] very little is known about the potential of metal and nitrogen-rich salts of **95**. Therefore, we decided to undertake the full characterization (both analytical and energetic) of **95** and the comprehensive characterization and study of the energetic properties and stability of (alkali and alkaline earth) metal

and nitrogen-rich salts containing the HBT²⁻ anion. In addition, due to the interesting energetic properties of the methylated 5,5′-azotetrazole derivatives presented in the previous chapter (i.e., 1,1′-dimethyl- and 2,2′-dimethyl-5,5′-azotetrazole), we decided to study two previously unreported (hydrazino-) bridged bistetrazoles, namely, 1,1′-dimethyl- and 2,2′-dimethyl-5,5′-hydrazinebistetrazole.

8.2 Synthesis

5-Amino-1*H*-tetrazole (5-At) was oxidized in sodium hydroxide solution by potassium permanganate yielding sodium 5,5′-azotetrazolate pentahydrate (**NaZT**),^[13] which was isolated and reacted overnight with an excess of magnesium powder in aqueous solution and subsequently treated with acid yielding 5,5′-hydrazinebistetrazole (**HBT**, **95**),^[6-8] which precipitated as a white powder on cooling. The methylated derivative 1,1′-dimethyl-5,5′-hydrazinebistetrazole monohydrate (**1,1DMHBTh**, **97**) was synthesized by reduction of the azo-bridge in the corresponding azo-derivative (*Chapter VII*) under similar conditions (see Scheme 8.1) in a relatively low yield (≤37%) and its synthesis is currently being optimized to apply the method for the synthesis of the isomer 2,2′-dimethyl-5,5′-hydrazinebistetrazole (**2,2DMHBT**, **98**). Methylation of the sodium salt of **95** with methyl iodide or dimethyl sulfate afforded only mixtures of the different methylated isomers as proven by NMR spectroscopy, similarly to the alkylation of 5-substituted tetrazolate salts,^[14] but in this case the two isomers could not be separated efficiently due to the similar solubility of the two isomers in the tested solvents (water, ethylacetate, acetonitrile, acetone, benzene and ethanol).



Scheme 8.1 Synthesis of 5,5′-hydrazinebistetrazole derivatives.

The free acid **95** is a strong acid and can accordingly be deprotonated by a suitable base. Thus, we synthesized salts containing the HBT^{2-} anion and nitrogen-rich cations such as ammonium (**AHBT**, **99**), hydrazinium (**HHBT**, **100**), guanidinium (**GHBT**, **101**) and aminoguanidinium (**AGHBT**, **102**) by acid-base reactions. The synthesis of **102** produced crystals of a compound, which was identified by its Raman spectrum and molecular structure as carboxyamino-guanidine betaine monohydrate (**CAGh**, **114**) (see Figure 8.2), which was to all effects the starting material of the reaction sold as aminoguanidinium carbonate^[15] The non-readily availability of a suitable source of the nitrogen-richer diamino- (DAG^+) and triaminoguaninium (TAG^+) cations rendered the synthesis of **DAGHBT** (**103**) and **TAGHBT** (**104**) unfeasible. On one side, reaction of silver 5,5′-hydrazinebistetrazolate (**AgHBT**, **115**) with the corresponding halogenide salt did not result in the expected precipitation of a silver halide due to the high insolubility of **115**, which is in contrast with the synthesis of analogous salts of **96** using silver *N,N*-bis(1-tetrazolate-5-yl)-amine (**121**, **116**).^[16] On the other side, reaction between a guanidinium sulphate salt and barium 5,5′-hydrazinebistetrazolate (**BaHBT**, **113**), resulted in precipitation of barium sulphate, however, the resulting compounds (**103** and **104**) were, in contrast to salts of **BTA** (**96**) prepared by the analogous method,^[10] not obtained in pure form. Therefore, every effort to improve the synthesis of these salts was abandoned.

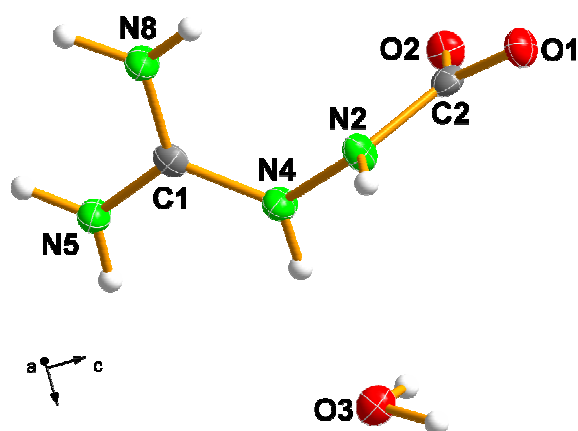


Figure 8.2 Molecular structure of carboxyamino-guanidine betaine monohydrate (**CAGh**, **114**).

Reaction of **95** with a metal hydroxide ($\text{M}^{x+}(\text{OH})_x$, where $\text{M}^{x+} = \text{Li}^+, \text{Na}^+, \text{K}^+, \text{Rb}^+, \text{Cs}^+, \text{Mg}^{2+}, \text{Ca}^{2+}, \text{Sr}^{2+}, \text{Ba}^{2+}$) either in water or in alcoholic solution yielded the corresponding alkali and alkaline earth metal salts. The synthesis of the salts containing the HBT^{2-} anion needs to be carried out under nitrogen due to the readily oxidation of the compounds to the 5,5′-azotetrazolate salts (ZT^{2-}) in solution, whereas in the solid state the compounds are much more stable (see energetic discussion in section 8.3.5). However, we took advantage of the readily oxidation of these salts to suggest a new method for the synthesis of 5,5′-azotetrazolate salts with alkali and alkaline earth metals and nitrogen-rich bases, which avoids the hazard of using highly sensitive **94**.^[1,2]

8.3 Characterization

All compounds were characterized by analytical (elemental analysis and mass spectrometry) and spectroscopic methods (IR/Raman and NMR: ^1H , ^{13}C and ^{15}N when possible). The already reported metal and nitrogen-rich 5,5'-azotetrazolate salts were synthesized and characterized only by elemental analysis and IR and since they have already been discussed elsewhere in detail,^[17] we will omit them from the following discussion. Lastly, the signals for the cations in the nitrogen-rich salts of **95** are well established and their discussion will also be omitted here.

8.3.1 Spectroscopic Discussion

The ^1H NMR spectrum of **95** shows fast exchange between the protons in $\text{DMSO-}d_6$ and one only averaged signal at 9.6 ppm is observed. This low field resonances in comparison to 5-amino-1*H*-tetrazole (5-At) puts into perspective the higher acidity of the ring protons in **95** in respect to 5-At and might explain the failure of the attempted synthesis of the corresponding nitrate and perchlorate salts of **95** by direct reaction with the concentrated acids. **97** shows similar shifts to **95** for the hydrazine-bridge protons (~9.5 ppm), in addition to the CH_3 group resonance at 3.8 ppm (**97**). Deprotonation of **95** to form the HBT^{2-} anion (compounds **99-113**) results in a shift in the resonances of the hydrazine moiety hydrogen atoms to high field (~7.0 ppm).

The tetrazole carbon signal observed at 159.6 ppm in **95** is shifted to low field in comparison to the methylated derivative **97** (157.2 ppm) and to high field in respect to sodium 5,5'-azotetrazolate (173.1 ppm),^[2] keeping in with the shift observed in 5-amino-1*H*-tetrazole salts.^[18] In the ^{13}C NMR the tetrazolate ring carbon atoms in **99-113** resonate at lower field (~167 ppm) as a consequence of the deshielding effect produced by the delocalization of the negative charge. Figure 8.3 shows the ^{13}C NMR spectrum of the strontium salt (**SrHBT**, **112**) at different times. As mentioned above, the HBT^{2-} anion oxidizes readily to the ZT^{2-} anion in solution. A proof for this is that when the pure compound (e.g., **112**) is dissolved in $\text{DMSO-}d_6$, the solvent turns slightly yellow as it dissolves. However, the ^{13}C NMR (of a diluted sample) looks clean and after 1 day a resonance at ~173 ppm starts to become visible. This signal increases in intensity upon time and the initial signal at ~167 ppm ends up disappearing indicating full oxidation of the HBT^{2-} to the ZT^{2-} anion. This is an interesting fact, specially in the solid state since it changes the energetic properties of the compound (see energetic discussion in section 8.3.5).

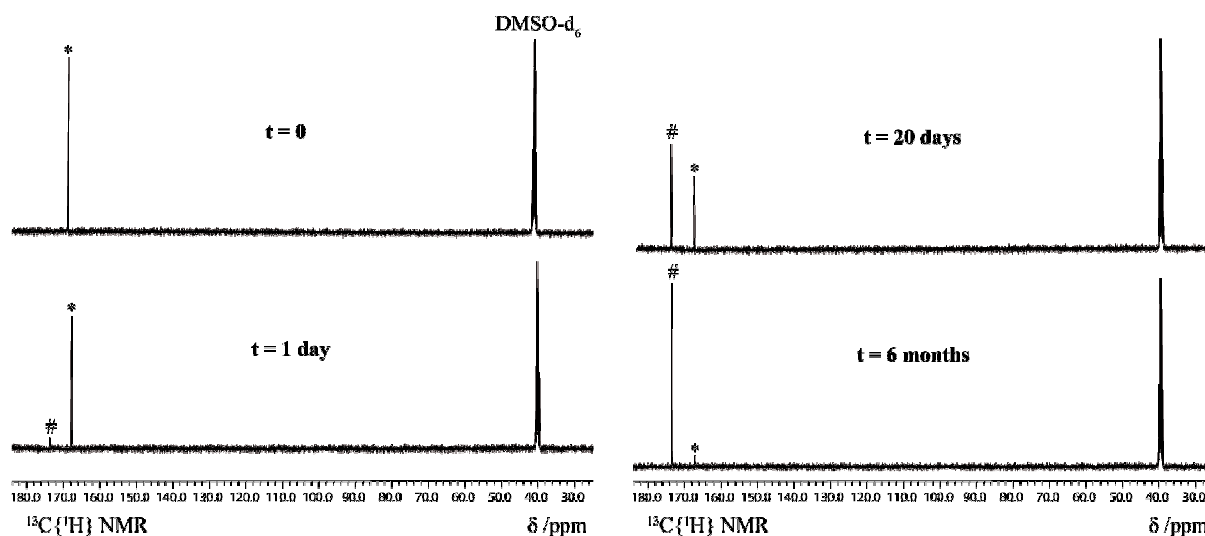


Figure 8.3 Monitoring of the oxidation of **112** to the 5,5'-azotetrazolate salt (**SrZT**, **117**) by $^{13}\text{C}\{^1\text{H}\}$ NMR in $\text{DMSO-}d_6$ (# and * denote **117** and **112**, respectively).

No signals were observed in the ^{14}N NMR of all compounds and they were too insoluble to record a ^{15}N NMR (natural abundance). The lack of protons in the vicinity of nitrogen atoms did not allow to observe the resonances of the tetrazole ring nitrogen atoms in the ^{15}N solid state NMR (the only resonance observed was that of the hydrazine nitrogen atoms at ~ -297 ppm). The only exception to this is **HBT** (**95**, Figure 8.4). The spectrum shows the typical rotational side bands (marked on the plot with an asterisk) observed in solid state NMR (two of which would fall in the positive range of the spectrum and are not showed for simplicity purposes). In contrast to NMR in solution where one would expect fast proton exchange resulting in N1 (N1^i) and N2 (N2^i) (see X-ray labeling scheme) being equivalent to N3 (N3^i) and N4 (N4^i), respectively, and in consequence, a total of three signals due to the symmetry of the molecule, in the solid state the proton is fixed to N4 (N4^i), making N1 (N1^i) and N2 (N2^i) no longer equivalent to N3 (N3^i) and N4 (N4^i). Taking into consideration the symmetry between both halves of the molecules, observed in the molecular structure (symmetry code: (i) 1-x, y, 2.5-z), one would expect five signals, which are experimentally observed and can be assigned as follows: the signal at highest field (-298.5 ppm) can be easily assigned to the hydrazine nitrogen atom, N1 and N4 are both attached to a carbon atom and one would expect them to be similar, but the proton induced shift (PIS), already observed in solution for similar compounds,^[19] shifts N4 to higher field (-179.0 vs. -110.9 ppm). Finally, the PIS is also reflected on the nitrogen atom closest to the proton in question, making N3 to have a more negative shift than the chemically similar N2 (-25.0 vs. -6.9 ppm). Regardless of the obvious structural similarities between **95**, **97** and **98**, several attempts to measure a solid state ^{15}N NMR for the methylated derivatives resulted fruitless regardless of the long pulse delay, measuring time and program used.

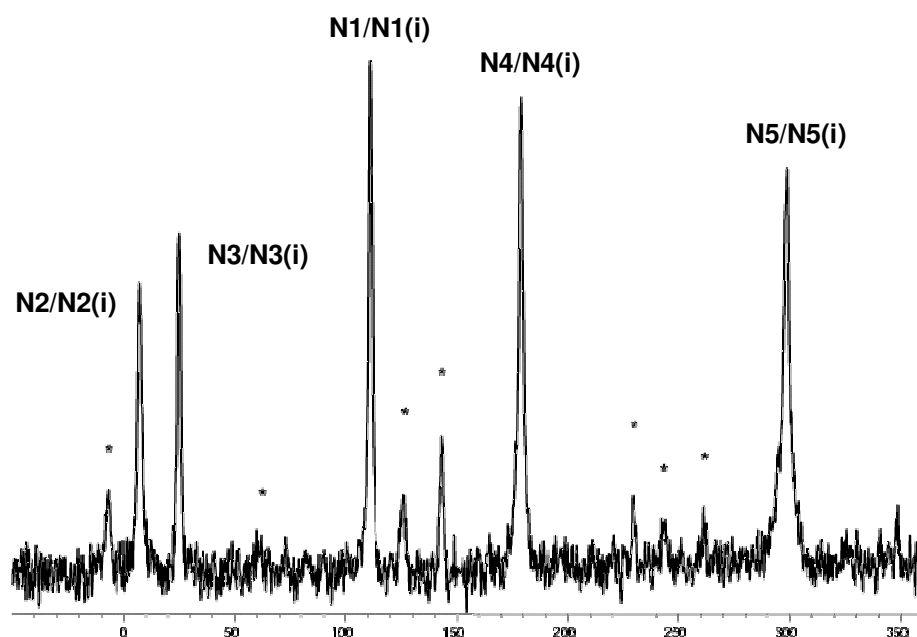


Figure 8.4 Solid state ^{15}N NMR of **95** (the rotational side bands are marked with an asterisk). See X-ray discussion for labeling scheme.

8.3.2 Vibrational spectroscopy

Table 8.A1 shows a comparison of the calculated and experimental vibrational spectra with the corresponding intensities for **95** (see experimental part for more details). Due to the obvious similarities in the structure of **95**, **97** and **98** their vibrational spectra will be discussed together here, whereas these of salts containing the HBT^{2-} anion (**99-113**) will be discussed separately. In the IR spectra of the neutral 5,5′-azotetrazoles there is a set of very strong bands in the N–H region around 3000 cm^{-1} corresponding to the stretching of the hydrazine and ring N–H bonds (one broad band in the Raman spectra). The $\nu(\text{C}_{\text{ring}}-\text{N}_{\text{hydr.}})_{\text{oop}}$ vibration is observed at $\sim 1650\text{ cm}^{-1}$. The N–N and C–N ring stretches appear as bands of moderate intensity in the range between 1400 and 1000 cm^{-1} ($\nu(\text{N}-\text{N})$) and ~ 1500 and 1050 cm^{-1} ($\nu(\text{C}-\text{N})$), respectively. The deformation of the ring and the hydrazine moiety are seen as peaks of medium intensity at ~ 1270 and $\sim 1370\text{ cm}^{-1}$ (identical shifts in the IR). Unfortunately, the strongest band in the Raman spectrum of **95** at 170 cm^{-1} (Figure 8.A1) was not found by our calculations and therefore we were not able to assign it. A similar band of high intensity is also observed in the Raman spectrum of **97** at $\sim 200\text{ cm}^{-1}$.

Deprotonation of **95** to yield the HBT^{2-} anion in compounds **99-113** results in obvious differences in the IR and Raman shifts. Figure 8.5 show representative IR and Raman spectra for some of the compounds reported here containing the HBT^{2-} anion (**110**, **111**, **112** and **113**). With some variations in the shifts, all spectra look very similar, as expected. The spectra of salts **99-110** look clearly

different from those of alkaline earth metal salts **111-113**. The main differences arise from differences in the structure of the salts (see section 8.3.3 *Molecular Structures*). The most intense signals in the IR spectra of alkaline earth metal salts of **95** are broad bands in the X–H (X = O and N) region between $\sim 3600\text{--}2800\text{ cm}^{-1}$ corresponding to the crystal water and hydrazine-bridge (obscured) protons stretching modes. In addition, the in-the-plane carbon-hydrazine nitrogen stretch (C1–N5 and C2–N10) is seen at $\sim 1630\text{ cm}^{-1}$ (Raman inactive) and the deformation modes (in- and out-of-the-plane) for the hydrazine moiety and ring C–N and N–N stretching modes are observed in the range between 1540 and 1380 cm^{-1} . In the Raman spectra the most intense signal correspond to stretching modes in the tetrazole rings at $\sim 1070\text{ cm}^{-1}$.

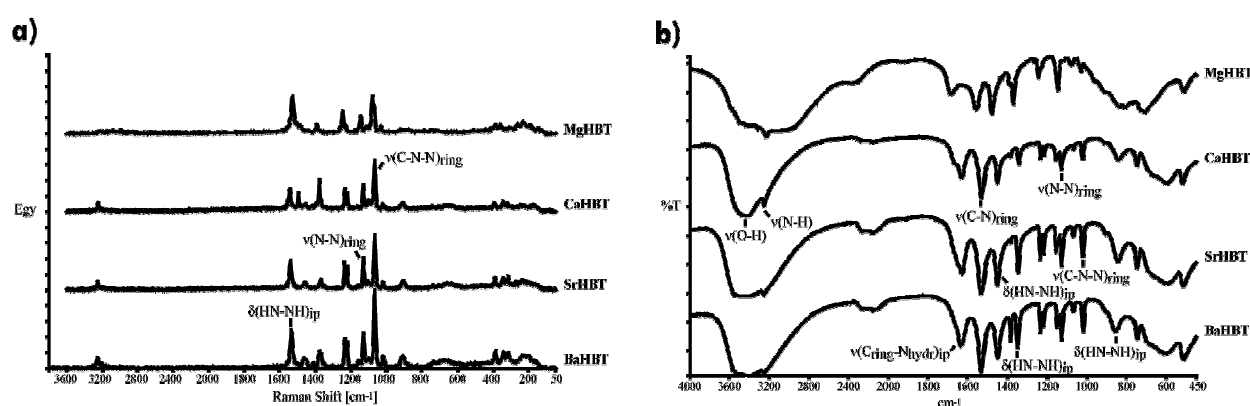


Figure 8.5 a) Raman and b) IR panel plot spectra for alkaline earth metal salts of **95**.

Lastly, in addition to the signals commented above for all compounds, many other bands of lower intensity can be observed in both IR and Raman spectra, which can be assigned as follows: $735\text{--}750\text{ cm}^{-1}$ [$\omega(\text{HN-NH})$], $\sim 845\text{ cm}^{-1}$ [$\delta(\text{HN-NH})_{ip}$], $\sim 1020\text{ cm}^{-1}$ [$\nu(\text{C-N-N})_{ring}$], $\sim 1070\text{ cm}^{-1}$ [$\nu(\text{C-N-N})_{ring}$ & $\nu(\text{N-N})_{ring}$], $\sim 1130\text{ cm}^{-1}$ [$\nu(\text{N-N})_{ring}$], $\sim 1370\text{ cm}^{-1}$ [$\delta(\text{HN-NH})_{ip}$ & $\nu(\text{N-N})_{ring}$], 1384 cm^{-1} [$\delta(\text{HN-NH})_{oop}$ & $\nu(\text{N-N})_{ring}$], $1450\text{--}1460\text{ cm}^{-1}$ [$\delta(\text{HN-NH})_{ip}$ & $\nu(\text{N-N})_{ring}$], $1530\text{--}1540\text{ cm}^{-1}$ [$\delta(\text{HN-NH})_{ip}$ & $\nu(\text{C-N})_{ring}$], $\sim 1630\text{ cm}^{-1}$ [$\nu(\text{C}_{ring}\text{--N}_{hydr})_{ip}$].^[19, 20]

8.3.3 Molecular Structures

The X-ray crystallographic data of the compounds were collected on an Oxford Diffraction Xcalibur 3 diffractometer equipped with a CCD detector using graphite-monochromated Mo K α radiation ($\lambda = 0.71073\text{ \AA}$). No absorption correction was applied to the data sets. The structure were solved by direct methods (SHELXS-97 and SIR97) and refined by means of full-matrix least-squares procedures using SHELXL-97.^[21] The geometry for the coordination around the cations is tabulated in *Appendix B*. All non-hydrogen atoms were refined anisotropically. All calculations were carried out

using the program package G03W.^[22] The structure and frequency calculations were performed with Becke's B3 three parameter hybrid functional using the LYP correlation function (B3LYP) and are tabulated in Table 8.A3.^[23] For all atoms H, C, N and O a correlation consistent polarized double-zeta basis set was used (cc-pVDZ).^[24] Since the structure of **95** show many interesting unique features (e.g., high density), its structure will be discussed in detail, however, since many of the HBT²⁻ salts have similar structures, only the distinctive features will be highlighted below.

The bond distances and angles in **95** (Tables 8.B2 and 8.B4) match nicely the literature reported values for structurally similar compounds such as 1,5-diamino-1*H*-tetrazole^[25] and 5-amino-1*H*-tetrazole monohydrate.^[26] In **95** half of the molecule can be generated by symmetry ((i): 1-x, y, 2.5-z) and, in contrast to the structurally similar 5,5′-azotetrazolate salts (*Chapter VII*), that contain an azo (N=N) bridge, which forces the two tetrazole rings to be coplanar,^[2] the sp³ character of the hydrazine bridging-moiety does not allow it for them to lay on the same plane (torsion angle C1ⁱ–N5ⁱ–N5–C1 = 115.2(2)°).

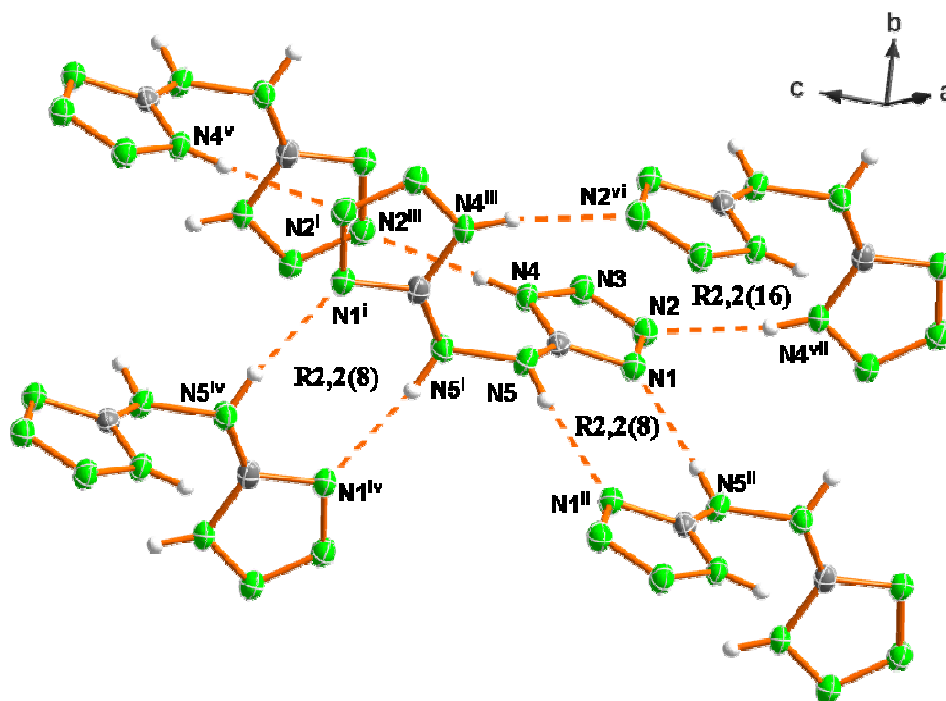


Figure 8.6 Hydrogen-bonding around the molecule in the crystal structure of **95** (Diamond picture, symmetry codes: (i) 1-x, y, 2.5-z; (ii) 1-x, -1-y, 2-z; (iii) x, -y, 0.5+z; (iv) x, -1-y, 0.5+z; (v) 1-x, -y, 3-z; (vi) 1-x, -y, 2-z; (vii) x, -y, -0.5+z).

Figure 8.6 shows the hydrogen bonds formed between **HBT** (**95**) molecules. Only two crystallographically independent (strong) hydrogen bonds (N4...N2ⁱ = 2.917(2) Å and N5...N1ⁱⁱ = 2.941(2) Å; symmetry codes: (i) 1+x, y, z; (ii) -1-x, 1-y, -z) are formed (Table 8.B6) but every molecule participates in the formation of up to eight hydrogen bonds with N3 being the only

electronegative atom that does not form any strong interaction ($N4^{ix} \cdots N3 = 3.258(2) \text{ \AA}$; symmetry code: (ix) 0.5-x, 0.5-y, 2-z). All hydrogen bonds are characterized by a great directionality with angles between donor-hydrogen-acceptor which vary between $166(2)$ and $168(2)^\circ$. The nomenclature introduced by Bernstein et al.^[27] in combination with the computer program *RPLUTO*^[28] are useful to explain the relatively complicated hydrogen-bonding networks found in the crystal structure of **95**. In the graph-set notation the unitary hydrogen-bonding network is given by $N_1 = C1,1(4)C1,1(5)$. Apart from other chain patterns, **95** participates in the formation of ring graph-sets, the most important ones being an **R2,2(8)** motif by using N1 and N5 and a larger **R2,2(16)** pattern including N2, N1, N5, $N5^i$, $N4^i$, $N2^{vi}$ and $N4^{vii}$ (symmetry codes: (i) 1-x, y, 2.5-z; (vi) 1-x, -y, 2-z; (vii) x, -y, -0.5+z) (Table 8.B1). The extensive hydrogen-bonding in the structure together with the great strength of the same results in a structure with a high density as calculated from the X-ray measurement ($\rho_{\text{calc}} = 1.841 \text{ g cm}^{-3}$), not to mention the good thermal stability and the unexpected low sensitivity to impact and friction regardless of its high nitrogen content of 83.3 % (see energetic discussion in section 8.3.4).

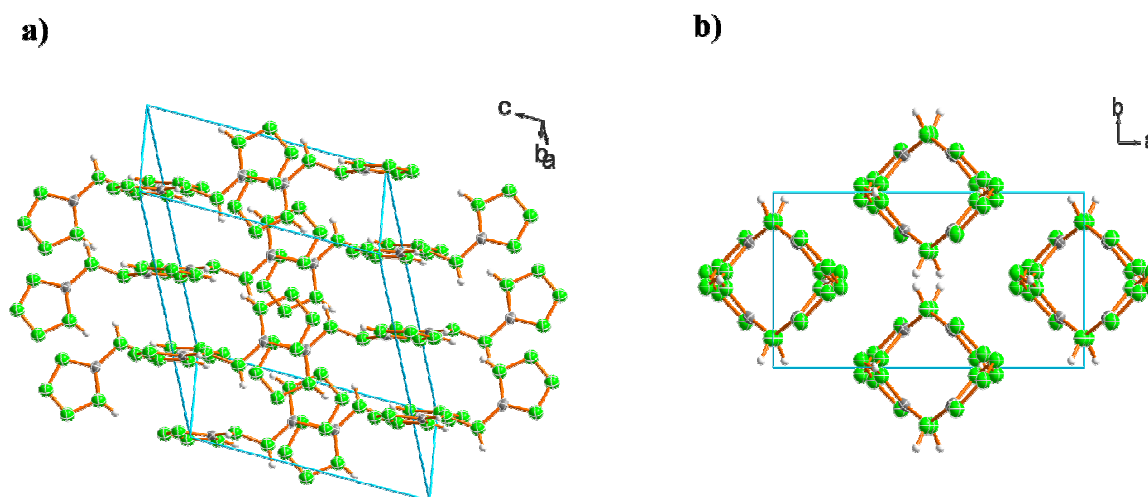


Figure 8.7 a) Unit cell of **95** showing the layers formed by the tetrazole moieties and b) View of the unit cell of **95** along the c -axis showing the gaps left by the molecules.

The torsion angle between the two aromatic rings may explain why the compound does not crystallize in layers as it would be expected, for example, for the parent 5,5'-azotetrazole (**75**). However, the tetrazole rings belonging to one half of the molecule arrange themselves in layers interacting with the subsequent layers by π -stacking with distance between layers of $\sim 3.3 \text{ \AA}$, while the other half of the molecule also stacks forming layers in a different direction (see Figure 8.7a). Figure 8.7b represents a view of the unit cell along the c -axis showing the gaps between molecules. These gaps ($\sim 3.9 \text{ \AA}$) may be interesting from the point of view of studying the properties of **95** as a nitrogen-rich ligand with transition metals such as Ti, Fe, Co, Ni, Cu, Zn, Ag or Pd.

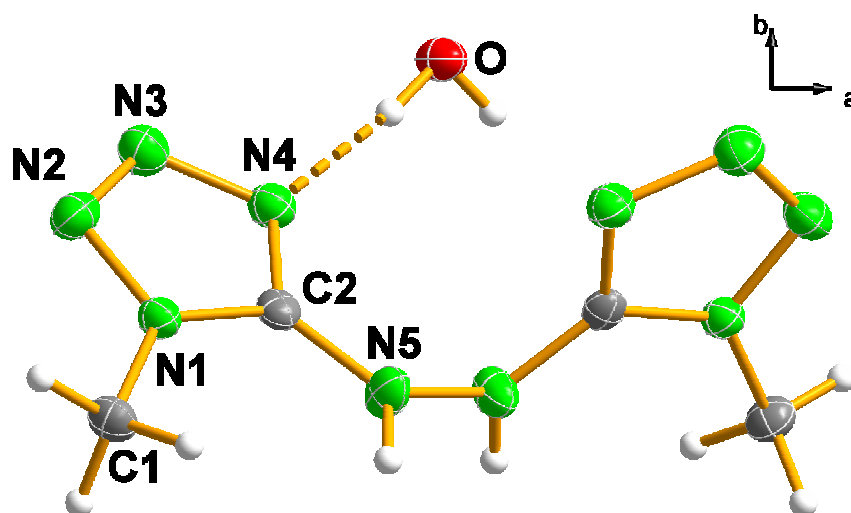


Figure 8.8 Asymmetric unit of **97** with the labelling scheme.

97 (Figure 8.8) crystallizes in a monoclinic cell in the centrosymmetric space group $C2/m$ as the monohydrated species. As expected from the space group, half of the molecule can be generated by symmetry (symmetry code: (ii) $1-x, y, 1-z$) and the oxygen atoms are placed in special positions. The dihedral angle $C1-N5-N5^{ii}-C1^{ii}$ has a value of $94.6(2)^\circ$, which is smaller in comparison to **95** ($115.2(2)^\circ$). The formal replacement of the two hydrogen atoms in **95** by two methyl groups in **97** limits the formation of hydrogen bridges and the two hydrogen bonds found in the structure (Table 8.B6) are formed by the water molecules. These are represented in a view of the unit cell of the compound in Figure 8.9. Molecules of **97** are connected over water molecules acting as hydrogen bond donors ($O \cdots N4^{ii} = 2.748(2) \text{ \AA}$) or over water molecules with the hydrazine bridge nitrogen atoms as the donor atoms ($N5 \cdots O^i = 2.783(3) \text{ \AA}$; symmetry code: (i) $x, -1+y, z$), yielding a very similar structure to that of 1,1'-dimethyl-5,5'-azotetrazole monohydrate (**1,1DMZTh**, Chapter VII). Graph-set analysis using *RPLUTO* reveals the formation of two dimeric **D1,1(2)** interaction, which form a **C1,2(5)** and a **C2,2(9)** chain motifs at the primary level. The former chain pattern goes from the hydrogen atom on $N5$ to O^i , whereas the latter extends from one of the hydrogen atoms on O^i over $N4$ to $N4^{ii}$. At the secondary level, two chain graph-sets of the type **C2,2(X)** ($X = 6, 7$) are found by interaction of the two hydrogen bonds found in the structure starting at O^i over $N4$ and finishing at $N5$ and $N5^{ii}$, respectively.

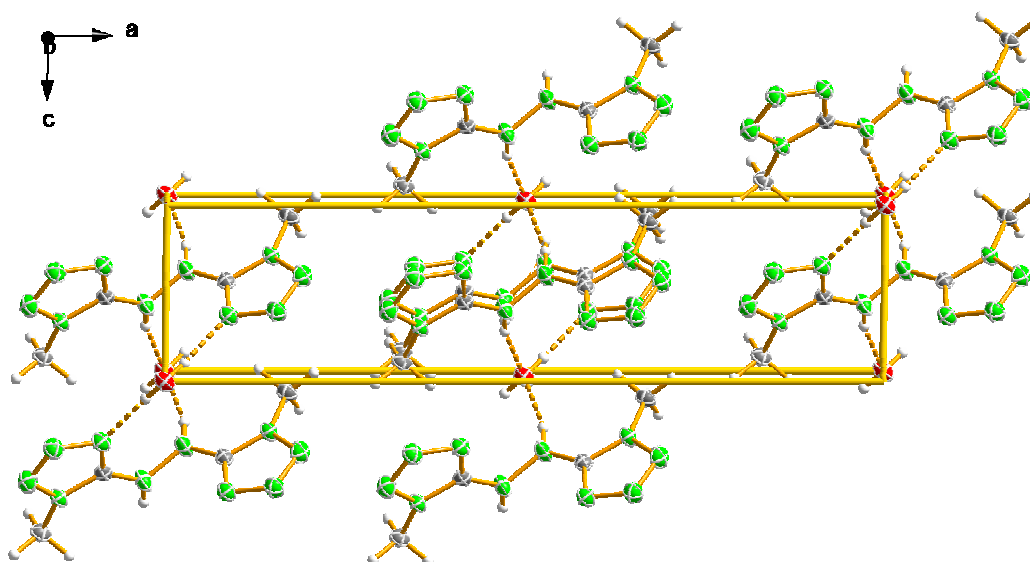


Figure 8.9 View of the unit cell of **97** along the *b*-axis showing the hydrogen-bonding (dotted lines). Symmetry codes: (i) $x, -1+y, z$; (ii) $1-x, y, 1-z$.

The N–N bond distances in the anions of HBT²⁻ salts **99–113** (1.299(2)–1.366(2) Å) are between N–N single bonds (1.454 Å) and N=N double bonds (1.245 Å)^[29] (Tables 8.B2 and 8.B3). This indicates conjugation of the negative charge throughout the aromatic rings as seen in the crystal structures of other salts containing the same anion.^[11] The distances between the two bridging nitrogen atoms (N5–N5ⁱⁱⁱ = 1.422(8)–1.432(2) Å and N6–N6^{iv} = 1.428(3)–1.442(2) Å) are relatively long (N–N single bond = 1.454 Å),^[29] longer than the analogous N–N distances observed in the free acid **95**^[6,7] by ~0.06 Å, in which no conjugation between the two aromatic rings and the bridging nitrogen atoms is observed. Lastly, the coordination numbers and distances described below for compounds **105–113** are keeping in with other metal salts with anionic nitrogen heterocycles.^[2,25,26,30]

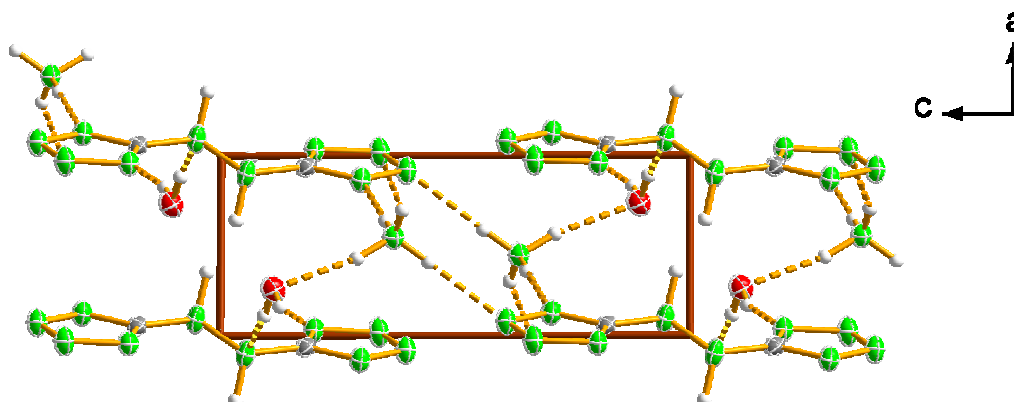


Figure 8.10 View of the unit cell of **99** along the *b*-axis showing the formation of non-planar layers connected by hydrogen-bonding (dotted lines).

99 crystallizes as the dihydrated species forming non-planar layers as represented in Figure 8.10, which are connected by hydrogen bonds to water molecules and ammonium cations. Similarly to other compounds containing the HBT^{2-} anion (see discussion below), there exists disorder in the structure. The average configuration of the anion presents tetrazole rings which sit on parallel planes. When one of the protons on N5 points upwards, the proton on N5^{iv} (symmetry code: (iv) $2-x, 1-x, -z$) points downwards and vice versa (i.e., the protons on the hydrazine-bridge are only half occupied). The water molecule oxygen atoms have three small electron density (protons) in the vicinity, two of which show approximately half occupied (49 and 51%) and one full occupied positions.

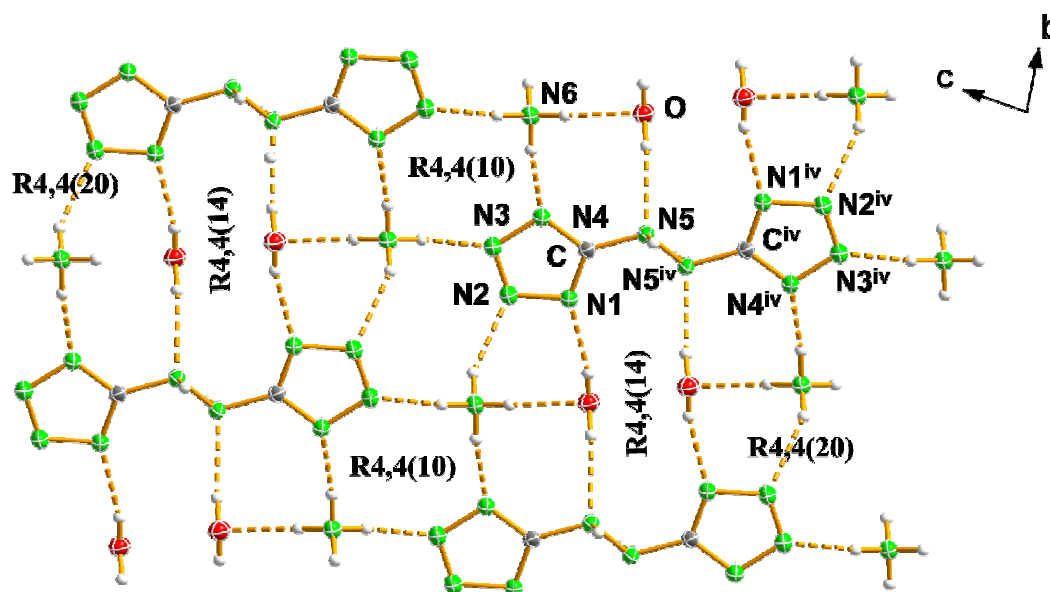


Figure 8.11 Hydrogen-bonding in the crystal structure of **99** with the labelling scheme showing the formation of some characteristic graph-sets (symmetry code: (iv) $2-x, 1-x, -z$).

Figure 8.11 shows the hydrogen-bonding in the structure of **99**. Every nitrogen atom is involved in the formation of hydrogen bonds of different strength (see Table B8.6). In one of the two possible configurations the compound adopts, water molecules are hydrogen bond donors interacting with the hydrazine-bridge nitrogen atoms with $\text{O} \cdots \text{N5} = 2.942(3) \text{ \AA}$ and in the other configuration they accept a hydrogen bond from the hydrazine-bridge nitrogen atoms with $\text{N5} \cdots \text{O} = 2.932(3) \text{ \AA}$. Using graph-set nomenclature one of the two possible configurations (represented in Figure 8.11) shows dimeric interactions of the type **D1,1(2)** and **C1,1(3)** chain motifs, which combine at the primary level with themselves to form finite patterns with the label **D2,2(X)** ($X = 4, 8, 10$) and **C2,2(6)** chain graph-sets, respectively. At the secondary level, many **D2,2(X)** ($X = 4-9$) finite patterns, **C2,2(X)** ($X = 6, 10, 11$), **C2,3(5)** and **C3,3(X)** ($X = 7, 9, 11, 13$) chain networks and **R4,4(X)** ($X = 10, 14, 20$) ring graph-sets are found. For example, the **R4,4(10)** motifs are formed by the interaction of two HBT^{2-} anions over two ammonium cations ($\text{N6} \cdots \text{N3}^{\text{ii}} = 2.942(3)$ and

$N6\cdots N2^{iii} = 2.966(3)$ Å; symmetry codes: (ii) $-x+3, -y+1, -z+1$; (iii) $x, y+1, z$). The **R4,4(14)** graph-sets are generated by the interaction of two anions with two water molecules *via* the hydrogen bond between O and N5 mentioned above and the shortest contact in the structure ($O\cdots N1^{iii} = 2.791(3)$ Å). Lastly, the **R4,4(20)** patterns are yielded by the interaction of two ammonium cations with N2 and N4 of the anion.

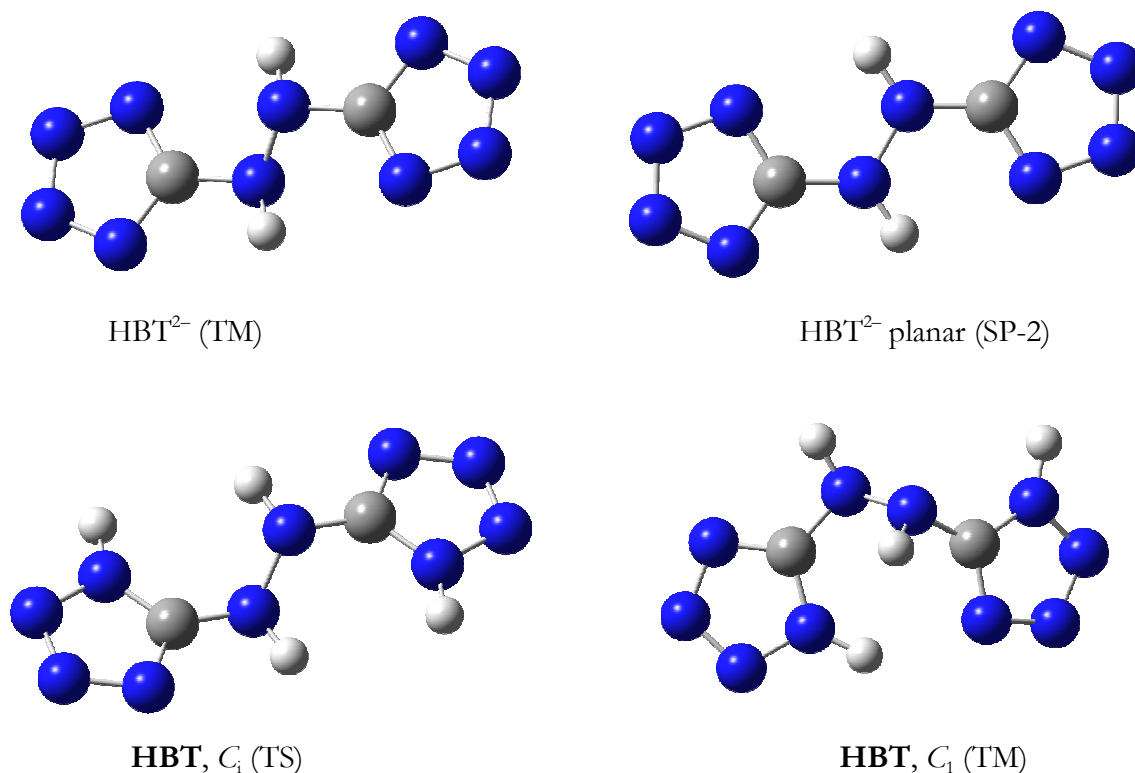


Figure 8.12 Optimized structures (B3LYP/cc-pVDZ) of HB T^{2-} , HB T^{2-} planar, **HB T** (**95**) C_i and **HB T** (**95**) C_1 .

The barium salt (**113**) was the first salt containing the HB T^{2-} anion, which was structurally characterized in this work and shows an anomalous structure. The cations lie on special positions so that half of the water molecules can be generated by symmetry (symmetry code: (i) $x, y, 2-z$). Due to the heavy barium atoms in **113** no electron density for the hydrazine-bridge hydrogen atoms was present in the solution file and, thus, these protons could not be found in the electron density map. In the solid state (see Figure 8.13) “coplanarity” between the two tetrazole rings in the anions is observed, which is in contrast with other previously reported compounds containing the **HB T** (**95**) moiety^[6,11] as well as with some of the compounds described below. In order to explain the “apparent coplanarity” of the two rings calculations were done. Table 8.A3 presents the computational results obtained for the gas-phase structure of the 5,5′-azotetrazolate anion (ZT^{2-}), 5,5′-azotetrazole (**75**) (Figure 8.A2), non-planar (HB T^{2-}) and planar (HB T^{2-} planar) 5,5′-hydrazinebistetrazolate anion and planar (**HB T** (**95**) C_i) and non-planar (**HB T** (**95**) C_1) 5,5′-

hydrazinebistetrazole (see Figure 8.12). Four of the six computed structures are true minima (TM) i.e., the number of imaginary frequencies equals zero. This results are in agreement with the previously reported structures of 5,5'-azotetrazolate salts,^[2,3,31] 5,5'-azotetrazole,^[27] 5,5'-hydrazinebistetrazolate salts^[11] and 5,5'-hydrazinebistetrazole,^[6,7] When the structure of **95** is optimized so that to have a planar geometry, i.e., C_i symmetry, one negative frequency is found and the structure where both tetrazole rings are coplanar is a transition state (TS) in the gas phase. Lastly, the optimized structure of the HBT²⁻ anion in which both rings are coplanar shows two negative frequencies indicating that, in the gas phase, this is a saddle point of second order (SP-2) and not the most stable conformation.

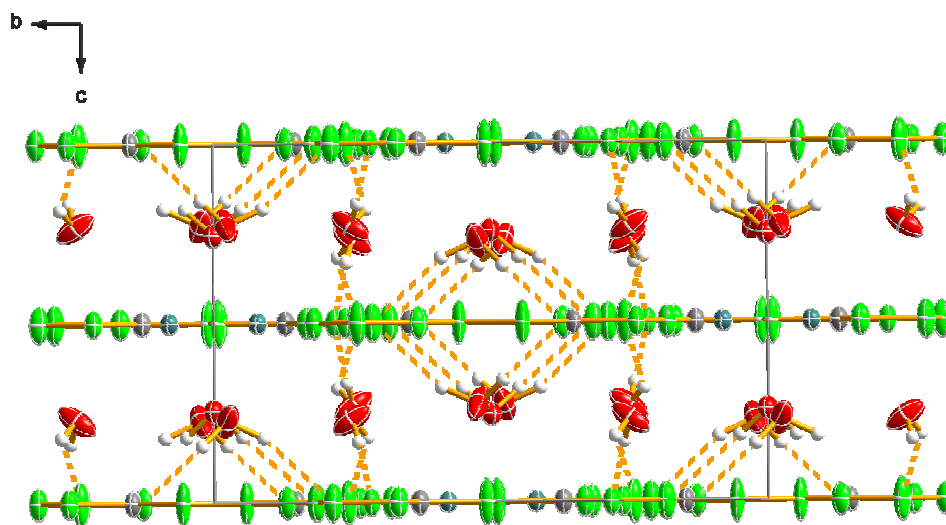
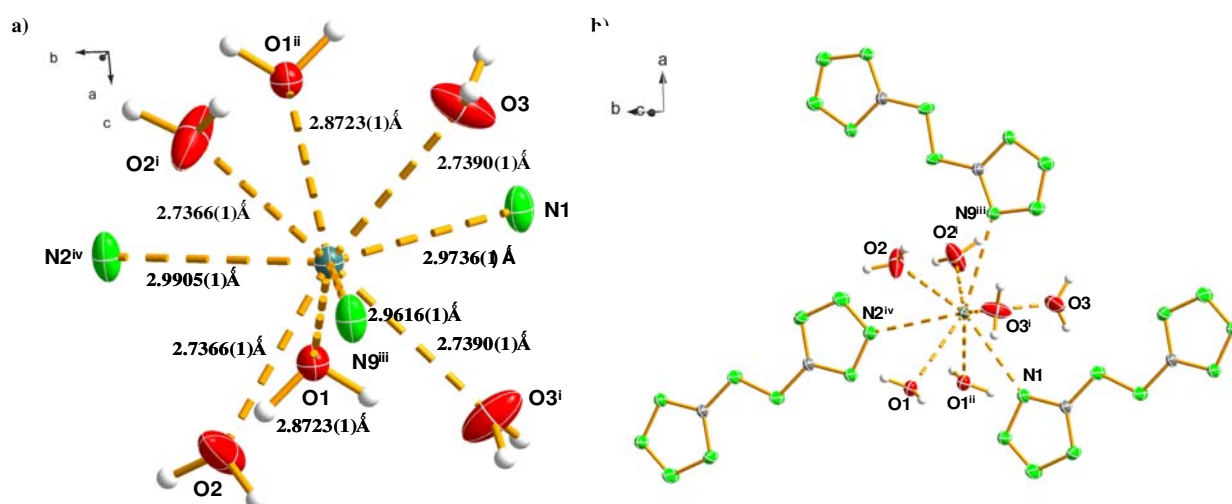


Figure 8.13 View of the unit cell of **113** along the a -axis showing “planar” parallel layers of anions connected through hydrogen bonds (dotted lines) to water molecules.

As represented in Figure 8.13, the layers of anions are connected to one another by strong very directional hydrogen bonds (see Table 8.B7) to water molecules ($O2 \cdots N4^{vii} = 2.900(1) \text{ \AA}$; symmetry code: (vii) $0.5+x, 0.5-y, 2.5-z$). Water molecules hydrogen-bond ring nitrogen atoms of the tetrazolate anion from the top and from the bottom in five out of the eight ring nitrogen atoms with distances between 2.9 and 3.0 \AA and angles between $147(1)$ and $176(2)^\circ$. This is a similar coordination mode to that of the water molecules in metal 5,5'-azotetrazolate salts.^[32a] The hydrazine bridge nitrogen atoms N5 and N10 are not involved in any hydrogen bond interaction. The next electronegative atom that would be available to form a hydrogen bond is O2, placed at more than 3.5 \AA away from N5 (sum of the van der Waals radii $r_O + r_N = 3.07 \text{ \AA}$).^[33] The lack of formation of hydrogen bonds by the hydrazine-bridge nitrogen atoms does not allow to assign the electron density for the hydrogen atoms attached to these nitrogen atoms and is in contrast with the salts of **95** reported previously where strong hydrogen bonds to the hydrazine hydrogen atoms are always present.^[6,7,11] The hydrogen-bonding networks identified by *RPLUTO* are of the type

D1,1(2) some of which are part of other **D1,2(3)** and **D2,2(X)** ($X = 8, 10$) dimeric interactions and one forms a **C2,2(11)** chain pattern and an **R2,4(8)** motif (all of them at the primary level). The ring motif is formed by two water molecules connecting two anions ($O1 \cdots N7^{vi} = 2.910(1) \text{ \AA}$; symmetry code: (vi) $1-x, 1-y, -1+z$). In addition, there exists a characteristic graph-set for this salt of the type **D2,1(3)** formed by a water molecule, which hydrogen-bonds to a nitrogen atom of the anion ($O3 \cdots N6 = 2.900(1) \text{ \AA}$) and to another water molecule ($O3 \cdots N3^{iii} = 2.983(1) \text{ \AA}$; symmetry code: (iii) $0.5+x, 0.5-y, 1.5-z$). At the secondary level the only graph-sets found by the program are finite chains with the label **D2,2(X)** ($X = 4, 5, 9, 10$). Lastly, the coordination number around the metal centre in **113** is nine (Figure 8.14) and is completed by interaction to six water molecules (half of which are generated by symmetry) and three tetrazolate rings. The distances between the water oxygen atoms and the barium atoms vary between $2.737(1)$ and $2.871(1) \text{ \AA}$, whereas the distances to the nitrogen atoms are slightly longer in the range $2.962(1)$ to $2.990(1) \text{ \AA}$. A report of the distances and angles for the coordination around the barium cations is presented in *Appendix B* (Table 8.B14).



above in mind and this observation, we conclude that the “apparent coplanarity” of the two tetrazole rings found in **111**, **112** and **113** is due to disorder in the crystal structure. A solution and detailed discussion of the same is out of the scope of this work and will thus be omitted.

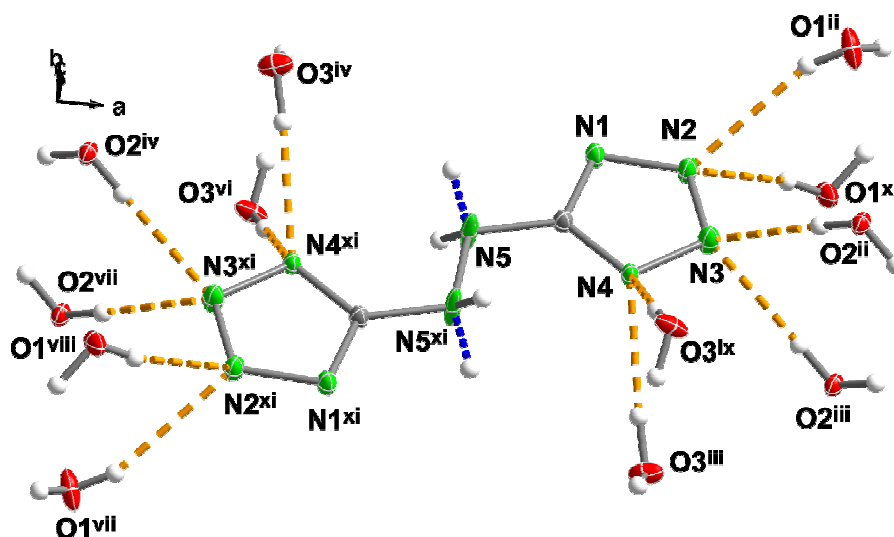


Figure 8.15 Hydrogen-bonding around the HBT^{2-} anion in the crystal structure of **112** showing the elongated ellipsoids for the hydrazine-bridge nitrogen atoms and the split hydrogen atoms. Symmetry codes: (ii) $0.5+x, 0.5-y, 0.5+y$; (iii) $0.5-x, -0.5+y, -0.5+z$; (iv) $-0.5+x, 0.5-y, 0.5-z$; (vi) $-0.5+x, 0.5-y, -0.5+z$; (vii) $-0.5-x, -0.5+y, -0.5+z$; (viii) $-0.5-x, -0.5+y, 0.5+z$; (ix) $0.5-x, -0.5+y, 0.5-z$; (x) $0.5+x, 0.5-y, -0.5-z$; (xi) $-x, -y, -z$.

On the other side, the hydrogen bond distances between donor and acceptor atom are (as discussed for **113**) in the range 2.9 to 3.0 Å and with the exception of one weaker hydrogen bond between water molecules ($\text{O1}\cdots\text{O3}^{\text{vi}} = 3.072(2)$ Å; symmetry code: (vi) $-0.5+x, 0.5-y, -0.5+z$) with an angle of $120(2)^\circ$, also very directional ($158(3)\text{--}180(3)^\circ$). Lastly, with the exception of the **D2,1(3)** graph-set, all the hydrogen-bonding networks discussed for **113** are also present in the structure of **112**.

The coordination number around the cation in **112** is nine as in **113** (Figure 8.16), but as a consequence of the smaller radius of Sr^{2+} in comparison to the Ba^{2+} cation, the contacts are shorter. Six of the distances are shorter and correspond to coordination of the strontium cations to water molecules with distances between 2.558(2) and 2.697(2) Å, whereas the contacts to the nitrogen atoms (three in total) are looser in the range 2.833(2) to 2.871(2) Å (Table 8.B13). Lastly, an interesting detail in the structure is the coordination found in a layer of the compound (Figure 8.A4), where every cation participates in the formation of the three Sr–N contacts mentioned above yielding hexagonal motifs. The space delimited by four anions and four cations is occupied

by crystal water coordinating from above and below the plane of the layers. As expected due to the high similarity of the structures, **111** and **113** also form similar hexagonal motifs.

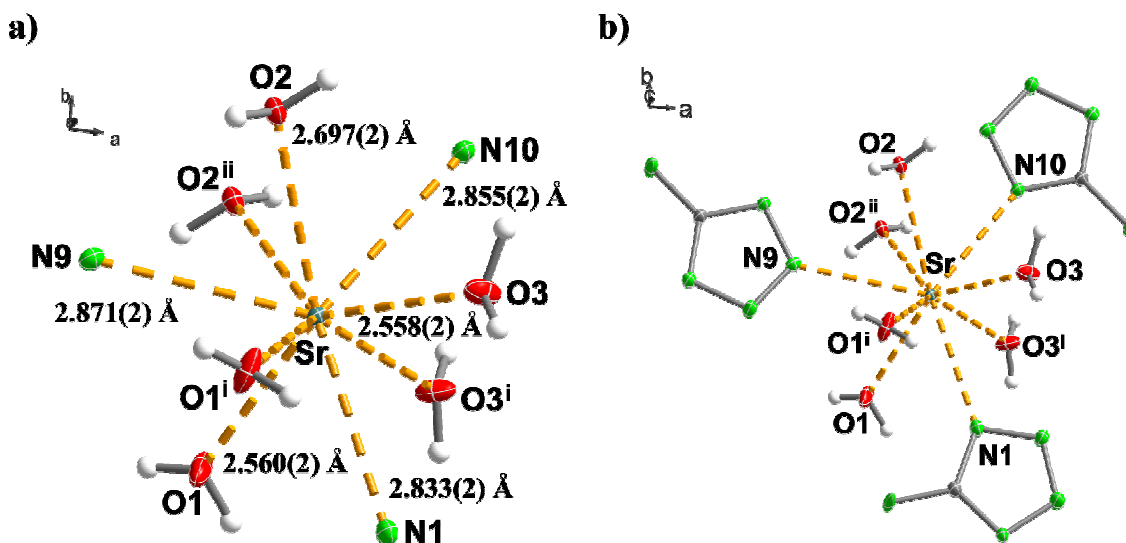


Figure 8.16 a) Simplified and b) Full coordination (the hydrazine-bridge hydrogen atoms are omitted) around the metal centre in **112**. Symmetry codes: (i) $x, y, -z$; (ii) $-x, 1-y, -z$.

The relatively small electron density of calcium allowed to find the hydrazine-bridge protons in **111**, which, similarly to **112** occupy split positions, as suggested by the elongated ellipsoids of the corresponding nitrogen atoms (N5 and N6). Figure 8.A5 shows a view of the unit cell of the compound along the c -axis where the “apparent coplanarity” of the tetrazole rings is obvious. The similarities in the packing between **111** and **112** and **113** are manifested, first of all, by the similar cell parameters ($a \sim 7$, $b \sim 11$ and $c \sim 14$ Å) found in the three compounds, which decrease with the smaller size of the cation (**113** > **112** > **111**) and for the coordination to the metal centre. Two cations are connected by two bridging water molecules (Figure 8.A5), which are generated by symmetry ($\text{Ca}-\text{O1} = \text{Ca}-\text{O1}^{\text{ii}} = 2.570(1)$ Å; symmetry code: (ii) $-x, -y, -z$). Each cation has a coordination number of nine (Figure 8.17) with short distances to oxygen atoms in the range $2.408(1)$ to $2.570(1)$ Å and longer contacts to nitrogen atoms between $2.788(2)$ and $2.806(2)$ Å (Table 8.B12). Finally, a total of five hydrogen bonds are found in the structure, which are analogous to those discussed for **112** and **113** but slightly more directional ($161(2)$ – $179(2)^\circ$) and slightly shorter ($\text{O1} \cdots \text{N3} \sim 2.9$ Å). As a consequence the hydrogen-bonding networks (except for the **D2,1(3)** graph-set found in **113**) are to practical effects identical (e.g., the **R2,4(8)** graph-set is formed by the hydrogen bond $\text{O3} \cdots \text{N7}^{\text{ii}} = 2.901(2)$ Å; symmetry code: (ii) $0.5+x, 0.5-y, 0.5+z$).

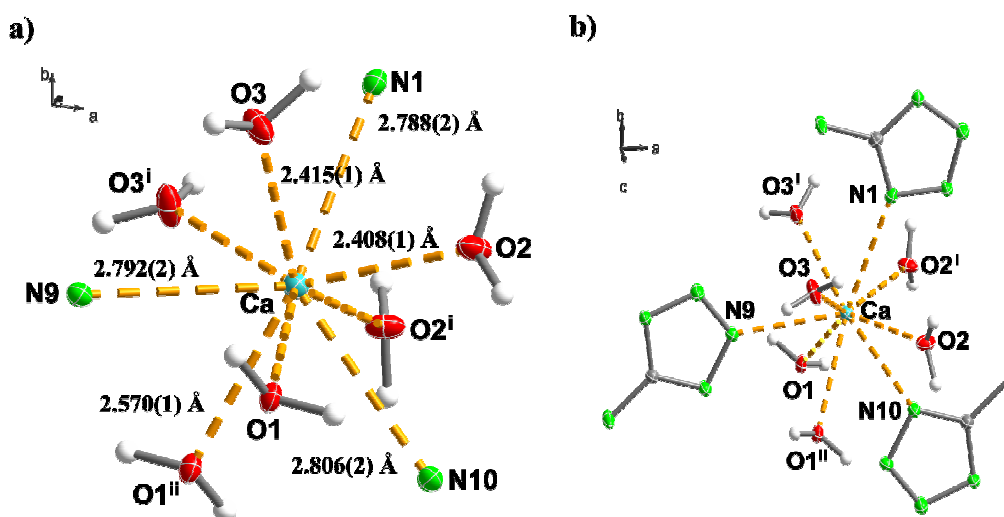


Figure 8.17 a) Simplified and b) Full coordination (the hydrazine-bridge hydrogen atoms are omitted) around the metal centre in **111**. Symmetry codes: (i) $x, y, -z$; (ii) $-x, -y, -z$.

The magnesium salt (**MgHBT**, **110**) is the first of the series, which does not present the disorder commented above for the rest of the alkaline earth metal salts of **95**. **110** crystallizes in a triclinic cell (space group $P\bar{1}$) in contrast to **111**, **112** and **113** and, regardless of the smaller size of the Mg^{2+} cation in comparison to Ca^{2+} , Sr^{2+} and Ba^{2+} , it forms the largest cell (1220 \AA^3) due to the higher amount of crystal water molecules in the structure (6.5 in **110** vs. 5 in the remainder of the alkaline earth metal salts). The tetrazole rings are unequivocally non-planar with an angle of $\sim 40^\circ$ between them and the asymmetric unit (Figure 8.18) is formed by two crystallographically independent anions, two cations and thirteen molecules of water.

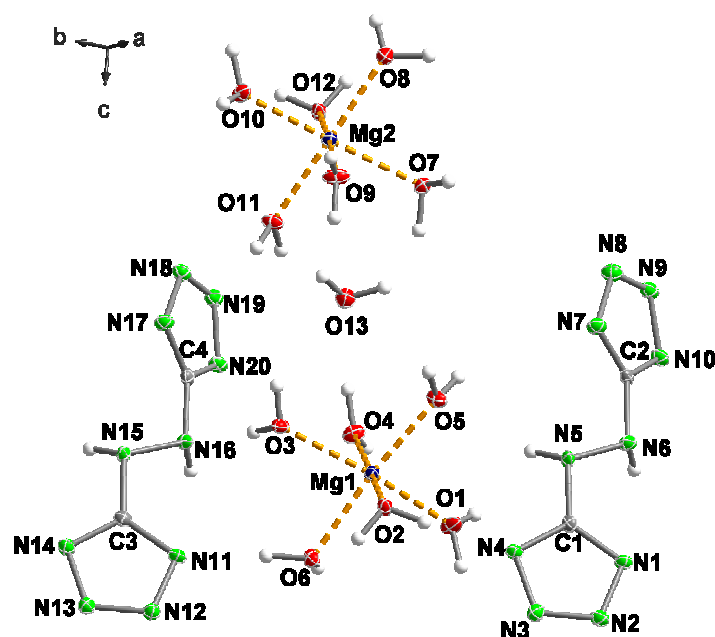


Figure 8.18 Asymmetric unit of **110** with the labeling scheme (the hydrogen bonds between the water molecules and O13 have been omitted for clarity purposes).

Each cation in **110** is surrounded by six water molecules with very little variation in the contact distances (~ 2.0 – 2.1 Å, Table 8.B11) forming slightly distorted octahedrons, whereas the remaining water molecule links two octahedrons by hydrogen bonds to water molecules ($O9\cdots O13 = 2.708(2)$ Å and $O4\cdots O13 = 2.717(2)$ Å). Figure 8.A6 shows a view of the unit cell of **110** along the *a*-axis where the anions are oriented approximately parallel to the *c*-direction without contacts between nitrogen and magnesium atoms. However, every nitrogen atom in the structure (including the hydrazine-bridge atoms N5/15 and N6/16) is involved in hydrogen-bonding forming a total of 28 $O\cdots N$ interactions to water molecules. Figure 8.19 shows the hydrogen-bonding around one of the two crystallographically independent HBT^{2-} anions (type **B**). One type of anion acts as a hydrogen bond acceptor ($O\cdots N$) with distances to the donor atom in the range 2.70–2.95 Å and as a hydrogen bond donor using the hydrazine-bridge nitrogen atoms ($N\cdots O$) with weaker interactions (~ 3.22 Å), whereas the other anion show somewhat different distances with $O\cdots N$ in the range 2.69–3.11 Å and $N\cdots O \sim 3.11$ Å. A complete record of these distances is found in Appendix B (Table 8.B7).

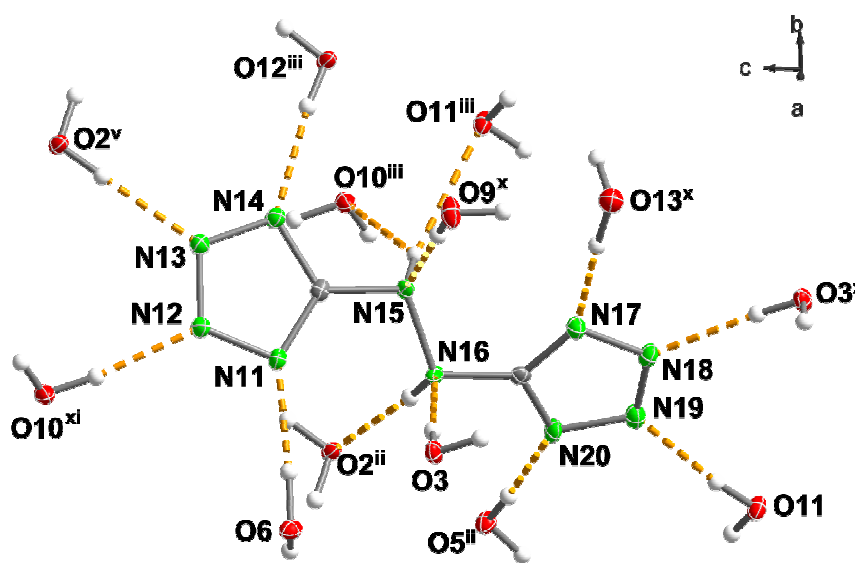


Figure 8.19 Hydrogen-bonding around the HBT^{2-} anion in the crystal structure of **110** showing the non-planar tetrazole rings. Symmetry codes: (ii) $-1+x, y, z$; (iii) $-x, 1-y, 1-z$; (v) $1-x, 1-y, 2-z$; (x) $1-x, 1-y, 1-z$; (xi) $x, y, 1+z$.

The lithium salt (**LiHBT**, **105**) crystallizes with three molecules of crystal water in analogy to lithium 5-nitrotetrazolate (*Chapter III*).^[34] Both crystallographically independent lithium atoms (Li1 and Li2) in the asymmetric unit have a coordination number of four (Figure 8.20) keeping in with other lithium salts.^[30b] Li1 has three contacts to nitrogen atoms and one to an oxygen atom of a water molecule, whereas Li2 is coordinated by three water molecules and has one contact to a nitrogen atom of an HBT^{2-} anion and both Li^+ cations show distorted tetrahedral geometries. Table

8.B8 contains summarized the distances and angles for the coordination around the two metal centers. The Li–N and Li–O distances are in the range 1.9–2.1 Å, as expected, although there exists a longer contact to a nitrogen atom (Li1–N9ⁱⁱ and Li2–N5 ~ 2.8 Å; symmetry code: (ii) 1-x, 1-y, 1-z). Figure 8.A7 shows a view of the packing in the unit cell of the compound. In contrast to the 5,5′-azotetrazolate analogue, where the anion is planar and the compound crystallizes forming layers, the two tetrazole rings in **105** are bent in respect to each other (C1–N5–N6–C2 = -140.1(1)°).

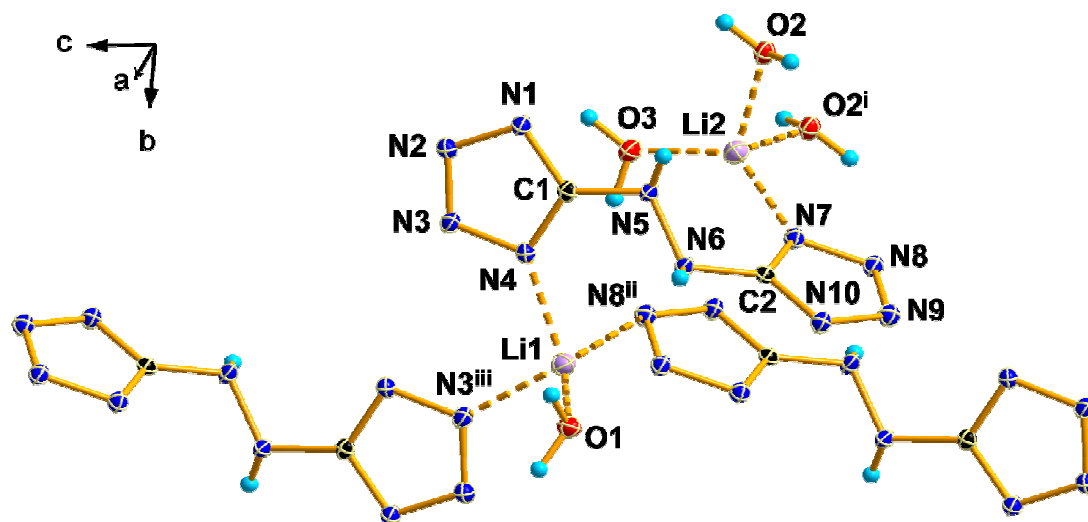


Figure 8.20 Coordination around the Li⁺ cations in the crystal structure of **105** and labeling scheme. The long Li–N contacts (~ 2.8 Å) have been omitted for the sake of simplicity. Symmetry codes: (i) 1-x, -y, 1-z; (ii) 1-x, 1-y, 1-z; (iii) 1-x, 1-y, 2-z.

In addition to contacts to the Li⁺ cations, there exist many hydrogen bonds in the structure of **105** (Table 8.B6). At the primary level there exist seven dimeric **D1,1(2)** and two ring **R2,2(12)** graph-sets, which combine at the secondary level to form many **D1,2(3)**, **D2,2(X)** (X = 4, 5, 8, 9), **D2,3(9)** and **D3,3(X)** (X = 9, 13, 15) finite patterns, chain **C2,2(X)** (X = 10–12) graph-sets and, more interestingly, ring **R2,1(3)** and **R2,4(8)** hydrogen-bonded networks. Figure 8.21 shows depicted a **R2,4(8)** and a **R2,2(12)** ring graph-sets formed by two HBT²⁻ anions and bridging water molecules (O1...N1ⁱⁱ = 2.963(1) Å, O1...N1^v = 2.933(1) Å; symmetry codes: (ii) -x, 1-y, 2-z; (v) x, 1+y, z) and by two HBT²⁻ anions (N5...N9ⁱ = 2.956(1) Å; symmetry code: (i) -x, 1-y, 1-z), respectively.

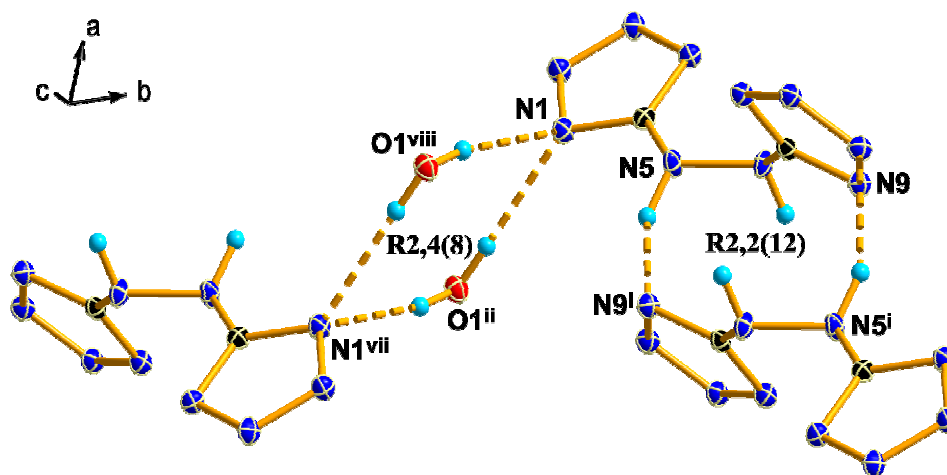


Figure 8.21 Characteristic hydrogen-bonding ring graph-sets in the crystal structure of **105**. Symmetry codes: (i) $-x, 1-y, 1-z$; (ii) $-x, 1-y, 2-z$; (vii) $-x, -y, 2-z$; (viii) $x, -1+y, z$.

In contrast to the lithium salt, the rubidium compound (**RbHBT**, **108**) does not contain crystal water in the structure. This and the larger size of the cation are reflected in the differences in the packing and the larger cell of the rubidium derivative ($833(1) \text{ \AA}^3$ *vs.* $468(1) \text{ \AA}^3$), respectively. Every single ring nitrogen atom in the HBT^{2-} anion of **108** is involved in coordination to Rb^+ cations. Figure 8.22 shows a view of the coordination around one of the two crystallographically independent cations (**Rb1**). **Rb1** has a coordination number of nine with distances to the metal center in the range $\text{Rb1-N} \sim 3.00\text{--}3.22 \text{ \AA}$ with the next nitrogen atom (**N9**) placed at $3.465(2) \text{ \AA}$, whereas **Rb2** shows nine contacts with distances in the range $\text{Rb2-N} \sim 2.95\text{--}3.26 \text{ \AA}$ and two not significantly longer interactions to **N1** and **N3** at $3.360(2)$ and $3.324(2) \text{ \AA}$, respectively (Table 8.B9).

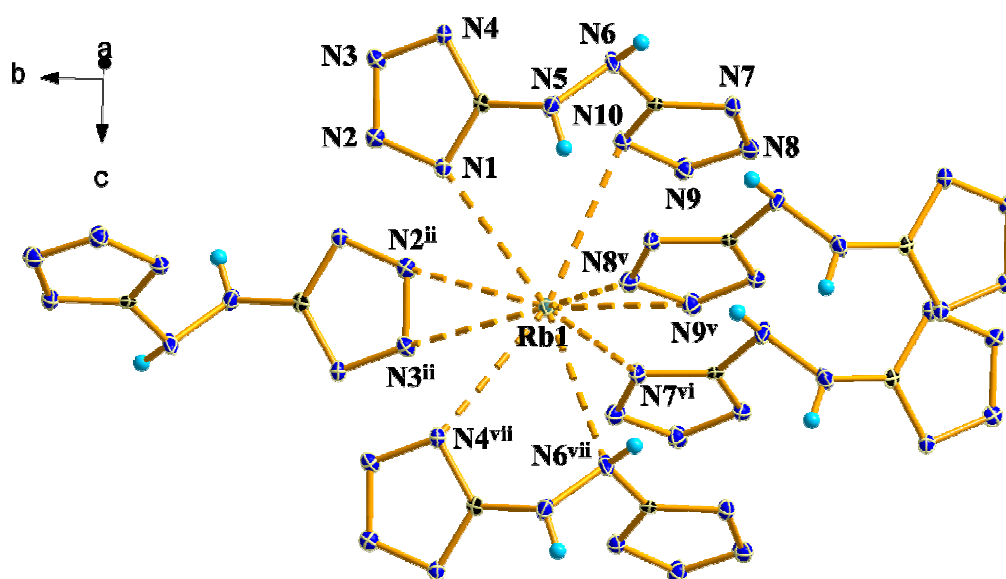


Figure 8.22 Coordination around the Rb^+ cations (**Rb1**) in the crystal structure of **108** and labeling scheme. Symmetry codes: (ii) $-x, 1-y, 2-z$; (v) $0.5+x, 0.5-y, 0.5+z$; (vi) $-0.5+x, 0.5-y, 0.5+z$; (vii) $x, y, 1+z$.

The dihedral angle C1–N5–N6–C2 with a value of $83.8(3)^\circ$ is as expected for salts containing the HBT²⁻ anion^[11] and comparable to the rest of the compounds reported here. The torsion of the two tetrazolate rings is also deciding in conditioning the packing (Figure 8.23). The tetrazolate rings with the labels C2 to N10 form layers along a direction that cuts the *a*-axis at an angle of $\sim 20^\circ$ and are connected among them by hydrogen bonds *via* one of the hydrazine-bridge nitrogen atoms with $N6 \cdots N9^{\text{ii}} = 3.104(3) \text{ \AA}$ (symmetry code: (ii) $0.5+x, 0.5-y, -0.5+z$) describing **C1,1(6)** chain graph-sets. Three weak ($3.10\text{--}3.25 \text{ \AA}$) hydrogen bonds are formed in total. In addition to the aforementioned hydrogen bond, the other hydrazine-bridge nitrogen atom (N5) forms two other hydrogen bonds, which describe **C1,1(5)** chain graph-sets, at the primary level. At the secondary level, **C2,2(X)** ($X = 6, 7, 10, 11$) motifs and one **R2,1(3)** ring network are being formed. For example, the latter is described by the hydrogen bridges formed by N5 and two (almost equidistant) nitrogen atoms belonging to the same tetrazolate ring ($N5 \cdots N8^{\text{i}} = 3.246(3)$ and $N5 \cdots N7^{\text{i}} = 3.179(3) \text{ \AA}$; symmetry code: (i) $0.5+x, 0.5-y, 0.5+z$).

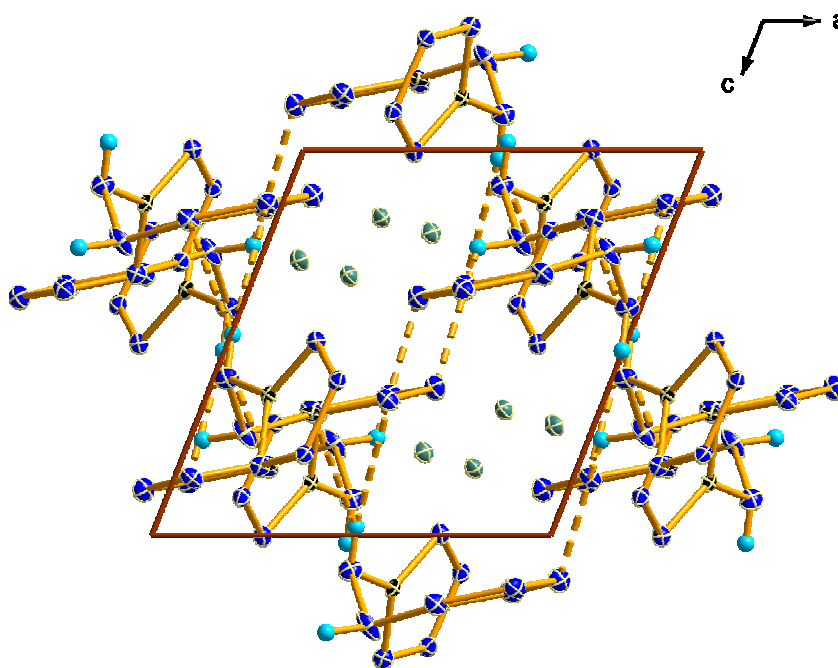


Figure 8.23 Tetrazolate layers and hydrogen-bonding (dotted lines) in the unit cell of **108**.

Cesium 5,5′-hydrazinebistetrazolate (**CsHBT**, **109**) is one of the few examples of a cesium salts with an azolate anion known in the literature.^[35,36] The two halves of the anion and the two Cs⁺ cations are crystallographically independent and are linked to each other by coordination. As represented in Figure 8.24 every one of the two cesium atoms is surrounded by five anions. Cs1 has a coordination number (CN) of 10+2 with ten distances to the nitrogen atoms in the range $3.2\text{--}3.4 \text{ \AA}$ and two longer contacts at $\sim 3.7 \text{ \AA}$ (not represented in Figure 8.24), whereas Cs2 interacts to the anions at distances of $3.1\text{--}3.5 \text{ \AA}$ with a CN of 11 (Table 8.B10). Figure 8.25a shows a view of the

unit cell of the compound along the *b*-axis where there is not evidence of aromatic π - π stacking between tetrazole rings. The tetrazole rings belonging to one anion are with torsion angles $C1-N5-N6-C2 = 83.4(3)^\circ$ almost perpendicular, similarly to **108**, which is in contrast with the solvated species in this and other studies.^[11]

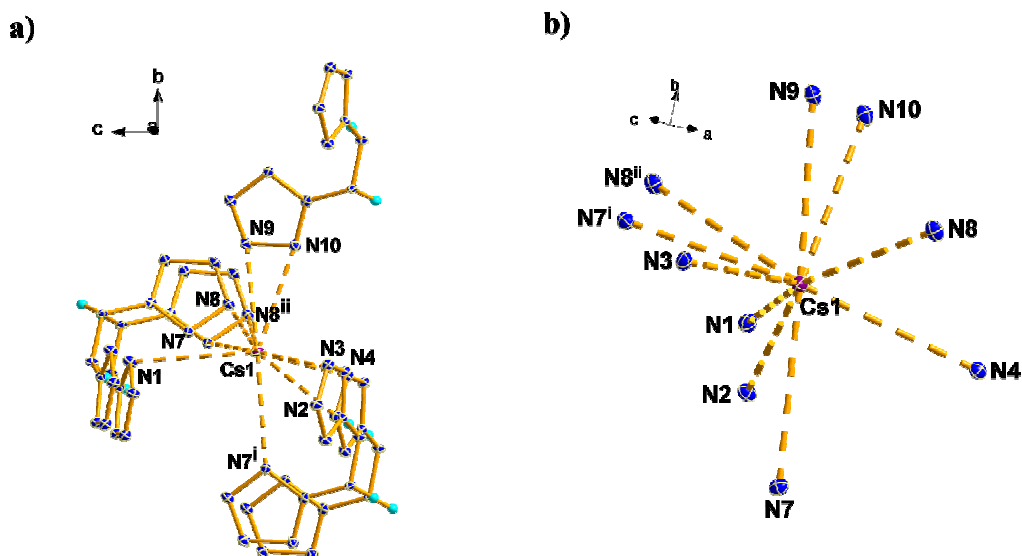


Figure 8.24 a) Full and b) simplified coordination around one of the Cs^+ cations ($Cs1$) in the crystal structure of **109**. Symmetry codes: (i) $-0.5+x, 0.5-y, 2-z$; (ii) $-1+x, y, z$.

In addition to the contacts to the metal, there exists two hydrogen bonds ($N5 \cdots N2 = 3.024(3)$, $N6 \cdots N4^i = 3.060(4)$ Å; symmetry code: (i) $2-x, 0.5+y, 1.5-z$) by using the hydrazine-bridge hydrogen atoms of one anion well within the sum of the van der Waals radii ($r_N + r_N = 3.10$ Å),^[37] which describe two **C1,1(5)** chain motifs at the primary level and **C2,2(X)** ($X = 7, 10$) graph-sets at the secondary. Also identified by the program *RPLUTO*, four anions combine through hydrogen-bonding to form a ring graph-set with the label **R4,4(17)**, again at the secondary level. Lastly, the distances and coordination numbers around the metal centers are in agreement with previously reported metal salts with azole-based anions.^[34-36]

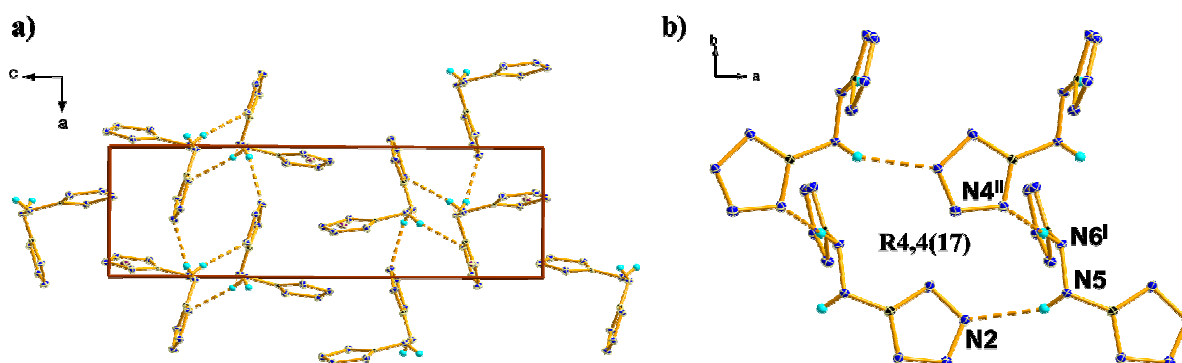


Figure 8.25 a) Hydrogen-bonding in the unit cell (view along the *b*-axis) and b) **R4,4(17)** hydrogen-bonding network in the crystal structure of **109**. Symmetry code: (i) $2-x, 0.5+y, 1.5-z$.

8.3.4 Thermal Stability and Energetic Properties of Nitrogen-rich 5,5'-Hydrazinebistetrazole Derivatives

The sensitivity to thermal stimuli of the nitrogen-rich compounds **2**, **4** and **6-9** was measured by differential scanning calorimetry (DSC) at a heating rate of 5 °C min⁻¹ (unless otherwise specified). Figure 8.26 shows a typical DSC curve for the nitrogen-richest compound in this work (**95**). The material has an excellent thermal stability decomposing at 208 °C (DSC on-set) without melting. The dimethyl derivative **97** has a similar decomposition point at 202 °C in addition to an endothermic peak corresponding to the loss of the tightly-bound crystal water at 138 °C. The nitrogen-rich salts of **HBt** (**95**) with ammonium (**99**) and guanidinium (**101**) cations decompose both at temperatures above 190 °C and the crystal water in **99** is lost at ~110 °C, whereas the hydrazinium (**100**) and aminoguanidinium (**102**) salts show slow decomposition over a relatively broad range starting at ~150 °C (see Table 8.1).

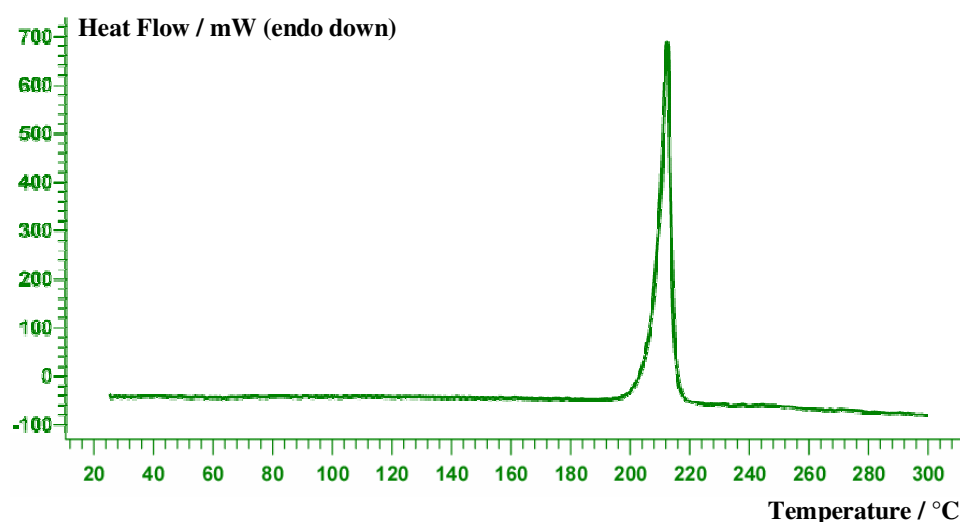


Figure 8.26 DSC plot of **95** at a heating rate of 2 °C min⁻¹. The compound decomposes exothermically without melting at 208 °C (DSC on-set).

Table 8.2 contains tabulated the friction (f), impact (i) and electrostatic discharge sensitivity results for the nitrogen-rich 5,5'-hydrazinebistetrazole derivatives. No detonation was observed in the drop hammer test at >30 J (**95** has an impact sensitivity of ~60 J) nor at the maximum setting in the friction tester (>360 N)^[38-40] with the exception of **95** (f = 108 N). **95**, its methylated derivative (**97**) and nitrogen-rich salts containing the HBT²⁻ anion (**99**, **100**, **101** and **102**) were (with the exception of **95**, which has a similar friction sensitivity to RDX or HMX) less sensitive to friction (f) and impact (i) than RDX or HMX (both f = 120 N and i = 7.4 J) and TNT (f = 355 N and i = 15 J).^[41] This is to be expected for compounds **95** and salts **99-102** because extensive hydrogen-bonding helps to stabilize a material and interesting since the two tunable properties of which the performance of a

material is proportional (density and heat of formation) are generally increased and only slightly decreased (less positive), respectively. Since the performance of an energetic material is most heavily dependent on density, increases in this property tend to outweigh the adverse affect on heat of formation caused by strong hydrogen-bonding.^[41] This is the principal reason why compounds that can form multiple hydrogen bonds are of interest as prospective insensitive materials with high densities and performances.^[42-43] The lower sensitivity of the methylated isomer **97** can be explained by the stabilization derived from the introduction of methyl groups (see *Chapter VI*) as well as the presence of one molecule of crystal water, which stabilize the material. Lastly, all nitrogen-rich 5,5'-hydrazinebistetrazole derivatives are safe for transport under the UN Recommendations on the Transport of Dangerous Goods as described in ref. [38].

Table 8.1 Physico-chemical properties of nitrogen-rich 5,5'-hydrazinebistetrazole derivatives.

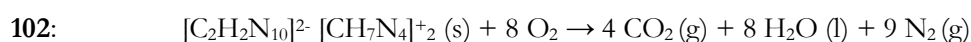
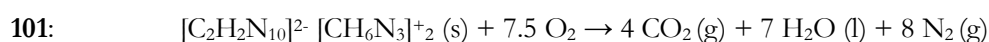
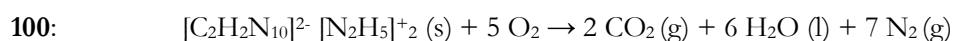
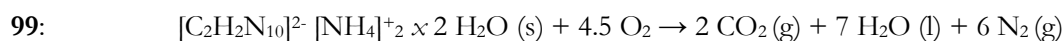
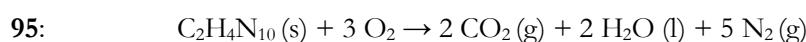
	95	99	100	101	102
Formula	C ₂ H ₄ N ₁₀	C ₂ H ₁₄ N ₁₂ O ₂	C ₂ H ₁₂ N ₁₄	C ₄ H ₁₄ N ₁₆	C ₄ H ₁₆ N ₁₈
Mol. Mass (g mol ⁻¹)	168.12	238.21	232.21	286.16	316.18
T _m (°C) ^a	-	-	154	-	142
T _d (°C) ^b	208	196	154-182	214	142-194
ΔH _{sub} / J mol ⁻¹ ^c	90				
N (%) ^d	83.3	70.6	84.5	78.3	79.7
Ω (%) ^e	-57.1	-60.4	-68.9	-96.8	-102.8
ρ (g cm ⁻³) ^f	1.841	1.622	1.598*	1.602*	1.618*
Δ _c U° / cal g ⁻¹ ^g	-2990(40) [-2396]	-3250(20)	-3320(15) [-3932]	-3280(15) [-3843]	-3390(20) [-3879]
Δ _c U° / kJ kg ⁻¹ ^h	4500(100) [2566]	2040(80) [4190]	3260(60) [5816]	1350(70) [3716]	2110(90) [4152]
Δ _c H° / kJ kg ⁻¹ ⁱ	4400(100) [2463]	1840(80) [3992]	3040(60) [5603]	1230(70) [3517]	1970(90) [3948]

^aChemical melting point and ^bDecomposition point (DSC onsets, β = 5 °C min⁻¹; ^cNitrogen percentage; ^dOxygen balance (ref. [44]); ^eX-ray or picnometer (*) density. ^fExperimentally determined (oxygen bomb calorimetry) enthalpy of combustion with uncertainty in curved brackets (). ^gExperimentally determined (back-calculated from ΔH_{comb.}) energy of formation; ^hExperimentally determined enthalpy of formation. ⁱCalculated values in square brackets []

The physico-chemical properties of the nitrogen-rich 5,5'-hydrazinebistetrazole derivatives are tabulated in Table 8.1. All compounds have high nitrogen contents in the range between 65.4% (**97**) and 84.4% (**100**) and, as expected from nitrogen-rich compounds, highly negative oxygen balances between -53.1% (**95**) and -90.6% (**97**) similar to TNT (Ω = -74.0%). The density, from the X-ray measurement, for **95** is exceptionally high in comparison to the parents 5-amino-1*H*-tetrazole^[25] and 1-5-diamino-1*H*-tetrazole,^[26] which have density values of ~0.3 g cm⁻³ lower and the values (calculated or determined by means of a picnometer) of **97**, **99**, **100**, **101** and **102** are higher than those of analogous 5,5'-azotetrazolate salts^[3] (see also *Chapter VII*) and comparable to the recently reported **BTA** (**96**) salts from Shreeve et al. with the same cations.^[10] The density values play a

determining role in the values for the detonation parameters of the compounds (see discussion below).

The energies of formation of the nitrogen-rich derivatives of **95** were back-calculated from the heat of combustion on the basis of their combustion equations (see below), Hess's Law, the known standard heats of formation for water and carbon dioxide^[45] and a correction for change in gas volume during combustion. The experimentally determined values for all materials are highly positive specially in the case of the free acid **95** (+4500(100) kJ kg⁻¹) and their heats of formation are comparable to that of bishydrazinium 5,5'-azotetrazolate for which $\Delta H_f^\circ \sim +3700$ kJ kg⁻¹.^[46]



Using the molecular formula, the energy of formation and either the calculated (from X-ray) or measured (from picnometer) density, the EXPLO5 code^[47] was used to determine the detonation parameters of the nitrogen-rich salts of **95**. The results are summarized in Table 8.2 together with the detonation parameters of **BTA (96)** salts: ammonium (**ABTA, 118**), hydrazinium (**HBTA, 119**), guanidinium (**GBTA, 120**), aminoguanidinium (**AGBTA, 121**), diaminoguanidinium (**DAGBTA, 122**) and triaminoguanidinium (**TAGBTA, 123**) for comparison purposes. The values presented in Table 8.2 for the detonation parameters of salts of **96** are all predicted based on isodesmic reactions [10] to calculate the heats of formation of the compounds and using the CHEETAH software.^[48] We used the EXPLO5 software with the following values for the empirical constants in the Becker-Kistiakowsky-Wilson equation of state (BKWN-EOS): $\alpha = 0.5$, $\beta = 0.176$, $\kappa = 14.71$ and $\theta = 6620$. In order to correlate the measured values for the physico-chemical properties and detonation parameters of the compounds, density functional (DFT) calculations were carried out using the program package G03W.^[22] The structure and frequency calculations were performed with Becke's B3 three parameter hybrid functional using the LYP correlation functional (B3LYP)^[23] for neutral **95**, whereas for the ionic compounds the electronic energies for all cations and the 5,5'-hydrazinebistetrazolate anion were calculated using Møller-Plesset perturbation theory truncated at

the second order (MP2)^[49] and were used unscaled. The results of the MP2 electronic energy calculations are tabulated in *Appendix A*, Table 8.A7. For all atoms in all calculations, the Dunning's correlation consistent polarized double-zeta basis set cc-pVDZ was used.^[50,51] The results of the DFT calculations for neutral **95** (see Table 8.A4) suffer of relatively large disagreement with the experimental values, possibly attributable to the low capacity of the B3LYP method to estimate satisfactory heats of formation for neutral molecules. However, the experimental and calculated values for the ionic salts (**99**, **100**, **101** and **102**) based on the MP2 method are in reasonable agreement and are also given in Table 8.2 in square [] brackets.

The experimentally obtained (from bomb calorimetry) detonation velocity of **95** ($D = 9463 \text{ m s}^{-1}$) is higher than that of octogen (HMX, $D = 9216 \text{ m s}^{-1}$) and comparable to the high explosive CL-20 at its maximum density ($D = 9632 \text{ m s}^{-1}$), regardless of the (although high) lower density of **95** in respect to CL-20 (1.841 g cm^{-3} *vs.* 2.020 g cm^{-3}). The detonation pressure of **95** ($P = 36.7 \text{ GPa}$) is between that of RDX ($P = 34.0 \text{ GPa}$) and that of HMX ($P = 38.2 \text{ GPa}$). Formal methylation of **95** to form **97** and **98**, would be expected to result in a decrease of the sensitivity towards shock and (specially interesting) towards friction (see discussion above) at the cost of sacrificing some performance. However, formation of the nitrogen-rich salts **99**, **100**, **101** and **102** containing the HBT²⁻ anion results in compounds, which are much less sensitive towards friction and impact^[52,53] than the free acid **95** (see also *Chapter III*), while still having high (calculated based on the MP2 method) detonation pressures and velocities above $\sim 30 \text{ GPa}$ and $\sim 9000 \text{ m s}^{-1}$, respectively (Table 8.2). The decrease of the predicted performance when comparing **95** with its nitrogen-rich salts is expected due to the lower density of the salts. This is a similar observation to that made for nitrogen-rich salts of 5-(5-nitrotetrazole-2-ylmethyl)-tetrazole (**NTTz**, *Chapter IX*), where the free acid is also relatively sensitive (towards impact) but formation of nitrogen-rich salts results in slightly decrease of the detonation parameters and the formation of insensitive (or less sensitive) materials. Furthermore, the (EXPLO5) detonation parameters of **95** and its salts fit nicely with and are higher than the calculated values for salts of **96** (CHEETAH)^[10] or those containing the ZT²⁻ anion (EXPLO5)^[3c] and the same nitrogen-rich cations (i.e., guanidinium (**GZT**, **124**), aminoguanidinium (**AGZT**, **125**), diaminoguanidinium (**DAGZT**, **126**) and triaminoguanidinium (**TAGZT**, **127**)). Lastly, it is important to point out that the systematic overestimation of the detonation parameters based on electronic energies is specially high when comparing the (MP2 method) computed values for 5,5'-azotetrazolate salts with those predicted by the Kamlet and Jacobs equations (Table 8.2), therefore, we believe the disagreement between computed and “experimental” detonation parameters for the 5,5'-hydrazinebistetrazole derivatives studied here to be justified.

Table 8.2 Initial safety testing results and calculated energetic performance of nitrogen-rich 5,5'-hydrazinebistetrazole (**95**) derivatives (using the EXPLO5 code) and comparison with analogous salts of **BTA** (**96**) and **H₂ZT** (**75**).

	T_{ex} (K) ^a	V_0 (L kg ⁻¹) ^b	P (GPa) ^c	D (m s ⁻¹) ^d	Shock (J) ^e	Friction (N) ^f	ESD (+/-) ^g	Thermal Shock
95	3568 [2539]	781 [782]	36.7 [27.7]	9464 [8523]	60	108	–	Deflagrates
97	<i>Compound not tested in bulk</i>				>100	>360	–	Burns
99	2938 [3849]	962 [960]	31.3 [39.4]	9423 [10330]	>30	>360	–	Deflagrates
100	2756 [3819]	935 [929]	29.0 [38.5]	9272 [10341]	>30	>360	–	Deflagrates
101	1880 [2928]	876 [870]	19.9 [29.2]	7914 [9159]	>30	>360	–	Deflagrates
102	2240 [3124]	893 [888]	24.6 [33.1]	8630 [9666]	>30	>360	–	Deflagrates
118^b			[21.6]	[8309]				
119^b			[34.9]	[9926]				
120^b			[17.5]	[7636]				
121^b			[22.9]	[8486]				
122^b			[23.6]	[8560]				
123^b			[23.9]	[8572]				
124^g	[3154]	975 [843]	15.4 [26.0]	6192 [8682]	32	>360		Burns
125^g	[3321]	999 [865]	16.6 [28.1]	6418 [8994]	15	>360		Deflagrates
126^g	[3432]	1026 [881]	20.4 [33.0]	7045 [9601]	4	>360		Deflagrates
127^g	[3644]	1058 [895]	24.2 [35.3]	7654 [9902]	4	60		Deflagrates

^aTemperature and ^bVolume of the explosion gases; ^cDetonation pressure; ^dDetonation velocity; ^eCritical diameter from Koenen (steel sleeve) test; ^fShock and friction sensitivities. Tests according to BAM methods (see ref. [38–40]); ^gRough sensitivity to electrostatic discharge: + sensitive, - insensitive. ^hOnly the detonation parameters (P and D) using the CHEETAH software have been reported for the salts of **96** (ref. [10]). ⁱThe detonation parameters for the salts of **H₂ZT** (**75**) are based on Kamlet and Jacobs equations and the gas volume was predicted using the ICT code (ref. [18b]).

Although the neutral 5,5'-hydrazinebistetrazole derivatives (**95** and **97**) are solids, which are perfectly stable towards oxidation when left in contact with air for extended periods of time, the nitrogen-rich salts containing the HBT²⁻ anion (**99**, **100**, **101** and **102**) might see their application limited regardless of their interesting energetic properties due to slow oxidation when left in contact with air. **99** and **101** turn yellow (oxidation to the 5,5'-azotetrazolate derivative) on standing in air for several days in an open beaker, whereas **100** and **102** contain both a (reducing) hydrazine moiety, which prevents oxidation and the materials are stable for at least several months when stored in closed containers. A way of taking advantage of the energetic properties of these compounds regardless of their susceptibility to oxidation would certainly prove useful. For example, it might be

suggested to sacrifice some of the performance of these materials by coating them (e.g., wax) or mixing them with a reducing agent (e.g., finely divided magnesium powder), depending on the application, making them more stable towards oxidation. Lastly, the high-nitrogen content, and high-performance and stability of **95** (among many other properties discussed herein) make the compound of prospective interest for use as a propellant or in propellant mixtures.

Due to the negative oxygen balances of all materials studied here, it is of interest to calculate mixtures with an oxidizer at a neutral oxygen balance in order to further increase the performance in comparison with the pure compounds. Thus, the detonation parameters for formulations of all 5,5'-hydrazinebistetrazole derivatives with an oxidizer such as ammonium nitrate (AN) or ammonium dinitramide (ADN) were calculated (Tables 8.A5 and 8.A6). From these studies it would be expected an increase in the detonation parameters of the lower-performing methylated derivatives **97** and **98** when mixing them with AN or ADN (a more notorious increase when using ADN as an oxidizer) similarly to what we observed in 5,5'-azobistetrazole derivatives (*Chapter VII*). The detonation parameters of the higher-performing compounds **95**, **99**, **100**, **101** and **102** are only decreased by adding an oxidizer, much more notoriously in the case of mixtures with AN. In summary, it makes sense to boost the performance of lower-performing compounds by adding an oxidizer due to their more highly negative oxygen balance, but the better “oxygen-balanced” nitrogen-rich compounds (**95**, **99**, **100**, **101** and **102**) are already outstandingly high-performing as the pure materials and formulations with an oxidizer do not do but decrease the performance values.

8.3.5 Thermal Stability and Energetic Properties of Metal Salts of **95**

In order to assess the energetic properties of alkali and alkaline earth metal salts of **95** (**105-113**) the thermal stability (from DSC measurements) and sensitivity towards thermal shock, friction and impact of each salt was experimentally determined (Table 8.3). In addition, due to the energetic character of the HBT²⁻ anion, the (constant volume) energy of combustion of all materials was also determined experimentally using oxygen bomb calorimetry. Lastly, the heats of combustion and formation were back-calculated from the combustion data.

Table 8.3 Physico-chemical properties of alkali and alkaline earth metal salts of **95**.

	101	102	103	104	105
Formula	C ₂ H ₈ N ₁₀ Li ₂ O ₃	C ₂ H ₃ N ₁₀ Na ₂ O _{0.5}	C ₂ H ₂ N ₁₀ K ₂	C ₂ H ₂ N ₁₀ Rb ₂	C ₂ H ₂ N ₁₀ Cs ₂
MW (g mol ⁻¹)	234.11	221.03	243.97	335.87	431.86
Impact (J) ^a	>30	~30	~30	~30	~30
Friction (N) ^a	>360	>360	>360	>360	>360
Electrostatics ^b	–	–	–	–	–
Flame slow heat.	Deflagrates	Explodes	Explodes	Explodes	Explodes
Flame fast heat.	Burns	Burns	Deflagrates	Deflagrates	Deflagrates
Flame color	Red	Orange	Purple	Lila	Pink
N (%) ^c	59.9	63.4	57.3	41.6	32.4
Ω (%) ^d	-47.8	-50.7	-45.9	-33.3	-25.9
Endotherms (°C) ^e	124 (-H ₂ O), 191 (mp)	~110 (-H ₂ O)			
Exothermic Dec. (°C) ^f	216, 324	262, 300	236	230	240
-Δ _c U (cal g ⁻¹) ^g	2460(20)	1960(20)	1970(40)	1210(30)	1060(20)
-Δ _c H° (kJ mol ⁻¹) ^b	2400(20)	1800(20)	2010(40)	1690(30)	1910(20)
Δ _f H° (kJ mol ⁻¹) ⁱ	-120(100)	80(90)	-370(160)	345(110)	280(80)
	106	107	108	109	
Formula	C ₂ H ₁₅ N ₁₀ O _{6.5} Mg	C ₂ H ₁₂ N ₁₀ O ₅ Ca	C ₂ H ₁₂ N ₁₀ O ₅ Sr	C ₂ H ₁₂ N ₁₀ O ₅ Ba	
MW (g mol ⁻¹)	307.55	296.26	343.80	394.00	
Impact (J) ^a	>30	>30	>30	>30	
Friction (N) ^a	>360	>360	>360	>360	
Electrostatics ^b	–	–	–	–	
Flame slow heat.	Burns	Burns	Burns	Burns	
Flame fast heat.	Deflagrates	Deflagrates	Deflagrates	Deflagrates	
Flame color	White	Red	Red	Green	
N (%) ^c	45.6	47.3	40.7	35.6	
Ω (%) ^d	-31.3	-32.4	-27.9	-24.4	
Endotherms (°C) ^e	142–158	140–160	150–185	128–154	
Exothermic Dec. (°C) ^f	220, 250	220, 260	276	260	
-Δ _c U (cal g ⁻¹) ^g	2000(20)	1300(20)	1360(20)	1310(20)	
-Δ _c H° (kJ mol ⁻¹) ^b	2560(20)	1590(20)	1940(20)	2150(20)	
Δ _f H° (kJ mol ⁻¹) ⁱ	955(70)	1530(70)	1140(100)	895(70)	

^a Impact and friction sensitivities determined by standard BAM methods (see reference [38–40]). ^b Rough sensitivity to 20 kV electrostatic discharge (ESD testing): + sensitive, - insensitive from an HF-Vacuum-Tester type VP 24. ^c Nitrogen content. ^d Oxygen balance, calculated according to reference [44]. ^{e,f} Melting (or water loss) and decomposition points (DSC onset) from measurement with $\beta = 5$ °C min⁻¹. ^g Experimental (constant volume) energy of combustion. ^h Experimental molar enthalpy of combustion. ⁱ Molar enthalpy of formation.

Apart from **107**, **108** and **109**, which form as the anhydrous species, the alkali metal salts **105** and **106** show loss of water at ~120 °C in the DSC apparatus, whereas the crystal water is more tightly bound in the case of the alkaline earth salts and lost at temperatures as high as ~185 °C (DSC off-set of **112**). The lithium salt (**105**) is the only material, which melts (m. p. = 191 °C) with almost concomitant decomposition at ~ 216 °C, whereas the rest of the compounds decompose without melting at or above 220 °C. The decomposition points of the metal salts in this study are (generally) at least as high as those of alkali salts of 5-amino-1*H*-tetrazole^[35a] and 5,5'-azotetrazole.^[2] Thermogravimetric (TG) analysis confirmed the results obtained by DSC. Figure 8.27 shows a typical TG curve for **113**. The loss of the five molecules of crystal water adds to 21.14% of the

sample weight (calculated: 21.34%) and at the decomposition point the weight loss is 66.49% so that the weight of the residue left in the TG pan is 12.35% of the original sample.

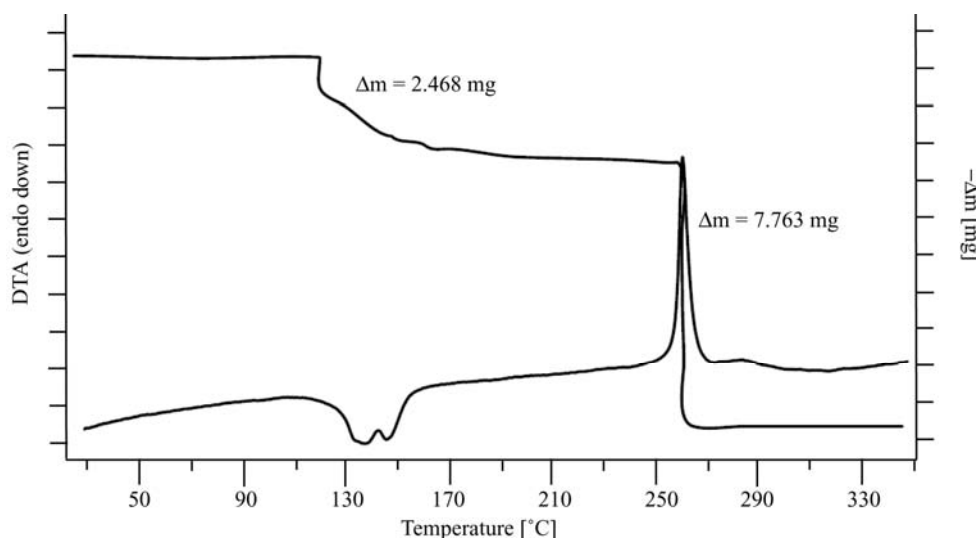


Figure 8.27 TG curve of **113** showing the DTA curve (left axis) and the loss of mass (right axis) for a measurement at $\beta = 5\text{ }^{\circ}\text{C min}^{-1}$ (sample weight = 11.675 mg).

In addition to DSC analysis, all compounds were tested in the “flame test”, once by placing the material over a thick metal spatula at ~5 cm of the open flame of a *Bunsen* burner (“slow heating”) and once by using a thinner spatula and heating the compound by direct contact with the flame (“fast heating”, Figure 8.28). “Slow heating” of alkali metal salts **105-109** resulted in deflagration with little smoke (Li salt) and low (Na and K) or loud (Rb and Cs) explosions. “Slow heating” of the alkaline earth metal salts **110-113** results in a less vigorous reaction and the compounds burn normally giving the corresponding color for the metal atom. On the other side, “fast heating” resulted in a less violent reaction for the alkali metal salts and a more vigorous one for the alkaline earth metal salts. **105** and **106** burned nicely with almost no smoke producing a red and an orange flame, respectively whereas the heavier alkali metal salts showed a more violent response deflagrating giving the typical color for the metal cation, namely purple, lilac and pink. These results are in agreement with the higher sensitivity toward oxidation of the heavier alkali metal salts (**107**, **108** and **109**). Whereas powders of **105** and **106** are stable in air for several weeks without appreciable oxidation, **107**, **108** and **109** oxidize readily to the yellow 5,5′-azotetrazolate salts after a few hours. Thus, we assume that heating in the flame accelerates the process of oxidation to the azo derivatives, for which the expected response in the “flame test” is an explosion.^[2] An explanation for this observation can be that the crystal water stabilizes the materials and prevents oxidation, which would fit with the low susceptibility of the alkaline earth salts towards oxidation (all contain ≥ 5 molecules of crystal water and are stable, at least, for several months).

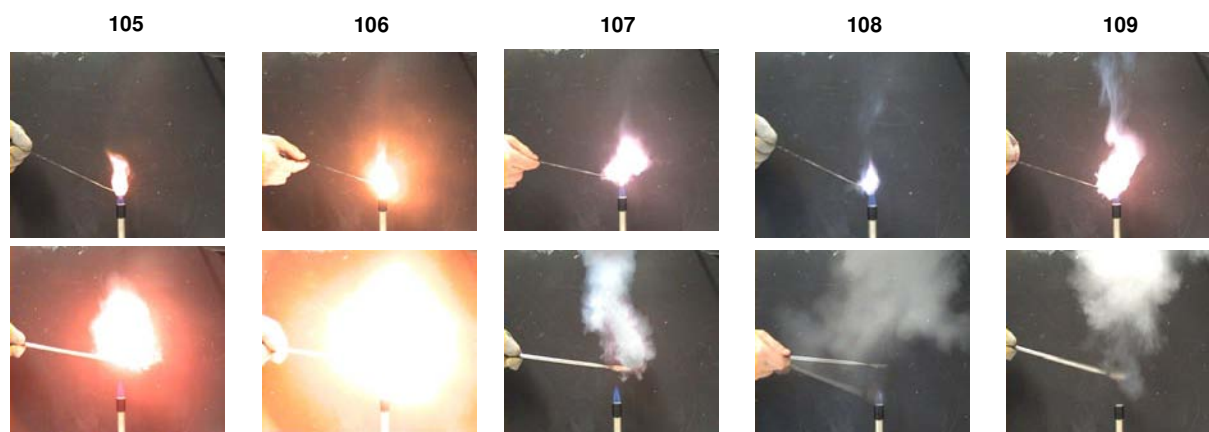
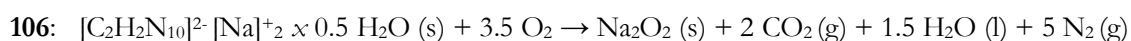
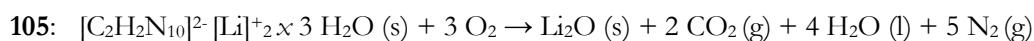


Figure 8.28 “Flame tests” for alkali metal salts, “fast heating” (top) and “slow heating” (bottom).

Impact (*i*), friction (*f*) and electrostatic discharge sensitivity data for metal salts of **95** is also summarized in Table 8.3. None of the compounds turned out to be sensitive to either impact or friction. The friction sensitivities, with values of >360 N classify the salts as insensitive and most (if not all) of the materials were insensitive (or less sensitive) to a shock stimulus of 30 J (salts **106-109** showed non-explosive decomposition). These results are in contrast with those observed for metal 5,5'-azotetrazolate salts. Whereas compounds with the ZT²⁻ anion are more prone to contain crystal water, which makes them insensitive towards the above-mentioned stimuli but are expected to have sensitivity values comparable to primary explosives as the anhydrous materials (e.g., barium 5,5'-azotetrazolate), the heavier alkali metal salts containing the HBT²⁻ anion (**107**, **108** and **109**) do not incorporate crystal water and are regardless insensitive or less sensitive compounds.

As mentioned above, due to the energetic nature of the compounds in this study, the constant volume energies of combustion ($\Delta_c U$) of **105–113** were measured using oxygen bomb calorimetry. The standard molar enthalpies of combustion ($\Delta_c H^\circ$) were calculated using the equation $\Delta_c H^\circ = \Delta_c U + \Delta nRT$ (where Δn is the difference between the number of moles of gases in the products and the reactants). The standard energies of formation of **105–113** ($\Delta_f H^\circ$) were back-calculated from the energy of combustion on the basis of the combustion equations shown below, Hess's Law and the known standard heats of formation for the reaction products.^[54] The energies of combustion obtained from sets of four measurements are in the rule more negative than those of metal salts of 5-amino-1*H*-tetrazole,^[35a] whereas the standard heats of formation are comparatively more positive (less negative) keeping in with the better (or less negative) oxygen balance of the compounds reported here.



- 107: $[\text{C}_2\text{H}_2\text{N}_{10}]^{2-} [\text{K}]^+_2 (\text{s}) + 4.5 \text{ O}_2 \rightarrow 2 \text{ KO}_2 (\text{s}) + 2 \text{ CO}_2 (\text{g}) + \text{H}_2\text{O} (\text{l}) + 5 \text{ N}_2 (\text{g})$
- 108: $[\text{C}_2\text{H}_2\text{N}_{10}]^{2-} [\text{Rb}]^+_2 (\text{s}) + 4.5 \text{ O}_2 \rightarrow 2 \text{ RbO}_2 (\text{s}) + 2 \text{ CO}_2 (\text{g}) + \text{H}_2\text{O} (\text{l}) + 5 \text{ N}_2 (\text{g})$
- 109: $[\text{C}_2\text{H}_2\text{N}_{10}]^{2-} [\text{Cs}]^+_2 (\text{s}) + 4.5 \text{ O}_2 \rightarrow 2 \text{ CsO}_2 (\text{s}) + 2 \text{ CO}_2 (\text{g}) + \text{H}_2\text{O} (\text{l}) + 5 \text{ N}_2 (\text{g})$
- 110: $[\text{C}_2\text{H}_2\text{N}_{10}]^{2-} \text{Mg}^{2+} \times 6.5 \text{ H}_2\text{O} (\text{s}) + 2.5 \text{ O}_2 \rightarrow \text{MgO} (\text{s}) + 2 \text{ CO}_2 (\text{g}) + 7.5 \text{ H}_2\text{O} (\text{l}) + 5 \text{ N}_2 (\text{g})$
- 111: $[\text{C}_2\text{H}_2\text{N}_{10}]^{2-} \text{Ca}^{2+} \times 5 \text{ H}_2\text{O} (\text{s}) + 2.5 \text{ O}_2 \rightarrow \text{CaO} (\text{s}) + 2 \text{ CO}_2 (\text{g}) + 6 \text{ H}_2\text{O} (\text{l}) + 5 \text{ N}_2 (\text{g})$
- 112: $[\text{C}_2\text{H}_2\text{N}_{10}]^{2-} \text{Sr}^{2+} \times 5 \text{ H}_2\text{O} (\text{s}) + 2.5 \text{ O}_2 \rightarrow \text{SrO} (\text{s}) + 2 \text{ CO}_2 (\text{g}) + 6 \text{ H}_2\text{O} (\text{l}) + 5 \text{ N}_2 (\text{g})$
- 113: $[\text{C}_2\text{H}_2\text{N}_{10}]^{2-} \text{Ba}^{2+} \times 5 \text{ H}_2\text{O} (\text{s}) + 2.5 \text{ O}_2 \rightarrow \text{BaO} (\text{s}) + 2 \text{ CO}_2 (\text{g}) + 6 \text{ H}_2\text{O} (\text{l}) + 5 \text{ N}_2 (\text{g})$

8.4 ESPs of **95** and its Methylated Derivatives

The electrostatic potentials (ESPs) were computed at optimized structures at the B3LYP/6-31G(d) level of theory using the program package HyperChem 7.0.^[56] Figures 8.29 and 8.30 and Figures 8.A8 and 8.A9 illustrate the electrostatic potentials for the 0.001 electron/bohr³ isosurface of electron density evaluated at the B3LYP level of theory for **95** and for its methylated derivatives for comparison. In the figures, the colors range from -0.07 to +0.07 hartrees with green denoting extremely electron-deficient regions ($V(\mathbf{r}) > 0.01$ hartree) and red denoting electron-rich regions ($V(\mathbf{r}) < -0.01$ hartrees). It has recently been found by Politzer et al.^[56] and extensively used and further developed by Rice et al.^[57] that the patterns of the computed electrostatic potential on the surface of molecules in general can be related to the sensitivity of the bulk material. While in nitro and aza systems the regions of positive potential are almost universally more extensive in area, in the subset they are also stronger than the negative, contrary to the usual situation. This atypical imbalance between stronger positive regions and weaker negative ones can be related to the impact sensitivity of a compound. The electrostatic potential at any point \mathbf{r} is given by the following equation in which Z_A is the charge on nucleus A, located at \mathbf{R}_A :

$$V(\mathbf{r}) = \sum \{Z_A / (|\mathbf{R}_A - \mathbf{r}|)\} - \int (\rho(\mathbf{r}') \, d\mathbf{r}') / (|\mathbf{r}' - \mathbf{r}|)$$

The relative strengths and size of the regions of positive and negative electrostatic potential on the surfaces of energetic molecules are of great importance. Typically, for organic molecules in general, the negative regions cover a smaller portion of the total surface area but are significantly stronger (in terms of average magnitudes) than the positive ones. In the case of energetic molecules, on the other hand, the positive regions are still larger but now also stronger than the negative. Politzer et al. were able to show^[56] that impact sensitivity can be expressed as a function of the extend of this

anomalous reversal of the strengths of the positive and negative surface potentials. The calculated electrostatic potentials of **95** (Figure 8.29), both isomers (1-Me and 2-Me) of dimethyl-5,5'-hydrazinebistetrazole **97** and **98** (Figure 8.30), 1,2-dimethyl-5,5'-hydrazinebistetrazole (Figure 8.A8), and both isomers of di(X)-methyl-5,5'-1,2-dimethylhydrazinebistetrazole (X = 1, 2) (Figure 8.A9) are shown.

Comparing the methylated derivatives with **95**, which is expected to be more sensitive, the most obvious feature of the ESPs in all four figures appears to be the region over the center of the molecule (i.e., over the hydrazine N–N bond). For both isomers of di-methyl-5,5'-1,2-dimethylhydrazinebistetrazole (Figure 8.A9) the region over the central N–N hydrazine bond actually shows a negative potential whereas for 1,2-dimethyl-5,5'-hydrazinebistetrazole this central region has almost zero electrostatic potential (Figure 8.A8). For **95** (Figure 8.29) and for **97** (Figure 8.30) the regions over the center of the molecule are now clearly positive. While the positive regions for **95** are still larger than the negative regions they are now also stronger (Figure 8.29). It is also interesting to note that for the dimethyl-5,5'-hydrazinebistetrazole isomers the 1-methyl derivative (**97**) can be expected to be more sensitive than the 2-methyl isomer (**98**, Figure 8.30). From the computed electrostatic potentials one would predict the following decreasing impact sensitivity: **95** > **97** and **98** > 1,2-dimethyl-5,5'-hydrazinebistetrazole > di(X)-methyl-5,5'-1,2-dimethylhydrazinebistetrazole. The obvious limitation in the preparation of the derivatives methylated on the hydrazine-bridge nitrogen atoms did not allow to correlate experimental data for this compounds with that obtained from this study, however the experimental values for the impact sensitivity of **95** (~60 J) and **97** (>100 J) are in agreement with the predictions.

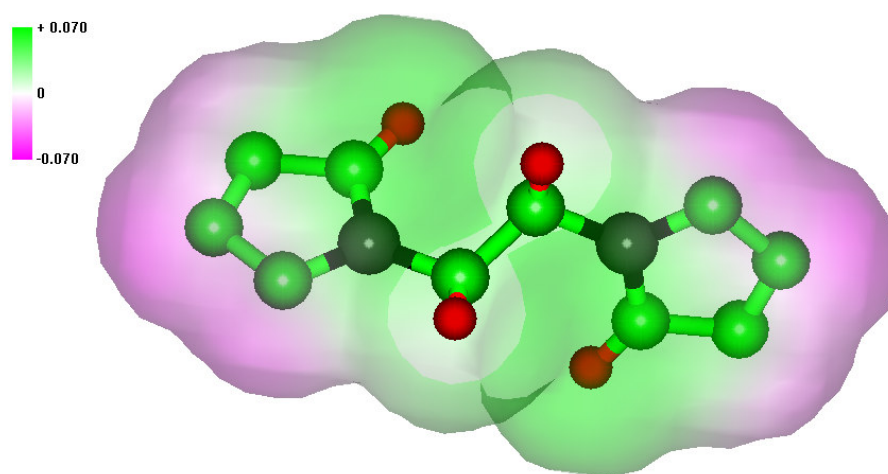


Figure 8.29 Electrostatic potential (ESP) of **95** for the 0.001 electron/bohr³ isosurface. Legend for the color ranges of the ESPs are given above (top left corner) and range from -0.07 to +0.07 hartrees (a.u.).

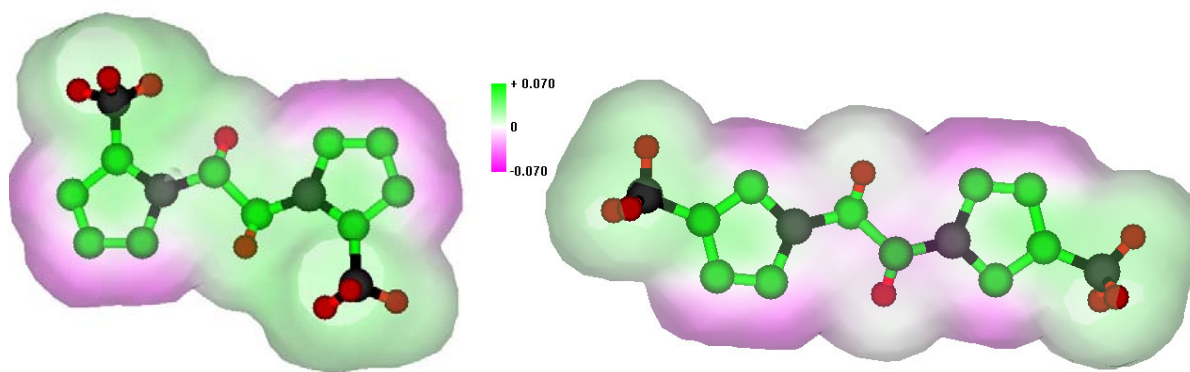


Figure 8.30 Electrostatic potential (ESP) for **97** (left) and **98** (right) for the 0.001 electron/bohr³ isosurface. Legend for the color ranges of the ESPs are given above (top left corner) and range from -0.07 to +0.07 hartrees (a.u.).

8.5 Koenen (Steel Sleeve Test) of **95**

The Koenen (steel sleeve) test^[59] was used in order to test the sensitivity of **95** to intense heat under confinement. Figure 8.31 shows pictures for a typical test using a port diameter of 8 mm and 15 g of **95**. As expected from the high detonation parameters of the compound, the steel sleeve was completely shredded by the explosion. RDX and HMX show similar behaviour under the same test using the same critical diameter.^[41] According to Table 7.A4 (*Chapter VII*), **95** can be classified as a type G explosive (it destroys the steel sleeve but not the screw top).

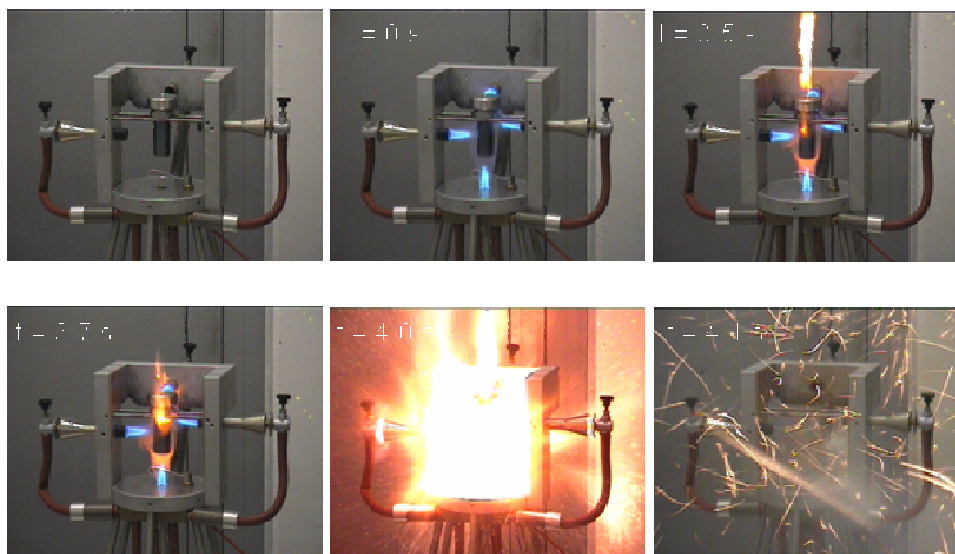


Figure 8.31 Steel sleeve (Koenen) test on 15 g of **95** (port diameter: 8 mm).

8.6 Long-term Stability and Response to Thermal Shock of **95**

The long-term thermal stability of **95** was measured by thermal safety calorimetry using a Systag FlexyTSC instrument^[60] in combination with a RADEX V5 oven and the SysGraph software. The samples size was ~300 mg and the tests were conducted in glass test-vessels. In addition to pure **95**, an homogeneous mixture of the same with copper powder (Cu) was also tested in order to simulate the conditions found in shell-casing in many propellants applications. Figure 7.23 (*Chapter VII*) shows typical TSC curves for **95** and guanazinium 5,5'-azotetrazolate (**GzZT**). Pure **95** is perfectly stable at ~40 °C below its decomposition temperature over a period of 48 hours. This can be extrapolated to a shelf-life of above 50 years for the compound. As for the mixture with copper powder, **95** shows some decomposition after heating at 170 °C for 6 hours but the color of the sample before and after the 48 hours remains the same, which indicates that the decomposition is minor. Thus, we conclude that **95** shows good long-term stability at high temperatures, which is the basic requirement for possible application. Apart from some minor decomposition for mixtures of **95**/Cu, the shell-casing simulation samples show reasonable long-term stability as well.

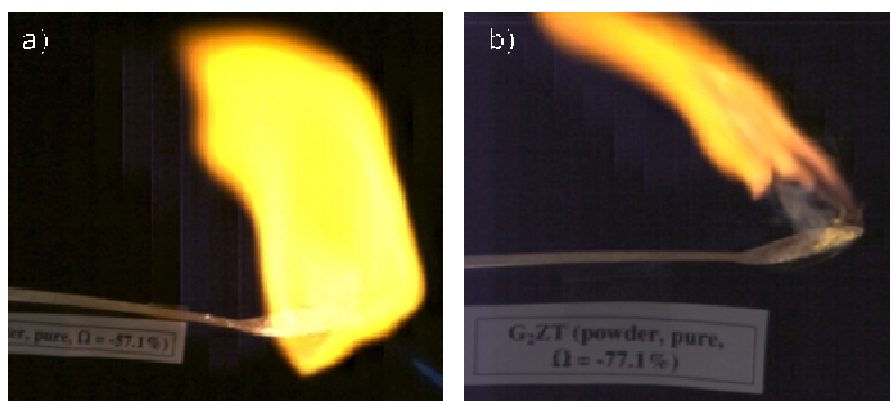


Figure 8.32 Smokeless combustion of **95** *vs.* non-smokeless combustion of guanazinium 5,5'-azotetrazolate (**GzZT**, *Chapter VII*). The compounds were tested as the pure powders.

The responses to thermal shock of **95** and mixtures with ammonium nitrate (AN) and ammonium dinitramide (ADN) in an approximately neutral oxygen balance were assessed by putting the compounds in contact with a flame (Table 7.A5, *Chapter VII*). The neat powder of **95** deflagrated giving a large yellow flame with no smoke in contrast to nitrogen-rich salts of the compound, which deflagrate giving a much brighter flame, as represented in Figure 8.33. When the compound was pressed into a pellet and held into a flame, **95** deflagrated rapidly with almost no smoke. A mixture of **95** with an oxidizer (AN or ADN) burned smokeless. Lastly, the combustion of **95** (neat powder or pellet) and **95** + ADN ($\Omega \sim 0\%$) was self-sustaining (i.e., the heat of source did not need to be kept applying after initiation).

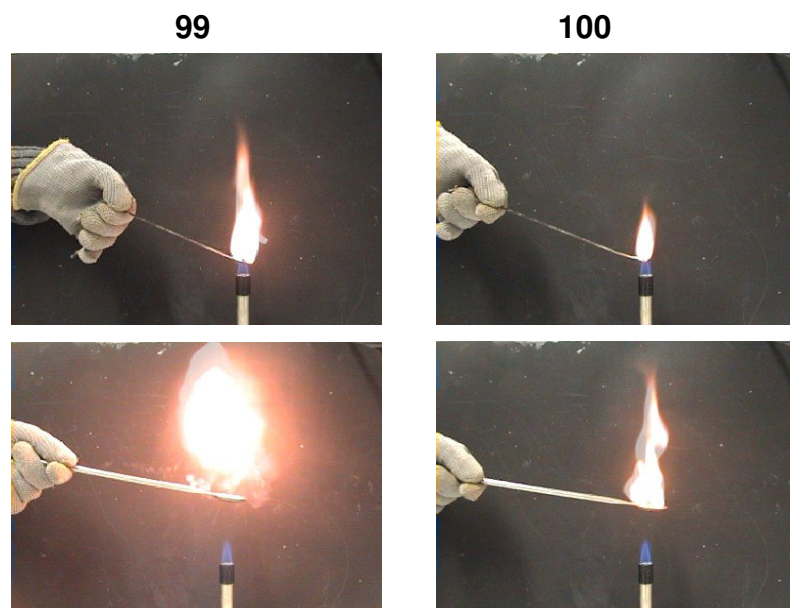


Figure 8.33 “Flame tests” for ammonium (**99**) and hydrazinium (**100**) salts of **95**, “fast heating” (top) and “slow heating” (bottom).

8.7 Decomposition Experiments of **95**

Figure 8.34 shows the IR spectra of the decomposition gases for **95** and **GzZT** (*Chapter VII*). Only NH_3 and HCN could be detected in these measurements. In addition to these gases, the MS measurements also showed the formation of large amounts of N_2 gas, as expected from the high nitrogen content of the compound.

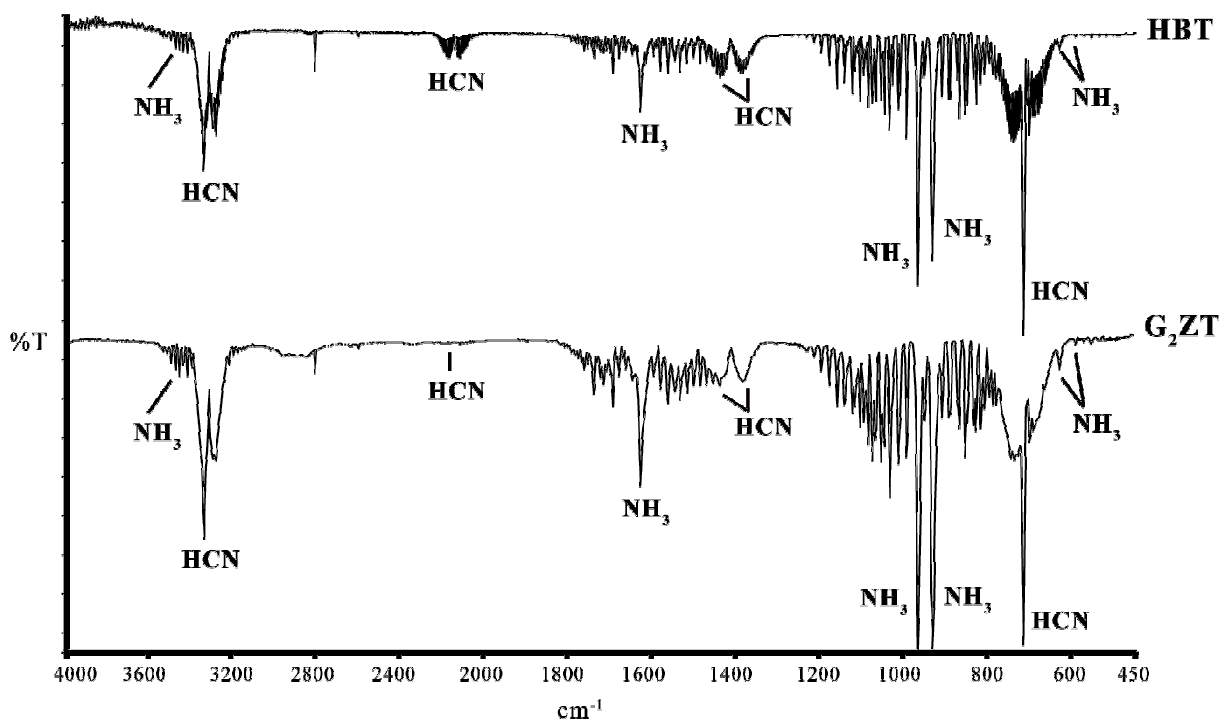


Figure 8.34 IR spectra of the decomposition gases of **HBT** (**95**, top) and **GzZT** (bottom, *Chapter VII*).

The ICT code^[61] was also used to predict the gases formed upon decomposition of **95** (Figure 8.A10). The code predicted and overestimated amount of NH₃ in comparison to the experimental results discussed above and, as mentioned for other compounds in this work (e.g., see *Chapter VII*), the amount of HCN formed is nearly neglected by the calculations, when in fact it is formed in relatively large amounts (not measured in this work).

8.8 Conclusions

5,5'-Hydrazinebistetrazole (**95**) is a useful and interesting old energetic material, which has now been studied in detail. The compound has a surprising high density comparable to that of RDX, great performance, low sensitivity, good stability, etc., which make it a prospective candidate to find application in gas generators, propellants or additives in solid rockets as low-smoke propellant ingredients. Furthermore, **95** is currently being further investigated by the U. S. Army. The moderate friction sensitivity value of **95** (108 N) can be reduced by forming the methylated isomers **97** and **98**, which are expected to be insensitive nitrogen-rich compounds with lower but still fairly high performances. Several nitrogen-rich salts of **95** with ammonium, hydrazinium and guanidinium cations and with alkali and alkaline earth metals were synthesized. The nitrogen-rich compounds have high detonation parameters and are yet insensitive materials, however, they oxidize slowly to the 5,5'-azotetrazolate salts on time, which limits their range of application. This might be overcome either by coating the material with wax or using a reducing agent (e.g., Mg powder) depending on the application. On the other side, we took advantage of the susceptibility of salts based on the HBT²⁻ anion towards oxidation to the azotetrazolate salts to suggest an alternative method for a safer synthesis of several interesting (previously reported) salts based on the latter anion, which avoid the use of highly sensitive **94** (see *8.9 Experimental Section*). Alkali metal salts of **95** are very sensitive toward oxidation even in the solid state. In contrast, the solid alkaline earth metal salts of **95** do not show oxidation after storing the materials under air for several months, which supposes a clear advantage over the alkali metal salts and suggests their potential use as coloring agents in pyrotechnic compositions (e.g., Sr to generate red color). Lastly, the energetic properties of all materials has been discussed in detail and the crystal structure of the compounds was analyzed in the formalism of graph-set analysis of hydrogen-bonding networks, indicating distinctive hydrogen-bonding playing a major role to determine the high crystal density of **95**.

8.9 Experimental Section

Caution! *Although we had no difficulties handling the compounds described here, tetrazoles and their derivatives are nevertheless energetic materials and the explosive properties of the compounds described herein are not well established. We recommend the synthesis to be carried out only by expert personnel, wearing protective gear (i.e., Kevlar gloves, wrist protectors, leather jacket, helmet, ear plugs...) and using conductive equipment, specially when working on a larger scale.*

General. All chemical reagents and solvents were obtained from Sigma-Aldrich Inc. or Acros Organics (analytical grade) and were used as supplied. Sodium 5,5'-azotetrazolate pentahydrate was prepared according to a literature known procedure^[13] and 1,1-dimethyl- and 2,2'-dimethyl-5,5'-azotetrazoles were prepared as described in *Chapter VII*. ¹H, ¹³C, and ¹⁵N NMR spectra were recorded on a JEOL Eclipse 400 instrument in DMSO-*d*₆ at or near 25 °C. The chemical shifts are given relative to tetramethylsilane (¹H, ¹³C) or nitromethane (¹⁵N) as external standards and coupling constants are given in Hertz (Hz). Infrared (IR) spectra were recorded on a Perkin-Elmer Spectrum One FT-IR instrument as KBr pellets at 20 °C.^[62] Transmittance values are qualitatively described as “very strong” (vs), “strong” (s), “medium” (m) and “weak” (w). Raman spectra were recorded on a Perkin-Elmer Spectrum 2000R NIR FT-Raman instrument equipped with a Nd:YAG laser (1064 nm). The intensities are reported as percentages of the most intense peak and are given in parentheses. Elemental analyses were performed with a Netsch Simultaneous Thermal Analyzer STA 429. Melting points were determined by differential scanning calorimetry (Linseis DSC PT-10 instrument^[63] calibrated with standard pure indium and zinc). Measurements were performed at a heating rate of 5 °C min⁻¹ in closed aluminum sample pans with a 1 µm hole in the top for gas release under a nitrogen flow of 20 mL min⁻¹ with an empty identical aluminum sample pan as a reference.

Long Term Stability Tests

The long term stability tests were performed with a Systag FlexyTSC (thermal safety calorimetry)^[60] in combination with a RADEX V5 oven and the SysGraph software. The tests were run on a ~500 mg sample of either **95** or an homogeneous mixture of **95** with copper powder in glass test-vessels at atmospheric pressure. The samples were tempered at ~180 °C for a period of 48 hours.

Bomb Calorimetry

For the calorimetric measurements of the picrate salts, a Parr 1356 bomb calorimeter (static jacket) equipped with a Parr 207A oxygen bomb for the combustion of highly energetic materials was used.^[64] A Parr 1755 printer, furnished with the Parr 1356 calorimeter, was used to produce a permanent record of all activities within the calorimeter. The samples (~200 mg each) were carefully mixed with ~800 mg analytical grade benzoic acid and carefully pressed into pellets, which were subsequently burned in a 3.05 MPa atmosphere of pure oxygen. The experimentally determined constant volume energies of combustion ($\Delta_c U_{(\text{exp.})}$) were obtained as the averages of three to five single measurements with standard deviations

calculated as a measure of experimental uncertainty. The calorimeter was calibrated by the combustion of certified benzoic acid in an oxygen atmosphere at a pressure of 3.05 MPa.

Synthesis of 5,5'-Hydrazinebistetrazole (95): Sodium 5,5'-azotetrazolate pentahydrate (50.00 g, 166.63 mmol) was dissolved in 1.4 L water before an excess of magnesium powder (28.71 g, 1.18 mol) was added to the yellow solution. The reaction mixture was refluxed for 6 hours and left to cool down to room temperature under a stream of nitrogen. The excess magnesium powder was filtered along with some magnesium hydroxide, which precipitated on cooling (this operation has to be carried out quickly in order to prevent oxidation of sodium 5,5'-hydrazinobistetrazolate) into a side-arm flask containing 160 (1.58 mol) mL of half-concentrated HCl (once the filtrate came into contact with the HCl no oxidation of the hydrazino-bridged compound was observed). A white solid immediately formed and the side-arm flask was shaken thoroughly to favour the precipitation of the product. The slightly yellow powder was filtered off, washed thoroughly with water and with acetone yielding the desired product as a white powder (26.64 g, 95.2 %). Crystals of the compound suitable for structure determination were grown by dissolving a small amount of the solid in boiling water and letting to cool slowly. C₂H₄N₁₀ (calc./found, %): C 14.29/14.07, H 2.40/2.61, N 83.31/82.34, m. p. (Büchi B-540, uncorrected): 207.1-208.1 °C, DSC (Linseis DSC PT-10, 2 °C/min, °C): 208 (dec.); ¹H NMR (DMSO-d₆, 400.18 MHz, 25°C, TMS) δ/ppm: 9.62 (4H, s, NH), ¹³C{¹H} NMR (DMSO-d₆, 100.63 MHz, 25°C, TMS) δ/ppm: 159.61 (s, CN₃); Raman $\tilde{\nu}$ / cm⁻¹ (rel. int.): 2998(19) 1648(19) 1609(71) 1549(14) 1372(65) 1274(53) 1203(9) 1119(19) 1063(93) 1049(91) 811(13) 573(9) 392(31) 361(11) 235(22) 170(100); IR $\tilde{\nu}$ / cm⁻¹ (KBr, rel. int.): 3206(m) 3118(m) 3033(s) 2997(s) 2887(s) 2760(m) 2674(m) 2635(m) 1645(s) 1625(s) 1528(m) 1408(w) 1376(m) 1273(m) 1128(w) 1109(w) 1070(m) 1061(m) 999(m) 853(m) 820(m) 735(m) 685(m) 670(m) 664(m) 574(m). **Decomposition Experiments.** MS (EI): *m/z* = 12 (0.1, C⁺), 14 (0.6, N⁺), 16 (1.2, NH₂⁺), 17 (3.6, NH₃⁺), 26 (3.2, CN⁺), 27 (20.4, HCN⁺) and 28 (100.0, N₂⁺); IR (Gas): $\tilde{\nu}$ (cm⁻¹) = 3332 (w, NH₃), 3336 (s, HCN), 3282 (s, HCN), 2168 (w, HCN), 2102 (w, HCN), 1621 (m, NH₃), 1431 (w, HCN), 1380 (w, HCN), 965 (vs, NH₃), 926 (vs, NH₃), 732 (s, HCN), 710 (vs, HCN), 679 (s, HCN).

Synthesis of 1,1'-Dimethyl-5,5'-hydrazinebistetrazole Monohydrate (97): 1,1'-Dimethylazobistetrazole (0.785 g, 4.61 mmol) was dissolved in 40 mL hot water and an excess of magnesium powder (0.350 g, 13.40 mmol) was added. The reaction mixture was heated to reflux, under exclusion of air, and turned brown initially. After having reacted overnight the solution was colorless and was filtered hot under vacuum using a *Schlenk* frit. Colorless crystals of the compounds precipitated on cooling, which were filtered and left to air-dry. Elemental analysis showed the presence of one molecule of crystal water (0.370 g, 37%). C₄H₁₀N₁₀O (calc./found): C 22.43 / 22.17, H 4.71 / 4.70, N 65.39 / 64.75; DSC (5 °C/min, °C): 138 (m.p., -H₂O), 202 (dec.); *m/z* (DEI⁺, xenon, 6 keV, m-NBA matrix): 197.1 (M+H); ¹H NMR (DMSO-d₆, 400.18 MHz, 25°C, TMS) δ/ppm: 9.51 (2H, s, NH-NH), 3.80 (6H, s, CH₃), 3.31 (2H, s, H₂O); ¹³C{¹H} NMR (DMSO-d₆, 100.63 MHz, 25°C, TMS) δ/ppm: 157.2 (2C, C-NH), 33.0 (2C, CH₃); ¹⁴N{¹H} NMR (DMSO-d₆, 40.55 MHz, 25°C, MeNO₂) δ/ppm: -285 (2N, Δ*v*_{1/2} = 5400 Hz, NH-NH); Raman $\tilde{\nu}$ / cm⁻¹ (rel. int.): 3426(13) 3039(28) 2966(98) 2784(21) 1639(35) 1608(78) 1559(37) 1460(51) 1398(69) 1326(78)

1273(100) 1228(33) 1160(26) 1102(94) 1036(43) 969(34) 828(97) 701(25) 655(30) 471(67) 348(26) 232(85) 205(85) 104(14) 75(13); IR $\tilde{\nu}$ / cm^{-1} (KBr, rel. int.): 3700(w) 3129(vs) 3047(vs) 2969(vs) 2377(w) 2197(w) 1995(w) 1645(s) 1606(s) 1520(m) 1457(s) 1396(m) 1316(m) 1272(w) 1243(w) 1217(w) 1158(w) 1106(m) 1037(m) 968(m) 832(m) 791(w) 730(m) 704(s) 684(m) 656(w) 623(w) 508(w).

Synthesis of Ammonium 5,5'-Hydrazinebistetrazolate Dihydrate (99): 40 mL of a 25% ammoniac solution were loaded in a 100 mL *Schlenk* flask and the solution was flushed with a stream of nitrogen for a short time. **95** (2.079 g, 12.4 mmol) was added portion-wise keeping the flow of nitrogen and under stirring and the reaction mixture was left to react over 15 minutes yielding a clear colorless solution. The solvent was carefully stripped by slow evaporation under nitrogen yielding the pure compound as the dehydrated species (2.854 g, 97%). DSC (5 $^{\circ}\text{C min}^{-1}$, $^{\circ}\text{C}$): ~ 111 ($-\text{H}_2\text{O}$), 196 (Dec.); IR (KBr, cm^{-1}) $\tilde{\nu} = 3129(\text{m})$ 2995(m) 1699(w) 1626(w) 1553(m) 1483(m) 1426(vs) 1376(s) 1226(m) 1206(m) 1152(w) 1138(m) 1120(m) 1075(m) 1024(m) 997(s) 938(m) 791(s) 727(s) 611(s) 582(s); Raman (400 mW, 25 $^{\circ}\text{C}$, cm^{-1}) $\tilde{\nu} = 3137(11)$ 2986(101) 1714(3) 1521(25) 1487(8) 1418(6) 1402(8) 1379(5) 1246(4) 1227(18) 1208(17) 1153(5) 1140(6) 1124(20) 1074(48) 1018(9) 941(5) 726(4) 397(9) 349(10) 235(19) 188(18); ^1H NMR ($\text{DMSO}-d_6$, 25 $^{\circ}\text{C}$) δ 7.8 (s, 2H, NH–NH), 5.5 (s, 8H, $[\text{NH}_4]^+$); ^{13}C NMR ($\text{DMSO}-d_6$, 25 $^{\circ}\text{C}$) δ 164.7 (2C, C_{ring}); m/z (FAB $^+$, xenon, 6 keV, glycerin matrix): 167.0 (100, $[\text{C}_2\text{H}_3\text{N}_{10}]^-$), 335.0 (68, $[\text{C}_2\text{H}_4\text{N}_{10} \cdot \text{C}_2\text{H}_3\text{N}_{10}]^-$); m/z (FAB $^+$, xenon, 6 keV, glycerin matrix): 18.3 (3, $[\text{NH}_4]^+$); $\text{C}_2\text{H}_{14}\text{N}_{12}\text{O}_2$ (238.14) calc.: C 10.08, H 5.92, N 70.56%; found: C 10.21, H 5.83, N 70.54%.

Synthesis of Hydrazinium 5,5'-Hydrazinebistetrazolate (100): A *Schlenk* flask was loaded with 20 mL distilled water, which had been freed of oxygen by flushing nitrogen gas through the solution over 10 min. A solution of 24% hydrazine (5.34 g, 40.0 mmol) was added into the flask and **95** (1.681 g, 10.0 mmol) was added portion-wise under a stream of nitrogen. The reaction mixture was stirred for 30 min. at room temperature and the solvent was stripped under high vacuum yielding the pure compound (9.1 mmol, 91%). DSC (5 $^{\circ}\text{C min}^{-1}$, $^{\circ}\text{C}$): ~ 154 –182 (m.p.+ Dec.); IR (KBr, cm^{-1}) $\tilde{\nu} = 3269(\text{m})$ 3162(w) 2971(w) 2836(m) 2703(m) 2612(m) 2139(vw) 1650(vw) 1615(m) 1552(m) 1523(s) 1467(s) 1416(m) 1360(s) 1271(vw) 1222(m) 1100(vs) 1061(m) 1013(m) 959(s) 809(m) 758(m) 717(m) 598(s) 592(s) 568(s); Raman (400 mW, 25 $^{\circ}\text{C}$, cm^{-1}) $\tilde{\nu} = 3169(7)$ 2986(68) 1645(9) 1549(17) 1515(24) 1478(12) 1411(12) 1388(21) 1366(15) 1231(35) 1118(19) 1056(100) 1009(20) 961(26) 815(13) 748(11) 412(10) 230(23); ^1H NMR ($\text{DMSO}-d_6$, 25 $^{\circ}\text{C}$) δ 8.0 (s, 2H, NH–NH), 5.9 (s, $\sim 10\text{H}$, $[\text{H}_2\text{N}-\text{NH}_3]^+$); ^{13}C NMR ($\text{DMSO}-d_6$, 25 $^{\circ}\text{C}$) δ 167.4 (2C, C_{ring}); m/z (FAB $^+$, xenon, 6 keV, glycerin matrix): 84.0 (12, $[\text{CH}_2\text{N}_5]^-$), 118.1 (3, HCN–gly), 124.1 (3, $[\text{C}_2\text{H}_2\text{N}_7]^-$), 166.0 (17, $[\text{C}_2\text{H}_2\text{N}_{10}]^2-$), 167.0 (100, $[\text{C}_2\text{H}_3\text{N}_{10}]^-$), 259.1 (12, $\text{C}_2\text{H}_4\text{N}_{10}$ –gly), 335.0 (46, $[\text{C}_2\text{H}_4\text{N}_{10} \cdot \text{C}_2\text{H}_3\text{N}_{10}]^-$); $\text{C}_2\text{H}_{12}\text{N}_{14}$ (232.14) calc.: C 10.34, H 5.21, N 84.45%; found: C 10.33, H 5.11, N 83.93%.

Synthesis of Guanidinium 5,5'-Hydrazinebistetrazolate (101). 20 mL water were added into a *Schlenk* flask and degassed by flushing nitrogen over 10 min. Guanidinium carbonate (0.629 g, 3.5 mmol) and an equivalent amount of **95** (0.587 g, 3.5 mmol) were suspended in the water and the reaction mixture was stirred for 30 min. at room temperature and under a stream of nitrogen with concomitant gas evolution

(CO₂). The clear colorless solution formed after this time was heated to 60 °C and evaporated to dryness under high vacuum yielding a slightly yellow solid (0.980 g, 98%). DSC (5 °C min⁻¹, °C): 214 (Dec.); IR (KBr, cm⁻¹) $\tilde{\nu}$ = 3336(w) 3153(m) 1650(s) 1585(w) 1548(w) 1466(w) 1399(vw) 1365(w) 1270(vw) 1240(vw) 1216(vw) 1087(vs) 1015(m) 961(w) 747(m) 737(m) 617(s) 606(s) 578(s); Raman (400 mW, 25 °C, cm⁻¹) $\tilde{\nu}$ = 3259(6) 2986(101) 1523(27) 1360(7) 1227(16) 1214(18) 1162(8) 1125(17) 1060(59) 1009(77) 860(10) 735(10) 549(23) 517(15) 375(13) 332(12) 203(13); ¹H NMR (DMSO-*d*₆, 25 °C) δ 7.1 (s, 8H, NH₂-C-NH₂, C-NH₂, HN-NH); ¹³C NMR (DMSO-*d*₆, 25 °C) δ 167.9 (2C, C_{ring}); *m/z* (FAB⁻, xenon, 6 keV, glycerin matrix): 84.0 (4, [CH₂N₅]⁻), 118.1 (3, HCN-gly), 166.0 (12, [C₂H₂N₁₀]²⁻), 167.0 (100, [C₂H₃N₁₀]⁻), 259.0 (28, C₂H₄N₁₀-gly), 335.0 (8, [C₂H₄N₁₀ · C₂H₃N₁₀]⁻); C₄H₁₄N₁₆ (268.16) calc.: C 16.77, H 4.93, N 78.30%; found: C 16.48, H 4.98, N 74.75%.

Synthesis of Aminoguanidinium 5,5'-Hydrazinebistetrazolate (102): 20 mL of water were degassed by flushing nitrogen through it over 10 min. and loaded into a 50 mL *Schlenk* flask. Aminoguanidinium bicarbonate¹ (0.861 g, 6.3 mmol) and **95** (0.532 g, 3.2 mmol) were added forming a suspension, which turned into a clear solution after stirring for 30 min. at room temperature (gas evolution!). The solvent was removed under high vacuum in a warm water bath yielding the pure compound as a off-yellow solid (0.985 g, 97%). DSC (5 °C min⁻¹, °C): ~142-194 (m.p. + Dec.); IR (KBr, cm⁻¹) $\tilde{\nu}$ = 3411(w) 3327(m) 3269(m) 3165(m) 3046(m) 2787(vw) 2231(vw) 2206(vw) 2094(vw) 1666(s) 1645(s) 1586(w) 1457(w) 1397(m) 1240(vw) 1203(w) 1177(w) 1164(w) 1110(m) 1077(w) 1054(w) 1037(w) 1007(m) 769(m) 738(vs) 632(s) 616(s); Raman (400 mW, 25 °C, cm⁻¹) $\tilde{\nu}$ = 3231(8) 2986(90) 1652(11) 1574(13) 1512(53) 1233(40) 1105(23) 1048(100) 956(37) 820(13) 616(15) 537(14) 513(27) 406(13) 373(35) 336(15) 225(36); ¹H NMR (DMSO-*d*₆, 25 °C) δ 7.7 (s, 4H, NH₂-C-NH₂), 7.1 (s, 1H, -NH-), 4.8 (s, 2H, NH₂); ¹³C NMR (DMSO-*d*₆, 25 °C) δ 159.5 (2C, C_{ring}); *m/z* (FAB⁻, xenon, 6 keV, glycerin matrix): 167.0 (42, [C₂H₃N₁₀]⁻); *m/z* (FAB⁺, xenon, 6 keV, glycerin matrix): 75.1 (35, [CH₇N₄]⁺); C₄H₁₆N₁₈ (316.18) calc.: C 15.18, H 5.10, N 79.72%; found: C 15.24, H 5.11, N 78.90%.

Synthesis of Lithium 5,5'-Hydrazinebistetrazolate Trihydrate (105): Lithium hydroxide (0.096 g, 4.0 mmol) was dissolved in 10 mL water degassed by bubbling nitrogen gas through it over ~ 15 minutes. Neat **95** (0.336 g, 2.0 mmol) was added portionwise under a stream of nitrogen. After 15 minutes reaction time all the insoluble material had dissolved yielding a clear colorless solution. This was heated shortly to reflux and the solvent was removed under high vacuum and at 50 °C yielding the lithium salt as a white powder in nearly quantitative yield (0.457 g). Single crystals of the product suitable for X-ray analysis were obtained by slow evaporation of a water solution of the compound under a nitrogen flow. DSC (5 °C min⁻¹, °C): ~127 (-H₂O), ~193-228 (m.p. + dec.); IR (KBr, cm⁻¹) $\tilde{\nu}$ = 3498(w) 3292(w) 3251(w) 3200(vw) 2993(w) 2888(vw) 1641(m) 1625(m) 1573(s) 1527(m) 1489(w) 1409(vw) 1366(vs) 1273(w) 1248(w) 1217(w) 1154(w) 1135(w) 1128(w) 1109(vw) 1071(w) 1061(vw) 1019(w) 999(w) 850(vw) 758(vw) 733(m) 683(w) 650(vw) 628(vw) 609(w); Raman (400 mW, 25 °C, cm⁻¹) $\tilde{\nu}$ = 3294(18) 3252(15) 2986(100) 1638(10) 1609(18) 1583(11) 1537(59)

¹ The aminoguanidinium bicarbonate from ACROS was in fact carboxyaminoguanidine betaine^[15] (see discussion above).

1487(16) 1409(8) 1367(23) 1287(11) 1274(14) 1249(39) 1219(25) 1177(10) 1137(35) 1085(29) 1072(84) 1049(35) 1023(18) 857(21) 762(12) 675(6) 572(7) 392(22) 374(15) 348(15) 236(20) 171(44); ^1H NMR (DMSO- d_6 , 25°C) δ 8.00 (s, 2H, NH–NH), 4.83 (s, ~10H, H₂O); ^{13}C NMR (DMSO- d_6 , 25 °C) δ 164.4 (2C, C_{ring}); m/z (FAB⁺, xenon, 6 keV, glycerin matrix): 84.0 (4, [CH₂N₅]⁺), 118.1 (3, HCN-gly), 124.1 (3, [C₂H₂N₇]⁺), 166.0 (5, [C₂H₂N₁₀]²⁺), 167.0 (29, [C₂H₃N₁₀]⁺), 173.0 (12, [C₂H₂N₁₀Li]⁺), 189.1 (9, [C₂H₂N₁₀LiO]³⁺), 259.1 (7, C₂H₄N₁₀-gly), 265.0 (6, C₂H₃N₁₀Li-gly), 271.1 (3, C₂H₂N₁₀Li₂-gly); C₂H₈N₁₀O₃Li₂ (234.11) calc: C 10.25, H 3.44, N 59.81%; found: C 10.96, H 3.58, N 63.19%.

Synthesis of Sodium 5,5'-Hydrazinebistetrazolate Hemihydrate (106): **95** (0.336 g, 2.0 mmol) was suspended in 10 mL degassed water (see above) and reacted with neat sodium hydroxide (0.160 g, 4.0 mmol) under a flow of nitrogen. After ~ 20 minutes reaction time a light clear yellow solution formed and the solvent was removed under high vacuum leaving behind a light yellow powder of the compound, which could be recrystallized from dry ethanol/water (0.416 g, 80%). DSC (5 °C min⁻¹, °C): ~100-120 (-H₂O), 268 (dec.); IR (KBr, cm⁻¹) $\tilde{\nu}$ = 3228(m) 1632(vw) 1549(s) 1474(vs) 1360(s) 1218(w) 1118(s) 1062(w) 1010(m) 833(w) 762(w); Raman (400 mW, 25 °C, cm⁻¹) $\tilde{\nu}$ = 3428(1) 3198(11) 2986(100) 1566(22) 1511(12) 1390(15) 1245(36) 1231(10) 1144(7) 1120(19) 1060(83) 1008(5) 939(7) 780(8) 705(8) 543(3) 400(11) 371(9) 222(16); ^1H NMR (DMSO- d_6 , 25°C) δ 6.9 (s, 2H, NH–NH), 3.9 (s, ~6H, H₂O); ^{13}C NMR (DMSO- d_6 , 25 °C) δ 167.6 (2C, C_{ring}); m/z (FAB⁺, xenon, 6 keV, glycerin matrix): 84.0 (6, [CH₂N₅]⁺), 118.1 (3, HCN-gly), 124.1 (2, [C₂H₂N₇]⁺), 166.0 (8, [C₂H₂N₁₀]²⁺), 167.0 (38, [C₂H₃N₁₀]⁺), 189.0 (41, [C₂H₂N₁₀Na]⁺), 205.0 (19, [C₂H₂N₁₀NaO]³⁺), 259.0 (10, C₂H₄N₁₀-gly), 281.0 (21, C₂H₃N₁₀Na-gly); C₂H₃N₁₀O_{0.5}Na₂ (221.03) calc.: C 10.86, H 1.37, N 63.35%; found: C 11.16, H 1.61, N 63.31%.

Synthesis of Potassium 5,5'-Hydrazinebistetrazolate (107): Potassium hydroxide (0.224 g, 4.0 mmol) was dissolved in 15 mL degassed water in a *Schlenk* flask and reacted with **95** (0.336 g, 2.0 mmol) for 15 minutes under a stream of nitrogen until all material had dissolved. At this point, the flask was connected to a *Schlenk* line and the solvent was removed at reduced pressure yielding the compound as a white powder (0.568 g, 96%). The compound oxidizes readily to the yellow azotetrazolate salt and was stored under nitrogen. DSC (5 °C min⁻¹, °C): 243 (Dec.); IR (KBr, cm⁻¹) $\tilde{\nu}$ = 3301(w) 3237(w) 1625(vw) 1561(w) 1490(m) 1469(s) 1360(s) 1345(vs) 1204(w) 1144(vw) 1130(m) 1114(w) 1081(vw) 1054(w) 1014(m) 917(s) 849(m) 768(s) 736(w) 718(m) 681(s) 606(m); Raman (400 mW, 25 °C, cm⁻¹) $\tilde{\nu}$ = 3305(32) 3238(16) 2986(59) 1562(5) 1488(90) 1473(24) 1381(29) 1362(10) 1346(6) 1281(5) 1227(6) 1208(66) 1145(11) 1131(15) 1119(17) 1078(21) 1048(100) 1016(7) 925(4) 852(8) 761(6) 733(6) 683(8) 499(6) 446(17) 393(6) 376(10) 353(41) 212(37) 170(11); ^1H NMR (DMSO- d_6 , 25°C) δ 8.1 (s, 2H, NH–NH), 4.7 (s, ~4H, H₂O); ^{13}C NMR (DMSO- d_6 , 25 °C) δ 163.9 (2C, C_{ring}); m/z (FAB⁺, xenon, 6 keV, glycerin matrix): 84.0 (18, [CH₂N₅]⁺), 118.0 (5, HCN-gly), 124.0 (3, [C₂H₂N₇]⁺), 166.0 (8, [C₂H₂N₁₀]²⁺), 167.1 (58, [C₂H₃N₁₀]⁺), 204.9 (100, [C₂H₂N₁₀K]⁺), 258.9 (9, C₂H₄N₁₀-gly), 334.8 (30, [C₂H₄N₁₀ · C₂H₃N₁₀]⁺), 372.8 (12, [C₂H₂N₁₀K · C₂H₄N₁₀]⁺); C₂H₂N₁₀K₂ (243.97) calc.: C 9.84, H 0.83, N 57.40%; found: C 9.77, H 1.09, N 57.04%.

Synthesis of Rubidium 5,5'-Hydrazinebistetrazolate (108): Rubidium carbonate (0.460 g, 2.0 mmol) was suspended in 15 mL degassed water in a 25 mL *Schlenk* flask under a flow of nitrogen. **95** (0.336 g, 2.0 mmol) was added neat forming a suspension, which was carefully warmed up with a heatgun (carbon dioxide evolution was observed). The reaction mixture was stirred and gently warmed up until the gas evolution had ceased and it was shortly brought to reflux. After removing the solvent under high vacuum, the compound was obtained as a white powder in quantitative yield (0.760 g). The compound turns completely yellow after little hours and was stored under nitrogen. Single crystals were obtained when nitrogen was blown over a freshly prepared solution of the material. DSC (5 °C min⁻¹, °C): 246 (Dec.); IR (KBr, cm⁻¹) $\tilde{\nu}$ = 3344(vw) 3286(m) 2933(vw) 1622(w) 1592(vw) 1530(s) 1488(w) 1468(vs) 1386(w) 1347(w) 1262(vw) 1243(vw) 1203(w) 1181(w) 1121(m) 1107(w) 1086(m) 1053(m) 1009(m) 890(s) 832(s) 782(s) 761(s) 730(m) 696(m) 637(s); Raman (400 mW, 25 °C, cm⁻¹) $\tilde{\nu}$ = 3351(13) 3289(28) 2986(100) 1539(18) 1488(57) 1409(5) 1374(15) 1349(7) 1204(28) 1183(26) 1140(9) 1122(21) 1108(11) 1088(9) 1045(86) 915(5) 833(7) 782(7) 731(7) 697(7) 641(9) 559(8) 545(5) 450(9) 387(11) 355(15) 273(6) 211(35) 159(7) 103(2); ¹H NMR (DMSO-*d*₆, 25 °C) δ 7.9 (s, 2H, NH–NH), ¹³C NMR (DMSO-*d*₆, 25 °C) δ 163.9 (2C, C_{ring}); *m/z* (FAB⁺, xenon, 6 keV, glycerin matrix): 84.0 (7, [CH₂N₅]⁺), 118.0 (3, HCN-gly), 124.1 (2, [C₂H₂N₇]⁺), 166.0 (5, [C₂H₂N₁₀]²⁺), 167.0 (35, [C₂H₃N₁₀]⁺), 250.8 (33, [C₂H₂N₁₀Rb]⁺), 259.0 (6, C₂H₄N₁₀-gly), 342.8 (13, C₂H₃N₁₀Cs-gly); C₂H₂N₁₀Rb₂ (335.87) calc.: C 7.15, H 0.60, N 41.69%; found: C 7.39, H 0.74, N 42.20%.

Synthesis of Cesium 5,5'-Hydrazinebistetrazolate (109): **95** (0.336 g, 2.0 mmol) was suspended in 15 mL degassed water and reacted with cesium carbonate (0.652 g, 2.0 mmol) under a stream of nitrogen. The reaction mixture was gently warmed up to induce the formation of carbon dioxide until the gas evolution had stopped. The solvent was removed by blowing nitrogen gas over the solution producing single crystals of the cesium salt suitable for diffraction studies in quantitative yield (0.950 g). DSC (5 °C min⁻¹, °C): 246 (Dec.); IR (KBr, cm⁻¹) $\tilde{\nu}$ = 3232(vw) 2798(vw) 2409(vw) 2211(vw) 2072(vw) 1632(vw) 1508(w) 1473(w) 1435(vw) 1382(s) 1358(w) 1210(vw) 1180(m) 1146(m) 1107(vw) 1064(w) 1039(m) 1025(w) 798(w) 774(s) 727(vs); Raman (400 mW, 25 °C, cm⁻¹) $\tilde{\nu}$ = 3243(6) 3209(10) 2987(51) 1542(13) 1510(47) 1489(14) 1371(14) 1217(48) 1174(10) 1104(30) 1041(100) 991(10) 888(9) 767(9) 754(9) 607(6) 422(18) 363(9) 353(10) 242(40) 150(11); ¹H NMR (DMSO-*d*₆, 25 °C) δ 6.7 (s, 2H, NH–NH), ¹³C NMR (DMSO-*d*₆, 25 °C) δ 168.3 (2C, C_{ring}); *m/z* (FAB⁺, xenon, 6 keV, glycerin matrix): 84.0 (6, [CH₂N₅]⁺), 118.0 (3, HCN-gly), 124.1 (2, [C₂H₂N₇]⁺), 166.0 (6, [C₂H₂N₁₀]²⁺), 167.0 (32, [C₂H₃N₁₀]⁺), 259.0 (8, C₂H₄N₁₀-gly), 298.8 (42, [C₂H₂N₁₀Cs]⁺), 390.8 (18, C₂H₃N₁₀Cs-gly); C₂H₂N₁₀Cs₂ (431.86) calc.: C 5.56, H 0.47, N 32.43%; found: C 5.56, H 0.60, N 32.47%.

Synthesis of Magnesium 5,5'-Hydrazinebistetrazolate Hexahemihydrate (110): **95** (0.478 g, 2.84 mmol) was suspended in 5 mL water and treated with one equivalent of magnesium hydroxide (0.165 g, 2.84 mmol). The reaction mixture was refluxed for 1.5 hrs. under a stream of nitrogen and left to cool to room temperature. The solvent was stripped under high vacuum (10⁻³ mbar) yielding a sticky mass, which was recrystallized from the minimum amount of hot water. Slightly yellow crystals of the product suitable for X-ray analysis separated upon slow cooling of the hot solution. These were filtered, washed with acetone and ether and dried under vacuum yielding the magnesium salt, which was pure by elemental analysis (0.549 g,

69%). $\text{C}_2\text{H}_{15}\text{N}_{10}\text{O}_{6.5}\text{Mg}$ (307.55 g mol⁻¹) calcd.: C 7.82, H 4.92, N 45.60%; found: C 7.90, H 4.73, N 45.92%; DSC (5 °C min⁻¹, °C): 142–158 (loss H₂O), 220 and 250 (dec); IR (KBr, cm⁻¹) $\tilde{\nu}$ = 3505(s) 3395(s) 3319(s) 3230(vs) 3054(s) 2330(w) 1687(m) 1557(m) 1530(m) 1480(s) 1371(m) 1263(w) 1245(w) 1146(m) 1077(w) 1028(w) 960(w) 908(m) 837(m) 806(m) 713(s) 513(m); Raman (400 mW, 25 °C, cm⁻¹) $\tilde{\nu}$ = 3231(3) 3082(3) 2986(100) 2663(1) 2409(1) 1530(47) 1485(10) 1393(11) 1264(8) 1248(28) 1233(10) 1180(4) 1145(21) 1111(9) 1079(47) 1067(35) 1031(9) 888(5) 739(5) 387(11) 361(10) 262(11) 231(14) 193(11) 150(7); ¹H NMR (DMSO-*d*₆, 25 °C) δ /ppm: 7.3 (s, 2H, NH–NH), 3.9 (s, ~12H, H₂O); ¹³C NMR (DMSO-*d*₆, 25 °C) δ /ppm: 166.2 (2C, C_{ring}); ¹⁴N NMR (DMSO-*d*₆, 25 °C) δ /ppm: –270 (2N, NH–NH); *m/z* (FAB[–], xenon, 6 keV, glycerine matrix): 83.0 (6, [CHN₅]^{2–}), 118.1 (4, HCN-gly), 124.1 (2, [C₂H₂N₇][–]), 167.1 (19, [C₂H₃N₁₀][–]), 205.1 (7, [C₂HN₁₀MgO]^{3–}), 259.1 (5, C₂H₄N₁₀-gly), 281.1 (18, C₂H₂N₁₀Mg-gly).

Synthesis of Calcium 5,5'-Hydrazinebistetrazolate Pentahydrate (111): **95** (0.354 g, 2.11 mmol) was suspended in 5 mL water in an *Schlenk* flask under a stream of nitrogen and treated with calcium hydroxide (0.156 g, 2.11 mmol). The reaction mixture was heated to boiling and stirred for 2 hrs. Colorless crystals of the desired compound suitable for X-ray structure analysis precipitated upon slow cooling to room temperature and the solution was stored in a refrigerator overnight. The solid that precipitated was filtered under vacuum and washed with acetone and ether. No further purification was necessary (0.481 g, 77%). $\text{C}_2\text{H}_{12}\text{N}_{10}\text{O}_5\text{Ca}$ (296.30 g mol⁻¹) calcd.: C 8.10, H 4.08, N 47.30%; found: C 8.13, H 4.01, N 46.40%; DSC (5 °C min⁻¹, °C): 140–160 (loss H₂O), 220 and 260 (dec); IR (KBr, cm⁻¹) $\tilde{\nu}$ = 3428(vs) 3251(s) 2170(w) 1631(m) 1531(s) 1451(m) 1384(w) 1343(m) 1234(w) 1217(w) 1158(m) 1146(w) 1129(m) 1067(w) 1022(m) 909(w) 839(m) 750(m) 600(m) 519(m); Raman (400 mW, 25 °C, cm⁻¹) $\tilde{\nu}$ = 3251(11) 1546(29) 1497(24) 1456(10) 1377(41) 1236(29) 1220(24) 1131(35) 1100(14) 1089(14) 1066(65) 1022(10) 909(11) 646(9) 396(11) 346(12) 324(11) 248(9) 173(9); ¹H NMR (DMSO-*d*₆, 25 °C) δ /ppm: 7.0 (s, 2H, NH–NH), 3.8 (s, ~10H, H₂O); ¹³C NMR (DMSO-*d*₆, 25 °C) δ /ppm: 167.1 (2C, C_{ring}); *m/z* (FAB[–], xenon, 6 keV, glycerine matrix): 83.0 (8, [CHN₅]^{2–}), 118.1 (6, HCN-gly), 124.1 (3, [C₂H₂N₇][–]), 167.1 (35, [C₂H₃N₁₀][–]), 214.0 (3), 221.0 (7, [C₂HN₁₀CaO]^{3–}), 259.1 (8, C₂H₄N₁₀-gly), 297.1 (28).

Synthesis of Strontium 5,5'-Hydrazinebistetrazolate Pentahydrate (112): **95** (0.354 g, 2.11 mmol) was charged in a *Schlenk* flask under a stream of nitrogen and suspended in 5 mL water. Neat strontium hydroxide octahydrate (0.541 g, 2.11 mmol) was added and the initial suspension dissolved upon heating. The solution was kept at reflux and stirred for 3 hours and left to slowly crystallize by switching off the oil bath, first at room temperature and then in the fridge yielding crystals of the strontium salt, which were used to measure the crystal structure. The slightly brown solid was filtered and let to air-dry. No further purification was required (0.661 g, 91%). $\text{C}_2\text{H}_{12}\text{N}_{10}\text{O}_5\text{Sr}$ (343.84 g mol⁻¹) calcd.: C 6.99, H 3.52, N 40.74%; found: C 7.09, H 3.46, N 40.59%; DSC (5 °C min⁻¹, °C): 150–185 (loss H₂O), 276 (m.p. + dec); IR (KBr, cm⁻¹) $\tilde{\nu}$ = 3416(vs) 3255(vs) 2260(w) 2166(w) 1628(m) 1533(vs) 1451(s) 1384(w) 1346(m) 1236(m) 1219(m) 1154(m) 1144(m) 1129(m) 1068(w) 1021(m) 843(m) 749(m) 598(s) 515(s); Raman (400 mW, 25 °C, cm⁻¹) $\tilde{\nu}$ = 3301(3) 3256(11) 1541(37) 1460(10) 1367(14) 1238(35) 1222(30) 1131(40) 1108(12) 1066(70) 1021(10) 908(12) 738(6) 657(8) 393(16) 346(16) 319(17) 273(11) 237(12); ¹H NMR (DMSO-*d*₆, 25 °C) δ /ppm: 6.9 (s,

2H, NH–NH), 3.7 (s, ~10H, H₂O); ¹³C NMR (DMSO-*d*₆, 25 °C) δ/ppm: 167.2 (2C, C_{ring}); *m/z* (FAB⁺, xenon, 6 keV, glycerine matrix): 83.0 (4, [CHN₅]²⁺), 118.1 (3, HCN-gly), 124.1 (2, [C₂H₂N₇]⁺), 167.1 (28, [C₂H₃N₁₀]⁺), 259.1 (7, C₂H₄N₁₀-gly), 269.0 (2, [C₂HN₁₀SrO]³⁺).

Synthesis of Barium 5,5'-Hydrazinebistetrazolate Pentahydrate (113). *Method A:* **95** (0.168 g, 1.0 mmol) was suspended in 5 mL water and reacted with sodium hydroxide (0.080 g, 2.0 mmol) under a stream of nitrogen. The resulting solution was heated to 65 °C and a solution of barium chloride dihydrate (0.249 g, 1.0 mmol) in 5 mL water was added at this temperature. The reaction mixture was stirred for further 15 min, left to cool slowly to room temperature and stored in the fridge overnight yielding prismatic colorless crystals of the product, which were filtered and stored under nitrogen (0.058 g, 19%).

Method B: Alternatively, a *Schlenk* flask was charged with **95** (0.385 g, 2.29 mmol) and 8 mL water under a stream of nitrogen. Barium hydroxide octahydrate (0.723 g, 2.29 mmol) was added. The suspension was refluxed for 1 hr. under a stream of nitrogen after which time all the insoluble material had dissolved. The solution was left to slowly cool to room temperature while keeping a nitrogen flow and stored in the fridge overnight yielding prismatic colorless crystals of the compound, which were filtered and allowed to air-dry (0.559 g, 80%). C₂H₁₂N₁₀O₅Ba (422.01 g mol⁻¹) calcd.: C 6.09, H 3.07, N 35.54%; found: C 6.16, H 3.02, N 35.59%; DSC (5 °C min⁻¹, °C): ~130–154 (loss H₂O), 260 (m.p. + dec); IR (KBr, cm⁻¹) $\tilde{\nu}$ = 3408(vs) 3255(vs) 2258(w) 2150(w) 1636(m) 1532(vs) 1450(s) 1384(m) 1349(m) 1235(m) 1219(m) 1149(m) 1128(m) 1068(w) 1019(m) 856(m) 748(m) 736(m) 603(s) 514(s); Raman (200 mW, 25 °C, cm⁻¹) $\tilde{\nu}$ = 3255(13) 2986(85) 1536(48) 1464(12) 1410(6) 1376(21) 1236(37) 1222(33) 1157(9) 1130(44) 1098(12) 1066(100) 1018(14) 909(15) 682(10) 389(22) 344(20) 318(20) 233(16); ¹H NMR (DMSO-*d*₆, 25 °C) δ 6.9 (s, 2H, NH–NH), 3.6 (s, ~10H, H₂O); ¹³C NMR (DMSO-*d*₆, 25 °C) δ 167.3 (2C, C_{ring}); *m/z* (FAB⁺, xenon, 6 keV, m-NBA matrix) 167.0 [C₂H₃N₁₀]⁺.

Improved Synthesis of Ammonium 5,5'-Azotetrazolate: 95 (0.500 g, 3.0 mmol) were suspended in 10 mL methanol and a slight stream of ammoniac gas was bubbled through the suspension for 15 min. The reaction mixture turned immediately slightly yellow and after further stirring under air formed a bright yellow solution of the product which was rotavaporated down to dryness leaving a pure yellow residue of the product in quantitative yield (0.594 g). C₂H₈N₁₂ (calc./found, %): C 12.03/11.82, H 4.02/3.97, N 84.06/83.21.

Improved Synthesis of Hydrazinium 5,5'-Azotetrazolate: 95 (0.160 g, 0.952 mmol) was suspended in 2 mL water and 5 mL methanol before hydrazine hydrate was added (0.096 g, 1.918 mmol). The initial colourless solution turned yellow immediately and the reaction mixture was stirred for 4 hours at reflux. After this time the solvent was evaporated to dryness giving the desired compound as a yellow powder (0.217 g, quantitative yield). C₂H₁₀N₁₄ (calc./found, %): C 10.44/10.45, H 4.38/5.02, N 85.19/85.49.

General Procedure for the Improved Synthesis of Metal 5,5'-Azotetrazolate Salts: 95 was suspended in water and reacted with an equivalent amount of a suitable metal hydroxide forming a yellow solution. The reaction mixture was shortly brought to reflux and the solvent was stripped off at 70 °C. The crude compound

was recrystallized from the minimum amount of water yielding the corresponding azotetrazolate in yields between 80 and 90 %. (The synthesis of the alkaline earth metal salts requires longer reaction times and the product precipitates out of the reaction mixture).

8.10 References

- [1] a) A. Hammerl, G. Holl, M. Kaiser, T. M. Klapötke, P. Mayer, H. Piotrowsky, M. Vogt, *Z. Naturforsch.* **2001**, *56b*, 847-856. b) A. Hammerl, G. Holl, M. Kaiser, T. M. Klapötke, P. Mayer, H. Piotrowsky, M. Vogt, *Z. Naturforsch.* **2001**, *56b*, 857 – 870. c) H.-G. Ang, W. Fraenk, K. Karaghiosoff, T. M. Klapötke, H. Nöth, J. Sprott, M. Suter, M. Vogt, M. Warchhold. *Z. Anorg. Allg. Chem.* **2002**, *628*, 2901-2906.
- [2] A. Hammerl, G. Holl, M. Kaiser, T. M. Klapötke, P. Mayer, H. Nöth, H. Piotrowski, M. Warchhold, *Eur. J. Inorg. Chem.* **2002**, 834-845.
- [3] a) T. M. Klapötke, C. Miró Sabaté, Particles, Crystals, Composites, ICT Symposium, Pfinztal (Berghausen), March 13 – 14, **2007**. b) T. M. Klapötke, C. Miró Sabaté, *Chem. Mater.* **2008**, *20*(5), 1750-1763. c) A. Hammerl, M. A. Hiskey, G. Holl, T. M. Klapötke, K. Polborn, J. Stierstorfer, J. J. Weigand, *Chem. Mater.* **2005**, *17*(14), 3784-3793.
- [4] G. Holl, T. M. Klapötke, J. J. Weigand, DE 10,2004,014,044, 2005.
- [5] J. Thiele, *Just. Lieb. Ann. Chem.* **1898**, *303*, 57-75.
- [6] T. M. Klapötke, C. Miró Sabaté, *Z. Anorg. Allg. Chem.* **2007**, *633*, 2671–2677.
- [7] T. M. Klapötke, C. Miró Sabaté, *Chem. Mater.* **2008**, *20*(11), 3629-3637.
- [8] a) R. J. Spear, P. P. Elischer, *Aust. J. Chem.* **1982**, *35*(1), 1–13. b) D. J. Whelan, R. J. Spear, R. W. Read, *Thermochim. Acta* **1984**, *80*(1), 149-163.
- [9] a) M. A. Hiskey, D. E. Chavez, D. L. Naud, S. F. Son, H. L. Berghout, C. A. Bolme, *Proceedings of the 27th International Pyrotechnics Seminar*, 2000, Los Alamos, NM, USA, 3-14. b) M. A. Hiskey, D. E. Chavez, D. L. Naud, US 6,214,139, 2001. c) S. P. Burns, J. W. Halpin, G. K. Williams, P. S. Khandhadia, D. L. Hordos, J. Newell, WO 038,803, 2007. d) J. W. Halpin, S. P. Burns, WO 041,384, 2007. e) T. M. Klapötke, P. Mayer, K. Polborn, J. Stierstorfer, J. J. Weigand, *New Trends in Research of Energetic Materials, Proceedings of the 9th Seminar*, 2006, Pardubice, Czech Republic, 641-651. f) M. Friedrich, J. C. Gálvez-Ruiz, T. M. Klapötke, P. Mayer, B. Weber, J. J. Weigand, *Inorg. Chem.* **2005**, *44*(22), 8044-8052.
- [10] Y. Gao, H. Gao, B. Twamley, J. M. Shreeve, *Adv. Mater.* **2007**, *19*, 2884-2888.
- [11] A. Hammerl, G. Holl, M. Kaiser, T. M. Klapötke, H. Piotrowski, *Z. Anorg. Allg. Chem.* **2003**, *629*(12–13), 2117–2121.
- [12] a) G. O. Reddy, A. K. Chatterjee, *J. Hazard. Mater.* **1984**, *9*(3), 291-303. b) D. J. Whelan, R. J. Spear, R. W. Read, *Thermochim. Acta* **1984**, *80*(1), 149-163.
- [13] (a) J. Thiele, *Just. Lieb. Ann. Chem.* **1892**, *270*, 54-63. (b) J. Thiele, J. T. Marais, *Just. Lieb. Ann. Chem.* **1893**, *273*, 144-160. (c) J. Thiele, *Ber.* **1893**, *26*, 2645-2646.
- [14] R. A. Henry, W. G. Finnegan, *J. Am. Chem. Soc.* **1954**, *76*, 923-924.
- [15] T. Kolev, R. Petrova, *Acta Crystallogr.* **2003**, *E59*(4), o447-o449.

- [16] T. M. Klapötke, J. Stierstorfer, unpublished results.
- [17] A. Hammerl, *Ph. D. Thesis*, Ludwig-Maximilian Univ. Munich, **2001**.
- [18] a) M. von Denffer, G. Heeb, T. M. Klapötke, G. Kramer, G. Spiess, J. M. Welch, *Propellants, Explos. Pyrotech.* **2005**, *30*(3), 191-195. b) J. J. Weigand, PhD Thesis, Ludwig-Maximilians Universität München, **2005**, 184.
- [19] K. Karaghiosoff, T. M. Klapötke, P. Mayer, C. Miró Sabaté, A. Penger, J. M. Welch, *Inorg. Chem.* **2008**, *47*, 1007–1019.
- [20] N. B. Colthup, L. H. Daly, S. E. Wiberley, *Introduction to Infrared and Raman Spectroscopy*, Academic Press, Boston, **1990**.
- [21] (a) Programs for Crystal Structure Analysis (Release 97-2). Sheldrick, G.M. Institut für Anorganische Chemie der Universität, Tammanstrasse 4, D-3400 Göttingen, Germany, **1998**. (b) A. Altomare, M. C. Burla, M. Camalli, G. L. Cascarano, C. Giacovazzo, A. Guagliardi, A. G. G. Moliterni, G. Polidori, R. Spagna, *J. Appl. Crystallogr.* **1999**, *32*, 115-119.
- [22] Gaussian 03, Revision A.1, M. J. Frisch, G. W. Trucks, H. B. Schlegel, G. E. Scuseria, M. A. Robb, J. R. Cheeseman, J. A. Montgomery Jr., T. Vreven, K. N. Kudin, J. C. Burant, J. M. Millam, S. S. Iyengar, J. Tomasi, V. Barone, B. Mennucci, M. Cossi, G. Scalmani, N. Rega, G. A. Petersson, H. Nakatsuji, M. Hada, M. Ehara, K. Toyota, R. Fukuda, J. Hasegawa, M. Ishida, T. Nakajima, Y. Honda, O. Kitao, H. Nakai, M. Klene, X. Li, J. E. Knox, H. P. Hratchian, J. B. Cross, C. Adamo, J. Jaramillo, R. Gomperts, R. E. Stratmann, O. Yazyev, A. J. Austin, R. Cammi, C. Pomelli, J. W. Ochterski, P. Y. Ayala, K. Morokuma, G. A. Voth, P. Salvador, J. J. Dannenberg, V. G. Zakrzewski, S. Dapprich, A. D. Daniels, M. C. Strain, O. Farkas, D. K. Malick, A. D. Rabuck, K. Raghavachari, J. B. Foresman, J. V. Ortiz, Q. Cui, A. G. Baboul, S. Clifford, J. Cioslowski, B. B. Stefanov, G. Liu, A. Liashenko, P. Piskorz, I. Komaromi, R. L. Martin, D. J. Fox, T. Keith, M. A. Al-Laham, C. Y. Peng, A. Nanayakkara, M. Challacombe, P. M. W. Gill, B. Johnson, W. Chen, M. W. Wong, C. González, J. A. Pople, Gaussian, Inc., Pittsburgh PA, **2003**.
- [23] A. D. Becke, A. Savin, H. Stoll, H. Preuss, *Chem. Phys. Lett.* **1989**, *157*(3), 200–206.
- [24] a) D. E. Woon, T. H. Dunning Jr., *J. Chem. Phys.* **1993**, *98*(2), 1358–1371; b) R. A. Kendall, T. H. Dunning Jr., R. J. Harrison, *J. Chem. Phys.* **1992**, *96*(9), 6796–6806; c) T. H. Dunning Jr., *J. Chem. Phys.* **1989**, *90*(2), 1007–1023; d) K. A. Peterson, D. E. Woon, T. H. Dunning Jr., *J. Chem. Phys.* **1994**, *100*(10), 7410–7415; e) A. Wilson, T. van Mourik, T. H. Dunning Jr., *J. Mol. Struct. (Theochem.)* **1997**, *388*, 339–349.
- [25] A. S. Lyakhov, P. N. Gaponik, S. V. Voitekhovich, *Acta Crystallogr.* **2001**, *C57*, 185–186.
- [26] D. D. Bray, J. G. White, *Acta Crystallogr.* **1979**, *B35*, 3089–3091.
- [27] J. Bernstein, R. E. Davis, L. Shimoni, N. L. Chang, *Angew. Chem. Int. Ed.* **1995**, *34*(15), 1555-1573.

[28] a) W. D. S. Motherwell, G. P. Shields, F. H. Allen, *Acta Crystallogr.* **2000**, B56(3), 466-473. b) W. D. S. Motherwell, G. P. Shields, F. H. Allen, *Acta Crystallogr.* **1999**, B55(6), 1044-1056. c) <http://www.ccdc.cam.ac.uk/support/documentation/rpluto/TOC.html>.

[29] N–N and N=N bond distances from: *International tables for X-ray crystallography*, Vol. C, Kluwer Academic Publisher, Dordrecht, **1992**.

[30] a) Etat Francais (J. Duguet) U.S.4566921 (January 28, **1986**). b) I. D. Brown, *Acta Cryst.* **1988**, B44, 545–553; c) J. Hitzbleck, G. B. Deacon, K. Ruhlandt-Senge, *Eur. J. Inorg. Chem.* **2007**, 4, 592–601; d) B. Lian, C. M. Thomas, O. L. Jr. Casagrande, T. Roisnel, J-F. Carpentier, *Polyhedron* **2007**, 26(14), 3817–3824; e) T. Zhang, C. Lu, J. Zhang, K. Yu, *Propellants, Explos., Pyrotech.* **2003**, 28(5), 271–276 ; f) N. C. Mosch-Zanetti, M. Ferbinteanu, J. Magull, *Eur. J. Inorg. Chem.* **2002**, 4, 950–956; g) I. Kobrsi, J. E. Knox, M. J. Heeg, H. B. Schlegel, C. H. Winter, *Inorg. Chem.* **2005**, 44(14), 4894–4896.

[31] C. Darwich, T. M. Klapötke, C. Miró Sabaté, *Propellants, Explos., Pyrotech.* **2007**, in press.

[32] a) A. Hammerl, T. M. Klapötke, H. Nöth, M. Warchhold, G. Holl, M. Kaiser, U. Ticmanis, *Inorg. Chem.* **2001**, 40(14), 3570–3575; b) T. M. Klapötke, C. Miró Sabaté, *Heteroat. Chem.* **2008**, 19(3), 301-306.

[33] R. Taylor, O. Kennard, *J. Am. Chem. Soc.* **1982**, 104, 5063–5070.

[34] T. M. Klapötke, C. Miró Sabaté, J. M. Welch, *J. Chem. Soc. Dalton Trans.* **2008**, submitted.

[35] a) V. Ernst, T. M. Klapötke, J. Stierstorfer *Z. Anorg. Allg. Chem.* **2007**, 633, 879-887. b) T. M. Klapötke, H. Radies, J. Stierstorfer, *Z. Naturforsch.* **2007**, 62b, 1343 –1352.

[36] T. M. Klapötke, C. Kuffer, P. Mayer, K. Polborn, A. Schulz, J. J. Weigand, *Inorg. Chem.* **2005**, 44(16), 5949-5958.

[37] A. Bondi, *J. Phys. Chem.* **1964**, 68(3), 441-451.

[38] Impact: Insensitive >40 J, less sensitive ≥ 35 J, sensitive ≥ 4 J, very sensitive ≤ 3 J; friction: Insensitive >360 N, less sensitive = 360 N, sensitive <360 N a. >80 N, very sensitive ≤ 80 N, extreme sensitive ≤ 10 N; According to the UN Recommendations on the Transport of Dangerous Goods (+) indicates: not safe for transport.

[39] <http://www.bam.de/>

[40] T. M. Klapötke, C. M. Rienäcker, *Propellants, Explos., Pyrotech.* **2001**, 26(1), 43–47.

[41] J. Köhler, R. Meyer, *Explosivstoffe* 9th ed.; Wiley-VCH: Weinheim, Germany, 1998.

[42] U. Bemm, H. Östmark, *Acta Crystallogr.* **1998**, C54, 1997–1999.

[43] M. S. Westwell, M. S. Searle, D. J. Wales, D. H. Williams, *J. Am. Chem. Soc.* **1995**, 117, 5013–5015.

[44] Calculation of the oxygen balance: $\Omega(\%) = (\text{O} - 2\text{C} - \text{H}/2 - x\text{AO}) 1600/\text{M}$; M = molecular mass.

[45] T. Shimanouchi, *Tables of Molecular Vibrational Frequencies Consolidated*; National Bureau of Standards: Washington, D.C., 1972; Vol. 1.

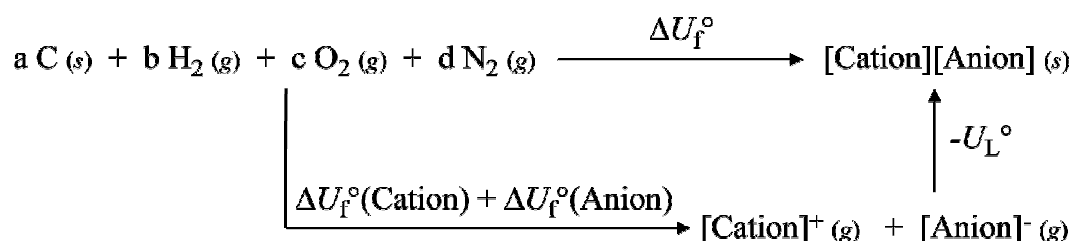
- [46] R. P. Singh, R. D. Verma, D. T. Meshri, J. M. Shreeve, *Angew.Chem., Int. Ed.* **2006**, *45*, 3584–3601, and references therein.
- [47] M. Suceca, *Propellants, Explos., Pyrotech.* **1991**, *16*, 197–202.
- [48] L. E. Fried, K. R. Glaesemann, W. M. Howard, P. C. Souers, 2004. *CHEETAH 4.0 User's Manual*, Lawrence Livermore National Laboratory.
- [49] J. A. Pople, R. Seeger, R. Krishnan, *Int. J. Quantum Chem., Symp.* **1977**, *11*, 149-163.
- [50] A. K. Rick, T. H. Dunning, J. H. Robert, *J. Chem. Phys.* **1992**, *96*, 6796-6806.
- [51] A. P. Kirk, E. W. David, T. H. Dunning, *J. Chem. Phys.* **1994**, *100*, 7410-7415.
- [52] G. I. Koldobskii, D. S. Soldatenko, E. S. Gerasimova, N. R. Khokhryakova, M. B. Shcherbinin, V. P. Lebedev and V. A. Obstrovskii, *Rus. J. Org. Chem.* **1997**, *33*(12), 1771-1783.
- [53] T. M. Klapötke, P. Mayer, C. Miró Sabaté, J. M. Welch, N. Wiegand, *Inorg. Chem.* **2007**, accepted.
- [54] NIST Chemistry WebBook, NIST Standard Reference Database Number 69 - March, **2003** Release, www version: <http://webbook.nist.gov/chemistry>.
- [55] *HyperChem 7.0*, Molecular Visualization and Simulation Program Package, Hypercube, Gainesville, FL, 2002.
- [56] a) P. Politzer, J. S. Murray, Computational Characterization of Energetic Materials, in: *Pauling's Legacy: Modern Modelling of the Chemical Bond*, Z. B. Maksic, W. J. Orville-Thomas (eds.), Theoretical and Computational Chemistry, **1999**, *6*, 347–363; b) P. Politzer, J. S. Murray, J. M. Seminario, P. Lane, M. E. Grice, M. C. Concha, *J. Mol. Struct.* **2001**, *573*, 1. c) J. S. Murray, P. Lane, P. Politzer, *Molec. Phys.* **1998**, *93*, 187; d) J. S. Murray, P. Lane, P. Politzer, *Mol. Phys.* **1995**, *85*, 1.
- [57] a) B. M. Rice, J. J. Hare, *J. Phys. Chem.* **2002**, *106A*, 1770. b) B. M. Rice in *Advanced Series in Physical Chemistry* **2005**, *16*, 335-367. c) B. M. Rice, S. Sahu, F. J. Owens, *J. Mol. Struct. (THEOCHEM)* **2002**, *583*, 69-72. d) B. M. Rice, D. Bressanini, G. F. Adams, R. C. Mowrey, M. Page, *Chem. Phys. Lett.* **1991**, *184*(4), 335-342.
- [58] http://www.sms-ink.com/products_koenen.html.
- [59] http://www.sms-ink.com/products_koenen.html.
- [60] <http://www.systag.ch>.
- [61] (a) *ICT-Thermodynamic Code*, v. 1.0, Fraunhofer-Institut für Chemische Technologie (ICT): Pfingztal, Germany, 1988-2000. (b) Webb, R.; Rooijen, M. van *Proceedings of the 29th International Pyrotechnics Seminar*, **2002**, 823-828. (c) Bathelt, H.; Volk, F. *27th International Annual Conference of ICT*, **1996**, *92*, 1-16.
- [62] <http://www.perkinelmer.com>.
- [63] http://www.linseis.net/html_en/thermal/dsc/dsc_pt10.php.
- [64] <http://www.parrinst.com>.

CHAPTER IX

SALTS OF 5-(5-NITROTETRAZOLE-2-YLMETHYL)-TETRAZOLE

9.1 Introduction

Due to the interesting energetic properties of tetrazoles and specially of bistetrazole derivatives (see *Chapters VII and VIII*) we decided to study a new family of bridged-bistetrazole derivatives based on the novel 5-(5-nitrotetrazole-2-ylmethyl)-tetrazolate (NTTz⁻) anion. This project started with the idea in mind that bistetrazoles are highly endothermic compounds and the nitro group in **129b** should confer the compounds a higher density in comparison with, for example, 5,5'-azotetrazolate salts. The combination of high endothermicities with high densities is important to reach high detonation parameters. This chapter is supposed to be a report on the on-going research on tetrazole chemistry and combine what has become two areas of expertise in the group: on one side 5-nitrotetrazole chemistry (*Chapter III*) and on the other the chemistry of simple 1*H*-tetrazole, which should allow to be derivatized and yield a new family of compounds with interesting energetic properties.



Scheme 9.1 General Born-Haber cycle for the formation of a CHNO-based salt.

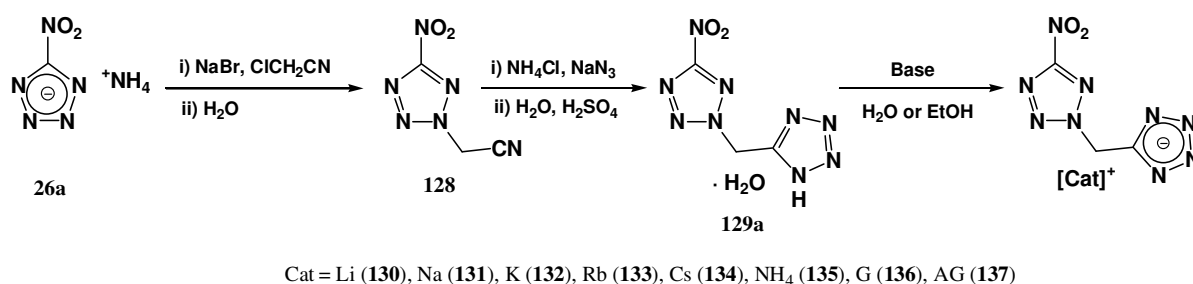
Scheme 9.1 shows a general Born-Haber cycle for an ionic compound made up of carbon, hydrogen, nitrogen and oxygen (CHNO). The (standard) energy of formation of a compound (ΔU_f°) is inversely proportional to the lattice energy (U_L° , Eqn. (1)) (i.e., the larger U_L° the smaller ΔU_f°) and the latter grows with the charge of the ions (in the case of ionic compounds) according to *Kapustinskii's equation* (Eqn. (2), where ν is the number of ions in the empirical formula, z is the anionic and cationic charge, respectively, r is the radius of the anion / cation and U_L is given in kJ mol^{-1}). It seems then reasonable to study compounds based on monoionic species rather than di- or polyvalent ions. We envision thus salts of **129b** to be highly endothermic and also high

performing compounds and hopefully their sensitivities will be low enough to allow safe transport, which is one of the main topics of discussion when looking at (for example) RDX replacements.^[1]

$$\Delta U_f^\circ = \Delta U_f^\circ(\text{Cation}) + \Delta U_f^\circ(\text{Anion}) - U_L^\circ \quad (1); \quad U_L = 1202.5 \times \frac{\nu \times z^+ \times z^-}{r^+ + r^-} \times \left(1 - \frac{0.345}{r^+ + r^-}\right) \quad (2)$$

9.2 Synthesis

Koldobskii et al.^[2] prepared 5-nitrotetrazole-2-ylacetonitrile (**NTAN**, **128**) from sodium 5-nitrotetrazolate (**NaNT**, **22**), however, we decided to use the (anhydrous) ammonium salt (**ANT**, **21a**) due to the hazards involved in the preparation of **22** (see *Chapter III*).^[3] A modified literature procedure^[4] for the synthesis of anhydrous **21a** was used, the main difference consisting in the extraction solvent. The last reported synthesis used dichloromethane (DCM) and dodecylamine. On one side, halogenated solvents are to be avoided on large scale synthesis due to the inherent toxicity of the same, on the other, dodecylamine is rather pricy and needs to be recycled every time. We came up with the use of ethylacetate as a cheap up-scalable alternative for the extraction process. **21a** is initially obtained as a cream-colored impure solid, which can be recrystallized. Recrystallization from methanol gives (in a reproducible way) the pure compound as the anhydrous species. This is also a clear advantage in respect to the published procedure^[4] where the compound forms as the hemihydrate and the crystal water can be removed by storing over P₄O₁₀ for several days (or weeks depending on the scale of the reaction). Crude (impure) **21a** product can be directly alkylated with bromoacetonitrile using DMF as the solvent (Scheme 9.2). After addition of water **128** precipitates as a slightly brown solid and after two recrystallizations from ethanol using active charcoal the compound is obtained as pure colorless needles in reproducible yields that vary around 50%. The 1,3-dipolar cycloaddition to form the tetrazole ring from the cyano group takes place when **128** is reacted with sodium azide and ammonium chloride in DMF and after work-up using diluted sulfuric acid a cream colored powder precipitates, which can be recrystallized from water using active charcoal into a colorless (slightly orange) pure crystalline solid. The product so-formed responds to the structure of 5-(5-nitrotetrazole-2-ylmethyl)-tetrazole monohydrate (**NTTzh**, **129a**) and not to the anhydrous compound as reported in the original procedure.^[2] The anhydrous compound (**NTTz**, **129b**) formed initially in an attempt to generate the nitrate and perchlorate salts of **129b** by reaction of **129a** with a small excess of the corresponding acid in ethanol and alternatively dehydration of **129a** yielded the anhydrous material quantitatively.

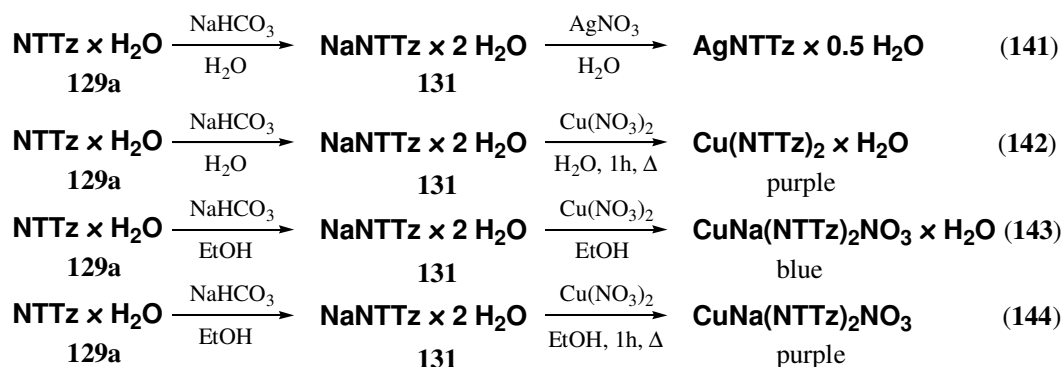


Scheme 9.2 Synthesis of **128**, **129a** and **129b** salts.

The synthesis of the **129b** salts proceeds by mere deprotonation of the tetrazole ring using a stoichiometric amount of either a suitable nitrogen-base (ammonium, guanidinium and aminoguanidinium) or a metal hydroxide/carbonate (Li, Na, K, Rb and Cs) in alcohol or aqueous solution. After slow evaporation of the solvent the salts are obtained in high yield and purity. The most important thing one should be careful with when synthesizing these compounds is not to heat up the reaction mixture. Apparently, the nitro-group in **129b** salts reacts very oxidant and the NMR spectra of the compounds are characterized by many other unidentified peaks apart from those of the pure compound (see NMR discussion). In contrast to hydrazinium 5-nitrotetrazolate,^[4] which can be easily synthesized by direct reaction of **21a** and hydrazine hydrate, reaction of **129a** with hydrazine to form the corresponding hydrazinium salt (**HNTTz**, **136**) results in gas evolution, also when the reaction is carried out at low temperatures (≥ -10 °C). Synthesis of the nitrogen-rich diaminoguanidinium (**DAGNTTz**, **139**) and triaminoguanidinium (**TAGNTTz**, **140**) salts by reaction of silver 5-(5-nitrotetrazole-2-ylmethyl)-tetrazolate (**AgNTTz**, **141**) with a suitable halogenide salts also failed due to the high insolubility of **141**.

The silver salt (**141**) precipitates as a hemihydrate when reacting the sodium salt (**NaNTTz**, **131**, generated *in situ* from **129a** and sodium bicarbonate) and silver nitrate in water (Scheme 9.3). In addition, due to the novelty of the anion and to the interest of copper salts with nitrogen-rich ligands for pyrotechnic applications we decided to prepare copper(II) 5-(5-nitrotetrazole-2-ylmethyl)-tetrazolate monohydrate (**CuNTTzh**, **142**). After 1 h reaction time at reflux the compound precipitates as a dark purple solid (Figure 9.1) with one molecule of water in the crystal structure. It is interesting to note that when the synthesis is carried out in ethanol instead of water, the expected copper(II) complex is not formed but instead an adduct between the expected complex and sodium nitrate (by-product of the reaction) precipitates out of the reaction mixture as a light purple solid. This solid obeys to the formula $\text{CuNa}(\text{NTTz})_2\text{NO}_3$ (**CuNaNTTzN**, **144**). We also noted that the reaction of **131** with copper(II) nitrate (both in water or ethanol), yields a blue solid, which turns purple on heating. We decided to analyze this solid, which obeys to the formula of the monohydrate species of **144** (**CuNaNTTzNh**, **143**). The different color of the anhydrous and

monohydrated complexes **144** and **143** suggests that the crystal water is most probably coordinated to the Cu^{2+} cations and is responsible for the change in color. Furthermore, the copper complexes are potentially very interesting energetic compounds due to their ease of initiation by a laser radiation (e.g., **144** was initiated by a laser powder of ~200 mW, resulting in a loud explosion).



Scheme 9.3 Synthesis of transition metal (Ag, Cu) salts of **129b**.



Figure 9.1 Pictures of a) **142**, b) **143** and c) **144**.

In addition to the energetic materials described above, due to the high value of halogenide salts or halogen substituted materials as educts for the synthesis of compounds of energetic interest,^[5,6] we decided to synthesize 2-(2-bromoethyl)-5-nitrotetrazole (**BENT**, **145**), which has a great potential for the synthesis of highly energetic molecules such as 2-(2-nitratoethyl)-5-nitrotetrazole (**NENT**, **146**), 2-(2-azidoethyl)-5-nitrotetrazole (**AENT**, **147**) or 2-(2-dinitramidoethyl)-5-nitrotetrazole (**DNENT**, **148**).

Lastly, the nitrogen-rich salts are perfectly stable solids at room conditions and are readily soluble in water or hot ethanol (moderately at room temperature). The alkali metal salts form as the hydrated species (even the heavier K, Rb and Cs salts), which is contrast with analogous salts containing the 5-nitrotetrazolate (NT^-) anion (see *Chapter III*).^[3] However, the Li and Na salts are very hygroscopic and slightly hygroscopic, respectively.

9.3 NMR Spectroscopy

All compounds were characterized by ^1H , ^{13}C , ^{14}N and (when suitable) ^{15}N NMR using $\text{DMSO-}d_6$. Alkylation of **21a** to form **128** results in a shift of the NT ring carbon atom to high field from 169.5^[4] to 166.3 ppm. In addition, the two new signals corresponding to the methylene carbon atom ($-\text{CH}_2-$) and the cyano group have resonances at 42.7 and 112.5 ppm, respectively. In the ^1H NMR spectrum the highly electron-withdrawing character of the two substituents (the NT ring on one side and the cyano group on the other) deshield the resonances for the protons on the methylene group to 6.31 ppm. Closing of the ring to form **129a** results in the cyano group resonance to disappear from the ^{13}C NMR spectrum and a tetrazole (Tz) resonance to show at 153.3 ppm. In addition, the resonances of the methylene group and the NT ring carbon atoms are shifted to low field at 167.1 and 49.0 ppm, respectively suggesting the greater electron-withdrawing character of the Tz ring in comparison to the CN group. A similar deshielding effect is also observed in the ^1H NMR spectrum of **129a**. The crystal water exchanges fast enough in the NMR solvent that only an average signal with the Tz ring proton is observed at 8.41 ppm. Deprotonation of the Tz ring to form the NT⁺Tz⁻ anion results in a high field shift of the resonance of the methylene group hydrogen atoms (see Experimental Part). The ^{13}C NMR resonances in the anion vary in ~ 1 ppm from the starting material (129b monohydrate) and are seen at ~ 166 , ~ 154 and ~ 50 ppm. At this point it must be said that the NT ring carbon atom resonances is very low in intensity and rather concentrated samples must be measured in order to see a good signal/noise ratio. This is a similar effect to that observed in salts containing the NT⁻ anion.^[3,4,7]

The only two resonances, which can be observed in the ^{14}N NMR of all compounds are a sharp signal at ~ 35 ppm (NO_2) and a broad band, which appears in the range -90 to -110 ppm, depending on the compound and can be assigned to the nitrogen atom crystallographically labelled as N2. The rest of the nitrogen atoms are either not observed or the resonances are so broad that any attempt of assignment is not feasible. The incredibly high solubility of all compounds in $\text{DMSO-}d_6$, allowed us to record a ^{15}N NMR for **128**, **129a** and for the guanidinium salt (**GNT⁺Tz⁻**, **137**) as a representative example of a salt containing the NT⁺Tz⁻ anion (Figure 9.2). The spectrum of **128** shows the six expected signals, which could be assigned by comparison with **21a**^[4] and 2-methyl-5-aminotetrazole (*Chapter VI*).^[8,9] The signal at the lowest field (+6.9 ppm) can be assigned as N4 (X-ray labels) due to the alkylation induced effect on N3,^[10-12] which shifts the signal for this nitrogen atom to -106.4 ppm and can be differentiated from N2 due to the larger coupling constant to the methylene group protons of the former ($^2J_{\text{NH}} = 2.51$ Hz *vs.* $^3J_{\text{NH}} = 1.76$ Hz). Apart from the nitro group, N5 is the only nitrogen atom, which does not show any coupling, as expected from the four bonds between this nitrogen and the next hydrogen atom. The cyano group nitrogen atom

resonance, is observed at the highest field (-121.9 ppm) with a coupling constant $^2J_{NH} = 1.51$ Hz. The formation of **129a** makes the latter signal disappear and instead two new broad signals of relative low intensity (due to the fast exchange of the ring proton in the NMR solvent) are observed at -21.9 (N7/N8) and -87.1 (N6/N9) ppm.^[4,10a] The rest of the nitrogen atoms have almost identical shifts to the starting material apart from the alkylated one (N3), which feels the effect caused by the change of substituent more strongly and is shifted from -106.4 to -86.9 ppm. Deprotonation of the tetrazole ring to form the NTTz^- anion results, as expected, in only small changes in the resonances for the NT ring nitrogen atoms. Once again, the substituted nitrogen atom (N3) is the only one that feels the electronic changes by the introduction of the negative charge and is now shifted to -92.8 ppm. However, the differences are much more notorious in the Tz moiety and all tetrazole ring nitrogen atoms are strongly deshielded in $\sim +20$ ppm (N7/N8: +4.9 ppm and N6/N9: -64.4 ppm).

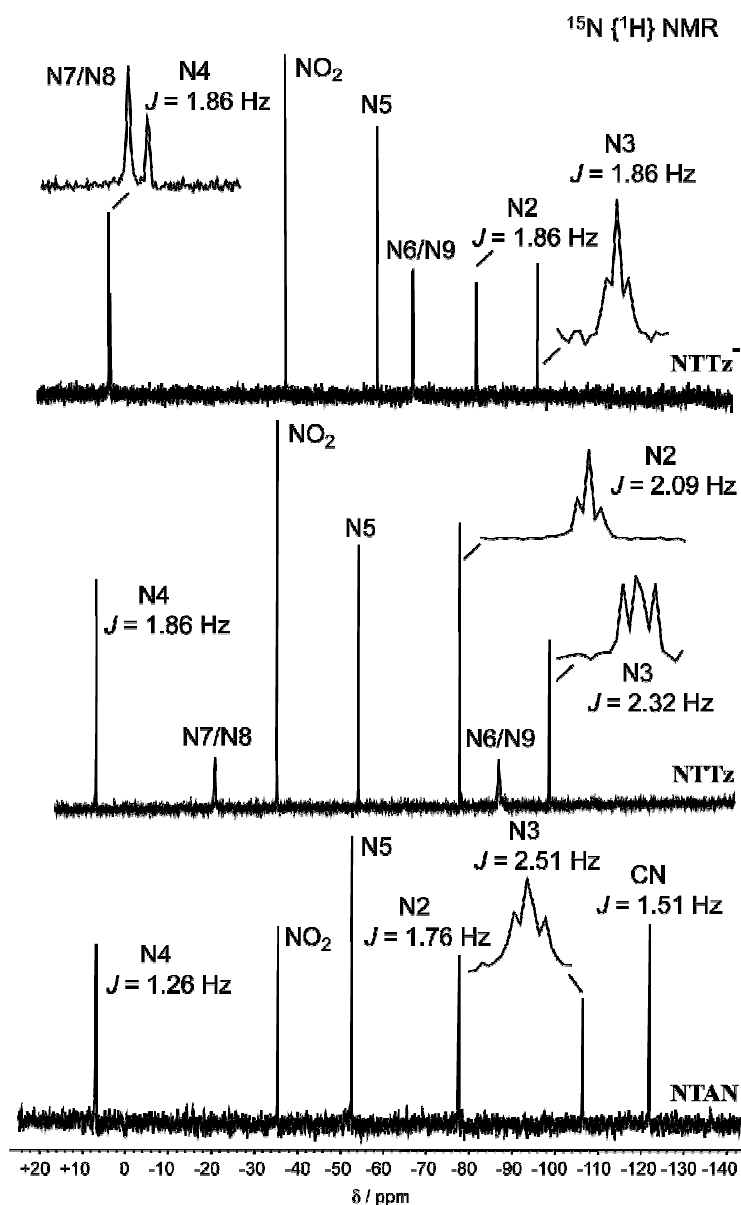


Figure 9.2 ^{15}N NMR spectra of **128**, **129b** and **137** (see X-ray labels).

Lastly, as commented in the synthesis section many signals corresponding to decomposition products appear in the NMR spectra when heating **129a** with an alkali metal hydroxide or carbonate base. They are to be found at the following resonances: ^1H NMR $\delta = 5.87, 4.32, 3.43, 1.33$ and 1.04 ppm; ^{13}C NMR $\delta = 66.7, 55.9, 48.5, 18.4$ and 14.2 ppm and ^{14}N -NMR $\delta = -359$ ppm. We believe that opening of the second tetrazole ring takes place with possible elimination of nitrogen and the formation of an ammonium salt, as proven by the sharp signal in the ^{14}N NMR spectrum. This opening should be base-catalyzed since **129b** itself can be cooked in water or ethanol without appreciable decomposition.

9.4 Vibrational Spectroscopy

Computational Methods. All quantum chemical calculations were carried out using the Gaussian03W software package.^[13] The IR and Raman frequencies of the 5-(5-nitrotetrazole-2-ylmethyl)-tetrazolate (NTTz⁻) anion were calculated using Becke's B3 three parameter hybrid function with an LYP correlation function (B3LYP)^[14] and were scaled by a factor of 0.9613 as described by Radom et al.^[15]

All salts were qualitatively identified by vibrational spectroscopy (IR and Raman). The vibration modes associated with the cations are well-known and will therefore be omitted from the following discussion. Those of the NTTz⁻ anion are reported here for the first time and will thus be discussed in detail. In order to establish a characteristic set of vibrations for the NTTz⁻ anion, we calculated the vibrational (both IR and Raman) frequencies for the NTTz⁻ anion together with the corresponding intensities (IR) and activities (Raman), by means of quantum chemical methods (see *Computational Methods* discussion above). The calculations are supposed to facilitate the assignment of the bands observed in the measured spectra of the compounds as well as to help to identify coupled modes. These coupled modes are of interest because they can be used to derive information about the structure of the NTTz⁻ anion and its interaction with the cations in the solid state. Table 9.1 contains tabulated the scaled, calculated frequencies and the intensity (IR) or activity (Raman) of the bands. The experimentally observed vibrations were averaged and are also tabulated in Table 9.1 with the corresponding standard deviation (in curved brackets), intensities and activities and tentative assignment (by comparison to the computed vibrational energies).

Remarkably, most of the frequencies obtained from the computational results were observed in the vibrational spectra of the compounds with reasonably good agreement between the observed and calculated values. It is also of note that the observed frequencies assigned to the NTTz⁻ anions in the vibrational spectra occur at fairly consistent energies as indicated by the reasonably low

standard deviations. Therefore it is expected the observed geometry of the NTTz^- anion in the **129b** salts to be very similar in all compounds in this study. This prediction is confirmed by the X-ray diffraction measurements (see Table 9.2 for a report on distances and angles in the anion).

Table 9.1 Calculated (corrected) and experimental frequencies with the corresponding intensities (IR) and activities (Raman) and tentative assignment for the NTTz^- anion.

	ν_{calc} (cm^{-1}) ^a	ν_{meas} (cm^{-1}) ^b (IR / Raman)	IR intensity ^c (Calc / Obs)	Raman activity ^d (Calc / Obs)	Mode Assignment ^e
1	62	- / 90(3)	3.2 / -	0.6 / w	$\tau(\text{NO}_2) + \tau(\text{NT-ring})$
2	320	- / 310(5)	1.9 / -	2.3 / w	$\tau(\text{CH}_2)$
3	351	- / 346(5)	0.9 / -	1.4 / w	$\tau(\text{CH}_2)$
4	530	548(6) / 548(8)	2.2 / w	4.2 / m	$\omega(\text{NO}_2)$
5	646	656(2) / n.o.	17.2 / m	2.3 / n.o.	$\nu(\text{NO}_2) + \nu(\text{NT-ring}) + \nu(\text{Tz-ring})$
6	669	684(1) / 686(4)	6.9 / w	4.4 / m	$\nu(\text{NO}_2) + \nu(\text{NT-ring}) + \nu(\text{Tz-ring})$
7	696	705(2) / n.o.	2.0 / w	0.3 / n.o.	$\nu(\text{NT-ring}) + \nu(\text{Tz-ring})$
8	722	n.o. / n.o.	37.0 / n.o.	2.4 / n.o.	$\nu(\text{N6-N7-N8})$
9	727	752(1) / n.o.	30.1 / m	0.6 / n.o.	$\nu(\text{N6-N7-N8})$
10	765	759(1) / 759(6)	1.6 / w	2.5 / m	$\nu(\text{NO}_2) + \nu(\text{NT-ring})$
11	795	785(1) / 774(1)	8.1 / w	0.6 / w	$\omega(\text{CH}_2)$
12	825	846(3) / 844(1)	92.5 / s	1.8 / w	$\delta(\text{NO}_2)$
13	1020	1031(3) / n.o.	3.9 / w	4.3 / n.o.	$\delta(\text{C3-N9-N8})_{\text{Tz-ring}}$
14	1042	1048(8) / 1032(3)	5.6 / w	47.9 / s	$\delta(\text{N6-C3-N9})_{\text{Tz-ring}}$
15	1048	1070(2) / 1070(2)	4.6 / w	14.1 / m	$\delta(\text{N4-N5-C1})_{\text{NT-ring}}$
16	1086	1101(3) / 1099(2)	2.1 / w	41.2 / m	$\nu_{\text{as}}(\text{N-N})_{\text{NT-ring}} + \omega(\text{CH}_2)$
17	1133	1125(9) / 1105(1)	8.6 / w	5.7 / m	$\nu(\text{N6-N7})_{\text{Tz-ring}} + \nu(\text{N8-N9})_{\text{Tz-ring}}$
18	1163	1145(1) / 1145(3)	9.6 / w	3.6 / m	$\nu(\text{N7-N8})_{\text{Tz-ring}} + \nu_{\text{sym}}(\text{CH}_2)$
19	1220	1219(1) / 1195(3)	10.7 / w	49.1 / s	$\omega(\text{CH}_2) + \nu(\text{N4-N5})$
20	1268	n.o. / n.o.	37.3 / n.o.	8.2 / n.o.	$\nu_{\text{as}}(\text{CH}_2)$
21	1279	1278(1) / 1280(1)	28.6 / m	8.5 / m	$\nu(\text{CH}_2)$
22	1313	1297(1) / 1298(1)	3.1 / w	26.9 / w	$\nu(\text{C1-N2}) + \nu(\text{N2-N3})$
23	1316	1325(5) / 1320(3)	106.0 / s	7.0 / m	$\nu(\text{C1-N5}) + \nu_{\text{sym}}(\text{NO}_2)$
24	1374	1342(6) / 1341(7)	39.7 / m	33.9 / m	$\delta(\text{CH}_2)$
25	1400	1419(2) / 1421(2)	24.9 / s	2.1 / w	$\nu(\text{C3-N})_{\text{Tz-ring}}$
26	1415	1437(3) / 1445(2)	1.2 / m	26.7 / s	$\nu(\text{C2-C3})_{\text{Tz-ring}}$
27	1451	1488(2) / 1489(2)	22.7 / s	58.5 / m	$\nu(\text{C-N})_{\text{NT-ring}} + \nu(\text{N-N})_{\text{NT-ring}}$
28	1590	1558(3) / 1560(4)	220.1 / s	7.1 / m	$\nu_{\text{as}}(\text{NO}_2)$
29	2961	n.o. / 2974(5)	20.0 / n.o.	132.0 / m	$\nu_{\text{sym}}(\text{CH}_2)$
30	3026	3022(8) / 3024(5)	2.6 / m	60.9 / m	$\nu_{\text{as}}(\text{CH}_2)$

^aCalculated frequencies scaled by 0.9613. ^bAverage values of measured (IR and Raman) frequencies with standard deviations in curved brackets (n.o. = not observed). ^cCalculated intensities and observed intensities (IR). ^dCalculated and observed activities (Raman). ^eTentative assignment of the vibrational modes (ν = stretching, δ = in-plane bending, γ = out-of-plane bending, ω = in plane rocking, τ = torsion, as = asymmetric and sym = symmetric).

The asymmetric C–H stretching mode for the methylene moiety is observed, in average, as a sharp band of moderate intensity at $\sim 3020 \text{ cm}^{-1}$ (IR and Raman), whereas the symmetric stretch appears as a band of medium intensity at $\sim 2975 \text{ cm}^{-1}$ in the Raman spectra and is IR inactive. The asymmetric nitro group stretching is observed at $\sim 1560 \text{ cm}^{-1}$, which is shifted to higher energies in respect to nitrogen-rich 5-nitrotetrazolate salts^[4] ($\sim 1540 \text{ cm}^{-1}$), similarly to neutral 5-nitro-2H-

tetrazole (**5-NT**, see *Chapter III*). The symmetric N–O stretch combines with a C1–N5 stretching vibration in the NT ring (strong band in the IR, moderate intensity in the Raman at $\sim 1325\text{ cm}^{-1}$). The NT ring C–N and N–N stretching modes have strong intensity in the IR spectra of the compounds, are observed at $\sim 1490\text{ cm}^{-1}$ and are shifted to higher energies in respect to the Tz ring vibrations (two bands at ~ 1440 and 1420 cm^{-1}). Also at higher energy is the deformation of the NT ring ($\delta(\text{N4–N5–C1}) \sim 1070\text{ cm}^{-1}$) in respect to those of the Tz ring ($\delta(\text{N6–C3–N9})$ and $\delta(\text{C3–N9–N8}) \sim 1040$ and 1030 cm^{-1} , respectively). One of the most intense signals corresponds to the deformation of the NO_2 group at $\sim 845\text{ cm}^{-1}$, only slightly shifted in respect to **5-NT** and its salts ($\sim 840\text{ cm}^{-1}$). Lastly, there exists a set of bands of lower intensity, which can be assigned as follows: $750\text{--}650\text{ cm}^{-1}$ (out-of-plane bending of the NT and Tz rings), $\sim 550\text{ cm}^{-1}$ (in-plane rocking of the NO_2 group) and $<350\text{ cm}^{-1}$ (torsion modes of the CH_2 and NO_2 moieties and the NT ring).

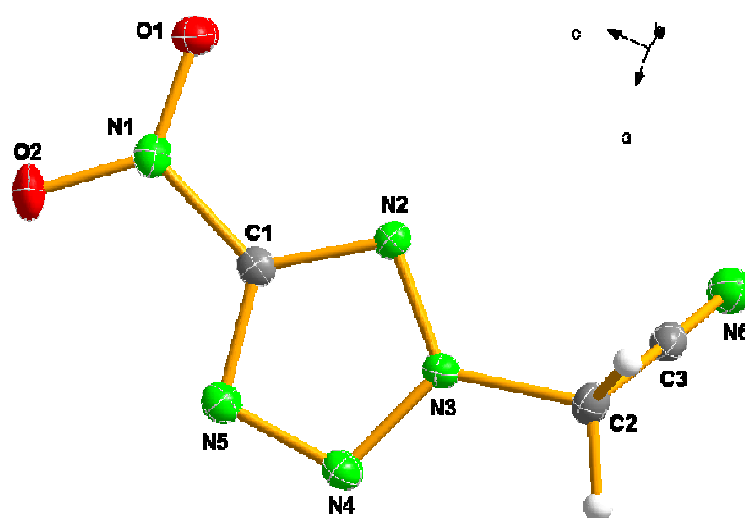
9.5 Molecular Structures

Single crystals of the compounds described here suitable for X-ray diffraction studies were obtained as described in *9.9 Experimental Section*. Intensity data were collected on an Oxford XCalibur 3 CCD diffractometer equipped with a molybdenum X-ray tube and a highly oriented graphite monochromator. The structures were solved by direct methods using SIR97 and refined by means of full-matrix least-squares procedures using SHELXL-97.^[16] All non-hydrogen atoms were refined anisotropically by full-matrix least-squares methods. Details concerning data collection and refinement are summarized in *Appendix C*. All hydrogen atoms were located from difference Fourier maps and were refined isotropically. Selected bond distances and angles in the tetrazole rings of the compounds synthesized in this work are shown in Table 9.2.

Alkylation of **21a** with bromoacetonitrile proceeds selectively at N3 yielding **128** as it is usual for 5-substituted tetrazoles bearing an electron-withdrawing group.^[17] As expected, the acetonitrile moiety is not coplanar to the tetrazole ring as indicated by the dihedral angle $\text{N4–N3–C2–C3} = 124.9(1)^\circ$ (Figure 9.3). One of the two methylene hydrogen atoms points only slightly out of the plane of the ring (*ca.* 4°). The ring distances and angles fit nicely with other tetrazoles with electron-withdrawing substituents^[18,19] and the cyano bond distance ($\text{C3–N6} = 1.139(2)\text{ \AA}$) is in the expected range for a C–N triple bond.^[20]

Table 9.2 Selected bond lengths [Å] and angles [°] for nitrogen-rich 5-nitrotetrazole derivatives.

Parameter	128	129a	NH ₄ N ⁺ TTz (A)	NH ₄ N ⁺ TTz (B)	138 (A)	138 (B)	145
N1–O1	1.225(1)	1.217(3)	1.223(2)	1.217(2)	1.225(3)	1.228(3)	1.216(4)
N1–O2	1.220(1)	1.228(2)	1.222(2)	1.227(2)	1.220(3)	1.221(3)	1.226(4)
N1–C1	1.448(1)	1.444(3)	1.444(2)	1.447(2)	1.455(3)	1.450(3)	1.455(4)
N2–C1	1.319(1)	1.316(3)	1.315(2)	1.311(2)	1.315(3)	1.321(3)	1.317(4)
N2–N3	1.325(1)	1.326(2)	1.320(2)	1.321(2)	1.328(3)	1.322(3)	1.326(4)
N3–N4	1.332(1)	1.331(3)	1.324(2)	1.329(2)	1.330(3)	1.328(3)	1.334(4)
N4–N5	1.317(1)	1.317(3)	1.323(2)	1.317(2)	1.323(3)	1.324(3)	1.321(4)
N5–C1	1.336(1)	1.336(3)	1.330(2)	1.328(2)	1.328(3)	1.329(4)	1.331(4)
N3–C2	1.462(1)	1.458(3)	1.467(2)	1.478(2)	1.486(4)	1.468(4)	1.464(4)
C2–C3	1.471(2)	1.491(3)	1.484(2)	1.486(2)	1.475(4)	1.493(4)	1.513(4)
C3–A ^a	1.138(2)	1.318(3)	1.331(2)	1.328(2)	1.324(3)	1.330(3)	1.940(3)
N6–N7		1.362(3)	1.352(2)	1.339(2)	1.347(3)	1.362(3)	
N8–N7		1.299(2)	1.308(2)	1.313(2)	1.323(3)	1.308(3)	
N9–N8		1.345(3)	1.345(2)	1.342(2)	1.342(3)	1.359(3)	
N9–C3		1.328(3)	1.324(2)	1.325(2)	1.326(3)	1.323(3)	
O1–N1–O2	125.9(1)	125.7(2)	126.0(1)	125.4(1)	125.7(3)	125.2(3)	126.0(3)
O1–N1–C1	116.7(1)	117.7(2)	117.0(1)	118.2(1)	117.3(3)	117.2(3)	117.1(3)
O2–N1–C1	117.4(1)	116.6(2)	116.9(1)	116.3(1)	117.0(3)	117.7(3)	116.9(3)
N2–C1–N1	122.2(1)	122.0(2)	121.0(1)	122.0(1)	122.2(3)	122.1(3)	121.3(3)
C1–N2–N3	99.4(1)	99.7(2)	100.1(1)	99.7(1)	99.7(2)	99.7(2)	99.7(3)
N2–N3–N4	114.7(1)	114.3(2)	114.1(1)	114.1(1)	114.2(2)	114.5(2)	114.1(3)
N5–N4–N3	105.8(1)	106.0(2)	106.1(1)	106.1(1)	105.9(2)	105.9(2)	106.2(3)
N4–N5–C1	104.6(1)	104.6(2)	104.3(1)	104.2(1)	104.5(2)	104.5(2)	104.2(3)
N5–C1–N1	122.4(1)	122.6(2)	123.7(1)	122.2(1)	122.1(3)	122.5(3)	123.4(3)
N2–N3–C2	123.1(1)	123.5(2)	123.1(1)	122.4(1)	121.8(2)	123.4(3)	122.4(3)
N4–N3–C2	122.2(1)	121.8(2)	122.5(1)	123.5(1)	123.7(2)	122.1(3)	122.8(3)
N3–C2–C3	110.0(1)	112.3(2)	112.2(1)	110.3(1)	111.9(3)	109.7(2)	111.7(3)
N2–C1–N5	115.4(1)	115.3(2)	115.2(1)	115.8(1)	115.7(2)	115.4(2)	115.8(3)
A–C3–C2 ^a	177.8(1)	126.2(2)	124.3(1)	122.8(1)	123.8(3)	124.0(3)	111.6(2)
C3–N6–N7		106.0(2)	104.4(1)	104.6(1)	104.5(2)	104.6(2)	
N6–N7–N8		109.9(2)	109.4(1)	109.1(1)	109.3(2)	109.3(2)	
N7–N8–N9		106.8(2)	109.2(1)	109.7(1)	108.9(2)	109.0(2)	
C3–N9–N8		108.5(2)	105.0(1)	104.1(1)	105.0(2)	105.1(2)	
N6–C3–N9		108.8(2)	111.9(1)	112.4(1)	112.4(2)	111.9(2)	
N9–C3–C2		124.9(2)	123.7(1)	124.7(1)	123.7(3)	124.1(2)	

^aA = N6 except for **145** where A = Br.**Figure 9.3** Asymmetric unit of **128** with the labeling scheme.

The lack of hydrogen atoms attached to an electronegative atom does not allow the formation of classical hydrogen bonds. However the $-\text{CH}_2-$ fragment participates in the formation of a non-classical hydrogen bridge with the cyano group nitrogen atom of another molecule with $\text{C2}\cdots\text{N6}^i = 3.314(2) \text{ \AA}$ (symmetry code: (i) $0.5+x, -0.5-y, -z$) only slightly below the sum of the van der Waals radii ($r_{\text{C}} + r_{\text{N}} = 3.32 \text{ \AA}$).^[21] This non-classical hydrogen bond (Table 9.2) link **128** molecules into dimer pairs and is responsible for the formation of the wavy layers represented in Figure 9.4, which account for the relatively efficient packing. The high density of the material (1.747 g cm^{-3}), regardless of the lack of extensive hydrogen-bonding puts into perspective that there are many other factors than influence the density (and thus the energetic properties) of a compound, in this case the nitro-group increases the value of the density as seen in other nitro-compounds.^[22,23] For comparison, the density of 2-methyl-5-amino-tetrazole, which should form some hydrogen bonds with the amino group is only 1.360 g cm^{-3} (*Chapter VI*).^[8]

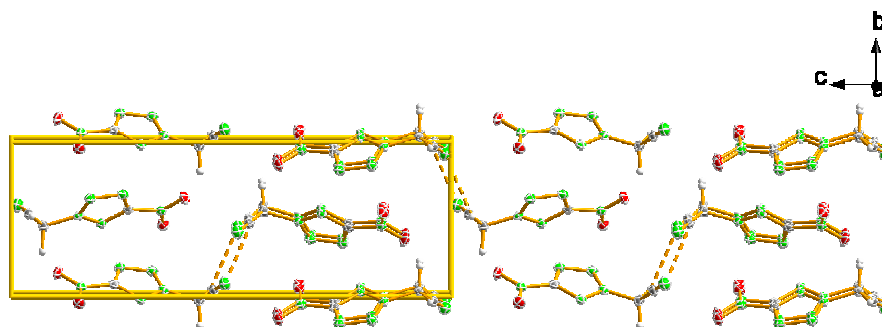


Figure 9.4 View of the double cell C $[-1 \dots +1]$ along the a -axis showing the formation of dimer pairs in the crystal structure of **128**.

In analogy to **128**, alkylation of **21a** with 1,2-dibromoethane also proceeds selectively at N3 yielding **145**. Figure 9.5 shows a view of the asymmetric unit of the compound where the bromomethyl fragment ($\text{C3H}_2\text{Br}$) points to the opposite direction than the cyano group in **128** with a similar dihedral angle ($\text{N4-N3-C2-C3} = -139.7(3)^\circ$ *vs.* $124.9(1)^\circ$ in **128**). Both compounds crystallize in the same crystal system (Orthorhombic, $P2_12_12_1$) but **145** has a much larger unit cell volume due to the larger volume of the bromomethyl in comparison to the cyano group. The C2–C3 distance is with $1.513(4) \text{ \AA}$, longer than the same distance in the rest of the compounds in this study in 0.02 to 0.04 whereas the largest bond distance is observed for the bond between C3 and the large bromine atoms at $1.940(3) \text{ \AA}$, as expected.^[20]

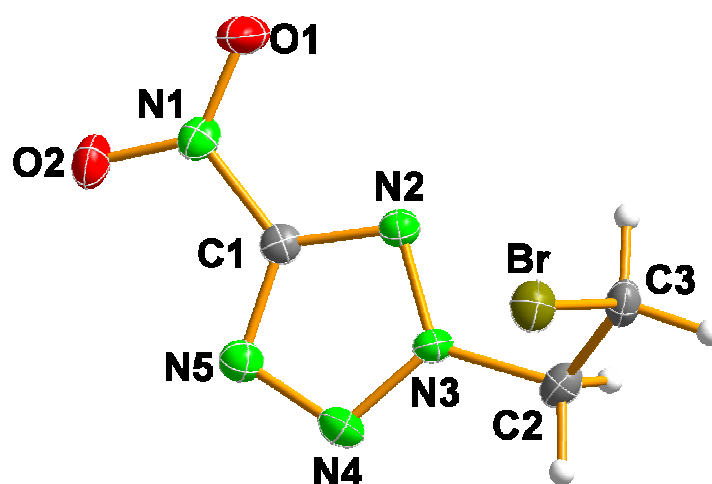


Figure 9.5 Asymmetric unit of **145** with the labeling scheme.

The only interaction between molecules in the structure apart from covalent forces are non-classical hydrogen bonds with low directionality between one of the methylene group hydrogen atoms and an oxygen atom of a nitro group with $C2 \cdots O1^i = 3.104(4) \text{ \AA}$ (symmetry code: (i) $0.5-x, -y, 0.5+z$). This hydrogen bridges link the **145** molecules into infinite chains along the c -axis as represented in Figure 9.6.

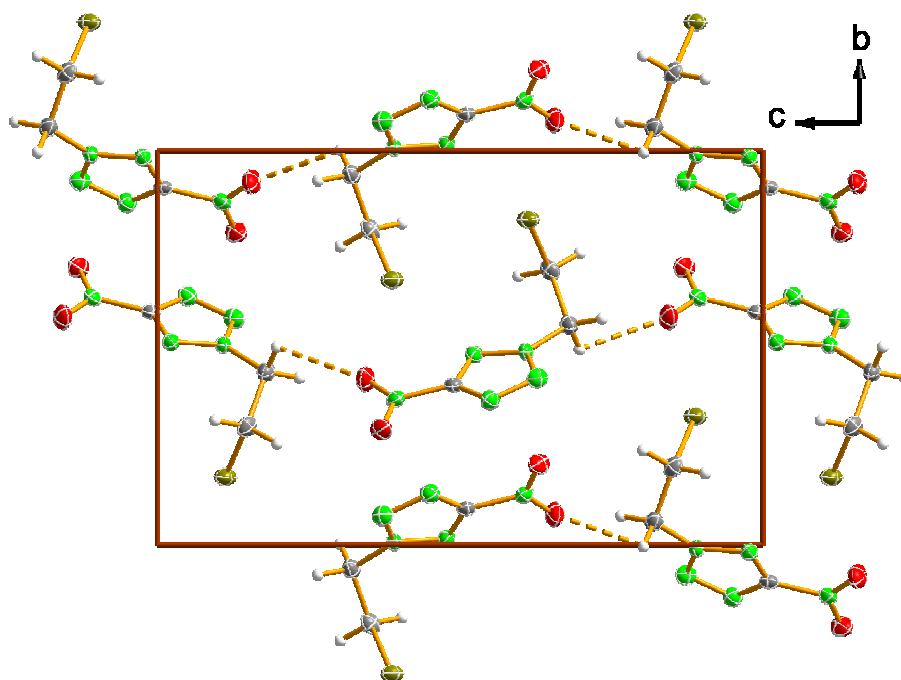


Figure 9.6 View of the unit cell of **145** along the a -axis.

Reaction of **128** with “hydrazoic acid” yields 5-(5-nitrotetrazolo-2-ylmethyl)tetrazole (**129b**), which after recrystallization from water forms as the monohydrated species (**129a**), in contrast to the literature where the compound is described to form as the anhydrous material.^[2] Closing to form the

second tetrazole ring results in a slight increase in the density of the compound to 1.796 g cm^{-3} , well above the density of nitrogen-bridged bistetrazoles (*Chapters VII and VIII*),^[12b,24,25] with the only exception of 5,5'-hydrazinebistetrazole, which has a similar value.^[25,26] The dihedral angle N4–N3–C2–C3 is with $111.9(2)^\circ$ smaller than that of the cyano compound. As represented in Figure 9.7, the tetrazole ring is protonated at N9 as it is common for 5-substituted tetrazoles with electron donating substituents.^[27,28] The distances and angles in the structure (apart from C3...N6) are in agreement with **128** and keeping in with other neutral compounds containing a 5-nitrotetrazole ring^[29] or a tetrazole ring.^[10a,12b,27]

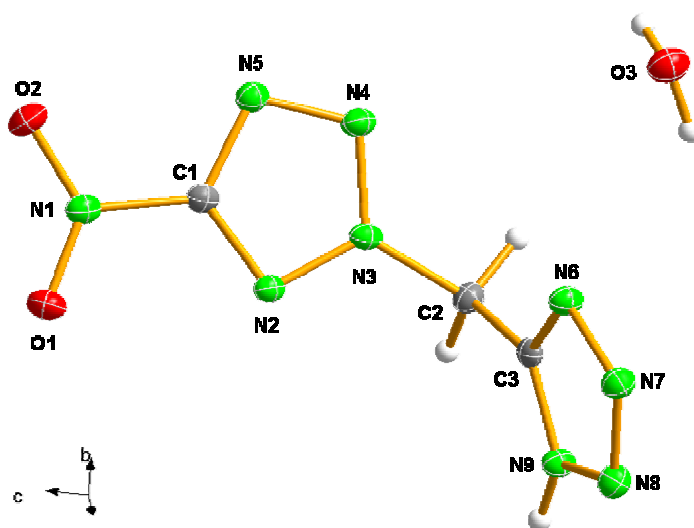


Figure 9.7 Asymmetric unit of **129a** with the labeling scheme.

Regardless of the non-planarity of the two tetrazole rings the high density value of the compound indicates a relatively efficient packing, partly due to the effect of the nitro group, as mentioned above. Figure 9.8 shows the hydrogen bonding in the crystal structure of the compound. There exists three classical and one non-classical hydrogen bonds (see Table 9.2). Using graph-set notation,^[30,31] the primary level (N_7) hydrogen bonding network is described by one dimeric and two chain motifs. The former is of the type **D1,1(2)** and is described by the hydrogen bonds between water molecules and tetrazole rings ($\text{O3}\cdots\text{N8}^i = 3.008(3) \text{ \AA}$; symmetry code: (i) $-1+x, 1+y, z$), whereas the latter take the labels **C1,1(2)** and **C1,1(4)** and are formed by the hydrogen bond between water molecules ($\text{O3}\cdots\text{O3}^{ii} = 2.796(2) \text{ \AA}$; symmetry code: (ii) $-x, -0.5+y, -z$) and between tetrazole rings ($\text{N9}\cdots\text{N6}^{iii} = 2.771(3) \text{ \AA}$; symmetry code: (iii) $x, -1+y, z$), respectively. Both chain networks extend forming infinite chains along the *b*-axis. At the secondary level, finite patterns of the type **D3,3(X)** ($X = 7, 8$) are found. The former are described by the two different hydrogen bonds formed by the water molecules, which connect tetrazole rings with other water molecules, whereas the larger patterns extend from H5 (on O3) to a symmetry equivalent hydrogen atom over two

tetrazole rings describing part of the ring patterns represented in Figure 9.8. Lastly, the non-classical hydrogen bond is formed by one of the methylene hydrogen atoms and a water molecule with $C2\cdots O3^{iii} = 3.118(3)$ Å.

Table 9.3 Hydrogen-bonding geometry in nitrogen-rich 5-nitrotetrazole derivatives.

D–H \cdots A	D–H (Å)	H \cdots A (Å)	D \cdots A (Å)	D–H \cdots A (°)
128				
C2–H1 \cdots N6 ⁱ	0.98(1)	2.73(1)	3.314(2)	118(1)
129a				
O3–H5 \cdots N8 ⁱ	0.85(3)	2.26(3)	3.008(3)	147(3)
O3–H4 \cdots O3 ⁱⁱ	0.88(4)	1.93(4)	2.796(3)	170(3)
N9–H3 \cdots N6 ⁱⁱⁱ	0.89(3)	1.92(3)	2.771(3)	159(2)
C2–H3 \cdots O3 ⁱⁱⁱ	0.94(2)	2.69(2)	3.118(3)	109(2)
135				
N21–H5 \cdots N17	0.95(2)	1.97(2)	2.911(2)	170(2)
N21–H5 \cdots N16	0.95(2)	2.52(2)	3.302(2)	139(1)
O5–H15 \cdots N7	0.91(2)	1.99(2)	2.882(2)	168(2)
N19–H12 \cdots O5	0.95(3)	1.91(3)	2.847(2)	167(2)
O6–H9 \cdots N15	0.91(2)	1.85(2)	2.7551(2)	173(2)
N21–H8 \cdots N18 ⁱ	0.96(2)	2.14(2)	2.987(2)	146(2)
N21–H8 \cdots O6 ⁱⁱ	0.96(2)	2.60(2)	3.151(2)	117(1)
N21–H6 \cdots N16 ⁱⁱ	0.91(2)	2.15(2)	3.016(2)	160(2)
N21–H7 \cdots O6 ⁱⁱⁱ	0.99(2)	1.84(2)	2.807(2)	167(2)
N19–H14 \cdots N2 ⁱⁱⁱ	0.87(2)	2.18(2)	3.020(2)	163(2)
N19–H14 \cdots O1 ⁱⁱⁱ	0.87(2)	2.62(2)	3.130(2)	119(2)
N19–H11 \cdots O5 ^{iv}	1.03(3)	1.86(3)	2.877(2)	167(2)
N19–H13 \cdots O4 ^v	0.89(3)	2.14(3)	2.946(2)	150(2)
O5–H16 \cdots N6 ^{vi}	0.90(2)	1.99(2)	2.884(2)	174(2)
O6–H10 \cdots N9 ^{vii}	0.88(2)	1.96(2)	2.831(2)	167(2)
138				
N22–H10 \cdots N9	0.93(3)	2.12(3)	3.023(4)	166(2)
N19–H5 \cdots N7 ⁱ	0.86(3)	2.24(3)	3.053(4)	158(3)
N21–H9 \cdots N7 ⁱ	0.84(2)	2.39(2)	3.166(4)	152(2)
N21–H9 \cdots O4 ⁱⁱ	0.84(2)	2.48(2)	3.030(3)	123(2)
N22–H11 \cdots N6 ⁱⁱ	0.88(3)	2.25(3)	3.046(4)	151(3)
N19–H6 \cdots N16 ⁱⁱⁱ	0.90(3)	2.07(3)	2.962(4)	171(2)
N20–H7 \cdots N15 ⁱⁱⁱ	0.88(3)	2.17(4)	3.007(4)	160(3)
N24–H15 \cdots N18 ^{iv}	0.91(4)	1.99(4)	2.882(4)	164(3)
N25–H16 \cdots N17 ^{iv}	0.88(3)	2.20(3)	3.051(4)	163(2)
N23–H13 \cdots N8 ^v	0.85(3)	2.29(3)	3.039(4)	147(2)
N24–H14 \cdots N8 ^v	0.87(3)	2.37(3)	3.046(4)	135(3)
N23–H12 \cdots N7 ^{vii}	0.87(4)	2.63(4)	3.099(4)	115(3)
N20–H8 \cdots N2 ^{viii}	0.84(3)	2.47(3)	3.238(4)	152(3)

Symmetry codes for **128**: (i) 0.5+x, -0.5-y, -z; (ii) -x, -0.5+y, -z; (iii) x, -1+y, z. **135**: (i) 1-x, 2-y, -z; (ii) -x, 2-y, -z; (iii) x, 1+y, z; (iv) 1-x, 2-y, 1-z; (v) x, 1+y, 1+z; (vi) 2-x, 1-y, 1-z; (vii) 1-x, 1-y, -z; **138**: (i) -0.5+x, 0.5-y, -0.5+z; (ii) 0.5+x, 0.5-y, -0.5+z; (iii) -x, 1-y, 3-z; (iv) -1+x, y, z; (v) -1.5+x, 0.5-y, 0.5+z; (vii) -0.5+x, 0.5-y, 0.5+z; (viii) 1+x, y, z.

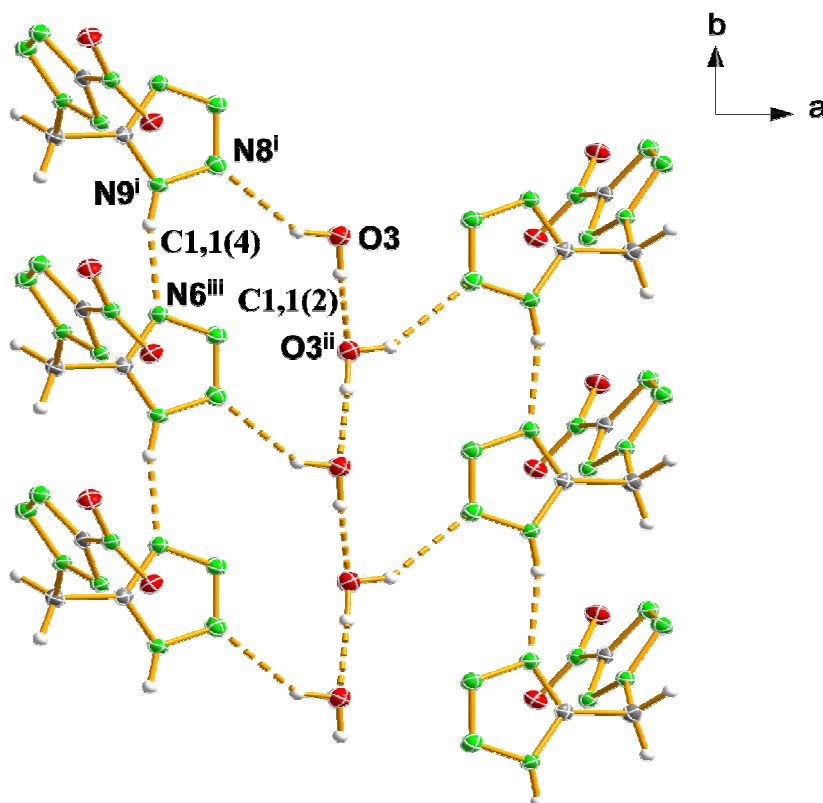


Figure 9.8 Hydrogen bonding in the crystal structure of **129a** (view along the *c*-axis). Symmetry codes: (i) -1+x, 1+y, z; (ii) -x, -0.5+y, -z; (iii) x, -1+y, z; (iii) -1+x, y, z.

135 forms, similarly to **21a** as a (mono)hydrate (Figure 9.9) and similarly to the rest of the salts in this study containing the NT⁺Tz⁻ anion (see discussion below) the asymmetric unit is formed by two formula units with very dissimilar angles between NT and Tz rings (N4–N3–C2–C3 = 139.4(1)° and N13–N12–C5–C6 = 6.4(1)°). There exists π -stacking between the Tz rings of one of the two crystallographically independent molecules along a direction nearly parallel to the *a*-axis. In addition, two consecutive anions belonging to the same stack are connected by strong unclassical hydrogen bonds (C2...O1^{viii} = 3.164(2) Å; symmetry code: (viii) 1+x, y, z) formed by the methylene group protons and one of the nitro group oxygen atoms of a NT ring.

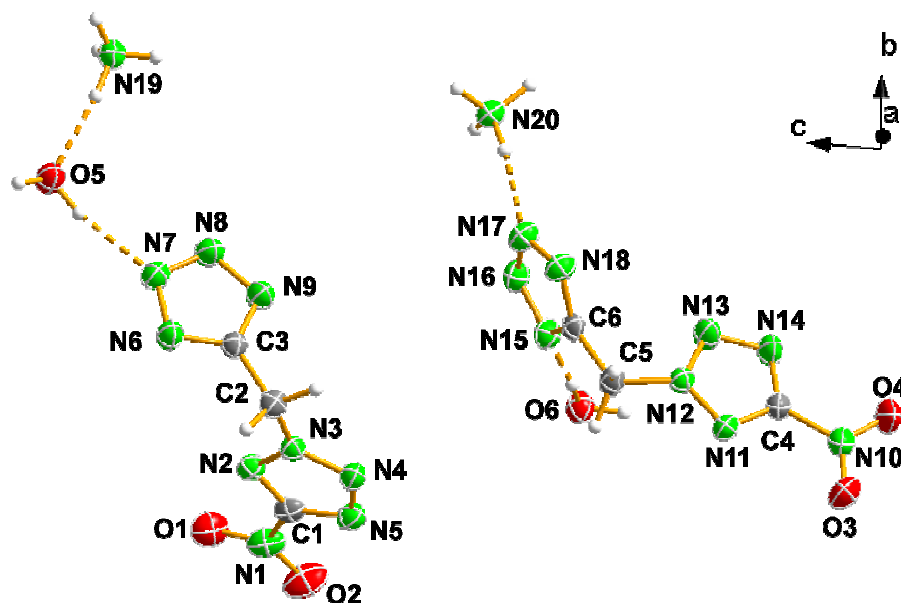


Figure 9.9 Asymmetric unit of **135** with the labeling scheme.

Whereas all nitrogen atoms in the Tz ring are hydrogen bond acceptors, N2 is the only nitrogen atom in the NT ring involved in the formation of hydrogen bonds ($\text{N19} \cdots \text{N2}^{\text{iii}} = 3.020(2) \text{ \AA}$; symmetry code: (iii) $x, 1+y, z$). Up to fourteen strong-to-medium hydrogen bonds are formed, most of which have distances between donor and acceptor atoms in the range 2.8-2.9 \AA (Table 9.2). The combination of the fourteen **D1,1(2)** dimeric interactions mentioned above yield many **D2,2(X)** ($X = 4, 5, 7, 8, 10, 11$) finite chains, one **C2,2(6)** chain pattern and several ring graph-sets with the labels **R2,1(3)**, **R2,4(8)** and **R4,4(X)** ($X = 10, 12$). Some of these networks are represented in Figure 9.10. The ammonium cations form one long ($\text{N21} \cdots \text{N16} = 3.302(2) \text{ \AA}$) and one short ($\text{N21} \cdots \text{N17} = 2.911(2) \text{ \AA}$) hydrogen bonds by using the same proton, which describe the above-mentioned **R2,1(3)** pattern. The combination of this long hydrogen bond between N21 and N16 and N21 and the same atom of another molecule ($\text{N21} \cdots \text{N16}^{\text{ii}} = 3.016(2) \text{ \AA}$; symmetry code: (ii) $x, 2-y, -z$) yields a larger ring pattern with the descriptor **R2,4(8)**. However, the combination of the short hydrogen bond mentioned above between N21 and N17 with the latter between N21 and N16^{ii} yields an **R4,4(10)** graph-set, similar to the one formed in **21a**.^[4]

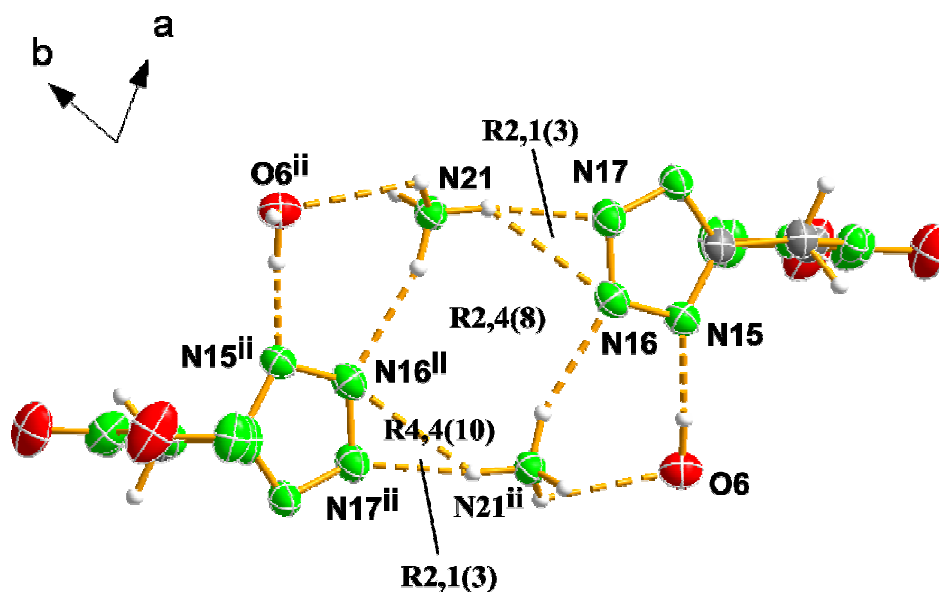


Figure 9.10 Ring graph-sets in the crystal structure of **135**. Symmetry code: (ii) $-x, 2-y, -z$.

138 contains, in analogy to **135** and the metal salts containing the same anion (see below), two crystallographically independent formula units as represented in Figure 9.11. While the distances and angles for the NT ring are similar to **128** or **129a**, formation of the $\text{N}^+\text{T}^-\text{Tz}^-$ anion results in shortening of the N6–N7 distance and lengthening of N7–N8 in the other tetrazole ring, in agreement with an increase of the aromaticity in comparison with the free acid favored by the delocalization of the negative charge. The dihedral angles between both tetrazole rings (N4–N3–C2–C3 and N13–N12–C5–C6) have very different values in the two molecules, which form the asymmetric unit (100° *vs.* 165°), which can be explained by their different environments.

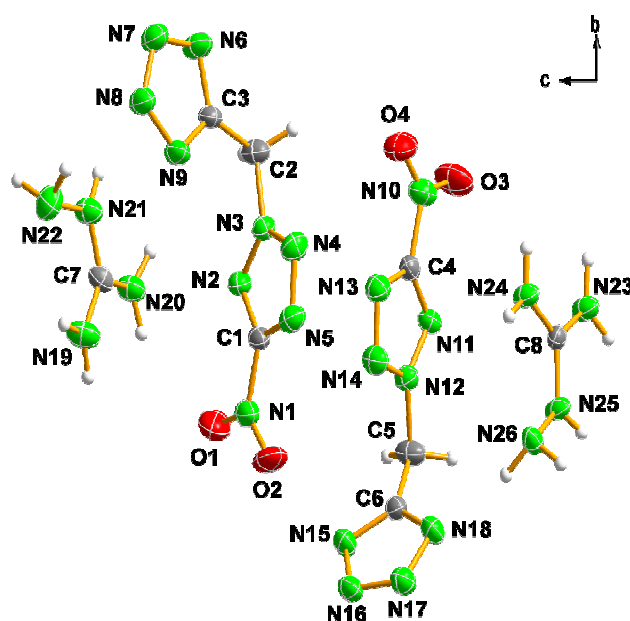


Figure 9.11 Asymmetric unit of **138** with the labeling scheme.

Figure 9.12 shows the hydrogen-bonding around the anion of one of the two crystallographically independent molecules. All nitrogen atoms in the Tz ring of the molecule are involved in the formation of strong hydrogen bonds, however, only N2 of the NT moiety is hydrogen-bonded to a cation and N4 and N5 interact only covalently to N13^{viii} and N14^{viii} (symmetry code: (viii) $1+x, y, z$) of a second anion, placed at *ca.* 3.1–3.2 Å. The aminoguanidinium cation forms the usual intermolecular hydrogen bond ($N20 \cdots N22 = 2.706(4)$ Å) observed for other salts with the same cation^[4,22] with the label **S(5)** (primary level). The rest of the hydrogen bonds describe common **D1,1(2)** finite patterns, which combine at the secondary level generating **D2,1(3)** and **D2,2(X)** ($X = 4-8, 10, 11, 13$) dimeric interactions, **C2,2(X)** ($X = 6-9, 11, 13, 14$) chain and **R1,2(6)** and **R2,2(7)** ring graph-sets. For example, the **R1,2(6)** networks are described by interaction of two amino groups in the cation with the same nitrogen atom in the anion ($N19 \cdots N7^i = 3.053(4)$ Å and $N21 \cdots N7^i = 3.166(4)$ Å; symmetry code: (i) $-0.5+x, 0.5-y, -0.5+z$), whereas the side-on interaction via hydrogen-bonding of another anion with two amino groups of a second cation ($N19 \cdots N16^{iii} = 2.962(4)$ Å and $N20 \cdots N15^{iii} = 3.007(4)$ Å; symmetry code: (iii) $-x, 1-y, 3-z$) is responsible for the formation of an **R2,2(7)** network. In addition, there exist many other hydrogen bonds (see Table 9.2), such as the one formed by one of the nitro-group oxygen atoms ($N21 \cdots O4^{ii} = 3.030(3)$ Å; symmetry code: (ii) $0.5+x, 0.5-y$). Lastly, the bridging $-CH_2-$ moieties are involved in the formation of weak unclassical hydrogen bonds (e.g., $C2 \cdots N22^{iv} = 3.407(5)$ Å; symmetry code: (iv) $-1+x, y, z$), which have been omitted from Figure 9.12 for the sake of simplicity.

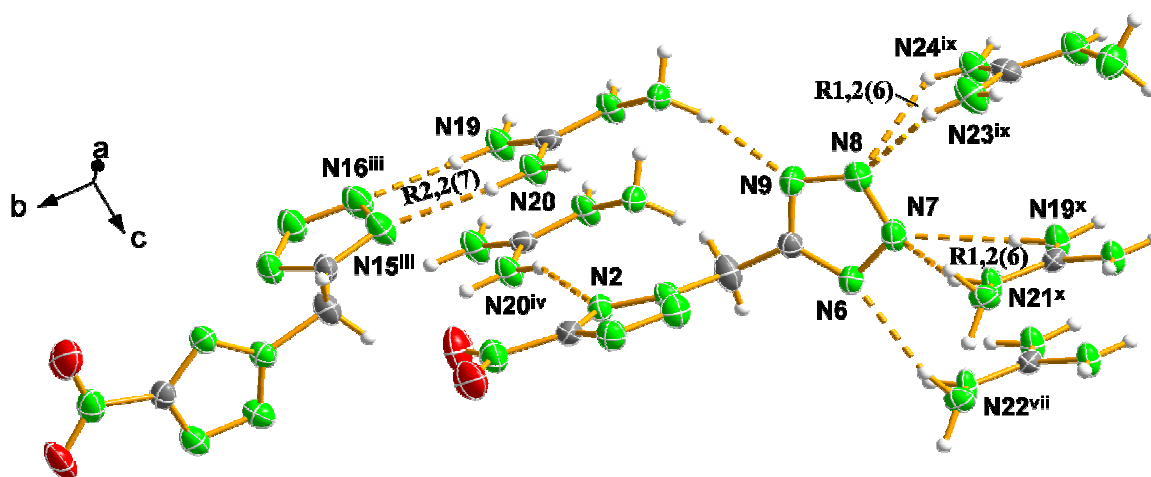


Figure 9.12 Hydrogen-bonding around the anion in the crystal structure of **138** showing the formation of some characteristic ring-patterns. Symmetry codes: (iii) $-x, 1-y, 3-z$; (iv) $-1+x, y, z$; (vii) $-0.5+x, 0.5-y, 0.5+z$; (ix) $1.5+x, 0.5-y, -0.5+z$; (x) $0.5+x, 0.5-y, 0.5+z$.

Table 9.4 Selected bond lengths [Å] and angles [°] for **132** and **133**.

Parameter	132 (A)	132 (B)	133 (A)	133 (B)
N1–O1	1.224(1)	1.218(1)	1.221(3)	1.226(3)
N1–O2	1.221(1)	1.221(1)	1.221(3)	1.220(2)
N1–C1	1.447(1)	1.450(1)	1.444(3)	1.440(3)
N2–C1	1.319(1)	1.319(1)	1.308(3)	1.319(3)
N2–N3	1.320(1)	1.317(1)	1.322(2)	1.321(2)
N3–N4	1.326(1)	1.327(1)	1.321(2)	1.325(2)
N4–N5	1.320(1)	1.320(1)	1.326(3)	1.324(3)
N5–C1	1.334(1)	1.329(1)	1.331(3)	1.325(3)
N3–C2	1.473(1)	1.476(1)	1.475(3)	1.468(3)
C2–C3	1.490(1)	1.484(1)	1.485(3)	1.498(3)
C3–N6	1.328(1)	1.326(1)	1.322(3)	1.322(3)
N6–N7	1.353(1)	1.345(1)	1.347(3)	1.356(3)
N8–N7	1.304(1)	1.311(1)	1.317(3)	1.326(3)
N9–N8	1.348(1)	1.346(1)	1.345(3)	1.349(3)
N9–C3	1.326(1)	1.330(1)	1.319(3)	1.307(3)
O1–N1–O2	125.7(1)	125.9(1)	125.9(2)	125.6(2)
O1–N1–C1	117.2(1)	118.0(1)	117.4(2)	117.3(2)
O2–N1–C1	117.0(1)	115.9(1)	116.6(2)	117.1(2)
N2–C1–N1	121.2(1)	122.2(1)	123.2(2)	121.6(2)
C1–N2–N3	99.7(1)	99.7(1)	100.0(2)	99.9(2)
N2–N3–N4	114.3(1)	114.3(1)	114.3(2)	114.4(2)
N5–N4–N3	106.4(1)	106.1(1)	105.9(2)	105.8(2)
N4–N5–C1	104.1(1)	104.2(1)	104.3(2)	104.7(2)
N5–C1–N1	123.1(1)	122.2(1)	121.4(2)	123.2(2)
N2–N3–C2	122.8(1)	121.9(1)	122.3(2)	122.8(2)
N4–N3–C2	122.7(1)	123.6(1)	123.3(2)	122.6(2)
N3–C2–C3	111.1(1)	110.8(1)	110.8(2)	111.5(2)
N2–C1–N5	115.5(1)	115.4(1)	115.4(2)	115.1(2)
N6–C3–C2	124.5(1)	123.4(1)	123.2(2)	123.8(2)
C3–N6–N7	104.3(1)	104.2(1)	104.0(2)	104.1(2)
N6–N7–N8	109.5(1)	109.7(1)	109.2(2)	109.3(2)
N7–N8–N9	109.2(1)	109.0(1)	109.3(2)	109.4(2)
C3–N9–N8	104.7(1)	104.7(1)	104.2(2)	104.3(2)
N6–C3–N9	112.1(1)	112.1(1)	113.2(2)	112.7(2)
N9–C3–C2	123.3(1)	124.3(1)	123.6(2)	123.5(2)

132 crystallizes, in analogy to the rubidium salt (see below) but in contrast to alkali salts of 5-nitrotetrazole,^[3] with one molecule of crystal water in the structure in the same space group (*P*-1) and very similar cell parameters (the largest difference is observed in the length of the *c*-axis due to the smaller size of K⁺ in comparison to Rb⁺). The asymmetric unit is also formed by two formula units but in this case all the atoms in one of the formula units are crystallographically independent, whereas for the other unit the NT and Tz moieties have different symmetries. Figure 9.13 shows the coordination around one type of K⁺ cations (K1) with the labeling scheme. The coordination around K1 is six and is completed by interaction to two water molecules and three anions one of which acts as a chelate ligand (N2...K1 = 2.868(1) Å and O1...K1 = 3.002(1) Å) as it is usual for the NT moiety.^[3,4] The distances around K1 vary in the range 2.75–3.00 Å, whereas K2 forms up to

eight interactions, six of which are in the same range as observed for K1 and two longer contacts at ~ 3.15 Å. Table 9.5 presents a complete summary of the bond distances for the coordination around the two K^+ cations whereas the corresponding angles are summarized in *Appendix B* (Table 9.B3).

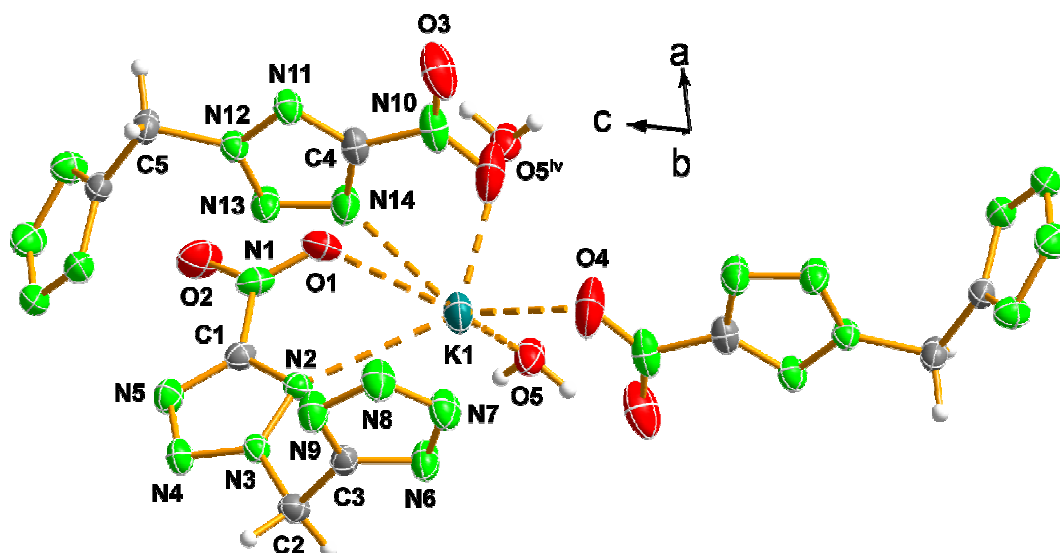


Figure 9.13 Coordination around one of the K^+ cations in the crystal structure of **132** with labeling scheme. Symmetry code: (iv) 3-x, 2-y, -1-z.

Table 9.5 Selected bond distances for the coordination around the K^+ cations in **132**.

K1–O5	2.783(1)	K1–O1	3.002(1)	K2–N16 ⁱⁱ	2.999(1)
K1–O4	2.799(1)	K2–O6	2.744(1)	K2–N4	3.089(1)
K1–O5 ^{iv}	2.819(1)	K2–N17	2.765(1)	K2–N16	3.130(1)
K1–N2	2.868(1)	K2–O6 ⁱ	2.874(1)	K2–N5 ⁱⁱ	3.172(1)
K1–N14	2.965(1)	K2–N18	2.897(1)		

Symmetry codes for **132**: (i) 2-x, 1-y, -z; (ii) 2-x, 2-y, -z; (iii) 1-x, 2-y, -z; (iv) 3-x, 2-y, -1-z; (v) 3-x, 1-y, -1-z.

The packing in the structure is rather complex due to the non-planarity of the anions (dihedral angle $N4-N3-C2-C3 = -137.9(1)^\circ$ and $N13-N12-C5-C6 = -6.5(1)^\circ$) and is characterized by “rhombi” formed between cations and water molecules: the cations with the label K1 are connected to each other over water molecules in a direction approximately parallel to the *a*-axis forming the subunits represented in Figure 9.14. These subunits are bridged with each other over the “rhombi” that K2 forms in turn with other water molecules. Apart from the non-classical $C\cdots N$ and $C\cdots O$ hydrogen bonds with average distances of ~ 3.2 Å, there exist four other type of hydrogen bonds (see Table 9.6) formed by the two water molecules and the Tz moiety, two long ones with O5 as the donor atom (~ 3.0 Å) and two shorter bridges formed by O6 (~ 2.8 Å). All these hydrogen bonds form **D1,1(2)** finite patterns (Table 9.B1), which combine at the secondary level yielding many **D2,2(5)** graph-sets and a **R4,4(10)** ring network. The latter is formed by two Tz moieties hydrogen-

bonded over water molecules ($\text{O5} \cdots \text{N6}^{\text{iii}} = 3.010(1) \text{ \AA}$ and $\text{O5} \cdots \text{N7}^{\text{iv}} = 2.949(1) \text{ \AA}$; symmetry codes: (iii) $2-x, 2-y, -1-z$; (iv) $-1+x, 2+y, 1+z$).

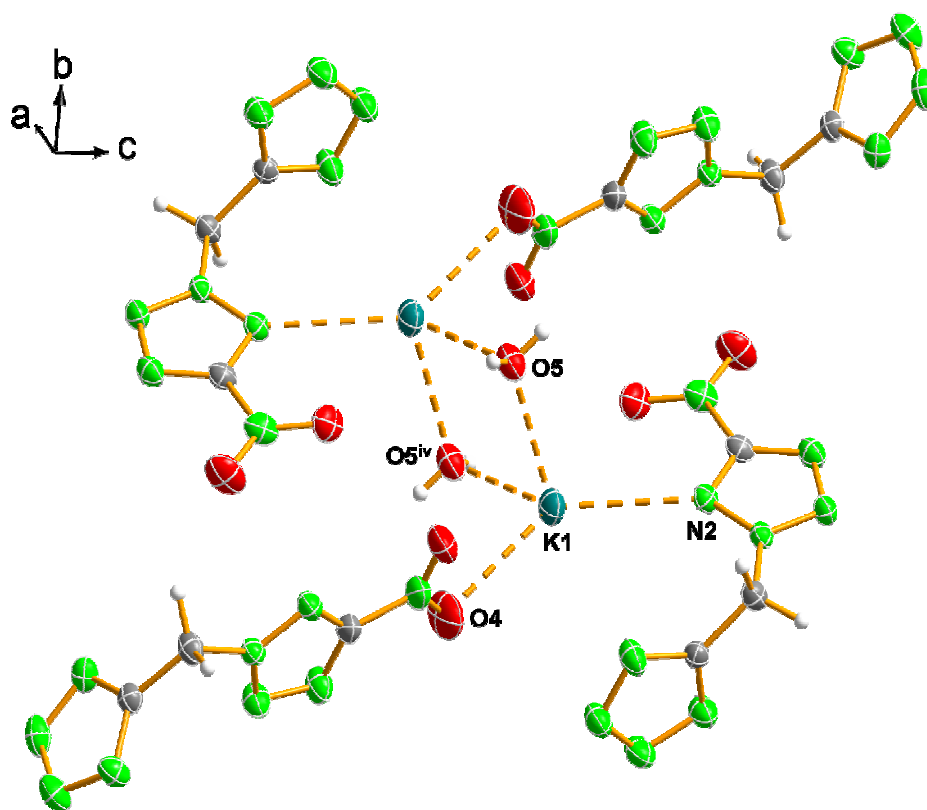


Figure 9.14 Packing in the crystal structure of **132**. Symmetry code: (iv) $3-x, 2-y, -1-z$.

Table 9.6 Hydrogen-bonding geometry in **132** and **133**.

D–H \cdots A	D–H (\AA)	H \cdots A (\AA)	D \cdots A (\AA)	D–H \cdots A ($^\circ$)
132				
O6–H6 \cdots N6 ⁱ	0.83(2)	1.93(2)	2.743(1)	166(2)
O6–H5 \cdots N9 ⁱⁱ	0.85(2)	2.04(2)	2.878(1)	168(2)
O5–H7 \cdots N6 ⁱⁱⁱ	0.80(2)	2.22(2)	3.010(1)	172(2)
O5–H8 \cdots N7 ^{iv}	0.77(2)	2.19(2)	2.949(1)	169(2)
C2–H1 \cdots O1 ^v	0.99(1)	2.40(1)	3.205(1)	138(1)
C5–H5 \cdots N16 ^{vi}	0.96(2)	2.73(2)	3.221(1)	112(1)
133				
O5–H7 \cdots N15 ⁱ	0.76(3)	2.24(3)	3.006(3)	178(3)
O5–H8 \cdots N16 ⁱⁱ	0.80(4)	2.15(4)	2.946(3)	166(4)
O6–H5 \cdots N18 ⁱⁱⁱ	0.83(4)	2.03(4)	2.835(3)	161(3)
O6–H6 \cdots N6 ⁱⁱⁱ	0.81(3)	1.99(3)	2.777(4)	164(3)
C5–H4 \cdots O3 ^{iv}	0.95(2)	2.40(2)	3.197(3)	141(2)

132: (i) $x, -1+y, z$; (ii) $2-x, 1-y, -z$; (iii) $2-x, 2-y, -1-z$; (iv) $-1+x, 2+y, 1+z$; (v) $-2+x, 1+y, 1+z$; (vi) $1-x, 3-y, -z$. **133:** (i) $-1-x, 2-y, 1-z$; (ii) $-1+x, y, z$; (iii) $-x, 2-y, -z$; (iv) $x, y+1, z$.

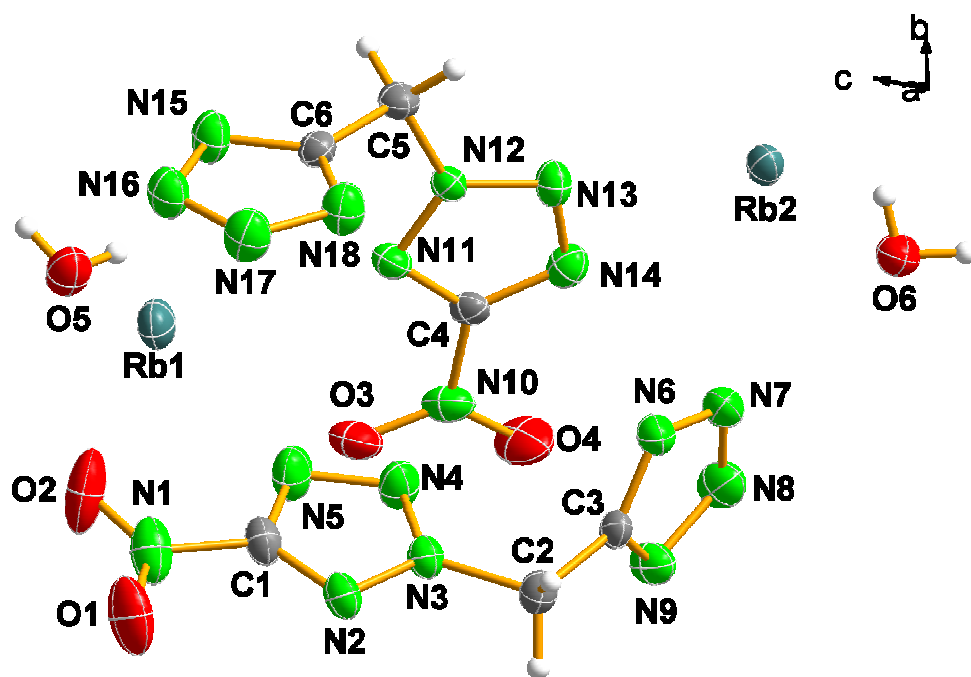


Figure 9.15 Asymmetric unit of **133** with labeling scheme.

133 also crystallizes as the monohydrate compound with two crystallographically independent molecules in the asymmetric unit (Figure 9.15). In one of the two moieties both tetrazole rings are nearly perpendicular to each other (dihedral angle $\text{N4-N3-C2-C3} = -4.3(3)^\circ$), whereas in the second molecule the rings are rotated by $44.2(3)^\circ$, similarly to **132**. In the unit cell there exist π -stacking along a direction approximately parallel to the b -axis between tetrazole and nitrotetrazole rings of two different molecules. The water molecules are involved in strong hydrogen bonds to the tetrazole nitrogen atoms (Table 9.6) forming dimeric interactions of the type **D1,1(2)**, which combine to form **D2,2(5)** finite patterns (Table 9.B2). More interestingly, O5 is involved in the formation of ring **R4,4(10)** graph-sets ($\text{O5} \cdots \text{N15}^{\text{i}} = 3.006(3) \text{ \AA}$ and $\text{O5} \cdots \text{N16}^{\text{ii}} = 2.946(3) \text{ \AA}$; symmetry codes: (i) $-1-x, 2-y, 1-z$; (ii) $-1+x, y, z$). In addition, there exists one non-classical hydrogen bond between the methylene carbon atom and a nitro-group oxygen atom ($\text{C5} \cdots \text{O3}^{\text{iv}} = 3.197(3) \text{ \AA}$; symmetry code: (iv) $x, y+1, z$) forming infinite chains along the b -axis. The NT ring is exclusively involved in the coordination to the metal center. Table 9.7 contains tabulated the distances for the coordination around the Rb^+ cations and the corresponding angles are summarized in Table 9.B4. The two crystallographically independent rubidium atoms (Rb1 and Rb2) show 5 and 3 long contacts in the range $3.4\text{--}3.6 \text{ \AA}$ and 6 and 8 shorter contacts at $2.9\text{--}3.3 \text{ \AA}$, respectively so that the total coordination around the rubidium cations is 11. Figure 9.16 shows the short contacts ($<3.2 \text{ \AA}$) around Rb1, where the coordination is completed by interaction to two water molecules and three NT moieties, one of which chelates the metal center ($\text{N11} \cdots \text{Rb1} = 2.998(2) \text{ \AA}$ and $\text{O3} \cdots \text{Rb1} = 3.162(2) \text{ \AA}$).

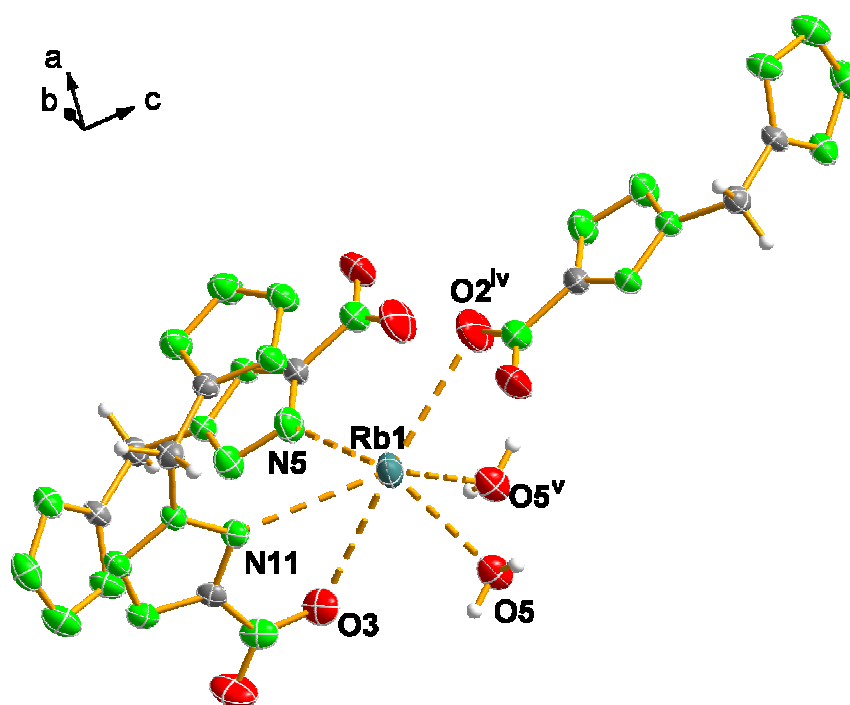


Figure 9.16 Coordination around one of the Rb⁺ cations (Rb1) in the crystal structure of **133** (only short contacts are shown for the sake of simplicity). Symmetry codes: (iv) -x, 1-y, 1-z; (v) -1-x, 1-y, 1-z.

Table 9.7 Selected bond distances for the coordination around the Rb⁺ cations in **133**.

Rb1–O5	2.912(2)	Rb1–O2	3.528(2)	Rb2–N7	3.110(2)
Rb1–O2 ^{iv}	2.941(2)	Rb1–N1 ^{iv}	3.569(2)	Rb2–N13	3.185(2)
Rb1–O5 ^v	2.977(2)	Rb1–O1 ^{vi}	3.627(2)	Rb2–N14 ⁱ	3.299(2)
Rb1–N11	2.998(2)	Rb2–N8 ⁱ	2.899(2)	Rb2–N7 ⁱ	3.327(2)
Rb1–N5	3.119(2)	Rb2–O6	2.930(2)	Rb2–N8 ⁱⁱ	3.416(2)
Rb1–O3	3.161(2)	Rb2–N9 ⁱⁱ	2.994(2)	Rb2–N6 ⁱⁱⁱ	3.580(2)
Rb1–N15	3.349(2)	Rb2–O6 ⁱⁱⁱ	3.002(2)	Rb2–N6	3.592(2)
Rb1–O1 ^{iv}	3.505(2)				

Symmetry codes for **133**: (i) -1-x, 2-y, -z; (ii) x, 1+y, z; (iii) -x, 2-y, -z; (iv) -x, 1-y, 1-z; (v) -1-x, 1-y, 1-z; (vi) -1+x, 1+y, z; (vii) 1+x, -1+y, z.

9.6 Energetic Properties

Computational Methods. Electronic energies for all cations and the 5-(5-nitrotetrazole-2-ylmethyl)-tetrazolate anion were calculated using Møller-Plesset perturbation theory truncated at the second order (MP2)^[32] and were used unscaled. The results of the MP2 electronic energy calculations are tabulated in *Appendix A* Table 9.A1. For all atoms in all calculations, the correlation consistent polarized double-zeta basis set cc-pVDZ was used.^[33]

The thermal stability of all compounds was determined by DSC measurements. In addition, the sensitivity of all compounds to impact, friction and thermal shock was also experimentally

determined. For all CHNO compounds the constant volume energy of combustion was determined experimentally using oxygen bomb calorimetry. In addition, for the nitrogen-rich salts **135**, **137** and **138** we predicted the energies of combustion on the basis of calculated electronic energies (see computational methods section and Table 9.A1) and an estimation of lattice enthalpy^[34] using similar methods to those reported elsewhere.^[35] The measured and predicted thermochemical properties for the nitrogen-rich 5-nitrotetrazole derivatives are summarized in Table 9.8. From the energies of formation back-calculated from experimental combustion data, molecular formulas and densities (from X-ray or picnometer measurements) the detonation pressure and velocity of each material were predicted using the EXPLO5 computer code.^[36]

DSC measurements on small samples of each energetic material (~1 mg) show distinctive melting points for all CHNO compounds apart from **137**, which melts with concomitant decomposition (Table 9.8). **128** has the lowest melting point at 118 °C and a high thermal stability up to 210 °C (liquid range = 92 °C). The rest of the CHNO compounds have also excellent thermal stabilities up to 196 (**137**) to 214 °C (**129b** and **129a**). Both **129b** and **129a** melt at ~170 °C and **129a** shows in addition an endothermic peak corresponding to the crystal water (99 °C), which is lost at higher temperatures than in **135** (83 °C). The melting points of CHNO compounds are lower than those of metal salts containing the NT⁺Tz⁻ (this chapter) or the NT⁻^[3] anions and are comparable to those observed for non-ionic liquid heterocycle based salts containing the NT⁻ anion.^[4,37-39] In comparison to commonly used explosives the compounds studied here have melting points higher than that of TNT (81 °C) but lower than that of RDX (204 °C), whereas the thermal stabilities are comparable to that of RDX, which decomposes at a temperature of 230 °C. The metal salts (Li, Na, K, Rb, Cs and Ag) have decomposition points, which vary within a relatively narrow range (168-192 °C) and are generally lower than those observed for alkali metal salts with the 5-At⁻^[40] or ZT²⁻^[41] anions (Table 9.9). With the exception of **134**, which shows a small melting endotherm just prior to melting, they all decompose without melting, in contrast to metal salts with the NT⁻ anion and have slightly lower thermal stabilities.^[3]

In addition to DSC analysis the response of all compounds to fast heating in a flame was tested. **128** burns smoothly without smoke whereas the rest of the CHNO compounds deflagrate (TNT and RDX explode under similar conditions). As for the alkali and the silver metal salts, two different “flame tests” were conducted. In the common “flame test” the compounds were put into direct contact with the flame by means of a thin metal spatula (“fast heating” test), whereas in the “slow heating” test, the materials were loaded on a thick metal spoon with the flame of the burner ~5 cm away from it. The response was the same for all salts: in the “fast heating” test, i.e., the compounds deflagrated giving the usual color for the metal cation (yellow in the case of **141**), whereas a slower

heating mode resulted in a loud explosion (in all cases without smoke). The copper salts (Table 9.10) showed a somewhat different thermal response and both “fast” and “slow” heating resulted in a smokeless deflagration reaction. In the case of **142** the expected green color was observed, whereas the presence of sodium in **143** and **144** was obvious due to the intense yellow coloration of the flame.

Table 9.8 Physico-chemical properties of nitrogen-rich salts of **129b**.

	128	129a	135	137	138
Formula	C ₃ H ₂ N ₆ O ₂	C ₃ H ₅ N ₉ O ₃	C ₃ H ₈ N ₁₀ O ₃	C ₄ H ₈ N ₁₂ O ₂	C ₄ H ₉ N ₁₃ O ₂
Mol. Mass (g mol ⁻¹)	154.09	215.05	232.16	256.09	271.10
T _m (°C) ^a	118	167	83	191	128
T _d (°C) ^b	210	214	206	196	201
N (%) ^c	54.5	58.6	60.33	65.6	67.1
N + O (%) ^d	75.3	80.9	81.0	78.1	78.9
Δ (%) ^e	-51.9	-40.9	-48.2	-62.5	-61.9
ρ (g cm ³) ^f	1.747	1.796	1.594	1.642*	1.633
ΔU _{comb.} / cal g ⁻¹ ^{g,h}	-3044(4)	-2436(12)	2524(9)	-3066(8) [-3065]	-3063(22) [-3122]
ΔU _f / kJ kg ⁻¹ ^{h,i}	3298(17)	1482(51)	664(36)	2322(32) [2319]	2380(90) [2621]
ΔH _f / kJ kg ⁻¹ ^{h,j}	3218(17)	1385(51)	552(36)	2215(32) [2213]	2271(90) [2511]

^aChemical melting point and ^bDecomposition point (DSC onsets) from measurement with $\beta = 5$ °C min⁻¹; ^cNitrogen percentage; ^dCombined oxygen and nitrogen contents; ^eOxygen balance according to ref. [42]; ^fDensity from X-ray measurements or picnometer (*); ^gExperimentally determined (oxygen bomb calorimetry) constant volume energy of combustion; ^hUncertainty in curved () brackets, calculated (MP2) values in squared [] brackets; ⁱExperimentally determined (back-calculated from ΔU_{comb.}) energy of formation; ^jExperimentally determined enthalpy of formation.

Data collected for friction and impact sensitivity testing are summarized in Table 9.9 for the **129b** metal salts and in Table 9.11 for the nitrogen-rich 5-nitrotetrazole derivatives. Crystalline **128** is a sensitive compound towards impact (>7 J) similarly to RDX (7.5 J) and very sensitive towards friction (18 N), more than the high-performing cage explosive CL-20 (48 N),^[43] regardless of its “inoffensive” response to thermal shock (only normal burning, see above). This is an interesting observation, which puts into perspective that there is no real correlation between friction and impact sensitivity values and the response to the “flame test”, therefore, potentially energetic compounds, which do not show a vigorous reaction in the flame ought to never be underestimated since they might be easily initiated by other stimuli (e.g., impact or friction). Formation of the tetrazole ring in **129a** results in a less endothermic compound due to the presence of crystal water (see discussion below), which is however equally sensitive towards impact (crystalline material: >8 J). So far the anhydrous material (**129b**) has not been study in bulk and current work is being directed towards the determination of the explosive properties of this material, which could turn out to be a high-performing primary explosive, similarly to 5-azido-1*H*-tetrazole.^[28,44] Surprisingly, regardless of its high impact sensitivity, **129a** is hardly shock sensitive. The crystalline compound decomposes non-explosively in the range 120 to 360 N. The sensitivity values of **129a** are comparable to those of the

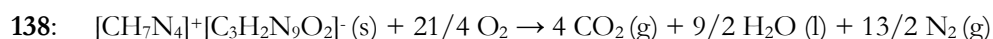
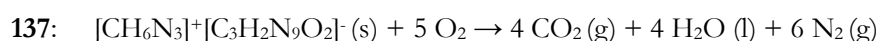
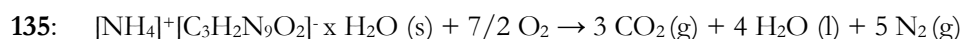
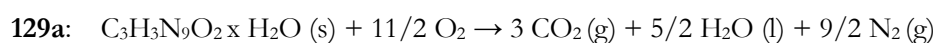
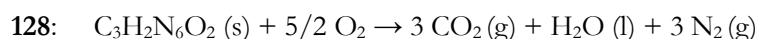
high explosive tetrytol (a mixture of TNT and tetryl, $i = 5$ J and $f = 353$ N)^[43] but the performance is much higher. Formation of the nitrogen-rich **135**, **137** and **138** salts translate in a notorious decrease in the sensitivity values. All compounds are insensitive to impact (>30 J) and are also expected to be insensitive to friction (>360 N), which can be explained by de formation of extensive hydrogen-bonding in the crystal structure (see X-ray structure discussion above).^[45] On the other side, the impact sensitivity of the alkali metal salts of **129b** correlates well with the size of the cation ($\text{Li} > \text{Na} \sim \text{Rb} > \text{K} > \text{Cs}$), with the exception of the Rb salt, which is more sensitive than expected. We had already observed a similar anomaly in the high sensitivity of the Rb salt when studying alkali metal salts of 5-nitrotetrazole (**5HNT**, see *Chapter III*).^[3,29] This might have to do with the tendency of both rubidium salts to form large thick crystals. Large crystals can break more easily (e.g., by dropping a weight on them) and the tension produced by the breaking of the crystals might induce the explosion. The values for the impact sensitivity vary between 4 J (**130**) and 15 J (**134**) and are in the range between commonly used primary explosives (technical grade lead diazide: 3.0-6.5 J) and secondary explosives (TNT: 15 J).^[43] As expected from transition metal salts with nitrogen-rich anions, the silver salt is the most sensitive compound in this study with an impact sensitivity of 3.5 J. Both **142** and **143** (monohydrate) have similar impact sensitivities (7.5 and 8.0 J, respectively), and as expected, the anhydrous copper salt (**144**) is (slightly) more sensitive to the same stimulus (6.0 J). These values are approximately between those of the primary explosive lead diazide or the sensitive secondary explosive PETN (3 J) and that of HMX (7.4 J).^[43]

Table 9.9 Physico-chemical properties of alkali metal salts of **129b**.

	130	131	132	133	134
Formula	$\text{LiC}_3\text{H}_5\text{N}_9\text{O}_{3.5}$	$\text{NaC}_3\text{H}_6\text{N}_9\text{O}_4$	$\text{KC}_3\text{H}_4\text{N}_9\text{O}_3$	$\text{RbC}_3\text{H}_4\text{N}_9\text{O}_3$	$\text{CsC}_3\text{H}_4\text{N}_9\text{O}_3$
MW (g mol ⁻¹)	230.07	255.13	255.12	299.59	329.01
Impact (J) ^a	>4.0	>6.0	>8.0	>6.0	>15
Friction (N) ^a	n.d. ^g	n.d. ^g	n.d. ^g	n.d. ^g	n.d. ^g
Flame (slow heat.) ^b	exp.	exp.	exp.	exp.	exp.
Flame (fast heat.) ^c	defl.	defl.	defl.	defl.	defl.
Color ^d	red	yellow	lilac	red	lilac
Combustion ^e	+	+	+	+	+
N (%) ^f	54.8	49.4	49.8	42.1	36.3
N+O (%) ^g	79.1	74.6	68.8	58.1	50.1
Δ (%) ^b	-41.7	-37.6	-37.6	-32.0	-27.7
m.p. (°C) ⁱ	-	-	-	-	183
Dec. (°C) ^j	180	192	184	170	186

^a Impact and friction sensitivities determined by standard BAM methods (see references [46-48]); ^{b,c} Response to “slow” and “fast heating”, respectively in the “flame test”, exp. = explosion and defl. = deflagration; ^d Color in the flame; ^e Smokeless (+) and non-smokeless (-) combustion in the flame; ^f Nitrogen content. ^g Combined nitrogen and oxygen contents. ^b Oxygen balance, calculated according to reference [42]. ^{i,j} Melting and decomposition points (DSC onset) from measurement with $\beta = 5$ °C min⁻¹. ^gn.d.. = not determined (compound under study).

In addition to the sensitivity data, which allow to decide whether a material is safe for transport or not and to classify it (e.g., primary or secondary explosive), the performance of a compound, commonly defined as its detonation pressure and velocity, is also of utmost interest. The energies of combustion obtained from the bomb calorimetry measurements, were used to back-calculate the energies of formation of the CHNO compounds, which were in turn combined with the density (either calculated from the X-ray experiments or experimentally determined using a picnometer) and the molecular formula to calculate the detonation parameters using the EXPLO5 computer-code.^[36] The energies of formation of **128**, **129a**, **135**, **137** and **138** were back-calculated on basis of the general combustion equations for CHNO compounds (see below), Hess's Law, the standard heats of formation for water and carbon dioxide^[49] and a correction for change in gas volume during combustion. Due to the reasonably large standard deviations for several sets of experimental combustion enthalpy measurements,^[10a] the enthalpies of combustion for the ionic based materials (**135**, **137** and **138**) were additionally predicted on the basis of known methods, utilizing calculated electronic energies and an approximation of lattice enthalpy,^[34] in an attempt to validate the experimentally determined values.



The experimentally determined energies of formation for the CHNO compounds in this study have highly positive values. **128** has the most positive one (3298(17) kJ kg⁻¹) comparable to bishydrazinium 5,5'-azotetrazolate,^[50] whereas the hydrated species **129a** (1482(51) kJ kg⁻¹) and **135** (664(36) kJ kg⁻¹) have the least positive. Once again, a comparison of the physico-chemical properties of the CHNO compounds studied here is useful to assess their suitability for application. The density values vary between ~1.6 and 1.8 g cm⁻³, well in the range of commonly used explosives (TNT: 1.654 g cm⁻³ and RDX: 1.800 g cm⁻³). In addition, all materials have better (less negative) oxygen balances than TNT (-74%), which vary in the range from ~-40 to -60% and excellent combined oxygen plus nitrogen balances (>75%).

Table 9.10 Physico-chemical properties of transition metal (Ag and Cu) salts of **129b**.

	141	142	143	144
Formula	AgC ₃ H ₃ N ₉ O _{2.5}	C ₆ H ₆ N ₁₈ O ₅ Cu	C ₆ H ₆ N ₁₉ O ₈ CuNa	C ₆ H ₄ N ₁₉ O ₇ CuNa
MW (g mol ⁻¹)	312.98	473.77	558.77	540.75
Impact (J) ^a	>3.5	>7.5	>8.0	>6.0
Friction (N) ^a	n.d. ^g	n.d. ^g	n.d. ^g	n.d. ^g
Flame (slow heat.) ^b	exp.	defl.	defl.	defl.
Flame (fast heat.) ^c	defl.	defl.	defl.	defl.
Color ^d	yellow	green	green	green
Combustion ^e	+	+	+	+
N (%) ^f	40.3	53.2	47.6	49.2
N+O (%) ^g	53.1	70.1	70.5	69.9
Δ (%) ^b	-30.7	-39.8	-25.8	-26.6
m.p. (°C) ⁱ	-	-	-	-
Dec. (°C) ^j	193	250	n.d. ^g	n.d. ^g

^a Impact and friction sensitivities determined by standard BAM methods (see references [46-48]); ^{b,c} Response to “slow” and “fast heating”, respectively in the “flame test”, exp. = explosion and defl. = deflagration; ^d Color in the flame; ^e Smokeless (+) and non-smokeless (-) combustion in the flame; ^f Nitrogen content. ^g Combined nitrogen and oxygen contents. ^b Oxygen balance, calculated according to reference [42]. ^{i,j} Melting and decomposition points (DSC onset) from measurement with $\beta = 5\text{ °C min}^{-1}$. ^gn.d.. = not determined (compound under study).

Table 9.11 Initial safety testing results and predicted energetic performance of nitrogen-rich 5-nitrotetrazole derivatives using the EXPLO5 code.

Compnd.	T_{ex} (K) ^a	V_0 (L kg ⁻¹) ^b	P_{det} (GPa) ^c	D (ms ⁻¹) ^d	Impact (J) ^e	Friction (N) ^e	Thermal Shock
128	4561	689	29.5	8356	>7	18	Burns
129a	3617	766	28.7	8326	>8	120-360 ^f	Deflagrates
135	3032	819	21.3	7658	>30	n.d. ^g	Deflagrates
137	3266 [3264]	780 [780]	24.3 [24.4]	8066 [8063]	>30	n.d. ^g	Deflagrates
138	3242 [3356]	797 [797]	25.0 [25.6]	8202 [8268]	>30	n.d. ^g	Deflagrates

^aTemperature of the explosion gases; ^bVolume of the explosion gases; ^cDetonation pressure; ^dDetonation velocity; ^eTests according to BAM methods (see references [46-48]). ^fnon-explosive decomposition. ^gn.d.. = not determined (compound under study).

The detonation parameters of the CHNO compounds were predicted on the basis of the experimentally determined energies of formation (Table 9.11). The EXPLO5 code, using the following values for the empirical constants in the Becker-Kistiakowsky-Wilson equation of state (BKWN-EOS): $\alpha = 0.5$, $\beta = 0.176$, $\kappa = 14.71$ and $\theta = 6620$, was used. **135** has a relatively low detonation velocity of 7658 m s^{-1} , due to the negative effect of the crystal water on the energy of formation, which is nevertheless higher than that of picric acid (7350 m s^{-1}) and only marginally lower than that of nitroglycerin (7717 m s^{-1}).^[43] However, the rest of the compounds have detonation velocities above 8000 m s^{-1} , which are higher than those of nitrogen-bridged bistetrazoles (*Chapter VII*)^[12b,24] and comparable to those of widely used high explosives such as TEX (8231 m s^{-1}).

¹),^[43] regardless of the higher density of the latter (1.99 g cm⁻³), and their lower sensitivity values suggests their potential for energetic applications. In comparison to other nitrogen-rich compounds for which predicted performance data is reported the materials in this study (excepting **135**) are predicted to perform as well as or outperform substituted triazolium^[51] and tetrazolium^[52] salts.

Table 9.12 Thermodynamic and explosive properties of formulations of nitrogen-rich salts of **129b** with ammonium nitrate (AN).

	AN + 128 ^a	AN + 129a ^b	AN + 135 ^c	AN + 137 ^d	AN + 138 ^e
ρ (g cm ⁻³) ^f	1.729	1.747	1.685	1.703	1.701
M (g mol ⁻¹)	100.77	124.62	124.15	122.28	125.91
Ω (%) ^g	-0.1	-0.1	0.2	0.2	0.3
ΔU°_f / kJ kg ⁻¹ ^h	-2261	-2475	-2948	-2805	-2791
ΔH°_f / kJ kg ⁻¹ ⁱ	-2383	-2602	-3080	-2936	-2923
T_{ex} / K ^j	3432	3207	3023	3111	3103
V_0 / L kg ⁻¹ ^k	890	907	934	933	938
P / GPa ^l	28.1	27.2	24.3	25.9	26.0
D / m s ⁻¹ ^m	8440	8322	8011	8226	8246

^a72% AN + 28% **128**; ^b67% AN + 33% **129a**; ^c71% ADN + 29% **135**; ^d76% ADN + 24% **137**; ^e76% ADN + 24% **138**;

^fDensity from EXPLO5; ^gOxygen balance according to ref. [42]; ^hCalculated energy of formation; ⁱCalculated enthalpy of formation; ^jTemperature of the explosion gases; ^kVolume of the explosion gases; ^lDetonation pressure; ^mDetonation velocity.

The detonation parameters for formulations of all CHNO compounds with an oxidant such as ammonium nitrate (AN) or ammonium dinitramide (ADN) were also calculated in order to further increase the performance of these materials. The results of the EXPLO5 calculations are tabulated in Tables 9.12 and 9.13. The formulations calculated were composed of compound and oxidant in oxygen neutral ratios. When using AN as the oxidizer, the energies of formation of the mixtures are highly negative (-2200 to -3000 kJ kg⁻¹) and the program predicts only small improvements in the performance data. The largest increase is calculated to be for the lowest-performing ammonium salt. However, formulations with ADN, have only slightly negative energies of formation and better densities, which translates in higher detonation parameters. For example, the detonation velocities and pressures (excepting those of **135**) for mixtures of the CHNO compounds with ADN have values around 8900 m s⁻¹ and 33.0 GPa, respectively, perfectly comparable to RDX/ADN mixtures ($D = 9091$ m s⁻¹, $P = 34.9$ GPa).

Table 9.13 Thermodynamic and explosive properties of formulations of nitrogen-rich salts of **129b** with ammonium dinitramide (ADN).

	ADN + 128 ^a	ADN + 129a ^b	ADN + 135 ^c	ADN + 137 ^d	ADN + 138 ^e
ρ (g cm ⁻³) ^f	1.788	1.803	1.733	1.760	1.758
M (g mol ⁻¹)	133.97	159.57	161.87	162.36	166.72
Ω (%) ^g	-0.1	-0.1	-0.1	0.2	0.3
ΔU°_f / kJ kg ⁻¹ ^h	-360	-85	-474	-99	-82
ΔH°_f / kJ kg ⁻¹ ⁱ	-242	-210	-604	-229	-213
T_{ex} / K ^j	4343	4038	3864	4029	3982
V_0 / L kg ⁻¹ ^k	826	850	877	872	877
P / GPa ^l	33.5	33.4	30.1	32.5	31.7
D / m s ⁻¹ ^m	8943	8960	8675	8930	8825

^a67% ADN + 33% **128**; ^b61% ADN + 39% **129a**; ^c65% ADN + 35% **135**; ^d71% ADN + 29% **137**; ^e71% ADN + 29% **138**;

^fDensity from EXPLO5; ^gOxygen balance according to ref. [42]; ^hCalculated energy of formation; ⁱCalculated enthalpy of formation; ^jTemperature of the explosion gases; ^kVolume of the explosion gases; ^lDetonation pressure; ^mDetonation velocity.

Lastly, it is important to point out that all literature performance values have been predicted based solely on theoretical heat of formation values (similar to the method used to predict the detonation parameters of the salts in this study). However, it has been shown that the calculated values are systematically overestimated.^[53] On the other side, performance values from experimentally determined heats of formation, like those used here, tend to underestimate the real performance of a material. Therefore, we conclude that the compounds in this study should perform at least as well as commonly used energetic materials.

9.7 Decomposition Gases

The ICT code^[54] was used to predict the heats of explosion as well as the gases formed upon decomposition of the nitrogen-rich 5-nitrotetrazole derivatives using the molecular formula, the density (either from X-ray or picnometer measurements) and the experimentally determined heats of formation (back-calculated from the heats of combustion) in kJ mol⁻¹ of **128** ($\Delta H^\circ_f = +496$ kJ mol⁻¹), **129a** ($\Delta H^\circ_f = +298$ kJ mol⁻¹), **135** ($\Delta H^\circ_f = +128$ kJ mol⁻¹), **137** ($\Delta H^\circ_f = +567$ kJ mol⁻¹) and **138** ($\Delta H^\circ_f = +616$ kJ mol⁻¹). The results of the calculations are summarized in Table 9.14 and in *Appendix A* (Figures 9.A1 and 9.A2) together with the corresponding results for commonly used high explosives such as RDX and TEX.

Table 9.14 Predicted decomposition gases and heats of explosion of nitrogen-rich 5-nitrotetrazole derivatives and comparison with known high explosives (using the ICT code).^a

Compound	CO ₂	H ₂ O	N ₂	CO	H ₂	NH ₃	CH ₄ ^b	HCN	C	$\Delta H_{\text{ex}} / \text{cal g}^{-1}$ ^c
128	138.8	107.1	541.7	20.1	0.2	4.3	0.3	0.3	186.9	1489
129a	72.7	184.5	574.8	10.7	0.3	13.2	0.4	0.4	142.5	1196
135	16.8	214.7	562.4	6.4	1.1	49.2	3.5	0.8	144.9	1011
137	4.2	135.0	594.2	3.2	1.4	74.6	6.7	0.9	179.6	1099
138	3.0	128.6	598.5	2.7	1.5	88.0	7.5	0.9	169.1	1094
RDX	292.6	232.8	373.9	21.5	0.2	5.1	-	0.3	72.7	1593
TEX	405.4	199.8	211.4	27.5	0.2	0.3	-	-	152.2	1237

^aThe amount of gases formed at 298 K is given in grams of gas per kilogram of energetic compound; ^bNo methane (RDX and TEX) and no hydrogen cyanide (TEX) were predicted by the code; ^cHeat of explosion.

The high nitrogen content of the compounds is reflected in the high amounts of molecular nitrogen predicted by the code ($\sim 540\text{--}600 \text{ g kg}^{-1}$), which is the main decomposition product, and supports that nitrogen-rich compounds derive their energy from (among other factors) their high nitrogen contents, whereas classical explosives such as RDX and TEX derive their energy from the oxidation of the carbon back-bone, which is the main decomposition product predicted for TEX (405.4 g kg^{-1}) and together with the formation of relatively large amounts of nitrogen (373.9 g kg^{-1}), is also one of the main products, which are expected from the explosion of RDX (292.6 g kg^{-1}). After nitrogen, carbon soot is (in the rule) the main decomposition product predicted for the decomposition of the 5-nitrotetrazole derivatives ($\sim 140\text{--}190 \text{ g kg}^{-1}$, comparable to TEX) followed by water ($\sim 110\text{--}215 \text{ g kg}^{-1}$), the amount of which is, as expected, higher for the hydrated compounds (**129a** and **135**). It is interesting to note that the amounts of carbon dioxide calculated decrease notoriously in the direction **128** to **138**, which is in agreement with an increase in the nitrogen content of the compounds from 54.5 to 67.1% (see Table 9.8), and is also reflected in an increase (in the same direction) in the amounts of ammoniac formed. The amounts of carbon dioxide expected from the explosion of the ionic salts is below 20 g kg^{-1} , whereas the amount of ammoniac for the same compounds are higher due to the ammonium cation (**135**) and the many amino groups in the guanidinium salts (**137** and **138**) and vary between ~ 50 and 90 g kg^{-1} . On the other side, the amounts of highly toxic gases (i.e., carbon monoxide and hydrogen cyanide) are in the rule expected to be fairly low for all nitrogen-rich compounds (below ~ 20 and 1 g kg^{-1} , respectively). Lastly, the heats of explosion have all values above 1000 cal g^{-1} , are in most cases comparable to TEX and that of **128** (1489 cal g^{-1}) is only slightly lower than that of RDX (1593 cal g^{-1}).

9.8 Conclusions

An alternative procedure for the synthesis of anhydrous ammonium 5-nitrotetrazolate (**21a**) is introduced, which shortens the time and lowers the prize involved in the preparation of the compound at the same time that using non-halogenated solvents, which is advantageous for up-scaling. **21a** was used as a starting material for the synthesis of two previously reported 5-nitrotetrazole derivatives (**128** and **129b**), which have now (for the first time) been energetically characterized and **129b** has been considered for the synthesis of energetic salts with alkali and transition (Ag and Cu) metals and nitrogen-rich cations (ammonium, guanidinium and aminoguanidinium). Apart from the lithium (**130**) and the sodium (**131**) salts, which draw water on time, the rest of the alkali salts have good energetic properties, comparable to 5,5'-azotetrazole and 5-nitrotetrazole metal salts. In addition, **141** has sensitivity values comparable to commonly used primaries (e.g., lead diazide) but with devoid of highly toxic metals. Interestingly, the copper salts with the NTTz^- anion described here have the capacity to be initiated by a laser beam, which makes them of interest for safe (non-accidental) initiation.

On the other side, the nitrogen-rich **129b** salts are highly endothermic compounds, have high performances and nevertheless decreased sensitivity values, which might be of interest for future application as insensitive or less sensitive high-performing nitrogen-rich materials. Lastly, we presented the synthesis and characterization of **145**, which is expected to be a valuable starting material for the synthesis of neutral HEDMs by replacement of the bromine atom by energetic moieties such as nitrato ($-\text{O}-\text{NO}_2$), azido ($-\text{N}_3$) or dinitramido ($-\text{N}(\text{NO}_2)_2$).

9. 9 Experimental Section

Caution! *Although no problems occurred during the synthesis and handling of the materials studied in this work, some of the compounds are highly endothermic and have high densities, which could cause severe damage to the surroundings in case of explosion. **128**, **129a** and **129b** are highly sensitive towards impact and some of the metal salts are very sensitive towards friction also. We recommend the synthesis of the compounds to be only undertaken by expert personnel with proper safety measures and wearing safety equipment such as Kevlar gloves, leather coat, face shield and ear plugs, in particular when working on a larger scale.*

General Method. All chemicals and solvents (analytical grade) were used as supplied by Sigma-Aldrich Inc. Ammonium 5-nitrotetrazolate (anhydrous) was prepared by a literature modified procedure^[4] as described below and 5-nitrotetrazole-2-ylacetonitrile, 5-(5-nitrotetrazole-2-ylmethyl)-tetrazole monohydrate and 2-(2-bromoethyl)-5-nitrotetrazole were prepared according to a published procedure.^[2] ¹H, and ¹³C NMR spectra were recorded on a JEOL Eclipse 400 instrument in DMSO-*d*₆ at or near 25 °C. The chemical shifts are given relative to tetramethylsilane as external standard. Infrared (IR) spectra were recorded on a Perkin-Elmer Spectrum One FT-IR instrument as KBr pellets at 20 °C.^[55] Transmittance values are qualitatively described as “very strong” (vs), “strong” (s), “medium” (m) and “weak” (w). Raman spectra were recorded on a Perkin-Elmer Spectrum 2000R NIR FT-Raman instrument equipped with a Nd:YAG laser (1064 nm). The intensities are reported as percentages of the most intense peak and are given in parentheses. Elemental analyses were performed with a Netsch Simultaneous Thermal Analyzer STA 429. Melting points were determined by differential scanning calorimetry (Linseis DSC PT-10 instrument,^[56] calibrated with standard pure indium and zinc). Measurements were performed at a heating rate of 5 °C min⁻¹ in closed aluminum sample pans with a 1 µm hole in the top for gas release under a nitrogen flow of 20 mL min⁻¹ with an empty identical aluminum sample pan as a reference. Lastly, the mass spectrometry measurements were conducted on a JEOL MStation JMS 700 machine.^[57]

Bomb Calorimetry. For all calorimetric measurements, a Parr 1356 bomb calorimeter (static jacket) equipped with a Parr 207A oxygen bomb for the combustion of highly energetic materials was used.^[58] A Parr 1755 printer, furnished with the Parr 1356 calorimeter, was used to produce a permanent record of all activities within the calorimeter. The samples (~200 mg each) were carefully mixed with ~800 mg analytical grade benzoic acid and pressed into pellets, which were subsequently burned in a 3.05 MPa atmosphere of pure oxygen. The experimentally determined constant volume energies of combustion were obtained as the averages of five single measurements. The calorimeter was calibrated by the combustion of certified benzoic acid in an oxygen atmosphere at a pressure of 3.05 MPa.

Synthesis of 5-Nitrotetrazole-2-ylacetonitrile (128**):** Anhydrous ammonium 5-nitrotetrazole (17.775 g, 126 mmol) and sodium bromide (13.418 g, 131 mmol) were dissolved in 86 mL DMF. Chloroacetonitrile (16.6 mL, 212 mmol) was added carefully at room temperature and the reaction mixture was stirred at 90-95 °C for 4 h. After this time a brown solution had formed with undissolved inorganic salts, which were filtered and washed with 2-3 mL DMF. Addition of 210 mL water to the brown filtrate solution resulted in the

precipitation of the brown crude product. Recrystallization from ethanol (2x70 mL) in the presence of active charcoal, resulted in the formation of the compound as colorless needle-like crystals suitable for X-ray measurements (8.96 g, 46%). $C_3H_2N_6O_2$ (154.08 g mol⁻¹, calc./found): C 23.37 / 23.42, H 1.31 / 1.43, N 54.55 / 54.83; DSC (5 °C min⁻¹, °C): 118 (m.p.), 210 (dec.); m/z (DEI⁺, xenon, 6 keV, m-NBA matrix): 155.2 ([128+H]⁺); ¹H NMR (DMSO-*d*₆, 399.78 MHz, 25°C, TMS) δ/ppm: 6.31 (2H, s, CH₂); ¹³C{¹H} NMR (DMSO-*d*₆, 100.52 MHz, 25°C, TMS) δ/ppm: 166.3 (1C, C-NO₂), 112.5 (1C, CN), 42.7 (1C, CH₂); ¹⁴N NMR (DMSO-*d*₆, 28.91 MHz, 25 °C, MeNO₂) δ/ppm: -35 (1N, Δ*ν*_{1/2} ~ 300 Hz), -110 (1N, Δ*ν*_{1/2} ~ 1875 Hz); ¹⁵N NMR (DMSO-*d*₆, 27.37 MHz, 25 °C, MeNO₂) δ/ppm: 6.9 (1N, t, ³*J*_{NH} = 1.26 Hz, N4), -35.4 (1N, s, NO₂), -52.5 (1N, s, N5), -77.6 (1N, t, ³*J*_{NH} = 1.76 Hz, N2), -106.4 (1N, t, ²*J*_{NH} = 2.51 Hz, N3), -121.9 (1N, t, ²*J*_{NH} = 1.51 Hz, CN); Raman $\tilde{\nu}$ / cm⁻¹ (rel. int.) 2994(23) 2949(55) 2267(36) 1565(30) 1491(40) 1464(17) 1419(100) 363(28) 1323(21) 1296(22) 1230(26) 137(29) 1072(18) 1031(66) 953(13) 942(13) 845(15) 790(27) 775(19) 690(13) 546(18) 416(37) 359(36) 350(39) 319(26) 226(30); IR $\tilde{\nu}$ / cm⁻¹ (KBr, rel. int.): 3429(w) 2993(m) 2948(m) 2880(w) 2266(vw) 1732(vw) 1618(vw) 1565(s) 1484(w) 1417(m) 1368(w) 1325(m) 1261(w) 1228(w) 1137(vw) 1105(w) 1071(w) 1055(w) 1030(m) 1007(w) 941(w) 848(m) 786(w) 690(w) 670(w) 657(w) 611(vw) 546(vw) 500(vw).

Synthesis of 5-(5-Nitrotetrazole-2-ylmethyl)-tetrazole Monohydrate (129a): Sodium azide (1.300 g, 20 mmol) was added to a solution of **128** (3.08 g, 20 mmol) and ammonium chloride (1.070 g, 20 mmol) in 30 mL DMF. The reaction mixture was stirred for 1 h at room temperature and for 5 h at 50-70 °C giving a brown solution with a white precipitate. The insoluble inorganic salts were filtered and washed with little DMF and the solvent evaporated to dryness in a rotatory evaporator giving a brown oil. The oil was taken into 50 mL water and reacted with ~3 mL diluted (10%) sulphuric acid until no more precipitation was observed. The brown product was recrystallized from 40 mL water in the presence of active charcoal yielding the pure monohydrate compound as colorless crystals. (2.300 g, 53%). $C_3H_5N_9O_3$ (215.13 g mol⁻¹, calc./found): C 16.75 / 16.87, H 2.34 / 2.47, N 58.60 / 58.67; DSC (5 °C min⁻¹, °C): 99 (-H₂O), 167 (m.p.) 214 (dec.); m/z (DEI⁺, xenon, 6 keV, m-NBA matrix): 198.2 ([129b+H]⁺); ¹H NMR (DMSO-*d*₆, 270.16 MHz, 25°C, TMS) δ/ppm: 8.41 (1H, s, NH), 6.48 (2H, s, CH₂), 3.78 (2H, s, H₂O); ¹³C{¹H} NMR (DMSO-*d*₆, 67.63 MHz, 25°C, TMS) δ/ppm: 167.1 (1C, C-NO₂), 153.3 (1C, C-Tz), 49.0 (1C, CH₂); ¹⁴N NMR (DMSO-*d*₆, 26.88 MHz, 25 °C, MeNO₂) δ/ppm: -34 (1N, Δ*ν*_{1/2} ~ 793 Hz, NO₂); ¹⁵N NMR (DMSO-*d*₆, 40.50 MHz, 25 °C, MeNO₂) δ/ppm: 6.5 (1N, t, ³*J*_{NH} = 1.86 Hz, N4), -21.1 (2N, s, N7/N8), -35.4 (1N, s, NO₂), -54.3 (1N, s, N5), -77.3 (1N, t, ³*J*_{NH} = 2.09 Hz, N2), -86.9 (2N, s, N6/N9), -98.7 (1N, t, ²*J*_{NH} = 2.32 Hz, N3); ¹⁵N{¹H} NMR (DMSO-*d*₆, 40.30 MHz, 25 °C, MeNO₂) δ/ppm: 6.4 (1N, N4), -21.9 (2N, N7/N8), -35.4 (1N, NO₂), -54.3 (1N, N5), -77.9 (1N, N2), -87.1 (2N, N6/N9), -98.7 (1N, N3); Raman $\tilde{\nu}$ / cm⁻¹ (rel. int.) 3023(8) 1590(6) 1561(11) 1488(23) 1470(6) 1454(6) 1416(38) 1361(8) 1347(6) 1329(6) 1320(8) 1303(7) 1241(18) 1227(10) 1135(10) 1116(14) 1071(16) 1029(43) 940(3) 842(5) 810(10) 776(10) 675(7) 544(4) 452(5) 372(8) 348(16) 312(12) 284(8) 206(13) 179(12); IR $\tilde{\nu}$ / cm⁻¹ (KBr, rel. int.): 3559(m) 3418(w) 3342(w) 3022(m) 2982(w) 2879(w) 2727(w) 2636(w) 2515(w) 1747(vw) 1640(w) 1590(w) 1561(s) 1487(m) 1454(w) 1419(m) 1384(w) 1361(w) 1348(w) 1329(m) 1261(w) 1238(w) 1226(w) 1134(w) 1117(m) 1067(m) 1028(w) 1006(w) 938(w) 904(w) 850(m) 808(w) 768(w) 718(w) 694(w) 657(w) 546(w) 474(w).

Synthesis of 5-(5-Nitrotetrazole-2-ylmethyl)-tetrazole (129b). *Method A:* The compound was accidentally obtained when trying to protonate **129a** either with nitric or perchloric acids. A typical and reproducible procedure using nitric acid follows: **129a** (0.202 g, 0.94 mmol) was dissolved in 5 mL ethanol and 65% concentrated nitric acid (0.109 g, 1.13 mmol) was added to the solution. The reaction mixture was shortly heated to boiling and left to cool. After 1 h standing **129b** formed as a colorless crystalline compound, which was filtered and dried under vacuum (0.120 g, 64%).

Method B: Alternatively, the crystal water in the hydrated species **129a** can be quantitatively removed by heating the compound to 60 °C for several days under high vacuum ($\sim 10^{-3}$ mbar). $C_3H_3N_9O_2$ (197.11 g mol⁻¹, calc./found): C 18.27 / 17.98, H 1.53 / 1.30, N 63.96 / 64.07; DSC (5 °C min⁻¹, °C): 168 (m.p.), 214 (dec.); ¹H NMR (DMSO-*d*₆, 400.18 MHz, 25°C, TMS) δ /ppm: 6.62 (2H, s, CH₂); ¹³C{¹H} NMR (DMSO-*d*₆, 100.63 MHz, 25°C, TMS) δ /ppm: 166.1 (1C, C-NO₂), 152.4 (1C, C-Tz), 47.8 (1C, CH₂); ¹⁴N NMR (DMSO-*d*₆, 28.92 MHz, 25 °C, MeNO₂) δ /ppm: -35 (1N, $\Delta\nu_{1/2} \sim 150$ Hz, NO₂), -104 (1N, $\Delta\nu_{1/2} \sim 900$ Hz, N₂); Raman $\tilde{\nu}$ / cm⁻¹ (rel. int.) 3008(9) 2972(15) 1562(9) 1488(16) 1470(7) 1455(7) 1416(22) 1363(7) 1344(7) 1321(7) 1308(7) 1235(14) 1134(8) 1114(9) 1069(12) 1029(24) 842(7) 808(8) 777(9) 672(7) 452(9) 371(11) 346(14) 311(12) 280(10) 206(12) 89(5) 13(6); IR $\tilde{\nu}$ / cm⁻¹ (KBr, rel. int.): 3557(w) 3338(w) 3142(w) 3023(m) 3007(m) 2972(m) 2878(m) 2777(m) 2732(m) 2640(m) 2512(m) 2355(vw) 1749(w) 1640(vw) 1588(m) 1560(s) 1487(m) 1470(vw) 1453(w) 1441(w) 1419(s) 1384(w) 1362(m) 1347(w) 1329(s) 1321(m) 1308(w) 1247(w) 1234(w) 1224(w) 1134(w) 1117(s) 1104(m) 1067(s) 1028(m) 1006(w) 936(w) 893(w) 849(s) 844(w) 807(w) 767(m) 717(w) 694(w) 673(vw) 667(w) 656(w) 542(w) 457(w) 450(w) 418(vw).

Synthesis of Lithium 5-(5-Nitrotetrazole-2-ylmethyl)-tetrazolate Monohemihydrate (130): **129a** (0.200 g, 0.93 mmol) and lithium carbonate (0.035 g, 0.93 mmol) were suspended in 5 mL water. The reaction mixture was stirred for 1 h at room temperature resulting in gas evolution (CO₂). After most of the insoluble solid had dissolved, the solution was filtered and the solvent was removed under high vacuum ($\sim 10^{-3}$ mbar) and at room temperature to yield the lithium salt as a slightly brown powder. No further purification was necessary. (0.172 g, 88%). $C_3H_3N_9O_{3.5}Li$ (230.06 g mol⁻¹, calc./found): C 15.64 / 15.68, H 2.19 / 2.03, N 54.78 / 54.10; DSC (5 °C min⁻¹, °C): 81 (H₂O), 180 (dec.); m/z (FAB-, xenon, 6 keV, m-NBA matrix) 202.1 ([130-H⁺]), 196.1 (NTTz), 114.0 (NT⁻); m/z (FAB+, xenon, 6 keV, m-NBA matrix) 7.3 (Li⁺); ¹H NMR (DMSO-*d*₆, 399.78 MHz, 25°C, TMS) δ /ppm: 6.12 (2H, s, CH₂), 3.39 (3H, s, H₂O); ¹³C{¹H} NMR (DMSO-*d*₆, 100.52 MHz, 25°C, TMS) δ /ppm: 165.9 (1C, C-NO₂), 154.3 (1C, C-Tz), 50.8 (1C, CH₂); ¹⁴N NMR (DMSO-*d*₆, 28.89 MHz, 25 °C, MeNO₂) δ /ppm: -34 (1N, $\Delta\nu_{1/2} \sim 80$ Hz, NO₂), -90 (1N, $\Delta\nu_{1/2} \sim 430$ Hz, N₂); Raman $\tilde{\nu}$ / cm⁻¹ 3426(1) 2554(1) 2448(1) 1753(2) 1565(4) 1477(9) 1415(16) 1315(4) 1218(5) 1125(4) 1083(4) 1030(10) 890(2) 843(3) 774(4) 688(3) 450(3) 413(3) 349(4) 196(4) 91(1); IR $\tilde{\nu}$ / cm⁻¹ (KBr, rel. int.): 3586(vs) 3507(vs) 3346(vs) 3247(vs) 2875(w) 2732(w) 2544(vw) 2481(vw) 2281(w) 2228(w) 2168(w) 1862(vw) 1669(m) 1565(vs) 1496(m) 1487(m) 1442(m) 1417(s) 1384(w) 1354(w) 1340(m) 1321(s) 1298(w) 1262(w)

1238(w) 1214(w) 1166(w) 1129(w) 1119(w) 1084(w) 1071(w) 1056(w) 1033(w) 948(w) 939(w) 846(s) 823(w) 813(w) 762(m) 742(w) 710(w) 692(m) 662(m) 571(m) 478(m).

Synthesis of Sodium 5-(5-Nitrotetrazole-2-ylmethyl)-tetrazolate Dihydrate (131): The compound was prepared as **130** from **129a** (0.200 g, 0.93 mmol) an sodium bicarbonate (0.078 g, 0.93 mmol) as a slightly brown crystalline solid (0.175 g, 74%). $C_3H_6N_9O_4Na$ (255.04 g mol⁻¹, calc./found): C 14.11 / 13.95, 2.37 / 2.18, N 49.41 / 48.99; DSC (5 °C min⁻¹, °C): 125 (H₂O), 192 (dec.); m/z (FAB⁻, xenon, 6 keV, m-NBA matrix) 218.9 ([131-H⁺]), 196.0 (NTTz⁻), 114.0 (NT⁻); m/z (FAB⁺, xenon, 6 keV, m-NBA matrix) 23.1 (Na⁺); ¹H NMR (DMSO-*d*₆, 400.18 MHz, 25°C, TMS) δ/ppm: 6.20 (2H, s, CH₂), 3.83 (4H, s, H₂O); ¹³C{¹H} NMR (DMSO-*d*₆, 100.52 MHz, 25°C, TMS) δ/ppm: 165.7 (1C, C-NO₂), 154.2 (1C, C-Tz), 50.5 (1C, CH₂); ¹⁴N NMR (DMSO-*d*₆, 28.91 MHz, 25 °C, MeNO₂) δ/ppm: -34 (1N, Δ*v*_{1/2} ~ 289 Hz, NO₂), -91 (1N, Δ*v*_{1/2} ~ 1705 Hz, N₂); Raman $\tilde{\nu}$ / cm⁻¹ (rel. int.) 3425(1) 3020(9) 2966(9) 1568(28) 1493(27) 1479(53) 1466(26) 1446(27) 1425(78) 1370(18) 1337(23) 1323(21) 1281(20) 1221(20) 1192(25) 1163(26) 1145(30) 1098(23) 1090(22) 1072(24) 1046(43) 1035(44) 948(16) 848(23) 825(23) 773(25) 755(23) 710(18) 692(21) 557(16) 545(15) 452(17) 378(18) 355(21) 315(20) 291(16) 207(12); IR $\tilde{\nu}$ / cm⁻¹ (KBr, rel. int.): 3379(s) 3016(m) 2964(m) 2876(w) 2287(vw) 1676(m) 1566(vs) 1559(vs) 1491(m) 1478(m) 1465(w) 1442(m) 1422(s) 1384(w) 1343(w) 1322(vs) 1280(w) 1219(w) 1191(w) 1138(w) 1089(w) 1071(w) 1054(w) 1044(w) 1033(w) 947(w) 844(vs) 824(w) 793(w) 758(m) 709(w) 691(m) 655(m) 627(w) 474(w).

Synthesis of Potassium 5-(5-Nitrotetrazole-2-ylmethyl)-tetrazolate Monohydrate (132): The potassium salt was obtained as the lithium compound from **129a** (0.200 g, 0.93 mmol) and potassium bicarbonate (0.093 g, 0.93 mmol) in 3 mL ethanol as a colorless powder (0.220 g, 96%). Crystals of the product suitable for X-ray analysis were obtained by slow evaporation of an aqueous solution of the compound under a stream of nitrogen. $C_3H_4N_9O_3K$ (253.01 g mol⁻¹, calc./found): C 14.22 / 14.53, H 1.59 / 1.81, N 49.81 / 48.66; DSC (5 °C min⁻¹, °C): 89 (H₂O), 184 (dec.); m/z (FAB⁻, xenon, 6 keV, m-NBA matrix) 234.9 ([KNTTz-H⁺]), 196.0 (NTTz⁻), 114.0 (NT⁻); m/z (FAB⁺, xenon, 6 keV, m-NBA matrix) 39.1 (K⁺); ¹H NMR (DMSO-*d*₆, 400.18 MHz, 25°C, TMS) δ/ppm: 6.26 (2H, s, CH₂), 4.70 (2H, s, H₂O); ¹³C{¹H} NMR (DMSO-*d*₆, 100.52 MHz, 25°C, TMS) δ/ppm: 166.2 (1C, C-NO₂), 154.2 (1C, C-Tz), 50.4 (1C, CH₂); ¹⁴N NMR (DMSO-*d*₆, 28.91 MHz, 25 °C, MeNO₂) δ/ppm: -34 (1N, Δ*v*_{1/2} ~ 227 Hz, NO₂), -89 (1N, Δ*v*_{1/2} ~ 1360 Hz, N₂); Raman $\tilde{\nu}$ / cm⁻¹ (rel. int.) 3020(6) 2971(7) 1568(11) 1492(11) 1479(26) 1467(10) 1446(10) 1425(43) 1371(4) 1337(6) 1323(6) 1282(4) 1221(5) 1193(7) 1163(7) 1145(9) 1099(6) 1089(5) 1072(7) 1046(17) 1035(20) 948(2) 847(5) 825(4) 773(6) 756(4) 692(4) 545(4) 451(3) 378(4) 355(6) 315(7) 290(4) 206(6) 95(3); IR $\tilde{\nu}$ / cm⁻¹ (KBr, rel. int.): 3401(m) 3016(w) 2965(w) 2925(w) 2878(w) 2737(w) 2638(w) 2510(w) 1676(w) 1627(w) 1567(s) 1559(s) 1491(w) 1478(w) 1465(w) 1442(w) 1422(m) 1384(w) 1359(w) 1345(w) 1323(s) 1280(w) 1234(w) 1219(w) 1192(w) 1139(w) 1133(w) 1117(w) 1096(w) 1089(w) 1071(m) 1065(w) 1054(w) 1044(w) 1028(w) 947(w) 898(w) 844(s) 825(w) 759(w) 738(w) 709(w) 691(w) 655(w) 627(w) 556(w) 472(w).

Synthesis of Rubidium 5-(5-Nitrotetrazole-2-ylmethyl)-tetrazolate Monohydrate (133): The compound was prepared from **129a** (0.187 g, 0.87 mmol) and rubidium carbonate (0.100 g, 0.44 mmol) in 5 mL ethanol as described above for the other metal salts. Concentration by slow evaporation of the solvent yielded the compound as slightly red crystals, which were used for the diffraction measurements (0.170 g, 66%). $C_3H_4N_9O_3Rb$ (299.59 g mol⁻¹, calc./found): C 12.03 / 11.99, H 1.34 / 1.17, N 42.08 / 42.13; DSC (5 °C min⁻¹, °C): 102 (H₂O), 170 (dec.); m/z (FAB⁻, xenon, 6 keV, m-NBA matrix) 280.9 ([RbNTTz-H⁺]⁻), 196.0 (NTTz⁻), 114.0 (NT⁻); m/z (FAB⁺, xenon, 6 keV, m-NBA matrix) 84.9 (Rb⁺); ¹H NMR (DMSO-*d*₆, 400.18 MHz, 25 °C, TMS) δ/ppm: 6.20 (2H, s, CH₂), 3.83 (2H, s, H₂O); ¹³C{¹H} NMR (DMSO-*d*₆, 100.52 MHz, 25 °C, TMS) δ/ppm: 165.7 (1C, C-NO₂), 154.2 (1C, C-Tz), 50.5 (1C, CH₂); ¹⁴N NMR (DMSO-*d*₆, 28.91 MHz, 25 °C, MeNO₂) δ/ppm: -34 (1N, Δ*v*_{1/2} ~ 289 Hz, NO₂), -91 (1N, Δ*v*_{1/2} ~ 1705 Hz, N₂); Raman $\tilde{\nu}$ / cm⁻¹ (rel. int.) 3015(9) 2967(10) 1564(15) 1492(18) 1478(41) 1466(16) 1444(15) 1423(77) 1373(5) 1334(10) 1279(7) 1222(7) 1190(13) 1160(11) 1145(17) 1096(9) 1071(8) 1045(29) 1034(32) 846(8) 825(7) 773(8) 754(7) 692(7) 556(4) 451(4) 375(7) 350(10) 315(10) 290(7) 204(6); IR $\tilde{\nu}$ / cm⁻¹ (KBr, rel. int.): 3385(s) 3014(m) 2964(w) 2927(w) 2874(w) 2738(w) 2562(w) 2510(w) 2384(w) 2217(w) 1868(w) 1670(w) 1626(w) 1566(s) 1558(s) 1491(m) 1477(m) 1465(w) 1440(m) 1421(s) 1384(w) 1371(w) 1356(w) 1341(m) 1322(s) 1278(m) 1235(w) 1220(w) 1189(w) 1137(m) 1088(m) 1071(m) 1054(m) 1044(m) 1032(m) 946(w) 844(s) 824(m) 758(s) 737(w) 709(m) 691(m) 655(m) 620(m) 556(m) 473(w).

Synthesis of Cesium 5-(5-Nitrotetrazole-2-ylmethyl)-tetrazolate Monohydrate (134): As described for **130**, **129a** (0.200 g, 0.92 mmol) and cesium carbonate (0.123 g, 0.45 mmol) were reacted in 5 mL ethanol and after concentration by slow evaporation of the solvent the cesium salt separated as slightly red crystals (0.174 g, 54%). $C_3H_4N_9O_3Cs$ (347.03 g mol⁻¹, calc./found): C 10.38 / 10.24, H 1.16 / 1.08, N 36.32 / 35.98; DSC (5 °C min⁻¹, °C): ~100 (H₂O), 183 (m.p.), 186 (dec.); m/z (FAB⁻, xenon, 6 keV, m-NBA matrix) 328.8 ([CsNTTz-H⁺]⁻), 196.0 (NTTz⁻), 114.0 (NT⁻); m/z (FAB⁺, xenon, 6 keV, m-NBA matrix) 133.0 (Cs⁺); ¹H NMR (DMSO-*d*₆, 400.18 MHz, 25 °C, TMS) δ/ppm: 6.20 (2H, s, CH₂), 3.83 (2H, s, H₂O); ¹³C{¹H} NMR (DMSO-*d*₆, 100.52 MHz, 25 °C, TMS) δ/ppm: 165.7 (1C, C-NO₂), 154.2 (1C, C-Tz), 50.5 (1C, CH₂); ¹⁴N NMR (DMSO-*d*₆, 28.91 MHz, 25 °C, MeNO₂) δ/ppm: -34 (1N, Δ*v*_{1/2} ~ 289 Hz, NO₂), -91 (1N, Δ*v*_{1/2} ~ 1705 Hz, N₂); Raman $\tilde{\nu}$ / cm⁻¹ (rel. int.) 3426(1) 3016(1) 2857(1) 1554(3) 1469(7) 1433(3) 1419(5) 1346(2) 1211(2) 1181(3) 1089(3) 1068(3) 1049(2) 1032(6) 844(2) 766(2) 683(2) 333(3) 312(3) 274(3); IR $\tilde{\nu}$ / cm⁻¹ (KBr, rel. int.): 3401(w) 3015(w) 2977(w) 2925(w) 2875(w) 2554(w) 2484(w) 2395(w) 2212(w) 2165(w) 2107(w) 2061(w) 1640(w) 1621(w) 1553(s) 1483(m) 1468(w) 1432(m) 1418(m) 1405(m) 1354(w) 1347(m) 1330(m) 1280(w) 1210(w) 1179(w) 1142(w) 1128(w) 1089(w) 1067(w) 1047(w) 1031(w) 1022(w) 927(w) 848(s) 819(w) 773(w) 763(m) 701(m) 682(w) 658(w) 554(w) 466(w).

Synthesis of Ammonium 5-(5-Nitrotetrazole-2-ylmethyl)-tetrazolate Monohydrate (135). **129a** (0.136 g, 0.6 mmol) was dissolved in 2 mL 35% concentrated ammonia and the solution was heated shortly to boiling. The solvent was left to slowly evaporate yielding X-ray quality crystals of the pure compound (0.134 g, 97%). $C_3H_7N_{10}O_{2.5}$ (215.15 g mol⁻¹, calc./found): C 16.15 / 16.08, H 3.47 / 3.50, N 60.33 / 60.49; DSC (5 °C min⁻¹, °C): 82 (H₂O), 206 (dec.); m/z (DEI⁺, xenon, 6 keV, m-NBA matrix): 198.2 ([NTTzH]⁺);

^1H NMR (DMSO- d_6 , 399.78 MHz, 25°C, TMS) δ /ppm: 7.21 (4H, s, NH_4^+), 6.20 (2H, s, CH_2), 3.63 (2H, s, H_2O); $^{13}\text{C}\{^1\text{H}\}$ NMR (DMSO- d_6 , 100.63 MHz, 25°C, TMS) δ /ppm: 166.1 (1C, C- NO_2), 154.2 (1C, C-Tz), 50.4 (1C, CH_2); ^{14}N NMR (DMSO- d_6 , 28.92 MHz, 25 °C, MeNO_2) δ /ppm: -34 (1N, $\Delta\nu_{1/2} \sim 133$ Hz, NO_2), -89 (1N, $\Delta\nu_{1/2} \sim 977$ Hz, N2), -359 (1N, $\Delta\nu_{1/2} \sim 6$ Hz, NH_4^+); Raman $\tilde{\nu}$ / cm^{-1} (rel. int.) 3426(1) 3019(7) 2969(11) 2912(4) 2559(3) 1562(24) 1491(32) 1477(48) 1466(30) 1445(30) 1421(76) 1336(26) 1318(25) 1280(22) 1221(25) 1196(30) 1156(26) 1142(31) 1105(26) 1070(28) 1045(39) 1031(51) 948(19) 845(26) 823(25) 773(28) 754(25) 691(24) 542(19) 451(20) 374(21) 349(25) 312(23) 290(19) 206(15) 92(1); IR $\tilde{\nu}$ / cm^{-1} (KBr, rel. int.): 3584(m) 3295(s) 3193(s) 3013(s) 2509(w) 2284(w) 2179(w) 2079(w) 1802(w) 1680(m) 1620(m) 1566(s) 1557(s) 1490(s) 1474(s) 1437(s) 1418(s) 1343(m) 1320(s) 1278(m) 1237(w) 1219(w) 1195(w) 1146(w) 1135(w) 1101(w) 1070(w) 1043(w) 1029(w) 948(w) 844(s) 823(m) 761(m) 752(m) 708(w) 690(m) 654(m) 554(m) 474(w).

Synthesis of Guanidinium 5-(5-Nitrotetrazole-2-ylmethyl)-tetrazolate (137): 129a (0.176 g, 0.8 mmol) was suspended in 5 mL water and reacted with guanidinium carbonate (0.074 g, 0.4 mmol) causing gas evolution. The slightly yellow solution was shortly heated to boiling and the solvent was left to evaporate yielding the pure compound as colorless feathery material (0.189 g, 95%). $\text{C}_4\text{H}_8\text{N}_{12}\text{O}_2$ (256.19 g mol^{-1} , calc./found): C 18.74 / 18.81, H 3.15 / 3.19, N 65.62 / 65.68; DSC (5 °C min^{-1} , °C): 191 (m.p.), 196 (dec.); m/z (FAB $^-$, xenon, 6 keV, m-NBA matrix) 256.0 ([137- H^+]), 196.0 (NTTz $^-$), 114.0 (NT $^-$); m/z (FAB $^+$, xenon, 6 keV, m-NBA matrix) 60.1 ([NH_4] $^+$); ^1H NMR (DMSO- d_6 , 400.18 MHz, 25°C, TMS) δ /ppm: 7.47 (6H, s, NH_2), 6.32 (2H, s, CH_2); $^{13}\text{C}\{^1\text{H}\}$ NMR (DMSO- d_6 , 100.63 MHz, 25°C, TMS) δ /ppm: 166.1 (1C, C- NO_2), 158.5 (1C, C(NH_2) $_3^+$), 155.0 (1C, C-Tz), 50.4 (1C, CH_2); ^{14}N NMR (DMSO- d_6 , 28.92 MHz, 25 °C, MeNO_2) δ /ppm: -33 (1N, $\Delta\nu_{1/2} \sim 150$ Hz, NO_2), -94 (1N, $\Delta\nu_{1/2} \sim 850$ Hz, N2); ^{15}N NMR (DMSO- d_6 , 40.50 MHz, 25 °C, MeNO_2) δ /ppm: 4.9 (2N, s, N7/N8), 4.5 (1N, t, $^3J_{\text{NH}} = 1.86$ Hz, N4), -35.4 (1N, s, NO_2), -56.3 (1N, s, N5), -64.4 (2N, s, N6/N9), -78.9 (1N, t, $^3J_{\text{NH}} = 1.86$ Hz, N2), -92.8 (1N, t, $^2J_{\text{NH}} = 1.86$ Hz, N3), -306.7 (2N, t, $^1J_{\text{NH}} = 91.14$ Hz, $=\text{NH}_2^+$); $^{15}\text{N}\{^1\text{H}\}$ NMR (DMSO- d_6 , 40.30 MHz, 25 °C, MeNO_2) 5.6 (2N, s, N7/N8), 5.3 (1N, N4), -34.6(1N, NO_2), -55.5 (1N, N5), -63.6 (2N, N6/N9), -78.1 (1N, N2), -92.0 (1N, N3), -305.9 (2N, $=\text{NH}_2^+$); Raman $\tilde{\nu}$ / cm^{-1} (rel. int.) 3427(2) 3326(1) 3030(3) 2974(5) 2549(1) 1563(5) 1487(7) 1422(13) 1361(3) 1322(2) 1298(3) 1221(3) 1192(4) 1128(4) 1099(2) 1072(3) 1056(4) 1035(15) 1010(8) 845(2) 825(3) 774(3) 683(2) 526(4) 450(2) 375(3) 350(4) 314(2) 285(3) 207(4); IR $\tilde{\nu}$ / cm^{-1} (KBr, rel. int.): 3443(s) 3153(m) 3029(m) 2880(w) 2222(w) 1647(s) 1562(s) 1486(m) 1434(w) 1421(m) 1384(w) 1360(w) 1336(w) 1327(m) 1297(w) 1219(w) 1191(w) 1123(m) 1098(m) 1071(m) 1054(m) 1034(m) 939(w) 846(m) 824(w) 759(m) 735(w) 705(w) 683(w) 658(w) 569(w) 542(w) 513(w) 469(w)

Synthesis of Aminoguanidinium 5-(5-Nitrotetrazole-2-ylmethyl)-tetrazolate (138): 129a (0.171 g, 0.82 mmol) was suspended in 5 mL water and reacted with aminoguanidinium bicarbonate (0.109 g, 0.82 mmol). The slightly yellow solution was left to evaporate to dryness giving the pure compound as brownish feathery material (0.207 g, 93%). Crystals suitable for X-ray analysis were obtained when ether was left to slowly diffuse into a saturated solution of the compound in methanol. $\text{C}_4\text{H}_9\text{N}_{13}\text{O}_2$ (271.20 g mol^{-1} , calc./found): C 17.71 / 17.72, H 3.36 / 3.59, N 67.15 / 67.43; DSC (5 °C min^{-1} , °C): 128 (m.p.), 201 (dec.);

m/z (FAB⁻, xenon, 6 keV, m-NBA matrix) 271.0 ([138-H⁺]), 196.0 (NTTz⁻), 114.0 (NT⁻); m/z (FAB⁺, xenon, 6 keV, m-NBA matrix) 346.2 (AG₂NTTz⁺), 75.1 (AG⁺); ¹H NMR (DMSO-*d*₆, 400.18 MHz, 25°C, TMS) δ/ppm: 8.68 (1H, s, NH), 7.31 (2H, s, C=NH₂⁺), 6.90 (2H, s, C-NH₂), 6.17 (2H, s, CH₂), 4.70 (2H, s, N-NH₂); ¹³C{¹H} NMR (DMSO-*d*₆, 100.63 MHz, 25°C, TMS) δ/ppm: 165.4 (1C, C-NO₂), 158.5 (1C, C(NH₂)₂⁺(NH-NH₂)), 154.0 (1C, C-Tz), 50.3 (1C, CH₂); ¹⁴N NMR (DMSO-*d*₆, 28.92 MHz, 25 °C, MeNO₂) δ/ppm: -34 (1N, Δ*v*_{1/2} ~ 160 Hz, NO₂), -94 (1N, Δ*v*_{1/2} ~ 800 Hz, N₂); Raman $\tilde{\nu}$ / cm⁻¹ (rel. int.) 3281(6) 3024(4) 2978(6) 2913(4) 2125(8) 1555(27) 1473(44) 1419(47) 1346(32) 1197(37) 1147(35) 1105(39) 1068(42) 1030(56) 969(42) 843(39) 818(38) 763(39) 685(37) 553(35) 340(29) 304(27) 87(3); IR $\tilde{\nu}$ / cm⁻¹ (KBr, rel. int.): 3597(m) 3427(s) 3371(s) 3342(s) 3283(s) 3177(s) 3023(s) 2886(m) 2408(w) 2243(w) 2196(w) 1675(s) 1593(m) 1554(s) 1488(m) 1473(m) 1439(m) 1418(s) 1385(w) 1367(w) 1349(m) 1329(s) 1320(m) 1312(m) 1277(w) 1246(w) 1209(m) 1196(m) 1145(m) 1117(m) 1104(m) 1085(m) 1068(m) 1029(m) 981(m) 945(m) 849(s) 840(m) 819(m) 785(w) 758(w) 703(m) 685(m) 656(m) 630(m) 613(m) 547(m) 463(m).

Synthesis of Silver 5-(5-Nitrotetrazole-2-ylmethyl)-tetrazolate Hemihydrate (141): 129a (0.200 g, 0.93 mmol) was suspended in 5 mL water and reacted with sodium bicarbonate (0.078 g, 0.93 mmol) at room temperature until all solids had dissolved and no further gas evolution was observed. The slightly yellow solution was added drop-wise to a previously prepared solution of silver nitrate (0.157 g, 0.93 mmol) in 10 mL water producing the immediate precipitation of a white (**highly sensitive!!**) powder. The precipitate was carefully filtered, washed with methanol and left to air-dry. C₃H₃N₉O_{2.5}Ag (312.98 g mol⁻¹, calc./found): C 11.51 / 11.20, H 0.97 / 0.84, N 40.27 / 38.28; DSC (5 °C min⁻¹, °C): 92 (H₂O), 193 (dec.); Raman $\tilde{\nu}$ / cm⁻¹ (rel. int.) 3427(0) 1564(2) 1483(6) 1413(10) 1311(3) 1219(5) 1090(4) 1028(7) 774(3) 681(2) 542(3) 372(2); IR $\tilde{\nu}$ / cm⁻¹ (KBr, rel. int.): 3399(m) 3072(m) 3015(m) 2964(m) 2676(m) 2563(m) 2089(w) 1971(w) 1915(w) 1688(s) 1602(m) 1583(m) 1567(s) 1558(s) 1492(w) 1478(w) 1453(m) 1422(s) 1384(m) 1323(s) 1293(s) 1187(w) 1128(w) 1100(w) 1072(m) 1044(w) 1027(m) 1000(w) 935(m) 845(m) 811(w) 759(w) 707(s) 684(m) 668(m) 554(w) 354(w) 335(w) 308(w) 302(w).

Synthesis of Copper Di-5-(5-nitrotetrazole-2-ylmethyl)-tetrazolate Monohydrate (142): 129a (0.200 g, 0.93 mmol) and sodium bicarbonate (0.078 g, 0.93 mmol) were suspended in 5 mL water and reacted for 30 min at room temperature until the insoluble solids had dissolved (carbon dioxide evolution could be observed). The slightly yellow solution was carefully added to a second solution containing copper(II) nitrate trihydrate (0.104 g, 0.43 mmol) in 10 mL water, producing the immediate precipitation of a blue solid. The suspension was then refluxed for 1 h resulting in the blue precipitate to turn purple. At this point the purple solid was filtered, washed with ethanol and left to air-dry (0.145 g, 72%). C₆H₆N₁₈O₅Cu (473.00 g mol⁻¹, calc./found): C 15.22 / 14.97, H 1.28 / 1.15, N 53.29 / 52.67; DSC (5 °C min⁻¹, °C): ~90 (H₂O), 250 (dec.); m/z (DEI⁺, xenon, 6 keV, m-NBA matrix) 197.3 (NTTz, neutral); Raman $\tilde{\nu}$ / cm⁻¹ (rel. int.) 3424(1) 3036(4) 2978(8) 1565(23) 1503(23) 1473(28) 1415(41) 1359(26) 1310(26) 1239(26) 1215(27) 1125(27) 1069(26) 1030(40) 840(26) 814(27) 775(27) 544(20) 454(22); IR $\tilde{\nu}$ / cm⁻¹ (KBr, rel. int.): 3636(vw) 3434(m) 3035(m) 2975(m) 1731(w) 1638(w) 1563(s) 1502(w) 1481(m) 1473(w) 1433(m) 1416(m) 1384(w) 1355(w)

1319(m) 1262(w) 1212(w) 1176(w) 1154(w) 1094(m) 1068(m) 1034(m) 953(w) 841(s) 803(m) 754(m) 728(vw) 703(w) 686(w) 659(w) 544(vw) 466(w).

Synthesis of Copper(II) Sodium Di-5-(5-nitrotetrazole-2-ylmethyl)-tetrazolate Nitrate Monohydrate (143): A suspension of **129a** (0.200 g, 0.93 mmol) and sodium bicarbonate (0.078 g, 0.93 mmol) in 10 mL ethanol was carefully heated (under gas evolution) to form a clear yellowish solution. This solution was added dropwise to a second solution containing copper(II) nitrate trihydrate (0.104 g, 0.43 mmol) in 10 mL ethanol, producing the precipitation of a blue compound, which was immediately filtered, washed with fresh ethanol and left to air-dry (0.195 g, 79 %). $C_6H_6N_{19}O_8CuNa$ (558.77 g mol⁻¹, calc./found): C 12.90 / 12.83, H 1.08 / 1.26, N 47.64 / 47.51

Synthesis of Copper(II) Sodium Di-5-(5-nitrotetrazole-2-ylmethyl)-tetrazolate Nitrate (144): **129a** (0.200 g, 0.93 mmol) and sodium bicarbonate (0.078 g, 0.93 mmol) were suspended in 10 mL ethanol and heated until all solids had dissolved. The resulting solution was added drop-wise to a previously prepared solution of copper(II) nitrate trihydrate (0.104 g, 0.43 mmol) in 10 mL ethanol and the resulting suspension was refluxed for 1 h. The initially blue precipitate turned purple and this was filtered, washed with ethanol and air-dried (0.180 g, 76%). $C_6H_4N_{19}O_7CuNa$ (calc./found): C 13.32 / 13.06, H 0.75 / 0.93, N 49.21 / 48.99; IR $\tilde{\nu}$ / cm⁻¹ (KBr, rel. int.) 3435(m) 3037(w) 2974(w) 2868(w) 1628(w) 1557(s) 1502(w) 1481(w) 1414(s) 1384(s) 1320(s) 1243(w) 1215(w) 1133(w) 1069(w) 1032(w) 952(w) 841(s) 798(w) 783(w) 760(w) 703(w) 668(w) 540(w) 473(w).

Synthesis of 2-(2-Bromoethyl)-5-nitrotetrazolate (145): **21a** (1.037 g, 7.35 mmol) was dissolved in 4.4 mL DMF and reacted with 1,2-dibromoethane (2.764 g, 14.70 mmol). The colorless reaction mixture was heated to 80 °C for 4 h producing the precipitation of a colorless solid. After cooling the suspension was added to 20 mL of ice-cold water and the precipitate was filtered and washed with ice-cold water (3 x 10 mL) and ethanol (10 mL). After air-drying the compound was obtained as a colorless solid (0.652 g, 40%). $C_3H_4N_5O_2Br$ (222.00 g mol⁻¹, calc./found): C 16.23 / 15.92, H 1.82 / 1.52, N 31.54 / 31.45; DSC (5 °C min⁻¹, °C): 105 (m.p.), 206 (dec.); m/z (DCI⁺, Iso-butane): 222.0 (145, neutral); ¹H NMR (DMSO-*d*₆, 400.18 MHz, 25 °C, TMS) δ /ppm: 5.33 (2H, t, ³J_{HH} = 5.72 Hz, CH₂), 4.07 (2H, t, ³J_{HH} = 5.72 Hz, CH₂ Br); ¹³C{¹H} NMR (DMSO-*d*₆, 100.52 MHz, 25 °C, TMS) δ /ppm: 166.0 (1C, C-NO₂), 56.1 (1C, CH₂), 29.1 (1C, CH₂Br); ¹⁴N NMR (DMSO-*d*₆, 28.91 MHz, 25 °C, MeNO₂) δ /ppm: -34 (1N, $\Delta\nu_{1/2}$ ~ 90 Hz, NO₂), -93 (1N, $\Delta\nu_{1/2}$ ~ 480 Hz, N₂); Raman $\tilde{\nu}$ / cm⁻¹ (rel. int.) 3034(11) 3020(20) 2977(34) 2956(35) 1559(15) 1483(25) 1437(41) 1419(75) 1371(7) 1322(8) 1297(7) 1254(13) 1226(8) 1193(24) 1117(10) 1070(8) 1032(54) 958(4) 882(4) 838(5) 774(8) 687(3) 578(51) 540(7) 471(10) 424(16) 354(9) 276(16) 244(10) 172(4); IR $\tilde{\nu}$ / cm⁻¹ 3033(m) 3019(m) 2976(w) 2955(w) 2874(w) 2839(w) 2805(vw) 2734(w) 2679(vw) 2548(w) 2483(w) 2441(w) 2392(w) 2379(w) 2304(w) 2257(w) 2227(w) 2136(w) 1860(w) 1839(w) 1609(w) 1558(vs) 1493(m) 1483(s) 1473(m) 1458(w) 1437(vs) 1426(s) 1420(s) 1403(m) 1390(w) 1374(m) 1355(m) 1345(m) 1328(s) 1298(s) 1255(s) 1225(m) 1192(m) 1116(w) 1070(s) 1031(s) 957(s) 881(s) 847(s) 838(s) 773(w) 701(w) 685(m) 661(s) 577(s) 539(m) 469(s).

9.10 References

- [1] a) T. L. Brown, H. E. Lemay, B. E. Bursten in *Chemistry: The Central Science*, New Jersey: Prentice Hall, 2000. b) A. F. Kapustinskii, *Z. Phys. Chem.* **1933**, B22, 257. c) A. F. Kapustinskii, *Zhur. Fiz. Khim.* **1943**, 5, 59. c) A. F. Kapustinskii in *Lattice energy of ionic crystals. Quart. Rev. Chem. Soc.* **1956**, 10, 283–294.
- [2] G. I. Koldobskii, D. S. Soldatenko, E. S. Gerasimova, N. R. Khokhryakova, M. B. Shcherbinin, V. P. Lebedev and V. A. Obstrovskii, *Rus. J. Org. Chem.*, **1997**, 33(12), 1771-1783.
- [3] T. M. Klapötke, C. Miró Sabaté, J. M. Welch, *J. Chem. Soc. Dalton. Trans.* **2008**, manuscript in preparation.
- [4] T. M. Klapötke, P. Mayer, C. Miró Sabaté, J. M. Welch, N. Wiegand, *Inorg. Chem.* **2008**, ASAP.
- [5] C. Darwich, K. Karagiosoff, T. M. Klapötke, C. Miró Sabaté, *Z. Anorg. Allg. Chem.* **2008**, 634, 61-68.
- [6] T. M. Klapötke, C. Miró Sabaté, *Z. Anorg. Allg. Chem.* **2008**, manuscript in preparation.
- [7] H. Xue, H. Gao, B. Twamley, J. M. Shreeve, *Chem. Mater.* **2007**, 19, 1731-1739.
- [8] a) T. M. Klapötke, C. Miró Sabaté, A. Penger, M. Rusan, J. M. Welch, *Chem. Eur. J.* **2008**, manuscript in preparation. b) J. H. Bryden, *Acta Crystallogr.* **1956**, 9, 874-878.
- [9] W. Bocian, J. Jazwinski, W. Kozminski, L. Stefaniak, G. A. Webb, *J. Chem. Soc. Perkin Trans. 2*, **1994**, 6, 1327-1332.
- [10] a) K. Karagiosoff, T. M. Klapötke, P. Mayer, C. Miró Sabaté, A. Penger, J. M. Welch, *Inorg. Chem.* **2008**, 47, 1007-1019. b) C. Darwich, T. M. Klapötke, C. Miró Sabaté, *Chem. Eur. J.* **2008**, ASAP.
- [11] J. C. Gálvez-Ruiz, G. Holl, K. Karagiosoff, T. M. Klapötke, K. Löhnwitz, P. Mayer, H. Nöth, K. Polborn, C. J. Rohbogner, M. Suter, J. J. Weigand, *Inorg. Chem.* **2005**, 44(12), 4237 - 4253.
- [12] a) T. M. Klapötke, C. Miró Sabaté, *Z. Anorg. Allg. Chem.* **2008**, 634, 1017-1024. b) T. M. Klapötke, C. Miró Sabaté, *Chem. Mater.* **2008**, 20(5), 1750-1763.
- [13] Gaussian 03, Revision A.1: M. J. Frisch, G. W. Trucks, H. B. Schlegel, G. E. Scuseria, M. A. Robb, J. R. Cheeseman, J. A. Montgomery, T. Jr. Vreven, K. N. Kudin, J. C. Burant, J. M. Millam, S. S. Iyengar, J. Tomasi, V. Barone, B. Mennucci, M. Cossi, G. Scalmani, N. Rega, G. A. Petersson, H. Nakatsuji, M. Hada, M. Ehara, K. Toyota, R. Fukuda, J. Hasegawa, M. Ishida, T. Nakajima, Y. Honda, O. Kitao, H. Nakai, M. Klene, X. Li, J. E. Knox, H. P. Hratchian, J. B. Cross, C. Adamo, J. Jaramillo, R. Gomperts, R. E. Stratmann, O. Yazyev, A. J. Austin, R. Cammi, C. Pomelli, J. W. Ochterski, P. Y. Ayala, K. Morokuma, G. A. Voth, P. Salvador, J. J. Dannenberg, V. G. Zakrzewski, S. Dapprich, A. D. Daniels, M. C. Strain, O. Farkas, D. K. Malick, A. D. Rabuck, K. Raghavachari, J. B. Foresman, J. V. Ortiz, Q. Cui, A. G. Baboul, S. Clifford, J. Cioslowski, B. B. Stefanov, G. Liu, A. Liashenko, P. Piskorz, I. Komaromi, R. L. Martin, D. J. Fox, T. Keith, M. A. Al-Laham, C. Y. Peng, A. Nanayakkara, M. Challacombe, P. M. W. Gill, B. Johnson, W. Chen, M. W. Wong, C. Gonzalez, J. A. Pople, Gaussian, Inc. Pittsburgh PA, 2004.
- [14] B. Michlich, A. Savin, H. Stoll, H. Preuss, *Chem. Phys. Lett.* **1989**, 157, 200-206.

- [15] A. P. Scott, L. Radom, *J. Phys. Chem.* **1996**, *100*, 16502-16513.
- [16] a) G. M. Sheldrick, *Programs for Crystal Structure Analysis (Release 97-2)*, Goettingen, Germany, 1998. b) A. Altomare, M. C. Burla, M. Camalli, G. L. Cascarano, C. Giacovazzo, A. Guagliardi, A. G. G. Moliterni, G. Polidori, R. Spagna, *J. Appl. Crystallogr.*, **1999**, *32*, 115-119.
- [17] a) G. F. Holland, J. N. Pereira, *J. Med. Chem.* **1967**, *10*(2), 149-154. b) M. Prhac, J. Kobe, *Tetrahedron Lett.* **1990**, *31*(13), 1925-1928. c) W. Holzer, J. C. Jäger, *Monats. Chem.* **1992**, *123*(11), 1027-1036. d) A. Schmidpeter, G. Jochem, *Z. Naturforsch.* **1993**, *B48*(1), 93-97. e) J. Boivin, E. B. Henriët, S. Z. Zard, *J. Am. Chem. Soc.* **1994**, *116*(21), 9739-9740. f) J. Boivin, E. B. Henriët, S. Z. Zard, Rhone-Poulenc Chimie SA, EP 685,442 **1995**. g) I. P. Beletskaya, D. V. Davydov, M. S. Gorovoy, *Tetrahedron Lett.* **2002**, *43*(35), 6221-6223. h) M. V. Reinov, M. A. Yurovskaya, D. V. Davydov, A. V. Streletskii, *Chem. Heterocycl. Compd.* **2004**, *40*(2), 188-193. i) T. Zhou, Z. C. Chen, *J. Chem. Res.* **2004**, *6*, 404-405. j) M. D. Cullen, B. L. Deng, T. L. Hartman, K. M. Watson, R. W. Jr. Buckheit, C. Pannecouque, E. De Clercq, M. Cushman, *J. Med. Chem.* **2007**, *50*(20), 4854-4867. k) W. Zhang, F. Zhao, T. Liu, M. Yuan, Z. M. Wang, S. Gao, *Inorg. Chem.* **2007**, *46*(7), 2541-2555.
- [18] a) S. Bernhardt, M. J. Crawford, T. M. Klapötke, H. Radies, H. *Proceed. 10th New Trends Res. Energ. Mater. Sem.*, Pardubice, Czech Republic, Apr. 25-27, University of Pardubice, **2007**, *2*, 532-540. b) E. O. John, R. D. Willett, R. L. Scott, R. L. Kirchmeier, J. M. Shreeve, *Inorg. Chem.* **1989**, *28*, 893-897. c) T. M. Becker, J. A. Krause-Bauer, C. L. Homrighausen, M. Orchin, *Polyhedron* **1999**, *18*, 2563-2571.
- [19] a) H. P. H. Arp, A. Decken, J. Passmore, D. J. Wood, *Inorg. Chem.* **2000**, *39*, 1840-1848. b) E. J. Graeber, B. Morosin, *Acta Crystallogr.* **1983**, *C39*, 567-570.
- [20] A. F. Holleman, E. Wiberg, N. Wiberg in *Lehrbuch der Anorganischen Chemie*, 101 Auflage, (Eds.: Walter de Gruyter), Berlin, Germany, 1995.
- [21] A. Bondi, *J. Phys. Chem.* **1964**, *68*(3), 441-451.
- [22] M. Göbel, T. M. Klapötke, P. C. Thumbs, *Proceed. 9th New Trends Res. Energ. Mater. Sem.*, Pardubice, Czech Republic, Apr. 19-21, University of Pardubice, **2007**, *1*, 127-134. b) M. Göbel, T. M. Klapötke, *Z. Anorg. Allg. Chem.* **2007**, *633*, 1006 - 1017.
- [23] M. Göbel, K. Karaghiosoff, T. M. Klapötke, *Angew. Chem.* **2006**, *118*(36), 6183-6186; *Intl. Ed.* **2006**, *45*, 6037 - 6040.
- [24] M. A. Hiskey, A. Hammerl, G. Holl, T. M. Klapötke, K. Polborn, J. Stiersdorfer, J. J. Weigand, *Chem. Mater.*, **2005**, *17*, 3784 - 3793.
- [25] T. M. Klapötke, C. Miró Sabaté, *Chem. Mater.*, **2008**, *20*(11), 3629-3637.
- [26] T. M. Klapötke, C. Miró Sabaté, *Z. Anorg. Allg. Chem.* **2007**, *633*, 2671-2677.
- [27] D. D. Bray, J. G. White, *Acta Crystallogr.* **1979**, *B35*, 3089-3091.
- [28] J. Stierstorfer, T. M. Klapötke, A. Hammerl, R. D. Chapman, *Z. Anorg. Allg. Chem.* **2008**, *634*(6-7), 1051-1057.

- [29] T. M. Klapötke, C. Miró Sabaté, J. Stierstorfer, *Chem. Commun.* **2008**, manuscript in preparation.
- [30] J. Bernstein, R. E. Davis, L. Shimoni and N.-L. Chang, *Angew. Chem. Int. Ed. Engl.*, **1995**, *34*, 1555-1573.
- [31] RPLUTO, Cambridge Crystallographic Data Centre, Cambridge, UK, 2000, <http://www.ccdc.cam.ac.uk/prods/rputo>.
- [32] J. A. Pople, R. Seeger, R. Krishnan, *Int. J. Quantum Chem., Symp.* **1977**, *11*, 149-163.
- [33] a) A. K. Rick, T. H. Dunning, J. H. Robert, *J. Chem. Phys.* **1992**, *96*, 6796-6806. b) A. O. Kirk, E. W. David, T. H. Dunning, *J. Chem. Phys.* **1994**, *100*, 7410-7415.
- [34] a) H. D. B. Jenkins, D. Tudela, L. Glasser, *Inorg. Chem.* **2002**, *41*, 2364-2367. b) H. D. B. Jenkins, H. K. Roobottom, J. Passmore, L. Glasser, *Inorg. Chem.* **1999**, *38*, 3609-3620.
- [35] H. Gao, C. Ye, C. M. Piekarski, J. M. Shreeve, *J. Phys. Chem.* **2007**, *C111*, 10718-10731.
- [36] M. Suceca, *Propellants, Explos., Pyrotech.* **1991**, *16*, 197-202.
- [37] a) H. Xue, J. M. Shreeve, *Adv. Mater.* **2005**, *17*, 2142-2146. b) H. Xue, B. Twamley, J. M. Shreeve, *Inorg. Chem.* **2005**, *44*, 7009-7013.
- [38] a) L. D. Redman, R. J. Spear, Report MRL-R-901; Materials Research Laboratory: Australia, 1983; 1-27. b) W. H. Gilligan, M. J. Kamlet, Report NSWC/WOL/TR 76-146; White Oak Laboratory: Silver Spring, MD, USA, 1976; 1-15.
- [39] a) H. Xue, H. Gao, B. Twamley, J. M. Shreeve, *Eur. J. Inorg. Chem.* **2006**, *15*, 2959-2965. b) H. Xue, Y. Gao, B. Twamley, J. M. Shreeve, *Inorg. Chem.* **2005**, *44*, 5068-5072. c) X. Jin, M. Shao, H. Huang, J. Wang, Y. Zhu, *Huaxue Tongbao* **1982**, 336-337. d) M. B. Talawar, J. S. Chhabra, A. P. Agrawal, S. N. Asthana, K. U. B. Rao, H. Singh, *J. Hazard. Mater.* **2004**, *113*, 27-33.
- [40] V. Ernst, T. M. Klapötke, J. Stierstorfer, *Z. Anorg. Allg. Chem.* **2007**, *633*, 879-887.
- [41] A. Hammerl, G. Holl, M. Kaiser, T. M. Klapötke, P. Mayer, H. Nöth, H. Piotrowski, M. Warchhold, *Eur. J. Inorg. Chem.* **2002**, 834 - 845.
- [42] Oxygen balance for a compound with the formula $C_xH_yO_zM_t$: $\Omega(\%) = -1600/MW (2x + y/2 + t - z)$; M = metal and MW = molecular weight.
- [43] J. Köhler and R. Mayer, in *Explosivstoffe*, ed. Wiley-VCH, Weinheim, Germany, 9th edn., 1998.
- [44] A. Hammerl, T. M. Klapötke, H. Nöth, M. Warchhold, G. Holl, *Propellants, Explos., Pyrotech.*, **2003**, *28(4)*, 165-173.
- [45] A. K. Sikder, N. Sikder, *J. Hazard. Mater.* **2004**, *A112*, 1-15 and references therein.
- [46] Impact: Insensitive >40 J, less sensitive ≥ 35 J, sensitive ≥ 4 J, very sensitive ≤ 3 J; friction: Insensitive >360 N, less sensitive = 360 N, sensitive <360 N a. >80 N, very sensitive ≤ 80 N, extreme sensitive ≤ 10 N;

According to the UN Recommendations on the Transport of Dangerous Goods (+) indicates: not safe for transport.

[47] <http://www.bam.de>.

[48] T. M. Klapötke and C. M. Rienäcker, *Propellants, Explos., Pyrotech.* **2001**, 26, 43-47.

[49] NIST Chemistry WebBook, NIST Standard Reference Database Number 69 - March, **2003** Release, www version: <http://webbook.nist.gov/chemistry>.

[50] a) A. Hammerl, T. M. Klapötke, H. Nöth and M. Warchhold, G. Holl, M. Kaiser, *Inorg. Chem.* **2001**, 40, 3570 - 3575. b) G. Holl, T. M. Klapötke, J. J. Weigand, DE 014,044 **2004**.

[51] C. Darwich, T. M. Klapötke, J. M. Welch, M. Suceca, *Propellants, Explos., Pyrotech.* **2007**, 32, 235-243.

[52] P. N. Gaponik, O. A. Ivashkevich, V. A. Krasitskii, A. A. Tuzik, A. I. Lesnikovich, *Russ. J. Gen. Chem.* **2002**, 72, 1457-1462.

[53] H. Gao, C. Ye, C. M. Piekarski, J. M. Shreeve, *J. Phys. Chem.* **2007**, C111, 10718-10731.

[54] a) *ICT-Thermodynamic Code, Version 1.0*, Fraunhofer-Institut für Chemische Technologie (ICT): Pfinztal/Berghausen, Germany, 1988–2000. b) R. Webb, M. van Rooijen, *Proceed. 29th Int. Pyrotech. Sem.*, Westminster, CO, July 14-19, 2002; International Pyrotechnics Society, **2002**, 823–828. c) H. Bathelt, F. Volk, *27th Int. Ann. Conf. ICT*, **1996**, 92, 1–16.

[55] <http://www.perkinelmer.com>.

[56] http://www.linseis.net/html_en/thermal/dsc/dsc_pt10.php.

[57] <http://www.jeol.co.kr>.

[58] <http://www.parrinst.com>.

Table 3.A1 Calculated (ν_{calc}) and measured (ν_{meas}) IR and Raman frequencies with tentative assignment for the NT⁻ anion.

	ν_{calc} (cm ⁻¹) ^a	ν_{meas} (cm ⁻¹) ^b (IR / Raman)	Mode Assignment ^c
1	1538	1540 / 1540	$\nu_{\text{asym}}(\text{NO}_2)$
2	1396	1440 / n.o.	$\nu_{\text{asym}}(\text{N1-C-N4})$
3	1383	1420 / 1420	$\nu_{\text{sym}}(\text{NO}_2) + \nu_{\text{sym}}(\text{N1-C-N4})$, “in phase”
4	1294	1320 / 1320	$\nu_{\text{sym}}(\text{NO}_2) + \nu_{\text{sym}}(\text{N1-C-N4})$, “out of phase”
5	1182	1170 / 1160	$\nu_{\text{asym}}(\text{ring})$
6	1163	1160 / n.o.	$\nu_{\text{sym}}(\text{ring}) + \nu_{\text{sym}}(\text{NO}_2)$, “in phase”
7	1024	1050 / 1060	$\delta(\text{N1-C-N4}) + \nu_{\text{sym}}(\text{NO}_2)$, “in phase”
8	1018	1025 / 1030	$\delta_{\text{asym}}(\text{ring})$
9	821	840 / 840	$\delta(\text{NO}_2) + \delta(\text{N1-C-N4})$, “in phase”
10	763	770 / 770	$\gamma(\text{NO}_2) + \gamma(\text{N1-C-N4})$, “out of phase”
11	718	730 / 730	$\gamma(\text{ring})$ “in phase”
12	664	675 / n.o.	$\gamma(\text{ring})$ “out of phase”
13	522	530 / 540	$\omega(\text{NO}_2) + \omega(\text{ring})$, “out of phase”
14	439	470 / n.o.	$\nu(\text{C-N5}) + \delta(\text{NO}_2)$
15	242	n.o. / 250	$\omega(\text{NO}_2) + \omega(\text{ring})$, “in phase”
16	218	n.o. / 230	$\gamma(\text{N1-C-N4})$

^a Calculated frequencies according to reference [49]. ^b Measured frequencies, average values from IR and Raman spectra of alkali metal salts of 5-nitro-2*H*-tetrazole, n.o. not observed. ^c Approximate description of vibrational modes: ν = stretching, δ = in-plane bending, γ = out-of-plane bending, ω = in plane rocking (see X-ray discussion for labeling scheme).

Computational Methods

Table 3.A2 CBS-4M results.

	p.g.	$-H^{298}$ / a.u.	$-G^{298}$ / a.u.	NIMAG
5-nitro-1 <i>H</i> -tetrazole	C_s	462.190261	462.227578	0
5-nitro-2 <i>H</i> -tetrazole	C_s	462.195276	462.232789	0
H		0.500991	0.514005	0
C		37.786156	37.803062	0
N		54.522462	54.539858	0
O		74.991202	75.008515	0

Table 3.A3 Literature values for atomic $\Delta H_f^{\circ 298}$ / kcal mol⁻¹

	Ref. [53]	NIST ^[54]
H	52.6	52.1
C	170.2	171.3
N	113.5	113.0
O	60.0	59.6

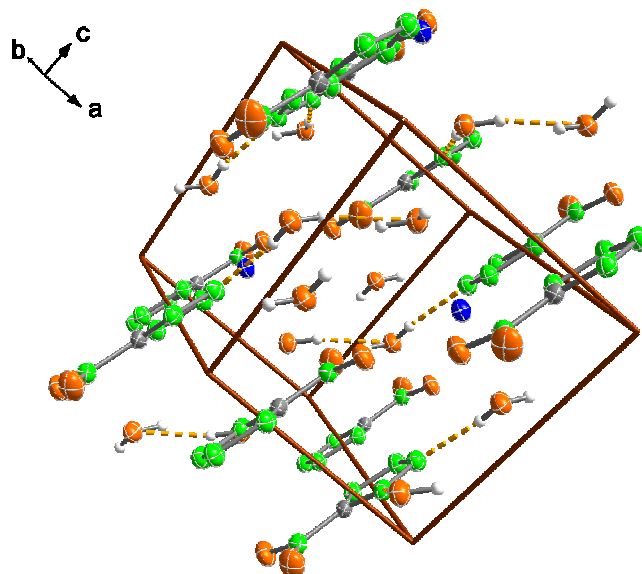
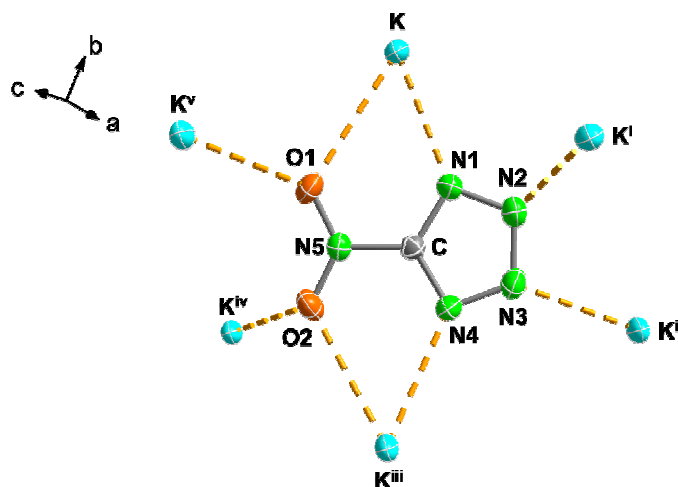
Table 3.A4 Enthalpies ($\Delta_f H^\circ$) of the gas-phase species M and enthalpy of sublimation (ΔH_{sub}) of 5-nitro-2*H*-tetrazole (**31**).^[55]

M	M	$\Delta_f H^\circ(\text{g,M}) / \text{kcal mol}^{-1}$	T_m / K	$\Delta H_{\text{sub}} / \text{kcal mol}^{-1}$
5-nitro-1 <i>H</i> -tetrazole	CHN ₅ O ₂	+87.1	-	-
5-nitro-2 <i>H</i> -tetrazole	CHN ₅ O ₂	+84.0	374	16.8

Table 3.A5 Solid state energy ($\Delta_f U^\circ$) and enthalpy ($\Delta_f H^\circ$) of formation of 5-nitro-2*H*-tetrazole (**31**).

	$\Delta_f H^\circ(\text{s}) / \text{kcal mol}^{-1}$	Δn	$\Delta_f U^\circ(\text{s}) / \text{kcal mol}^{-1}$	M / g mol ⁻¹	$\Delta_f U^\circ(\text{s}) / \text{kJ kg}^{-1}$	$\Delta_f H^\circ(\text{s,M}) / \text{kcal mol}^{-1}$
31	+67.2	-4	+69.5	115.07	+2527.1	+67.2

$$\Delta U_m = \Delta H_m - \Delta n RT \quad (\Delta n \text{ being the change of moles of gaseous components})$$

**Figure 3.A1** View of the unit cell of **23** showing the hydrogen-bonding (symmetry codes: (ii) 2-x, 1-y, 2-z; (iii) 1-x, -y, 2-z; (vii) 1-x, 1-y, 1-z; (viii) 2-x, 1-y, 1-z).**Figure 3.A2** Packing around the anion in the crystal structure of **24** with the numbering scheme (symmetry codes: (i) 1+x, y, z; (ii) 1+x, 0.5-y, -0.5+z; (iii) 1-x, -0.5+y, 0.5-z; (iv) -x, -0.5+y, 0.5-z; (v) x, 0.5-y, 0.5+z).

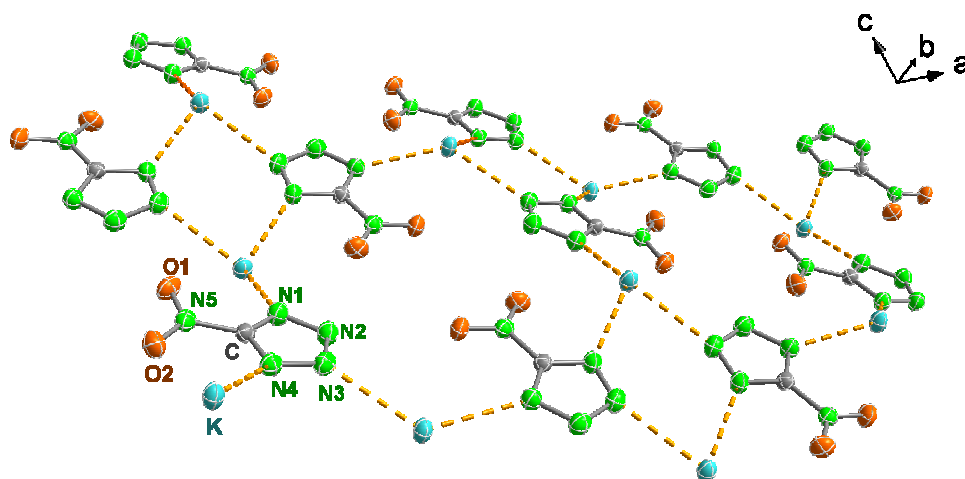


Figure 3.A3 View of a “layer” in the crystal structure of **24** showing the contacts between the anions and the K^+ cations (the contacts to the oxygen atoms have been ignored for the sake of simplicity).

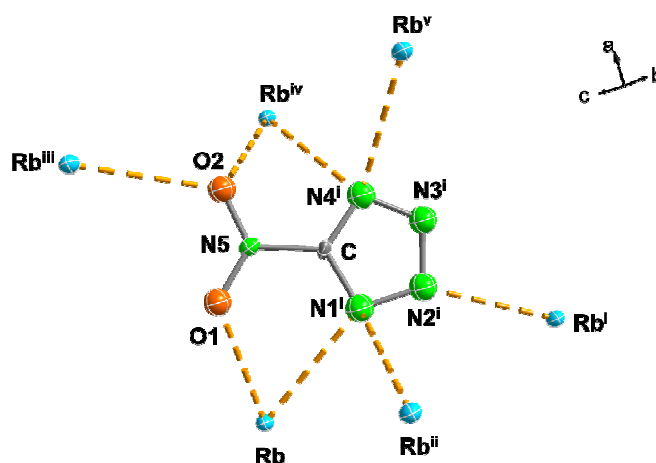


Figure 3.A4 Packing around the anion in the crystal structure of **25** with the numbering scheme (symmetry codes: (i) $x, 1-y, -0.5+z$; (ii) $x, -y, -0.5+z$; (iii) $0.5+x, -0.5+y, z$; (iv) $0.5+x, 0.5+y, z$; (v) $0.5+x, 0.5-y, -0.5+z$).

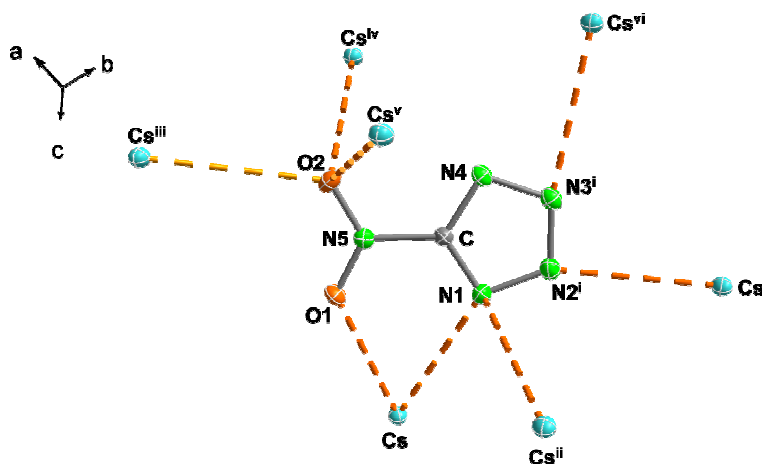


Figure 3.A5 Packing around the anion in the crystal structure of **26** with the numbering scheme (symmetry codes: (i) $-x, 1+y, 0.5-z$; (ii) $-x, y, 0.5-z$; (iii) $0.5-x, -0.5+y, 0.5-z$; (iv) $0.5-x, 0.5+y, 0.5-z$; (v) $x, 2-y, -0.5+z$; (vi) $x, 3-y, -0.5+z$).

Table 4.A1 Calculated (C_1 point group) and observed (IR and Raman) frequencies ($250\text{ cm}^{-1} > \nu > 2000\text{ cm}^{-1}$) with assignment.

42	43	44	45a	46a	47	B3LYP (IR/Ra) ^[a]	Assignment ^[b]
	289 w, 303 w / 304(18)	302 w / 306(16)	285 w, 296 w / -			294 (12/1)	$\omega(\text{N-NH}_2)$
- / 357(18)	350 m / -	350 w / 332(13)	360 w / 333(2)		- / 338(20)	342 (13/3)	$\omega(\text{N-NH}_2)$ $\delta(\text{C-NH}_2)$
	548 m / -		558 w / -	- / 538(6)		549 (29/1)	$\delta(\text{C-NH}_2)$
587 w / 590(12)	586 m / 589(15)	587 w / 588(12)	587 w / 594(2)	588 w / 591 (7)	587 w / 588(11)	587 (231/4)	$\omega(\text{C-NH}_2)$
- / 618(11)	- / 627(25)	626 m / 629(18)		625 w / 623(7)		629 (30/8)	$\omega(\text{C-NH}_2)$ & $\nu(\text{N-C-N})_{\text{ring}}$
649 m / 650(32)		636 w / 651(34)	643 m / 647(2)	- / 647(13)	648 w / 649(31)	655 (10/1)	$\delta(\text{C-N-N})_{\text{ring}}$ & $\omega(\text{C-NH}_2)$
712 w / -	719 m / 716(19)	712 w / -		712 w / -	712 w / -	707 (52/2)	$\delta(\text{C-N-N})_{\text{ring}}$ & $\omega(\text{C-NH}_2)$
			726 w / -			747 (12/17)	$\nu(\text{N-NH}_2)$
777 w / 775(56)	775 m / 775(18)	778 w / 777(48)	774 m / 780(5)	780 w / 782(26)	778 w / 777(48)	794(30/3)	$\delta(\text{N-N-C})_{\text{ring}}$
881 w / 890(8)			872 w / -			866 (150/8)	$\omega(\text{C-NH}_2)$
	- / 916(11)		- / 919(9)		- / 911(7)	929 (95/3)	$\omega(\text{N-NH}_2)$
1022 w / -			1029 w / 1058(23)	1031 w / 1051(31)	1032 m / 1047(11)	1033 (17/4)	$\nu(\text{N-N})_{\text{ring}}$
1099 m / -	1082 m / -	1087 vs / 1084(18) 1144 s / 1134(10)	1078 w / 1084(18) 1157 w / 1160(2)	1101 m / -	1097 w / 1090(3)	1095 (15/1)	$\delta(\text{N-N-C})_{\text{ring}}$
			1192 w / 1160(2)	1173 w / 1162 (10)	1178 s / 1174(10)	1146 (27/4)	$\delta(\text{C-NH}_2)$ & $\nu(\text{N-N})_{\text{ring}}$
1331 w / -	1327 s / -	1332 w / 1334(13)	- / 1348(3)	1343 w / -	1343 w / -	1178 (3/9)	$\delta(\text{C-NH}_2)$
					1431 m /	1331 (2/5)	$\omega(\text{C-NH}_2)$
1423 w / 1417(13)	1423 m / 1425(20)	1424 w / 1426(14)		1444 s / 1447(14) 1545 s /	1421(15), 1437(18)	1434 (31/7)	$\nu(\text{C-N})_{\text{ring}}$ & $\delta(\text{C-NH}_2)$
1536 w / -	1538 m / -		1532 w / -	1546 (15)	1537 m / -	1533 (37/5)	$\nu(\text{C-N})_{\text{ring}}$ & $\nu(\text{N-NH}_2)$
1574 w / -	1578 m / -	- / 1580(10)			- / 1577(9)	1587 (37/3)	$\nu(\text{C-N})_{\text{ring}}$ & $\gamma(\text{C-NH}_2)$
1604 w / -			1592 m / 1615(1)		1613 w / -	1607 (53/6)	$\gamma(\text{C-NH}_2)$
1660 s / -	1656 s / 1652(2)	1658 vs / 1649(11)	1663 s / -	1657 s / 1662(10)	1658 vs / 1649(10)	1656 (217/6)	$\nu(\text{C-NH}_2)$ & $\gamma(\text{C-NH}_2)$
1699 s / 1667(15)						1672 (42/54)	$\nu(\text{C-N})_{\text{ring}}$ & $\nu(\text{C-NH}_2)$
- / 1713(21)	1704 s / 1703(20)	1699 s / 1710(27)	1708 s / 1710(2)	1700 s / 1712(10)	1699 m / 1706(20)	1706 (113/16)	$\gamma(\text{N-NH}_2)$ & $\nu(\text{C-NH}_2)$

[a] calculated IR intensities in km mol^{-1} , [b] calculated Raman scattering activities in $\text{\AA}^4 \text{amu}^{-1}$.

Table 4.A2 Calculated electronic and zero point energies (MP2/aug-cc-pVDZ).

Compound	Formula	p. g. ^[a]	- <i>E</i> / a. u. ^[b]	<i>zpe</i> / kcal mol ⁻¹ ^[c]	<i>NIMAG</i> ^[d]
Methylguanazinium	C ₃ H ₉ N ₆ ⁺	<i>C</i> ₁	446.81332	94.5	0
Azide	N ₃ ⁻	<i>D</i> _{∞h}	163.858800	6.3	0
Nitrate	NO ₃ ⁻	<i>D</i> _{3h}	279.761750	9.0	0
Perchlorate	ClO ₄ ⁻	<i>T</i> _d	759.637931	9.4	0
5,5'-Azotetrazolate	C ₂ N ₁₀ O ₂ ⁻	<i>C</i> ₁	622.12846	35.1	0
5-Nitrotetrazolate	CN ₅ O ₂ ⁻	<i>C</i> _{2v}	461.17921567	22.6	0
Dinitramide	N ₃ O ₄ ⁻	<i>C</i> ₂	463.977162	17.9	0
Carbon Monoxide	CO	<i>C</i> _{∞v}	113.054970	3.0	0
Water	H ₂ O	<i>C</i> _{2v}	76.260910	13.4	0
Dihydrogen	H ₂	<i>D</i> _{∞h}	1.156216	6.4	0
Dinitrogen	N ₂	<i>D</i> _{∞h}	109.280650	3.1	0
Carbon Dioxide	CO ₂	<i>D</i> _{∞h}	188.169700	7.1	0
Dioxygen	O ₂	<i>D</i> _{∞h}	150.004290	2.0	0
Hydrogen Chloride	HCl	<i>C</i> _{∞v}	460.251823	4.3	0

[a] Point group; [b] Electronic energy (Hartrees); [c] Zero point energy; [d] Number of imaginary frequencies.

Table 4.A3 Thermodynamic and explosive properties of formulations of **42**, **43** and **47** with ammonium nitrate (AN).

	AN + 42 ^[a]	AN + 43 ^[b]	AN + 47 ^[c]
ρ (g cm ⁻³) ^[d]	1.667	1.709	1.702
<i>M</i> (g mol ⁻¹)	95.52	106.69	128.11
Ω (%) ^[e]	-0.1	+0.1	+0.1
ΔU_f° / kJ kg ⁻¹ ^[f]	-3123	-3252	-2652
ΔH_f° / kJ kg ⁻¹ ^[g]	-3259	-3382	-2782
<i>T</i> _{ex} / K ^[h]	3018	3060	3250
<i>V</i> ₀ / L kg ⁻¹ ^[i]	963	948	934
<i>P</i> / GPa ^[j]	24.5	26.2	26.8
<i>D</i> / m s ⁻¹ ^[k]	8070	8267	8325

[a] 83% AN + 17% **42**; [b] 76% AN + 24% **43**; [c] 69% AN + 31% **47**; [d] Density from X-ray measurements; [e] Oxygen balance according to ref. [66]; [f] Calculated energy of formation (EXPLO5); [g] Calculated enthalpy of formation (EXPLO5); [h] Temperature of the explosion gases; [i] Volume of the explosion gases; [j] Detonation pressure; [k] Detonation velocity.

Table 4.A4 Thermodynamic and explosive properties of formulations of **45a**, **45b**, **46a** and **46b** with ammonium nitrate (AN).

	AN + 45a ^[a]	AN + 45b ^[b]	AN + 46a ^[c]	AN + 46b ^[d]
ρ (g cm ⁻³) ^[e]	1.696	1.697	1.689	1.692
M (g mol ⁻¹)	144.88	138.21	123.50	115.92
Ω (%) ^[f]	0.0	+0.5	-0.2	+0.4
ΔU_f° / kJ kg ⁻¹ ^[g]	-2875	-2931	-2860	-2967
ΔH_f° / kJ kg ⁻¹ ^[h]	-3009	-3064	-2992	-3088
T_{ex} / K ^[i]	3148	3098	3171	3091
V_0 / L kg ⁻¹ ^[j]	954	952	946	941
P / GPa ^[k]	26.6	26.2	26.3	25.7
D / m s ⁻¹ ^[l]	8321	8274	8282	8202

[a] 82% AN + 18% **45a**; [b] 83% AN + 17% **45b**; [c] 76% AN + 24% **46a**; [d] 78% AN + 22% **46b**; [e] Density from X-ray measurements; [f] Oxygen balance according to ref. [66]; [g] Calculated energy of formation (EXPLO5); [h] Calculated enthalpy of formation (EXPLO5); [i] Temperature of the explosion gases; [j] Volume of the explosion gases; [k] Detonation pressure; [l] Detonation velocity.

Table 4.A5 Thermodynamic and explosive properties of formulations of **42**, **43** and **47** with ammonium dinitramide (ADN).

	ADN + 42 ^[a]	ADN + 43 ^[b]	ADN + 47 ^[c]
ρ (g cm ⁻³) ^[d]	1.722	1.767	1.752
M (g mol ⁻¹)	133.95	143.51	165.16
Ω (%) ^[e]	-0.2	+0.1	-0.1
ΔU_f° / kJ kg ⁻¹ ^[f]	-180	-638	-207
ΔH_f° / kJ kg ⁻¹ ^[g]	-316	-767	-335
T_{ex} / K ^[h]	3984	3932	4092
V_0 / L kg ⁻¹ ^[i]	902	890	881
P / GPa ^[j]	31.3	33.0	33.0
D / m s ⁻¹ ^[k]	8837	8989	8988

[a] 79% ADN + 21% **42**; [b] 71% ADN + 29% **43**; [c] 73% ADN + 27% **47**; [d] Density from X-ray measurements; [e] Oxygen balance according to ref. [66]; [f] Calculated energy of formation (EXPLO5); [g] Calculated enthalpy of formation (EXPLO5); [h] Temperature of the explosion gases; [i] Volume of the explosion gases; [j] Detonation pressure; [k] Detonation velocity.

Table 4.A6 Thermodynamic and explosive properties of formulations of **45a**, **45b**, **46a** and **46b** with ammonium dinitramide (ADN).

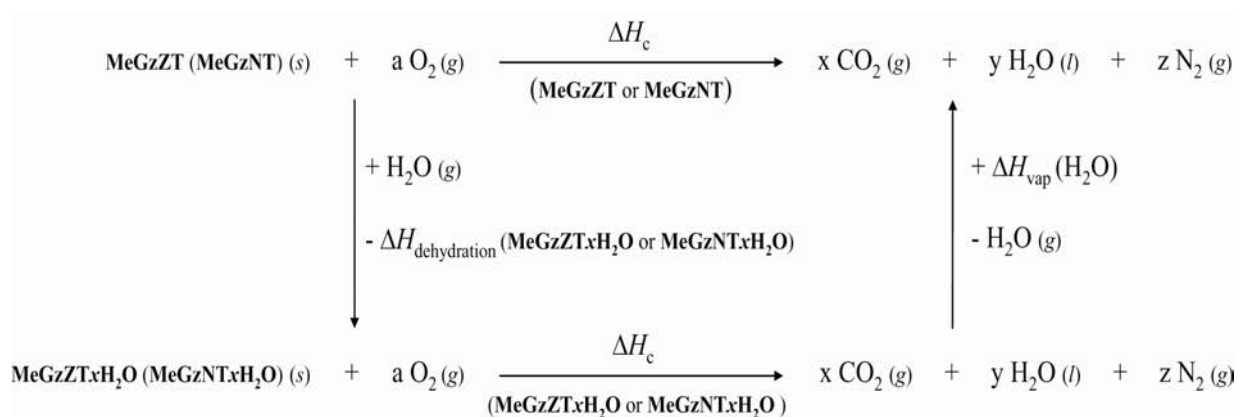
	ADN + 45a ^[a]	ADN + 45b ^[b]	ADN + 46a ^[c]	ADN + 46b ^[d]
ρ (g cm ⁻³) ^[e]	1.757	1.759	1.743	1.748
M (g mol ⁻¹)	193.66	186.70	163.83	156.22
Ω (%) ^[f]	+0.1	+0.5	-0.3	+0.2
ΔU_f° / kJ kg ⁻¹ ^[g]	+72	+57	-165	-187
ΔH_f° / kJ kg ⁻¹ ^[h]	-61	-76	-296	-317
T_{ex} / K ^[i]	4126	4096	4085	3999
V_0 / L kg ⁻¹ ^[j]	892	888	888	879
P / GPa ^[k]	33.7	33.5	32.9	31.5
D / m s ⁻¹ ^[l]	9077	9044	8991	8801

[a] 78% ADN + 22% **45a**; [b] 79% ADN + 21% **45b**; [c] 71% ADN + 29% **46a**; [d] 73% ADN + 27% **46b**; [e] Density from X-ray measurements; [f] Oxygen balance according to ref. [66]; [g] Calculated energy of formation (EXPLO5); [h] Calculated enthalpy of formation (EXPLO5); [i] Temperature of the explosion gases; [j] Volume of the explosion gases; [k] Detonation pressure; [l] Detonation velocity.

Computational Methods

The electronic energies for all anions and the methylguanazinium cation were calculated using Møller-Plesset perturbation theory truncated at the second order (MP2) and were used unscaled. The results of the MP2 electronic energy calculations are tabulated in Table 4.A2. For all atoms in all calculations, the correlation consistent polarized double-zeta basis set cc-pVDZ was used. For **45b** monohydrate and **46b** monohydrate the following approximation was used: the calculated (MP2 method) electronic energies were used to predict the heats of combustion of the anhydrous **45b** and **46b** assuming that $\Delta H_{\text{hydration}} \ll \Delta H_c$ in the Born-Haber cycle shown in Scheme 4.A1. The unit cell volume (V) for **45b** and **46b** was approximated as being that of the monohydrate compounds minus the volume of the number of waters in the unit cell ($V(\text{H}_2\text{O}) = 0.02496 \text{ nm}^3$).^[59] Since the temperatures of water loss (DSC) for **45b** monohydrate and **46b** monohydrate are relatively close to 100 °C, it is assumed that the interactions in the crystal structure are similar enough to those found in liquid water and the above approximation is valid. Typical values for hydration energies in similar compounds have values of ca. -20 cal g^{-1} and are smaller than 1% of the combustion energies.^[30b] In addition, errors in the combustion measurements are estimated at ~5%, therefore, disregarding the hydration enthalpy is justified. On the other hand, the volume of the unit cell has little effect on the predicted values (errors of ~5% in the volume produce errors of ~2% in the calculated energies of formation). In addition, the energies of formation calculated

for the anhydrous species **45b** and **46b** were used to calculate their detonation parameters using the (X-ray) densities of the monohydrate salts. This is justified by our experience that crystal water has generally little effect on the density values.^[30,60] Lastly, a similar method to the one used here has already been described before.^[60,61]



Scheme 4.A1 Born-Haber energy cycle for the calculation of the heat of combustion of **45b** and **46b** (**45a**: $a = 12.5$, $x = 8$, $y = 10$, $z = 11$; **45b**: $a = 12.5$, $x = 8$, $y = 9$, $z = 11$; **46a**: $a = 5.25$, $x = 4$, $y = 5.5$, $z = 5.5$ and **46b**: $a = 5.25$, $x = 4$, $y = 4.5$, $z = 5.5$).

Table 5.A1 Results of the quantum chemical calculations (MP2/cc-pVDZ).

Compound	Formula	p.g. ^a	-E / a.u. ^b	zpe / kcal mol ⁻¹ ^c	NIMAG ^d
5-Amino-1 <i>H</i> -tetrazolium	CN ₅ H ₄ ⁺	C _{2v}	313.177864	47.6	0
1-Methyl-5-amino-1 <i>H</i> -tetrazolium	C ₂ H ₆ N ₅ ⁺	C ₁	352.373507	65.1	0
2-Methyl-5-amino-1 <i>H</i> -tetrazolium	C ₂ H ₆ N ₅ ⁺	C ₁	352.381769	65.6	0
1,4-Dimethyl-5-amino-1 <i>H</i> -tetrazolium	C ₃ H ₈ N ₅ ⁺	C _s	391.568749	82.8	0
1,3-Dimethyl-5-amino-1 <i>H</i> -tetrazolium	C ₃ H ₈ N ₅ ⁺	C ₁	391.577017	83.2	0
1,5-Diamino-1 <i>H</i> -tetrazolium	CN ₆ H ₅ ⁺	C ₁	368.373816	58.3	0
1,5-Diamino-4-methyl-1 <i>H</i> -tetrazolium	C ₂ N ₆ H ₇ ⁺	C ₁	407.568995	75.6	0
Guanazinium	C ₂ H ₇ N ₆ ⁺	C ₁	407.617543	76.8	0
Methylguanazinium	C ₃ H ₉ N ₆ ⁺	C ₁	446.813320	94.5	0
Picrate	C ₆ H ₂ N ₃ O ₇ ⁻	C _s	918.319590	62.3	0
Carbon Monoxide	CO	C _{∞v}	113.054970	3.0	0
Water	H ₂ O	C _{2v}	76.260910	13.4	0
Dihydrogen	H ₂	D _{∞h}	1.156216	6.4	0
Dinitrogen	N ₂	D _{∞h}	109.280650	3.1	0
Carbon Dioxide	CO ₂	D _{∞h}	188.169700	7.1	0
dioxygen	O ₂	D _{∞h}	150.004290	2.0	0

^a Point group; ^b Electronic energy (Hartrees); ^c Zero point energy; ^d Number of imaginary frequencies.

Table 5.A2 Thermodynamic and explosive properties of formulations of azolium picrate salts with ammonium nitrate (AN).

	AN + 59 ^a	AN + 60 ^b	AN + 61 ^c	AN + 62 ^d	AN + 63 ^e
ρ (g cm ⁻³) ^f	1.755	1.721	1.719	1.705	1.704
M (g mol ⁻¹)	145.56	139.55	139.55	135.05	135.05
Ω (%) ^g	+0.1	0.0	0.0	+0.1	+0.1
ΔU°_f / kJ kg ⁻¹ ^h	-3276	-3467	-3473	-3608	-3617
ΔH°_f / kJ kg ⁻¹ ⁱ	-3389	-3583	-3589	-3726	-3735
T_{ex} / K ^j	3124	3085	3084	3048	3044
V_0 / L kg ⁻¹ ^k	885	900	900	911	911
P / GPa ^l	26.2	25.4	25.4	25.0	25.0
D / m s ⁻¹ ^m	8165	8103	8095	8071	8065
	AN + 64 ⁿ	AN + 65 ^o	AN + 66 ^p	AN + 67 ^q	
ρ (g cm ⁻³) ^f	1.732	1.714	1.728	1.714	
M (g mol ⁻¹)	149.77	143.17	143.17	138.22	
Ω (%) ^g	+0.1	+0.1	+0.1	+0.3	
ΔU°_f / kJ kg ⁻¹ ^h	-3091	-3323	-3423	-3572	
ΔH°_f / kJ kg ⁻¹ ⁱ	-3208	-3441	-3540	-3691	
T_{ex} / K ^j	3197	3132	3078	3034	
V_0 / L kg ⁻¹ ^k	891	905	905	915	
P / GPa ^l	26.2	25.6	25.7	25.3	
D / m s ⁻¹ ^m	8176	8137	8141	8110	

^a72% AN + 28% **59**; ^b76% AN + 24% **60**; ^c76% AN + 24% **61**; ^d79% AN + 21% **62**; ^e79% AN + 21% **63**; ^fDensity from X-ray measurements; ^gOxygen balance according to ref. 36; ^hCalculated energy of formation (EXPLO5); ⁱCalculated enthalpy of formation (EXPLO5); ^jTemperature of the explosion gases; ^kVolume of the explosion gases; ^lDetonation pressure; ^mDetonation velocity. ⁿ72% AN + 28% **64**; ^o76% AN + 24% **65**; ^p76% AN + 24% **66**; ^q79% AN + 21% **67**.

Table 5.A3 Thermodynamic and explosive properties of formulations of azolium picrate salts with ammonium dinitramide (ADN).

	ADN + 59 ^a	ADN + 60 ^b	ADN + 61 ^c	ADN + 62 ^d	ADN + 63 ^e
ρ (g cm ⁻³) ^f	1.819	1.781	1.780	1.764	1.763
M (g mol ⁻¹)	188.69	183.24	183.24	180.76	180.76
Ω (%) ^g	-0.3	-0.1	-0.1	-0.4	-0.4
ΔU°_f / kJ kg ⁻¹ ^h	-827	-899	-906	-945	-955
ΔH°_f / kJ kg ⁻¹ ⁱ	-936	-1010	-1017	-1058	-1069
T_{ex} / K ^j	4008	3995	3993	3987	3983
V_0 / L kg ⁻¹ ^k	819	833	833	843	843
P / GPa ^l	32.6	31.7	31.6	31.4	31.4
D / m s ⁻¹ ^m	8808	8758	8753	8755	8756
	ADN + 64 ⁿ	ADN + 65 ^o	ADN + 66 ^p	ADN + 67 ^q	
ρ (g cm ⁻³) ^f	1.790	1.773	1.790	1.776	
M (g mol ⁻¹)	193.80	187.61	187.61	184.68	
Ω (%) ^g	-0.3	+0.1	+0.1	-0.1	
ΔU°_f / kJ kg ⁻¹ ^h	-605	-725	-845	-900	
ΔH°_f / kJ kg ⁻¹ ⁱ	-715	-838	-959	-1015	
T_{ex} / K ^j	4097	4050	3983	3972	
V_0 / L kg ⁻¹ ^k	827	839	839	847	
P / GPa ^l	32.3	31.9	32.1	31.9	
D / m s ⁻¹ ^m	8811	8792	8808	8807	

^a66% ADN + 34% **59**; ^b71% ADN + 29% **60**; ^c71% ADN + 29% **61**; ^d74% ADN + 26% **62**; ^e74% ADN + 26% **63**;

^fDensity from X-ray measurements; ^gOxygen balance according to ref. 36; ^hCalculated energy of formation (EXPLO5);

ⁱCalculated enthalpy of formation (EXPLO5); ^jTemperature of the explosion gases; ^kVolume of the explosion gases;

^lDetonation pressure; ^mDetonation velocity. ⁿ66% ADN + 34% **64**; ^o71% ADN + 29% **65**; ^p71% ADN + 29% **66**;

^q74% ADN + 26% **67**.

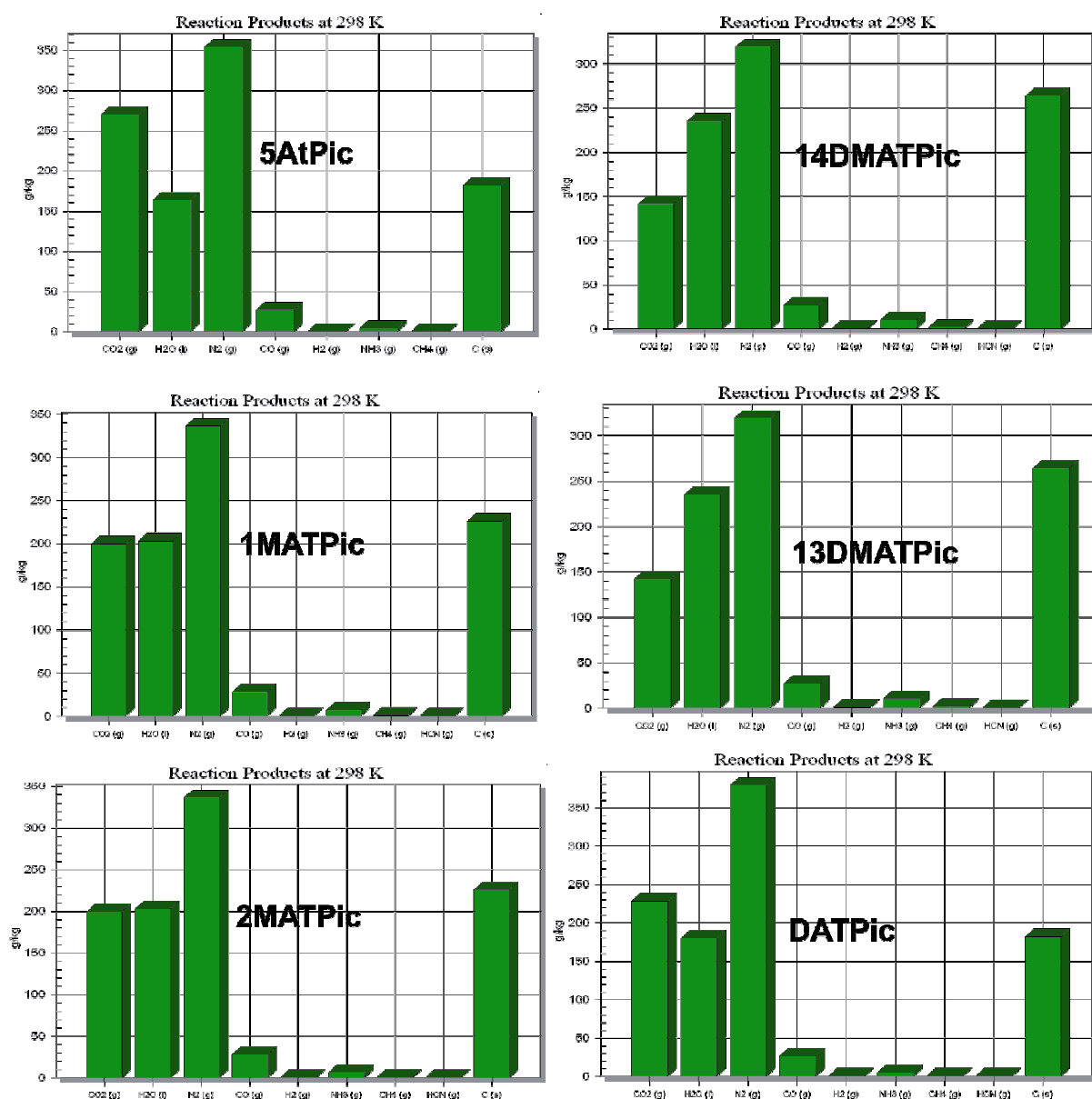


Figure 5.A1 Predicted decomposition gases for picrate salts 59, 60, 61, 62, 63 and 64 using the ICT-code.

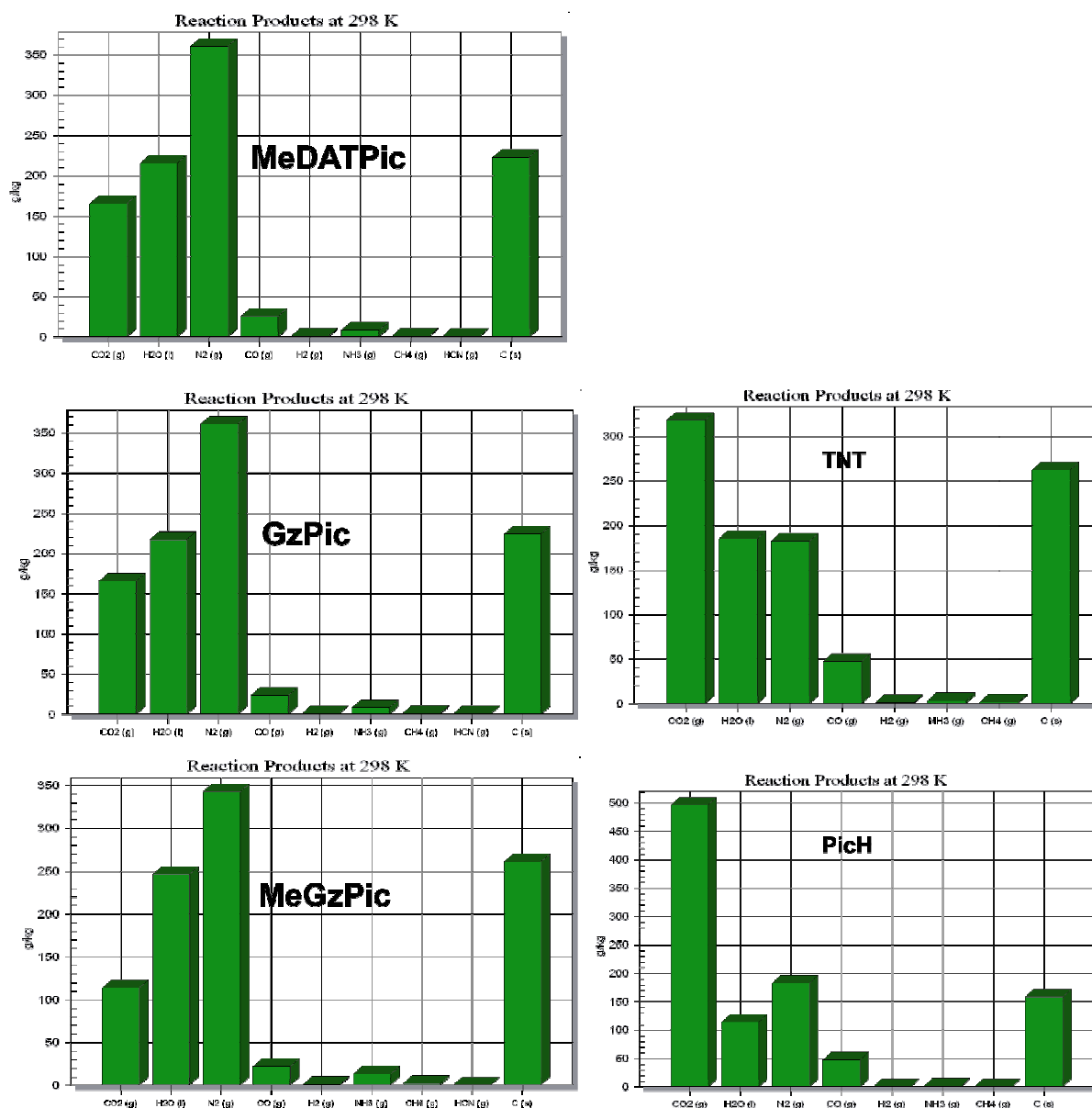


Figure 5.A2 Predicted decomposition gases for picrate salts **65**, **66**, **67** and for TNT and picric acid (PicH) using the ICT-code.

Table 6.A1 Calculated electronic and zero point energies (MP2/aug-cc-pVDZ).

Species	Formula	p. g. ^[a]	- <i>E</i> / a. u. ^[b]	<i>zpe</i> / kcal mol ⁻¹ ^[c]	<i>NIMAG</i> ^[d]
2-Methyl-5-aminotetrazolium	C ₂ H ₆ N ₅ ⁺	C ₁	352.381769	65.6	0
1,3-Dimethyl-5-aminotetrazolium	C ₃ H ₈ N ₅ ⁺	C ₁	391.577017	83.2	0
Nitrate	NO ₃ ⁻	D _{3h}	279.761750	9.0	0
Perchlorate	ClO ₄ ⁻	T _d	759.637931	9.4	0
Azide	N ₃ ⁻	D _{∞h}	163.858800	6.3	0
Dinitramide	N ₃ O ₄ ⁻	C ₂	463.977162	17.9	0
Carbon Monoxide	CO	C _{∞v}	113.054970	3.0	0
Water	H ₂ O	C _{2v}	76.260910	13.4	0
Dihydrogen	H ₂	D _{∞h}	1.156216	6.4	0
Dinitrogen	N ₂	D _{∞h}	109.280650	3.1	0
Carbon Dioxide	CO ₂	D _{∞h}	188.169700	7.1	0
Dioxygen	O ₂	D _{∞h}	150.004290	2.0	0
Hydrogen Chloride	HCl	C _{∞v}	460.251823	4.3	0

[a] Point group; [b] Electronic energy (Hartrees); [c] Zero point energy; [d] Number of imaginary frequencies.

Table 6.A2 Predicted thermochemical data.

Compnd.	ΔH_L (kJ mol ⁻¹) ^[a]	ΔH_r (kJ mol ⁻¹) ^[b]	$\Delta_c H_m^\circ$ (kJ mol ⁻¹) ^[c]
11	519.53	-2448.03	-1956.87
12	530.44	-2158.22	-1754.74
71	514.45	-2754.11	-2408.41
72	493.97	-3043.91	-2621.68
73	522.98	-3210.64	-2857.22
74	485.50	-2938.09	-2621.14

[a] Predicted lattice enthalpy; [b] Gas-phase heat of reaction from calculated (MP2/aug-cc-pVDZ) electronic energies of ions and combustion products; [c] Predicted standard molar enthalpy of combustion.

Table 6.A3 Thermodynamic and explosive properties of formulations of the energetic salts with ammonium nitrate (AN).

	AN + 12 ^[a]	AN + 71 ^[b]	AN + 73 ^[c]	AN + 74 ^[d]
ρ (g cm ⁻³) ^[e]	1.687	1.685	1.683	1.676
M (g mol ⁻¹)	107.93	103.08	92.20	123.46
Ω (%) ^[f]	-0.2	-0.1	+0.4	+0.3
ΔU°_f / kJ kg ⁻¹ ^[g]	-2597	-3238	-3129	-2723
ΔH°_f / kJ kg ⁻¹ ^[h]	-2725	-3366	-3263	-2851
T_{ex} / K ^[i]	3282	3112	3050	3256
V_0 / L kg ⁻¹ ^[j]	930	943	960	928
P / GPa ^[k]	26.4	25.7	25.7	25.8
D / m s ⁻¹ ^[l]	8283	8212	8228	8214

[a] 66% AN + 34% **12**; [b] 76% AN + 24% **71**; [c] 84% AN + 16% **73**; [d] 69% AN + 31% **74**; [e] Density from X-ray measurements; [f] Oxygen balance according to ref. [36]; [g] Calculated energy of formation; [h] Calculated enthalpy of formation; [i] Temperature of the explosion gases; [j] Volume of the explosion gases; [k] Detonation pressure; [l] Detonation velocity.

Table 6.A4 Thermodynamic and explosive properties of formulations of the energetic salts with ammonium dinitramide (ADN).

	ADN + 12 ^[a]	ADN + 71 ^[b]	ADN + 73 ^[c]	ADN + 74 ^[d]
ρ (g cm ⁻³) ^[e]	1.733	1.739	1.742	1.722
M (g mol ⁻¹)	139.28	139.15	130.47	159.61
Ω (%) ^[f]	-0.3	-0.1	+0.1	+0.1
ΔU°_f / kJ kg ⁻¹ ^[g]	-272	-622	-136	-292
ΔH°_f / kJ kg ⁻¹ ^[h]	-399	-748	-270	-417
T_{ex} / K ^[i]	4060	3966	4012	4075
V_0 / L kg ⁻¹ ^[j]	878	884	897	873
P / GPa ^[k]	31.2	31.2	32.0	30.7
D / m s ⁻¹ ^[l]	8788	8778	8880	8726

[a] 60% ADN + 40% **12**; [b] 71% ADN + 29% **71**; [c] 80% ADN + 20% **73**; [d] 63% ADN + 37% **74**; [e] Density from X-ray measurements; [f] Oxygen balance according to ref. [36]; [g] Calculated energy of formation; [h] Calculated enthalpy of formation; [i] Temperature of the explosion gases; [j] Volume of the explosion gases; [k] Detonation pressure; [l] Detonation velocity.

Table 7.A1 Thermodynamic and explosive properties of formulations of 5,5'-azotetrazole derivatives with ammonium nitrate (AN).

	AN + 81 ^a	AN + 82 ^b	AN + 83 ^c	AN + 84 ^d	AN + 85 ^e	
ρ (g cm ⁻³) ^f	1.671	1.654	1.683	1.719	1.699	
M (g mol ⁻¹)	142.69	168.29	157.07	145.98	153.49	
Ω (%) ^g	+0.2	-0.3	+0.0	-0.4	-0.1	
ΔU°_f / kJ kg ⁻¹ ^h	-3132	-2784	-2964	-2826	-3381	
ΔH°_f / kJ kg ⁻¹ ⁱ	-3266	-2917	-3100	-2962	-3517	
T_{ex} / K ^j	2987	3290	3010	3030	2824	
V_0 / L kg ⁻¹ ^k	953	964	953	949	956	
P / GPa ^l	24.5	26.4	24.7	26.4	24.1	
D / m s ⁻¹ ^m	8034	8329	8063	8301	7993	
	AN + 86 ^a	AN + 87 ^a	AN + 88 ^b	AN + 89 ^d	AN + 91a ^e	AN + 92 ⁱ
ρ (g cm ⁻³) ^f	1.673	1.669	1.660	1.695	1.686	1.685
M (g mol ⁻¹)	133.09	133.09	146.01	139.05	100.57	100.57
Ω (%) ^g	-0.1	-0.1	-0.4	-0.2	+0.1	+0.1
ΔU°_f / kJ kg ⁻¹ ^h	-3019	-3051	-2631	-2893	-2888	-2833
ΔH°_f / kJ kg ⁻¹ ⁱ	-3148	-3184	-2767	-3029	-3019	-2965
T_{ex} / K ^j	3064	3052	3121	2991	3117	3142
V_0 / L kg ⁻¹ ^k	949	949	949	948	938	938
P / GPa ^l	24.6	24.4	24.5	24.8	25.6	25.7
D / m s ⁻¹ ^m	8062	8041	8066	8079	8199	8206

^a82% AN + 18% **81**; ^b79% AN + 21% **82**; ^c78% AN + 22% **83**; ^d79% AN + 21% **84**; ^e73% AN + 27% **85**; ^f83% AN + 17% **86**; ^g83% AN + 17% **87**; ^h79% AN + 21% **88**; ⁱ75% AN + 25% **89**; ^j82% AN + 18% **91a**; ^k82% AN + 18% **92**;

^fDensity from X-ray measurements; ^gOxygen balance according to EXPLO5; ^hCalculated energy of formation; ⁱCalculated enthalpy of formation; ^jTemperature of the explosion gases; ^kVolume of the explosion gases; ^lDetonation pressure; ^mDetonation velocity.

Table 7.A2 Thermodynamic and explosive properties of formulations of 5,5'-azotetrazole derivatives with ammonium dinitramide (ADN).

	ADN + 81 ^a	ADN + 82 ^b	ADN + 83 ^c	ADN + 84 ^d	ADN + 85 ^e	
ρ (g cm ⁻³) ^f	1.727	1.705	1.737	1.783	1.754	
M (g mol ⁻¹)	190.98	218.16	206.75	191.60	197.07	
Ω (%) ^g	+0.4	+0.2	-0.2	+0.1	+0.1	
ΔU°_f / kJ kg ⁻¹ ^h	-242	+31	-196	-19	-919	
ΔH°_f / kJ kg ⁻¹ ⁱ	-372	-101	-334	-155	-1055	
T_{ex} / K ^j	4000	4206	3960	3963	3620	
V_0 / L kg ⁻¹ ^k	890	904	894	885	900	
P / GPa ^l	31.1	31.9	31.6	33.6	30.3	
D / m s ⁻¹ ^m	8792	8911	8761	9044	8701	
	ADN + 86 ^a	ADN + 87 ^a	ADN + 88 ^b	ADN + 89 ^d	ADN + 91a ^r	ADN + 92 ^s
ρ (g cm ⁻³) ^f	1.729	1.725	1.713	1.750	1.745	1.744
M (g mol ⁻¹)	180.38	180.38	194.33	181.70	139.48	139.48
Ω (%) ^g	-0.2	-0.2	+0.1	-0.2	+0.2	+0.2
ΔU°_f / kJ kg ⁻¹ ^h	-52	-92	+213	-251	+56	+123
ΔH°_f / kJ kg ⁻¹ ⁱ	-183	-224	+77	-387	-74	-7
T_{ex} / K ^j	4057	4041	4086	3866	4112	4144
V_0 / L kg ⁻¹ ^k	885	885	886	890	872	872
P / GPa ^l	31.3	31.1	30.9	31.2	32.4	32.6
D / m s ⁻¹ ^m	8807	8786	8778	8791	8932	8939

^a78% ADN + 22% **81**; ^b75% ADN + 25% **82**; ^c73% ADN + 27% **83**; ^d75% AN + 25% **84**; ^e68% ADN + 32% **85**;
^f79% ADN + 21% **86**; ^g79% ADN + 21% **87**; ^h75% ADN + 25% **88**; ⁱ70% ADN + 30% **89**; ^j78% AN + 22% **91a**;
^k78% AN + 22% **92**; ^lDensity from X-ray measurements; ^mOxygen balance according to EXPLO5; ⁿCalculated energy of formation; ^oCalculated enthalpy of formation; ^pTemperature of the explosion gases; ^qVolume of the explosion gases; ^rDetonation pressure; ^sDetonation velocity.

Table 7.A3 Explosive properties of 5,5'-hydrazinebistetrazole (**HB**T, *Chapter VIII*) and **84** and comparison with common high explosives and formulations with commonly used oxidizers and high explosives (calculated using the EXPLO5 code).

Compound	Ratio (%) ^a	Ω (%) ^b	ρ (g cm ³) ^c	P (GPa) ^d	D (m s ⁻¹) ^e
HB T	100	-57.1	1.841	36.7	9463
84	100	-77.1	1.708	27.7	8702
TNT	100	-74.0	1.654	20.5	7171
Picric Acid	100	-45.4	1.767	24.9	7660
TEX	100	-42.7	1.990	30.8	8231
RDX	100	-21.6	1.800	34.0	8885
HMX	100	-21.6	1.905	38.2	9216
CL-20	100	-11.0	2.020	44.5	9632
HB T + AN	26:74	-0.1	1.753	30.6	8746
HB T + ADN	31:69	+0.1	1.818	35.3	9191
HB T + NF	39:61	+0.3	1.620	28.0	8370
HB T + TNM	46:54	+0.2	1.731	32.7	8822
HB T + RDX	70:30	-46.4	1.829	34.4	9019
HB T + HMX	30:70	-32.2	1.886	37.0	9134
HB T + HMX	70:30	-46.5	1.860	36.4	9215
HB T + HMX	50:50	-39.4	1.873	36.1	9053
HB T + CL-20	30:70	-24.8	1.979	42.5	9532
HB T + CL-20	70:30	-43.3	1.900	37.8	9250
HB T + CL-20	50:50	-34.0	1.940	39.6	9335
84 + AN	21:79	-0.4	1.719	26.4	8300
84 + ADN	25:75	+0.1	1.783	33.5	9044
84 + NF	32:68	+0.5	1.552	24.7	7991
84 + TNM	39:61	-0.2	1.665	29.1	8450
84 + RDX	50:50	-49.4	1.754	29.7	8522
84 + RDX	30:70	-38.3	1.772	30.5	8541
84 + HMX	30:70	-38.2	1.846	33.5	8808
84 + CL-20	50:50	-44.0	1.873	33.4	8746
84 + CL-20	30:70	-30.8	1.939	38.7	9225

^aPercentage of compound (**HB**T or **84**) and either oxidizer (AN, ADN, NF, TNM) or high explosive (RDX, HMX, CL-20); ^bOxygen balance (EXPLO5); ^cDensity (EXPLO5); ^dDetonation pressure and ^eDetonation velocity.

Table 7.A4 Fragmentation degree for the Koenen (steel-sleeve) test.⁵⁴

Types of Fragments	Description	Result
0	Thimble is unchanged	—
A	Thimble plate is dented in	—
B	Thimble plate and sides are dented in	—
C	Thimble plate is broken	—
D	Thimble is teared up	—
E	Thimble is put in two parts	—
F	Thimble is destroyed in three or more big pieces, which can be connected	Explosion
G	Thimble is destroyed into little pieces, top is undamaged	Explosion
H	Thimble is damaged in a lot of little pieces, the top is damaged too	Explosion

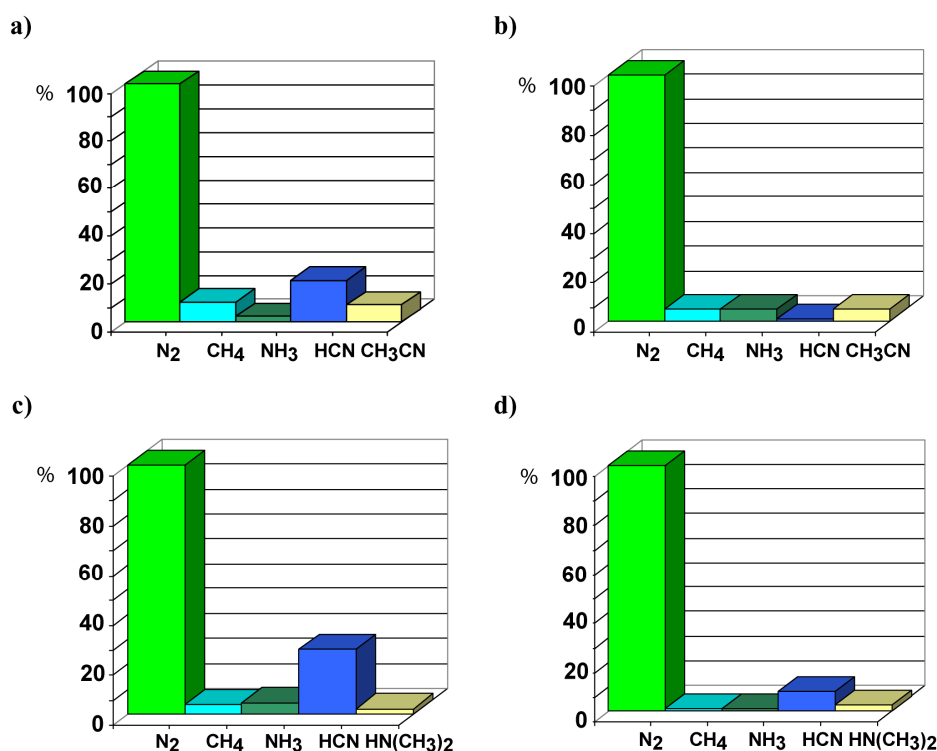
Table 7.A5 Response to thermal shock of 5,5'-hydrazinebistetrazole (**HBT**, *Chapter VIII*) and **84** and mixtures with AN and ADN^a.

	Neat (powder)	Neat (pellet)	+AN ^b	+ADN ^b
HBT	deflagrates (s)	deflagrates (s)	s (1:3)	s (1:2)
84	deflagrates (n.s.)	burns (n.s.)	s (1:4)	s (1:3)

^as and n.s. = smokeless and non-smokeless combustion, respectively. ^bThe compound:AN and compound:ADN mixtures are given in parentheses.

Table 7.A6 Results of the DFT calculations (MP2/aug-cc-pVDZ).⁵⁵

compound	Formula	p.g	- <i>E</i> / a.u.	<i>zpe</i> / kcal mol ⁻¹	<i>NIMAG</i>
14DMAT ⁺	C ₃ H ₈ N ₅ ⁺	C _s	391.568749	82.81	0
13DMAT ⁺	C ₃ H ₈ N ₅ ⁺	C ₁	391.577017	83.20	0
MeDAT ⁺	C ₂ H ₇ N ₆ ⁺	C ₁	407.569321	75.64	0
Gz ⁺	C ₂ H ₇ N ₆ ⁺	C ₁	407.617541	76.80	0
Scz ⁺	CH ₆ N ₃ O ⁺	C ₁	280.234194	59.26	0
ZT ²⁻	C ₂ N ₁₀ ²⁻	C ₁	622.128460	35.10	0
Oxygen	O ₂	D _{∞h}	150.320042	10.0	0
Carbon Dioxide	CO ₂	D _{∞h}	188.580940	30.5	0
Water	H ₂ O	D _{∞h}	76.419736	56.1	0
Nitrogen	N ₂	D _{∞h}	109.524129	14.6	0

**Figure 7.A1** Experimental normalized molar percentage of decomposition gases as estimated by mass spectrometry for nitrogen-rich azotetrazolate salts a) **81**, b) **86**, c) **83** and d) **88**.

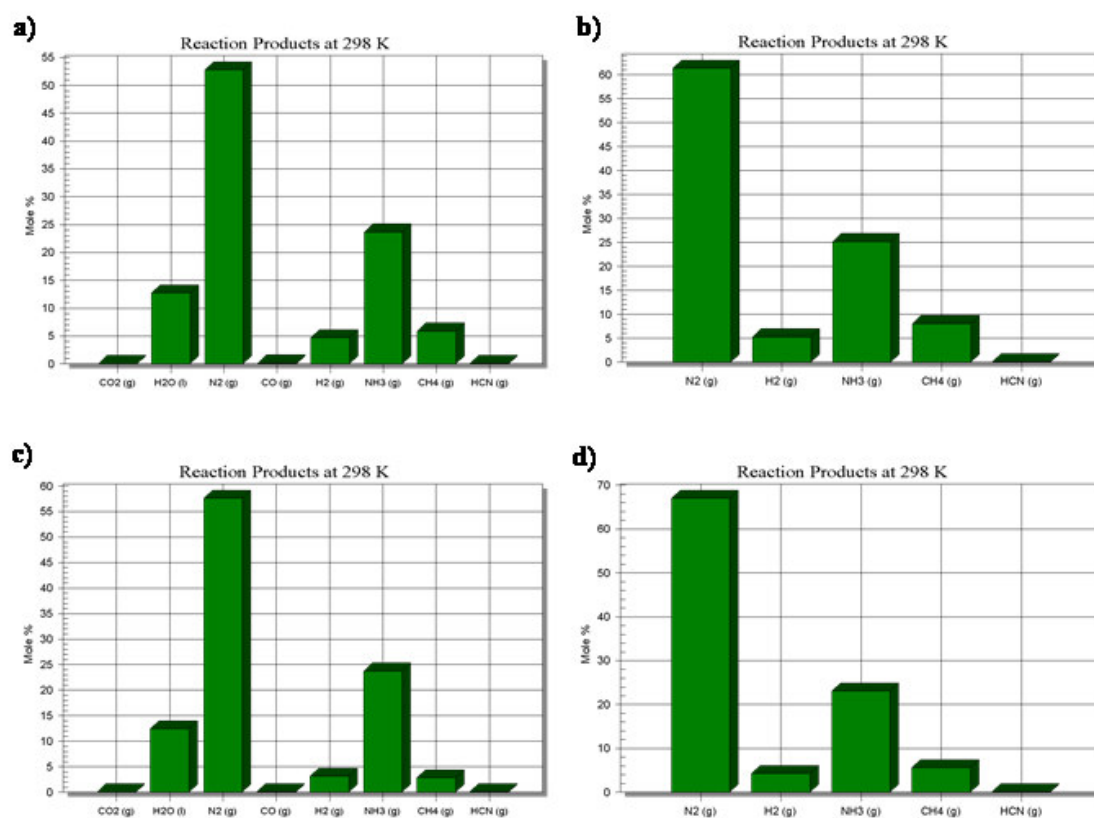


Figure 7.A2 Predicted molar percentage of decomposition gases using the ICT code for nitrogen-rich azotetrazolate salts a) **81**, b) **86**, c) **83** and d) **88**.

Table 8.A1 Calculated (C_1 point group) and observed (IR and Raman) frequencies ($\nu > 500 \text{ cm}^{-1}$) for **95**.

IR	Raman	B3LYP (IR/Ra) ^a	assignment ^b
		551 (78/1)	
574 m	573 (9)	557 (100/1)	$\omega(\text{ring-H})$
685 m, 670 m		670 (16/3)	$\delta(\text{HNNH})_{\text{oop}}$
735 m		715 (50/0)	$\omega(\text{HNNH})$
		721 (7/0)	
		726 (6/0)	
		744 (1/1)	
		748 (0/1)	
820 m		834 (206/2)	$\delta(\text{HNNH})_{\text{ip}}$
		838 (0/5)	
		1002 (16/5)	
999 m		1005 (34/1)	$\nu(\text{N-N})_{\text{ring}}$
		1011 (6/2)	
		1012 (6/8)	
1061 m	1063 (93)	1068 (8/21)	$\nu(\text{C-N-N})_{\text{ring}}$
1070 m		1072 (41/4)	$\nu(\text{N-N})_{\text{ring}}$
1109 w		1109 (4/5)	$\nu(\text{N-N})_{\text{ring}}$
1128 w		1128 (6/4)	$\nu(\text{N-N})_{\text{ring}}$
		1182 (2/3)	
	1274 (53)	1273 (1/3)	$\delta(\text{NNH})_{\text{ring}}$ & $\nu(\text{N-N})_{\text{ring}}$
1273 m		1275 (32/0)	$\delta(\text{NNH})_{\text{ring}}$ & $\nu(\text{N-N})_{\text{ring}}$
	1372 (65)	1372 (1/23)	$\delta(\text{HNNH})_{\text{oop}}$ & $\nu(\text{N-N})_{\text{ring}}$
1376 m		1372 (65/11)	$\delta(\text{HNNH})_{\text{ip}}$ & $\nu(\text{N-N})_{\text{ring}}$
		1416 (12/9)	
1408 w		1426 (24/1)	$\delta(\text{HNNH})_{\text{ip}}$ & $\nu(\text{N-N})_{\text{ring}}$
1528 m		1530 (39/1)	$\delta(\text{HNNH})_{\text{ip}}$ & $\nu(\text{C-N})_{\text{ring}}$
		1530 (2/4)	
1625 s		1634 (38/70)	$\nu(\text{C}_{\text{ring}}-\text{N}_{\text{hydr}})_{\text{ip}}$
1645 s	1648 (19)	1648 (427/11)	$\nu(\text{C}_{\text{ring}}-\text{N}_{\text{hydr}})_{\text{oop}}$
		3473 (16/69)	
		3475 (34/163)	
		3635 (94/63)	
		3635 (86/68)	

^a calculated IR intensities in km mol^{-1} , calculated Raman scattering activities in $\text{\AA}^4 \text{ amu}^{-1}$.^b ip = in phase, oop = out of phase**Table 8.A2** Results of the DFT calculations (B3LYP/cc-pVDZ) on **95**.

	$-E / \text{a.u.}$	$\text{zpe} / \text{kJ mol}^{-1}$	<i>NIMAG</i>	<i>point group</i>	$\Delta H^\circ_{\text{f}} / \text{kJ mol}^{-1}$
$\text{C}_2\text{H}_4\text{N}_{10}$	626.035407	283.8	0	C_2	
O_2	150.334042	9.9	0	$D_{\infty\text{h}}$	0
CO_2	188.598469	30.5	0	$D_{\infty\text{h}}$	-393.5
H_2O	76.420627	55.4	0	$D_{\infty\text{h}}$	-241.8
N_2	109.533376	14.7	0	$D_{\infty\text{h}}$	0

Table 8.A3 Computational results (B3LYP/cc-pVDZ) of bridged bistetrazoles.

	ZT ²⁻	H ₂ ZT	HBT ²⁻	HBT ²⁻ , planar	95, C _i	95, C ₁
$-E$ / a.u.	623.631700	624.808041	624.839139	624.822819	626.015826	626.034231
$E_{\text{rel.}}$ / kcal mol ⁻¹			0.0	10.2	11.5	0.0
p.g. NIMAG	C _{2h} 0	C _{2h} 0	C _i 0	C _{2h} 2, -568 cm ⁻¹ , -558 cm ⁻¹	C _i 1, -59 cm ⁻¹	C ₁ 0
$\tilde{\nu}_{pe}$ / kcal mol ⁻¹	36.3	52.6	52.0	50.4	67.5	68.2
$d(\text{N-N})$ / Å	1.270	1.267	1.474	1.406	1.479	1.424
$\tau(\text{CNNC})$ / ° ^a	180.0	180.0	180.0	180.0	180.0	85.6
$\tau(\text{NCNN})$ / ° ^a	0.0	0.0	47, -139	0	62.8	145, -38, 90, -90
μ / D	0.0	0.0	0.0	0.0	0.0	6.7
stat. point ^b	TM	TM	TM	SP-2	TS	TM

^a τ = torsion angle; ^bstat. point = stationary point, TM = true minimum, TS = transition state, SP-n = saddle point of nth order.

Predicted performance of 95. Using the DFT^c calculated values and the experimentally known structural parameters (see X-ray discussion) we calculated the thermodynamic and energetic properties of 5,5-hydrazinebistetrazole (**95**) following the procedure described earlier in the literature [32-33, 34-39]. The calculated thermodynamic and explosive properties of **95** are summarized in Table 8.A4.

Table 8.A4 Thermodynamic and explosive properties of 5,5'-hydrazinebistetrazole (**95**).

ρ / g cm ⁻³ ^a	1.841	$\Delta U_{\text{f}}^{\circ}$ / kJ kg ⁻¹ ^f	+2566
MW / g mol ⁻¹	168.1	Ω / % ^g	-57.1
$T_{\text{dec.}}$ / °C ^b	207	T_{ex} / K ^b	2539
ΔH_{sub} / kJ mol ⁻¹ ^c	90	P / GPa ⁱ	27.7
$\Delta H_{\text{comb.}}$ / kJ mol ⁻¹ ^d	-1685	D / m s ⁻¹ ^j	8523
$\Delta H_{\text{f}}^{\circ}$ / kJ mol ⁻¹ ^e	+414	V_0 / L kg ⁻¹ ^k	782

^a Density from X-ray measurement. ^b Decomposition point (DSC onset) from measurement at 5 °C min⁻¹. ^c Enthalpy of sublimation calculated according to ref 48. ^d Calculated constant pressure enthalpy of combustion. ^e Enthalpy of formation. ^f Calculated energy of formation. ^g Oxygen balance, calculated according to ref 49. ^h Temperature of the explosion gases. ⁱ Detonation pressure. ^j Detonation velocity. ^k Volume of the explosion gases.

Table 8.A5 Thermodynamic and explosive properties of formulations of nitrogen-rich hydrazinebistetrazolate salts with ammonium nitrate (AN).

	AN + 99 ^a	AN + 100 ^b	AN + 101 ^c	AN + 102 ^d
ρ (g cm ⁻³) ^e	1.697	1.693	1.699	1.701
M (g mol ⁻¹)	119.56	115.03	119.19	127.25
Ω (%) ^f	-0.1	-0.5	+0.2	-0.2
ΔU°_f / kJ kg ⁻¹ ^g	-2809	-2658	-3326	-3117
ΔH°_f / kJ kg ⁻¹ ^h	-2951	-2802	-3464	-3258
T_{ex} / K ⁱ	3097	3020	2832	2906
V_0 / L kg ⁻¹ ^j	982	979	964	969
P / GPa ^k	27.1	25.7	24.3	25.0
D / m s ⁻¹ ^l	8420	8236	8022	8117

^a75% AN + 25% **99**; ^b77% AN + 23% **100**; ^c81% AN + 19% **101**; ^d80% AN + 20% **102**; ^eDensity from EXPLO5;^fOxygen balance according to ref. 48; ^gCalculated energy of formation; ^hCalculated enthalpy of formation;ⁱTemperature of the explosion gases; ^jVolume of the explosion gases; ^kDetonation pressure; ^lDetonation velocity.**Table 8.A6** Thermodynamic and explosive properties of formulations of nitrogen-rich hydrazinebistetrazolate salts with ammonium dinitramide (ADN).

	ADN + 99 ^a	ADN + 100 ^b	ADN + 101 ^c	ADN + 102 ^d
ρ (g cm ⁻³) ^e	1.752	1.751	1.759	1.762
M (g mol ⁻¹)	158.30	153.26	162.97	170.18
Ω (%) ^f	-0.1	+0.2	-0.5	+0.2
ΔU°_f / kJ kg ⁻¹ ^g	-150	86	-501	-321
ΔH°_f / kJ kg ⁻¹ ^h	-293	-59	-640	-461
T_{ex} / K ⁱ	3917	3908	3730	3801
V_0 / L kg ⁻¹ ^j	930	921	906	909
P / GPa ^k	33.1	32.6	31.4	31.9
D / m s ⁻¹ ^l	9038	8978	8830	8891

^a70% ADN + 30% **99**; ^b73% ADN + 27% **100**; ^c76% ADN + 24% **101**; ^d76% ADN + 24% **102**; ^eDensity from EXPLO5; ^fOxygen balance according to ref. 48; ^gCalculated energy of formation; ^hCalculated enthalpy of formation;ⁱTemperature of the explosion gases; ^jVolume of the explosion gases; ^kDetonation pressure; ^lDetonation velocity.

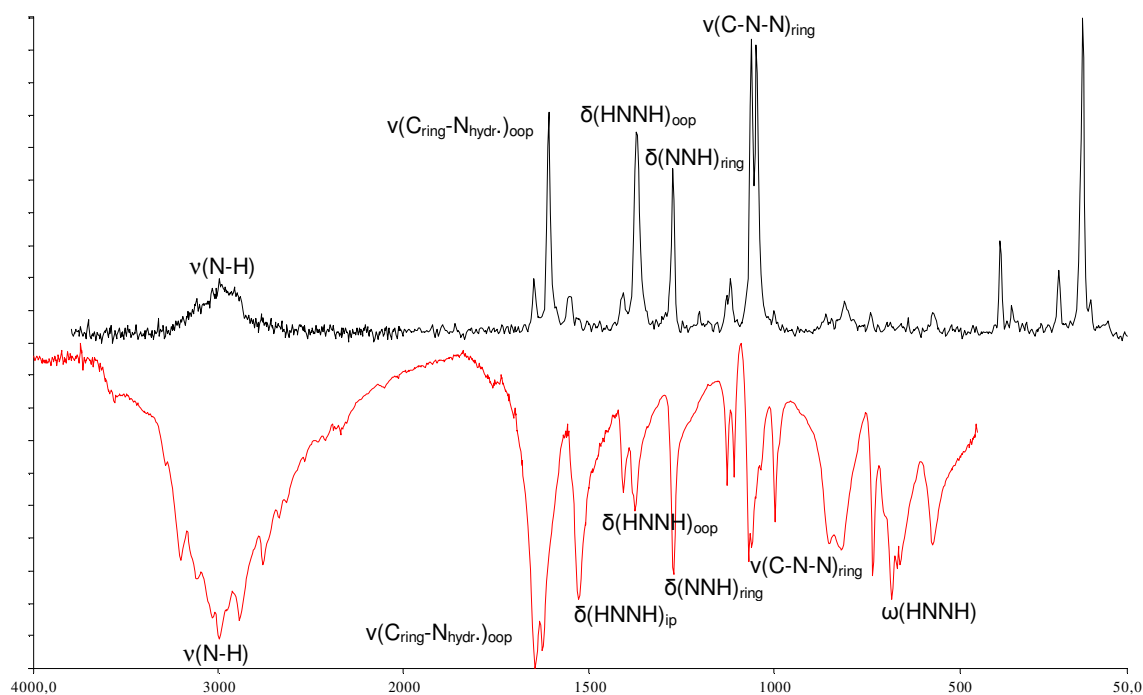


Figure 8.A1 Raman (top) and IR (bottom) of **95** indicating the most important bands.

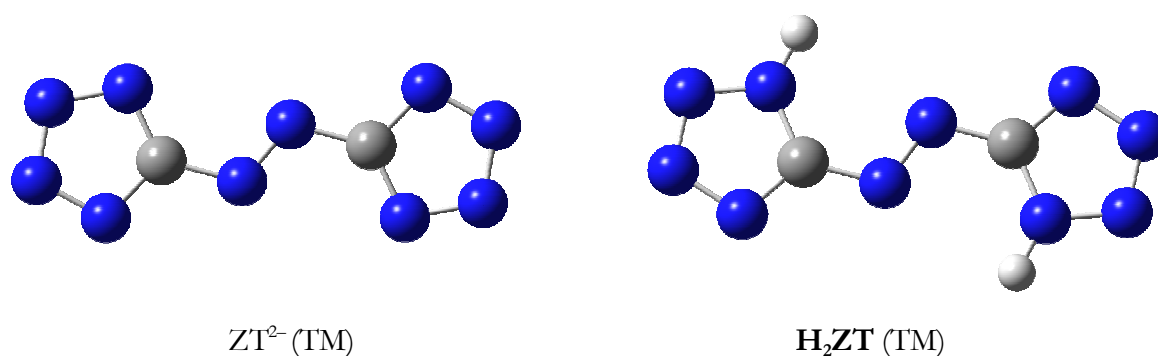


Figure 8.A2 Optimized structures (B3LYP/cc-pVDZ) of the ZT^{2-} anion (left) and H_2ZT (**75**, right).

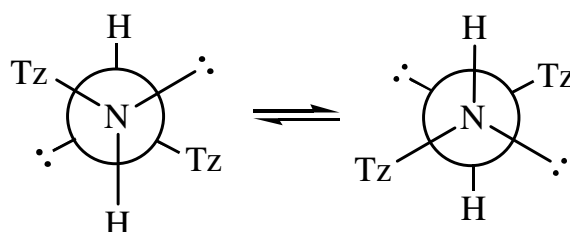


Figure 8.A3 Equilibrium between the two possible configurations of the tetrazole rings in alkaline earth salts of 5,5'-hydrazinebistetrazole (Tz = tetrazole). View along the NH–NH bond.

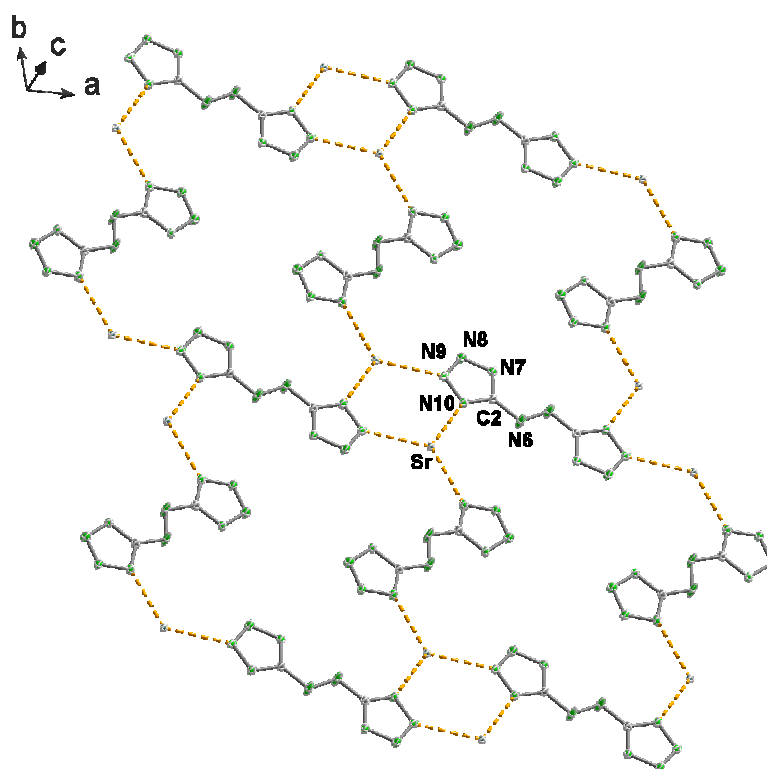


Figure 8.A4 Coordination to the Sr^{2+} cations in a layer in the crystal structure of **112** (the water molecules have been omitted for simplicity sake).

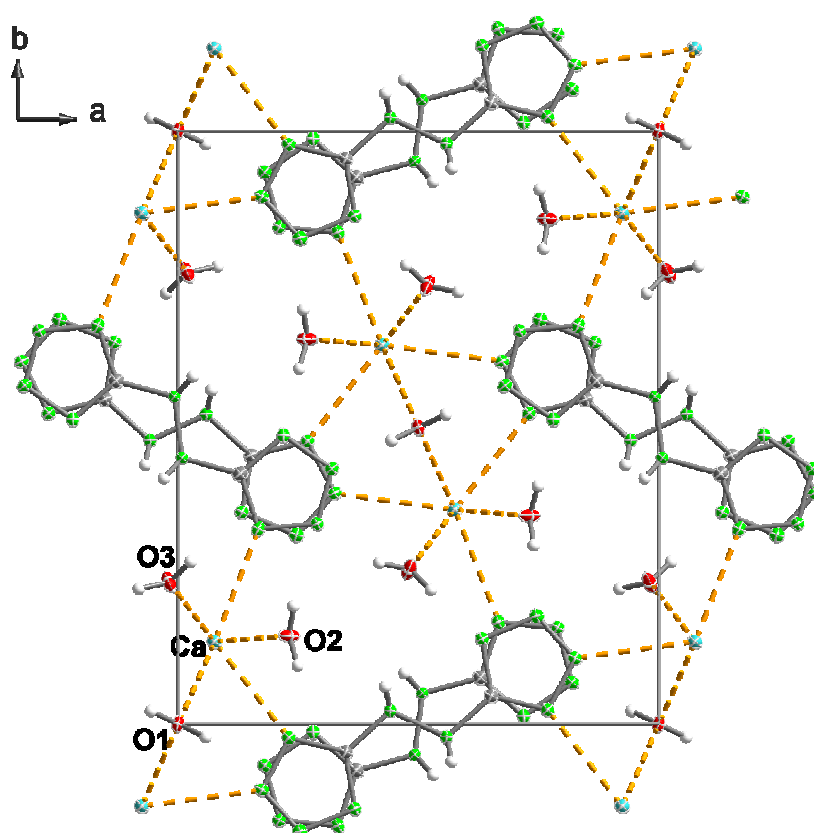


Figure 8.A5 View of the unit cell of **111** along the c -axis showing the “apparent coplanarity” between tetrazole rings and the contacts to the calcium atoms (dotted lines).

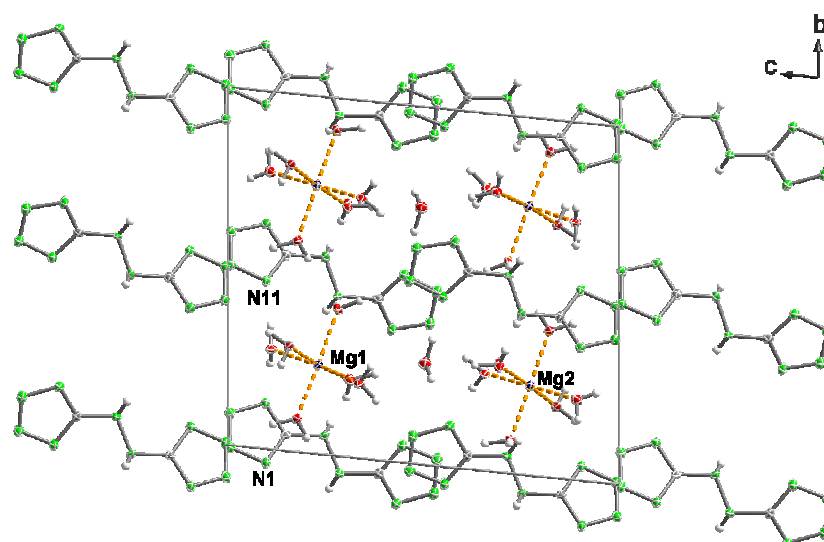


Figure 8.A6 View of the unit cell of **110** along the a -axis showing the contacts to the Mg^{2+} cations (dotted lines).

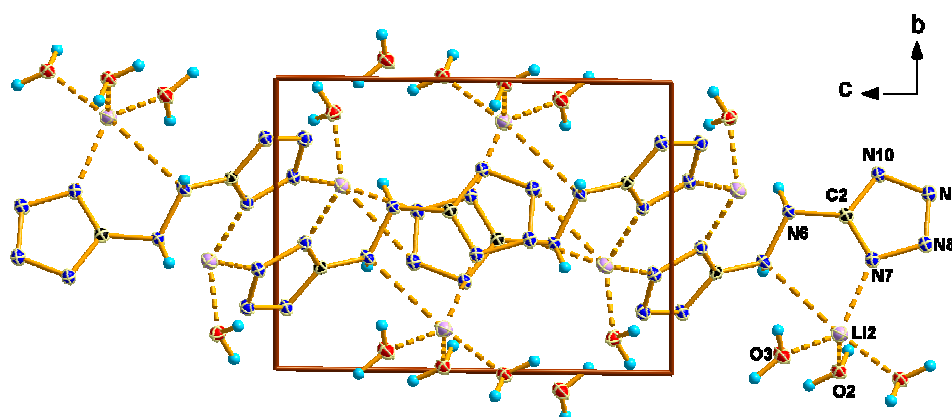


Figure 8.A7 View of the unit cell of **105** along the a -axis showing the coordination to the Li^+ cations (dotted lines).

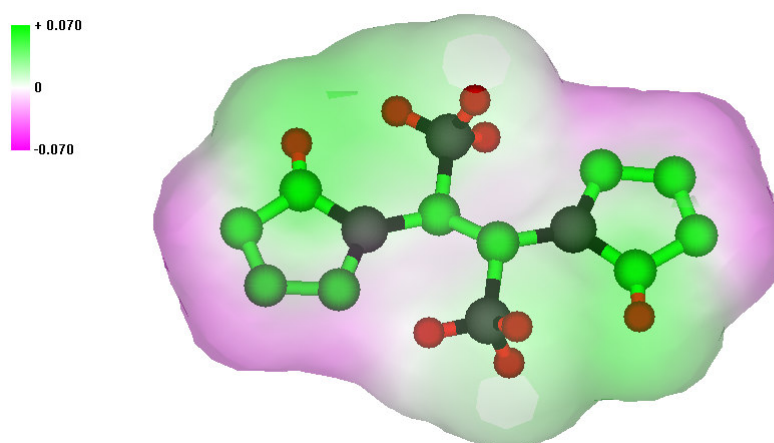


Figure 8.A8 Electrostatic potential (ESP) of 1,2-dimethylhydrazine bistetrazole for the 0.001 electron/ bohr^3 isosurface. Legend for the color ranges of the ESPs are given above (top left corner) and range from -0.07 to +0.07 hartrees (a.u.).

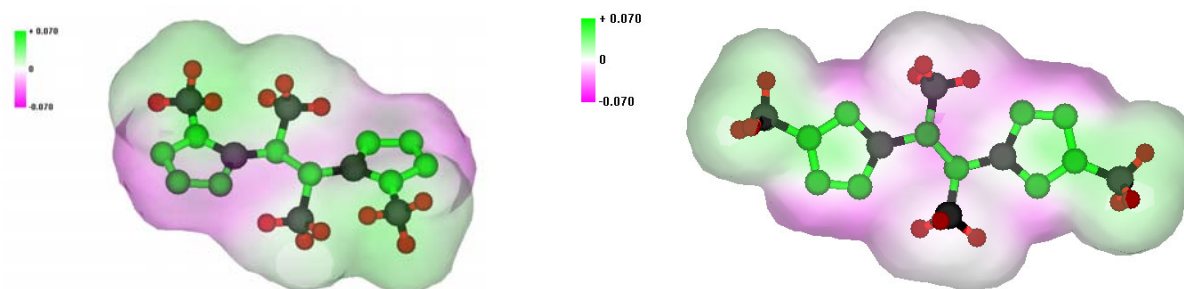


Figure 8.A9 Electrostatic potential (ESP) of both isomers of 1,2-dimethylhydrazine bis(methyl)tetrazole for the 0.001 electron/bohr³ isosurface. Legend for the color ranges of the ESPs are given above (top left corner) and range from -0.07 to +0.07 hartrees (a.u.). Left: 1,2-dimethylhydrazine bis(1-methyl)tetrazole, right: 1,2-dimethylhydrazine bis(2-methyl)tetrazole.

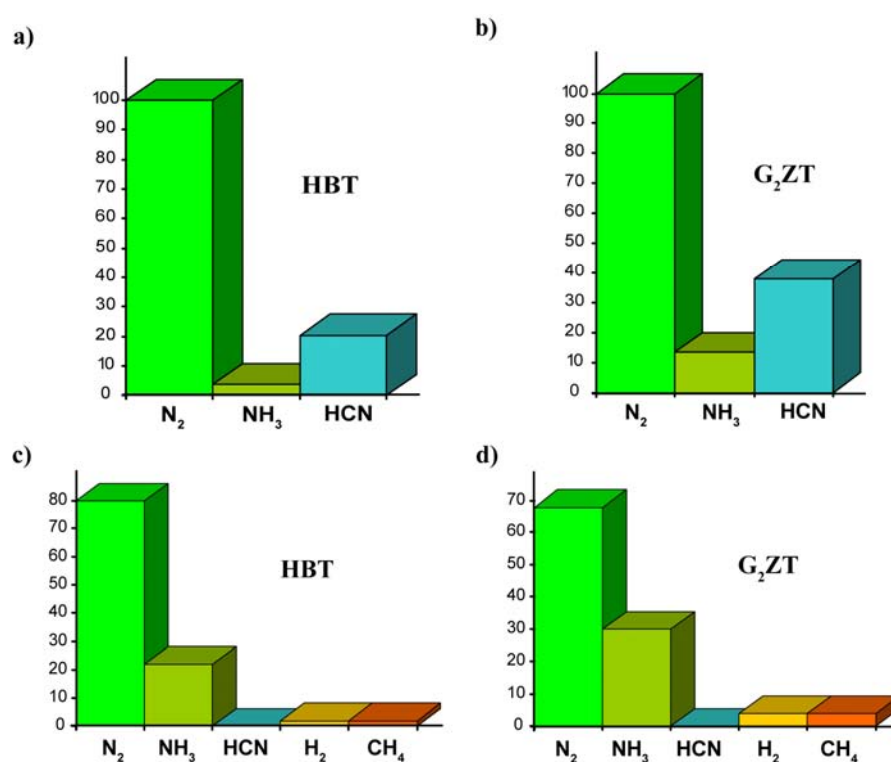


Figure 8.A10 Molar percentages of the decomposition gases of **95** and **GzZT** (*Chapter VII*): experimental using MS (top, normalized) and calculated using the ICT computer-code (bottom). The experimental percentages of HCN in a) and b) are highly overestimated due to the ease of ionization of the same.

Table 9.A1 Calculated electronic and zero point energies (MP2/aug-cc-pVDZ).

Compound	Formula	p. g. ^[a]	- <i>E</i> / a. u. ^[b]	<i>zpe</i> / kcal mol ⁻¹ ^[c]	<i>NIMAG</i> ^[d]
NTTz ⁻	C ₃ H ₂ N ₉ O ₂ ⁺	<i>C</i> ₁	756.812759	57.5	0
Ammonium	NH ₄ ⁺	<i>T</i> _d	56.739780	31.2	0
Guanidinium	C(NH ₂) ₃ ⁺	<i>D</i> _{3h}	205.218051	55.3	0
Aminoguanidinium	C(NH-NH ₂)(NH ₂) ₂ ⁺	<i>C</i> ₁	260.403398	66.2	0
Carbon Monoxide	CO	<i>C</i> _{∞v}	113.054970	3.0	0
Water	H ₂ O	<i>C</i> _{2v}	76.260910	13.4	0
Dihydrogen	H ₂	<i>D</i> _{∞h}	1.156216	6.4	0
Dinitrogen	N ₂	<i>D</i> _{∞h}	109.280650	3.1	0
Carbon Dioxide	CO ₂	<i>D</i> _{∞h}	188.169700	7.1	0
Dioxygen	O ₂	<i>D</i> _{∞h}	150.004290	2.0	0

[a] Point group; [b] Electronic energy (Hartrees); [c] Zero point energy; [d] Number of imaginary frequencies.

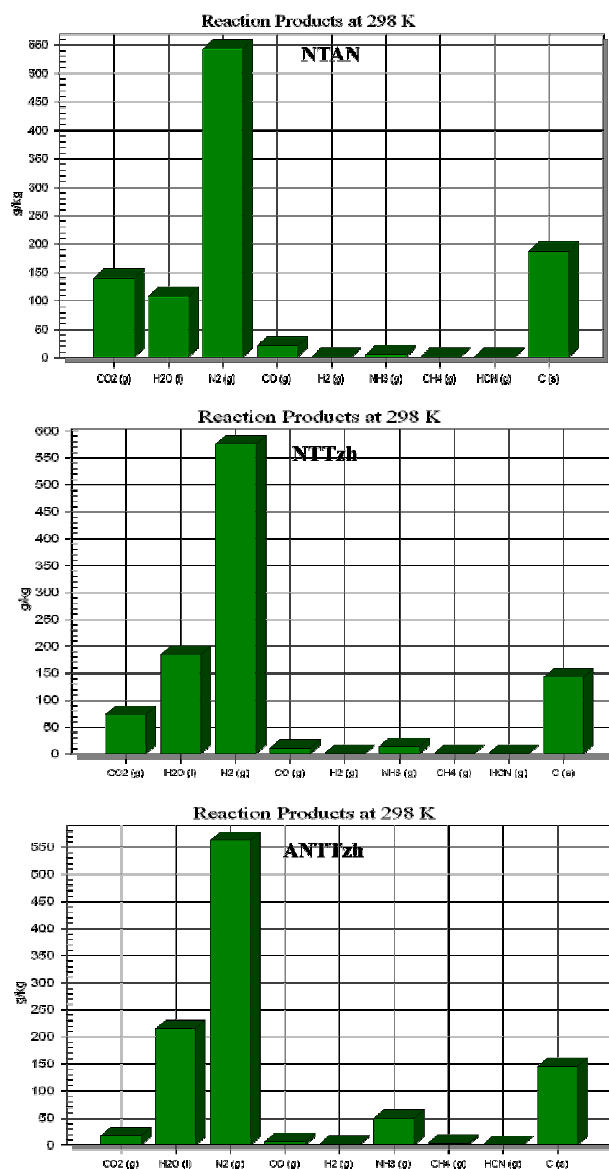


Figure 9.A1 Predicted decomposition gases for NTAN (128), NTTzh (129a) and ANTTzh (135) using the ICT-code.

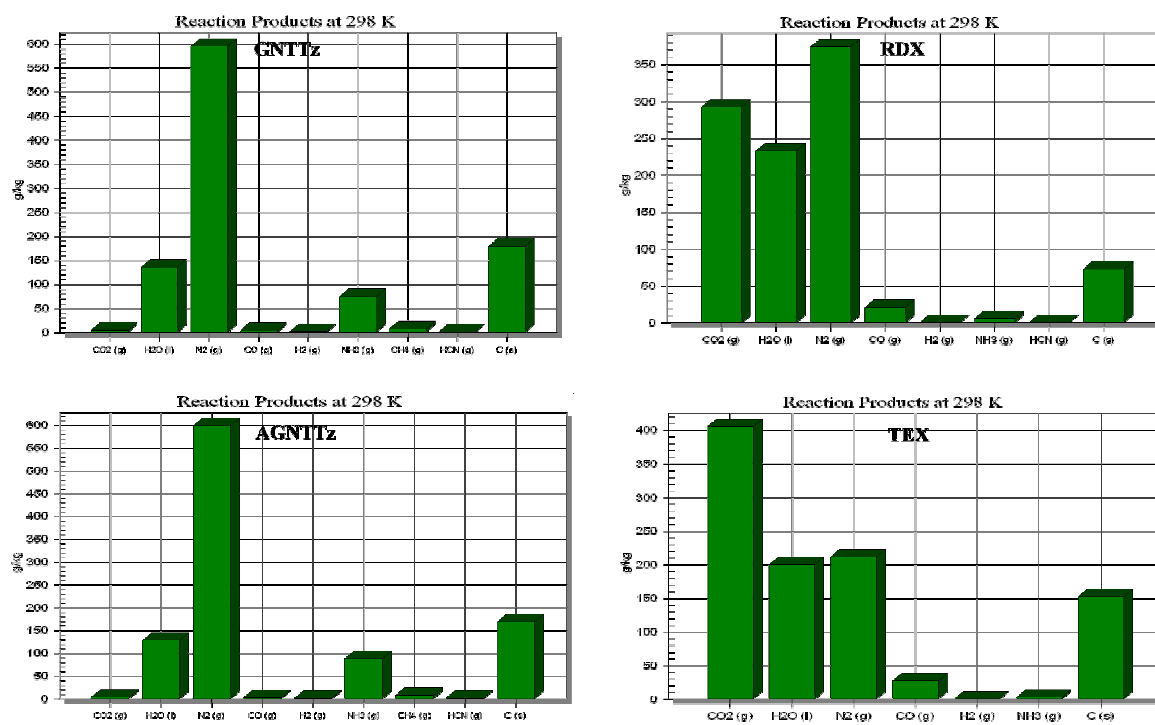


Figure 9.A2 Predicted decomposition gases for **GNTTz (137)**, **AGNTTz (138)**, **RDX** and **TEX** using the ICT-code.

Table 3.B1 Graph-set matrix for selected hydrogen bonds in lithium 5-nitro-2*H*-tetrazolate. First level motifs on-diagonal and second level graph-sets off-diagonal.

D–H...A	A	B	C	D	E	F
O4–H1...N4 (A)	D1,1(2)					
O5–H5...N3 (B)	D2,2(4)	D1,1(2)				
O3–H3...N2 ⁱ (C)	D2,2(4)	D2,2(5)	D1,1(2)			
O5–H6...O3 ⁱ (D)		D2,2(5)	D2,2(4)	D1,1(2)		
O3–H4...O4 ^{iv} (E)	D2,2(4)		D2,2(5)	D2,2(4)	D1,1(2)	
O4–H2...O5 ^v (F)	D2,2(5)	D2,2(4)		D2,2(4)	D2,2(4)	D1,1(2)

Symmetry codes: (i) 2-x, -y, 1-z; (iv) x, 0.5-y, 0.5+y; (v) 2-x, -y, -z.

Table 3.B2 Graph-set matrix for selected hydrogen bonds in sodium 5-nitro-2*H*-tetrazolate. First level motifs on-diagonal and second level graph-sets off-diagonal.

D–H...A	O4–H1...O3	O4–H1...N4 ⁱⁱⁱ	O3–H1...N3 ^v	O3–H1...O4 ^{vi}
O4–H1...O3	D1,1(2)			
O4–H1...N4 ⁱⁱⁱ	D2,2(4)	D1,1(2)		
O3–H1...N3 ^v	D2,2(5)	D2,2(4)	D1,1(2)	
O3–H1...O4 ^{vi}	R2,2(4)	D2,2(5)	D2,2(4)	D1,1(2)

Symmetry codes: (iii) 1-x, -y, 2-z; (v) x, y, -1+z; (vi) 1+x, y, z.

Table 3.B3 Graph-set matrix for medium to strong hydrogen bonds in the crystal structure of 5-nitro-2*H*-tetrazole. First level motifs on-diagonal and second level graph sets off-diagonal.

D–H...A	N2–H1...N4	N7–H2...O3 ⁱ	N7–H2...N3 ⁱⁱ
N2–H1...N4	D1,1(2)		
N7–H2...O3 ⁱ	D3,2(9)	C1,1(6)	
N7–H2...N3 ⁱⁱ	D3,3(7)		C1,1(4)

Symmetry codes: (i) -x, 0.5+y, -z; (ii) 1-x, 0.5+y, 1-z.

Table 3.B4 Selected coordination geometry around the metal centre in lithium, sodium and potassium 5-nitro-2*H*-tetrazolate (some of the bond angles geometry for the potassium salt have been omitted for simplicity purposes).

Bond distances (Å)					
22					
N1–Li	2.105(2)	O3–Li	1.928(2)	O5–Li	1.999(2)
O1–Li	2.736(2)	O4–Li	1.957(2)		
23^a					
Na–N1	2.467(2)	Na–O3	2.370(2)	Na–N2 ^v	2.441(2)
Na–O1	2.641(2)	Na–O4	2.385(2)	Na–O1 ^{vi}	2.470(2)
24^b					
K–O1	3.1628(1)	K–O2 ^{vii}	3.0368(1)	K–N3 ^{ix}	2.8454(1)
K–N1	2.8182(1)	K–N4 ^{vii}	2.8328(1)	K–N2 ^x	2.9097(1)
K–O1 ^{vi}	2.9557(1)	K–O2 ^{viii}	2.9446(1)		

...

...	Bond angles (°)				
22					
N2–N1–Li	131.9(1)	O3–Li–O5	103.2(1)	O4–Li–N1	122.7(1)
C–N1–Li	124.7(1)	O4–Li–O5	99.4(1)	O5–Li–N1	100.1(1)
O3–Li–O4	115.1(1)	O3–Li–N1	111.8(1)		
23 ^a					
O3–Na–O4	168.2(1)	O3–Na–O1 ^{vi}	88.9(1)	C–N1–Na	117.6(1)
O3–Na–N2 ^v	92.2(1)	O4–Na–O1 ^{vi}	86.9(1)	N2–N1–Na	137.4(1)
O4–Na–N2 ^v	99.4(1)	N5–O1–Na	118.0(1)	O4–Na–O1	83.6(1)
O3–Na–N1	89.6(1)	N2 ^v –Na–O1 ^{vi}	121.7(1)	N2 ^v –Na–O1	164.4(1)
O4–Na–N1	86.1(1)	N1–Na–O1 ^{vi}	137.2(1)	N1–Na–O1	63.8(1)
N2 ^v –Na–N1	101.0(1)				
24 ^b					
N1–K–N4 ^{vii}	124.67(4)	O1 ^{vi} –K–N1 ^{vi}	90.40(3)	N3 ^{ix} –K–O2 ^{viii}	131.17(4)
N1–K–N2 ^x	84.53(4)	O2 ^{viii} –K–N1 ^{vi}	155.04(3)	N2 ^x –K–O2 ^{viii}	134.11(4)
N3 ^{ix} –K–N2 ^x	93.80(4)	O1–K–N1 ^{vi}	66.34(3)	O2 ^{vii} –K–O2 ^{viii}	107.47(4)
N4 ^{vii} –K–O1 ^{vi}	102.11(4)	O1 ^{vi} –K–O1	110.29(3)	N4 ^{vii} –K–O1	141.30(4)
O2 ^{vii} –K–O1 ^{vi}	84.53(3)	O2 ^{viii} –K–O1	122.16(3)	N3 ^{ix} –K–O1	78.92(3)
O2 ^{vii} –K–O1	130.03(3)	N1–K–N1 ^{vi}	100.02(4)	N2 ^x –K–O1	68.00(4)
O2 ^{vii} –K–N1 ^{vi}	66.14(3)	N3 ^{ix} –K–N1 ^{vi}	71.63(4)		

Symmetry codes for ^a**23**: (v) x, y, -1+z; (vi) 1+x, y, z; ^b**24**: (vi) x, 0.5-y, -0.5+z; (vii) 1-x, 0.5+y, 0.5-z; (viii) -x, 0.5+y, 0.5-z; (ix) -1+x, 0.5-y, 0.5+z; (x) -1+x, y, z.

Table 3.B5 Selected coordination geometry around the metal centre in rubidium and cesium 5-nitro-2H-tetrazolate salts.

Bond distances (Å)					
25^c					
Rb–O2	2.937(6)	Rb–O2 ^{vi}	3.490(8)	Rb–O1 ^{viii}	3.001(7)
Rb–N3	3.022(8)	Rb–N1 ^{vii}	3.231(6)	Rb–N4 ^{ix}	3.138(5)
Rb–N4 ⁱ	3.139(6)	Rb–N1 ^{viii}	3.038(6)	Rb–N3 ^{ix}	3.521(9)
Rb–O1 ^{vi}	2.930(6)				
26^d					
Cs–O1	3.112(2)	Cs–O2 ^{viii}	3.362(2)	Cs–N2 ^x	3.490(3)
Cs–N1	3.325(2)	Cs–N4 ^{viii}	3.635(2)	Cs–N1 ^{xi}	3.349(2)
Cs–O2 ⁱⁱⁱ	3.333(2)	Cs–N3 ^{ix}	3.204(2)	Cs–N1 ^{xii}	3.210(3)
Cs–O2 ^{vii}	3.230(2)				

Symmetry codes for ^c**25**: (i) x, 1-y, -0.5+z; (vi) -0.5+x, 0.5+y, z; (vii) -0.5+x, 0.5-y, -0.5+z; (viii) -0.5+x, -0.5+y, z; (ix) x, -1+y, z; ^d**26**: (iii) 0.5-x, -0.5+y, 0.5-z; (vii) 0.5-x, 0.5+y, 0.5-z; (viii) x, 2-y, 0.5+z; (ix) x, 3-y, 0.5+z; (x) -x, 2-y, 1-z; (xi) x, 1+y, z; (xii) -x, y, 0.5-z.

Table 3.B6 Selected coordination geometry around the Ca²⁺ cations in calcium 5-nitro-2*H*-tetrazolate.

Bond distances (Å)					
Ca1–O10	2.352(2)	Ca1–O7	2.382(1)	Ca1–O6	2.417(1)
Ca1–O8	2.368(1)	Ca1–O5	2.404(1)	Ca1–O1	2.553(1)
Ca1–O9	2.379(1)				
Bond angles (°)					
O10–Ca1–O8	122.79(6)	O8–Ca1–O5	81.00(5)	O5–Ca1–O6	136.33(5)
O10–Ca1–O9	77.03(6)	O9–Ca1–O5	124.69(6)	O10–Ca1–O1	78.56(5)
O8–Ca1–O9	77.51(6)	O7–Ca1–O5	76.62(5)	O8–Ca1–O1	153.66(5)
O10–Ca1–O7	113.70(6)	O10–Ca1–O6	150.04(6)	O9–Ca1–O1	94.64(5)
O8–Ca1–O7	108.36(6)	O8–Ca1–O6	75.34(5)	O7–Ca1–O1	70.88(5)
O9–Ca1–O7	158.69(5)	O9–Ca1–O6	85.27(5)	O5–Ca1–O1	122.81(5)
O10–Ca1–O5	73.23(5)	O7–Ca1–O6	76.81(5)	O6–Ca1–O1	79.00(5)

Table 4.B1 Selected hydrogen bonding and iodine-hydrogen contact parameters for **α -GzI (55a)**, distances in Å, angles in °, symmetry codes: (i) 1.5-x, 0.5-y, 1-z; (ii) x, 1+y, z; (iii) 1-x, -y, 1-z; (iv) -0.5+x, 0.5-y, -0.5+z; (v) 1.5-x, -0.5-y, 1-z; (vi) 1.5-x, -0.5+y, 1.5-z).

D-H...A	D-H	H...A	D-A	D-H-A
N1-H1...N8 ⁱ	0.75(2)	2.31(2)	2.873(2)	132(2)
N1-H1...I1 ⁱⁱ	0.75(2)	3.17(2)	3.770(2)	139(2)
N3-H2...I2	0.87(2)	2.86(2)	3.703(2)	162(2)
N3-H3...I3 ⁱⁱⁱ	0.84(3)	2.80(3)	3.593(2)	158(2)
N6-H4...I1 ⁱⁱⁱ	0.87(3)	3.08(2)	3.686(2)	128(2)
N6-H5...N3 ⁱⁱⁱ	0.86(3)	2.42(3)	3.270(3)	169(2)
N5-H6...I1 ⁱⁱ	0.80(3)	2.93(3)	3.672(2)	156(2)
N5-H7...I2 ^{iv}	0.82(3)	2.89(3)	3.634(2)	152(2)
N7-H8...N2 ⁱ	0.79(2)	2.28(2)	2.878(2)	134(2)
N7-H8...I2 ⁱ	0.79(2)	3.14(2)	3.736(2)	135(2)
N9-H9...I1 ^v	0.87(3)	2.83(3)	3.660(2)	161(2)
N9-H10...I2 ^{vi}	0.82(3)	2.87(3)	3.648(2)	160(2)
N12-H12...N9 ^v	0.81(3)	2.44(3)	3.201(3)	157(2)
N11-H13...I3	0.85(2)	2.94(2)	3.686(2)	148(2)
N11-H14...I2 ⁱ	0.76(3)	2.94(3)	3.636(2)	153(2)
N5-H7...N6	0.82(3)	2.60(2)	2.860(3)	100(2)
N11-H13...N12	0.85(2)	2.56(2)	2.861(3)	102(2)

Table 4.B2 Selected hydrogen bonding and iodine-hydrogen contact parameters for **β -GzI (55b)**, distances in Å, angles in °, symmetry codes: (i) x, 0.5+y, 0.5+z; (ii) 1-x, 1-y, z; (iii) x, -0.5+y, -0.5+z; (iv) 0.5-x, -0.5+y, 1+z; (v) 1-x, 0.5-y, -0.5+z; (vi) 0.5-x, y, 0.5+z; (vii) -0.5+x, 0.5-y, 1+z; (viii) 0.5+x, 0.5-y, 1+z).

D-H...A	D-H	H...A	D-A	D-H-A
N7-H8...N2 ⁱ	0.79(4)	2.24(4)	2.831(4)	132(4)
N7-H8...I1 ⁱⁱ	0.79(4)	3.22(4)	3.821(3)	134(3)
N1-H1...N8 ⁱⁱⁱ	0.76(5)	2.24(5)	2.833(4)	136(4)
N1-H1...I2 ^{iv}	0.76(5)	3.25(5)	3.812(3)	134(4)
N3-H2...I1 ^v	0.86(5)	2.92(5)	3.753(3)	163(4)
N9-H9...I2 ^{vi}	0.95(5)	2.89(5)	3.780(3)	157(3)
N9-H1...I1 ^{vii}	0.74(4)	2.97(4)	3.710(3)	176(4)
N3-H3...I2 ⁱⁱ	0.93(5)	2.94(5)	3.800(3)	155(3)
N5-H6...I2 ^{iv}	0.75(4)	2.91(4)	3.624(4)	160(4)
N11-H14...I2	0.79(4)	3.00(4)	3.757(4)	160(3)
N5-H7...I1	0.89(4)	2.84(4)	3.669(3)	155(3)
N11-H13...I1 ⁱⁱ	0.81(5)	2.94(5)	3.678(4)	153(5)
N12-H11...I1 ^{viii}	0.79(5)	3.14(4)	3.774(3)	139(3)
N6-H4...I2 ^{viii}	1.02(4)	2.85(4)	3.781(3)	152(3)
N6-H5...I2 ⁱⁱ	0.96(4)	2.79(4)	3.709(3)	159(3)
N12-H12...I1	0.92(5)	3.15(5)	3.744(3)	124(3)
N5-H7...N6	0.89(4)	2.56(4)	2.872(5)	102(3)
N11-H14...N12	0.79(4)	2.52(4)	2.848(5)	107(3)

Table 4.B3 Selected hydrogen bonding and iodine-hydrogen contact parameters for **41** (distances in Å, angles in °, symmetry codes: (i) -x-1, -y+2, -z+1; (ii) x, y+1, z; (iii) -x, -y+2, -z+1; (iv) -x-1, -y+3, -z+2; (v) x-1, y+1, z).

D–H•••A	D–H	H•••A	D–A	D–H–A
N6–H7•••N5 ⁱ	0.91(5)	2.66(6)	3.563(5)	172(5)
N6–H6•••I1 ⁱⁱ	0.890(6)	2.89(5)	3.609(5)	138(6)
N5–H8•••I1 ⁱⁱⁱ	0.78(5)	2.83(5)	3.607(5)	170(5)
N5–H9•••I1	0.89(5)	2.77(5)	3.631(5)	163(5)
N3–H4•••N2 ^{iv}	0.93(5)	2.09(6)	2.983(6)	161(5)
N3–H5•••N6	0.70(5)	2.52(5)	2.872(6)	114(6)
N3–H5•••I1 ^v	0.70(5)	3.12(5)	3.634(5)	133(5)

Table 4.B4 Selected hydrogen bonds for **42** (distances in Å, angles in °, symmetry codes: (i) x, -y+1/2, z-1/2; (ii) -x, 1-y, 1-z; (iii) x-1, -y+1/2, z+1/2; (iv) x-1, y, z; (v) x, -y+1/2, z+1/2; (vi) -1-x, 1-y, 1-z; (vii) -x, 1-y, -z).

D–H•••A	D–H	H•••D	D–A	∠(D–H–A)
N6–H6A•••N4	0.95(4)	2.51(3)	2.855(4)	101(2)
N12–H12A•••N10	0.89(4)	2.54(4)	2.855(4)	101(3)
N4–H4B•••N11	0.93(4)	2.43(4)	3.248(5)	147(3)
N10–H10B•••N04	0.95(4)	2.11(4)	3.028(4)	161(3)
N6–H6A•••N01	0.95(4)	2.03(4)	2.893(4)	150(3)
N5–H5B•••N04	0.90(4)	2.02(4)	2.914(4)	169(3)
N11–H11A•••N3 ⁱ	0.94(3)	2.03(4)	2.956(4)	173(3)
N4–H4A•••N06 ⁱⁱ	0.87(3)	2.18(3)	3.038(4)	166(3)
N12–H12B•••N01 ⁱⁱⁱ	0.93(3)	1.93(3)	2.861(4)	173(3)
N10–H10A•••N03 ^{iv}	0.91(3)	2.18(4)	2.994(5)	148(3)
N5–H5A•••N9 ^v	0.88(3)	2.14(4)	3.009(4)	169(3)
N12–H12A•••N06 ^{vi}	0.89(4)	2.15(4)	2.968(4)	152(3)
N11–H11B•••N03 ^{vii}	0.90(4)	2.05(4)	2.815(4)	141(3)

Table 4.B5 Selected hydrogen bonds for **43** (distances in Å, angles in °, symmetry codes: (i) 1-x, -y, 2-z; (ii) x+1, y, z; (iii) 1-x, -y, 1-z; (iv) 2+x, -1+y, z; (v) -1-x, 1-y, 2-z; (vii) x+1, y-1, z).

D–H•••A	D–H	H•••D	D–A	∠(D–H–A)
N4–H4B•••O3 ⁱ	0.91(2)	2.32(2)	3.075(2)	140(2)
N4–H4B•••O3 ⁱⁱ	0.91(2)	2.34(2)	3.026(2)	131(2)
N6–H6A•••O2 ⁱ	0.84(2)	2.04(2)	2.818(2)	153(2)
N5–H5B•••O3	0.89(2)	2.04(2)	2.911(2)	169(2)
N5–H5A•••N3 ⁱⁱⁱ	0.87(2)	2.17(2)	3.019(2)	164(2)
N6–H6B•••O2 ^{iv}	0.85(2)	2.31(2)	2.893(2)	126(2)
N6–H6B•••O1 ^{iv}	0.85(2)	2.46(2)	3.312(2)	173(2)
N5–H5B•••N4	0.89(2)	2.60(2)	2.869(2)	99(1)
N4–H4A•••O2 ^{vii}	0.93(2)	2.31(2)	3.113(2)	144(2)

Table 4.B6 Selected hydrogen bonds for **44** (distances in Å, angles in °, symmetry codes: (i) -1-x, 1-y, 1-z; (ii) 1-x, -y, 1-z; (iii) -x, 1-y, 1-z; (iv) -x, -y, 1-z; (v) -0.5-x, 0.5-y, -z).

D-H...A	D-H	H...D	D-A	∠(D-H-A)
N5-H5B...N4	0.76(3)	2.63(3)	2.855(3)	100(2)
N6-H6A...O3	0.80(3)	2.24(3)	2.943(4)	148(3)
N5-H5B...O4 ⁱ	0.76(3)	2.52(3)	3.198(4)	150(3)
N5-H5B...O2 ⁱ	0.76(3)	2.62(3)	3.131(4)	126(3)
N6-H6B...O1 ⁱⁱ	0.76(3)	2.31(3)	3.055(4)	167(3)
N4-H4B...O4 ⁱⁱⁱ	0.80(3)	2.46(3)	3.111(3)	139(3)
N4-H4A...O3 ^{iv}	0.88(4)	2.31(4)	3.042(3)	141(3)
N5-H5A...N3 ^v	0.82(3)	2.23(3)	3.035(4)	168(3)

Table 4.B7 Selected hydrogen bonds for **45a** (distances in Å, angles in °, symmetry codes: (i) x, y, z+1; (ii) -x+1, -y+1, -z+1; (iii) -x+2, -y+1, -z+1; (iv) x+1, y-1, z+1; (v) -x+2, -y, -z+1; (vi) -x+2, -y+1, -z).

D-H...A	D-H	H...D	D-A	∠(D-H-A)
O1-H13...N22	0.81(3)	2.13(3)	2.910(3)	162(3)
N6-H6A...N4	0.87(2)	2.53(2)	2.854(2)	103(1)
N12-H12A...N10	0.90(2)	2.57(2)	2.860(2)	99(1)
N4-H4A...N11	0.92(2)	2.45(2)	3.139(3)	132(2)
N12-H12A...O1 ⁱ	0.90(2)	2.11(2)	2.927(2)	151(2)
N10-H10A...N17 ⁱ	0.90(2)	2.40(2)	3.082(2)	132(2)
N11-H11B...N13 ⁱ	0.88(2)	2.16(2)	3.034(2)	173(2)
N5-H5B...N19 ⁱⁱ	0.91(2)	2.03(2)	2.925(2)	167(2)
N10-H10B...N16 ⁱⁱ	0.89(2)	2.26(2)	3.062(3)	150(2)
N4-H4B...N5 ⁱⁱ	0.92(2)	2.30(2)	3.191(3)	164(2)
N4-H4A...N18 ⁱⁱ	0.92(2)	2.50(2)	3.073(2)	121(2)
N5-H5A...N9 ⁱⁱⁱ	0.89(2)	2.14(2)	2.993(2)	161(2)
N11-H11A...N3 ⁱⁱⁱ	0.88(2)	2.15(2)	3.007(2)	165(2)
N12-H12B...N15 ^{iv}	0.92(2)	2.03(2)	2.930(2)	166(2)
N6-H6B...N21 ^v	0.90(2)	1.97(2)	2.845(2)	165(2)
N6-H6A...O1 ^v	0.87(2)	2.28(2)	2.862(2)	124(2)
O1-H20...N14 ^{vi}	0.87(3)	2.05(3)	2.915(2)	168(2)

Table 4.B8 Selected hydrogen bonds for **46a** (distances in Å, angles in °, symmetry codes: (i) -1+x, y, z; (ii) 2-x, -y, 1-z; (iii) 1-x, 0.5+y, 1.5-z; (iv) 1-x, -0.5+y, 1.5-z; (v) 2-x, -0.5+y, 1.5-z).

D-H...A	D-H	H...D	D-A	∠(D-H-A)
N4-H4B...O3	0.91(2)	2.14(2)	2.986(2)	154(2)
O3-H7...N11	0.89(2)	1.92(2)	2.808(2)	172(2)
N6-H6A...N4	0.98(2)	2.55(2)	2.872(2)	99(1)
N6-H6A...N10 ⁱ	0.98(2)	2.04(2)	2.901(2)	145(1)
N4-H4A...N5 ⁱ	0.88(2)	2.67(2)	3.404(2)	141(1)
N5-H5B...N3 ⁱⁱ	0.85(2)	2.15(2)	2.977(2)	164(2)
N6-H6B...O3 ⁱⁱⁱ	0.88(2)	1.94(2)	2.798(2)	164(2)
N4-H4A...N8 ^{iv}	0.88(2)	2.70(2)	3.116(2)	110(1)
N5-H5A...N8 ^{iv}	0.87(2)	2.26(2)	3.125(2)	175(2)
O3-H8...N9 ^v	0.79(2)	2.58(2)	3.256(2)	144(2)

Table 4.B9 Selected hydrogen bonds for **47** (distances in Å, angles in °, symmetry codes: (i) x, 1.5-y, 0.5+z; (ii) -x, 0.5+y, 0.5-z; (iii) -x, -0.5+y, 0.5-z; (iv) x, 0.5-y, 0.5+z; (v) 1-x, -1.5+y, 0.5-z).

D–H•••A	D–H	H•••D	D–A	∠(D–H–A)
N5–H5B•••N4	0.89(2)	2.54(2)	2.841(3)	100(2)
N6–H6A•••O3 ⁱ	0.83(3)	2.37(3)	3.068(2)	142(2)
N4–H6B•••N8 ⁱ	0.90(2)	2.17(2)	3.041(2)	163(2)
N5–H5A•••N3 ⁱⁱ	0.86(3)	2.11(3)	2.966(3)	175(2)
N5–H5B•••O1 ⁱⁱ	0.89(2)	2.11(2)	2.968(3)	163(2)
N4–H4A•••O1 ⁱⁱⁱ	0.92(3)	2.38(3)	3.039(3)	129(2)
N4–H4A•••O1 ^{iv}	0.92(3)	2.55(3)	3.180(2)	126(2)
N6–H6B•••O3 ^v	0.87(3)	2.05(3)	2.851(2)	153(2)

Table 7.B1 Hydrogen-bonding geometry in 5,5'-azotetrazole derivatives.

D–H...A	D–H (Å)	H...A (Å)	D...A (Å)	D–H...A (°)
81				
O1–H1A...N4	0.85(4)	2.01(4)	2.850(5)	177(4)
O2–H2B...N10	0.81(4)	2.13(4)	2.933(5)	170(3)
N17–H17B...N1 ⁱ	0.86(3)	2.03(3)	2.889(4)	174(2)
N17–H17A...O2 ⁱ	0.86(3)	1.85(3)	2.739(4)	166(2)
N11–H11A...O1 ⁱⁱ	0.86(3)	1.85(3)	2.704(4)	170(2)
N11–H11B...N7 ⁱⁱ	0.86(3)	2.02(3)	2.876(4)	170(2)
O2–H2A...N3 ⁱⁱⁱ	0.95(6)	1.87(6)	2.793(4)	168(5)
O1–H1B...N9 ^v	0.99(5)	1.83(5)	2.818(4)	176(4)
82				
O3–H32...N6	0.98(3)	1.94(4)	2.899(2)	165(3)
O2–H21...N9	0.83(3)	2.05(3)	2.876(2)	172(3)
O1–H12...O2	0.90(3)	1.88(4)	2.776(2)	174(3)
N1–H1A...N8 ⁱ	0.96(3)	2.03(3)	2.974(2)	168(2)
N1–H1B...O1 ⁱⁱ	0.85(3)	1.95(3)	2.795(2)	176(2)
O1–H11...O2 ⁱⁱ	0.83(3)	1.93(3)	2.763(3)	180(3)
O3–H31...N7 ⁱⁱⁱ	0.88(3)	2.03(3)	2.894(2)	167(2)
O2–H22...O3 ^{iv}	0.95(4)	1.74(4)	2.687(2)	176(3)
83				
N11–H11A...N16	0.88(3)	2.63(1)	2.912(1)	100(3)
N11–H1B...O1 ^{viii}	0.91(1)	1.88(1)	2.784(1)	172(1)
N16–H16B...N1 ^{viii}	0.84(1)	2.43(1)	3.168(1)	146(1)
O1–H1B...N2 ^{viii}	0.88(1)	1.93(1)	2.832(1)	173(1)
N11–H11A...N4 ^{xiii}	0.88(1)	2.03(1)	2.892(2)	164(2)
O1–H1A...N1 ^{xiv}	0.80(1)	2.04(1)	2.806(1)	170(1)
N16–H16A...O1 ^{xv}	0.88(1)	2.19(1)	3.024(1)	159(1)
84				
N8–H2...N11	0.91(2)	2.550(2)	2.837(3)	99(2)
N11–H6...N7 ⁱ	0.88(2)	2.45(2)	3.277(2)	157(2)
N8–H1...N7 ⁱⁱ	0.88(2)	2.12(2)	2.981(2)	165(2)
85				
N8–H8B...O2	0.98(4)	1.75(4)	2.725(3)	174(3)
N6–H6B...N1 ⁱ	0.84(3)	2.17(3)	3.000(3)	171(3)
N7–H7...N5 ⁱⁱ	0.83(3)	2.19(4)	2.998(3)	165(3)
N8–H8C...N4 ⁱⁱ	0.98(4)	1.92(4)	2.864(3)	159(3)
N6–H6A...N2 ⁱⁱⁱ	0.87(3)	2.22(3)	3.088(4)	173(3)
N8–H8A...O1 ^{iv}	0.85(3)	2.23(3)	2.957(3)	144(3)
O2–H2B...N3 ^{iv}	0.93(5)	1.89(5)	2.803(3)	168(4)
N8–H8A...O1 ^v	0.85(3)	2.42(3)	3.038(4)	131(2)
O2–H2A...O1 ^{vi}	0.88(5)	1.87(5)	2.742(3)	174(4)
86				
N11–H11A...N3	0.87(1)	2.01(2)	2.860(2)	165(1)
N11–H11B...N7	0.93(1)	1.93(1)	2.849(2)	169(1)
N17–H17A...N2 ⁱⁱⁱ	0.84(1)	2.08(1)	2.922(2)	171(1)
N17–H17B...N8 ⁱⁱⁱ	0.92(1)	1.97(2)	2.885(2)	179(1)
88				
N11–H11A...N3 ^{vii}	0.80(2)	2.13(2)	2.929(3)	170(2)
N17–H17A...N2 ^{vii}	0.84(2)	2.04(2)	2.863(3)	165(3)
N11–H11B...N8 ^{viii}	0.95(3)	1.95(3)	2.884(3)	167(2)
N17–H17B...N7 ^{viii}	0.83(3)	2.03(2)	2.852(3)	168(3)
91a				
O1–H8...N4	0.92(2)	2.04(2)	2.992(2)	162(2)

Symmetry codes for **81**: (i) x, -0.5-y, 0.5+z; (ii) x, -0.5-y, -0.5+z; (iii) x, -1+y, z; (v) x, 1+y, z; Symmetry codes for **82**: (i) 0.5-x, -0.5+y, 0.5-z; (ii) 1.5-x, -0.5+y, 0.5-z; (iii) -x, 1-y, 1-z; (iv) 1-x, 1-y, 1-z. **83**: (viii) 1-x, 1-y, -z; (xiii) -1+x, y, -1+z; (xiv) x, 1+y, z; (xv) -1+x, y, z; **84**: (i) 1+x, y, z; (ii) -1-x, 1-y, -z. **85**: (i) 1-x, -y, 1-z; (ii) -1+x, -1+y, z; (iii) 1+x, y, z; (iv) 1-x, -y, 2-z; (v) -1+x, y, z; (vi) 2-x, -y, 2-z. **86**: (iii) 1-x, 1-y, 1-z; **88**: (vii) 1+x, y, z; (viii) 1-x, 1-y, 1-z.

Table 8.B1 Graph-set matrix for strong hydrogen bonds in **95**. First level motifs on-diagonal and second level graph sets off-diagonal.

Constituent H-bond	N4–H4•••N2 ⁱⁱⁱ	N5–H5•••N1 ^{vi}
N4–H4•••N2 ⁱⁱⁱ	C1,1(4)[R2,2(16)]	
N5–H5•••N1 ^{vi}	C2,2(7)[R2,2(16)][R2,2(8)]	C1,1(5)[R2,2(8)]

Symmetry codes: (iii) x, -y, 2.5+z; (vi) 1-x, -1-y, 2-z.

Table 8.B2 Bond distances (Å) in 5,5'-hydrazinebistetrazole derivatives.

Bond	95	97	99	105 (A)	105 (B)	108 (A)	108 (B)	109 (A)	109 (B)
N1–C2		1.463(2)							
C1–N1	1.327(2)	1.341(2)	1.329(3)	1.342(1)	1.394(1)	1.336(3)	1.400(3)	1.333(4)	1.388(4)
N1–N2	1.365(2)	1.367(2)	1.356(3)	1.359(1)	1.334(1)	1.357(3)	1.335(3)	1.369(4)	1.333(4)
N2–N3	1.288(2)	1.293(2)	1.308(3)	1.303(1)	1.353(1)	1.312(3)	1.361(3)	1.309(4)	1.378(3)
N3–N4	1.362(2)	1.371(2)	1.350(3)	1.358(1)	1.315(1)	1.365(3)	1.320(3)	1.357(4)	1.313(4)
N4–C1	1.333(2)	1.326(2)	1.331(3)	1.337(1)	1.356(1)	1.336(3)	1.355(3)	1.348(3)	1.364(3)
C1–N5	1.356(2)	1.350(2)	1.409(3)	1.375(1)	1.334(1)	1.396(3)	1.335(3)	1.385(4)	1.344(4)
N5–N5 ⁱ	1.391(2)	1.394(2)	1.441(4)	1.412(1)		1.432(3)		1.416(4)	

Symmetry codes for **95**: (i) 1-x, y, 2.5-z. **97**: (i) 1-x, -y, -z. **99**: (i) 2-x, 1-y, -z.

Table 8.B3 Selected bond distances (Å) for alkaline earth salts of 5,5'-hydrazinebistetrazole (**95**).

Bond	110 (A)	110 (B)	111	112	113
N1–N2 ^a	1.366(2)	1.363(2)	1.352(2)	1.345(3)	1.347(6)
N2–N3	1.299(2)	1.308(2)	1.306(2)	1.306(3)	1.301(6)
N3–N4	1.364(2)	1.352(2)	1.354(2)	1.356(3)	1.361(6)
N4–C1 ^a	1.341(2)	1.334(2)	1.328(2)	1.328(3)	1.316(6)
C1–N1	1.337(2)	1.329(2)	1.341(2)	1.342(3)	1.333(6)
C1–N5	1.388(2)	1.405(2)	1.391(3)	1.391(3)	1.397(6)
N5–N5 ^{iii b}	1.432(2)		1.426(3)	1.423(4)	1.422(8)
N6–N6 ^{iv b}		1.442(2)	1.428(3)	1.432(4)	1.431(9)
N6–C2	1.407(2)	1.407(2)	1.397(2)	1.390(3)	1.392(6)
C2–N7	1.335(2)	1.327(2)	1.330(2)	1.330(3)	1.324(6)
N7–N8 ^c	1.356(2)	1.356(2)	1.362(2)	1.361(3)	1.344(6)
N8–N9	1.305(2)	1.311(2)	1.300(2)	1.301(3)	1.307(6)
N9–N10 ^{iii d}	1.361(2)	1.351(2)	1.349(2)	1.351(3)	1.344(6)
C2–N10 ^{iii e}	1.332(2)	1.332(2)	1.338(2)	1.343(3)	1.336(6)

110: ^{a,c}no symmetry codes, N5–N5ⁱⁱⁱ = N5–N6 and N6–N6^{iv} = N15–N16. **111**: ^b(iii) -1-x, -y, -z; (iv) -x, 1-y, -z; ^d(ii) -x, -y, -z; ^e(ii) -x, -y, -z. **112**: ^b(iii) 1-x, 1-y, -z; (iv) -x, -y, -z; ^c(ii) -x, 1-y, -z; ^e(ii) -x, 1-y, -z; **113**: ^a(ii) 1-x, 1-y, -z; N1–N2ⁱⁱ. ^b(iii) 1-x, -y, -z; (iv) 2-x, 1-y, -z.

Table 8.B4 Bond angles (°) in 5,5'-hydrazinebistetrazole derivatives.

Angle	95	97	99	105 (A)	105 (B)	108 (A)	108 (B)	109 (A)	109 (B)
C1–N1–C2	111.8(1)	130.3(1)							
N2–N1–C2	105.6(1)	121.7(1)							
N3–N2–N1	108.9(1)	106.6(1)	109.5(2)	109.88(8)	109.65(8)	109.7(2)	109.4(2)	110.4(2)	109.9(2)
N2–N3–N4	126.7(1)	110.9(1)	109.7(2)	109.93(8)	109.62(8)	109.9(2)	109.7(2)	109.4(2)	109.7(2)
N4–C1–N1	124.0(1)	109.1(1)	112.9(2)	112.61(9)	116.04(8)	113.5(2)	113.6(2)	113.1(3)	114.0(2)
N4–C1–N5	104.9(1)	127.2(1)	121.2(2)	125.01(9)	112.94(8)	122.6(2)	115.5(2)	120.1(3)	116.2(3)
N1–C1–N5	108.5(1)	123.6(1)	125.9(2)	122.22(9)	122.66(9)	123.8(2)	123.4(2)	126.8(3)	124.3(3)
C1–N1–N2	116.8(1)	107.8(1)	103.9(2)	103.73(8)	103.91(8)	103.7(2)	103.7(2)	103.2(2)	103.2(2)
C1–N4–N3		105.5(1)	104.0(2)	103.85(8)	103.77(8)	103.2(2)	103.8(2)	104.0(3)	103.6(2)
C1–N5–N5 ⁱ		118.3(1)	110.9(2)	116.04(8)		113.6(2)		114.0(2)	

Symmetry codes for **95**: (i) 1-x, y, 2.5-z. **97**: (i) 1-x, -y, -z. **99**: (i) 2-x, 1-y, -z.

Table 8.B5 Selected bond angles (°) for alkaline earth salts of 5,5'-hydrazinebistetrazole (**95**).

Angle	110 (A)	110 (B)	111	112	113
N1–C1–N5	125.9(2)	125.2(2)	123.4(2)	123.1(2)	122.7(4)
N2–N3–N4	109.7(1)	110.0(1)	109.7(1)	109.7(2)	109.6(4)
N7–C2–N6	124.6(2)	125.0(2)	123.3(2)	124.0(2)	125.3(4)
C2–N7–N8 ^a	102.7(1)	103.5(1)	103.4(1)	103.6(2)	104.0(4)
N9–N8–N7 ^a	110.7(1)	109.9(1)	109.9(1)	110.1(2)	109.7(4)
C1–N5–N5 ⁱⁱⁱ ^b	111.1(1)	111.2(1)	112.1(2)	112.3(2)	112.6(5)
C2–N6–N6 ^{iv} ^b	112.0(1)	112.3(1)	112.6(2)	112.7(2)	111.6(5)
N8–N9–N10 ⁱⁱ ^c	109.2(1)	109.2(1)	109.9(1)	109.5(2)	109.8(4)
C2–N10–N9 ⁱⁱ ^c	103.5(1)	104.1(1)	103.8(1)	104.0(2)	103.6(4)
N6–C2–N10 ⁱⁱ ^d	121.6(2)	121.7(2)	123.6(2)	123.4(2)	121.9(4)
N7–C2–N10 ⁱⁱ ^d	113.7(2)	113.1(2)	112.9(2)	112.6(2)	112.9(4)
N3–N4–C1 ^e	103.6(1)	103.6(1)	103.6(1)	103.5(2)	103.7(4)
N1–C1–N4 ^e	112.9(2)	113.3(2)	113.2(2)	113.0(2)	113.1(4)
N5–C1–N4 ^e	120.9(2)	121.3(2)	123.2(2)	123.9(2)	124.2(4)
N3–N2–N1 ^e	110.2(1)	109.4(1)	110.2(1)	110.1(2)	109.6(4)
C1–N1–N2 ^e	103.3(1)	103.6(1)	103.1(1)	103.5(2)	103.9(4)
N1–C1–N5–N5 ⁱⁱⁱ ^b	–168.9(2)	–163.1(2)	180.0(1)	180.0(2)	180.0(3)
N7–C2–N6–N6 ^{iv} ^b	–151.1(2)	–146.7(2)	180.0(1)	180.0(2)	180.0(3)

110: ^{a-c}no symmetry codes, N5ⁱⁱⁱ = N6 and N6^{iv} = N16. **111**: ^b(iii) -1-x, -y, -z; (iv) -x, 1-y, -z; ^c(ii) -x, -y, -z; ^d(ii) -x, -y, -z. **112**:

^a(ii) -x, 1-y, -z; ^b(iii) 1-x, 1-y, -z; (iv) -x, -y, -z; ^c(ii) -x, 1-y, -z. **113**: ^a(iii) 1-x, -y, -z; (iv) 2-x, 1-y, -z; ⁱ(ii) 1-x, 1-y, -z.

Table 8.B6 Hydrogen-bonding geometry in 5,5'-hydrazinebistetrazole derivatives.

D–H...A	D–H (Å)	H...A (Å)	D...A (Å)	D–H...A (°)
95				
N4–H4...N2 ⁱ	0.81(2)	2.13(2)	2.917(2)	166.(2)
N5–H5...N1 ⁱⁱ	0.86(2)	2.09(2)	2.941(2)	168.(2)
97				
N5–H5...O ⁱ	0.88(2)	1.92(2)	2.783(3)	165(1)
O–H4...N4 ⁱⁱ	0.86(2)	1.89(2)	2.748(2)	172(2)
99				
O–H2...N5	0.88(4)	2.09(3)	2.942(3)	162(3)
N5–H5A...O	0.95(4)	2.00(4)	2.932(3)	168(3)
N6–H6A...N4	0.95(4)	1.94(3)	2.884(3)	171(3)
N6–H6B...O ⁱ	0.90(3)	1.95(3)	2.833(3)	170(3)
N6–H6D...N3 ⁱⁱ	0.90(4)	2.04(4)	2.942(3)	174(3)
N6–H6C...N2 ⁱⁱⁱ	0.87(3)	2.16(4)	2.966(3)	154(3)
O–H1...N1 ⁱⁱⁱ	0.84(4)	2.06(3)	2.791(3)	162(3)
105				
N5–H5...N9 ⁱ	0.87(1)	2.21(1)	2.956(1)	144(1)
N6–H6...N2 ⁱⁱ	0.84(1)	2.41(1)	3.142(1)	145(1)
O3–H3B...N9 ⁱⁱⁱ	0.87(2)	2.06(2)	2.845(1)	149(2)
O3–H3B...N10 ⁱⁱⁱ	0.87(2)	2.67(2)	3.233(1)	123(1)
O2–H2B...N10 ⁱ	0.84(2)	2.02(2)	2.838(1)	166(2)
O1–H1A...N1 ⁱⁱ	0.83(2)	2.14(2)	2.963(1)	177(2)
O3–H3A...N2 ^{iv}	0.88(2)	1.92(2)	2.794(1)	173(2)
O1–H1B...N1 ^v	0.87(2)	2.07(2)	2.933(1)	169(2)
O2–H2A...O1 ^{vi}	0.85(2)	2.04(2)	2.859(1)	163(2)
108				
N5–H5...N8 ⁱ	0.75(2)	2.51(2)	3.246(3)	167(2)
N5–H5...N7 ⁱ	0.75(2)	2.51(2)	3.179(3)	149(2)
N6–H6...N9 ⁱⁱ	0.84(3)	2.58(3)	3.104(3)	122(2)
109				
N5–H5...N2	0.83(4)	2.27(4)	3.024(3)	153(3)
N6–H6...N4 ⁱ	0.82(4)	2.24(4)	3.060(4)	172(4)

Symmetry codes for **95**: (i) x, -y, 2.5+z; (ii) 1-x, -1-y, 2-z. **97**: (i) x, -1+y, z; (ii) 1-x, y, 1-z. **99**: (i) x+1, y, z; (ii) -x+3, -y+1, -z+1; (iii) x, y+1, z. **105**: (i) -x, 1-y, 1-z; (ii) -x, 1-y, 2-z; (iii) 1-x, 1-y, 1-z; (iv) 1-x, -y, 2-z; (v) x, 1+y, z; (vi) x, -1+y, z. **108**: (i) 0.5+x, 0.5-y, 0.5+z; (ii) 0.5+x, 0.5-y, -0.5+z. **109**: (i) 2-x, 0.5+y, 1.5-z.

Table 8.B7 Geometry for selected hydrogen bonds for alkaline earth salts of 5,5'-hydrazinebistetrazole (**95**).

D–H...A	D–H (Å)	H...A (Å)	D...A (Å)	D–H...A (°)
110				
O9–H9A...O13	0.84(2)	1.90(3)	2.708(2)	159(2)
O4–H4A...O13	0.89(3)	1.83(3)	2.717(2)	169(3)
O3–H3B...N16	0.83(2)	2.13(2)	2.956(3)	177(2)
O6–H11B...N11	0.91(3)	1.80(3)	2.706(2)	176(2)
N16–H16...O2 ⁱⁱ	0.86(2)	2.36(2)	3.219(2)	175(2)
N15–H15...O10 ⁱⁱⁱ	0.87(2)	2.53(2)	3.233(3)	138(2)
N15–H15...O11 ⁱⁱⁱ	0.87(2)	2.44(2)	3.199(2)	147(2)
O2–H2B...N13 ^v	0.85(2)	1.94(2)	2.782(2)	168(2)
O5–H5A...N20 ^{vi}	0.88(2)	1.85(2)	2.729(2)	174(2)
O10–H2B...N12 ^{ix}	0.88(3)	1.86(3)	2.733(2)	172(2)
O9–H9B...N15 ^x	0.82(2)	2.10(2)	2.926(3)	179(2)
O3–H3A...N18 ^x	0.83(2)	1.95(2)	2.770(2)	175(2)
111				
O1–H1...N3 ⁱ	0.88(2)	2.04(2)	2.922(1)	175(2)
O2–H2A...N4 ⁱ	0.87(2)	2.01(2)	2.880(1)	176(2)
O2–H2B...N8 ⁱⁱ	0.81(2)	2.10(2)	2.906(2)	172(2)
O3–H3B...N7 ⁱⁱ	0.86(2)	2.04(2)	2.901(2)	179(2)
O3–H3A...N2 ⁱⁱⁱ	0.82(2)	2.14(2)	2.936(2)	161(2)
112				
O3–H3B...N4 ⁱ	0.84(3)	2.05(3)	2.886(2)	176(2)
O3–H3A...N8 ⁱⁱ	0.77(3)	2.18(3)	2.934(2)	167(2)
O1–H1B...N7 ⁱⁱⁱ	0.81(3)	2.09(3)	2.901(2)	180(3)
O2–H2...N3 ^{iv}	0.80(2)	2.14(2)	2.935(2)	176(2)
O1–H1A...N2 ^v	0.71(3)	2.30(3)	2.978(2)	158(3)
O1–H1A...O3 ^{vi}	0.71(3)	2.65(3)	3.072(2)	120(2)
113				
O3–H3A...N6	0.83(1)	2.06(1)	2.900(1)	176(1)
O3–H3B...N3 ⁱⁱⁱ	0.85(1)	2.25(1)	2.983(1)	147(1)
O1–H1A...N7 ^v	0.84(1)	2.08(1)	2.933(1)	174(2)
O1–H1B...N7 ^{vi}	0.85(1)	2.10(1)	2.910(1)	169(2)
O2–H2A...N4 ^{vii}	0.86(1)	2.06(1)	2.900(1)	176(2)
O2–H2B...N8 ^{viii}	0.84(1)	2.30(1)	3.051(1)	151(1)

Symmetry codes for **110**: (ii) -1+x, y, z; (iii) -x, 1-y, 1-z; (v) 1-x, 1-y, 2-z; (vi) 1+x, y, z; (ix) x, y, -1+z; (x) 1-x, 1-y, 1-z; **111**: (i) 0.5-x, -0.5+y, 0.5-z; (ii) 0.5+x, 0.5-y, 0.5+z; (iii) -0.5+x, 0.5-y, 0.5+z; **112**: (i) 0.5-x, 0.5+y, 0.5+z; (ii) 0.5+x, 0.5-y, 0.5-z; (iii) 0.5-x, -0.5+y, -0.5+z; (iv) -0.5+x, 0.5-y, 0.5-z; (v) -0.5+x, 0.5-y, -0.5-z; (vi) -0.5+x, 0.5-y, -0.5+z; **113**: (iii) 0.5+x, 0.5-y, 1.5-z; (v) x, y, 1+z; (vi) 1-x, 1-y, -1+z; (vii) 0.5+x, 0.5-y, 2.5-z; (viii) 1-x, 1-y, 1+z.

Table 8.B8 Selected contact distances for the coordination around the Li⁺ atoms in **105**.

<i>Contact distances (Å)</i>			
Li1–O1	1.982(2)	Li2–N7	2.030(2)
Li1–N4	2.031(2)	Li2–O2	1.998(2)
Li1–N8 ⁱⁱ	2.070(2)	Li2–O3	1.907(2)
Li1–N3 ⁱⁱⁱ	2.092(2)	Li2–O2 ⁱ	1.996(2)

Symmetry codes: (i) 1-x, -y, 1-z; (ii) 1-x, 1-y, 1-z; (iii) 1-x, 1-y, 2-z.

Table 8.B9 Selected contact distances for the coordination around the Rb⁺ atoms in **108**.

<i>Contact distances (Å)</i>			
Rb1–N1	3.182(2)	Rb2–N1	3.360(2)
Rb1–N9	3.465(2)	Rb2–N2	3.213(2)
Rb1–N10	3.091(2)	Rb2–N3	3.324(2)
Rb1–N2 ⁱⁱ	2.998(2)	Rb2–N10	3.050(2)
Rb1–N3 ⁱⁱ	3.060(2)	Rb2–N3 ⁱ	2.949(2)
Rb1–N8 ^v	3.022(2)	Rb2–N4 ⁱ	3.243(2)
Rb1–N9 ^v	3.173(2)	Rb2–N1 ⁱⁱ	3.264(2)
Rb1–N7 ^{vi}	3.059(2)	Rb2–N2 ⁱⁱ	3.006(2)
Rb1–N4 ^{vii}	3.129(2)	Rb2–N4 ⁱⁱⁱ	3.105(2)
Rb1–N6 ^{vii}	3.216(2)	Rb2–N5 ⁱⁱⁱ	3.100(2)
		Rb2–N8 ^{iv}	3.263(2)

Symmetry codes: (i) -x, 1-y, 1-z; (ii) -x, 1-y, 2-z; (iii) -1+x, y, z; (iv) -0.5+x, 0.5-y, -0.5+z; (v) 0.5+x, 0.5-y, 0.5+z; (vi) -0.5+x, 0.5-y, 0.5+z; (vii) x, y, 1+z.

Table 8.B10 Selected contact distances for the coordination around the Cs⁺ atoms in **109**.

<i>Contact distances (Å)</i>			
Cs1–N9	3.179(3)	Cs2–N8	3.124(2)
Cs1–N4	3.467(3)	Cs2–N6	3.240(3)
Cs1–N8	3.232(3)	Cs2–N4	3.339(3)
Cs1–N10	3.240(3)	Cs2–N10	3.443(3)
Cs1–N2	3.354(3)	Cs2–N3 ^{iv}	3.155(3)
Cs1–N1	3.485(2)	Cs2–N10 ^{iv}	3.231(3)
Cs1–N7	3.425(3)	Cs2–N9 ^v	3.258(3)
Cs1–N3	3.443(3)	Cs2–N1 ^v	3.308(2)
Cs1–N7 ⁱ	3.212(2)	Cs2–N2 ^{vi}	3.338(2)
Cs1–N8 ⁱⁱ	3.382(3)	Cs2–N3 ^{vi}	3.375(3)
Cs1–N2 ⁱⁱⁱ	3.671(3)	Cs2–N1 ^{vii}	3.533(2)
Cs1–N7 ⁱⁱⁱ	3.696(3)		

Symmetry codes: (i) -0.5+x, 0.5-y, 2-z; (ii) -1+x, y, z; (iii) 0.5+x, 0.5-y, 2-z; (iv) 1+x, y, z; (v) 0.5+x, 1.5-y, 2-z; (vi) 2-x, 0.5+y, 1.5-z; (vii) 2.5-x, 1-y, -0.5+z.

Table 8.B11 Selected bond distances (Å) and angles (°) for the coordination around the Mg²⁺ cations in **110**.

A		B	
Mg1–O1	2.051(2)	Mg2–O9	2.047(2)
Mg1–O2	2.093(2)	Mg2–O8	2.060(2)
Mg1–O3	2.134(2)	Mg2–O11	2.061(2)
Mg1–O4	2.070(2)	Mg2–O12	2.075(2)
Mg1–O5	2.047(2)	Mg2–O10	2.081(2)
Mg1–O6	2.111(2)	Mg2–O7	2.120(2)
A		B	
O1–Mg1–O2	95.12(7)	O7–Mg2–O8	85.15(7)
O1–Mg1–O3	171.52(7)	O7–Mg2–O9	87.80(7)
O1–Mg1–O4	89.38(7)	O7–Mg2–O10	173.64(7)
O1–Mg1–O5	87.58(7)	O7–Mg2–O11	95.19(6)
O1–Mg1–O6	87.97(7)	O7–Mg2–O12	91.35(6)
O2–Mg1–O3	90.27(6)	O8–Mg2–O9	94.44(8)
O2–Mg1–O4	175.16(7)	O8–Mg2–O10	91.83(7)
O2–Mg1–O5	86.46(8)	O8–Mg2–O11	176.93(7)
O2–Mg1–O6	89.70(8)	O8–Mg2–O12	91.12(8)
O3–Mg1–O4	85.47(7)	O9–Mg2–O10	86.86(7)
O3–Mg1–O5	99.30(6)	O9–Mg2–O11	88.63(8)
O3–Mg1–O6	85.51(6)	O9–Mg2–O12	174.28(7)
O4–Mg1–O5	91.97(8)	O10–Mg2–O11	88.13(6)
O4–Mg1–O6	92.23(8)	O10–Mg2–O12	94.30(7)
O5–Mg1–O6	173.84(7)	O11–Mg2–O12	85.82(8)

Table 8.B12 Selected distances (Å) and angles (°) for the coordination around the Ca²⁺ cations in **111**.

Ca–O2	2.408(1)	Ca–O1	2.570(1)
Ca–O2 ⁱ	2.408(1)	Ca–N1	2.788(2)
Ca–O3	2.415(1)	Ca–N9	2.792(2)
Ca–O3 ⁱ	2.415(1)	Ca–N10	2.806(2)
Ca–O1 ⁱⁱ	2.570(1)		
O2–Ca–O1	82.08(3)	O3–Ca–N9	69.38(3)
O2 ⁱ –Ca–O1	133.54(3)	O1–Ca–N9	65.00(3)
O3–Ca–O1	82.16(3)	N1–Ca–N9	119.13(5)
O3 ⁱ –Ca–O1	133.76(3)	O2–Ca–N10	67.05(3)
O1 ⁱⁱ –Ca–O1	72.49(5)	O3–Ca–N10	135.55(3)
O2–Ca–N1	71.68(3)	O1–Ca–N10	67.43(3)
O3–Ca–N1	68.22(3)	N1–Ca–N10	120.89(5)
O1–Ca–N1	143.68(2)	N9–Ca–N10	119.97(5)
O2–Ca–N9	135.57(3)	O2–Ca–O3 ⁱ	139.88(4)
O2–Ca–O2 ⁱ	88.70(5)	O2 ⁱ –Ca–O3 ⁱ	77.63(4)
O2–Ca–O3	77.63(4)	O3–Ca–O3 ⁱ	88.89(5)

Symmetry codes: (i) x, y, -z; (ii) -x, -y, -z.

Table 8.B13 Selected distances (Å) and angles (°) for the coordination around the Sr²⁺ cations in **112**.

Sr–O3	2.558(2)	Sr–O2 ⁱⁱ	2.697(2)
Sr–O3 ⁱ	2.558(2)	Sr–N1	2.833(2)
Sr–O1	2.560(2)	Sr–N9	2.871(2)
Sr–O1 ⁱ	2.560(2)	Sr–N10	2.855(2)
Sr–O2	2.697(2)		
O3–Sr–O3 ⁱ	90.40(8)	O1–Sr–N1	68.34(5)
O3–Sr–O1	140.92(5)	O2–Sr–N1	142.16(4)
O3 ⁱ –Sr–O1	76.39(6)	O3–Sr–N10	67.29(4)
O3 ⁱ –Sr–O1 ⁱ	140.92(5)	O1–Sr–N10	134.53(4)
O1–Sr–O1 ⁱ	90.94(8)	O2–Sr–N10	67.88(4)
O3–Sr–O2	80.25(5)	N1–Sr–N10	121.72(6)
O3 ⁱ –Sr–O2	134.33(4)	O3–Sr–N9	134.62(4)
O1–Sr–O2	134.47(4)	O1–Sr–N9	70.36(5)
O1 ⁱ –Sr–O2	80.11(6)	O2–Sr–N9	64.55(3)
O2–Sr–O2 ⁱⁱ	75.44(7)	N1–Sr–N9	119.61(6)
O3–Sr–N1	72.64(4)	N9–Sr–N9	118.67(6)

Symmetry codes: (i) x, y, -z; (ii) -x, 1-y, -z.

Table 8.B14 Selected distances (Å) and angles (°) for the coordination around the Ba²⁺ cations in **113**.

Ba–O2 ⁱ	2.7366(1)	Ba–N2 ^{iv}	2.9905(1)
Ba–O1 ⁱⁱ	2.8723(1)	Ba–O3 ⁱ	2.7390(1)
Ba–O3	2.7390(1)	Ba–O1	2.8723(1)
Ba–N1	2.9736(1)	Ba–O2	2.7366(1)
Ba–N9 ⁱⁱⁱ	2.9616(1)		
O2–Ba–O2 ⁱ	93.5(1)	O3–Ba–N9 ⁱⁱⁱ	73.72(6)
O2–Ba–O3	142.2(1)	O1–Ba–N9 ⁱⁱⁱ	141.24(5)
O2–Ba–O3 ⁱ	75.2(1)	O2–Ba–N1	133.22(7)
O3–Ba–O3 ⁱ	91.8(1)	O3–Ba–N1	67.90(7)
O2–Ba–O1 ⁱⁱ	135.06(6)	O1–Ba–N1	67.29(5)
O3–Ba–O1 ⁱⁱ	78.75(7)	N9 ⁱⁱⁱ –Ba–N1	123.53(9)
O2–Ba–O1	78.41(8)	O2–Ba–N2 ⁱⁱ	71.50(7)
O2 ⁱ –Ba–O1	135.06(6)	O3–Ba–N2 ⁱⁱ	133.76(7)
O3–Ba–O1	134.48(6)	O1–Ba–N2 ⁱⁱ	63.97(5)
O1 ⁱⁱ –Ba–O1	77.2(1)	N9 ⁱⁱ –Ba–N2 ⁱⁱ	120.22(9)
O2–Ba–N9 ⁱⁱⁱ	68.60(8)	N1–Ba–N2 ⁱⁱ	116.25(9)

Symmetry codes: (i) x, y, 2-z; (ii) 1-x, 1-y, 2-z; (iii) 0.5+x, 0.5-y, 0.5+z; (iv) 1-x, -y, 2-z.

Table 9.B1 Graph-set matrix for selected hydrogen bonds in **132**. First level motifs on-diagonal and second level graph-sets off-diagonal.

D–H...A	O5–H7...N6 ⁱⁱⁱ	O5–H8...N7 ^{iv}	O6–H5...N9 ⁱⁱ	O6–H6...N6 ⁱ
O5–H7...N6 ⁱⁱⁱ	D1,1(2)			
O5–H8...N7 ^{iv}	R4,4(10)	D1,1(2)		
O6–H5...N9 ⁱⁱ	D2,2(5)	D2,2(5)	D1,1(2)	
O6–H6...N6 ⁱ	D2,2(5)	D2,2(5)	D2,2(5)	D1,1(2)

Symmetry codes for **132**: (i) x, -1+y, z; (ii) 2-x, 1-y, -z; (iii) 2-x, 2-y, -1-z; (iv) -1+x, 2+y, 1+z.

Table 9.B2 Graph-set matrix for selected hydrogen bonds in **133**. First level motifs on-diagonal and second level graph-sets off-diagonal.

D–H...A	O5–H7...N15 ⁱ	O5–H8...N16 ⁱⁱ	O6–H5...N18 ⁱⁱⁱ	O6–H6...N6 ⁱⁱⁱ
O5–H7...N15 ⁱ	D1,1(2)			
O5–H8...N16 ⁱⁱ	R4,4(10)	D1,1(2)		
O6–H5...N18 ⁱⁱⁱ	D2,2(5)	D2,2(5)	D1,1(2)	
O6–H6...N6 ⁱⁱⁱ	D2,2(5)	D2,2(5)	D2,2(5)	D1,1(2)

Symmetry codes for **133**: (i) -1-x, 2-y, 1-z; (ii) -1+x, y, z; (iii) -x, 2-y, -z.

Table 9.B3 Selected bond angles for the coordination around the K⁺ cations in **132**.

O5–K1–O4	103.68(3)	N6–K1–O3 ^v	74.45(3)	O6–K2–N5 ⁱⁱ	72.86(3)
O5–K1–O5 ^{iv}	83.99(3)	O5–K1–N10 ^v	85.95(3)	N17–K2–N5 ⁱⁱ	69.68(3)
O4–K1–O5 ^{iv}	85.23(4)	N2–K1–N10 ^v	140.76(3)	O6 ⁱ –K2–N5 ⁱⁱ	137.00(3)
O5–K1–N2	104.56(3)	N14–K1–N10 ^v	116.38(3)	N18–K2–N5 ⁱⁱ	141.92(3)
O4–K1–N2	138.61(3)	O1–K1–N10 ^v	164.03(3)	N16 ⁱⁱ –K2–N5 ⁱⁱ	75.44(3)
O5 ^{iv} –K1–N2	127.26(3)	N6–K1–N10 ^v	74.41(3)	N4–K2–N5 ⁱⁱ	119.73(3)
O5–K1–N14	150.92(3)	O3 ^v –K1–N10 ^v	20.51(3)	N16–K2–N5 ⁱⁱ	59.70(3)
O4–K1–N14	97.07(3)	O4–K1–N10 ^v	19.36(3)	O6–K2–N17 ⁱⁱⁱ	103.81(3)
O5 ^{iv} –K1–N14	77.61(3)	O5 ^{iv} –K1–N10 ^v	90.97(3)	N17–K2–N17 ⁱⁱⁱ	67.46(3)
N2–K1–N14	70.65(3)	O6–K2–N17	127.66(3)	O6 ⁱ –K2–N17 ⁱⁱⁱ	97.06(3)
O5–K1–O1	84.43(3)	O6–K2–O6 ⁱ	78.34(3)	N18–K2–N17 ⁱⁱⁱ	22.58(3)
O4–K1–O1	158.18(4)	N17–K2–O6 ⁱ	151.33(3)	N16 ⁱⁱ –K2–N17 ⁱⁱⁱ	161.56(3)
O5 ^{iv} –K1–O1	75.39(3)	O6–K2–N18	102.10(3)	N4–K2–N17 ⁱⁱⁱ	92.95(3)
N2–K1–O1	54.56(2)	N17–K2–N18	86.62(3)	N16–K2–N17 ⁱⁱⁱ	91.05(3)
N14–K1–O1	69.33(3)	O6 ⁱ –K2–N18	74.74(3)	N5 ⁱⁱ –K2–N17 ⁱⁱⁱ	120.22(3)
O5–K1–N6	122.45(3)	O6–K2–N16 ⁱⁱ	89.74(3)	O6–K2–N15 ⁱⁱ	81.86(3)
O4–K1–N6	71.40(3)	N17–K2–N16 ⁱⁱ	113.97(3)	N17–K2–N15 ⁱⁱ	134.89(3)
O5 ^{iv} –K1–N6	147.67(3)	O6 ⁱ –K2–N16 ⁱⁱ	73.16(3)	O6 ⁱ –K2–N15 ⁱⁱ	50.59(3)
N2–K1–N6	68.04(3)	N18–K2–N16 ⁱⁱ	142.60(3)	N18–K2–N15 ⁱⁱ	123.53(3)
N14–K1–N6	83.31(3)	O6–K2–N4	149.91(3)	N16 ⁱⁱ –K2–N15 ⁱⁱ	22.88(3)
O1–K1–N6	121.55(3)	N17–K2–N4	81.75(3)	N4–K2–N15 ⁱⁱ	70.63(3)
O5–K1–O3 ^v	70.04(3)	O6 ⁱ –K2–N4	74.89(3)	N16–K2–N15 ⁱⁱ	110.62(3)
O4–K1–O3 ^v	39.53(3)	N18–K2–N4	83.94(3)	N5 ⁱⁱ –K2–N15 ⁱⁱ	93.64(3)
O5 ^{iv} –K1–O3 ^v	101.62(3)	N16 ⁱⁱ –K2–N4	69.61(3)	N17 ⁱⁱⁱ –K2–N15 ⁱⁱ	145.99(3)
N2–K1–O3 ^v	130.53(3)	O6–K2–N16	131.14(3)		
N14–K1–O3 ^v	135.53(3)	N17–K2–N16	24.73(3)	N4–K2–N16	72.16(3)
O1–K1–O3 ^v	154.47(3)	O6 ⁱ –K2–N16	146.40(3)	N18–K2–N16	107.76(3)

Symmetry codes for **132**: (i) 2-x, 1-y, -z; (ii) 2-x, 2-y, -z; (iii) 1-x, 2-y, -z; (iv) 3-x, 2-y, -1-z; (v) 3-x, 1-y, -1-z.

Table 9.B4 Selected bond angles for the coordination around the Rb⁺ cations in **133**.

O2–Rb1–O1 ^{vi}	144.56(5)	N11–Rb1–N1 ^{iv}	145.01(5)	N14 ⁱ –Rb2–N7 ⁱ	58.82(5)
N1 ^{iv} –Rb1–O1 ^{vi}	90.47(6)	N5–Rb1–N1 ^{iv}	118.55(6)	N8 ⁱ –Rb2–N8 ⁱⁱ	72.11(6)
O5–Rb1–O2 ^{iv}	98.20(7)	O3–Rb1–N1 ^{iv}	162.97(5)	O6–Rb2–N8 ⁱⁱ	110.32(6)
O5–Rb1–O5 ^v	84.33(6)	N15–Rb1–N1 ^{iv}	79.29(5)	N9 ⁱⁱ –Rb2–N8 ⁱⁱ	23.04(5)
O2 ^{iv} –Rb1–O5 ^v	81.35(7)	O1 ^{iv} –Rb1–N1 ^{iv}	19.85(5)	O6 ⁱⁱⁱ –Rb2–N8 ⁱⁱ	93.27(5)
O5–Rb1–N11	109.20(6)	O2–Rb1–N1 ^{iv}	72.89(6)	N7–Rb2–N8 ⁱⁱ	157.53(5)
O2 ^{iv} –Rb1–N11	142.05(6)	O5–Rb1–O1 ^{vi}	66.55(5)	N13–Rb2–N8 ⁱⁱ	89.65(5)
O5 ^v –Rb1–N11	126.04(6)	O2 ^{iv} –Rb1–O1 ^{vi}	104.35(6)	N14 ⁱ –Rb2–N8 ⁱⁱ	125.50(5)
O5–Rb1–N5	151.15(6)	O5 ^v –Rb1–O1 ^{vi}	150.78(5)	N7 ⁱ –Rb2–N8 ⁱⁱ	93.19(5)
O2 ^{iv} –Rb1–N5	99.96(6)	N11–Rb1–O1 ^{vi}	65.66(5)	N8 ⁱ –Rb2–N6 ⁱⁱⁱ	118.11(6)
O5 ^v –Rb1–N5	76.50(6)	N5–Rb1–O1 ^{vi}	128.95(5)	O6–Rb2–N6 ⁱⁱⁱ	49.26(5)
N11–Rb1–N5	67.52(5)	O3–Rb1–O1 ^{vi}	98.96(4)	N9 ⁱⁱ –Rb2–N6 ⁱⁱⁱ	60.93(5)
O5–Rb1–O3	89.44(6)	N15–Rb1–O1 ^{vi}	61.01(5)	O6 ⁱⁱⁱ –Rb2–N6 ⁱⁱⁱ	77.56(5)
O2 ^{iv} –Rb1–O3	156.63(6)	O1 ^{iv} –Rb1–O1 ^{vi}	73.01(5)	N7–Rb2–N6 ⁱⁱⁱ	123.45(5)
O5 ^v –Rb1–O3	77.44(6)	N8 ⁱ –Rb2–O6	125.38(6)	N13–Rb2–N6 ⁱⁱⁱ	133.47(5)
N11–Rb1–O3	51.79(5)	N8 ⁱ –Rb2–N9 ⁱⁱ	91.32(6)	N14 ⁱ –Rb2–N6 ⁱⁱⁱ	107.07(5)
N5–Rb1–O3	65.65(5)	O6–Rb2–N9 ⁱⁱ	109.74(6)	N7 ⁱ –Rb2–N6 ⁱⁱⁱ	139.48(5)
O5–Rb1–N15	123.37(5)	N8 ⁱ –Rb2–O6 ⁱⁱⁱ	146.89(6)	N8 ⁱⁱ –Rb2–N6 ⁱⁱⁱ	63.00(5)
O2 ^{iv} –Rb1–N15	76.19(6)	O6–Rb2–O6 ⁱⁱⁱ	87.34(6)	N8 ⁱ –Rb2–N6	134.63(6)
O5 ^v –Rb1–N15	146.23(5)	N9 ⁱⁱ –Rb2–O6 ⁱⁱⁱ	70.30(6)	O6–Rb2–N6	78.23(5)
N11–Rb1–N15	66.97(5)	N8 ⁱ –Rb2–N7	114.54(6)	N9 ⁱⁱ –Rb2–N6	118.56(5)
N5–Rb1–N15	82.87(5)	O6–Rb2–N7	83.92(6)	O6 ⁱⁱⁱ –Rb2–N6	48.80(5)
O3–Rb1–N15	117.68(5)	N9 ⁱⁱ –Rb2–N7	136.59(6)	N7–Rb2–N6	21.68(5)
O5–Rb1–O1 ^{iv}	66.05(6)	O6 ⁱⁱⁱ –Rb2–N7	69.44(6)	N13–Rb2–N6	71.19(5)
O2 ^{iv} –Rb1–O1 ^{iv}	38.19(6)	N8 ⁱ –Rb2–N13	83.33(6)	N14 ⁱ –Rb2–N6	92.82(5)
O5 ^v –Rb1–O1 ^{iv}	98.13(6)	O6–Rb2–N13	148.38(5)	N7 ⁱ –Rb2–N6	111.67(5)
N11–Rb1–O1 ^{iv}	135.52(5)	N9 ⁱⁱ –Rb2–N13	79.12(5)	N8 ⁱⁱ –Rb2–N6	141.56(5)
N5–Rb1–O1 ^{iv}	137.42(5)	O6 ⁱⁱⁱ –Rb2–N13	66.63(5)	N6 ⁱⁱⁱ –Rb2–N6	106.51(4)
O3–Rb1–O1 ^{iv}	155.47(5)	N7–Rb2–N13	70.64(5)	N8 ⁱ –Rb2–O4 ⁱ	66.67(6)
N15–Rb1–O1 ^{iv}	79.36(5)	N8 ⁱ –Rb2–N14 ⁱ	67.56(5)	O6–Rb2–O4 ⁱ	59.56(5)
O5–Rb1–O2	137.32(6)	O6–Rb2–N14 ⁱ	69.08(6)	N9 ⁱⁱ –Rb2–O4 ⁱ	104.27(5)
O2 ^{iv} –Rb1–O2	54.57(7)	N9 ⁱⁱ –Rb2–N14 ⁱ	148.12(5)	O6 ⁱⁱⁱ –Rb2–O4 ⁱ	143.26(5)
O5 ^v –Rb1–O2	61.51(6)	O6 ⁱⁱⁱ –Rb2–N14 ⁱ	139.26(5)	N7–Rb2–O4 ⁱ	117.62(5)
N11–Rb1–O2	111.48(5)	N7–Rb2–N14 ⁱ	75.23(5)	N13–Rb2–O4 ⁱ	149.76(5)
N5–Rb1–O2	47.15(5)	N13–Rb2–N14 ⁱ	119.42(5)	N14 ⁱ –Rb2–O4 ⁱ	46.23(5)
O3–Rb1–O2	105.71(5)	N8 ⁱ –Rb2–N7 ⁱ	23.13(5)	N7 ⁱ –Rb2–O4 ⁱ	77.13(5)
N15–Rb1–O2	84.85(5)	O6–Rb2–N7 ⁱ	127.02(6)	N8 ⁱⁱ –Rb2–O4 ⁱ	84.84(5)
O1 ^{iv} –Rb1–O2	92.70(5)	N9 ⁱⁱ –Rb2–N7 ⁱ	109.29(5)	N6 ⁱⁱⁱ –Rb2–O4 ⁱ	68.92(4)
O5–Rb1–N1 ^{iv}	81.30(6)	O6 ⁱⁱⁱ –Rb2–N7 ⁱ	139.55(5)	N6–Rb2–O4 ⁱ	127.94(4)

Symmetry codes for **133**: (i) -1-x, 2-y, -z; (ii) x, 1+y, z; (iii) -x, 2-y, -z; (iv) -x, 1-y, 1-z; (v) -1-x, 1-y, 1-z; (vi) -1+x, 1+y, z; (vii) 1+x, -1+y, z.

Appendix C

Crystal Structure Solution and Refinement

Parameter	4	5	7
Empirical formula	C ₂ H ₆ N ₅	C ₂ H ₄ N ₅ O ₄ Cl	C ₂ H ₇ N ₁₀ O ₄ Cl
Formula weight [g mol ⁻¹]	99.10	197.54	270.63
Temperature / K	200(2)	200(2)	200(2)
$\lambda_{\text{MoK}\alpha}$ / Å	0.71073	0.71073	0.71073
Crystal size / mm	0.50x0.12x0.07	0.19x0.12x0.09	0.25x0.15x0.12
Crystal system	Orthorhombic	Monoclinic	Monoclinic
Space group	<i>Pnma</i>	<i>P2₁/n</i>	<i>P2₁/n</i>
<i>a</i> / Å	8.033(1)	5.362(1)	5.2615(1)
<i>b</i> / Å	6.524(1)	7.8310(9)	8.5311(2)
<i>c</i> / Å	9.231(2)	15.255(3)	21.4870(4)
<i>a</i> / °	90	90	90
β / °	90	91.39(2)	96.127(1)
γ / °	90	90	90
<i>V</i> _{uc} / Å ³	483.9(1)	640.5(2)	958.96(3)
<i>Z</i>	4	4	4
ρ_{calc} / g cm ⁻³	1.360	1.924	1.874
μ / mm ⁻¹	0.103	0.575	0.430
<i>F</i> (000)	208	578	552
θ range / °	3.80–28.00	2.70–27.90	3.73–27.48
Index ranges	–10 ≤ <i>h</i> ≤ 10 –8 ≤ <i>k</i> ≤ 8 –12 ≤ <i>l</i> ≤ 12	–7 ≤ <i>h</i> ≤ 5 –8 ≤ <i>k</i> ≤ 10 –19 ≤ <i>l</i> ≤ 19	–6 ≤ <i>h</i> ≤ 6 –11 ≤ <i>k</i> ≤ 10 –27 ≤ <i>l</i> ≤ 27
Reflections collected	3841	4609	9497
Independent reflections	631 (<i>R</i> _{int} = 0.1250)	1512 (<i>R</i> _{int} = 0.1387)	2166 (<i>R</i> _{int} = 0.0376)
Data/Restraints/Parameters	631/0/56	1512/0/116	2166/0/182
Goodness-of-fit on <i>F</i> ²	0.990	0.917	1.058
<i>R</i> ₁ (<i>F</i> > 2 σ (<i>F</i>)) ^a	0.0424	0.0583	0.0330
<i>R</i> ₁ (all data)	0.0633	0.1097	0.0395
<i>wR</i> ₂ [<i>F</i> > 2(<i>F</i>)]	0.1021	0.1201	0.0847
<i>wR</i> ₂ (all data) ^b	0.1168	0.1337	0.0890

^a*R*₁ = $\sum ||F_o| - |F_c|| / \sum |F_o|$. ^b*R*_w = $[\sum (F_o^2 - F_c^2) / \sum w(F_o^2)]^{1/2}$. ^c*w* = $[\sigma^2(F_o^2) + (\chi P)^2 + yP]^{-1}$, *P* = $(F_o^2 - 2F_c^2) / 3$.

Appendix C

Crystal Structure Solution and Refinement

Parameter	11	12	15
Empirical formula	C ₂ H ₆ N ₅ O ₄ Cl	C ₂ H ₇ N ₆ O ₃	C ₂ H ₆ N ₅ O _{4.5} ClAg
Formula weight [g mol ⁻¹]	199.57	162.11	315.44
Temperature / K	200(2)	200(2)	100(2)
$\lambda_{\text{MoK}\alpha}$ / Å	0.71073	0.71073	0.71073
Crystal size / mm	0.35x0.12x0.12	0.20x0.10x0.05	0.25x0.20x0.12
Crystal system	Monoclinic	Monoclinic	Monoclinic
Space group	<i>P</i> 2 ₁ / <i>c</i>	<i>P</i> 2 ₁ / <i>n</i>	<i>C</i> 2/ <i>c</i>
<i>a</i> / Å	5.162(1)	6.340(1)	13.303(2)
<i>b</i> / Å	12.705(1)	8.704(2)	11.616(2)
<i>c</i> / Å	11.022(1)	12.223(2)	12.019(2)
<i>a</i> / °	90	90	90
β / °	96.16(1)	99.88(3)	111.93(1)
γ / °	90	90	90
<i>V</i> _{uc} / Å ³	718.8(1)	664.6(2)	1723.0(4)
<i>Z</i>	4	4	8
ρ_{calc} / g cm ⁻³	1.844	1.620	2.432
μ / mm ⁻¹	0.519	0.150	2.651
<i>F</i> (000)	408	368	1224
θ range / °	4.50–30.06	4.00–30.00	4.70–26.00
Index ranges	–7 ≤ <i>h</i> ≤ 7 –17 ≤ <i>k</i> ≤ 17 –15 ≤ <i>l</i> ≤ 15	–8 ≤ <i>h</i> ≤ 8 –6 ≤ <i>k</i> ≤ 12 –17 ≤ <i>l</i> ≤ 14	–15 ≤ <i>h</i> ≤ 16 –14 ≤ <i>k</i> ≤ 13 –14 ≤ <i>l</i> ≤ 8
Reflections collected	9478	4643	4342
Independent reflections	2097 (<i>R</i> _{int} = 0.0339)	1926 (<i>R</i> _{int} = 0.0729)	1688 (<i>R</i> _{int} = 0.0729)
Data/Restraints/Parameters	2097/0/134	1502/0/124	1688/0/147
Goodness-of-fit on <i>F</i> ²	1.037	1.163	1.016
<i>R</i> ₁ (<i>F</i> > 2 σ (<i>F</i>)) ^a	0.0316	0.0507	0.0390
<i>R</i> ₁ (all data)	0.0348	0.0646	0.0543
<i>wR</i> ₂ [<i>F</i> > 2(<i>F</i>)]	0.0811	0.1398	0.0877
<i>wR</i> ₂ (all data) ^b	0.0838	0.1470	0.0966

^a*R*₁ = $\sum ||F_o| - |F_c|| / \sum |F_o|$. ^b*R*_w = $[\sum (F_o^2 - F_c^2) / \sum w(F_o^2)]^{1/2}$. ^c*w* = $[\sigma_c^2(F_o^2) + (\chi P)^2 + yP]^{-1}$, *P* = $(F_o^2 - 2F_c^2) / 3$.

Appendix C

Crystal Structure Solution and Refinement

Parameter	17	19	20
Empirical formula	C ₂ H ₅ N ₅ O ₄ ClAg	C ₁₂ H ₁₆ N ₁₃ O ₇ Ag	C ₆ H ₁₅ N ₁₆ O ₃ Ag
Formula weight [g mol ⁻¹]	306.43	562.25	467.21
Temperature / K	200(2)	200(2)	200(2)
$\lambda_{\text{MoK}\alpha}$ / Å	0.71073	0.71073	0.71073
Crystal size / mm	0.26x0.10x0.03	0.35x0.10x0.08	0.25x0.10x0.05
Crystal system	Monoclinic	Triclinic	Triclinic
Space group	<i>P</i> 2 ₁ / <i>c</i>	<i>P</i> -1	<i>P</i> -1
<i>a</i> / Å	6.519(5)	7.233(1)	7.179(1)
<i>b</i> / Å	7.089(5)	14.260(1)	11.380(1)
<i>c</i> / Å	18.378(5)	20.874(1)	11.440(1)
α / °	90	72.467(6)	64.68(1)
β / °	96.901(5)	83.214(5)	79.00(1)
γ / °	90	81.500(5)	79.87(1)
<i>V</i> _{UC} / Å ³	843.2(9)	2024.1(2)	824.6(1)
<i>Z</i>	4	4	2
ρ_{calc} / g cm ⁻³	2.414	1.845	1.882
μ / mm ⁻¹	2.700	1.065	1.273
<i>F</i> (000)	592	1128	468
θ range / °	3.63–27.00	3.80–30.06	3.73–30.00
Index ranges	-8 ≤ <i>h</i> ≤ 8 -9 ≤ <i>k</i> ≤ 9 -23 ≤ <i>l</i> ≤ 23	-10 ≤ <i>h</i> ≤ 10 -20 ≤ <i>k</i> ≤ 20 -29 ≤ <i>l</i> ≤ 29	-10 ≤ <i>h</i> ≤ 10 -16 ≤ <i>k</i> ≤ 16 -16 ≤ <i>l</i> ≤ 16
Reflections collected	6157	27799	11037
Independent reflections	1829 (<i>R</i> _{int} = 0.0280)	11729 (<i>R</i> _{int} = 0.0736)	4754 (<i>R</i> _{int} = 0.0414)
Data/Restraints/Parameters	1829/0/138	11729/0/720	4754/0/256
Goodness-of-fit on <i>F</i> ²	1.157	0.961	0.822
<i>R</i> ₁ (<i>F</i> > 2σ(<i>F</i>)) ^a	0.0292	0.0558	0.0313
<i>R</i> ₁ (all data)	0.0325	0.0984	0.0540
<i>wR</i> ₂ [<i>F</i> > 2(<i>F</i>)]	0.0725	0.1306	0.0609
<i>wR</i> ₂ (all data) ^b	0.0745	0.1434	0.0756

^a*R*₁ = $\sum ||F_o| - |F_c|| / \sum |F_o|$. ^b*R*_w = $[\sum (F_o^2 - F_c^2) / \sum w (F_o^2)]^{1/2}$. ^c*w* = $[\sigma^2 (F_o^2) + (\chi P)^2 + yP]^{-1}$, *P* = $(F_o^2 - 2F_c^2) / 3$.

Appendix C

Crystal Structure Solution and Refinement

Parameter	22	23	24
Empirical formula	CH ₆ N ₅ O ₅ Li	CH ₄ N ₅ O ₄ Na	CN ₅ O ₂ K
Formula weight [g mol ⁻¹]	175.05	173.08	153.16
Temperature / K	200(2)	200(2)	200(2)
$\lambda_{\text{MoK}\alpha}$ / Å	0.71073	0.71073	0.71073
Crystal size / mm	0.35x0.25x0.10	0.23x0.10x0.05	0.35x0.35x0.05
Crystal system	Monoclinic	Triclinic	Monoclinic
Space group	<i>P</i> 2 ₁ / <i>c</i>	<i>P</i> -1	<i>P</i> 2 ₁ / <i>c</i>
<i>a</i> / Å	7.656(5)	6.4192(3)	4.8229(1)
<i>b</i> / Å	13.063(5)	7.8838(2)	13.1492(4)
<i>c</i> / Å	7.354(5)	8.1896(3)	7.9381(2)
<i>a</i> / °	90	115.983(2)	90
β / °	100.636(5)	96.525(2)	96.384(2)
γ / °	90	110.192(2)	90
<i>V</i> _{UC} / Å ³	722.8(7)	331.99(2)	500.29(2)
<i>Z</i>	4	2	4
ρ_{calc} / g cm ⁻³	1.608	1.731	2.033
μ / mm ⁻¹	0.154	0.216	0.979
<i>F</i> (000)	360	176	304
θ range / °	3.86 – 32.40	3.20 – 27.45	4.03 – 27.49
Index ranges	-11 ≤ <i>h</i> ≤ 11 -19 ≤ <i>k</i> ≤ 19 -10 ≤ <i>l</i> ≤ 10	-8 ≤ <i>h</i> ≤ 8 -10 ≤ <i>k</i> ≤ 10 -10 ≤ <i>l</i> ≤ 10	-6 ≤ <i>h</i> ≤ 6 -17 ≤ <i>k</i> ≤ 15 -10 ≤ <i>l</i> ≤ 10
Reflections collected	21279	4683	6534
Independent reflections	2471 (<i>R</i> _{int} = 0.0307)	1501 (<i>R</i> _{int} = 0.0599)	1141 (<i>R</i> _{int} = 0.0717)
Data/Restraints/Parameters	2471/0/133	1501/4/114	1141/0/83
Goodness-of-fit on <i>F</i> ²	1.063	1.074	1.087
<i>R</i> ₁ (<i>F</i> > 2σ(<i>F</i>)) ^a	0.0298	0.0437	0.0283
<i>R</i> ₁ (all data)	0.0422	0.0573	0.0340
<i>wR</i> ₂ [<i>F</i> > 2(<i>F</i>)]	0.0804	0.1198	0.0693
<i>wR</i> ₂ (all data) ^b	0.0868	0.1300	0.0724

^a*R*₁ = $\sum ||F_o| - |F_c|| / \sum |F_o|$. ^b*R*_w = $[\sum (F_o^2 - F_c^2) / \sum w (F_o^2)]^{1/2}$. ^c*w* = $[\sigma_c^2 (F_o^2) + (xP)^2 + yP]^{-1}$, *P* = $(F_o^2 - 2F_c^2) / 3$.

Appendix C

Crystal Structure Solution and Refinement

Parameter	25	26	28
Empirical formula	CN ₅ O ₂ Rb	CN ₅ O ₂ Cs	C ₂ H ₁₂ N ₁₀ O ₁₀ Ca
Formula weight [g mol ⁻¹]	199.53	246.91	376.30
Temperature / K	100(2)	100(2)	100(2)
$\lambda_{\text{MoK}\alpha}$ / Å	0.71073	0.71073	0.71073
Crystal size / mm	0.20x0.15x0.05	0.23x0.09x0.06	0.25x0.15x0.5
Crystal system	Monoclinic	Monoclinic	Orthorhombic
Space group	<i>C1c</i>	<i>C2c</i>	<i>Pna2</i>
<i>a</i> / Å	11.9135(5)	15.9926(5)	6.8960(2)
<i>b</i> / Å	5.1626(2)	4.8284(1)	32.575(1)
<i>c</i> / Å	8.6760(3)	14.7039(4)	6.2399(2)
α / °	90	90	90
β / °	93.82(1)	104.607(3)	90
γ / °	90	90	90
V_{UC} / Å ³	532.4(2)	1098.72(5)	1401.73(8)
<i>Z</i>	4	4	4
ρ_{calc} / g cm ⁻³	2.489	2.986	1.783
μ / mm ⁻¹	9.222	6.666	0.525
<i>F</i> (000)	376	896	776
θ range / °	4.30 – 28.66	4.35 – 28.71	3.75 – 26.00
Index ranges	-15 ≤ <i>h</i> ≤ 15 -6 ≤ <i>k</i> ≤ 6 -11 ≤ <i>l</i> ≤ 11	-20 ≤ <i>h</i> ≤ 21 -6 ≤ <i>k</i> ≤ 5 -18 ≤ <i>l</i> ≤ 19	-8 ≤ <i>h</i> ≤ 8 -40 ≤ <i>k</i> ≤ 40 -7 ≤ <i>l</i> ≤ 7
Reflections collected	1649	3054	13446
Independent reflections	918 (<i>R</i> _{int} = 0.0212)	1262 (<i>R</i> _{int} = 0.0218)	1516 (<i>R</i> _{int} = 0.0435)
Data/Restraints/Parameters	918/2/82	1262/0/82	1516/1/256
Goodness-of-fit on <i>F</i> ²	1.035	1.042	1.184
<i>R</i> ₁ (<i>F</i> > 2 σ (<i>F</i>)) ^a	0.0318	0.0183	0.0223
<i>R</i> ₁ (all data)	0.0345	0.0212	0.0264
<i>wR</i> ₂ [<i>F</i> > 2(<i>F</i>)]	0.0802	0.0446	0.0421
<i>wR</i> ₂ (all data) ^b	0.0809	0.0452	0.0445

^a*R*₁ = $\sum ||F_o| - |F_c|| / \sum |F_o|$. ^b*R*_w = $[\sum (F_o^2 - F_c^2) / \sum w(F_o^2)]^{1/2}$. ^c*w* = $[\sigma^2(F_o^2) + (\chi P)^2 + yP]^{-1}$, *P* = $(F_o^2 - 2F_c^2) / 3$.

Appendix C

Crystal Structure Solution and Refinement

Parameter	31	41	42
Empirical formula	CHN ₅ O ₂	C ₃ H ₉ N ₆ I	C ₃ H ₉ N ₉
Formula weight [g mol ⁻¹]	115.07	256.05	171.16
Temperature / K	200(2)	100(2)	200(2)
$\lambda_{\text{MoK}\alpha}$ / Å	0.71073	0.71073	0.71073
Crystal size / mm	0.25x0.11x0.05	0.30x0.20x0.20	0.30x0.25x0.03
Crystal system	Monoclinic	Triclinic	Monoclinic
Space group	<i>P</i> 2 ₁	<i>P</i> -1	<i>P</i> 2 ₁ / <i>c</i>
<i>a</i> / Å	5.3358(4)	6.094(3)	9.457(1)
<i>b</i> / Å	9.4799(7)	7.086(5)	17.418(1)
<i>c</i> / Å	8.3190(8)	10.820(2)	9.913(1)
<i>a</i> / °	90	99.83(3)	90
<i>β</i> / °	106.989(9)	93.82(3)	95.86(1)
<i>γ</i> / °	90	114.98(6)	90
<i>V</i> _{uc} / Å ³	402.44(6)	412.24(5)	1624.4(2)
<i>Z</i>	4	2	8
ρ_{calc} / g cm ⁻³	1.899	2.063	1.399
μ / mm ⁻¹	0.174	3.826	0.107
<i>F</i> (000)	232	244	720
θ range / °	3.99 – 23.98	3.73–25.99	3.68–27.00
Index ranges	-6 ≤ <i>h</i> ≤ 6 -10 ≤ <i>k</i> ≤ 10 -9 ≤ <i>l</i> ≤ 9	-7 ≤ <i>h</i> ≤ 7 -8 ≤ <i>k</i> ≤ 8 -13 ≤ <i>l</i> ≤ 13	-12 ≤ <i>h</i> ≤ 12 -22 ≤ <i>k</i> ≤ 22 -12 ≤ <i>h</i> ≤ 12
Reflections collected	3448	4339	16405
Independent reflections	673 (<i>R</i> _{int} = 0.0406)	1623 (<i>R</i> _{int} = 0.0457)	3539 (<i>R</i> _{int} = 0.0818)
Data/Restraints/Parameters	673/1/153	1623/0/127	3539/0/277
Goodness-of-fit on <i>F</i> ²	1.035	0.860	1.040
<i>R</i> ₁ (<i>F</i> > 2σ(<i>F</i>)) ^a	0.0220	0.0285	0.0632
<i>R</i> ₁ (all data)	0.0345	0.0411	0.1145
<i>wR</i> ₂ [<i>F</i> > 2(<i>F</i>)]	0.0401	0.0435	0.1424
<i>wR</i> ₂ (all data) ^b	0.0447	0.0446	0.1463

^a*R*₁ = $\sum ||F_o| - |F_c|| / \sum |F_o|$. ^b*R*_w = $[\sum (F_o^2 - F_c^2) / \sum w(F_o^2)]^{1/2}$. ^c*w* = $[\sigma^2(F_o^2) + (xP)^2 + yP]^2$, *P* = $(F_o^2 - 2F_c^2) / 3$.

Appendix C

Crystal Structure Solution and Refinement

Parameter	43	44	45a
Empirical formula	C ₃ H ₉ N ₇ O ₃	C ₃ H ₉ N ₆ O ₄ Cl	C ₈ H ₂₀ N ₂₂ O
Formula weight [g mol ⁻¹]	191.15	228.60	440.39
Temperature / K	100(2)	200(2)	100(2)
$\lambda_{\text{MoK}\alpha}$ / Å	0.71073	0.71073	0.71073
Crystal size / mm	0.30x0.25x0.20	0.15x0.08x0.08	0.20x0.20x0.15
Crystal system	Triclinic	Triclinic	Triclinic
Space group	<i>P</i> -1	<i>P</i> -1	<i>P</i> -1
<i>a</i> / Å	5.318(1)	5.793(1)	7.741(5)
<i>b</i> / Å	6.718(1)	7.613(1)	10.464(5)
<i>c</i> / Å	11.236(3)	11.080(2)	12.074(5)
α / °	81.11(2)	83.12(1)	82.12(1)
β / °	86.44(2)	86.87(1)	88.46(1)
γ / °	73.83(1)	69.61(2)	73.49(1)
<i>V</i> _{uc} / Å ³	380.9(2)	454.7(1)	928.7(8)
<i>Z</i>	2	2	2
ρ_{calc} / g cm ⁻³	1.667	1.669	1.575
μ / mm ⁻¹	0.144	0.425	0.122
<i>F</i> (000)	200	236	460
θ range / °	3.90–26.99	3.75–26.99	3.73–27.00
Index ranges	–6 ≤ <i>h</i> ≤ 6 –8 ≤ <i>k</i> ≤ 8 –14 ≤ <i>l</i> ≤ 14	–7 ≤ <i>h</i> ≤ 7 –9 ≤ <i>k</i> ≤ 9 –14 ≤ <i>l</i> ≤ 14	–9 ≤ <i>h</i> ≤ 9 –13 ≤ <i>k</i> ≤ 13 –15 ≤ <i>l</i> ≤ 14
Reflections collected	8544	4932	9549
Independent reflections	1668 (<i>R</i> _{int} = 0.0271)	1968 (<i>R</i> _{int} = 0.0282)	3794 (<i>R</i> _{int} = 0.0504)
Data/Restraints/Parameters	1668/0/154	1968/0/163	3794/0/360
Goodness-of-fit on <i>F</i> ²	1.100	1.103	1.027
<i>R</i> ₁ (<i>F</i> > 2σ(<i>F</i>)) ^a	0.0343	0.0416	0.0363
<i>R</i> ₁ (all data)	0.0421	0.0651	0.0666
<i>wR</i> ₂ [<i>F</i> > 2(<i>F</i>)]	0.0947	0.1067	0.0993
<i>wR</i> ₂ (all data) ^b	0.1008	0.1220	0.1319

^a*R*₁ = $\sum ||F_o| - |F_c|| / \sum |F_o|$. ^b*R*_w = $[\sum (F_o^2 - F_c^2) / \sum w(F_o^2)]^{1/2}$. ^c*w* = $[\sigma^2(F_o^2) + (\chi P)^2 + yP]^{-1}$, *P* = $(F_o^2 - 2F_c^2) / 3$.

Appendix C

Crystal Structure Solution and Refinement

Parameter	46a	47	55a
Empirical formula	C ₄ H ₁₁ N ₁₁ O ₃	C ₃ H ₉ N ₉ O ₄	C ₂ H ₇ N ₆ I
Formula weight [g mol ⁻¹]	261.20	235.16	242.02
Temperature / K	100(2)	200(2)	200(2)
$\lambda_{\text{MoK}\alpha}$ / Å	0.71073	0.71073	0.71073
Crystal size / mm	0.35x0.10x0.05	0.35x0.15x0.04	0.30x0.20x0.20
Crystal system	Monoclinic	Monoclinic	Monoclinic
Space group	<i>P</i> 2 ₁ / <i>c</i>	<i>P</i> 2 ₁ / <i>c</i>	<i>C</i> 2/ <i>c</i>
<i>a</i> / Å	5.104(1)	9.8919(4)	23.0810(1)
<i>b</i> / Å	13.233(1)	4.4530(2)	10.9450(1)
<i>c</i> / Å	16.220(1)	21.4998(8)	12.9370(2)
<i>a</i> / °	90	90	90
β / °	91.06(1)	95.32(1)	116.610(1)
γ / °	90	90	90
<i>V</i> _{UC} / Å ³	1095.4(2)	943.0(2)	2922.09(5)
<i>Z</i>	4	4	16
ρ_{calc} / g cm ⁻³	1.584	1.657	2.201
μ / mm ⁻¹	0.134	0.147	4.312
<i>F</i> (000)	544	488	1824
θ range / °	3.97–32.53	3.81–27.00	3.70–27.00
Index ranges	–7 ≤ <i>h</i> ≤ 7 –19 ≤ <i>k</i> ≤ 19 –24 ≤ <i>l</i> ≤ 24	–12 ≤ <i>h</i> ≤ 12 –5 ≤ <i>k</i> ≤ 5 –27 ≤ <i>l</i> ≤ 27	–29 ≤ <i>h</i> ≤ 29 –13 ≤ <i>k</i> ≤ 13 –16 ≤ <i>l</i> ≤ 16
Reflections collected	15103	8842	15552
Independent reflections	3730 (<i>R</i> _{int} = 0.0581)	2046 (<i>R</i> _{int} = 0.0577)	3187 (<i>R</i> _{int} = 0.0215)
Data/Restraints/Parameters	3730/0/207	2046/0/181	3187/0/220
Goodness-of-fit on <i>F</i> ²	1.007	1.065	1.075
<i>R</i> ₁ (<i>F</i> > 2σ(<i>F</i>)) ^a	0.0433	0.0440	0.0143
<i>R</i> ₁ (all data)	0.0885	0.0789	0.0183
<i>wR</i> ₂ [<i>F</i> > 2(<i>F</i>)]	0.1004	0.0851	0.0317
<i>wR</i> ₂ (all data) ^b	0.1118	0.1015	0.0335

^a*R*₁ = $\sum ||F_o| - |F_c|| / \sum |F_o|$. ^b*R*_w = $[\sum (F_o^2 - F_c^2) / \sum w (F_o^2)]^{1/2}$. ^c*w* = $[\sigma^2 (F_o^2) + (xP)^2 + yP]^{-1}$, *P* = $(F_o^2 - 2F_c^2) / 3$.

Appendix C

Crystal Structure Solution and Refinement

Parameter	55b	60	62
Empirical formula	C ₂ H ₇ N ₆ I	C ₈ H ₈ N ₈ O ₇	C ₉ H ₁₀ N ₈ O ₇
Formula weight [g mol ⁻¹]	242.02	328.22	342.25
Temperature / K	200(2)	200(2)	200(2)
$\lambda_{\text{MoK}\alpha}$ / Å	0.71073	0.71073	0.71073
Crystal size / mm	0.25x0.20x0.04	0.35x0.25x0.20	0.35x0.25x0.20
Crystal system	Orthorombic	Triclinic	Monoclinic
Space group	<i>Aba2</i>	<i>P</i> -1	<i>P2</i> ₁ / <i>c</i>
<i>a</i> / Å	12.7221(2)	5.895(1)	14.862(1)
<i>b</i> / Å	11.0301(2)	10.126(1)	5.7352(4)
<i>c</i> / Å	20.5901(1)	11.578(1)	16.839(1)
<i>a</i> / °	90	106.96(1)	90
β / °	90	100.88(1)	104.96(1)
γ / °	90	98.02(1)	90
<i>V</i> _{uc} / Å ³	2889.33(7)	635.1(1)	1386.7(2)
<i>Z</i>	16	2	4
ρ_{calc} / g cm ⁻³	2.226	1.716	1.639
μ / mm ⁻¹	4.361	0.152	0.143
<i>F</i> (000)	1824	336	704
θ range / °	2.70 – 20.00	4.16 – 30.06	3.91 – 30.07
Index ranges	-17 ≤ <i>h</i> ≤ 17 -15 ≤ <i>k</i> ≤ 15 -28 ≤ <i>l</i> ≤ 28	-8 ≤ <i>h</i> ≤ 8 -14 ≤ <i>k</i> ≤ 14 -16 ≤ <i>l</i> ≤ 16	-8 ≤ <i>h</i> ≤ 8 -20 ≤ <i>k</i> ≤ 20 -23 ≤ <i>l</i> ≤ 23
Reflections collected	18716	8662	17842
Independent reflections	4218 (<i>R</i> _{int} = 0.0302)	3712 (<i>R</i> _{int} = 0.0472)	4058 (<i>R</i> _{int} = 0.0761)
Data/Restraints/Parameters	4218/1/220	3712/0/240	4058/0/257
Goodness-of-fit on <i>F</i> ²	0.974	1.110	1.180
<i>R</i> ₁ (<i>F</i> > 2 σ (<i>F</i>)) ^a	0.0173	0.0437	0.0649
<i>R</i> ₁ (all data)	0.0193	0.0577	0.0951
<i>wR</i> ₂ [<i>F</i> > 2(<i>F</i>)]	0.0405	0.1192	0.1303
<i>wR</i> ₂ (all data) ^b	0.0413	0.1302	0.1475

^a*R*₁ = $\sum ||F_o| - |F_c|| / \sum |F_o|$. ^b*R*_w = $[\sum (F_o^2 - F_c^2) / \sum w(F_o^2)]^{1/2}$. ^c*w* = $[\sigma^2(F_o^2) + (xP)^2 + yP]^{-1}$, *P* = $(F_o^2 - 2F_c^2) / 3$.

Appendix C

Crystal Structure Solution and Refinement

Parameter	63	66	67
Empirical formula	C ₉ H ₁₀ N ₈ O ₇	C ₈ H ₉ N ₉ O ₇	C ₉ H ₁₁ N ₉ O ₇
Formula weight [g mol ⁻¹]	342.25	343.214	357.27
Temperature / K	100(2)	200(2)	100(2)
$\lambda_{\text{MoK}\alpha}$ / Å	0.71073	0.71073	0.71073
Crystal size / mm	0.30x0.15x0.04	0.35x0.25x0.03	0.20x0.05x0.05
Crystal system	Monoclinic	Triclinic	Monoclinic
Space group	<i>P</i> 2 ₁ / <i>c</i>	<i>P</i> -1	<i>P</i> 2 ₁ / <i>c</i>
<i>a</i> / Å	14.6340(4)	3.789(1)	13.030(1)
<i>b</i> / Å	5.9538(2)	12.833(1)	3.8299(2)
<i>c</i> / Å	16.3299(4)	13.935(1)	28.5923(2)
<i>a</i> / °	90	103.78(1)	90
<i>β</i> / °	102.396(3)	90.38(1)	99.184(5)
<i>γ</i> / °	90	96.94(1)	90
<i>V</i> _{UC} / Å ³	1389.62(7)	652.84(1)	1408.5(1)
<i>Z</i>	4	2	4
ρ_{calc} / g cm ⁻³	1.636	1.746	1.685
μ / mm ⁻¹	0.142	0.154	0.146
<i>F</i> (000)	704	352	736
θ range / °	3.65 – 26.00	3.93 – 29.99	3.69 – 27.00
Index ranges	±18, ±7, ±20	±4, ±15, ±17	±16, ±4, ±36
Reflections collected	13086	6632	13091
Independent reflections	2724	2560	3050
Data/Restraints/Parameters	2724/0/257	2560/0/253	3050/0/270
Goodness-of-fit on <i>F</i> ²	1.114	1.083	1.056
<i>R</i> _{int}	0.0505	0.0589	0.0702
<i>R</i> ₁ (<i>F</i> > 2σ(<i>F</i>)) ^a	0.0445	0.0542	0.0539
<i>R</i> ₁ (all data)	0.0780	0.0671	0.0919
<i>wR</i> ₂ [<i>F</i> > 2(<i>F</i>)]	0.0800	0.1445	0.1187
<i>wR</i> ₂ (all data) ^b	0.0941	0.1581	0.1210

^a*R*₁ = $\sum ||F_o| - |F_c|| / \sum |F_o|$. ^b*R*_w = $[\sum (F_o^2 - F_c^2) / \sum w(F_o^2)]^{1/2}$. ^c*w* = $[\sigma_c^2(F_o^2) + (\chi P)^2 + yP]^{-1}$, *P* = $(F_o^2 - 2F_c^2) / 3$.

Appendix C

Crystal Structure Solution and Refinement

Parameter	68	69	70
Empirical formula	C ₃ H ₇ N ₅	C ₂ H ₆ N ₅ O ₄ Cl	C ₃ H ₈ N ₅ I
Formula weight [g mol ⁻¹]	113.13	199.57	241.04
Temperature / K	200(2)	200(2)	100(2)
$\lambda_{\text{MoK}\alpha}$ / Å	0.71073	0.71073	0.71073
Crystal size / mm	0.15x0.09x0.04	0.40x0.40x0.30	0.12x0.10x0.05
Crystal system	Triclinic	Monoclinic	Orthorhombic
Space group	<i>P</i> -1	<i>P</i> 2 ₁ / <i>c</i>	<i>Pbca</i>
<i>a</i> / Å	6.256(1)	5.1623(5)	11.5016(4)
<i>b</i> / Å	6.765(1)	12.706(1)	10.3405(3)
<i>c</i> / Å	6.773(1)	11.022(1)	13.7744(5)
<i>a</i> / °	102.24(3)	90	90
β / °	97.96(3)	96.16(1)	90
γ / °	100.39(3)	90	90
<i>V</i> _{uc} / Å ³	270.91)	718.8(1)	1638.2(1)
<i>Z</i>	2	4	8
ρ_{calc} / g cm ⁻³	1.387	1.844	1.955
μ / mm ⁻¹	0.101	0.519	4.842
<i>F</i> (000)	120	408	912
θ range / °	3.13 – 27.00	4.50 – 26.00	3.94 – 26.00
Index ranges	-7 ≤ <i>h</i> ≤ 7 -8 ≤ <i>k</i> ≤ 8 -8 ≤ <i>l</i> ≤ 8	-6 ≤ <i>h</i> ≤ 6 -15 ≤ <i>k</i> ≤ 15 -13 ≤ <i>l</i> ≤ 13	-14 ≤ <i>h</i> ≤ 14 -12 ≤ <i>k</i> ≤ 12 -16 ≤ <i>l</i> ≤ 16
Reflections collected	2243	6888	9781
Independent reflections	1176	1412	1608
Data/Restraints/Parameters	1176/0/101	1412/0/134	1608/0/103
<i>R</i> _{int}	0.0213	0.0432	0.0265
Goodness-of-fit on <i>F</i> ²	1.128	1.088	1.073
<i>R</i> ₁ [<i>F</i> > 4σ(<i>F</i>)]	0.0410	0.0303	0.0143
w <i>R</i> ₂ (all data)	0.1126	0.0759	0.0371

$$^a R_1 = \Sigma ||F_o| - |F_c|| / \Sigma |F_o|. \quad ^b R_w = [\Sigma (F_o^2 - F_c^2) / \Sigma w (F_o^2)]^{1/2}. \quad ^c w = [\sigma_c^2 (F_o^2) + (\chi P)^2 + yP]^{-1}, P = (F_o^2 - 2F_c^2) / 3.$$

Appendix C

Crystal Structure Solution and Refinement

Parameter	71	72	73
Empirical formula	C ₃ H ₈ N ₆ O ₃	C ₃ H ₈ N ₅ O ₄	C ₃ H ₈ N ₈
Formula weight [g mol ⁻¹]	176.15	213.59	156.17
Temperature / K	100(2)	100(2)	100(2)
$\lambda_{\text{MoK}\alpha}$ / Å	0.71073	0.71073	0.71073
Crystal size / mm	0.40x0.25x0.10	0.35x0.35x0.10	0.20x0.05x0.05
Crystal system	Orthorhombic	Monoclinic	Monoclinic
Space group	<i>Pbca</i>	<i>P2₁/c</i>	<i>P2₁/n</i>
<i>a</i> / Å	9.9514(3)	7.3367(2)	6.4210(3)
<i>b</i> / Å	10.1725(3)	11.5310(3)	13.2989(4)
<i>c</i> / Å	14.7348(4)	10.5025(2)	8.2644(3)
<i>a</i> / °	90	90	90
<i>β</i> / °	90	101.868(2)	96.432(3)
<i>γ</i> / °	90	90	90
<i>V</i> _{uc} / Å ³	1491.6(1)	869.51(4)	701.27(5)
<i>Z</i>	8	4	4
ρ_{calc} / g cm ⁻³	1.569	1.632	1.479
μ / mm ⁻¹	0.137	0.435	0.112
<i>F</i> (000)	736	440	328
θ range / °	3.98 – 26.00	3.97 – 26.00	3.82 – 26.00
Index ranges	-12 ≤ <i>h</i> ≤ 12 -12 ≤ <i>k</i> ≤ 12 -18 ≤ <i>l</i> ≤ 18	-9 ≤ <i>h</i> ≤ 9 -14 ≤ <i>k</i> ≤ 14 -12 ≤ <i>l</i> ≤ 12	-7 ≤ <i>h</i> ≤ 7 -16 ≤ <i>k</i> ≤ 16 -10 ≤ <i>l</i> ≤ 10
Reflections collected	13993	8548	6682
Independent reflections	1464	1703	1373
Data/Restraints/Parameters	1464/0/119	1703/0/139	1373/0/133
<i>R</i> _{int}	0.0353	0.0234	0.0607
Goodness-of-fit on <i>F</i> ²	1.085	1.058	1.136
<i>R</i> ₁ [<i>F</i> > 4σ(<i>F</i>)]	0.0324	0.0307	0.0431
w <i>R</i> ₂ (all data)	0.0890	0.0904	0.0937

$$^a R_1 = \sum ||F_o| - |F_c|| / \sum |F_o|. \quad ^b R_w = [\sum (F_o^2 - F_c^2) / \sum w (F_o^2)]^{1/2}. \quad ^c w = [\sigma_c^2 (F_o^2) + (\chi P)^2 + yP]^{-1}, P = (F_o^2 - 2F_c^2) / 3.$$

Appendix C

Crystal Structure Solution and Refinement

Parameter	74	81	82
Formula	C ₃ H ₈ N ₈ O ₄	C ₈ H ₂₀ N ₂₀ O ₂	C ₈ H ₂₈ N ₂₀ O ₆
Formula weight [g mol ⁻¹]	220.17	428.44	500.51
Crystal size	0.25x0.20x0.20	0.05x0.02x0.02	0.17x0.12x0.06
T / K	150(2)	200(2)	200(2)
Crystal system	Monoclinic	Monoclinic	Monoclinic
Space group	<i>P</i> 2 ₁ / <i>c</i>	<i>P</i> 2 ₁ / <i>c</i>	<i>P</i> 2 ₁ / <i>n</i>
<i>a</i> / Å	13.3927(4)	14.441(3)	9.3101(3)
<i>b</i> / Å	8.0033(2)	9.277(2)	6.5383(2)
<i>c</i> / Å	9.0985(2)	16.014(3)	19.5637(5)
<i>a</i> / °	90	90	90
<i>β</i> / °	107.766(3)	113.01(3)	90.48(1)
<i>γ</i> / °	90	90	90
Volume / Å ³	928.72(4)	1974.7(7)	1190.84(6)
<i>Z</i>	4	4	2
<i>ρ</i> (g cm ⁻³)	1.575	1.441	1.396
<i>λ</i> (Mo Kα, Å)	0.71073	0.71073	0.71073
<i>μ</i> (mm ⁻¹)	0.141	0.114	528
reflns collected	9068	7180	5078
indep. reflns	1813	2045	1861
<i>R</i> _{int}	0.0251	0.0530	0.0292
obsd. reflns.	4435	3871	2709
F(000)	456	896	528
GOOF	1.080	1.066	1.039
n°. parameters	187	287	210
<i>R</i> ₁ / <i>wR</i> ₂ [<i>I</i> > 2σ(<i>I</i>)]	0.0298	0.0606, 0.1528	0.0459, 0.1199
<i>R</i> ₁ / <i>wR</i> ₂ (all data)	0.0895	0.1347, 0.1871	0.0720, 0.1356

$$^a R_1 = \Sigma ||F_o| - |F_c|| / \Sigma |F_o|. \quad ^b R_w = [\Sigma (F_o^2 - F_c^2) / \Sigma w (F_o^2)]^{1/2}. \quad ^c w = [\sigma_c^2 (F_o^2) + (\chi P)^2 + yP]^{-1}, P = (F_o^2 - 2F_c^2) / 3.$$

Appendix C

Crystal Structure Solution and Refinement

Parameter	83	84	85
Formula	C ₆ H ₁₈ N ₂₂ O ₂	C ₆ H ₁₄ N ₂₂	C ₄ H ₁₆ N ₁₆ O ₄
Formula weight [g mol ⁻¹]	430.35	394.32	352.33
Crystal size	0.1x0.05x0.04	0.30x0.20x0.05	0.29x0.13x0.07
T / K	200(2)	100(2)	100(2)
Crystal system	Triclinic	Triclinic	Triclinic
Space group	<i>P</i> -1	<i>P</i> -1	<i>P</i> -1
<i>a</i> / Å	7.505(2)	5.2619(9)	4.563(5)
<i>b</i> / Å	8.184(2)	6.698(2)	7.362(5)
<i>c</i> / Å	9.040(2)	1.1884(8)	11.334(5)
<i>α</i> / °	108.58(3)	102.05(4)	105.125(5)
<i>β</i> / °	112.70(3)	90.80(3)	90.933(5)
<i>γ</i> / °	98.25(3)	109.96(2)	102.871(5)
Volume / Å ³	462.3(1)	383.4(3)	357.2(5)
<i>Z</i>	1	1	1
<i>ρ</i> (g cm ⁻³)	1.546	1.708(1)	1.638
<i>λ</i> (Mo Kα, Å)	0.71073	0.71073	0.71073
<i>μ</i> (mm ⁻¹)	0.125	0.133	0.140
reflns collected	6358	3845	2480
indep. reflns	2232	1680	1311
<i>R</i> _{int}	0.0616	0.0314	0.0193
obsd. reflns.	2704	1079	1164
F(000)	224	204	184
GOOF	1.109	0.908	1.071
n°. parameters	172	164	141
<i>R</i> ₁ / <i>wR</i> ₂ [<i>I</i> > 2σ(<i>I</i>)]	0.0471, 0.1244	0.0365, 0.0764	0.0530, 0.1323
<i>R</i> ₁ / <i>wR</i> ₂ (all data)	0.0616, 0.1364	0.0666, 0.0849	0.0590, 0.1378

$$^a R_1 = \sum ||F_o| - |F_c|| / \sum |F_o|. \quad ^b R_w = [\sum (F_o^2 - F_c^2) / \sum w (F_o^2)]^{1/2}. \quad ^c w = [\sigma_c^2 (F_o^2) + (\alpha P)^2 + \beta P]^{-1}, P = (F_o^2 - 2F_c^2) / 3.$$

Appendix C

Crystal Structure Solution and Refinement

Parameter	86	88	91a
Formula	C ₈ H ₁₆ N ₂₀	C ₆ H ₁₄ N ₂₂	C ₄ H ₈ N ₁₀ O
Formula weight [g mol ⁻¹]	392.35	394.39	212.21
Crystal size	0.05x0.1x0.08	0.01x0.02x0.05	0.25x0.10x0.05
T / K	200(2)	200(2)	200(2)
$\lambda_{\text{MoK}\alpha}$ / Å	0.71073	0.71073	0.71073
Crystal system	Triclinic	Triclinic	Monoclinic
Space group	<i>P</i> -1	<i>P</i> -1	<i>C</i> 2/ <i>c</i>
<i>a</i> / Å	5.830(4)	5.840(5)	16.195(1)
<i>b</i> / Å	10.994(8)	11.008(5)	5.052(1)
<i>c</i> / Å	14.71(1)	14.727(5)	10.992(1)
α / °	99.93(1)	99.93(1)	90
β / °	93.64(1)	93.63(1)	94.27(1)
γ / °	98.72(1)	98.69(1)	90
Volume / Å ³	913.8(2)	918.0(9)	896.8(4)
<i>Z</i>	2	2	4
ρ (g cm ⁻³)	1.431	1.427	1.572
λ (Mo K α , Å)	0.71073	0.71073	0.71073
μ (mm ⁻¹)	0.108	0.111	0.125
reflns collected	10071	12572	4685
indep. reflns	2928	2961	972
<i>R</i> _{int}	0.0664	0.0423	0.0722
obsd. reflns.	3939	5347	540
F(000)	400	408	440
GOOF	1.024	1.018	0.922
n°. parameters	317	271	85
<i>R</i> ₁ (<i>F</i> > 2 σ (<i>F</i>)) ^a	0.0556	0.0618	0.0360
<i>R</i> ₁ (all data)	0.1008	0.1208	0.0722
<i>wR</i> ₂ [<i>F</i> > 2(<i>F</i>)]	0.1192	0.1573	0.0754
<i>wR</i> ₂ (all data) ^b	0.1446	0.1939	0.0845

^a $R_1 = \sum ||F_o| - |F_c|| / \sum |F_o|$. ^b $R_w = [\sum (F_o^2 - F_c^2) / \sum w(F_o^2)]^{1/2}$. ^c $w = [\sigma_c^2(F_o^2) + (\chi P)^2 + yP]^{-1}$, $P = (F_o^2 - 2F_c^2) / 3$.

Appendix C

Crystal Structure Solution and Refinement

Parameter	95	97	99
Chem. Formula	C ₂ H ₄ N ₁₀	C ₄ H ₁₀ N ₁₀ O	C ₂ H ₁₄ N ₁₂ O ₂
Formula weight [g mol ⁻¹]	168.15	214.22	238.26
Crystal Size (mm)	0.25x0.11x0.05	0.30x0.10x0.04	0.25x0.10x0.10
Crystal System	Monoclinic	Monoclinic	Triclinic
Space Group	<i>C</i> 2/ <i>c</i>	<i>C</i> 2/ <i>m</i>	<i>P</i> -1
<i>a</i> [Å]	12.401(3)	18.788(5)	3.8236(2)
<i>b</i> [Å]	5.5133(11)	5.254(5)	6.9671(5)
<i>c</i> [Å]	9.835(2)	4.617(5)	9.9199(6)
<i>a</i> (°)	90	90	80.478(5)
<i>β</i> (°)	115.57(3)	90.686(5)	88.652(4)
<i>γ</i> (°)	90	90	79.478(5)
<i>V</i> [Å ³]	606.6(9)	455.7(7)	256.23(3)
<i>Z</i>	4	2	2
$\rho_{\text{calc.}}$ [g/cm ³]	1.841	1.561	1.544
μ [mm ⁻¹]	0.146	0.123	0.130
<i>F</i> (000)	344	224	126
θ range [°]	3.64–27.50	4.03–30.10	3.94–27.00
λ (Mo K α , Å)	0.71073	0.71073	0.71073
Temp [K]	200(2)	100(2)	200(2)
Index Range	-15 ≤ <i>h</i> ≤ 16 -7 ≤ <i>k</i> ≤ 7 -12 ≤ <i>l</i> ≤ 12	-26 ≤ <i>h</i> ≤ 26 -7 ≤ <i>k</i> ≤ 7 -6 ≤ <i>l</i> ≤ 6	-4 ≤ <i>h</i> ≤ 4 -8 ≤ <i>k</i> ≤ 8 -12 ≤ <i>l</i> ≤ 12
Refl. Collected	1330	3048	5803
Refl. Unique	701	1330	1107
<i>R</i> (int.)	0.0234	0.0334	0.0236
Data/restr./param.	701/0/64	1330/1/89	1107/0/109
GOOF	1.061	0.888	1.287
<i>R</i> _{<i>i</i>} , <i>wR</i> ₂ [<i>I</i> > 4 σ (<i>I</i>)]	0.0381, 0.0924	0.0327, 0.0582	0.0488, 0.1191
<i>R</i> _{<i>i</i>} , <i>wR</i> ₂ (all data)	0.0525, 0.0982	0.0529, 0.0588	0.0566, 0.1207

$$^a R_1 = \sum ||F_o| - |F_c|| / \sum |F_o|. \quad ^b R_w = [\sum (F_o^2 - F_c^2) / \sum w(F_o^2)]^{1/2}. \quad ^c w = [\alpha^2 (F_o^2) + (\chi P)^2 + \gamma P]^{-1}, P = (F_o^2 - 2F_c^2) / 3.$$

Appendix C

Crystal Structure Solution and Refinement

Parameter	105	108	109
Chem. Formula	C ₂ H ₈ N ₁₀ O ₃ Li ₂	C ₂ H ₂ N ₁₀ Rb ₂	C ₂ H ₂ N ₁₀ Cs ₂
Formula weight [g mol ⁻¹]	234.06	337.08	431.96
Crystal Size (mm)	0.30x0.20x0.20	0.25x0.10x0.05	0.35x0.25x0.20
Crystal System	Triclinic	Monoclinic	Orthorombic
Space Group	<i>P</i> -1	<i>P</i> 2 ₁ / <i>n</i>	<i>P</i> 2 ₁ 2 ₁ 2 ₁
<i>a</i> [Å]	6.7522(4)	6.5093(2)	6.0662(1)
<i>b</i> [Å]	7.7880(3)	20.3928(6)	8.5638(2)
<i>c</i> [Å]	10.0091(4)	6.7479(2)	17.8315(4)
<i>a</i> (°)	83.827(3)	90	90
<i>β</i> (°)	75.925(4)	111.490(4)	90
<i>γ</i> (°)	66.539(4)	90	90
<i>V</i> [Å ³]	468.30(4)	833.46(4)	926.34(3)
<i>Z</i>	2	4	4
$\rho_{\text{calc.}}$ [g/cm ³]	1.660	2.686	3.097
μ [mm ⁻¹]	0.139	11.720	7.850
<i>F</i> (000)	240	632	776
θ range [°]	4.20–30.11	3.72–25.99	4.06–27.50
λ (Mo K α , Å)	0.71073	0.71073	0.71073
Temp [K]	100(2)	100(2)	100(2)
Index Range	-9 ≤ <i>h</i> ≤ 9 -10 ≤ <i>k</i> ≤ 10 -14 ≤ <i>l</i> ≤ 14	-8 ≤ <i>h</i> ≤ 8 -25 ≤ <i>k</i> ≤ 25 -8 ≤ <i>l</i> ≤ 8	-7 ≤ <i>h</i> ≤ 7 -11 ≤ <i>k</i> ≤ 11 -23 ≤ <i>l</i> ≤ 23
Refl. collected	13435	8242	10135
Refl. unique	2743	1633	2118
<i>R</i> (int.)	0.0252	0.0251	0.0187
Data/restr./param.	2743/0/186	1633/0/135	2118/0/135
GOOF	1.104	1.026	1.301
<i>R</i> _{<i>i</i>} , <i>wR</i> ₂ [<i>I</i> > 4 σ (<i>I</i>)]	0.0316, 0.0898	0.0149, 0.0340	0.0139, 0.0338
<i>R</i> _{<i>i</i>} , <i>wR</i> ₂ (all data)	0.0410, 0.0933	0.0209, 0.0363	0.0143, 0.0340

$$^a R_1 = \sum ||F_o| - |F_c|| / \sum |F_o|. \quad ^b R_w = [\sum (F_o^2 - F_c^2) / \sum w (F_o^2)]^{1/2}. \quad ^c w = [\alpha^2 (F_o^2) + (\chi P)^2 + \gamma P]^{-1}, P = (F_o^2 - 2F_c^2) / 3.$$

Appendix C

Crystal Structure Solution and Refinement

Parameter	110	111	112
Empirical formula	C ₂ H ₁₅ N ₁₀ O _{6.5} Mg	C ₂ H ₁₂ N ₁₀ O ₅ Ca	C ₂ H ₁₂ N ₁₀ O ₅ Sr
Formula weight [g mol ⁻¹]	307.55	296.30	343.84
Temperature / K	100(2)	100(2)	100(2)
Crystal size / mm	0.30x0.15x0.10	0.25x0.10x0.10	0.11x0.10x0.09
Crystal system	Triclinic	Orthorhombic	Orthorhombic
Space group	<i>P</i> -1	<i>Pnnm</i>	<i>Pnnm</i>
<i>a</i> / Å	7.037(5)	11.0655(2)	11.173(5)
<i>b</i> / Å	12.621(5)	13.6701(3)	13.869(5)
<i>c</i> / Å	13.969(5)	6.8527(1)	7.057(5)
<i>a</i> / °	83.915(5)	90	90
<i>β</i> / °	81.558(5)	90	90
<i>γ</i> / °	87.464(5)	90	90
<i>V</i> _{UC} / Å ³	1219.8(1)	1036.58(3)	1093.51(2)
<i>Z</i>	4	4	4
<i>ρ</i> _{calc} / g cm ⁻³	1.675	1.898	2.088
<i>μ</i> / mm ⁻¹	0.198	0.648	4.971
<i>F</i> (000)	644	616	688
Θ range / °	3.70–27.00	3.68–27.00	3.72–27.00
Index ranges	-8 ≤ <i>h</i> ≤ 8 -12 ≤ <i>k</i> ≤ 16 -17 ≤ <i>l</i> ≤ 17	-14 ≤ <i>h</i> ≤ 14 -17 ≤ <i>k</i> ≤ 17 -8 ≤ <i>l</i> ≤ 8	-14 ≤ <i>h</i> ≤ 14 -17 ≤ <i>k</i> ≤ 17 -9 ≤ <i>l</i> ≤ 9
Refl. collected	8965	10976	11448
Independent refl.	5215	1230	1286
Data/Restr./Param.	5215/0/472	1230/0/130	1286/0/130
GOOF	0.816	1.030	1.092
<i>R</i> _{int}	0.0230	0.0360	0.0296
<i>R</i> ₁ (<i>F</i> > 2σ(<i>F</i>)) ^a	0.0314	0.0231	0.0163
<i>R</i> ₁ (all data)	0.0665	0.0315	0.0241
<i>wR</i> ₂ [<i>F</i> > 2(<i>F</i>)]	0.0670	0.0553	0.0362
<i>wR</i> ₂ (all data) ^b	0.0735	0.0586	0.0408

^a*R*₁ = Σ ||*F*_o| - |*F*_c|| / Σ |*F*_o|. ^b*R*_w = [Σ (*F*_o² - *F*_c²) / Σ *w* (*F*_o)²]^{1/2}. ^c*w* = [σ_c² (*F*_o)² + (*xP*)² + *yP*]⁻¹, *P* = (*F*_o² - 2*F*_c²) / 3.

Appendix C

Crystal Structure Solution and Refinement

Parameter	113	114	128
Empirical formula	C ₂ H ₁₂ N ₁₂ O ₅ Ba	C ₂ H ₈ N ₄ O ₃	C ₃ H ₂ N ₆ O ₂
Formula weight [g mol ⁻¹]	422.01	136.12	154.11
Temperature / K	100(2)	200(2)	200(2)
Crystal size / mm	0.20x0.12x0.07	0.20x0.10x0.10	0.35x0.20x0.03
Crystal system	Orthorhombic	Monoclinic	Orthorhombic
Space group	<i>Pnmm</i>	<i>P 2₁/c</i>	<i>P2₁2₁2₁</i>
<i>a</i> / Å	14.2461(3)	9.1213(6)	5.4521(3)
<i>b</i> / Å	11.2834(3)	4.8400(3)	6.1417(3)
<i>c</i> / Å	7.3188(2)	13.2259(8)	17.483(1)
<i>a</i> / °	90	90	90
<i>β</i> / °	90	92.779(6)	90
<i>γ</i> / °	90	90	90
<i>V</i> _{UC} / Å ³	1176.46(5)	583.20(6)	585.93(5)
<i>Z</i>	4	2	4
<i>ρ</i> _{calc} / g cm ⁻³	2.210	1.550	1.747
<i>μ</i> / mm ⁻¹	3.410	0.144	0.149
<i>F</i> (000)	752	288	312
Θ range / °	2.77–54.93	3.72–25.98	3.91–30.10
Index ranges	–18 ≤ <i>h</i> ≤ 18 –14 ≤ <i>k</i> ≤ 14 –9 ≤ <i>l</i> ≤ 8	–11 ≤ <i>h</i> ≤ 11 –5 ≤ <i>k</i> ≤ 5 –16 ≤ <i>l</i> ≤ 16	–7 ≤ <i>h</i> ≤ 7 –8 ≤ <i>k</i> ≤ 8 –24 ≤ <i>l</i> ≤ 24
Refl. collected	8665	5542	7761
Independent refl.	1444	1140	1033
Data/Restr./Param.	1444/0/118	1140/0/114	1033/0/108
GOOF	1.162	0.997	1.060
<i>R</i> _{int}	0.0300	0.0357	0.0298
<i>R</i> ₁ (<i>F</i> > 2σ(<i>F</i>)) ^a	0.0222	0.0283	0.0255
<i>R</i> ₁ (all data)	0.0244	0.0483	0.0344
<i>wR</i> ₂ [<i>F</i> > 2(<i>F</i>)]	0.0500	0.0672	0.0563
<i>wR</i> ₂ (all data) ^b	0.0508	0.0770	0.0622

^a*R*₁ = Σ ||*F*_o| – |*F*_c|| / Σ |*F*_o|. ^b*R*_w = [Σ (*F*_o² – *F*_c²) / Σ *w* (*F*_o)²]^{1/2}. ^c*w* = [σ_c² (*F*_o²) + (*xP*)² + *yP*]⁻¹, *P* = (*F*_o² – 2*F*_c²) / 3.

Appendix C

Crystal Structure Solution and Refinement

Parameter	129a	132	133
Empirical formula	C ₃ H ₅ N ₉ O ₃	C ₃ H ₄ N ₉ O ₃ K	C ₃ H ₄ N ₉ O ₃ Rb
Formula weight [g mol ⁻¹]	215.16	253.25	299.62
Crystal size (mm)	0.30x0.20x0.02	0.40x0.30x0.20	0.30x0.15x0.05
Crystal system	Monoclinic	Triclinic	Triclinic
Space group	<i>P</i> 2 ₁	<i>P</i> -1	<i>P</i> -1
<i>a</i> , Å	6.3238(5)	7.5296(3)	7.5556(4)
<i>b</i> , Å	4.9208(4)	7.6976(3)	7.5518(4)
<i>c</i> , Å	13.032(1)	17.6101(8)	18.2305(9)
α , deg	90	84.707(3)	78.960(5)
β , deg	101.132(9)	78.411(4)	85.340(4)
γ , deg	90	69.760(4)	71.073(5)
<i>V</i> , Å ³	397.90(6)	937.84(7)	965.55(9)
<i>Z</i>	2	2	4
<i>T</i> [K]	200(2)	200(2)	200(2)
ρ_{calc} , g cm ⁻³	1.796	1.794	2.061
μ , mm ⁻¹	0.157	0.580	5.141
<i>F</i> (000)	220	512	584
θ range / °	4.11–30.09	3.73–30.11	3.73–30.07
Index ranges	–8 ≤ <i>h</i> ≤ 8	–10 ≤ <i>h</i> ≤ 10	–10 ≤ <i>h</i> ≤ 10
	–6 ≤ <i>k</i> ≤ 6	–10 ≤ <i>k</i> ≤ 10	–10 ≤ <i>k</i> ≤ 10
	–18 ≤ <i>l</i> ≤ 18	–24 ≤ <i>l</i> ≤ 24	–25 ≤ <i>l</i> ≤ 25
Reflections collected	5172	5442	12858
Independent reflections	1273	4387	5580
<i>R</i> _{int}	0.0487	0.0156	0.0304
Reflections parameters	156	321	321
<i>S</i> on <i>F</i> ²	1.015	1.077	0.915
<i>R</i> ₁ (<i>F</i> > 2 σ (<i>F</i>)) ^a	0.0343	0.0264	0.0270
<i>R</i> ₁ (all data)	0.0503	0.0369	0.0321
<i>wR</i> ₂ [<i>F</i> > 2(<i>F</i>)]	0.0589	0.0672	0.0522
<i>wR</i> ₂ (all data) ^b	0.0611	0.0734	0.0553

^a*R*₁ = $\sum ||F_o| - |F_c|| / \sum |F_o|$. ^b*R*_w = $[\sum (F_o^2 - F_c^2) / \sum w(F_o^2)]^{1/2}$. ^c*w* = $[\sigma_c^2(F_o^2) + (\chi P)^2 + yP]^{-1}$, *P* = $(F_o^2 - 2F_c^2) / 3$.

Appendix C

Crystal Structure Solution and Refinement

Parameter	135	138	145
Empirical formula	C ₃ H ₈ N ₁₀ O ₃	C ₄ H ₉ N ₁₃ O ₂	C ₃ H ₄ N ₅ O ₂ Br
Formula weight [g mol ⁻¹]	232.19	271.24	222.02
Crystal size (mm)	0.30x0.30x0.20	0.35x0.35x0.03	0.40x0.20x0.10
Crystal system	Triclinic	Monoclinic	Orthorhombic
Space group	<i>P</i> -1	<i>P</i> 2 ₁ /n	<i>P</i> 2 ₁ 2 ₁ 2 ₁
<i>a</i> , Å	7.4710(4)	5.027(5)	5.094(5)
<i>b</i> , Å	7.8386(5)	30.882(5)	9.548(5)
<i>c</i> , Å	18.036(1)	14.223(5)	14.678(5)
α , deg	84.318(5)	90	90
β , deg	78.597(5)	92.413(5)	90
γ , deg	69.203(6)	90	90
<i>V</i> , Å ³	967.47(10)	2206(2)	713.9(8)
<i>Z</i>	4	4	4
<i>T</i> [K]	200(2)	200(2)	200(2)
ρ_{calc} , g cm ⁻³	1.594	1.633	2.066
μ , mm ⁻¹	0.138	0.135	5.715
<i>F</i> (000)	480	1120	432
θ range / °	4.06–26.00	3.90–24.00	4.23–24.00
	–9 ≤ <i>h</i> ≤ 9	–5 ≤ <i>h</i> ≤ 5	–5 ≤ <i>h</i> ≤ 5
Index ranges	–9 ≤ <i>k</i> ≤ 9	–35 ≤ <i>k</i> ≤ 35	–10 ≤ <i>k</i> ≤ 10
	–22 ≤ <i>l</i> ≤ 22	–16 ≤ <i>l</i> ≤ 16	–16 ≤ <i>l</i> ≤ 16
Reflections collected	9896	3459	6033
Independent reflections	3802	2083	683
<i>R</i> _{int}	0.0284	0.0652	0.0414
Reflections parameters	353	415	100
<i>S</i> on <i>F</i> ²	0.945	1.085	1.130
<i>R</i> ₁ (<i>F</i> > 2 σ (<i>F</i>)) ^a	0.0315	0.0381	0.0141
<i>R</i> ₁ (all data)	0.0572	0.0599	0.0166
<i>wR</i> ₂ [<i>F</i> > 2(<i>F</i>)]	0.0719	0.0831	0.0323
<i>wR</i> ₂ (all data) ^b	0.0797	0.0993	0.0338

^a*R*₁ = $\sum ||F_o| - |F_c|| / \sum |F_o|$. ^b*R*_w = $[\sum (F_o^2 - F_c^2) / \sum w(F_o^2)]^{1/2}$. ^c*w* = $[\sigma_c^2(F_o^2) + (\chi P)^2 + yP]^{-1}$, *P* = $(F_o^2 - 2F_c^2) / 3$.

Appendix D

List of Compounds

Compnd.	Short Name	Full Name
1	5-At	5-Amino-1 <i>H</i> -tetrazole
2	DAT	1,5-Diamino-1 <i>H</i> -tetrazole
3	1MAT	1-Methyl-5-amino-1 <i>H</i> -tetrazole
4	2MAT	2-Methyl-5-amino-1 <i>H</i> -tetrazole
5	5AtClO ₄	5-Amino-1 <i>H</i> -tetrazolium Perchlorate
6	5AtNO ₃	5-Amino-1 <i>H</i> -tetrazolium Nitrate
7	5AtClO ₄ *5At	5-Amino-1 <i>H</i> -tetrazolium Perchlorate 5-Amino-1 <i>H</i> -tetrazole
8	5AtNO ₃ *5At	5-Amino-1 <i>H</i> -tetrazolium Nitrate 5-Amino-1 <i>H</i> -tetrazole
9	1MATClO ₄	1-Methyl-5-Amino-1 <i>H</i> -tetrazolium Perchlorate
10	1MATNO ₃	1-Methyl-5-Amino-1 <i>H</i> -tetrazolium Nitrate
11	2MATClO ₄	2-Methyl-5-Amino-1 <i>H</i> -tetrazolium Perchlorate
12	2MATNO ₃	2-Methyl-5-Amino-1 <i>H</i> -tetrazolium Nitrate
13	Ag ₂ AtClO ₄	Disilver 5-Amino-1 <i>H</i> -tetrazolium Perchlorate
14	Ag ₂ AtNO ₃	Disilver 5-Amino-1 <i>H</i> -tetrazolium Nitrate
15	Ag1MATClO ₄	Silver 1-Methyl-5-Amino-1 <i>H</i> -tetrazolium Perchlorate Hemihydrate
16	Ag1MATNO ₃	Silver 1-Methyl-5-Amino-1 <i>H</i> -tetrazolium Nitrate
17	Ag2MATClO ₄	Silver 2-Methyl-5-Amino-1 <i>H</i> -tetrazolium Perchlorate
18	Ag2MATNO ₃	Silver 2-Methyl-5-Amino-1 <i>H</i> -tetrazolium Nitrate
19	Ag(DMIT) ₂ Pic	Bis-(1,4-dimethyl-5-iminotetrazole) Silver Picrate
20	Ag(1MAT) ₃ NO ₃	Tri-(1-Methyl-5-Amino-1 <i>H</i> -tetrazolo) Silver Nitrate
21a	ANT	Ammonium 5-Nitrotetrazolate
21b	ANTh	Ammonium 5-Nitrotetrazolate Hemihydrate
22	LiNT	Lithium 5-Nitrotetrazolate Trihydrate
23	NaNT	Sodium 5-Nitrotetrazolate Dihydrate
24	KNT	Potassium 5-Nitrotetrazolate
25	RbNT	Rubidium 5-Nitrotetrazolate
26	CsNT	Cesium 5-Nitrotetrazolate
27	MgNT	Magnesium 5-Nitrotetrazolate Hexahydrate
28	CaNT	Calcium 5-Nitrotetrazolate Hexahydrate
29	SrNT	Strontium 5-Nitrotetrazolate Pentahydrate
30	BaNT	Barium 5-Nitrotetrazolate Pentahydrate
31	5-NTH	5-Nitro-2 <i>H</i> -tetrazole
31b	-	5-Nitro-1 <i>H</i> -tetrazole
32	DAT	1,5-diamino-1 <i>H</i> -tetrazole
33	Gz	3,4,5-Triamino-1,2,4-triazole (Guanazine)
34	GzNT	Guanazinium 5-Nitrotetrazolate
35	GzPic	Guanazinium Picrate
36	GzZT	Guanazinium 5,5'-Azotetrazolate
37	GzDN	Guanazinium Dinitramide
38	GzClO ₄	Guanazinium Perchlorate
39	GzNO ₃	Guanazinium Nitrate
40	GzN ₃	Guanazinium Azide
41	MeGzI	Methylguanazinium Iodide
42	MeGzN ₃	Methylguanazinium Azide
43	MeGzNO ₃	Methylguanazinium Nitrate
44	MeGzClO ₄	Methylguanazinium Perchlorate
45a	MeGzZTxH ₂ O	Methylguanazinium 5,5'-Azotetrazolate Monoh.
45b	MeGzZT	Methylguanazinium 5,5'-Azotetrazolate
46a	MeGzNTxH ₂ O	Methylguanazinium 5-Nitrotetrazolate Monoh.

46b	MeGzNT	Methylguanazinium 5-Nitrotetrazolate
47	MeGzDN	Methylguanazinium Dinitramide
48	HOSA	Hydroxylamine- <i>O</i> -sulfonic Acid
49	TScz	Thiosemicarbazide
50	DAGCl	Diaminoguanidinium Chloride
51	DNPP	2,4-Dinitro- <i>O</i> -phenyoxyphtalimide
52	DI	Diimine
53	GzBr	Guanazinium Bromide
54	MeTSczI	Methylthiosemicarbazide Iodide
55a	α -GzI	α -Guanazinium Iodide
55b	β -GzI	β -Guanazinium Iodide
56	MeTScz	Methylthiosemicarbazide
57	14DMATI	1,4-Dimethyl-5-aminotetrazolium Iodide
58	PicH	Picric Acid
59	5AtPic	5-Amino-1 <i>H</i> -tetrazolium Picrate
60	1MATPic	1-Methyl-5-amino-1 <i>H</i> -tetrazolium Picrate
61	2MATPic	2-Methyl-5-amino-1 <i>H</i> -tetrazolium Picrate
62	14DMATPic	1,4-Dimethyl-5-amino-1 <i>H</i> -tetrazolium Picrate
63	13DMATPic	1,3-Dimethyl-5-amino-1 <i>H</i> -tetrazolium Picrate
64	DATPic	1,5-Diamino-1 <i>H</i> -tetrazolium Picrate
65	MeDATPic	1,5-Diamino-4-methyl-tetrazolium Picrate
66	GzPic	Guanazinium Picrate
67	MeGzPic	Methylguanazinium Picrate
68	14DMIT	1,4-Dimethyl-5-iminotetrazole
69	13DMIT	1,3-Dimethyl-5-iminotetrazole
70	13DMATI	1,3-Dimethyl-5-amino-1 <i>H</i> -tetrazolium Iodide
71	13DMATNO ₃	1,3-Dimethyl-5-amino-1 <i>H</i> -tetrazolium Nitrate
72	13DMATClO ₄	1,3-Dimethyl-5-amino-1 <i>H</i> -tetrazolium Perchlorate
73	13DMATN ₃	1,3-Dimethyl-5-amino-1 <i>H</i> -tetrazolium Azide
74	13DMATDN	1,3-Dimethyl-5-amino-1 <i>H</i> -tetrazolium Dinitramide
75	H ₂ ZT	5,5'-Azo(bis)tetrazole
76	5-HyTz	5-hydrazino-1 <i>H</i> -tetrazole
77	NaZT	Sodium 5,5'-Azotetrazolate
78	TMeATZT	1,4,5-trimethyltetrazolium 5,5'-azotetrazolate
79	5-AZT	5-amino-1 <i>H</i> -tetrazolium 5,5'-azotetrazolate
80	DATZT	1,5-diaminotetrazolium 5,5'-azotetrazolate
81	14DMATZTh	1,4-dimethyl-5-aminotetrazolium 5,5'-azotetrazolate Dihydrate
82	13DMATZTh	1,3-dimethyl-5-aminotetrazolium 5,5'-azotetrazolate Hexahydrate
83	MeDATZTh	1,5-diamino-4-methyltetrazolium 5,5'-azotetrazolate Dihydrate
84	GzZT	Guanazinium 5,5'-Azotetrazolate
85	SczZTh	Semicarbazidium 5,5'-azotetrazolate Dihydrate
86	14DMATZT	1,4-dimethyl-5-aminotetrazolium 5,5'-azotetrazolate
87	13DMATZT	1,3-dimethyl-5-aminotetrazolium 5,5'-azotetrazolate
88	MeDATZT	1,5-diamino-4-methyltetrazolium 5,5'-azotetrazolate
89	SczZT	Semicarbazidium 5,5'-azotetrazolate
90	AgZT	Silver 5,5'-Azotetrazolate
91a	11DMZT	1,1'-Dimethyl-5,5'-Azotetrazole
91b	11DMZTh	1,1'-Dimethyl-5,5'-Azotetrazole Monohydrate
92	22DMZT	2,2'-Dimethyl-5,5'-Azotetrazole
93	HZT	Bishydrazinium 5,5'-azotetrazolate
94	BaZT	Barium 5,5'-Azotetrazolate
95	HBT	5,5'-Hydrazinebistetrazole
96	BTA	<i>N,N</i> -bis(1 <i>H</i> -tetrazole-5-yl)-amine
97	11DMHBT	1,1'-Dimethyl-5,5'-Hydrazinebistetrazole Monohydrate
98	22DMHBT	2,2'-Dimethyl-5,5'-Hydrazinebistetrazole
99	AHBT	Ammonium 5,5'-Hydrazinebistetrazolate Monohydrate
100	HHBT	Hydrazinium 5,5'-Hydrazinebistetrazolate

101	GHBT	Guanidinium 5,5'-Hydrazinebistetrazolate
102	AGHBT	Aminoguanidinium 5,5'-Hydrazinebistetrazolate
103	DAGHBT	Diaminoguanidinium 5,5'-Hydrazinebistetrazolate
104	TAGHBT	Triaminoguanidinium 5,5'-Hydrazinebistetrazolate
105	LiHBT	Lithium 5,5'-Hydrazinebistetrazolate Trihydrate
106	NaHBT	Sodium 5,5'-Hydrazinebistetrazolate Hemihydrate
107	KHBT	Potassium 5,5'-Hydrazinebistetrazolate
108	RbHBT	Rubidium 5,5'-Hydrazinebistetrazolate
109	CsHBT	Cesium 5,5'-Hydrazinebistetrazolate
110	MgHBT	Magnesium 5,5'-Hydrazinebistetrazolate Hexahemihydrate
111	CaHBT	Calcium 5,5'-Hydrazinebistetrazolate Pentahydrate
112	SrHBT	Strontium 5,5'-Hydrazinebistetrazolate Pentahydrate
113	BaHBT	Barium 5,5'-Hydrazinebistetrazolate Pentahydrate
114	CAGh	Carboxyaminoguanidine Betaine Monohydrate
115	AgHBT	Silver 5,5'-Hydrazinebistetrazolate
116	AgBTA	Silver <i>N,N</i> -Bis(1 <i>H</i> -tetrazolate-5-yl)-amine
117	SrZT	Strontium 5,5'-Azotetrazolate
118	ABTA	Ammonium <i>N,N</i> -Bis(1 <i>H</i> -tetrazolate-5-yl)-amine
119	HBTA	Hydrazinium <i>N,N</i> -Bis(1 <i>H</i> -tetrazolate-5-yl)-amine
120	GBTA	Guanidinium <i>N,N</i> -Bis(1 <i>H</i> -tetrazolate-5-yl)-amine
121	AGBTA	Aminoguanidinium <i>N,N</i> -Bis(1 <i>H</i> -tetrazolate-5-yl)-amine
122	DAGBTA	Diaminoguanidinium <i>N,N</i> -Bis(1 <i>H</i> -tetrazolate-5-yl)-amine
123	TAGBTA	Triaminoguanidinium <i>N,N</i> -Bis(1 <i>H</i> -tetrazolate-5-yl)-amine
124	GZT	Guanidinium 5,5'-Azotetrazolate
125	AGZT	Aminoguanidinium 5,5'-Azotetrazolate
126	DAGZT	Diaminoguanidinium 5,5'-Azotetrazolate
127	TAGZT	Triaminoguanidinium 5,5'-Azotetrazolate
128	NTAN	5-Nitrotetrazole-2-ylacetonitrile
129a	NTTzh	5-(5-Nitrotetrazole-2-ylmethyl)-tetrazole Monohydrate
129b	NTTz	5-(5-Nitrotetrazole-2-ylmethyl)-tetrazole
130	LiNTTz	Lithium 5-(5-Nitrotetrazole-2-ylmethyl)-tetrazolate Monohemihydrate
131	NaNTTz	Sodium 5-(5-Nitrotetrazole-2-ylmethyl)-tetrazolate Dihydrate
132	KNTTz	Potassium 5-(5-Nitrotetrazole-2-ylmethyl)-tetrazolate Monohydrate
133	RbNTTz	Rubidium 5-(5-Nitrotetrazole-2-ylmethyl)-tetrazolate Monohydrate
134	CsNTTz	Cesium 5-(5-Nitrotetrazole-2-ylmethyl)-tetrazolate Monohydrate
135	ANTTzh	Ammonium 5-(5-Nitrotetrazole-2-ylmethyl)-tetrazolate Monohydrate
136	HNTTz	Hydrazinium 5-(5-Nitrotetrazole-2-ylmethyl)-tetrazolate
137	GNTTz	Guanidinium 5-(5-Nitrotetrazole-2-ylmethyl)-tetrazolate
138	AGNTTz	Aminoguanidinium 5-(5-Nitrotetrazole-2-ylmethyl)-tetrazolate
139	DAGNTTz	Diaminoguanidinium 5-(5-Nitrotetrazole-2-ylmethyl)-tetrazolate
140	TAGNTTz	Triaminoguanidinium 5-(5-Nitrotetrazole-2-ylmethyl)-tetrazolate
141	AgNTTz	Silver 5-(5-Nitrotetrazole-2-ylmethyl)-tetrazolate Hemihydrate
142	CuNTTzh	Copper(II) 5-(5-Nitrotetrazole-2-ylmethyl)-tetrazolate Monohydrate
143	CuNaNTTzNh	Copper(II) Sodium Di-5-(5-nitrotetrazole-2-ylmethyl)-tetrazolate Nitrate Monohydrate
144	CuNaNTTzN	Copper(II) Sodium Di-5-(5-nitrotetrazole-2-ylmethyl)-tetrazolate Nitrate
145	BENT	2-(2-Bromoethyl)-5-nitrotetrazolate
146	NENT	2-(2-Nitratoethyl)-5-nitrotetrazole
147	AENT	2-(2-Azidoethyl)-5-nitrotetrazole
148	DNENT	2-(2-Dinitramidoethyl)-5-nitrotetrazole

List of Abbreviations			
		t (NMR)	Triplet
		TEX	Dinitro-tetraoxa-diazaisowurtzitane
		THF	Tetrahydrofuran
a.u.	Atomic Units (Hartree)	vs (IR)	Very Strong
calcd.	Calculated	vw (IR)	Very Weak
CL-20	Hexanitrohexaaza- <i>iso</i> -wurtzitane	w (IR)	Weak
Dec.	Decomposition	Å	Amstrong (10 ⁻¹⁰ m)
DMF	Dimethylformamide	δ	Chemical Shift
DMSO	Dimethylsulphoxide	ρ	Density
DSC	Differential Scanning Calorimetry	Ω	Oxygen Balance
EI	Electronic Ionization	ν	Frequency
en	Ethylendiamine		
g	Gas Phase		
h	Hours		
HMX	High Melting Explosive		
Int.	Intensity	Abbreviations of Chemical Names	
IR	Infrared	AG ⁺	Aminoguanidinium
<i>J</i>	Coupling Constant	5-AtH ⁺	5-Amino-1 <i>H</i> -tetrazolium
l	Liquid Phase	BTA ²⁻	<i>N,N</i> -Bis(1 <i>H</i> -tetrazolate-5-yl)-amine
m (IR)	Medium	DAG ⁺	Diaminoguanidinium
m (NMR)	Multiplet	DATH ⁺	1,5-Diamino-1 <i>H</i> -tetrazolium
Me	Methyl Group	13DMAT ⁺	1,3-Dimethyl-5-aminotetrazolium
min	Minutes	14DMAT ⁺	1,4-Dimethyl-5-aminotetrazolium
m.p.	Melting Point	G ⁺	Guanidinium
MS	Mass Spectroscopy	Gz ⁺	Guanazinium
NMR	Nuclear Magnetic Resonance	HBT ²⁻	5,5'-Hydrazinebistetrazolate
NOE	Nuclear-Overhauser Effect	1MATH ⁺	1-Methyl-5-aminotetrazolium
PETN	Penta Erythritol Tetra Nitrate	2MATH ⁺	2-Methyl-5-aminotetrazolium
ppm	Part per Million	MeDAT ⁺	1,5-Diamino-4-methyltetrazolium
q	Quartet	MeGz ⁺	Methylguanazinium
RDX	Research Department Explosive	NT ¹⁻	5-Nitrotetrazolate
RT	Room Temperature	NT ¹ Tz ⁻	5-(5-Nitrotetrazole-2-ylmethyl)-tetrazolate
s (NMR)	Singlet	Scz ⁺	Semicarbazidium
s	Solid Phase	TAG ⁺	Triaminoguanidinium
s (IR)	Strong	ZT ²⁻	5,5'-Azotetrazolate
T	Temperature		

Curriculum Vitae

Name: Carlos H. Miró Sabaté
Address: Cimbernstr. 68, 81377 Munich
E-Mail: cmich@cup.uni-muenchen.de
Birth Date: 10 June 1981, Lleida (Spain)
Nationality: Spanish
Marital Status: Single

Education: 1987–1995 Primary School: Col·legi Públic Otogesa, Maials, SPAIN
1995–1999 Secondary School: I.B. Joan Oró, Lleida, SPAIN
1998–1999 COU (A levels): I.B. Joan Oró, Lleida, SPAIN
June 1999 High-School Diploma (Cum Laude), I.B. Joan Oró, Lleida, SPAIN
1999–2004 B. Sc. Degree in Chemistry, Universitat Autònoma de Barcelona SPAIN
2003–2004 Exchange year at Glasgow University, Glasgow, UK
Oct. 2004– Ph. D. at the Ludwig-Maximilian University, Munich, GERMANY

Languages knowledge: Catalan and Spanish – Native speaker
English, German and Italian – Fluent
French and Portuguese – Basic knowledge

Work

Experience: July–Sept. 2002 – KAO CORPORATION S.A. in Barberà del Vallès, SPAIN
July–Sept. 2003 – Catalysis and Synthesis Group at the Universitat Autònoma de Barcelona
Oct.–April 2003 – Organic Synthesis Research on the topic “Synthesis of ^{13}C -Chlorogenic Acid” at Glasgow University
Oct. 2004–Present – Doctoral research on the topic “Highly Energetic Materials Based on Tetrazoles” at the Ludwig-Maximilian University

Teaching

Experience: Introductory teaching lab instructor: Oct.–Feb. 2004, Oct.–Feb. 2005, Oct.–Feb. 2006 and Oct.–Feb. 2007
Teaching lab instructor 4th semester inorganic chemistry: Apr.–Aug. 2005, Apr.–Aug. 2006 and Apr.–Aug. 2007
Teaching lab instructor advanced inorganic chemistry: Mar. 2005, Sept. 2005, Mar. 2006, Sept. 2006, Mar. 2007 and Sept. 2007
Teaching lab instructor magisterium (LAF): Apr.–May 2008
Supervisor of 1 bachelor and 3 undergraduate research students

Memberships/Scholarships

and Awards: Socrates/Erasmus Student Mobility Program: Glasgow University, Sept. 2003–June 2004

Excellent Poster Presentation Award: ICT Symposium, Pfinztal, GERMANY, March 13–14, 2007

Dr. Klaus Römer Outstanding Graduate Student Award: Ludwig-Maximilian University, Munich, Dec. 2007

Member of the Gesellschaft Deutscher Chemiker (GDCh), 2008

Karl-Ziegler-Stiftung (GDCh) Scholarship, Sept. 2008

Great Poster Presentation Award: 11th International Seminar on New Trends in Research of Energetic Materials, Pardubice, CZECH REPUBLIC, April 09–11, 2008

Great Oral Presentation Award: 11th International Seminar on New Trends in Research of Energetic Materials, Pardubice, CZECH REPUBLIC, April 09–11, 2008

Collaborations:

TTCP Program (Energetic Materials)

Full List of Publications

Articles (A) in Peer Reviewed Journals

- The Energetic Double Salt Nitroguanidinium Nitrate-Guanidinium Nitrate (1/1),**
A1 G. Steinhauser, M-J. Crawford, C. Darwich, T. M. Klapötke, C. Miró Sabaté, J. Welch,
Acta Crystallogr., **2007**, *E63*, o3100–o3101.
- Structural and Preliminary Explosive Property Characterizations of New 3,4,5-Triamino-1,2,4-triazolium Salts,**
A2 C. Darwich, T. M. Klapötke, C. Miró Sabaté,
Propellants, Explos. Pyrotech., **2007**, in press.
- 5,5'-Hydrazinebistetrazole: an Oxidation-stable Nitrogen-rich Compound and Starting Material for the Synthesis of 5,5'-Azobistetrazolates,**
A3 T. M. Klapötke, C. Miró Sabaté,
Z. Anorg. Allg. Chem., **2007**, *633*, 2671–2677.
- Synthesis and characterisation of 3,4,5-triamino-1,2,4-triazolium and 1-methyl-3,4,5-triamino-1,2,4-triazolium iodides,**
A4 C. Darwich, K. Karaghiosoff, T. M. Klapötke, C. Miró Sabaté,
Z. Anorg. Allg. Chem., **2008**, *634*, 61–68.
- Salts of Methylated 5-Aminotetrazoles with Energetic Anions,**
A5 K. Karaghiosoff, T. M. Klapötke, P. Mayer, C. Miró Sabaté, A. Penger, J. M. Welch,
Inorg. Chem., **2008**, *47*, 1007–1019.
- Synthesis, Characterization and Explosive Properties of 1,3-Dimethyl-5-amino-1*H*-tetrazolium 5-Nitrotetrazolate,**
A6 T. M. Klapötke, C. Miró Sabaté, M. Rusan,
Z. Anorg. Allg. Chem., **2008**, *634*(4), 688–695.
- The Preparation and Characterization of Guanylurea Nitrate and Perchlorate Salts,**
A7 T. M. Klapötke, C. Miró Sabaté,
Heteroat. Chem., **2008**, *19*(3), 301–306.
- Nitrogen-rich Tetrazolium Azotetrazolate Salts: a New Family of Insensitive Energetic Materials,**
A8 T. M. Klapötke, C. Miró Sabaté,
Chem. Mater., **2008**, *20*(5), 1750–1763.
- 1,5-Diamino-4-methyltetrazolium 5-Nitrotetrazolate – Synthesis, Testing and Scale-up,**
A9 T. M. Klapötke, C. Miró Sabaté, J. M. Welch,
Z. Anorg. Allg. Chem., **2008**, *634*(5), 857–866.
- Synthesis and Spectroscopic Characterization of Azolium Picrate Salts,**
A10 T. M. Klapötke, C. Miró Sabaté,
Z. Anorg. Allg. Chem., **2008**, *634*, 1017–1024.
- Bistetrazoles: Nitrogen-rich, High-performing, Insensitive Energetic Compounds,**
A11 T. M. Klapötke, C. Miró Sabaté,
Chem. Mater., **2008**, *20*(11), 3629–3637. [ACS PRESS RELEASE](#)

- Simple, Nitrogen-rich, Energetic Salts of 5-Nitrotetrazole,**
 A12 T. M. Klapötke, P. Mayer, C. Miró Sabaté, J. M. Welch, N. Wiegand,
Inorg. Chem., **2008**, 47(13), 6014–6027.
- The Preparation and Crystal Structures of two Salts with the 5-Nitrotetrazolate Anion,**
 A13 T. M. Klapötke, C. Miró Sabaté, J. M. Welch,
Heteroat. Chem., **2008**, submitted.
- 1,2,4-Triazolium-Cation-Based Energetic Salts,**
 A14 C. Darwich, T. M. Klapötke, C. Miró Sabaté,
Chem. Eur. J., **2008**, 14, 5756–5771.
- Hydrogen-bonding Stabilization in Energetic Perchlorate Salts: 5-Amino-1*H*-tetrazolium Perchlorate and its Adduct with 5-Amino-1*H*-tetrazole,**
 A15 T. M. Klapötke, C. Miró Sabaté, J. Stierstorfer,
Z. Anorg. Allg. Chem., **2008**, in press.
- Hydrates of 5-Amino-1*H*-tetrazolium Halogenide Salts – Starting Materials for the Synthesis of Energetic Compounds,**
 A16 M. von Denffer, T. M. Klapötke, C. Miró Sabaté,
Z. Anorg. Allg. Chem., **2008**, submitted.
- Alkali Metal 5-Nitrotetrazolate Salts: Prospective Replacements for Service Lead(II)azide in Explosive Initiators,**
 A17 T. M. Klapötke, C. Miró Sabaté, J. M. Welch,
J. Chem. Soc. Dalton Trans., **2008**, submitted.
- Energetic Silver Salts with 5-Aminotetrazole Ligands,**
 A18 K. Karaghiosoff, T. M. Klapötke, C. Miró Sabaté,
Chem. Eur. J., **2008**, submitted.
- Nitrogen-rich Compounds in Pyrotechnics: Alkaline Earth Metal Salts of 5,5'-Hydrazinebistetrazole,**
 A19 K. Karaghiosoff, T. M. Klapötke, C. Miró Sabaté,
Eur. J. Inorg. Chem., **2008**, submitted.
- 1,2,4-Triazolium and Tetrazolium Picrate Salts: “On the way” from Nitroaromatic to Azole-based Energetic Materials,**
 A20 T. M. Klapötke, C. Miró Sabaté,
Chem. Mater., **2008**, submitted.

Oral (O) Presentations

- Synthesis of ¹³C-chlorogenic Acid.**
 O1 Hartley, R.; Miró Sabaté, C.,
 Glasgow University, May 2004.
- Energetic Salts of 5-Aminotetrazole, 1-Methyl-5-aminotetrazole and 1,4-Dimethyl-5-iminotetrazole.**
 O2 v. Denffer, M.; Klapötke, T. M.; Mayer, P.; Miró Sabaté, C.; Penger, A.; Welch, J. M.,
 4th Swiss Snow Symposium, Grindelwald, Switzerland, Febr. 24-26, 2006.
- Stable Salts of Methylated 5-Aminotetrazoles.**
 O3 Göbel, M.; Karaghiosoff, K.; Klapötke, T. M.; Miró, C.; Welch, J. M.,
 New Trends in Research of Energetic Materials, Proceedings of the Seminar, 9th, Pardubice, Czech Republic, Apr. 19-21, 2006, 202-213 (indexed by chemical abstracts).

- New Tetrazole Based Energetic Materials.**
 O4 Klapötke, T. M.; Mayer, P.; Miró, C.; Penger, A.; Welch, J. M.,
 Abstracts of Papers, 233rd ACS National Meeting, Chicago, IL, United States, March 25-29, 2007.
- Primary Explosives: Metal Salts of 5-Nitrotetrazole.**
 O5 Klapötke, T. M.; Miró Sabaté, C.,
 New Trends in Research of Energetic Materials, Proceedings of the Seminar, 10th, Pardubice, Czech Republic, Apr. 25-27, 2007, 191-200 (indexed by chemical abstracts).
- Bridged-bistetrazole Derivatives.**
 O6 Klapötke, T. M.; Miró Sabaté, C.,
 New Trends in Research of Energetic Materials, Proceedings of the Seminar, 11th, Pardubice, Czech Republic, Apr. 09-11, 2008, 234-245 (indexed by chemical abstracts). **TALK AWARD**
- Pyrotechnics, Propellants and Explosives. Advances on Nitrogen-rich Chemistry**
 O7 Klapötke, T. M.; Miró Sabaté, C.,
 2nd EuCheMS Chemistry Congress, Torino, Italy, Sept. 16-20, 2008.

Poster (P) Presentations

- T. M. Klapötke, C. Miró Sabaté,
Environmentally Friendly, Insensitive Tetrazolium Azotetrazolates,
 P1 Insensitive Energetic Materials – Particles, Crystals, Composites, ICT Symposium, Pfinztal (Berghausen), Germany, March 13-14, 2007. **POSTER AWARD**
- T. M. Klapötke, C. Miró Sabaté,
Stable Salts of Methylated Guanidines with Energetic Anions,
 P2 Energetic Materials – Characterisation and Performance of Advanced Systems, 38th Annual Conference of ICT, Karlsruhe, Germany, Jun. 26-29, 2007.
- C. Darwich, T. M. Klapötke, C. Miró Sabaté,
Energetic Guanazinium Salts,
 P3 Prospective Students Open House, Munich, Germany, Febr. 22, 2008.
- T. M. Klapötke, C. Miró Sabaté, M. Rusan, J. M. Welch,
Energetic Salts containing the Nitrogen-rich 2-Methyl- and 1,3-Dimethyl-5-amino-1H-tetrazolium Cations,
 P4 Abstracts of Papers, 235rd ACS National Meeting, New Orleans, LA, United States, Apr. 6-10, 2008.
- T. M. Klapötke, C. Miró Sabaté, J. M. Welch,
Alkali and Alkaline-earth Metal Salts of 5-Nitrotetrazole as Primary Explosives,
 P5 Abstracts of Papers, 235rd ACS National Meeting, New Orleans, LA, United States, Apr. 6-10, 2008.
- T. M. Klapötke, C. Miró Sabaté,
5,5'-Hydrazinebistetrazole and its Metal Salts: Promising Propellant and Pyrotechnic Ingredients,
 P6 New Trends in Research of Energetic Materials, Proceedings of the Seminar, 11th, Pardubice, Czech Republic, Apr. 09-11, 2008, 661-672 (indexed by chemical abstracts).
- T. M. Klapötke, C. Miró Sabaté,
Energetic Salts with the Guanylurea Cation,
 P7 New Trends in Research of Energetic Materials, Proceedings of the Seminar, 11th, Pardubice, Czech Republic, Apr. 09-11, 2008, 673-679 (indexed by chemical abstracts). **POSTER AWARD**